MSFC MPR-SAT-FE-71-2

cy 2

GEORGE C. MARSHALL SPACE FLIGHT CENTER

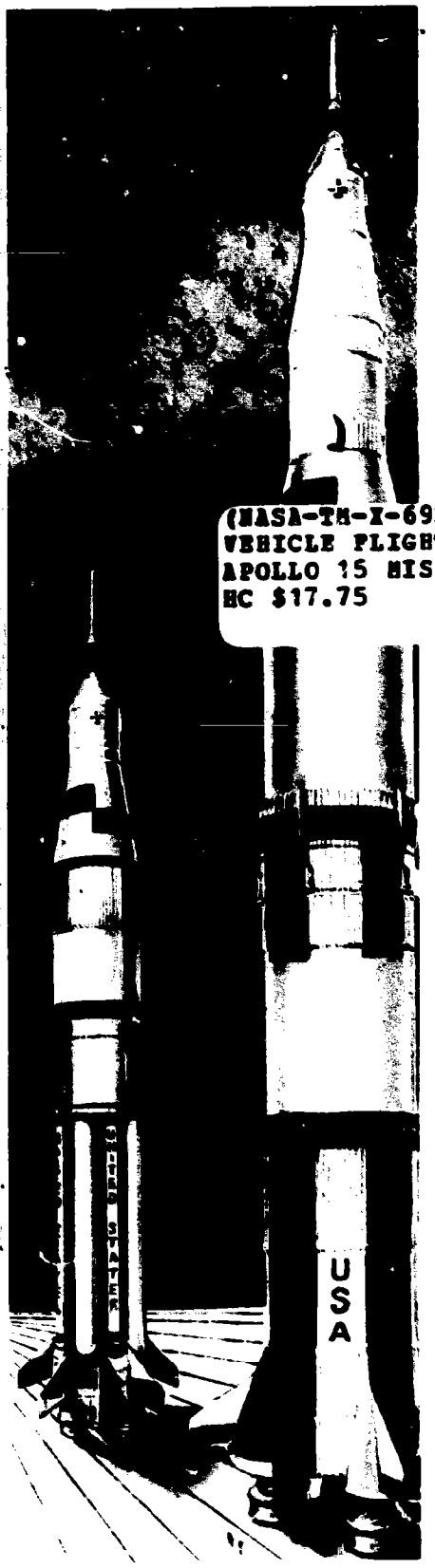

SATURN

MPR-SAT-FE-71-2

OCTOBER 28, 1971

(NASA-TM-X-69539) SATURN 5 LAUNCH VEHICLE FLIGHT EVALUATION REPORT, AS-510, APOLLO 15 MISSION (NASA) 312 p
HC $17.75 CSCL 22C G3/30

N73-33819
Unclas
19841

SATURN V LAUNCH VEHICLE FLIGHT EVALUATION REPORT-AS-510 APOLLO 15 MISSION

RECEIVED NASA STI FACILITY INPUT BRANCH NOV 1973

PREPARED BY

SATURN FLIGHT EVALUATION WORKING GROUP

NATIONAL AERONAUTICS AND SPACE ADMINISTRATION

MSFC - Form 774 (Rev October 1967)

GEORGE C. MARSHALL SPACE FLIGHT CENTER

MPR-SAT-FE-71-2

SATURN V LAUNCH VEHICLE

FLIGHT EVALUATION REPORT - AS-510

APOLLO 15 MISSION

PREPARED BY

SATURN FLIGHT EVALUATION WORKING GROUP

REPRODUCIBILITY OF THE ORIGINAL PAGE IS POOR

MPR-SAT-FE-71-2

V LAUNCH VEHICLE FLIGHT EVALUATION REPORT - AS-510

APOLLO 15 MISSION

BY

rn Flight Evaluation Working Group
ge C. Marshall Space Flight Center

ABSTRACT

Saturn V AS-510 (A o 15 Mission) was launched at 9:34:00 Eastern Daylight Time (ED on July 26, 1971, from Kennedy Space Center, Complex 39, Pad A. The vehicle lifted off on a launch azimuth of 90 degrees east of north and rolled to a flight azimuth of 80.088 degrees east of north. The launch vehicle successfully placed the manned spacecraft in the planned translunar coast mode. The S-IVB/IU impacted the lunar surface within the planned target area.

This was the first Apollo Mission to employ the Lunar Roving Vehicle (LRV) during Extravehicular Activity (EVA). The performance of the LRV was satisfactory and resulted in extended EVA, and greatly increased the crews lunar exploration capabilities.

All Mandatory and Desirable Objectives of this mission for the launch vehicle were accomplished except the precise determination of the lunar impact point. It is expected that this will be accomplished at a later date. No failures, anomalies, or deviations occurred that seriously affected the mission.

Any questions or comments pertaining to the information contained in this report are invited and should be directed to:

Director, George C. Marshall Space Flight Center
Huntsville, Alabama 35812
Attention: Chairman, Saturn Flight Evaluation Working Group, S&E-CSE-LA (Phone 205-453-2462)

PRECEDING PAGE BLANK NOT FILMED

TABLE OF CONTENTS

TABLE OF CONTENTS (CONTINUED)

TABLE OF CONTENTS (CONTINUED)

LIST OF ILLUSTRATIONS

LIST OF ILLUSTRATIONS (CONTINUED)

LIST OF ILLUSTRATIONS (CONTINUED)

LIST OF ILLUSTRATIONS (CONTINUED)

LIST OF TABLES

LIST OF TABLES (CONTINUED)

ACKNOWLEDGEMENT

This report is published by the Saturn Flight Evaluation Working Group, composed of representatives of Marshall Space Flight Center, John F. Kennedy Space Center, and MSFC's prime contractors, and in cooperation with the Manned Spacecraft Center. Significant contributions to the evaluation have been made by:

George C. Marshall Space Flight Center

Science and Engineering

Central Systems Engineering
Aero-Astrodynamics Laboratory
Astrionics Laboratory
Computation Laboratory
Astronautics Laboratory
Space Sciences Laboratory

Program Management

John F. Kennedy Space Center

Manned Spacecraft Center

The Boeing Company

McDonnell Douglas Astronautics Company

International Business Machines Company

North American Rockwell/Space Division

North American Rockwell/Rocketdyne Division

ABBREVIATIONS

ACN	Ascension Island
ACS	Alternating Current Power Supply
ALSEP	Apollo Lunar Surface Experiments Package
ANT	Antigua
AOS	Acquisition of Signal
APS	Auxiliary Propulsion System
ARIA	Apollo Range Instrument Aircraft
ASC	Accelerometer Signal Conditioner
BDA	Bermuda
BST	Boost
C&DC	Control and Display Console
CIF	Central Instrumentation Facility
CCS	Command and Communications System
CDDT	Countdown Demonstration Test
CECO	Center Engine Cutoff
CG	Center of Gravity
CM	Command Module
CNV	Cape Kennedy
CRO	Carnarvon
CRP	Computer Reset Pulse
CSM	Command and Service Module
CT4	Cape Telemetry 4
CVS	Continuous Vent System
CYI	Grand Canary Island
DAC	Data Acquisition Camera
DDAS	Digital Data Acquisition System
DEE	Digital Events Evaluator
DGU	Directional Gyro Unit
DO	Desirable Objective
DOM	Data Output Multiplexer
DTS	Data Transmission System
EBW	Exploding Bridge Wire
ECO	Engine Cutoff
ECP	Engineering Change Proposal
ECS	Environmental Control System
EDS	Emergency Detection System
EMR	Engine Mixture Ratio
EMU	Extra Vehicular Mobility Unit
EPO	Earth Parking Orbit
ESC	Engine Start Command
EST	Eastern Standard Time
ETC	Goddard Experimental Test Center
ETW	Error Time Word
EVA	Extra-Vehicular Activity
FCC	Flight Control Computer
FM/FM	Frequency Modulation/ Frequency Modulation
FMR	Flight Mission Rule
FRT	Flight Readiness Test
GBI	Grand Bahama Island

ABBREVIATIONS (CONTINUED)

GBS	Gas Bearing System
GDS	Goldstone
GG	Gas Generator
GOX	Gaseous Oxygen
GRR	Guidance Reference Release
GSE	Ground Support Equipment
GSFC	Goddard Space Flight Center
GTK	Grand Turk Island
GWM	Guam
HAW	Hawaii
HDA	Holddown Arm
HFCV	Helium Flow Control Valve
HSK	Honeysuckle Creek
ICD	Interface Control Document
IGM	Iterative Guidance Mode
IMU	Inertial Measurement Unit
IU	Instrument Unit
KSC	Kennedy Space Center
LCRU	Lunar Communication Relay Unit
LET	Launch Escape Tower
LH_2	Liquid Hydrogen
LM	Lunar Module
LMR	Launch Mission Rule
LOI	Lunar Orbit Insertion
LOS	Loss of Signal
LOX	Liquid Oxygen
LRV	Lunar Roving Vehicle
LSS	Lunar Soil Simulant
LUT	Launch Umbilical Tower
LV	Launch Vehicle
LVDA	Launch Vehicle Data Adapter
LVDC	Launch Vehicle Digital Computer
LVGSE	Launch Vehicle Ground Support Equipment
MAD	Madrid
MAP	Message Acceptance Pulse
MCC-H	Mission Control Center - Houston
MILA	Merritt Island Launch Area
ML	Mobile Launcher
MO	Mandatory Objective
MOV	Main Oxidizer Valve
MR	Mixture Ratio
MRCV	Mixture Ratio Control Valve
MSC	Manned Spacecraft Center
MSFC	Marshall Space Flight Center
MSFN	Manned Space Flight Network
MSS	Mobile Service Structure
MTF	Mississippi Test Facility
M/W	Methanol Water
NPSP	Net Positive Suction Pressure
NPV	Nonpropulsive Vent
NASA	National Aeronautics and Space Administration
OAT	Overall Test
OCP	Orbital Correction Program
OECO	Outboard Engine Cutoff
OFSO	Overfill Shutoff Sensor
OMPT	Postflight Trajectory
OT	Operational Trajectory
PACSS	Project Apollo Coordinate System Standards
PAFB	Patrick Air Force Base

PCM	Pulse Code Modulation
PCM/FM	Pulse Code Modulation/ Frequency Modulation
PEA	Platform Electronics Assembly
PIO	Process Input/Output
PLSS	Portable Life Support System
POI	Parking Orbit Insertion
PMR	Programed Mixture Ratio
PRA	Patrick Reference Atmosphere
PTCS	Propellant Tanking Computer System
PTC	Passive Thermal Control
PU	Propellant Utilization
RF	Radiofrequency
RFI	Radiofrequency Interference
RMS	Root Mean Square
RP-1	S-IC Stage Fuel
SA	Service Arm
SC	Spacecraft
SCFM	Standard Cubic Feet per Minute
SCIM	Standard Cubic Inch per Minute
SLA	Spacecraft/LM Adapter
SM	Service Module
SPS	Service Propulsion System
SPU	Signal Processing Unit
SRSCS	Secure Range Safety Command System
SSDO	Switch Selector and Discrete Output Register
SSE	Space Support Equipment
STDV	Start Tank Discharge Valve
SV	Space Vehicle
TCS	Thermal Conditioning System
TD&E	Transportation, Docking and Ejection
TEI	Transearth Injection
TEX	Corpus Christi (Texas)
TLC	Translunar Coast
TLI	Translunar Injection
TM	Telemetry
TMR	Triple Module Redundant
TSM	Tail Service Mast
TVC	Thrust Vector Control
UCR	Unsatisfactory Condition Report
USAE	U. S. Army Engineer
USB	Unified S-Band
UT	Universal Time
VA	Volt Amperes
VAN	Vanguard (ship)
VHF	Very High Frequency
WES	Waterways Experimental Station
Z	Zulu Time (equivalent to UT)

MISSION PLAN

The AS-510 flight (Apollo 15 Mission) is the tenth flight in the Apollo/Saturn V flight program, the fifth lunar landing mission, and the third landing planned for the lunar highlands. The primary mission objectives are: a) perform selenological inspection, survey, and sampling of materials in the Hadley-Appennine Region; b) deploy and activate the Apollo Lunar Surface Experiments Package (ALSEP); c) evaluate the capability of the Apollo equipment to provide extended lunar surface stay time, increased Extravehicular Activity (EVA), and surface mobility; and d) conduct inflight experiments and photographic tasks from lunar orbit. The crew consists of David R. Scott (Mission Commander), Alfred M. Worden, Jr. (Command Module Pilot), and James B. Irwin (Lunar Module Pilot).

The AS-510 Launch Vehicle (LV) is composed of the S-IC-10, S-II-10, and S-IVB-510 stages, and Instrument Unit (IU)-510. The Spacecraft (SC) consists of SC/Lunar Module Adapter (SLA)-19, Command Module (CM)-112, Service Module (SM)-112, and Lunar Module (LM)-10. The LM has been modified for this flight and will include the Lunar Roving Vehicle (LRV)-1.

Vehicle launch from Complex 39A at Kennedy Space Center (KSC) is along a 90 degree azimuth with a roll to a flight azimuth of approximately 80.088 degrees measured east of true north. Vehicle mass at ignition is 6,494,710 lbm.

The S-IC stage powered flight is approximately 159 seconds; the S-II stage provides powered flight for approximately 388 seconds. The S-IVB stage burn of approximately 145 seconds inserts the S-IVB/IU/SLA/LM/Command and Service Module (CSM) into a circular 90 n mi altitude (referenced to the earth equatorial radius) Earth Parking Orbit (EPO). Vehicle mass at orbit insertion is 309,816 lbm.

At approximately 10 seconds after EPO insertion, the vehicle is aligned with the local horizontal. Continuous hydrogen venting is initiated shortly after EPO insertion and the LV and CSM systems are checked in preparation for the Translunar Injection (TLI) burn. During the second or third revolution in EPO, the S-IVB stage is restarted and burns for approximately 356 seconds. This burn inserts the S-IVB/IU/SLA/LM/CSM into a near free-return, translunar trajectory.

Within 15 minutes after TLI, the vehicle initiates a maneuver to an inertial attitude hold for CSM separation, docking, and LM ejection. Following the attitude freeze, the CSM separates from the LV and the SLA panels are jettisoned. The CSM then transposes and docks to the LM. After docking, the CSM/LM is spring ejected from the S-IVB/IU. Following separation of the combined CSM/LM from the S-IVB/IU, the S-IVB/IU will perform a yaw maneuver and then an 80-second burn of the S-IVB Auxiliary Propulsion System (APS) ullage engines to propel the S-IVB/IU a safe distance away from the spacecraft. Subsequent to the completion of the S-IVB/IU evasive maneuver, the S-IVB/IU is placed on a trajectory such that it will impact the lunar surface in the vicinity of the Apollo 14 landing site. The impact trajectory is achieved by propulsive venting of liquid hydrogen (LH_2) and dumping of residual liquid oxygen (LOX) and by firing the APS engines. The S-IVB/IU impact will be recorded by the seismographs deployed during the Apollo 12 and 14 missions. S-IVB/IU lunar impact is predicted at approximately 79 hours 15 minutes after launch.

Several inflight experiments will be flown on Apollo 15. Several experiments are to be conducted by use of the Scientific Instrument Module (SIM) located in Sector I of the SM. A subsatellite is launched from the SIM into lunar orbit and several experiments are performed by it. The inflight experiments are conducted during earth orbit, translunar coast, lunar orbit, and transearth coast mission phases.

During the 75-hour 36-minute translunar coast, the astronauts will perform star-earth landmark sightings, Inertial Measurement Unit (IMU) alignments, general lunar navigation procedures, and possibly four midcourse corrections. At approximately 78 hours and 31 minutes, a Service Propulsion System (SPS), Lunar Orbit Insertion (LOI) burn of approximately 392 seconds is initiated to insert the CSM/LM into a 58 by 170 n mi altitude parking orbit. Approximately two revolutions after LOI a 22.9-second burn will adjust the orbit into an 8 by 60 n mi altitude. The LM is entered by astronauts Scott and Irwin, and checkout is accomplished. During the twelfth revolution in orbit, at 100.14 hours, the LM separates from the CSM and prepares for the lunar descent. The CSM is then inserted into an approximately 60 n mi circular orbit using a 3.9-second SPS burn. The LM descent propulsion system is used to brake the LM into the proper landing trajectory and maneuver the LM during descent to the lunar surface.

Following lunar landing, three EVA time periods of 7, 7, and 6 hours are scheduled during which the astronauts will explore the lunar surface in the LRV, examine the LM exterior, photograph the lunar surface, and deploy scientific instruments. Sorties in the LRV will be limited in radius such that the life support system capability will not be exceeded if LRV failure necessitates the astronauts walking back to the LM. Total stay time on the lunar surface is open-ended. with a planned maximum of 67 hours, depending upon the outcome of current lunar surface operations planning and of real-time operational decisions. After the EVA, the astronauts prepare the LM ascent propulsion system for lunar ascent.

The CSM performs a plane change approximately 8 hours before rendezvous. At approximately 171.7 hours, the ascent stage inserts the LM into a 9 by 46 n mi altitude lunar orbit. At approximately 173.5 hours the rendezvous and docking with the CSM are accomplished.

Following docking, equipment transfer, and decontamination procedures, the LM ascent stage is jettisoned and targeted to impact the lunar surface at a point near the Apollo 15 landing site, but far enough away so as not to endanger the scientific packages. During the second revolution before transearth injection, the CSM will perform an SPS maneuver to achieve a 55 by 75 n mi orbit. Shortly thereafter the subsatellite will be launched into the same orbit. Transearth Injection (TEI) is accomplished at the end of revolution 74 at approximately 223 hours and 46 minutes with a 139-second SPS burn.

During the 71-hour 12-minute transearth coast, the astronauts will perform navigation procedures, star-earth-moon sightings, and possibly three midcourse corrections. The SM will separate from the CM 15 minutes before reentry. Splashdown will occur in the Pacific Ocean 295 hours and 12 minutes after liftoff.

After the recovery operations, a biological quarantine is not imposed on the crew and CM. However, biological isolation garments will be available for use in the event of unexplained crew illness.

FLIGHT SUMMARY

The eighth manned Saturn V Apollo space vehicle, AS-510 (Apollo 15 Mission) was launched at 9:34:00 Eastern Daylight Time on July 26, 1971. The performance of the launch vehicle was satisfactory and at the time of this report, all MSFC objectives have been successfully accomplished except for the precise determination of the lunar impact point. Preliminary assessments indicate that the final impact solution will satisfy the mission objective.

The ground systems supporting the AS-510/Apollo 15 countdown and launch performed satisfactorily. System component failures and malfunctions requiring corrective action were corrected during countdown without causing unscheduled holds. Propellant tanking was accomplished satisfactorily. Damage to the pad, Launch Umbilical Tower (LUT) and support equipment was considered minimal.

The vehicle was launched on an azimuth 90 degrees east of north. A roll maneuver was initiated at 12.2 seconds that placed the vehicle on a flight azimuth 80.088 degrees east of north. The trajectory parameters from launch to Translunar Injection (TLI) were close to nominal. Earth Parking Orbit (EPO) insertion conditions were achieved 4.39 seconds earlier than nominal at a heading angle 0.143 degree less than nominal. TLI was achieved 0.88 second later than nominal. The trajectory parameters at Command and Service Module (CSM) separation deviated from nominal since the event occurred 94.3 seconds later than predicted.

All S-IC propulsion systems performed satisfactorily. In all cases, the propulsion performance was very close to nominal. Overall stage thrust was 0.47 percent lower than predicted. Total propellant consumption rate was 0.29 percent lower than predicted with the total consumed Mixture Ratio (MR) 0.35 percent higher than predicted. Specific impulse was 0.18 percent lower than predicted. Total propellant consumption from Holddown Arm (HDA) release to Outboard Engine Cutoff (OECO) was low by 0.03 percent. Center Engine Cutoff (CECO) was initiated by the Instrument Unit (IU) at 136.0 seconds. OECO, initiated by LOX low level sensors, occurred at 159.56 seconds which was 0.53 second later than predicted. The LOX residual at OECO was 31,135 lbm compared to the predicted 36,115 lbm. The fuel residual at OECO was 27,142 lbm compared to the predicted 29,404 lbm. The S-IC experienced a 1-1-2-1 start sequence rather than the planned 1-2-2 sequence. Since engine No. 1 had been replaced after the stage static test, it was expected that the planned start sequence would not be attained.

The S-II propulsion system performed satisfactorily throughout flight. The S-II Engine Start Command (ESC), as sensed at the engines, occurred at 161.95 seconds. CECO occurred as planned at 459.56 seconds, and OECO occurred at 549.06 seconds giving an outboard engine operating time of 387.11 or 1.16 seconds less than predicted. The earlier than predicted S-II OECO was a result of higher than predicted engine performance during the low Engine Mixture Ratio (EMR) portion of S-II boost. Four of the eight S-IC retro motors and all of the S-II ullage motors were removed for this flight; therefore, the S-IC/S-II separation sequence was revised. This sequence change extended the coast period between S-IC OECO and S-II ESC by one second. The S-IC/S-II separation sequence and S-II engine thrust buildup performance was satisfactory. The total stage thrust at the standard time slice (61 seconds after S-II ESC) was 0.05 percent below predicted. Total propellant flowrate, including pressurization flow, was 0.03 percent below predicted and the stage specific impulse was 0.02 percent below predicted at the standard time slice. Stage propellant mixture ratio was 0.03 percent above predicted. Engine cutoff transients were normal.

This was the second flight stage to incorporate a center engine LOX feedline accumulator system as a POGO suppression device. The operation of the accumulator system was effective in suppressing POGO type oscillations.

S-II hydraulic system performance was normal throughout the flight.

The S-IVB propulsion system operated satisfactorily throughout operational phase of first and second burns and had normal start and cutoff transients. S-IVB first burn time was 141.5 seconds which was 3.8 seconds less than predicted. Approximately 2.6 seconds of the shorter burn time can be attributed to higher S-IVB performance. The remainder can be attributed to S-IC and S-II stage performances. The engine performance during first burn, as determined from standard altitude reconstruction analysis, deviated from the predicted Start Tank Discharge Valve (STDV) +130-second time slice by 1.82 percent for thrust and 0.09 percent for specific impulse. The S-IVB stage first burn Engine Cutoff (ECO) was initiated by the Launch Vehicle Digital Computer (LVDC) at 694.7 seconds. The Continuous Vent System (CVS) adequately regulated LH_2 tank ullage pressure at an average level of 19.3 psia during orbit and the Oxygen/Hydrogen (O_2/H_2) burner satisfactorily achieved LH_2 and LOX tank repressurization for restart. Engine restart conditions were within specified limits. The restart at full open Mixture Ratio Control Valve (MRCV) position was successful.

Abnormal temperatures were noted in the turbine hot gas system between first burn ECO and second burn ESC. Most noticeable was the fuel turbine inlet temperature. During LH_2 chilldown in Time Base 6 (T_6), the temperature decreased from 130 to -10°F at second ESC. The oxidizer turbine inlet temperature also indicated a small decrease in temperature. In addition, fuel turbine inlet temperature indicated an abnormally fast temperature decrease after first burn ECO. The cause of the decrease in turbine inlet temperature was a small leak past the teflon seal of the gas generator fuel valve poppet.

S-IVB second burn time was 350.8 seconds which was 5.4 seconds less than predicted. The engine performance during second burn, as determined from the standard altitude reconstruction analysis, deviated from the predicted STDV +130-second time slice by 1.89 percent for thrust and 0.09 percent for specific impulse. Second burn ECO was initiated by the LVDC at 10,553.7 seconds (02:55:53.7). Subsequent to second burn, the stage propellant tanks and helium spheres were safed satisfactorily. Sufficient impulse was derived from LOX dump, LH_2 CVS operation and Auxiliary Propulsion System (APS) ullage burns to achieve a successful lunar impact.

The structural loads experienced during the S-IC boost phase were well below design values. The maximum bending moment was 80 x 10^6 lbf-in. at the S-IC LOX tank (30 percent of the design value). Thrust cutoff transients experienced by AS-510 were similar to those of previous flights. The maximum longitudinal dynamic responses at the IU were ±0.25 g and ±0.30 g at S-IC CECO and OECO, respectively. The magnitudes of the thrust cutoff responses are considered normal. During S-IC stage boost, 4 to 5 hertz oscillations were detected beginning at approximately 100 seconds. The maximum amplitude measured at the IU was ±0.06 g. Oscillations in the 4 to 5 hertz range have been observed on previous flights and are considered to be normal vehicle response to flight environment. POGO did not occur during S-IC boost. The S-II stage center engine LOX feedline accumulator successfully inhibited the 14 to 16 hertz POGO oscillations. A peak response of ±0.6 g was measured on engine No. 5 gimbal pad during steady-state engine operation. As on previous flights, low amplitude 11 hertz oscillations were experienced near the end of S-II burn. Peak engine No. 1 gimbal pad response was ±0.06 g. POGO did not occur during S-II boost. The POGO limiting backup cutoff system performed satisfactorily during the prelaunch and flight operations. The system did not produce any discrete outputs. The structural loads experienced during the S-IVB stage burns were well below design values. During first burn the S-IVB experienced low amplitude, 16 to 20 hertz oscillations. The amplitudes measured on the gimbal block were comparable to previous flights and well within the expected range of values. Similarly, S-IVB second burn produced intermittent low amplitude oscillations in the 12 to 16 hertz frequency range which peaked near second burn ECO.

The guidance and navigation system provided satisfactory end conditions for the boost to Earth Parking Orbit (EPO) and the boost to TLI. A navigation update was performed at the beginning of the second revolution, because the difference between the IU navigation vector and the tracking vector at Carnarvon exceeded the allowable tolerance defined in Flight Mission Rule (FMR) 7-11. The navigation differences following the update were small and were well within all allowable tolerances at TLI.

A negative shift of approximately 0.25 m/s (0.82 ft/s) occurred in the Z (down range) accelerometer output approximately one second before range zero. The probable cause of the shift was vibration which held the measuring head off null in the negative direction. The precise effect of

the shift on subsequent navigation errors has not been determined. The Launch Vehicle Data Adapter (LVDA) and LVDC performed satisfactorily with nominal values for component temperatures and power supply voltages.

The AS-510 control system was different from that of AS-509 because of redesigned filters and a revised gain schedule. These changes were made to stabilize structural dynamics caused by vehicle mass and structural changes and to improve wind and engine-out characteristics. The system performed satisfactorily. The Flight Control Computer (FCC), Thrust Vector Control (TVC) System, and Auxiliary Propulsion System (APS) satisfied all requirements for vehicle attitude control during the flight. Bending and slosh dynamics were adequately stabilized. The prelaunch programed yaw, roll, and pitch maneuvers were properly executed during S-IC boost. During the maximum dynamic pressure region of flight, the launch vehicle experienced winds that were slightly greater than the 95-percentile July wind from a 60-degree azimuth. The maximum average pitch engine deflection was in the maximum dynamic pressure region. The maximum average yaw engine deflection occurred with the initial yaw maneuver.

S-IC/S-II first and second plane separations were accomplished with no significant attitude deviations. The S-IC retro motors performed as expected. Separation distance was less than predicted because F-1 engine impulse "tailoff" was higher than expected. The effect of the closer S-II exhaust plume at engine start resulted in a more severe environment at the S-IC forward LOX dome and resulted in S-IC telemetry system damage. Analysis indicates that with an S-IC stage having only four retro motors, failure of one retro motor to ignite would result in marginal separation distance and in the 3σ case, recontact of the two stages. Consequently, S-IC-11 and subsequent stages will be equipped with eight retro motors rather than the planned four.

The AS-510 launch vehicle electrical systems and Emergency Detection System (EDS) performed satisfactorily throughout all phases of flight. Operation of the batteries, power supplies, inverters, Exploding Bridge Wire (EBW) firing units and switch selectors was normal.

Vehicle base pressure and base thermal environments, in general, were similar to those experienced on earlier flights. The environmental control system performance was satisfactory.

All data systems performed satisfactorily through the flight. Flight measurements from onboard telemetry were 99.8 percent reliable. Telemetry performance was normal except that the S-IC telemetry was lost after S-IC/S-II separation. Radiofrequency (RF) propagation was generally good, though the usual problems due to flame effects and staging were experienced and an additional dropout occurred when S-II stage flame impinged on the S-IC stage at S-II stage ignition. Usable Very High Frequency (VHF) data were received until 23,225 seconds (6:27:05). The Secure Range Safety Command Systems (SRSCS) on the S-IC, S-II, and S-IVB stages were ready to

perform their functions properly, on command, if flight conditions during launch phase had required destruct. The system properly safed the S-IVB on a command transmitted from Bermuda (BDA) at 701.5 seconds. The performance of the Command and Communications System (CCS) was excellent. Usable CCS telemetry data were received to 48,240 seconds (13:24:00) at which time the telemetry subcarrier was inhibited. Ascension (ACN), Canary Island (CYI), Goldstone (GDS), Madrid (MAD), and Merritt Island Launch Area (MILA) were receiving CCS signal carrier at S-IVB/IU lunar impact. Good tracking data were received from the C-Band radar, with Carnarvon (CRO) indicating final Loss of Signal (LOS) at 53,358 seconds (14:49:18).

All aspects of the S-IVB/IU lunar impact mission objectives were accomplished successfully with the possible exception of the precise determination of the impact point. Previous experience and the high quality and large quantity of tracking data indicate that the final impact solution will satisfy the remaining mission objective after additional analysis. At 285,881.55 seconds (79:24:41:55), the S-IVB/IU impacted the lunar surface at approximately 0.99 degree south latitude and 11.89 degrees west longitude with a velocity of 2577 m/s (8455 ft/s). This preliminary impact point is approximately 154 kilometers (83 n mi) from the target of 3.67 degrees south latitude and 7.58 degrees west longitude. The mission objectives were to maneuver the S-IVB/IU such that it would have at least a 50 percent probability of impacting the lunar surface with 350 kilometers (189 n mi) of the target, and to determine the actual impact point within 5 kilometers (2.7 n mi), and the time within 1 second. The AS-510 targeting philosophy for seismic experiment performance and data resolution defined "preferred," "acceptable," and "undesirable" impact regions about the Apollo 12 and Apollo 14 lunar seismometers. Although the impact location is not within the preferred region nor within the acceptable region of the Apollo 14 seismometer, the principle seismic experiment investigator reports that both seismometers gave valuable scientific data from the impact. The projected impact point resulting from the APS-1 maneuver was perturbed in an easterly direction by unplanned forces acting after the LOX dump. A first force was caused by the ambient helium pressurization spheres dumping through the ambient helium engine control sphere into the J-2 engine. Other forces were apparently caused by the IU thermal control system water valve operations and APS attitude engine reactions. Following the APS-2 maneuver, a small and gradually decreasing unbalanced force (also unplanned) acted during a 5-hour period to perturb the lunar impact to a point northwest of the target.

All Lunar Roving Vehicle (LRV) systems performed satisfactorily with the range capability being approximately twice the predicted value. The total range traversed was 27.9 kilometers at an average velocity of 9.3 km/hr; the maximum velocity was 13 km/hr and the maximum slopes negotiated were up to 12 degrees. The stopping distance was approximately 4.6 meters from 10 km/hr, and the braking and steering duty cycles were much less than predicted, with estimates of 5 percent of the time given by the crew. The LRV average energy consumation was 1.87 amp-hr/km with a total consumed energy of 52 amp-hr. The navigation system attained a Lunar Module (LM)

closure error of less than 0.2 kilometer on each traverse while gyro drift was negligible. The wander factor (LRV path deviation due to obstacles) plus wheel slip was approximately equal to the predicted value of 10 percent.

The following list of concerns was recorded during the lunar surface operation:

a. Battery No. 2 volt-ammeter was inoperative at first power up.

b. Forward steering was inoperative on Extravehicular Activity (EVA)-1 but was successfully activated on EVA-2 and 3.

c. Seat belt fastening was excessively time consuming.

d. Lunar Communication Relay Unit (LCRU) TV dropped out after LM liftoff.

e. The left front fender extension was missing after EVA-1.

MISSION OBJECTIVES ACCOMPLISHMENT

Table 1 presents the MSFC Mandatory Objectives and Desirable Objectives as defined in the "Saturn V Apollo 15/AS-510 Mission Implementation Plan," MSFC Document PM-SAT-8010.8 (Rev. A), dated March 5, 1971. An assessment of the degree of accomplishment of each objective is shown. Discussion supporting the assessment can be found in other sections of this report as shown in Table 1.

Table 1. Mission Objectives Accomplishment

NO.	MSFC MANDATORY OBJECTIVES (MO) AND DESIRABLE OBJECTIVES (DO)	DEGREE OF ACCOMPLISHMENT	DISCREPANCIES	PARAGRAPH IN WHICH DISCUSSED
1	Launch on a flight azimuth between 80 and 100 degrees and insert the S-IVB/IU/SC into the planned circular earth parking orbit (MO).	Complete	None	4.1, 9.1
2	Restart the S-IVB during either the second or third revolution and inject the S-IVB/IU/SC onto the planned translunar trajectory (MO).	Complete	None	4.2.3, 7.6
3	Provide the required attitude control for the S-IVB/IU/SC during TD&E (MO).	Complete	None	10.4.4
4	Perform an evasive maneuver after ejection of the CSM/LM from the S-IVB/IU (DO).	Complete	None	10.4.4
5	Impact the S-IVB/IU on the lunar surface within 350 kilometers of lat. 3.65°S, long. 7.58°W (DO).	Complete	None	17.5
6	Determine actual impact point within 5 kilometers and time of impact within one second (DO).	Probably Complete	Analysis not Complete	17.5
7	After final LV/SC separation, vent and dump the remaining gases and propellants to safe the S-IVB/IU (DO).	Complete	None	7.13

FAILURES, ANOMALIES AND DEVIATIONS

Evaluation of the launch vehicle and LRV data revealed seven deviations. There were no failures nor anomalies. The deviations are summarized in Table 2.

Table 2. Summary of Deviations

ITEM	VEHICLE SYSTEM	DEVIATION	PROBABLE CAUSE	SIGNIFICANCE	PARAGRAPH REFERENCE
1	Guidance/ Navigation	The difference between the IU navigation state vector and the tracking vector at Carnarvon exceeded the allowable tolerance defined by Flight Mission Rule (FMR) 7-11	(1) Propagation of insertion navigation errors, and (2) higher than predicted continuous vent system thrust during EPO.	None. A navigation update was performed at the beginning of the second revolution, 6371.59 seconds (1:46:11.59). The navigation differences following the update were small and well within all applicable tolerances at Translunar Injection (TLI).	9.2, 9.3
2	S-IC/S-II Separation	S-IC/S-II separation slower than predicted.	F-1 engine thrust decay longer than was used in separation prediction.	The pressure and thermal environment at the S-IC forward LOX dome due to the closer S-II exhaust plume was more severe than expected and resulted in S-IC non-critical telemetry system damage. To assure a safer, more positive separation, S-IC-11 and subsequent will be equipped with eight retro motors rather than the planned four.	10.6
3	Flight Program/ S-IVB Propulsion	LOX venting through the non-propulsive vent following earth parking orbit insertion.	Phase reinforcement of a slosh wave caused by the pitch maneuver to local horizontal resulted in LOX covering the vent line diffuser and venting through the LOX non-propulsive vent.	Approximately 500 lbm of LOX was vented. The AS-510 90 n mi earth orbit required an 18° pitch maneuver, which was greater than the 6 to 10° maneuver required for the 100 n mi orbit on previous flights. The unfavorable phasing condition will be corrected by reducing the commanded pitch turning rate from 0.4°/s to approximately 0.14°/s during the maneuver to local horizontal.	7.10.2, 10.4.2
4	S-IVB Propulsion	4500 lbf-s impulse from unplanned ambient helium dump through the J-2 engine.	A planned AS-510 sequence change had delayed the LH_2 ambient helium dump to later in the mission to reserve pressurizing gas for dumping additional propellants if more Δv were required to achieve lunar impact. However, it was not recognized that because of ambient helium and engine control bottle interconnection, the LH_2 ambient helium pressurant could not be retained beyond engine helium control bottle safing.	The resulting impulse devalued the IU state vector, which is the backup vector for lunar impact targeting. In cases where the backup is required, as on Apollo 14, impact outside the target radius of 380 km could have occurred. The impulse could also have caused added uncertainty in the primary vector which is computed from tracking data. Corrective action has been taken to return the dumping sequence to essentially the same operation as programed for previous flights.	7.13.4, 17.3
5	S-IVB Electrical	Forward No. 2 battery did not deliver the vendor guaranteed rating of 24.75 ampere hours. Depleted after supplying 22.21 ampere hours.	Unknown. Tests in process at vendor's factory for identification of possible deficiencies.	None. Mission requirements of the battery were achieved with adequate reserves.	11.4
6	Lunar Roving Vehicle (LRV)	Forward steering inoperative during first EVA.	All likely sources have been investigated. Further isolation is not possible because of LRV data limitation.	None. The first EVA was completed satisfactorily using only the rear steering. Forward steering was operative for the second and third EVA. No further investigation is planned for this item.	20.7.4, 20.8.4
7	LRV	Seat belts difficult to secure.	In the 1/6 g lunar environment the astronauts experienced less compression of their suits which resulted in a higher sitting position making seat belts difficult to secure.	Approximately 20 minutes of EVA time was lost due to extra time taken for securing seat belts. Seat belts will be modified to provide easier adjustment and operation.	20.11

SECTION 1

INTRODUCTION

1.1 PURPOSE

This report provides the National Aeronautics and Space Administration (NASA) Headquarters, and other interested agencies, with the launch vehicle and Lunar Roving Vehicle (LRV) evaluation results of the AS-510 flight (Apollo 15 Mission). The basic objective of flight evaluation is to acquire, reduce, analyze, evaluate and report on flight data to the extent required to assure future mission success and vehicle reliability. To accomplish this objective, actual flight problems are identified, their causes determined, and recommendations made for appropriate corrective action.

1.2 SCOPE

This report contains the performance evaluation of the major launch vehicle systems and LRV, with special emphasis on problems. Summaries of launch operations and spacecraft performance are included.

The official George C. Marshall Space Flight Center (MSFC) position at this time is represented by this report. It will not be followed by a similar report unless continued analysis or new information should prove the conclusions presented herein to be significantly incorrect. Reports covering special subjects will be published as required.

SECTION 2

EVENT TIMES

2.1 SUMMARY OF EVENTS

Range zero time, the basic time reference for this report is 09:34:00 Eastern Daylight Time (EDT) (13:34:00 Universal Time [UT]) July 26, 1971. Range time is the elapsed time from range zero time and, unless otherwise noted, is the time used throughout this report. All data, except as otherwise defined, presented in "Range Time" are the times at which the data were received at the telemetry ground station, i.e., actual time of occurrence at the vehicle plus telemetry transmission time. The Time-From-Base times are presented as elapsed vehicle time from start of time base. Vehicle time is the Launch Vehicle Digital Computer (LVDC) clock time. Figure 2-1 shows the conversion between ground station time and vehicle time.

Vehicle and ground times for each time base used in the flight sequence program and the signal for initiating each time base are presented in Table 2-1. Start times of T_0, T_1, and T_2 were nominal. T_3, T_4, and T_5 were initiated approximately 0.6 seconds late, 0.6 seconds early and 4.4 seconds early, respectively, due to variations in the stage burn times. These variations are discussed in Sections 5, 6 and 7 of this document. Start times of T_6 and T_7 were 6.2 seconds late and 0.9 second late, respectively. T_8, which was initiated by the receipt of a ground command, started 66.1 seconds late.

A summary of significant events for AS-510 is given in Table 2-2. The predicted times for establishing actual minus predicted times in Table 2-2 were taken from 40M33627B, "Interface Control Document Definition of Saturn SA-507 and Subs Flight Sequence Program" and from the "AS-510 Launch Vehicle Operational Trajectory for July 26, 1971, Launch".

2.2 VARIABLE TIME AND COMMANDED SWITCH SELECTOR EVENTS

Table 2-3 lists the switch selector events which were issued during the flight, but were not programed for specific times. The water coolant valve open and close switch selector commands were issued based on the condition of two thermal switches in the Environmental Control System (ECS). The output of these switches was sampled once every 300 seconds beginning nominally at 480 seconds, and a switch selector command was

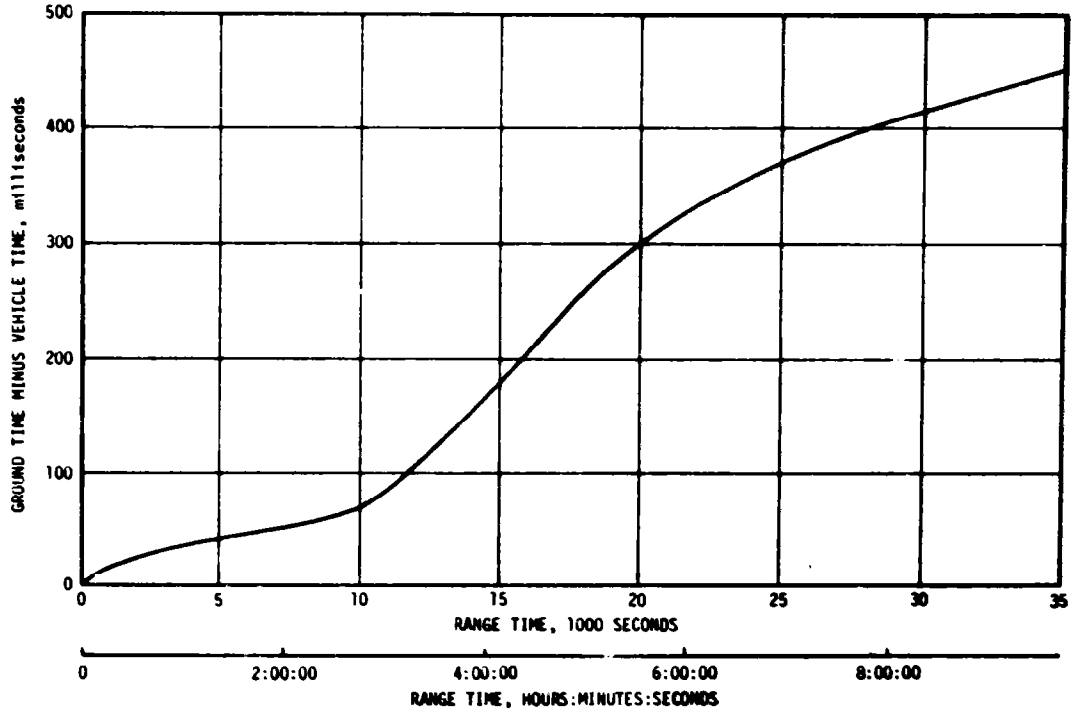

Figure 2-1. Ground Station Time to Vehicle Time Conversion

issued to open or close the water valve. The valve was opened if the temperature was too high and was closed if the temperature was too low. Data indicate the water coolant valve responded properly to temperature fluctuations.

Table 2-3 also contains the special sequence of switch selector events which were programed to be initiated by telemetry station acquisition and included the following calibration sequence:

FUNCTION	STAGE	TIME (SEC)
Telemetry Calibrator Inflight Calibrate, ON	IU	Acquisition + 60.0
TM Calibrate, ON	S-IVB	Acquisition + 60.4
TM Calibrate, OFF	S-IVB	Acquisition + 61.4
Telemetry Calibrator Inflight Calibrate, OFF	IU	Acquisition + 65.0

Table 2-1. Time Base Summary

TIME BASE	VEHICLE TIME SECONDS (HR:MIN:SEC)	GROUND TIME SECONDS (HR:MIN:SEC)	SIGNAL START
T_0	-16.94	-16.94	Guidance Reference Release
T_1	0.58	0.58	IU Umbilical Disconnect Sensed by LVDC
T_2	136.08	136.08	Down range velocity $\geq$ 500 m/s at T_1 +135.5 seconds as sensed by LVDC
T_3	159.58	159.58	S-IC OECO Sensed by LVDC
T_4	549.06	549.07	S-II OECO Sensed by LVDC
T_5	694.87	694.88	S-IVB ECO (Velocity) Sensed by LVDC
T_6	9624.83 (02:40:24.83)	9624.90 (02:40:24.90)	Restart Equation Solution
T_7	10,553.84 (02:55:53.84)	10,553.92 (02:55:53.92)	S-IVB ECO (Velocity) Sensed by LVDC
T_8	16,800.44 (04:40:00.44)	16,800.66 (04:40:00.66)	Initiated by Ground Command

Table 2-2. Significant Event Times Summary

ITEM	EVENT DESCRIPTION	RANGE TIME		TIME FROM BASE	
		ACTUAL SEC	ACT-PRED SEC	ACTUAL SEC	ACT-PRED SEC
1	GUIDANCE REFERENCE RELEASE (GRR)	-16.9	0.1	-17.5	0.2
2	S-IC ENGINE START SEQUENCE COMMAND (GROUND)	-8.9	0.0	-9.4	0.1
3	S-IC ENGINE NO.5 START	-6.5	0.0	-7.1	0.1
4	S-IC ENGINE NO.3 START	-6.3	0.1	-6.9	0.1
5	S-IC ENGINE NO.2 START	-6.3	0.0	-6.8	0.1
6	S-IC ENGINE NO.4 START	-6.1	0.0	-6.6	0.2
7	S-IC ENGINE NO.1 START	-6.0	0.0	-6.5	0.1
8	ALL S-IC ENGINES THRUST OK	-1.4	0.1	-2.0	0.2
9	RANGE ZERO	0.0		-0.6	
10	ALL HOLDDOWN ARMS RELEASED (FIRST MOTION)	0.3	0.0	-0.3	0.1
11	IU UMBILICAL DISCONNECT, START OF TIME BASE 1 (T1)	0.6	-0.1	0.0	0.0
12	BEGIN TOWER CLEARANCE YAW MANEUVER	1.7	0.0	1.1	0.1
13	END YAW MANEUVER	9.7	0.0	9.1	0.1
14	BEGIN PITCH AND ROLL MANEUVER	12.2	0.6	11.6	0.6
15	S-IC OUTBOARD ENGINE CANT	20.5	-0.2	20.0	0.0
16	END ROLL MANEUVER	23.0	-0.8	22.4	-0.7
17	MACH 1	65.0	0.6	64.4	0.7
18	MAXIMUM DYNAMIC PRESSURE (MAX Q)	82.0	1.7	81.4	1.8
19	S-IC CENTER ENGINE CUTOFF (CECO)	135.96	-0.11	135.38	-0.01
20	START OF TIME BASE 2 (T2)	136.1	-0.1	0.0	0.0
21	END PITCH MANEUVER (TILT ARREST)	156.9	1.0	20.9	1.2
22	S-IC OUTBOARD ENGINE CUTOFF (OECO)	159.56	0.53	23.48	0.62
23	START OF TIME BASE 3 (T3)	159.6	0.6	0.0	0.0

Table 2-2. Significant Event Times Summary (Continued)

ITEM	EVENT DESCRIPTION	RANGE TIME		TIME FROM BASE	
		ACTUAL SEC	ACT-PRED SEC	ACTUAL SEC	ACT-PRED SEC
24	START S-II LH2 TANK HIGH PRESSURE VENT MODE	159.7	0.6	0.1	0.0
25	S-II LH2 RECIRCULATION PUMPS OFF	159.7	0.5	0.2	0.0
26	S-IC/S-II SEPARATION COMMAND TO FIRE SEPARATION DEVICES AND RETRO MOTORS	161.2	0.5	1.7	0.0
27	S-II ENGINE START SEQUENCE COMMAND (ESC)	161.9	0.5	2.4	0.0
28	S-II ENGINE SOLENOID ACTIVATION (AVERAGE OF FIVE)	162.0	0.6	2.4	0.0
29	S-II IGNITION-STDV OPEN	163.0	0.6	3.4	0.0
30	S-II CHILLDOWN VALVES CLOSE	164.8	0.5	5.3	0.0
31	S-II MAINSTAGE	164.9	0.5	5.4	0.0
32	S-II HIGH (5.5) EMR NO. 1 ON	167.4	0.5	7.9	0.0
33	S-II HIGH (5.5) EMR NO. 2 ON	167.6	0.5	8.1	0.0
34	S-II SECOND PLANE SEPARATION COMMAND (JETTISON S-II AFT INTERSTAGE)	191.2	0.5	31.7	0.0
35	LAUNCH ESCAPE TOWER (LET) JETTISON	195.9	-0.5	36.3	-1.1
36	ITERATIVE GUIDANCE MODE (IGM) PHASE 1 INITIATED	202.6	2.0	43.0	1.4
37	S-II CENTER ENGINE CUTOFF (CECO)	459.56	0.52	299.98	-0.01
38	START OF ARTIFICIAL TAU MODE	483.7	-0.1	324.1	-0.6
39	S-II LOW ENGINE MIXTURE RATIO (EMR) SHIFT (ACTUAL)	483.9	1.5	324.3	0.9
40	END OF ARTIFICIAL TAU MODE	494.2	-0.8	334.6	-1.4
41	S-II OUTBOARD ENGINE CUTOFF (OECO)	549.06	-0.64	389.47	-1.19
42	S-II ENGINE CUTOFF INTERRUPT, START OF TIME BASE 4 (T4) (START OF IGM PHASE 3)	549.1	-0.6	0.0	0.0
43	S-IVB ULLAGE MOTOR IGNITION	549.9	-0.7	0.9	0.0

Table 2-2. Significant Event Times Summary (Continued)

ITEM	EVENT DESCRIPTION	RANGE TIME		TIME FROM BASE	
		ACTUAL SEC	ACT-PRED SEC	ACTUAL SEC	ACT-PRED SEC
44	S-II/S-IVB SEPARATION COMMAND TO FIRE SEPARATION DEVICES AND RETRO MOTORS	550.1	-0.6	1.0	0.0
45	S-IVB ENGINE START COMMAND (FIRST ESC)	550.2	-0.6	1.1	0.0
46	FUEL CHILLDOWN PUMP OFF	551.2	-0.7	2.2	0.0
47	S-IVB IGNITION (STDV OPEN)	553.2	-0.6	4.1	0.0
48	S-IVB MAINSTAGE	555.7	-0.6	6.6	0.0
49	START OF ARTIFICIAL TAU MODE	557.5	-1.3	8.5	-0.5
50	S-IVB ULLAGE CASE JETTISON	561.8	-0.7	12.8	0.0
51	END OF ARTIFICIAL TAU MODE	567.0	-1.1	17.9	-0.5
52	BEGIN TERMINAL GUIDANCE	663.0	-2.6	114.0	-1.9
53	END IGM PHASE 3	687.8	-4.0	138.7	-3.3
54	BEGIN CHI FREEZE	687.8	-4.0	138.7	-3.3
55	S-IVB VELOCITY CUTOFF COMMAND NO. 1 (FIRST ECO)	694.68	-4.40	-0.20	0.00
56	S-IVB VELOCITY CUTOFF COMMAND NO. 2	694.79	-4.39	-0.09	0.01
57	S-IVB ENGINE CUTOFF INTERRUPT, START OF TIME BASE 5 (T5)	694.9	-4.4	0.0	0.0
58	S-IVB APS ULLAGE ENGINE NO. 1 IGNITION COMMAND	695.1	-4.5	0.3	0.0
59	S-IVB APS ULLAGE ENGINE NO. 2 IGNITION COMMAND	695.2	-4.5	0.4	0.0
60	LOX TANK PRESSURIZATION OFF	696.0	-4.5	1.2	0.0
61	PARKING ORBIT INSERTION	704.7	-4.4	9.8	0.0
62	BEGIN MANEUVER TO LOCAL HORIZONTAL ATTITUDE	716.3	-3.3	21.4	1.1
63	S-IVB CONTINUOUS VENT SYSTEM (CVS) ON	753.9	-4.4	59.0	0.0
64	S-IVB APS ULLAGE ENGINE NO. 1 CUTOFF COMMAND	781.8	-4.5	87.0	0.0
65	S-IVB APS ULLAGE ENGINE NO. 2 CUTOFF COMMAND	781.9	-4.5	87.1	0.0

Table 2-2. Significant Event Times Summary (Continued)

ITEM	EVENT DESCRIPTION	RANGE TIME		TIME FROM BASE	
		ACTUAL SEC	ACT-PRED SEC	ACTUAL SEC	ACT-PRED SEC
66	BEGIN ORBITAL NAVIGATION	795.7	-3.9	100.8	0.5
67	BEGIN S-IVB RESTART PREPARATIONS, START OF TIME BASE 6 (T6)	9624.9	6.2	0.0	0.0
68	S-IVB O2/H2 BURNER LH2 ON	9666.2	6.2	41.3	0.0
69	S-IVB O2/H2 BURNER EXCITERS ON	9666.5	6.2	41.6	0.0
70	S-IVB O2/H2 BURNER LOX ON (HELIUM HEATER ON)	9666.9	6.2	42.0	0.0
71	S-IVB CVS OFF	9667.1	6.2	42.2	0.0
72	S-IVB LH2 REPRESSURIZATION CONTROL VALVE ON	9673.0	6.2	48.1	0.0
73	S-IVB LOX REPRESSURIZATION CONTROL VALVE ON	9673.2	6.2	48.3	0.0
74	S-IVB AUX HYDRAULIC PUMP FLIGHT MODE ON	9843.9	6.2	219.0	0.0
75	S-IVB LOX CHILLDOWN PUMP ON	9873.9	6.2	249.0	0.0
76	S-IVB LH2 CHILLDOWN PUMP ON	9878.9	6.2	254.0	0.0
77	S-IVB PREVALVES CLOSED	9883.9	6.2	259.0	0.0
78	S-IVB MIXTURE RATIO CONTROL VALVE OPEN	10075.0	6.2	450.1	0.0
79	S-IVB APS ULLAGE ENGINE NO. 1 IGNITION COMMAND	10121.2	6.2	496.3	0.0
80	S-IVB APS ULLAGE ENGINE NO. 2 IGNITION COMMAND	10121.3	6.2	496.4	0.0
81	S-IVB O2/H2 BURNER LH2 OFF (HELIUM HEATER OFF)	10121.7	6.2	496.8	0.0
82	S-IVB O2/H2 BURNER LOX OFF	10126.2	6.2	501.3	0.0
83	S-IVB LH2 CHILLDOWN PUMP OFF	10194.3	6.2	569.4	0.0
84	S-IVB LOX CHILLDOWN PUMP OFF	10194.5	6.2	569.6	0.0
85	S-IVB ENGINE RESTART COMMAND (FUEL LEAD INITIATION) (SECOND ESC)	10194.9	6.2	570.0	0.0
86	S-IVB APS ULLAGE ENGINE NO. 1 CUTOFF COMMAND	10197.9	6.2	573.0	0.0

Table 2-2. Significant Event Times Summary (Continued)

ITEM	EVENT DESCRIPTION	RANGE TIME		TIME FROM BASE	
		ACTUAL SEC	ACT-PRED SEC	ACTUAL SEC	ACT-PRED SEC
87	S-IVB APS ULLAGE ENGINE NO. 2 CUTOFF COMMAND	10198.0	6.2	573.1	0.0
88	S-IVB SECOND IGNITION (STDV OPEN)	10202.9	6.3	578.0	0.1
89	S-IVB MAINSTAGE	10205.4	6.3	580.5	0.1
90	ENGINE MIXTURE RATIO (EMR) CONTROL VALVE SHIFT (BEGIN VALVE MOVEMENT)	10259.4	6.8	634.5	0.6
91	S-IVB LH2 STEP PRESSURIZATION (SECOND BURN RELAY OFF)	10474.9	6.2	850.0	0.0
92	BEGIN TERMINAL GUIDANCE	10526.5	1.9	901.5	-4.4
93	BEGIN CHI FREEZE	10551.5	0.7	926.6	-5.6
94	S-IVB SECOND GUIDANCE CUTOFF COMMAND NO. 1 (SECOND ECO)	10553.69	0.87	-0.23	-0.03
95	S-IVB SECOND GUIDANCE CUTOFF COMMAND NO. 2	10553.79	0.87	-0.12	-0.02
96	S-IVB ENGINE CUTOFF INTERRUPT, START OF TIME BASE 7	10553.9	0.9	0.0	0.0
97	S-IVB CVS ON	10554.4	0.9	0.5	0.0
98	TRANSLUNAR INJECTION	10563.7	1.0	9.8	0.1
99	BEGIN ORBITAL NAVIGATION	10706.0	1.9	152.0	1.0
100	BEGIN MANEUVER TO LOCAL HORIZONTAL ATTITUDE	10706.2	2.1	152.3	1.2
101	S-IVB CVS OFF	10704.8	0.9	150.9	0.0
102	BEGIN MANEUVER TO TRANSPOSITION AND DOCKING ATTITUDE (TD&E)	11454.6	1.7	900.7	0.8
103	CSM SEPARATION	12147.2	94.3	1593.3	93.4
104	CSM DOCK	12829.5	176.6	2275.5	175.6
105	SC/LV FINAL SEPARATION	15481.2	128.3	4927.2	127.4
106	START OF TIME BASE 8 (T8)	16800.7	66.1	0.0	0.0
107	S-IVB APS ULLAGE ENGINE NO. 1 IGNITION COMMAND	16801.8	66.0	1.2	0.0
108	S-IVB APS ULLAGE ENGINE NO. 2 IGNITION COMMAND	16802.0	66.0	1.4	0.0

Table 2-2. Significant Event Times Summary (Continued)

ITEM	EVENT DESCRIPTION	RANGE TIME		TIME FROM BASE	
		ACTUAL SEC	ACT-PRED SEC	ACTUAL SEC	ACT-PRED SEC
109	S-IVB APS ULLAGE ENGINE NO. 1 CUTOFF COMMAND	16881.8	66.0	81.2	0.0
110	S-IVB APS ULLAGE ENGINE NO. 2 CUTOFF COMMAND	16882.0	66.0	81.4	0.0
111	INITIATE MANEUVER TO LOX DUMP ATTITUDE	17381.8	67.2	581.1	1.1
112	S-IVB CVS ON	17800.6	66.0	1000.0	0.0
113	BEGIN LOX DUMP	18080.6	66.0	1280.0	0.0
114	S-IVB CVS OFF	18100.6	66.0	1300.0	0.0
115	END LOX DUMP	18128.7	66.1	1328.0	0.0
116	H2 NONPROPULSIVE VENT (NPV) ON	18377.7	66.0	1577.0	0.0
117	INITIATE MANEUVER TO ATTITUDE REQUIRED FOR FINAL S-IVB APS BURN	19633.5	-160.9	2832.8	-226.9
118	S-IVB APS ULLAGE ENGINE NO. 1 IGNITION COMMAND	20760.7	66.3	3960.0	0.3
119	S-IVB APS ULLAGE ENGINE NO. 2 IGNITION COMMAND	20760.9	66.3	3960.2	0.3
120	S-IVB APS ULLAGE ENGINE NO. 1 CUTOFF COMMAND	21001.7	73.3	4201.0	7.3
121	S-IVB APS ULLAGE ENGINE NO. 2 CUTOFF COMMAND	21001.9	73.3	4201.2	7.3
122	2ND LUNAR IMPACT MANEUVER COMMAND	35,486.			
123	S-IVB APS IGNITION	36,001.			
124	S-IVB APS CUTOFF	36,072.			
125	MANEUVER TO LOX DUMP ATTITUDE	36,593.			
126	0.3 DEGREE/SECOND ROLL COMMAND	37,162.			
127	S-IVB/IU LUNAR IMPACT	285,881.6 (79:24:41.6)	-605.8	260,080.8 (74:08:40.8)	-539.5

Table 2-3. Variable Time and Command Switch Selector Events

FUNCTION	STAGE	RANGE TIME (SEC)	TIME FROM BASE (SEC)	REMARKS
Water Coolant Valve CLOSED	IU	481.4	T_3 +321.8	LVDC Function
Low (4.8) EMR No. 1	S-II	483.7	T_3 +324.1	LVDC Function
Low (4.8) EMR No. 2	S-II	483.9	T_3 +324.3	LVDC Function
Telemetry Calibrator Inflight Calibrate ON	IU	1095.8	T_5 +400.9	Acquisition by Canary Revolution 1
TM Calibrate ON	S-IVB	1096.2	T_5 +401.3	Acquisition by Canary Revolution 1
TM Calibrate OFF	S-IVB	1097.2	T_5 +402.3	Acquisition by Canary Revolution 1
Telemetry Calibrator Inflight Calibrate OFF	IU	1100.7	T_5 +405.9	Acquisition by Canary Revolution 1
Telemetry Calibrator Inflight Calibrate ON	IU	3191.8	T_5 +2496.9	Acquisition by Carnarvon Revolution 1
TM Calibrate ON	S-IVB	3192.2	T_5 +2497.3	Acquisition by Carnarvon Revolution 1
TM Calibrate OFF	S-IVB	3193.2	T_5 +2498.3	Acquisition by Carnarvon Revolution 1
Telemetry Calibrator Inflight Calibrate OFF	IU	3196.8	T_5 +2501.9	Acquisition by Carnarvon Revolution 1
Telemetry Calibrator Inflight Calibrate ON	IU	5351.8	T_5 +4656.9	Merged Data, Goldstone, Texas, MILA, Bermuda
TM Calibrate ON	S-IVB	5352.2	T_5 +4657.3	
TM Calibrate OFF	S-IVB	5353.2	T_5 +4658.3	
Telemetry Calibrator Inflight Calibrate OFF	IU	5356.8	T_5 +4661.9	
Telemetry Calibrator Inflight Calibrate ON	IU	10,773.9	T_7 +220.0	Acquisition by Hawaii TLI
TM Calibrate OFF	S-IVB	10,775.3	T_7 +221.4	Acquisition by Hawaii TLI
Telemetry Calibrator Inflight Calibrate ON	IU	10,778.9	T_7 +225.0	Acquisition by Hawaii TLI
Start of Time Base 8 (T_8)		16,800.7	T_8 +0.0	CCS Command
Water Coolant Valve OPEN	IU	16,980.7	T_8 +180.0	LVDC Function
Water Coolant Valve CLOSED	IU	17,280.7	T_8 +480.0	LVDC Function
Water Coolant Valve OPEN	IU	25,080.7	T_8 +8280.0	LVDC Function
Water Coolant Valve CLOSED	IU	25,380.8	T_8 +8580.1	LVDC Function
Water Coolant Valve CLOSED	IU	27,780.7	T_8 +10980.0	LVDC Function

SECTION 3

LAUNCH OPERATIONS

3.1 SUMMARY

The ground systems supporting the AS-510/Apollo 15 countdown and launch performed satisfactorily. System component failures and malfunctions requiring corrective action were corrected during countdown without causing unscheduled holds. Propellant tanking was accomplished satisfactorily. The space vehicle was launched on schedule at 09:34:00 Eastern Daylight Time (EDT) on July 26, 1971, from pad 39A of the Kennedy Space Center, Saturn Complex. Damage to the pad, Launch Umbilical Tower (LUT) and support equipment was considered minimal.

3.2 PRELAUNCH MILESTONES

A chronological summary of prelaunch milestones for the AS-510 launch is contained in Table 3-1.

3.3 COUNTDOWN EVENTS

The AS-510/Apollo 15 terminal countdown was picked up at T-28 hours on July 24, 1971, at 19:00:00 EDT. Scheduled holds were initiated at T-9 hours for a duration of 9 hours 34 minutes, and at T-3 hours 30 minutes for a duration of 1 hour. Launch occurred on schedule at 09:34:00 EDT on July 26, 1971, from pad 39A of the Kennedy Space Center (KSC), Saturn Launch Complex.

3.4 PROPELLANT LOADING

3.4.1 RP-1 Loading

The RP-1 system successfully supported countdown and launch without incident. Tail Service Mast (TSM) 1-2 fill and replenish was accomplished at T-13 hours and S-IC level adjust and fill line inert at about T-1 hour. Both operations were completed as planned. Launch countdown support consumed 212,060 gallons of RP-1.

Launch damage was not extensive or serious. The Ansul dry powder fire extinguisher system activated inadvertently in LUT room 4A. The Ansul system failure should be evaluated and design corrective action taken if required to prevent problem recurrence. Extensive cleanup was required.

Table 3-1. AS-510/Apollo 15 Prelaunch Milestones

DATE	ACTIVITY OR EVENT
May 18, 1970	S-II-10 Stage Arrival
June 13, 1970	S-IVB-510 Stage Arrival
June 26, 1970	Instrument Unit (IU)-510 Arrival
July 6, 1970	S-IC-10 Stage Arrival
July 8, 1970	Spacecraft/Lunar Module Adapter (SLA)-19 Arrival
July 8, 1970	S-IC Erection on Mobile Launcher (ML)-3
September 15, 1970	S-II Erection
September 16, 1970	S-IVB Erection
September 17, 1970	IU Erection
November 17, 1970	Lunar Module (LM)-10 Arrival
November 17, 1970	Launch Vehicle (LV) Electrical Systems Test
January 14, 1971	Command and Service Module (CSM)-112 Arrival
March 15, 1971	Lunar Roving Vehicle (LRV)-1 Arrival
April 15, 1971	LV Propellant Dispersion/Malfunction Overall Test (OAT) Complete
April 27, 1971	LV Service Arm OAT Complete
April 28, 1971	LRV Installation
May 8, 1971	Spacecraft (SC) Erection
May 11, 1971	Space Vehicle (SV)/ML Transfer to Pad 39A
June 7, 1971	SV Electrical Mate
June 9, 1971	SV OAT No. 1 (Plugs In) Complete
June 22, 1971	SV Flight Readiness Test (FRT) Completed
July 6, 1971	RP-1 Loading
July 13, 1971	Countdown Demonstration Test (CDDT) Completed (Wet)
July 14, 1971	CDDT Completed (Dry)
July 24, 1971	SV Terminal Countdown Started (T-28 Hours)
July 26, 1971	SV Launch

3.4.2 LOX Loading

As a result of an overloading condition discovered during the CDDT, the predicted S-IVB LOX mission load input to the Propellant Tanking Computer System (PTCS) was rescaled downward. This rescaling avoided a recalibration of the S-IVB stage Propellant Utilization Electronics Assembly (PUEA). There were no operational difficulties encountered by conducting the launch countdown with the PTCS operating with a modified full load point.

The LOX system supported countdown and launch satisfactorily. The fill sequence began with S-IVB fill command at 00:17:00 EDT, July 26, 1971, and was completed 2 hours 43 minutes later with all stage replenish normal at 03:00:00 EDT. Replenish was as planned. Minor LOX leaks were noted during loading operations and a pneumatic leak was discovered in the S-IVB main fuel valve actuator housing early in countdown.

S-II LOX loading, which was normal, started at T-7 hours 38 minutes and was completed at T-6 hours 57 minutes. The LOX tank Overfill Shutoff (OFSO) point sensor indicated a splashing wet condition as expected at T-33 minutes at the initiation of LOX helium injection. The OFSO sensor reached a maximum of 7.6 percent wet for one minute during the early part of helium injection. At T-12 minutes, the LOX OFSO sensor returned to a totally dry state and remained dry through the terminal sequence.

Total vehicle LOX consumption during launch countdown was 592,000 gallons.

The LOX storage area, cross-country and Mobile Launcher (ML) equipment was free of launch damage with the exception of minor blast damage to the LUT.

During valve complex maintenance on ML, July 20, 1971, a leak was discovered in the pneumatic actuator housing cover of the S-IVB main fill valve A207. The cover was removed, the actuator shaft lubricated and the valve cycled repeatedly. Minor leakage persisted after the cover was reinstalled. This condition did not affect valve operation and was accepted for launch.

During LOX loading operations on July 26, 1971, what appeared to be a minor seal leak was noted on the A126 replenish pump. The leak did not affect pump performance and pump bearing temperature remained normal throughout loading operations. Postlaunch tests are planned to determine source of leakage.

At the start of S-IC fast fill on July 26, 1971, filter A224 in the lower S-IC fill and drain line began leaking. The leak disappeared about 5 minutes later when the filter had completely chilled down. The filter lid gasket will be replaced during normal postlaunch filter element changeout.

3.4.3 LH_2 Loading

During CDDT, the S-IVB LH_2 Depletion Sensor No. 1 failed "wet" after LOX loading and prior to the start of LH_2 loading. Investigation disclosed that the level sensor control unit had been misadjusted during calibration such that its response to input changes was approximately 10 times too great. The controller was recalibrated. During inspection, prior to final cable reconnection, it was discovered that the unit coaxial connector teflon insulation had been punctured. The controller was removed and replaced.

The LH_2 system successfully supported countdown and launch. The fill sequence began with start of S-II loading at 03:11:00 EDT, July 26, 1971, and was completed 86 minutes later when all stage replenish was established at 04:37:00 EDT. S-II replenish was automatic until Terminal Countdown Start (TCDS) at T-187 seconds with one exception at T-3 hours, when both the S-II and S-IVB levels were temporarily controlled in the manual mode to obtain reference data in the event of a Propellant Utilization (PU) system failure. S-IVB replenish was controlled manually from T-1 hour until TCDS per the loading procedure. Two minor problems were encountered with the LUT vent lines; two leak alarms were noted during fill and replenish operations; and the S-IVB heat exchanger supply valve failed to open after launch. However, none of these affected loading operations. Launch damage was not excessive or serious. Launch countdown support consumed about 470,000 gallons of LH_2.

3.5 S-II INSULATION

Overall performance of the insulation system on the S-II-10 stage was satisfactory prior to and during launch of the AS-510. No anomalies of the insulation system from data readout and visual observation (operational television) were observed. Purge pressures and flows in the forward bulkhead uninsulated area and "J" ring area were satisfactory. Vacuum in the common bulkhead was recorded as 1.2 psia, well below the redline value of 5 psia.

The heat leak to the LH_2 was estimated to be approximately 65,000 BTU for the total mission. This was well within the allowable of 209,000 BTU.

A limited number of defects were noted in the external insulation during post-CDDT inspection. The defects included 12 foam divots (occurring primarily around the feedline areas), 3 cork insulation debonds, and 15 coating blisters. These defects were repaired within the allotted schedule time.

Post-CDDT inspection also revealed defects in the internal spray or ablative insulation. These defects were limited to approximately 4-square inch debonded areas at six locations and hairline cracks located in the

vicinity of the engine No. 3 area. The ablative insulation was considered acceptable based on structural and heating criteria and no rework was required.

All rework if required, however, could have been accomplished within a 24-hour turnaround interval.

3.6 GROUND SUPPORT EQUIPMENT

3.6.1 Ground/Vehicle Interface

In general, performance of the ground service systems supporting all stages of the launch vehicle was satisfactory. Overall damage to the pad, LUT, and support equipment from the blast and flame impingement was considered minimal. Detailed discussion of the Ground Support Equipment (GSE) is contained in KSC Apollo/Saturn V (AS-510) "Ground Support Evaluation Report."

The S-IVB J-2 engine start tank pressure reached 1400 psia during the plus time operation of Countdown Demonstration Test (CDDT). Flight Mission Rule 7-20 was changed from 1400 to 1450 psia for the first opportunity restart pressure limit in the start tank. The pressure remained below the launch redline and reached 1390 psia prior to restart.

The PTCS satisfactorily supported countdown and launch operations. There was no damage or system failures noted. During all-stage replenish at about T-2 hours 20 minutes, immediately after the S-IC LOX boiloff test, the tank was replenished to an indicated level of 100.16 percent flight mass. The level remained at this value for 20 minutes with the replenish valve closed before any noticeable change was observed. Subsequent operation of the replenish system was normal for the remainder of the countdown. A design investigation is recommended.

The Data Transmission System (DTS) satisfactorily supported countdown and launch. There were no failures or anomalies and no launch damage.

The Environmental Control System (ECS) performed satisfactorily throughout countdown and launch. Changeover from air to GN_2 purge occurred at 23:10:00 EDT, July 25, 1971, 24 minutes before resuming the count at T-9 hours. GN_2 purge was terminated at 09:44:00 EDT, July 26, 1971. One minor problem and one waiver condition were encountered during countdown operations but did not seriously affect system support. During inspection of the chiller solenoid valves at about T-21 hours, water was found in the connection compartment of chiller No. 1 valve A6973. The valve was replaced. The cover was left off so that if water entered the replacement it could drain off before the electrical terminals were shorted. Similar failures of this valve occurred on April 21, 1971, and June 23, 1971. Additional failure

analysis has been requested. S-IVB aft compartment temperature fell below specifications for about 1 hour on July 20, 1971 when ECS electrical wires were disconnected to allow replacement of failed ECS linear power controller components. Normal temperature was restored when power controller work was completed. A waiver request was prepared by S-IVB engineering to cover specification deviation. No adverse effects to the S-IVB were reported.

Launch damage was minor and confined to slightly scorched ducts and some loose anchor studs on the remote air plenum attached to the ECS room exterior wall.

The Holddown Arms (HDA) and Service Arm Control Switches (SACS) satisfactorily supported countdown and launch. All HDA released pneumatically within a 3-millisecond period. The retraction and explosive release lanyard pull was accomplished in advance of ordnance actuation with a 45-millisecond margin. The pneumatic release valves No. 1 and No. 2 opened simultaneously 24 milliseconds after the SACS armed signal. The SACS primary switches closed within 27 milliseconds of each other at 449 and 476 milliseconds after commit and the SACS secondary switches closed simultaneously 1.112 seconds after commit. Launch damage was minimal.

Overall performance of the Tail Service Masts (TSM) was satisfactory. Mast retraction times were nominal; 2.307 seconds for TSM 1-2, 2.151 seconds for TSM 3-2 and 2.688 seconds for TSM 3-4, measured from umbilical plate separation to mast retracted. There was a minimal amount of heat and blast damage to all masts.

At about T-6 hours 25 minutes the TSM 3-2 accumulator pressure meter (M4) indicated approximately 150 psig lower than the alternate monitoring facilities. This indicated that an end item component in the Launch Control Center (LCC) Panel had experienced some degradation. System pressure switch status was monitored as an indication of system readiness for the remainder of the countdown. Troubleshooting and corrective action were postponed until after launch.

The Preflight and Inflight Service Arms (S/A 1 through S/A 8) supported countdown satisfactorily. The performance of the Inflight Service Arms was within design parameters during terminal count and liftoff. Only expected minor damage, similar to previous launches, occurred on the lower Preflight Service Arms (S/A 1, 2, and 3). Damage on the Inflight Service Arms was also minor, with damage judged even less than on previous launches.

3.6.2 MSFC Furnished Ground Support Equipment

The S-IC Mechanical GSE performance for countdown and launch was nominal. Launch damage was negligible and only one minor problem occurred. The Ansul fire extinguisher activated, apparently due to launch vibrations, blanketing Mobile Launcher Room 4Ab equipment with chemical powder.

The S-IC electrical GSE satisfactorily supported countdown and launch. No failures or anomalies were noted in any of the electrical GSE systems. Launch damage was minor.

All ground power and battery equipment satisfactorily supported countdown from the start of precount through launch. All systems performed within acceptable limits. No significant damage occurred to ground power equipment during AS-510 launch. A minor problem occurred at T-48 hours when the S-IVB flight battery console intermittently printed out erroneous voltage values and channel numbers. The console was replaced and no problems were experienced with the replacement.

The Hazardous Gas Detection System (HGDS) became active in countdown and launch operations at 23:00:00 EDT, July 25, 1971, and maintained satisfactory support through liftoff with no significant system problems. The system continued to operate satisfactorily after launch and was secured at 13:30:00 EDT, July 26, 1971. There was no reportable launch damage to the HGDS or the HGDS sample lines.

The S-IC flight control system performed satisfactorily throughout prelaunch checkout and flight. One waivered exception was encountered. At about T-4 hours 30 minutes the No. 3 pitch actuator indicated a gain of 0.352 at switch point 2. Nominal at this point is 0.300 and the upper limit is 0.342. This condition had been anticipated. A waiver request dated May 12, 1971, increased the upper limit for No. 3 pitch actuator to 0.362. Because of this prior approval no impact to countdown operations resulted.

SECTION 4

TRAJECTORY

4.1 SUMMARY

The vehicle was launched on an azimuth 90 degrees east of north. A roll maneuver was initiated at 12.2 seconds that placed the vehicle on a flight azimuth of 80.088 degrees east of north. The reconstructed trajectory was generated by merging the following four trajectory segments: the ascent phase, parking orbit phase, injection phase, and post Translunar Injection (TLI) phase. The analysis for each phase was conducted separately with appropriate end point constraints to provide trajectory continuity. Available C-Band radar and Unified S-Band (USB) tracking data plus telemetered guidance velocity data were used in the trajectory reconstruction.

The trajectory parameters from launch to TLI were close to nominal. Earth parking orbit insertion conditions were achieved 4.39 seconds earlier than nominal at a heading angle 0.143 degree less than nominal. TLI was achieved 0.88 second later than nominal. The trajectory parameters at Command and Service Module (CSM) separation deviated from nominal since the event occurred 94.3 seconds later than predicted.

4.2 TRAJECTORY EVALUATION

4.2.1 Ascent Phase

The ascent phase spans the interval from guidance reference release through parking orbit insertion. The ascent trajectory was established by using telemetered guidance velocities as generating parameters to fit tracking data from five C-Band stations and one S-Band station. Approximately 15 percent of the C-Band tracking data and 10 percent of the S-Band tracking data were eliminated due to inconsistencies. The launch phase portion of the ascent phase, (liftoff to approximately 20 seconds), was established by constraining integrated telemetered guidance accelerometer data to the best estimate trajectory.

Actual and nominal altitude, surface range, and cross range for the ascent phase are presented in Figure 4-1. Actual and nominal space-fixed velocity and flight path angle during ascent are shown in Figure 4-2. Actual and nominal comparisons of total inertial accelerations are shown in Figure 4-3. The maximum acceleration during S-IC burn was 3.97 g.

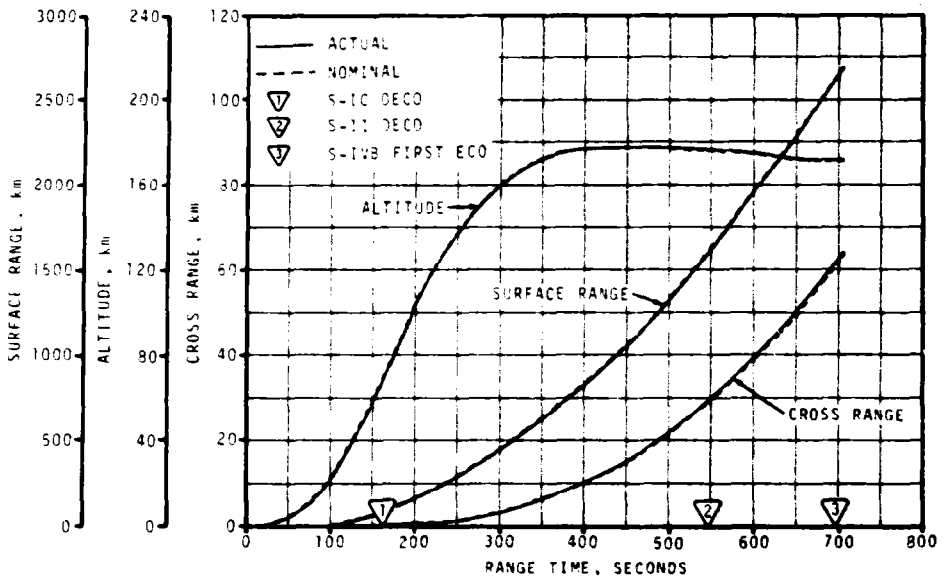

Figure 4-1. Ascent Trajectory Position Comparison

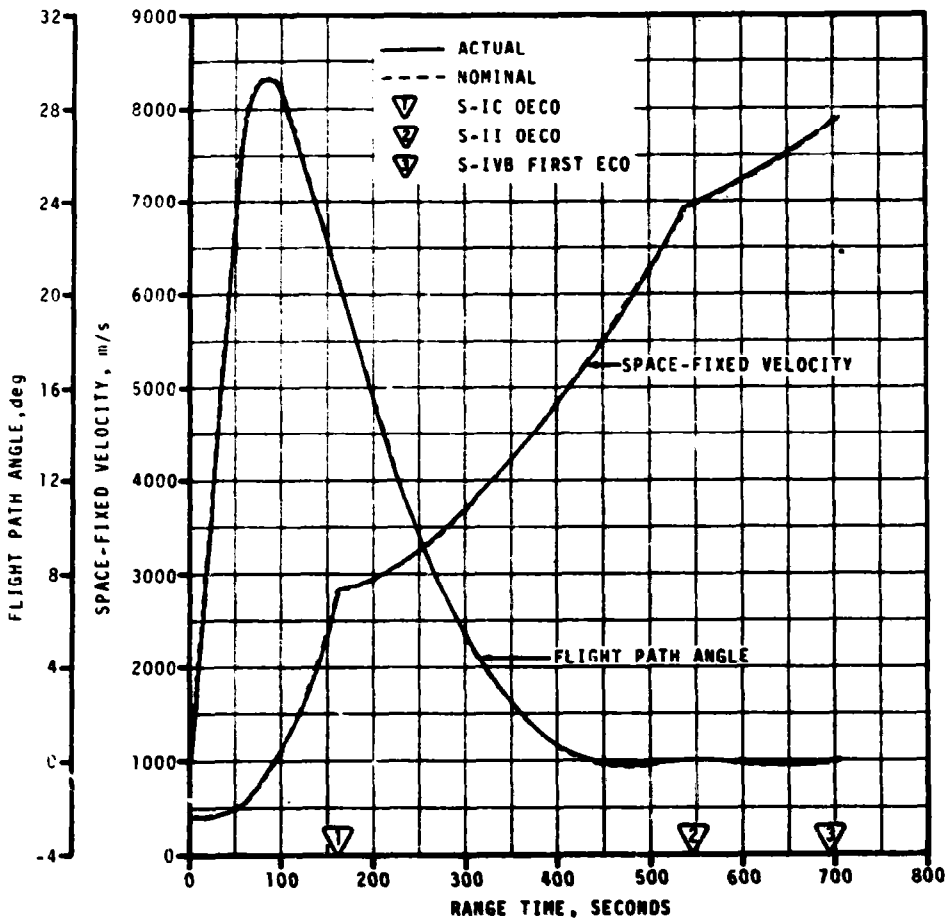

Figure 4-2. Ascent Trajectory Space-Fixed Velocity and Flight Path Angle Comparisons

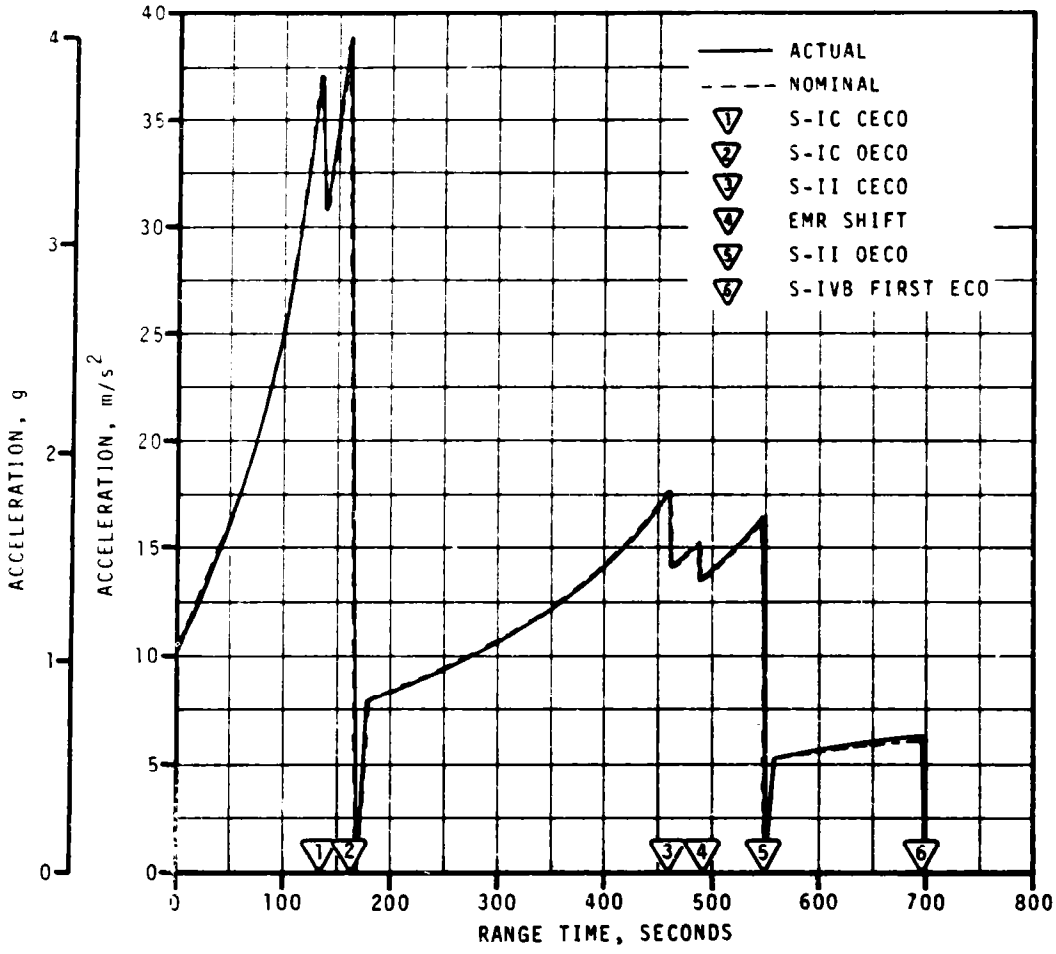

Figure 4-3. Ascent Trajectory Acceleration Comparison

Mach number and dynamic pressure are shown in Figure 4-4. These parameters were calculated using meteorological data measured to an altitude of 58.0 kilometers (31.3 n mi). Above this altitude, the measured data were merged into the U. S. Standard Reference Atmosphere.

Actual and nominal values of parameters at significant trajectory event times, cutoff events, and separation events are shown in Tables 4-1, 4-2, and 4-3, respectively.

4.2.2 Parking Orbit Phase

Orbital tracking was conducted by the NASA Manned Space Flight Network. Four C-Band stations (Merritt Island, two Bermuda radars and Carnarvon) provided six data passes. Two S-Band stations (Texas and Merritt Island) furnished two additional tracking passes.

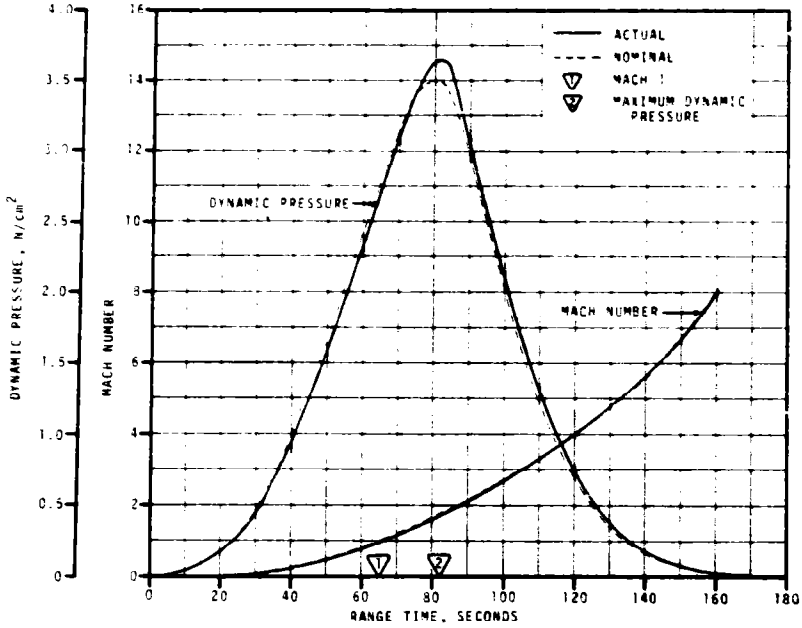

Figure 4-4. Dynamic Pressure and Mach Number Comparisons

The parking orbit trajectory was obtained by integrating a comprehensive orbit model with corrected insertion conditions forward to 10,010 seconds (2:46:50). The final insertion conditions were obtained through a differential correction procedure in the Orbital Correction Program (OCP) which adjusted the preliminary estimate of insertion conditions to final values in accordance with relative weights assigned to the tracking data. The orbital acceleration model was derived from telemetered guidance velocity data generated by the ST-124M-3 guidance platform.

A comparison of actual and nominal parking orbit insertion parameters is presented in Table 4-4. The ground track from insertion to S-IVB/CSM separation is given in Figure 4-5.

4.2.3 Injection Phase

The injection phase was generated by the integration of the telemetered guidance accelerometer data. These accelerometer data were initialized from a parking orbit state vector at 10,010 seconds (02:46:50) and were constrained to a state vector at TLI obtained from the post TLI trajectory. The S-Band tracking data available during the early portion of the injection phase were not used in the trajectory reconstruction because the data were inconsistent with parking orbit and translunar orbit tracking solutions.

Comparisons between the actual and nominal space-fixed velocity and flight path angle are shown in Figure 4-6. The actual and nominal total inertial acceleration comparisons are presented in Figure 4-7.

Table 4-1. Comparison of Significant Trajectory Events

EVENT	PARAMETER	ACTUAL	NOMINAL	ACT-NOM
First Motion	Range Time, sec	0.3	0.3	0.0
	Total Inertial Acceleration, m/s^2	10.61	10.74	-0.13
	(ft/s^2)	(34.81)	(35.24)	(-0.43)
	(g)	(1.08)	(1.10)	(-0.02)
Mach 1	Range Time, sec	65.0	64.4	0.6
	Altitude, km	7.8	7.7	0.1
	(n mi)	(4.2)	(4.2)	(0.0)
Maximum Dynamic Pressure	Range Time, sec	82.0	80.3	1.7
	Dynamic Pressure, N/cm^2	3.68	3.51	0.17
	(lbf/ft^2)	(768.58)	(733.08)	(35.50)
	Altitude, km	13.7	13.1	0.6
	(n mi)	(7.4)	(7.1)	(0.3)
Maximum Total Inertial Acceleration: S-IC	Range Time, sec	159.56	158.27	1.29
	Acceleration, m/s^2	38.97	37.90	1.07
	(ft/s^2)	(127.85)	(124.34)	(3.51)
	(g)	(3.97)	(3.86)	(0.11)
S-II	Range Time, sec	459.56	459.04	0.52
	Acceleration, m/s^2	17.55	17.59	-0.04
	(ft/s^2)	(57.58)	(57.71)	(-0.13)
	(g)	(1.79)	(1.79)	(0.0)
S-IVB 1st Burn	Range Time, sec	694.67	699.06	-4.39
	Acceleration, m/s^2	6.40	6.34	0.06
	(ft/s^2)	(21.00)	(20.80)	(0.20)
	(g)	(0.65)	(0.65)	(0.0)
S-IVB 2nd Burn	Range Time, sec	10,553.61	10,552.73	0.88
	Acceleration, m/s^2	13.93	13.49	0.44
	(ft/s^2)	(45.70)	(44.26)	(1.44)
	(g)	(1.42)	(1.38)	(0.04)
Maximum Earth-Fixed Velocity: S-IC	Range Time, sec	160.00	160.27	-0.27
	Velocity, m/s	2,388.9	2,379.5	9.4
	(ft/s)	(7,837.6)	(7,806.8)	(30.8)
S-II	Range Time, sec	550.00	550.79	-0.79
	Velocity, m/s	6,584.1	6,573.8	10.3
	(ft/s)	(21,601.4)	(21,567.6)	(33.8)
S-IVB 1st Burn	Range Time, sec	704.67	709.06	-4.39
	Velocity, m/s	7,389.1	7,389.5	-0.4
	(ft/s)	(24,242.5)	(24,243.8)	(-1.3)
S-IVB 2nd Burn	Range Time, sec	10,554.00	10,552.94	1.06
	Velocity, m/s	10,436.5	10,433.6	2.9
	(ft/s)	(34,240.5)	(34,231.0)	(9.5)

NOTE: Times used are vehicle times.

Table 4-2. Comparison of Cutoff Events

PARAMETER	ACTUAL	NOMINAL	ACT-NOM	ACTUAL	NOMINAL	ACT-NOM
	S-IC CECO (ENGINE SOLENOID)			S-IC OECO (ENGINE SOLENOID)		
Range Time, sec	135.96	136.07	-0.11	159.56	159.03	0.53
Altitude, km (n mi)	46.8 (25.3)	47.3 (25.5)	-0.5 (-0.2)	68.4 (36.9)	68.6 (37.0)	-0.2 (-0.1)
Space-Fixed Velocity, m/s (ft/s)	2,044.7 (6,708.3)	2,061.4 (6,763.1)	-16.7 (-54.8)	2,756.4 (9,043.3)	2,747.2 (9,013.1)	9.2 (30.2)
Flight Path Angle, deg	24.217	24.403	-0.186	21.266	21.523	-0.257
Heading Angle, deg	82.494	82.533	-0.039	82.129	82.215	-0.086
Surface Range, km (n mi)	48.1 (26.0)	48.7 (26.3)	-0.6 (-0.3)	90.0 (48.6)	89.5 (48.3)	0.5 (0.3)
Cross Range, km (n mi)	0.2 (0.1)	0.2 (0.1)	0.0 (0.0)	0.3 (0.2)	0.4 (0.2)	-0.1 (0.0)
Cross Range Velocity, m/s (ft/s)	3.9 (12.8)	5.6 (18.4)	-1.7 (-5.6)	6.8 (22.3)	10.4 (34.1)	-3.6 (-11.8)
	S-II CECO (ENGINE SOLENOID)			S-II OECO (ENGINE SOLENOID)		
Range Time, sec	459.56	459.04	0.52	549.06	549.70	-0.64
Altitude, km (n mi)	178.2 (96.2)	178.2 (96.2)	0.0 (0.0)	176.3 (95.2)	175.8 (94.9)	0.5 (0.3)
Space-Fixed Velocity, m/s (ft/s)	5,713.4 (18,744.8)	5,708.4 (18,728.3)	5.0 (16.5)	6,995.0 (22,949.5)	6,985.2 (22,917.3)	9.8 (32.2)
Flight Path Angle, deg	-0.285	-0.352	0.067	0.059	0.025	0.034
Heading Angle, deg	87.150	87.101	0.049	89.863	89.864	-0.001
Surface Range, km (n mi)	1,103.8 (596.0)	1,100.6 (594.3)	3.2 (1.7)	1,619.6 (874.5)	1,622.9 (876.3)	-3.3 (-1.8)
Cross Range, km (n mi)	16.1 (8.7)	15.8 (8.5)	0.3 (0.2)	29.5 (15.9)	29.1 (15.7)	0.4 (0.2)
Cross Range Velocity, m/s (ft/s)	121.6 (399.0)	118.0 (387.1)	3.6 (11.9)	181.4 (595.1)	179.2 (587.9)	2.2 (7.2)
	S-IVB 1ST GUIDANCE CUTOFF SIGNAL			S-IVB 2ND GUIDANCE CUTOFF SIGNAL		
Range Time, sec	694.67	699.06	-4.39	10,553.61	10,552.73	0.88
Altitude, km (n mi)	172.6 (93.2)	171.8 (92.8)	0.8 (0.4)	307.5 (166.0)	310.8 (167.8)	-3.3 (-1.8)
Space-Fixed Velocity, m/s (ft/s)	7,801.9 (25,596.6)	7,802.5 (25,598.8)	-0.6 (-2.0)	10,852.9 (35,606.6)	10,850.6 (35,599.1)	2.3 (7.5)
Flight Path Angle, deg	0.013	-0.002	0.015	6.952	7.142	-0.190
Heading Angle, deg	95.149	95.293	-0.144	72.782	72.930	-0.148
Surface Range, km (n mi)	2,605.4 (1,406.8)	2,633.6 (1,422.0)	-28.2 (-15.2)			
Cross Range, km (n mi)	61.9 (33.4)	62.2 (33.6)	-0.3 (-0.2)			
Cross Range Velocity, m/s (ft/s)	265.8 (872.0)	266.7 (875.0)	-0.9 (-3.0)			
Inclination, deg				29.685	29.696	-0.011
Descending Node, deg				108.419	108.453	-0.034
Eccentricity				0.9749	0.9750	-0.0001
C_3*, m^2/s^2 (ft^2/s^2)				-1,522,505 (-16,388,107)	-1,514,734 (-16,304,461)	-7,771 (-83,646)

NOTE: Times used are vehicle times.

* C_3 is twice the specific energy of orbit

$$C_3 = V^2 - \frac{2\mu}{R}$$

where V = Inertial Velocity
μ = Gravitational Constant
R = Radius vector from center of earth

Table 4-3. Comparison of Separation Events

PARAMETER	ACTUAL	NOMINAL	ACT-NOM
	S-IC/S-II SEPARATION		
Range Time, sec	161.2	160.8	0.4
Altitude, km (n mi)	70.1 (37.9)	70.4 (38.0)	-0.3 (-0.1)
Space-Fixed Velocity, m/s (ft/s)	2,762.2 (9,062.3)	2,753.4 (9,033.5)	8.8 (28.8)
Flight Path Angle, deg	21.021	21.251	-0.230
Heading Angle, deg	82.144	82.231	-0.087
Surface Range, km (n mi)	93.5 (50.5)	93.3 (50.4)	0.2 (0.1)
Cross Range, km (n mi)	0.3 (0.2)	0.4 (0.2)	-0.1 (0.0)
Cross Range Velocity, m/s (ft/s)	7.1 (23.3)	10.7 (35.1)	-3.6 (-11.8)
Geodetic Latitude, deg N	28.748	28.746	0.002
Longitude, deg E	-79.661	-79.663	0.002
	S-II/S-IVB SEPARATION		
Range Time, sec	550.1	550.8	-0.7
Altitude, km (n mi)	176.3 (95.2)	175.8 (94.9)	0.5 (0.3)
Space-Fixed Velocity, m/s (ft/s)	6,999.0 (22,962.6)	6,988.7 (22,928.8)	10.3 (33.8)
Flight Path Angle, deg	0.047	0.015	0.032
Heading Angle, deg	89.900	89.901	-0.001
Surface Range, km (n mi)	1,626.3 (878.1)	1,629.8 (880.0)	-3.5 (-1.9)
Cross Range, km (n mi)	29.7 (16.0)	29.3 (15.8)	0.4 (0.2)
Cross Range Velocity, m/s (ft/s)	182.0 (597.1)	179.7 (589.6)	2.3 (7.5)
Geodetic Latitude, deg N	29.843	29.847	-0.004
Longitude, deg E	-63.922	-63.886	-0.036
	S-IVB/CSM SEPARATION		
Range Time, sec	12,147.2	12,052.9	94.3
Altitude, km (n mi)	7,459.8 (4,028.0)	6,977.7 (3,767.7)	482.1 (260.3)
Space-Fixed Velocity, m/s (ft/s)	7,494.1 (24,586.9)	7,631.5 (25,037.7)	-137.4 (-450.8)
Flight Path Angle, deg	46.011	45.046	0.965
Heading Angle, deg	112.493	111.816	0.677
Geodetic Latitude, deg N	19.957	20.724	-0.767
Longitude, deg E	-62.502	-64.048	1.546

NOTE: Times used are vehicle times.

Table 4-4. Parking Orbit Insertion Conditions

PARAMETER	ACTUAL	NOMINAL	ACT-NOM
Range Time, sec	704.67	709.06	-4.39
Altitude, km (n mi)	172.6 (93.2)	171.8 (92.8)	0.8 (0.4)
Space-Fixed Velocity, m/s (ft/s)	7,803.7 (25,602.7)	7,804.0 (25,603.7)	-0.3 (-1.0)
Flight Path Angle, deg	0.015	0.000	0.015
Heading Angle, deg	95.531	95.674	-0.143
Inclination, deg	29.679	29.685	-0.006
Descending Node, deg	109.314	109.330	-0.016
Eccentricity	0.0003	0.0000	0.0003
Apogee*, km (n mi)	169.5 (91.5)	166.7 (90.0)	2.8 (1.5)
Perigee*, km (n mi)	166.0 (89.6)	166.5 (89.9)	-0.5 (-0.3)
Period, min	87.84	87.82	0.02
Geodetic Latitude, deg N	29.365	29.346	0.019
Longitude, deg E	-53.081	-52.791	-0.290

NOTE: Range Times used are times of occurrence at the vehicle, see Figure 2-1.

*Based on a spherical earth of radius 6,378.165 km (3,443.934 n mi).

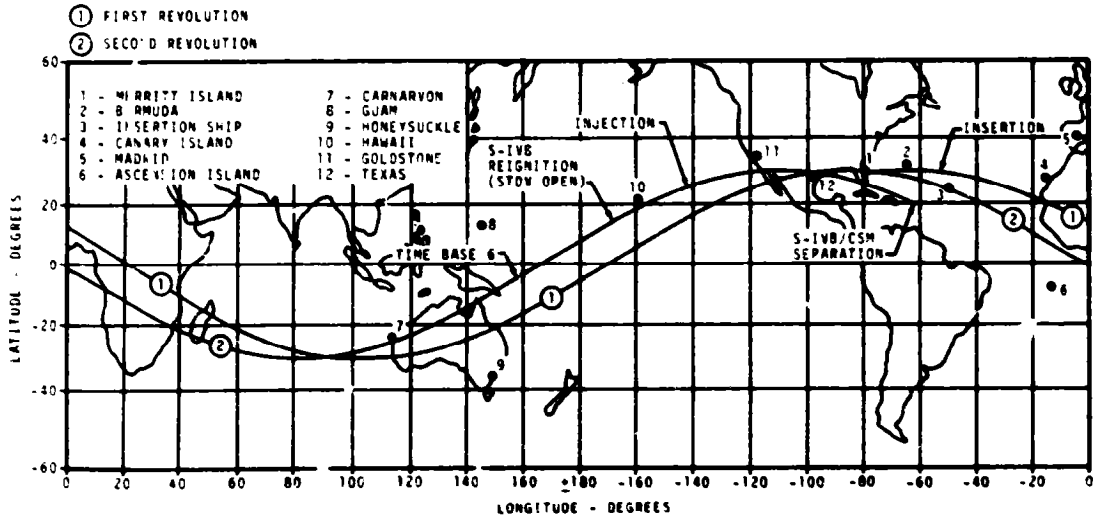

Figure 4-5. Launch Vehicle Ground Track

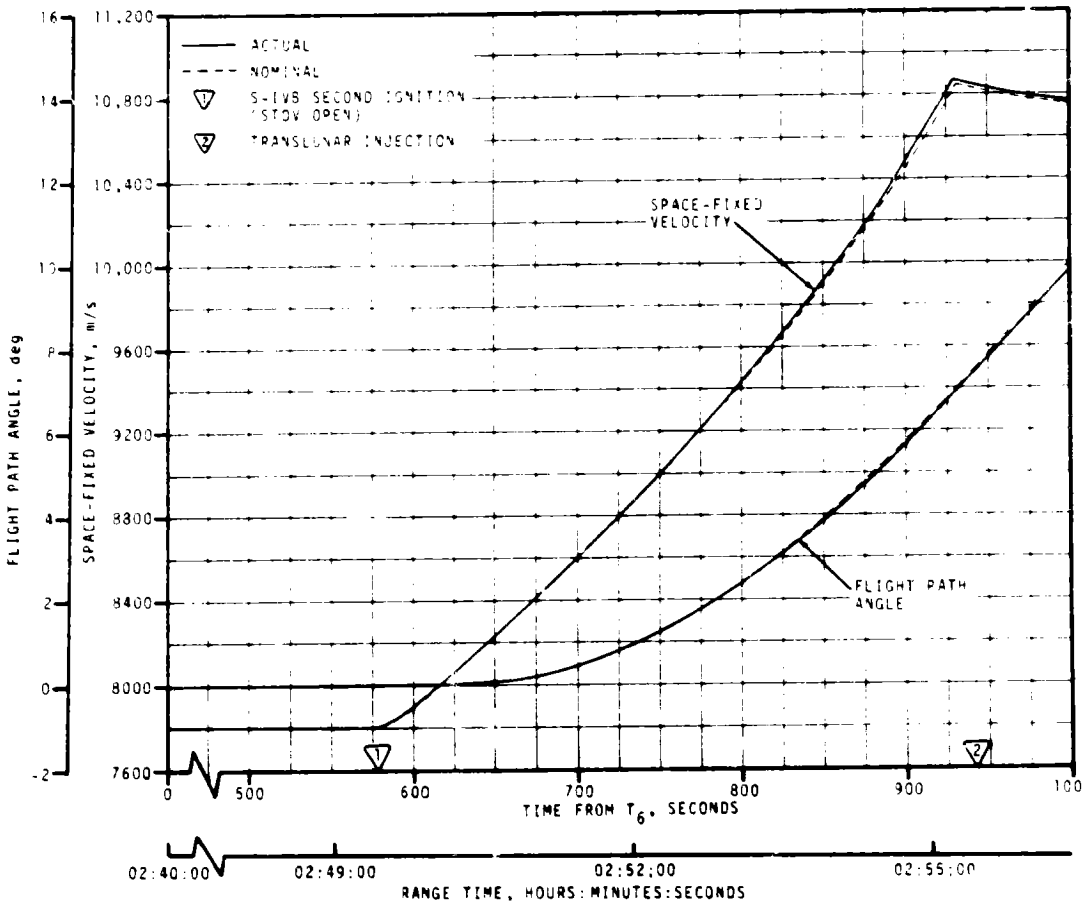

Figure 4-6. Injection Phase Space-Fixed Velocity and Flight Path Angle Comparisons

The space-fixed velocity was greater than nominal with deviations more noticeable towards the end of the time period. The actual and nominal targeting parameters at S-IVB second guidance cutoff are presented in Table 4-2. The actual and nominal translunar injection conditions are compared in Table 4-5.

4.2.4 Post TLI Phase

The post TLI trajectory spans the interval from translunar injection to S-IVB/CSM separation. Tracking data from two C-Band stations (Merritt Island and Bermuda) and three S-Band stations (Goldstone, Goldstone Wing

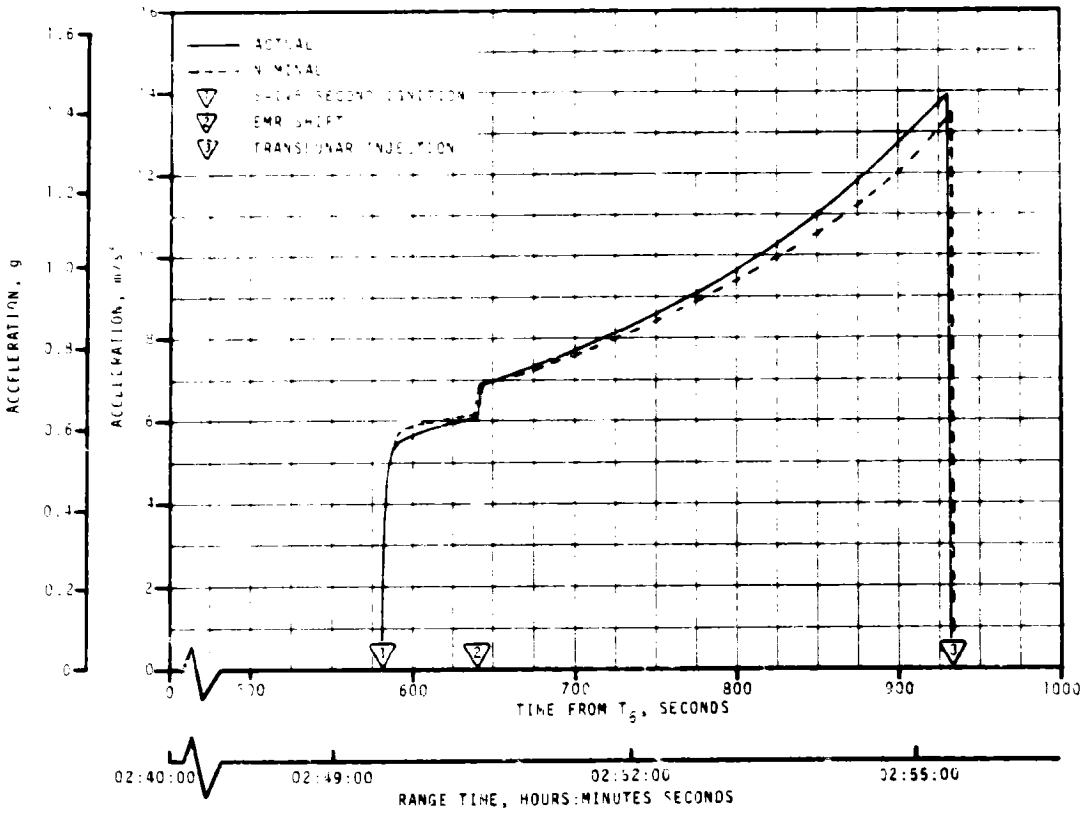

Figure 4-7. Injection Phase Acceleration Comparison

and Texas) were utilized in the reconstruction of this trajectory segment. Telemetered post TLI guidance velocity data were used to derive the post TLI nonpotential accelerations during this phase. The post TLI trajectory reconstruction utilizes the same methodology as outlined in paragraph 4.2.2. The S-IVB/CSM separation conditions are presented in Table 4-3.

Table 4-5. Translunar Injection Conditions

PARAMETER	ACTUAL	NOMINAL	ACT-NOM
Range Time, sec	10,563.69	10,562.74	0.95
Altitude, km (n mi)	321.1 (173.4)	324.8 (175.4)	-3.7 (-2.0)
Space-Fixed Velocity, m/s (ft/s)	10,845.6 (35,582.7)	10,842.3 (35,571.9)	3.3 (10.8)
Flight Path Angle, deg	7.408	7.596	-0.188
Heading Angle, deg	73.188	73.338	-0.150
Inclination, deg	29.684	29.696	-0.012
Descending Node, deg	108.418	108.452	-0.034
Eccentricity	0.9762	0.9761	0.0001
C_3, m^2/s^2 (ft^2/s^2)	-1,438,810 (-15,487,222)	-1,445,581 (-15,560,104)	6,771 (72,822)

NOTE: Times used are vehicle times.

SECTION 5

S-IC PROPULSION

5.1 SUMMARY

All S-IC propulsion systems performed satisfactorily. Overall stage thrust was 0.47 percent lower than predicted. Total propellant consumption rate was 0.29 percent lower than predicted with the total consumed Mixture Ratio (MR) 0.35 percent higher than predicted. Specific impulse was 0.18 percent lower than predicted. Total propellant consumption from Holddown Arm (HDA) release to Outboard Engine Cutoff (OECO) was low by 0.03 percent.

Center Engine Cutoff (CECO) was initiated by the Instrument Unit (IU) at 136.0 seconds which was 0.1 second earlier than planned. OECO, initiated by LOX low level sensors, occurred at 159.56 seconds which was 0.53 second later than predicted. The LOX residual at OECO was 31,135 lbm compared to the predicted 36,115 lbm. The fuel residual at OECO was 27,142 lbm compared to the predicted 29,404 lbm.

The S-IC experienced a 1-1-2-1 start sequence rather than the planned 1-2-2 sequence. Since engine No. 1 had been replaced after the stage static test, it was expected that the planned start sequence would not be attained.

Stage static tests have shown an inability to closely predict the starting time of an engine in the stage, based on acceptance test firing data, prior to its firing in the stage. The actual start sequence caused no problems.

Higher than normal LOX turbopump seal purge flowrate was experienced during the first 45 seconds of flight. Based on the GN_2 storage sphere pressure decay, the AS-510 flowrate was approximately 65 percent greater than the previous maximum flowrate for a similar system configuration (AS-509). It was known prior to flight that the engine No. 3 purge flowrate was higher than normal but within acceptable limits. The sphere capacity was adequate and all system requirement pressures were met. Therefore, the system performance is considered to have been normal in view of the acceptance history of engine No. 3.

The S-IC hydraulic system performed satisfactorily.

5.2 S-1C IGNITION TRANSIENT PERFORMANCE

The fuel pump inlet preignition pressure was 45.6 psia and within the F-1 engine model specification limits of 43.3 to 110 psia.

The LOX pump inlet preignition pressure and temperature were 83.3 psia and -287.3°F and were within F-1 engine model specification limits, as shown by Figure 5-1.

The planned 1-2-2 start was not attained. Engine position starting order was 5, 3, 2-4, 1. By definition, two engines are considered to start together if their combustion chamber pressures reach 100 psig in a 100-millisecond time period. Engine No. 1 had not been static fired on an S-IC stage so that only acceptance test times were available for the engine No. 1 start time prediction. Stage static tests have demonstrated an inability to closely predict the starting time of an engine in the stage, based upon acceptance test firing data, prior to its firing in the stage. The actual start sequence caused no problems. Thrust build-up rates were as expected, as shown in Figure 5-2.

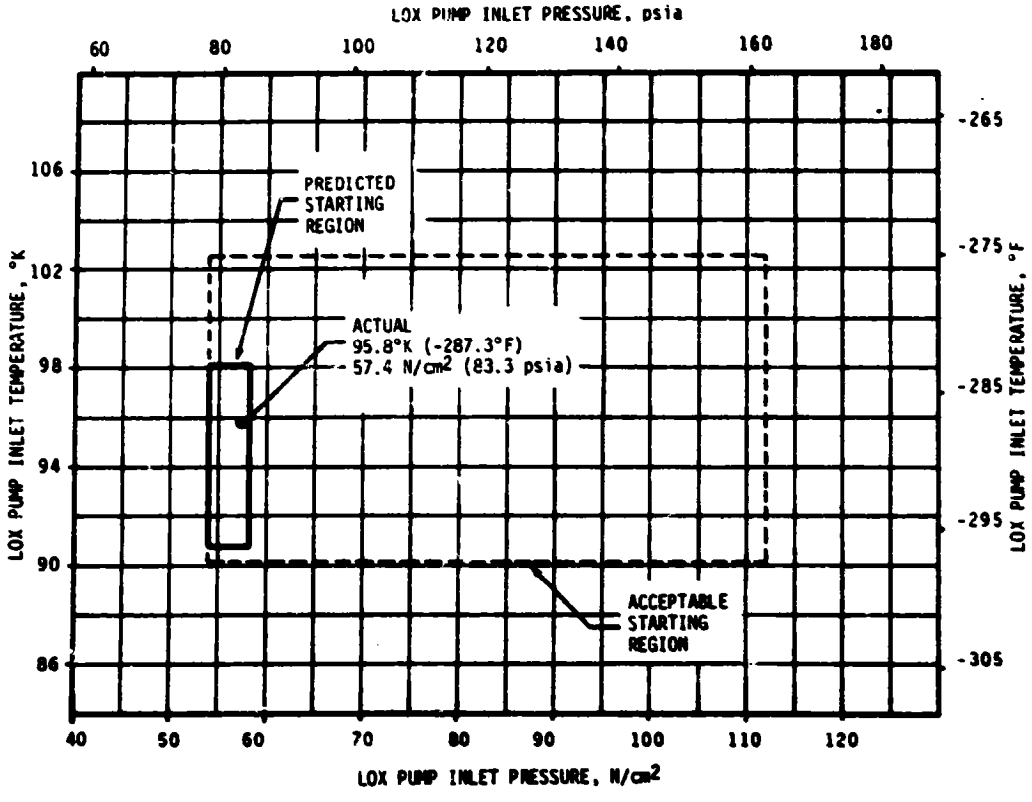

Figure 5-1. S-IC LOX Start Box Requirements

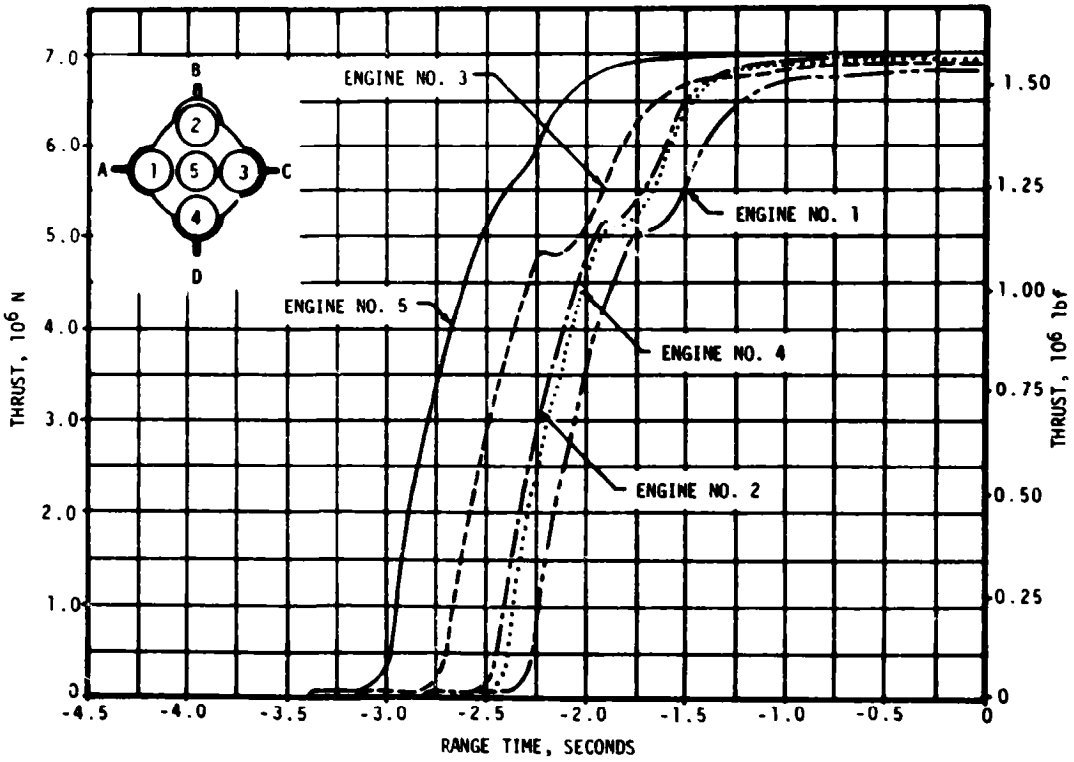

Figure 5-2. S-IC Engines Thrust Buildup

It should be expected during future S-IC operations that there is a low probability of obtaining a 1-2-2 start sequence if any engine is replaced after static firing.

5.3 S-IC MAINSTAGE PERFORMANCE

S-IC stage propulsion performance was satisfactory. The stage site thrust (averaged from time zero to OECO) was 0.47 percent lower than predicted. Total propellant consumption rate was 0.29 percent lower than predicted and the total consumed mixture ratio was 0.35 percent higher than predicted. The specific impulse was 0.18 percent lower than predicted. Total propellant consumption from HDA release to OECO was low by 0.03 percent. See Figure 5-3. For comparison of F-1 engine flight performance with predicted performance, the flight performance has been analytically reduced to standard conditions and compared to the predicted performance which is based on ground firings and also reduced to standard conditions. These values are shown in Table 5-1 and are at the 35 to 38-second time slice. The largest thrust deviation from the predicted value was -25.8 Klbf for engine No. 5. Engines No. 2,

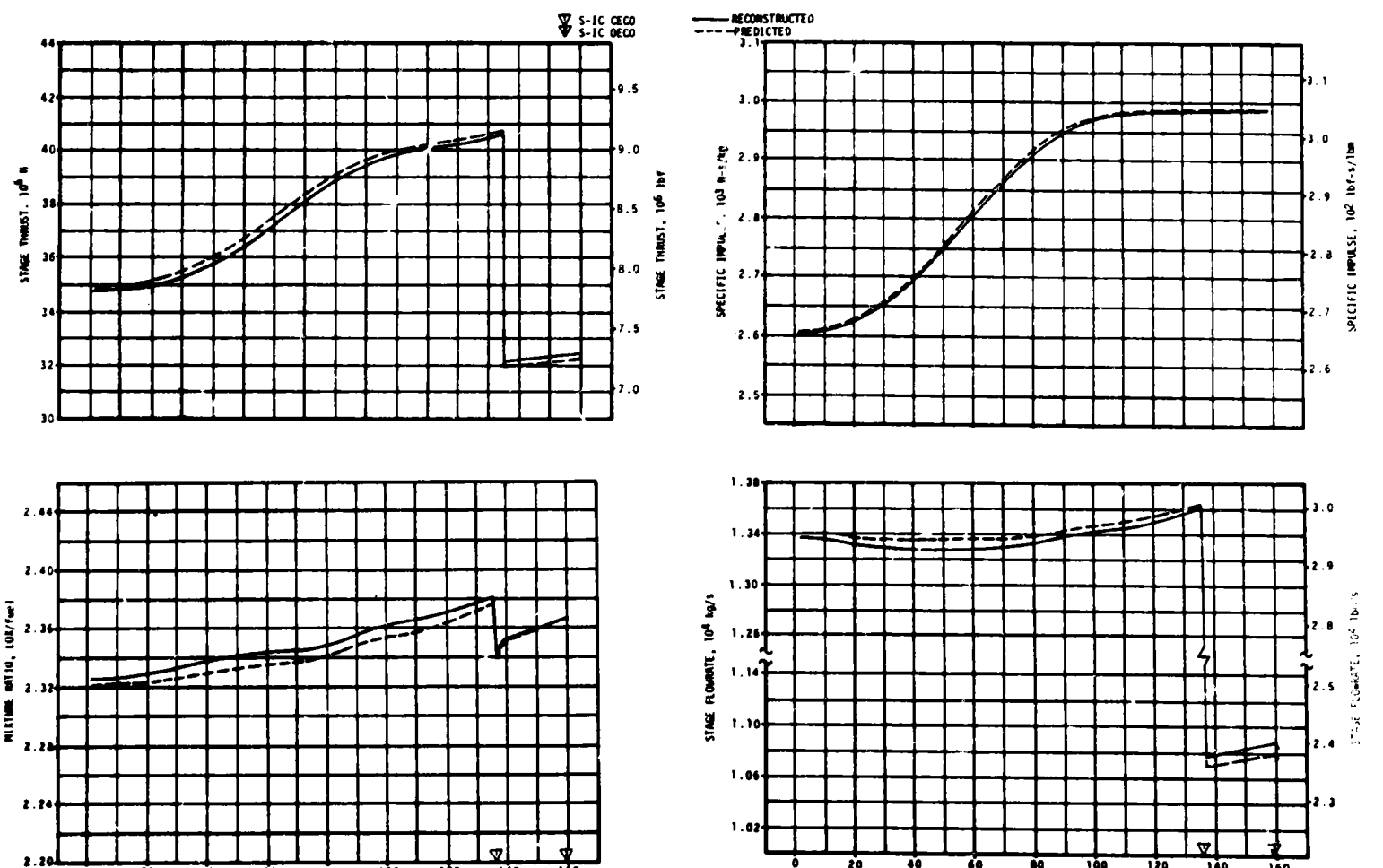

Figure 5-3. S-IC Stage Propulsion Performance

Table 5-1. S-IC Individual Standard Sea Level Engine Performance

PARAMETER	ENGINE	PREDICTED	RECONSTRUCTION ANALYSIS	DEVIATION PERCENT	AVERAGE DEVIATION PERCENT
Thrust 10J lbf	1	1521	1527	0.394	
	2	1522	1510	-0.788	
	3	1522	1510	-0.788	-0.683
	4	1522	1514	-0.526	
	5	1523	1497	-1.707	
Specific Impulse, lbf-s/lbm	1	265.6	265.7	0.0377	
	2	264.9	264.6	-0.113	
	3	264.3	263.9	-0.151	-0.113
	4	265.4	265.2	-0.0754	
	5	264.9	264.2	-0.264	
Total Flowrate l.?/s	1	5728	5747	0.332	
	2	5744	5705	-0.679	
	3	5758	5720	-0.660	-0.577
	4	5734	5709	-0.436	
	5	5749	5666	-1.444	
Mixture Ratio LOX/Fuel	1	2.271	2.271	0	
	2	2.275	2.268	-0.308	
	3	2.281	2.275	-0.263	-0.238
	4	2.263	2.257	-0.265	
	5	2.274	2.266	-0.352	

NOTE: Performance levels were reduced to standard sea level and pump inlet conditions. Data were taken from the 35 to 38-second time slice.

3, and 4 had lower thrust than predicted by 12.2, 11.8, and 7.5 Klbf, respectively. Engine No. 1 was high by 5.8 Klbf. The average of all five engines was 1512 Klbf compared to the predicted 1522 Klbf.

It should be noted that this was the first Saturn V stage to be launched with engines that had been reorificed to a new power level after stage static test without the benefit of a second stage static test to validate proper power level with the new orifices. Overall performance was sufficiently close to predicted values to verify the acceptability of reorificing engines without the benefit of a stage static test.

The turbopump LOX seal purge pressure, measured at engine No. 1 customer connect point, showed a higher than normal initial decay. This behavior has been attributed to engine No. 3 which exhibited a high purge flow-rate during acceptance tests. See paragraph 5.8 for further details. This caused no problems for the AS-510 flight.

5.4 S-IC ENGINE SHUTDOWN TRANSIENT PERFORMANCE

The F-1 engine thrust decay transient was normal. The combustion chamber pressure oscillogram for engine No. 3 showed that the pressure transducer sense tube was momentarily obstructed during shutdown. This phenomenon has been observed before during engine test firings and on AS-505 and caused no problem on AS-510.

The cutoff impulse, measured from cutoff signal to zero thrust, was 667,656 lbf-s for the center engine and 2,643,945 lbf-s for all outboard engines. These values are 4.3 and 10.8 percent, respectively, above the predicted values. For this analysis, thrust chamber pressure was assumed to go to zero four seconds after the engine cutoff command.

Due to the revised S-IC/S-II staging sequence used on this flight, a more complete definition of the F-1 engine thrust decay characteristic is desirable for flight data evaluation (see paragraph 10.6). Figure 5-4 presents the normalized thrust decay characteristics for the four outboard F-1 engines on the AS-510.

Center engine cutoff, initiated by a signal from the IU at 136.0 seconds, was 0.1 second earlier than planned. Outboard engine cutoff, initiated by a signal from the LOX low level sensors at 159.56 seconds, was 0.53 second later than the nominal predicted time of 159.03 seconds. Most of the OECO deviation, which was small when compared to the 3-sigma limits of +3.92, -3.38 seconds, can be attributed to low thrust.

The AS-510 and subsequent S-IC stages employ a 1.6 second LOX cutoff timer delay setting as compared to 1.2 seconds on AS-501 through AS-509. Increasing the timer setting allows an additional 6700 pounds of usable LOX residuals to be consumed. The LOX pump net positive suction head at the OECO signal ranged from 101 to 108 feet of LOX for the four outboard engines. This is well above the F-1 engine model specification minimum value of 65 feet.

5.5 S-IC STAGE PROPELLANT MANAGEMENT

The S-IC stage does not have an active propellant utilization system. Minimum residuals are obtained by attempting to load the mixture ratio expected to be consumed by the engines plus the predicted unusable residuals. Also, a small additional amount of usable fuel (fuel bias) is loaded to minimize maximum residuals. An analysis of the usable residuals experienced during a flight is a good measure of the performance of the passive propellant utilization system.

The residual LOX at OECO was 31,135 lbm compared to the predicted value of 36,115 lbm. The fuel residual at OECO was 27,142 lbm compared to the predicted value of 29,404 lbm. A summary of the propellants remaining at major event times is presented in Table 5-2.

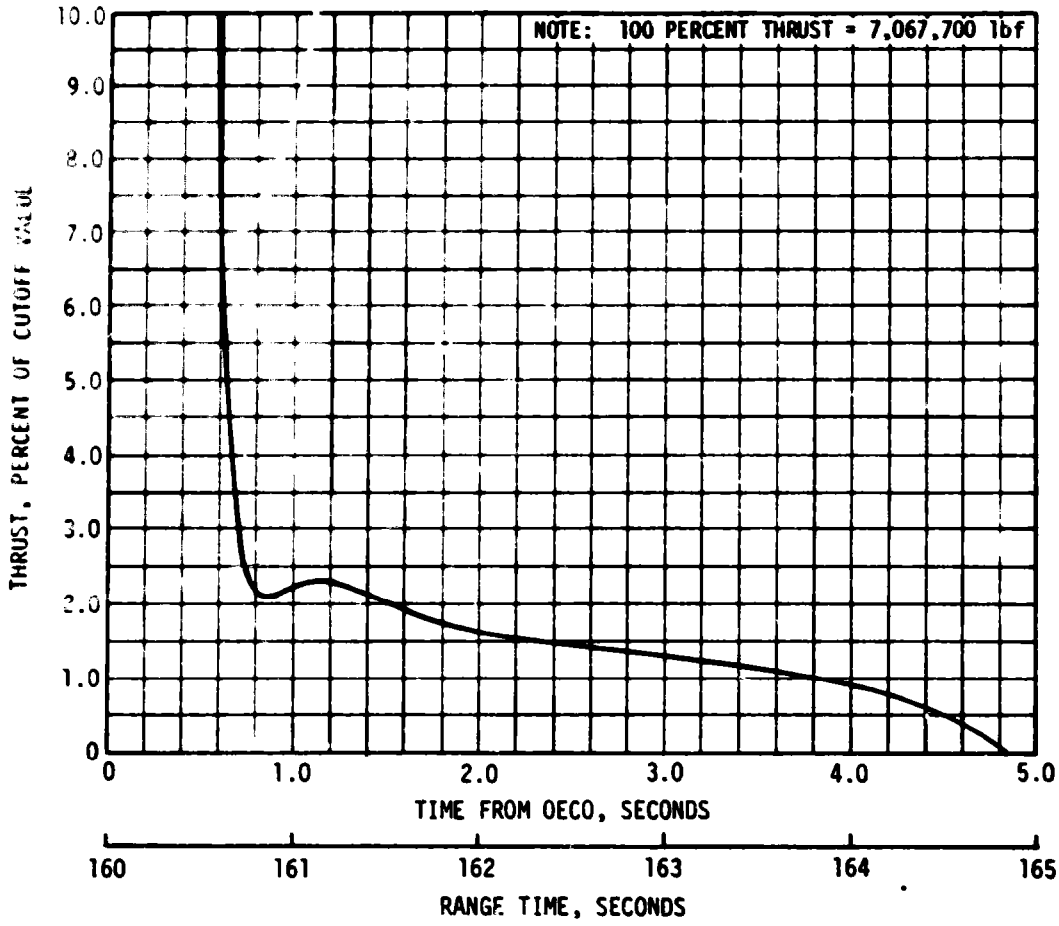

Figure 5-4. Normalized AS-510 Outboard Engine Thrust Decay Characteristic

5.6 S-IC PRESSURIZATION SYSTEMS

5.6.1 S-IC Fuel Pressurization System

The fuel tank pressurization system performed satisfactorily, keeping ullage pressure within acceptable limits during flight. Helium Flow Control Valves (HFCV) No. 1 through 4 opened as planned and HFCV No. 5 was not required.

The low flow prepressurization system was commanded on at -96.96 seconds and was cycled on a second time at -2.72 seconds. High flow pressurization, accomplished by the onboard pressurization system, performed as expected. Helium flow control valve No. 1 was commanded on at -2.70 seconds and was supplemented by the ground high flow prepressurization system until umbilical disconnect.

Table 5-2. S-IC Propellant Mass History

EVENT	PREDICTED, LBM		LEVEL SENSOR DATA, LBM		RECONSTRUCTED, LBM	
	LOX	FUEL	LOX	FUEL	LOX	FUEL
Ignition Command	3,310,079	1,413,921	-	1,410,798	3,312,030	1,410,798
Holddown Arm Release	3,241,889	1,395,058	-	1,378,599	3,238,286	1,389,703
CECO	420,640	192,289	-	195,373	428,798	195,688
OECO	36,115	29,404	-	26,572	31,135	27,142
Separation	30,585	26,457	-	-	25,369	24,023
Zero Thrust	30,457	26,368	-	-	25,236	23,929

NOTE: Predicted and reconstructed values do not include pressurization gas so they will compare with level sensor data.

Fuel tank ullage pressure was within the predicted limits throughout flight as shown in Figure 5-5. Helium flow control valves No. 2, 3, and 4 were commanded open during flight by the switch selector within acceptable limits. Helium bottle pressure was 2990 psia at -2.75 seconds and decayed to 500 psia at OECO. Total helium flowrate and heat exchanger performance were as expected.

Fuel pump inlet pressure was maintained above the required minimum Net Positive Suction Pressure (NPSP) during flight.

5.6.2 S-IC LOX Pressurization System

The LOX pressurization system performed satisfactorily and all performance requirements were met. The ground prepressurization system maintained ullage pressure within acceptable limits until launch commit. The on-board pressurization system performed satisfactorily during flight.

This was the first launch with ECP627 incorporated. This ECP redesigned the LOX tank vent and relief valves. This redesign was to correct a failure-to-close problem that occurred during the AS-508 launch. The redesign eliminated some potential mechanical interferences and added a second closing spring to the pneumatic actuator. Valve performance during the AS-510 CDDT and launch countdown was within requirements. The AS-508 problem is considered closed.

The prepressurization system was initiated at -71.96 seconds. Ullage pressure increased to the prepressurization switch band and flow was

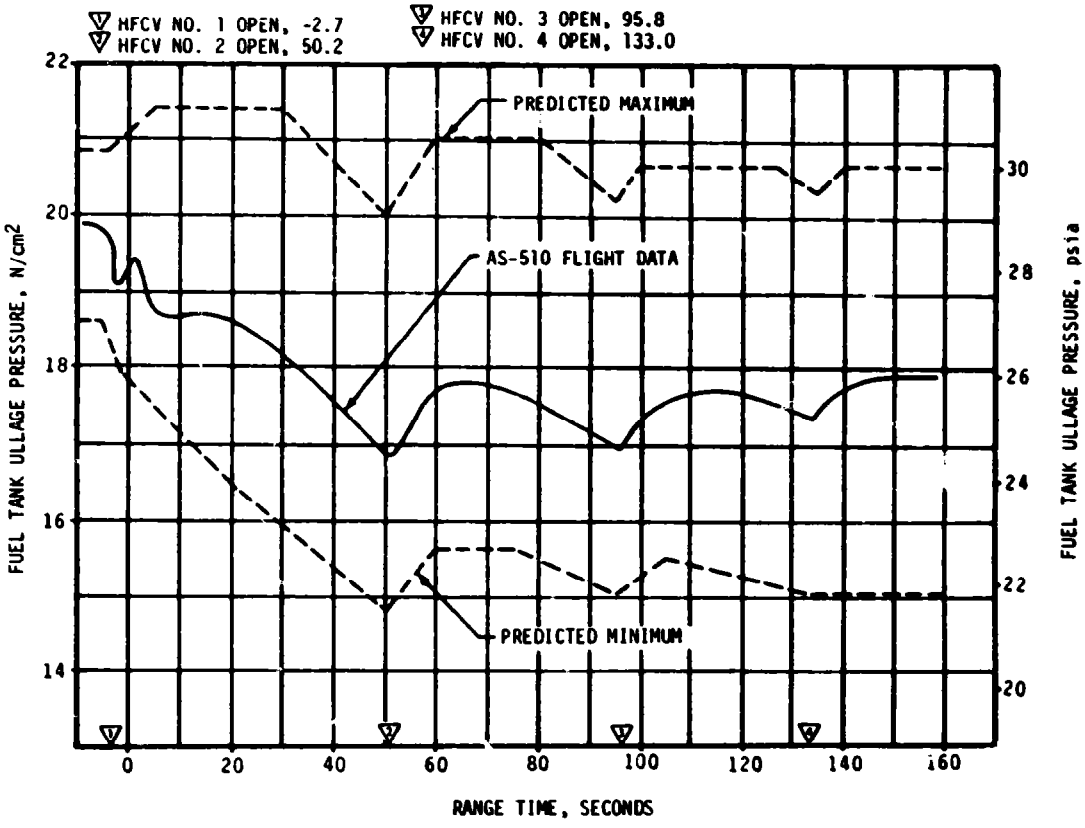

Figure 5-5. S-IC Fuel Tank Ullage Pressure

terminated at -57.58 seconds. The low flow system was cycled on three additional times at -41.59, -21.76, and -5.21 seconds. At -4.65 seconds the high flow system was commanded on and maintained ullage pressure within acceptable limits until launch commit.

Ullage pressure was maintained within the predicted limits as shown in Figure 5-6. GOX flowrate to the tank was as expected. The maximum GOX flowrate after the initial transient was 45.9 lbm/s at CECO.

The LOX pump inlet pressure met the minimum NPSP requirement throughout flight.

The performance of the heat exchangers was as expected.

5.7 S-IC PNEUMATIC CONTROL PRESSURE SYSTEM

The control pressure system functioned satisfactorily throughout the S-IC flight.

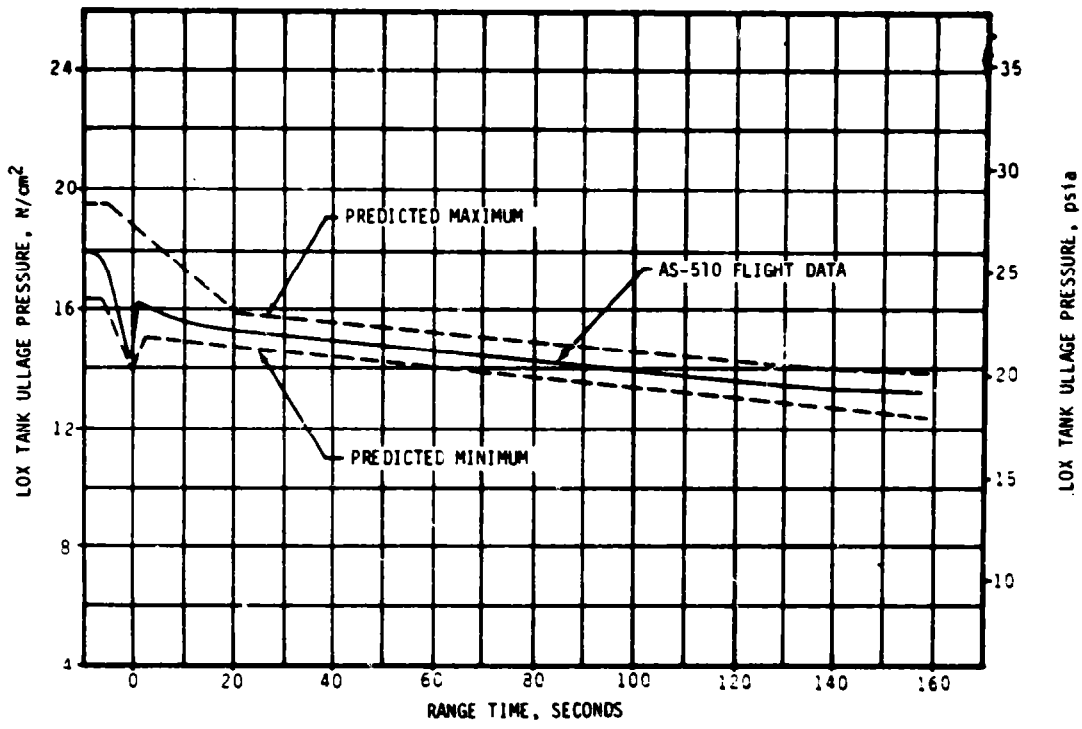

Figure 5-6. S-IC LOX Tank Ullage Pressure

Sphere pressure was 2942 psia at liftoff and remained steady until CECO when it decreased to 2830 psia. The decrease was due to center engine prevalve actuation. There was a further decrease to 2455 psia after OECO.

The engine prevalves were closed after CECO and OECO as required.

5.8 S-IC PURGE SYSTEMS

Performance of the purge systems was satisfactory during flight.

The turbopump LOX seal storage sphere pressure was 2950 psia at liftoff which was within the preignition limits of 2700 to 3300 psia. The sphere pressure was within the predicted envelope throughout flight and was 2200 psia at OECO.

Higher than normal purge flows were experienced during the first 45 seconds of flight. This was observed at the storage sphere pressure, Figure 5-7, and the engine No. 1 customer connect point pressure, Figure 5-8. Based on the storage sphere pressure decay, the flowrate was between 0.14 and 0.22 lbm/s. The previous maximum flowrate for a similar configuration was observed on AS-509. For that flight the

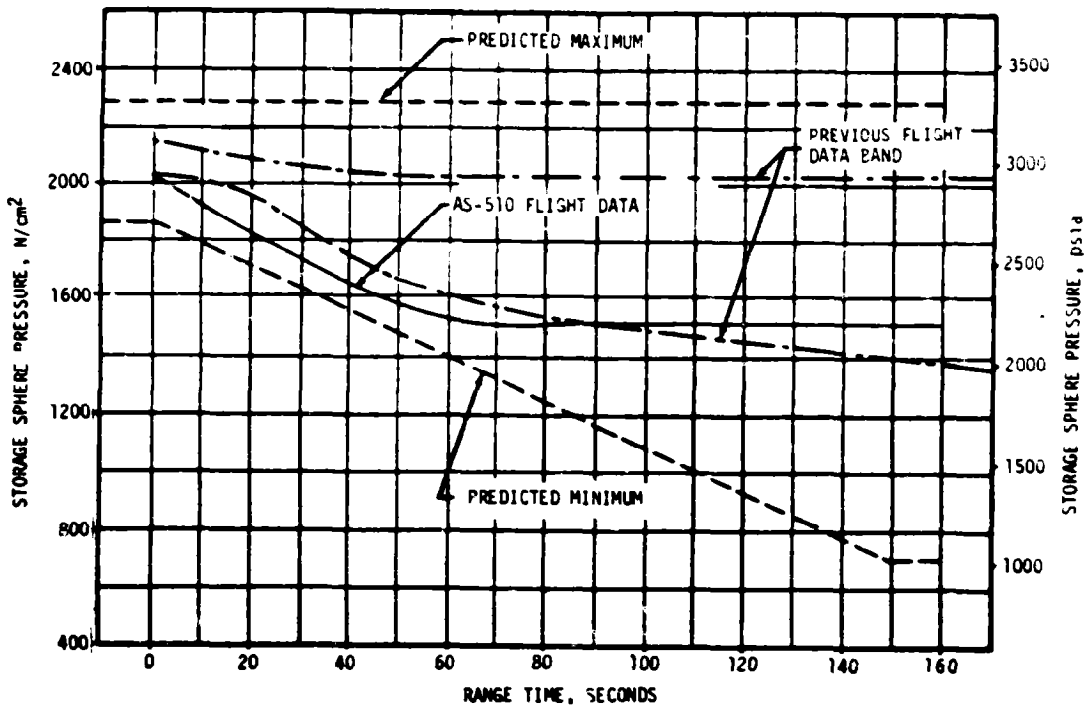

Figure 5-7. S-IC Purge Systems Storage Sphere Pressure

flowrate was between 0.08 and 0.13 lbm/s. The AS-510 flowrate represents approximately a 65 percent increase over the AS-509 flowrate.

Turbopump seal purge flowrate is measured during acceptance test, and is nominally less than 0.010 lbm/s during engine operation. However, engine No. 3 (position 3) exhibited a maximum purge flowrate of 0.0288 lbm/s during its acceptance testing. This corresponds to a maximum flowrate of 0.0334 lbm/s when corrected to account for acceptance test vehicle configuration differences. The high flowrate occurred between start transition and 55 seconds of mainstage, at which time the intermediate seal seated and the purge flowrate dropped to 0.0021 lbm/s. The acceptance test characteristics of engine No. 3 match the characteristics of the flight data.

The purpose of the purge is to provide a positive pressure in the turbopump intermediate seal to assist the carbon segmented dynamic intermediate seal to maintain a separation between the LOX seal cavity and No. 1 bearing lubrication seal vent low pressure areas.

The turbopump intermediate seal is a dynamic seal with carbon segments spring loaded to ride the turbopump shaft. During transition to mainstage speed the carbon segments are unseated from the shaft due to shaft

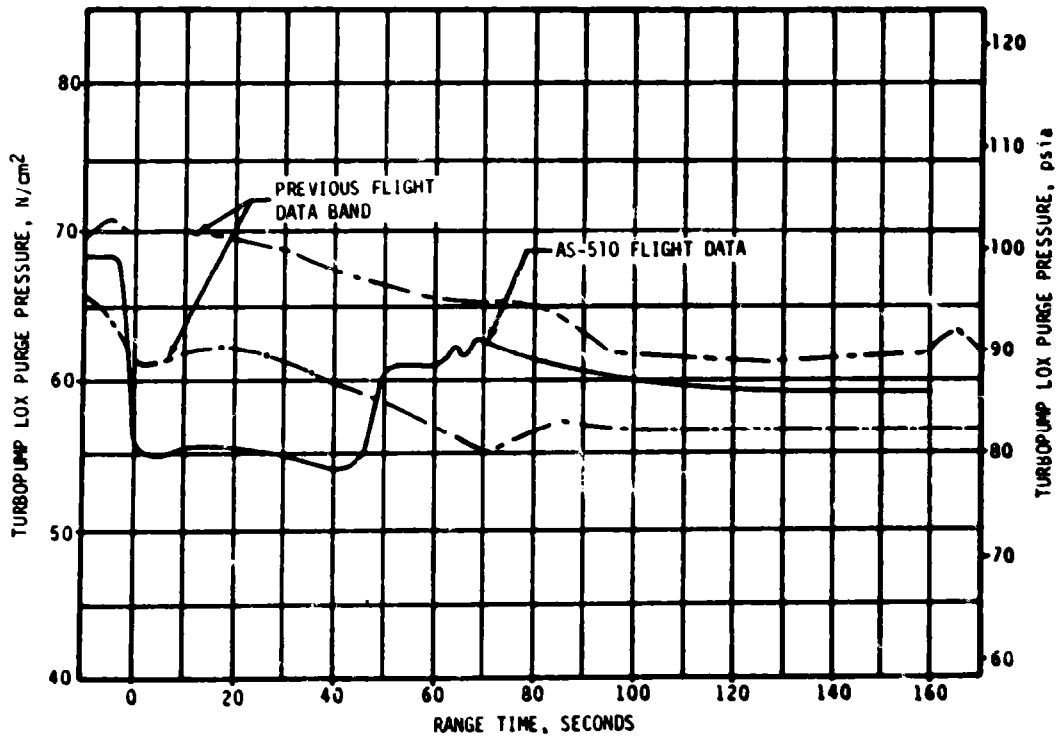

Figure 5-8. F-1 Engine Turbopump LOX Purge Pressure at Station 109, Engine No. 1

motion. The spring force aided by the purge pressure reseats the carbon segments usually within the first 30 to 50 seconds of mainstage operation. The amount of unseating of the seal and the recovery time vary with each engine. The results of this operating characteristic may be observed in the turbopump LOX seal purge pressure, which is characterized by a drop in pressure during initial operation due to increased purge gas flow through the seal. A high purge gas flowrate to any individual engine in the stage will be indicated by a drop in the No. 1 turbopump LOX seal pressure due to the common manifold system.

The turbopump LOX seal purge flowrate experienced during the AS-510 flight, although higher than experienced on previous flights, is considered normal in view of the acceptance test history of engine No. 3. The sphere capacity was adequate and all system pressure requirements were met.

5.9 S-IC POGO SUPPRESSION SYSTEM

The POGO suppression system performed satisfactorily during S-IC flight.

Outboard LOX prevalve temperature measurements indicated that the outboard LOX prevalve cavities were filled with gas prior to liftoff as

planned. The four resistance thermometers behaved during the AS-510 flight similarly to those on the AS-509 flight. The temperature measurements in the outboard LOX prevalve cavities remained warm (off scale high) throughout flight, indicating helium remained in the prevalves. The two thermometers in the center engine prevalve were cold, indicating LOX in this valve as planned. The pressure and flowrate in the system were nominal.

5.10 S-IC HYDRAULIC SYSTEM

The performance of the S-IC hydraulic system was satisfactory. All servoactuator supply pressures were within required limits.

The engine control system return pressures were within predicted limits and the engine hydraulic control valves operated as planned.

SECTION 6

S-II PROPULSION

6.1 SUMMARY

The S-II propulsion system performed satisfactorily throughout the flight. The S-II Engine Start Command (ESC), as sensed at the engines, occurred at 161.95 seconds. Center Engine Cutoff (CECO) occurred as planned at 459.56 seconds, and Outboard Engine Cutoff (OECO) occurred at 549.06 seconds giving an outboard engine operating time of 387.1 or 1.2 seconds less than predicted. The earlier than predicted S-II OECO was a result of the higher than predicted engine performance during the low Engine Mixture Ratio (EMR) portion of S-II boost.

Four of the eight S-IC retromotors and all of the S-II ullage motors were removed for this flight; therefore, the S-IC/S-II separation sequence was revised. This sequence change extended the coast period between S-IC OECO and S-II ESC by one second. The S-IC/S-II separation sequence and S-II engine thrust buildup performance was satisfactory.

The total stage thrust at the standard time slice (61 seconds after S-II ESC) was 0.05 percent below predicted. Total propellant flowrate, including pressurization flow, was 0.03 percent below predicted and the stage specific impulse was 0.02 percent below predicted at the standard time slice. Stage propellant mixture ratio was 0.03 percent above predicted. Engine Cutoff (ECO) transients were normal.

This was the second flight stage to incorporate a center engine LOX feedline accumulator system as a POGO suppression device. The operation of the device was effective in suppressing POGO type oscillations.

The propellant management system performance was satisfactory throughout propellant loading and flight and all parameters were within expected limits. Control of EMR was accomplished with the two-position pneumatically operated Mixture Ratio Control Valves (MRCV). The Instrument Unit (IU) velocity dependent low EMR command occurred 0.6 second earlier than the trajectory simulation. S-II OECO was initiated by the LOX depletion ECO sensors as planned.

The performance of the LOX and LH_2 tank pressurization systems was satisfactory. This was the first flight stage to utilize bootstrap pressurization line orifices in place of the regulators to control inflight pressurization of the propellant tanks. Ullage pressure in both tanks was adequate to meet or exceed engine inlet Net Positive Suction Pressure (NPSP) minimum requirements throughout mainstage.

The engine servicing, recirculation, helium injection, and valve actuation systems performed satisfactorily.

S-II hydraulic system performance was normal throughout the flight.

6.2 S-II CHILLDOWN AND BUILDUP TRANSIENT PERFORMANCE

The engine servicing operations required to condition the engines prior to S-II engine start were satisfactorily accomplished. Thrust chamber jacket temperatures were within predicted limits at both prelaunch and S-II ESC. Thrust chamber chilldown requirements were -200°F maximum at prelaunch commit and -150°F maximum at engine start. Thrust chamber temperatures ranged between -300 and -257°F at prelaunch commit and between -242 and -204°F at ESC. Thrust chamber temperature warmup rates during S-IC boost agreed closely with those experienced on previous flights.

Start tank system performance was satisfactory. Both temperature and pressure conditions of the engine start tanks were within the required prelaunch and engine start boxes as shown in Figure 6-1. Prelaunch and S-IC boost start tank temperature and pressure heat-up rates were normal and no indication of start tank relief valve operation was noted.

As a result of the countdown hold experienced during the AS-509 launch, a special start tank rechill test was conducted during the AS-510 Countdown Demonstration Test (CDDT). This special test was conducted to (1) establish criteria for a start tank rechill to increase the total countdown hold duration available, and (2) determine pressure decay (relief valve flow) characteristics of the start tank relief valves on the AS-510 S-II engines. The abbreviated start tank rechill was demonstrated to be a satisfactory procedure for extending the S-II hold capability to upwards of 5 hours. A period of 5 minutes is required to complete each rechill cycle. Each cycle yields an additional 38 minutes of hold time as shown in Figure 6-2. At least six such rechill cycles are available.

The pressure decay characteristics of the start tank relief valves were shown to be repeatable throughout the operating range during CDDT as shown in Figure 6-3. Only three of the five engines exhibited pressure decay and these were limited to a zone of 1365 to 1320 psia.

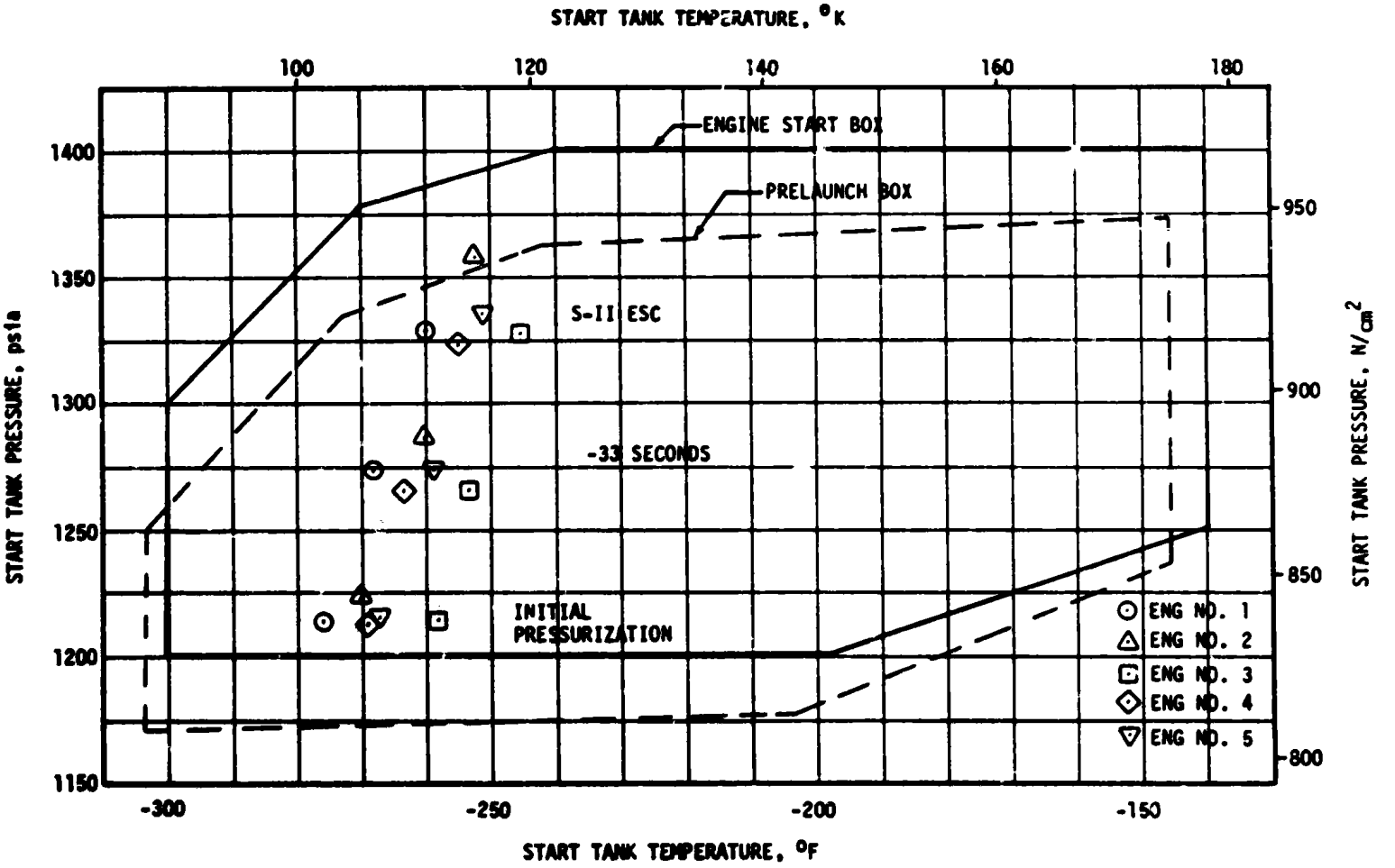

Figure 6-1. S-II Engine Start Tank Performance

During launch operations, all engine helium tank pressures were within the prelaunch and engine start limits of 2800 to 3450 psia. Engine helium tank pressures ranged between 2998 and 3090 psia prior to launch (at -19 seconds) and between 3120 and 3225 psia at S-II ESC.

The LOX and LH_2 recirculation systems used to chill the feed ducts, turbopumps, and other engine components performed satisfactorily during prelaunch and S-IC boost. Engine pump inlet temperatures and pressures at S-II ESC were well within the requirements as shown in Figure 6-4. The LOX pump discharge temperatures at S-II ESC were approximately 14°F subcooled, well below the 3°F subcooling requirement.

Deletion of the S-II ullage motors did not adversely affect the recirculation system. The engine inlet temperatures were similar to those of previous flights at S-II ESC. The characteristic temperature rise of the LOX pump discharge temperature between S-IC OECO and S-II ESC increased from approximately 1.5°F, as seen on previous flights, to approximately 2.5°F for this flight. This temperature rise difference was as predicted because of the additional one second coast time during S-IC/S-II separation.

Prepressurization of the propellant tanks was accomplished satisfactorily. Tank ullage pressures at S-II ESC were 41.2 psia for LOX and 28.4 psia for LH_2.

S-II ESC was received at 161.9 seconds and the Start Tank Discharge Valve (STDV) solenoid activation signal occurred 1.0 second later. The engine thrust buildup was satisfactory and well within the required thrust buildup envelope. All engines reached mainstage levels within 3.1 seconds after S-II ESC.

6.3 S-II MAINSTAGE PERFORMANCE

The propulsion reconstruction analysis showed that stage performance during mainstage operation was satisfactory. A comparison of predicted and reconstructed performance of thrust, specific impulse, total flowrate, and mixture ratio versus time is shown in Figure 6-5. Stage performance during the high EMR portion of flight (prior to CECO) was very close to predicted. At the time of ESC +61 seconds, total stage thrust was 1,169,661 lbf which was 648 lbf (0.05 percent) below the preflight prediction. Total propellant flowrate, including pressurization flow, was 2770.4 lbm/s; 0.03 percent below predicted. Stage specific impulse, including the effect of pressurization gas flowrate, was 422.2 lbf-s/lbm; 0.02 percent below predicted. The stage propellant mixture ratio was 0.03 percent above predicted.

Center engine cutoff was initiated at ESC +297.6 seconds as planned. This action reduced total stage thrust by 232,541 lbf to a level of 932,634 lbf. The EMR shift from high to low occurred 321.9 seconds after ESC. The change of EMR resulted in further stage thrust reduction and at ESC +350 seconds, the total stage thrust was 799,259 lbf; thus, a decrease

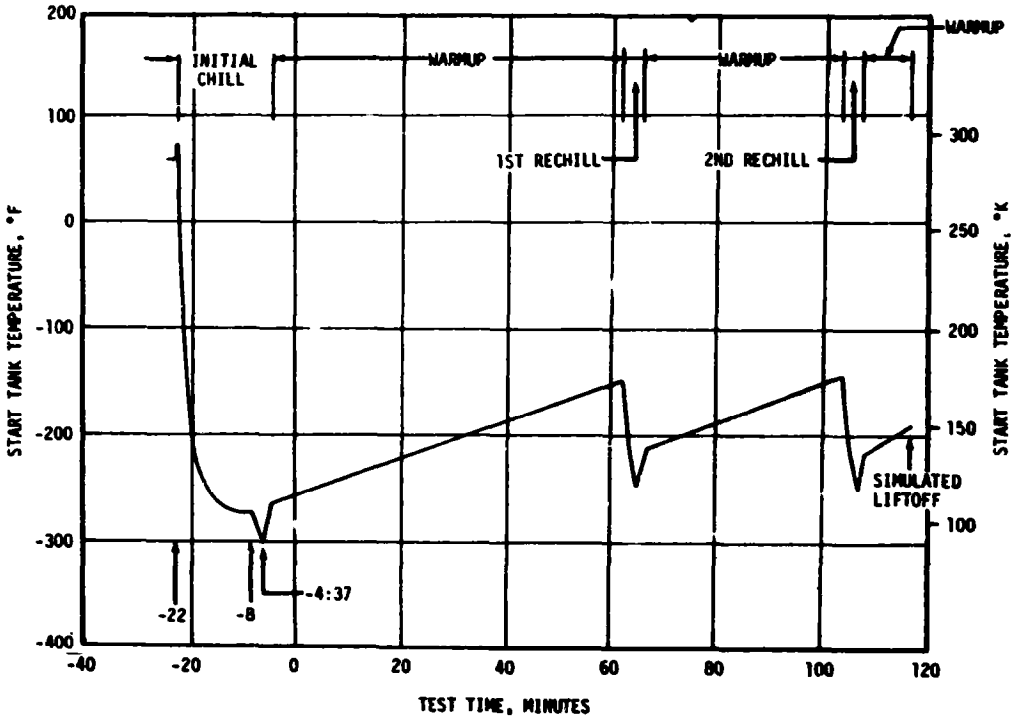

Figure 6-2. AS-510 CDDT Start Tank Rechill Performance (Engine No. 3)

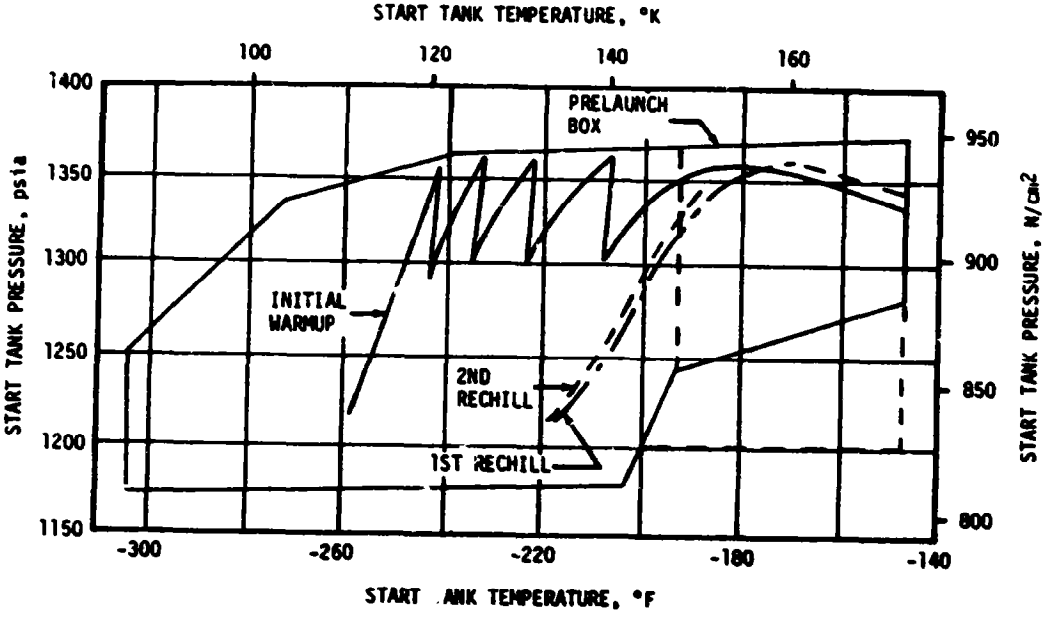

Figure 6-3. AS-510 CDDT Start Tank Preconditioning (Engine No. 3)

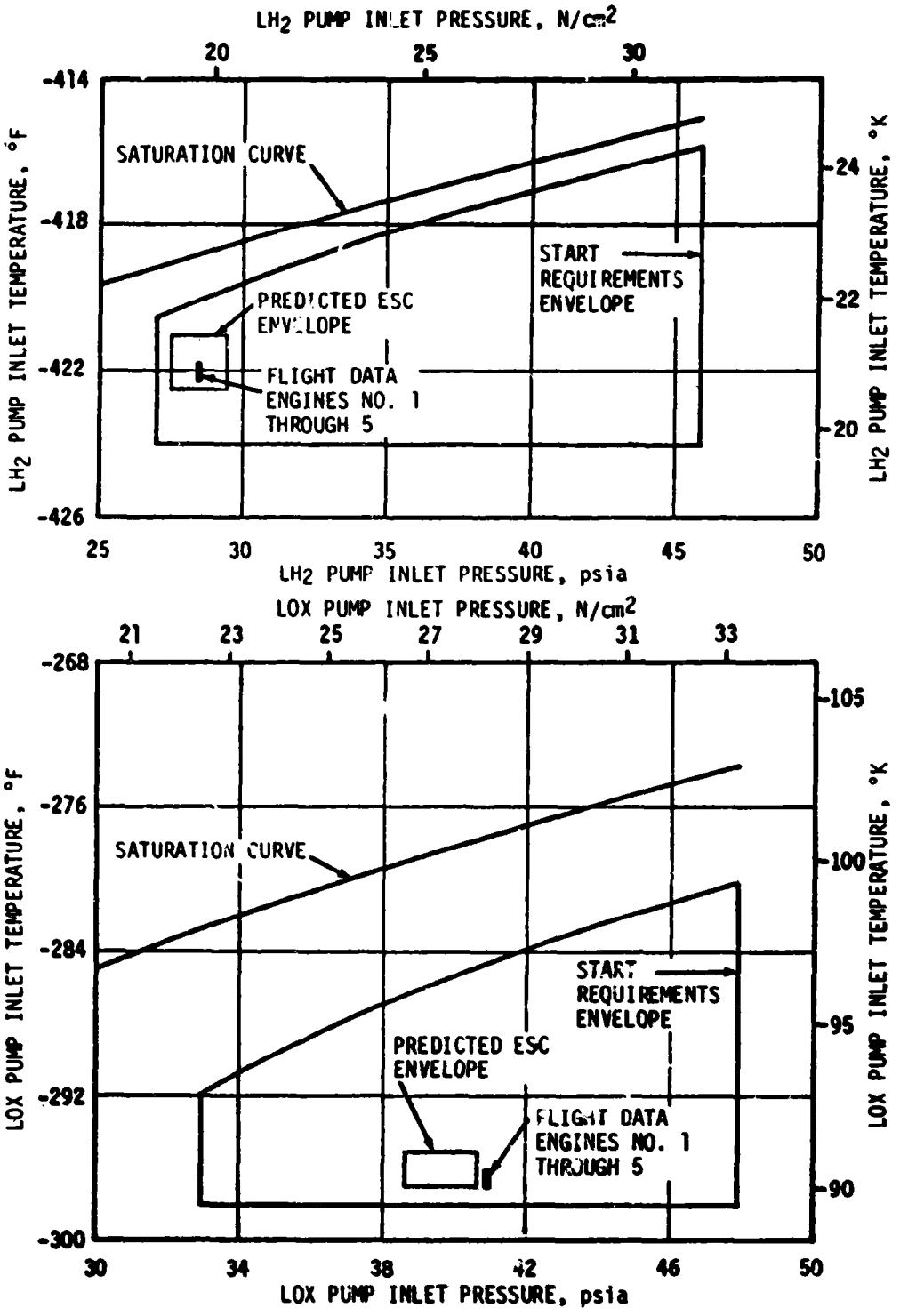

Figure 6-4. S-II Engine Pump Inlet Start Requirements

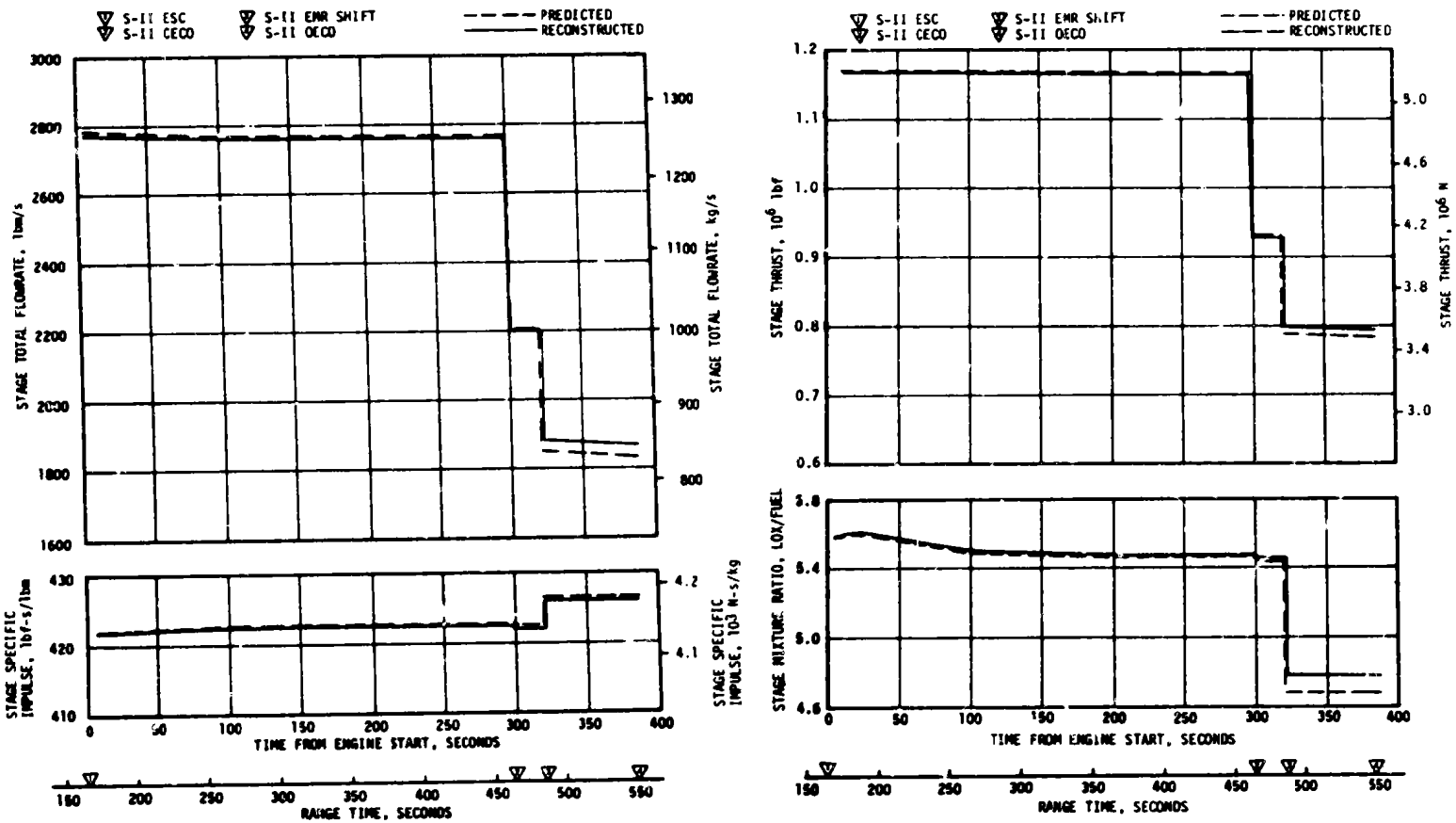

Figure 6-5. S-II Steady State Operation

in thrust of 133,375 lbf was indicated between high and low EMR operation. S-II burn duration was 387.1 seconds, which was 1.2 seconds less than predicted.

Individual J-2 engine data are presented in Table 6-1 for the ESC +61 second time slice. Good correlation between predicted and reconstructed flight performance is indicated by the small deviations. The performance levels shown in Table 6-1 have not been adjusted to standard J-2 altitude conditions and do not include the effects of pressurization flow.

Table 6-1. S-II Engine Performance

PARAMETER	ENGINE	PREDICTED	RECONSTRUCTION ANALYSIS	PERCENT INDIVIDUAL DEVIATION	PERCENT AVERAGE DEVIATION
Thrust, lbf	1	231,394	233,173	0.77	
	2	236,478	235,406	-0.45	
	3	235,256	234,833	-0.18	-0.05
	4	233,939	232,950	-0.42	
	5	233,243	233,300	0.02	
Specific Impulse, lbf-s/lbm	1	425.1	425.1	0	
	2	424.9	424.1	-0.19	
	3	423.7	423.7	0	-0.02
	4	424.6	424.6	0	
	5	424.1	424.4	0.07	
Engine Flowrate, lbm/s	1	544.3	548.5	0.77	
	2	556.6	555.0	-0.29	
	3	555.2	554.3	-0.16	-0.02
	4	551.0	548.7	-0.42	
	5	550.0	550.0	0	
Engine Mixture Ratio, LOX/LH_2	1	5.59	5.60	0.18	
	2	5.62	5.65	0.53	
	3	5.59	5.60	0.18	0.11
	4	5.57	5.58	0.18	
	5	5.56	5.53	-0.54	

NOTE: Performance levels at ESC +61 seconds. Values do not include effect of pressurization flow.

One minor engine performance shift was observed and attributed to a typical shift in Gas Generator (GG) oxidizer system resistance on engine No. 4. A 1500 lbf increase in thrust resulted from this performance shift.

6.4 S-II SHUTDOWN TRANSIENT PERFORMANCE

S-II OECO was initiated by the stage LOX depletion cutoff system as planned. The LOX depletion cutoff system again included a 1.5 second delay timer. As in previous flights (AS-504 and subsequent), this resulted in engine thrust decay (observed as a drop in thrust chamber pressure) prior to receipt of the cutoff signal. The precutoff decay was similar to that observed on AS-509 flight, but somewhat greater than experienced on AS-508. This was due to the incorporation of the two-position MRCV on AS-509 and subsequent vehicles.

Again, the largest thrust chamber pressure decay was noted on engine No. 1 with first indications of performance change visible at 0.95 second prior to cutoff signal. Total pressure decay on engine No. 1 was 210 psi while the decays of the other three outboard engines were 175 psi, as expected.

At S-II OECO total thrust was down to 548,783 lbf. Stage thrust dropped to 5 percent of this level within 0.4 second. The stage cutoff impulse through the 5 percent thrust level is estimated to be 101,700 lbf-s.

6.5 S-II STAGE PROPELLANT MANAGEMENT

Flight and ground loading performance of the propellant management system was nominal and all parameters were within expected limits, except for the apparent failure of the LH_2 60 percent liquid level point sensor. The S-II stage used a Propellant Utilization (PU) system with velocity dependent IU signals to command the two-position MRC.

The facility Propellant Tanking Control System (PTCS) and the stage propellant management system properly controlled S-II loading and replenishment. All loading redlines were easily met at the -187 second commit point. The new LOX redline (overfill shutoff sensor 5 percent wet) was met within 4 minutes after LOX tank helium injection was actuated, which is a 14 minute improvement over AS-509 (2 percent wet redline).

Open-loop control of EMR during flight was successfully accomplished with the MRCV. At ESC, helium pressure drove the valves to the engine start position corresponding to the 4.8 EMR. The high EMR (5.5) command was received at S-II ESC +5.6 seconds as expected. Helium pressure was thereby relieved and the return spring moved the valves to the high EMR position providing a nominal EMR of 5.5 for the first phase of the Programed Mixture Ratio (PMR).

The command to low EMR occurred at ESC +321.8 seconds; 0.6 second earlier than the MSFC trajectory time. The average EMR at the low position was 4.81 as compared to a predicted 4.71. This higher than planned low EMR operation when corrected to standard altitude conditions was within the 2 sigma ±0.06 mixture ratio tolerance. The EMR shift command time deviation is most likely attributable to use of an IU low EMR guidance presetting.

Outboard engine cutoff was initiated by the LOX tank propellant depletion system following a 1.5-second time delay at ESC +387.11 seconds, which is 1.16 seconds earlier than planned. The earlier OECO was the result of increased propellant flows at low EMR. Based on point sensor and flowmeter data, propellant residuals (mass in tanks and sump) at OECO were 1373 lbm LOX and 3750 lbm LH_2 versus 1396 lbm LOX and 2996 lbm LH_2 predicted. The high LH_2 residuals were the result of the higher than planned engine performance at low EMR. A +780 lbm LH_2 PU error at OECO remained within the estimated 3-sigma dispersion of ±2500 lbm LH_2.

Review of the LH_2 point sensor liquid level measurement revealed that the 60 percent sensor did not actuate in flight when the LH_2 level passed this sensor. Proper operation of the sensor, however, was observed during the ground loading operation. Therefore, it can be concluded that the sensor failed sometime between LH_2 loading and S-II boost. This sensor is used for flight evaluation only and has no other function in flight. The only other inflight failure of this sensor was observed during AS-502 flight.

Table 6-2 presents a comparison of propellant masses as measured by the PU probes and engine flowmeters. The best estimate propellant mass is based on integration of flowmeter data utilizing the propellant residuals determined from point sensor data. These mass values were 0.10 percent more than predicted for LOX and 0.04 percent more than predicted for LH_2.

6.6 S-II PRESSURIZATION SYSTEM

6.6.1 S-II Fuel Pressurization System

LH_2 tank ullage pressure, actual and predicted, is presented in Figure 6-6 for autosequence, S-IC boost, and S-II boost. The LH_2 vent valves were closed at -94.0 seconds and the ullage volume pressurized to 35.0 psia in approximately 20.1 seconds. One make-up cycle was required at approximately -44.0 seconds and the ullage pressure was increased to approximately 34.9 psia. Ullage pressure decayed to 34.1 psia at S-IC ESC at which time the pressure decay rate increased for about 20 seconds. The increased decay rate was attributed to an increase in ullage volume when the liquid level lowered at S-IC thrust buildup. This decay is normal and has been noted on previous launches.

Table 6-2. AS-510 Flight S-II Propellant Mass History

EVENT	PREDICTED, LBM (TRAJECTORY)		PU SYSTEM ANALYSIS, LBM *		ENGINE FLOW - METER INTEGRATION (BEST ESTIMATE), LBM	
	LOX	LH_2	LOX	LH_2	LOX	LH_2
Liftoff	835,500	158,675	835,013	158,732	836,366	158,735
S-II ESC	835,500	158,662	836,820	158,064	836,366	158,721
S-II PU Valve Step Cmd	104,076	24,809	103,700	24,900	102,707	24,957
2 Percent Point Sensor	15,795	4242	15,850	3831	16,428	4242
S-II OECO	1396	2996	1391	3223	1373	3750
S-II Residual After Thrust Decay	1124	2880	Data Not Usable	Data Not Usable	1082	3636

NOTE Table is based on mass in tanks and sump only. Propellant trapped external to tanks and LOX sump is not included.

*Liftoff data based on pressurized ground data system. All other PU System propellant quantities based on flight data system.

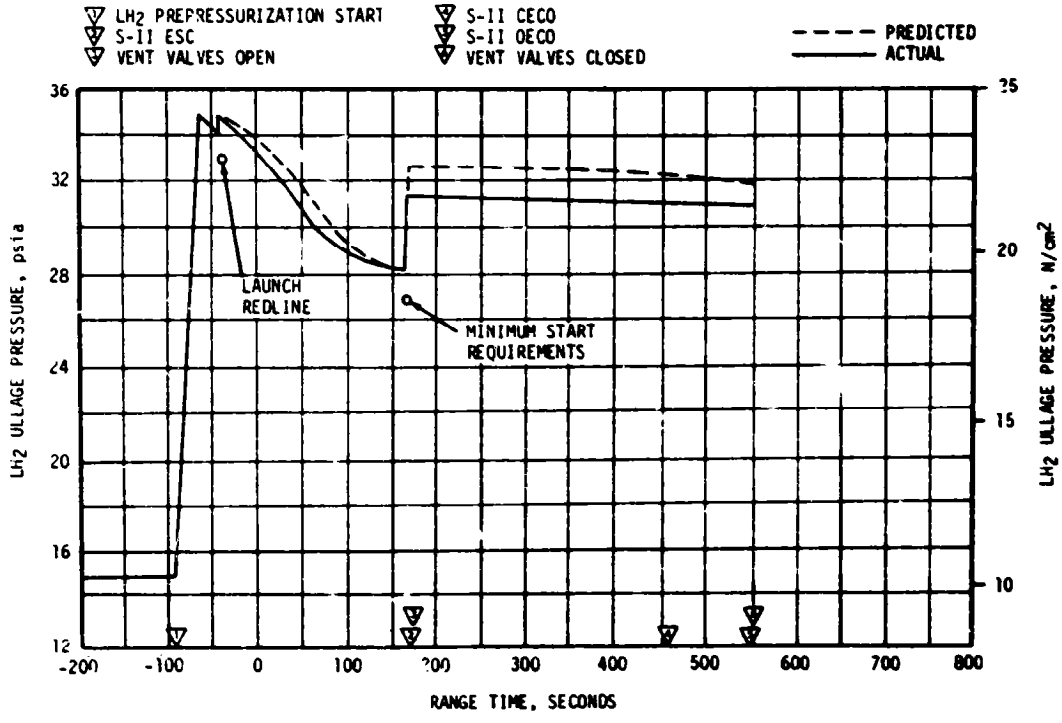

Figure 6-6. S-II Fuel Tank Ullage Pressure

The LH_2 tank ullage pressure redline commit time was changed from -30 seconds to -19 seconds for AS-510 and subsequent flights. This change was made because of a problem with the LOX tank vent valve during CDDT. This problem is discussed in paragraph 6.6.2.

The LH_2 vent valves opened during S-IC boost to control tank pressure; however, no main poppet operation was indicated. Differential pressure across the vent valve was maintained by the primary pilot valve within the allowable low mode band of 27.5 to 29.5 psid. Ullage pressure at engine start was 28.4 psia exceeding the minimum engine start requirement of 27.0 psia. The LH_2 vent valves were switched to the high vent mode prior to S-II ESC.

Ullage pressure during S-II boost has been previously controlled by a regulator installed in the LH_2 tank pressurization line. For this and subsequent flights, the regulator has been replaced by an orifice with maximum tank pressure controlled by the LH_2 vent valves. For this flight the ullage pressure was controlled by the LH_2 vent valves throughout the S-II boost period and remained within the 30.5 to 33.0 psia allowable band. The vent valves actuated open at 169.4 seconds and remained open until approximately 550.5 seconds. The ullage pressure was approximately 1.0 psi lower than predicted because the vent valves controlled the pressure at the reseat-level rather than the crack-level. This is an acceptable condition and no corrective action is planned.

Figure 6-7 shows LH_2 total inlet pressure, temperature, and NPSP for the J-2 engines. The parameters were close to the predicted values throughout the S-II flight period. NPSP remained above the minimum requirement throughout the S-II burn period.

6.6.2 S-II LOX Pressurization System

LOX tank ullage pressure, actual and predicted, is presented in Figure 6-8 for S-II burn. After a 2-minute cold helium chilldown flow through the LOX tank, the vent valves were closed at -184 seconds and the LOX tank was pressurized to the pressure switch setting of 38.7 psia in 34.8 seconds. The LOX tank ullage pressure increased to 40.0 psia because of common bulkhead flexure due to the LH_2 tank prepressurization. The LOX tank ullage pressure redline commit time was changed from -30 seconds to -19 seconds for this and subsequent flights because of the LOX vent valve problem that occurred during CDDT. This time change provides for a longer ullage pressure monitoring time before launch commit. The LOX vent valve No. 1 had an abnormally long closing time and did not fully close during the CDDT special accumulator test. Subsequent valve operations appeared to be normal including a special LOX ullage pressure decay test that was conducted during the CDDT. The LOX vent valve problem was attributed to frost accumulation on the poppet seat due to the valve being open during the 5 hours preceding the problem. The LOX vent valves were not replaced, but the countdown procedures incorporated a periodic cycling of the vent valves when operating at cryogenic temperatures.

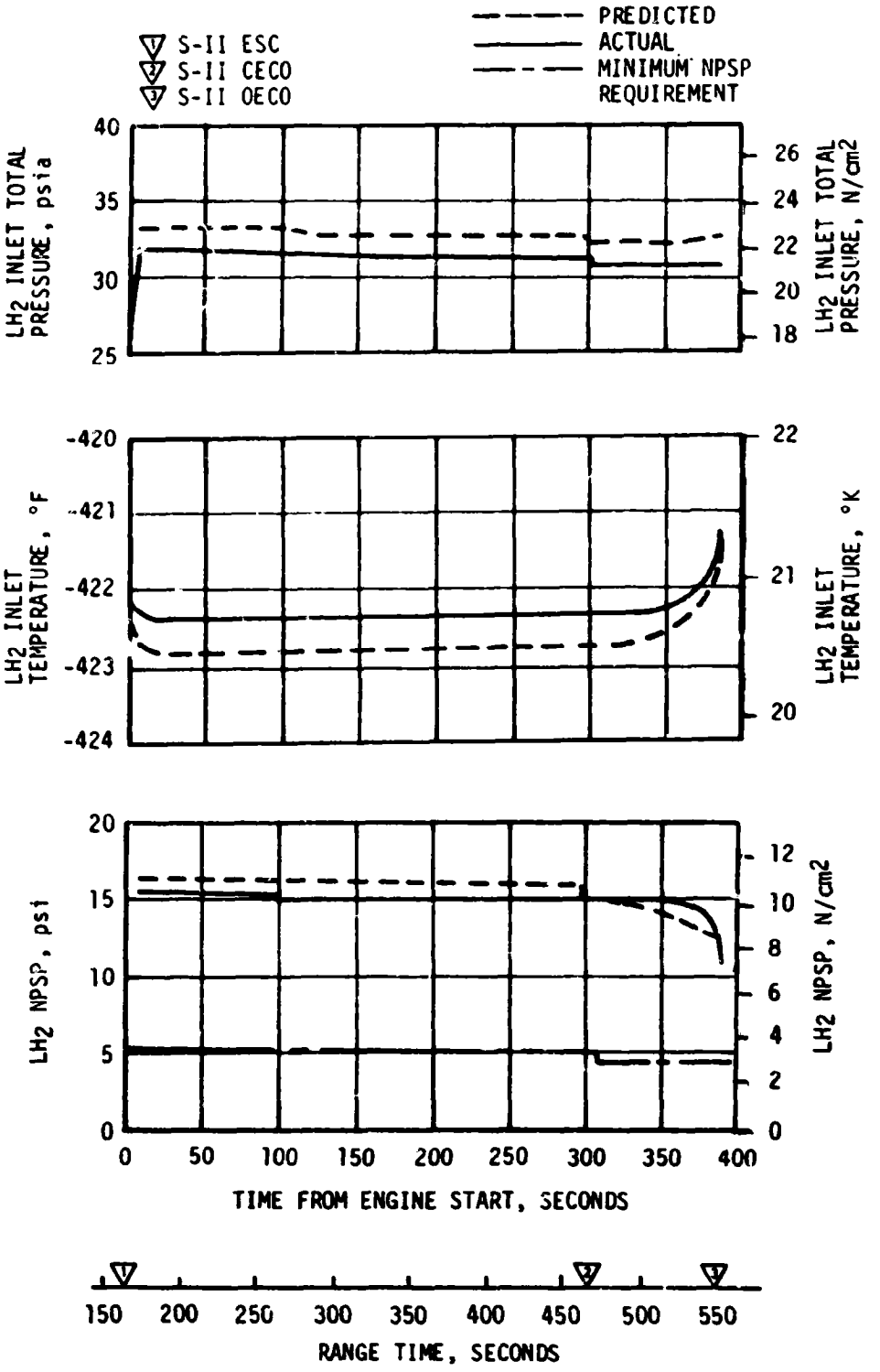

Figure 6-7. S-II Fuel Pump Inlet Conditions

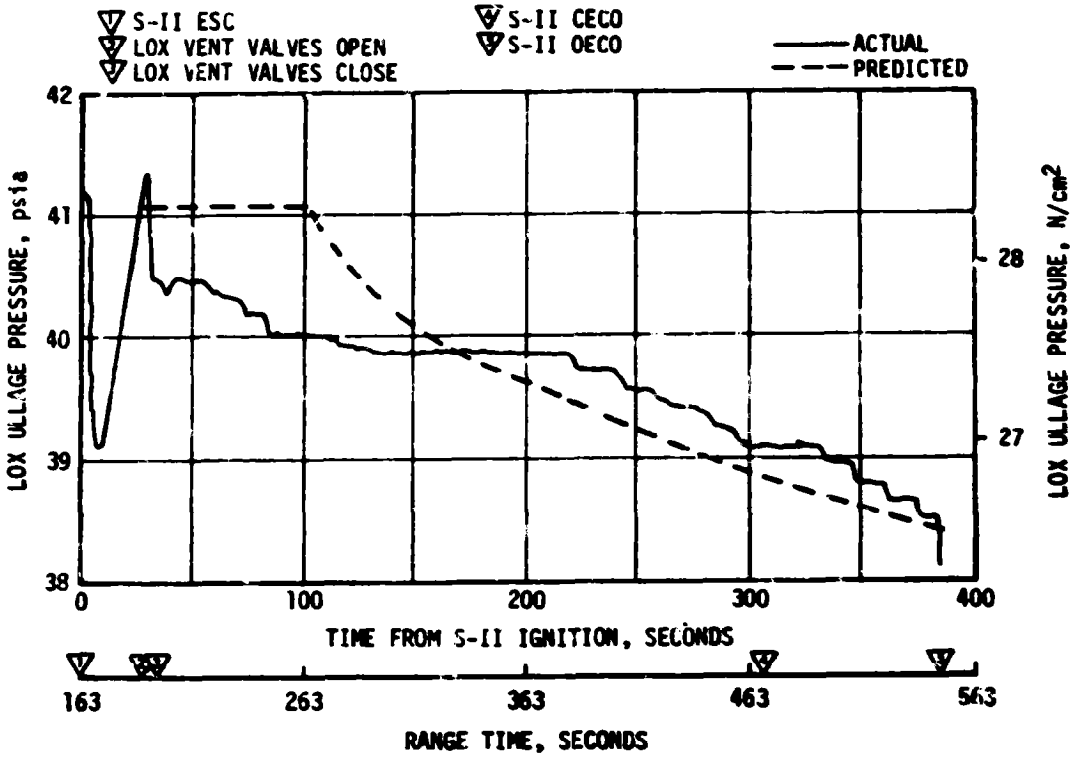

Figure 6-8. S-II LOX Tank Ullage Pressure

LOX tank ullage pressure just prior to S-II ESC was 41.2 psia. Since the pressure regulator for the LOX tank was also replaced by an orifice (similar to the LH_2 system), the LOX tank vent valves controlled the maximum tank pressure.

The LOX tank ullage pressure was within approximately 1 psi of the preflight prediction. Vent valve No. 1 opened, and after one cycle, remained open from 189 seconds until 198.8 seconds. Vent valve No. 2 had one open-close cycle at 191.3 seconds but otherwise remained closed. Ullage pressure decreased at a relatively constant rate to 38.3 psia at S-II OECO. LOX pump total inlet pressure, temperature, and NPSP are presented in Figure 6-9.

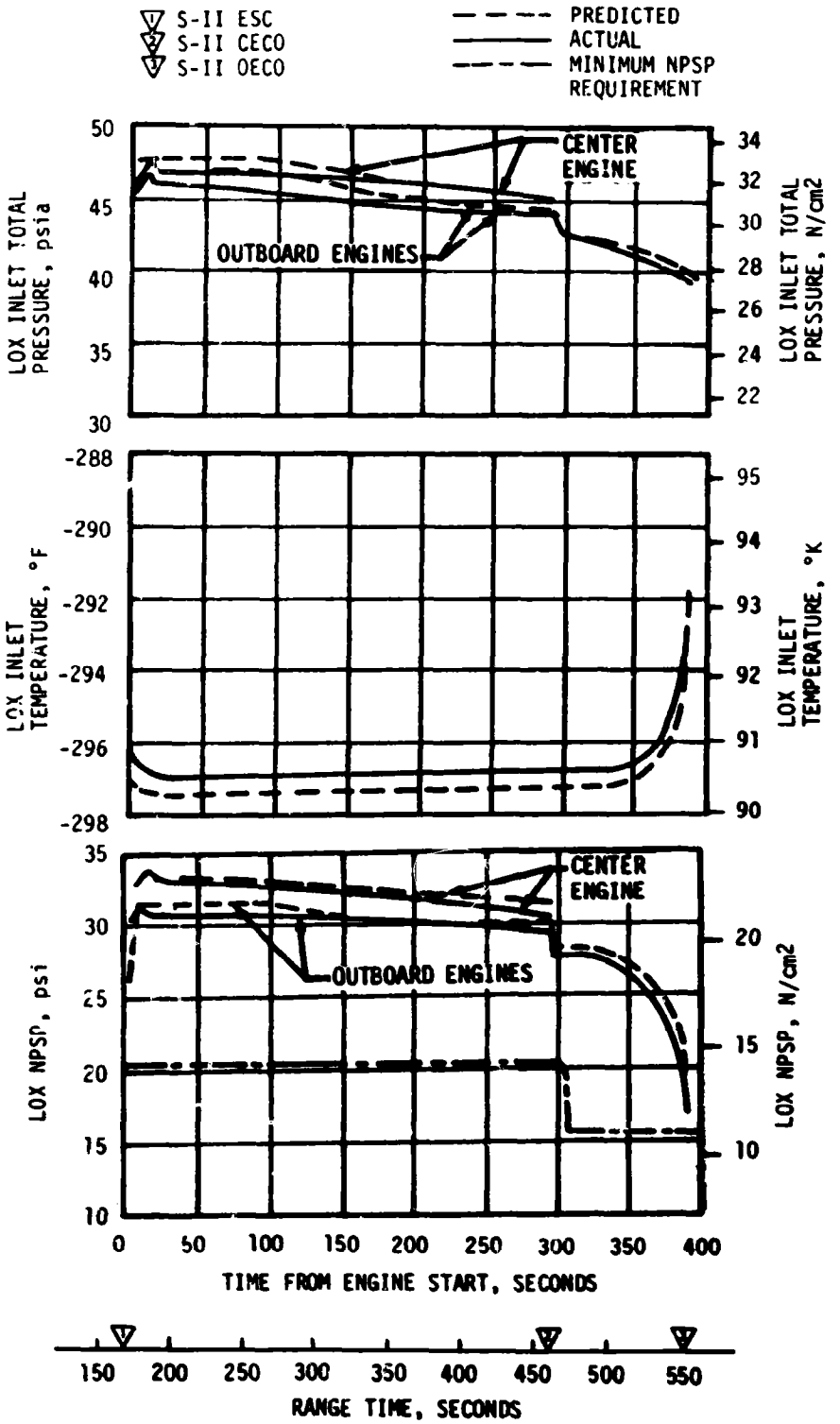

Figure 6-9. S-II LOX Pump Inlet Conditions

6.7 S-II PNEUMATIC CONTROL PRESSURE SYSTEM

The pneumatic control system functioned satisfactorily throughout the S-IC and S-II boost periods. Bottle pressure was 2910 psia at -30 seconds. The pressure decayed to 2490 psia after S-II OECO because of the allowed slight leakage and normal valve activities during S-II burn.

6.8 S-II HELIUM INJECTION SYSTEM

The performance of the helium injection system was satisfactory. The supply bottle was pressurized to 2900 psia prior to liftoff and by S-II ESC the pressure was 1720 psia. Helium injection average total flowrate during supply bottle blowdown (-30 to 163 seconds) was 67 scfm.

6.9 POGO SUPPRESSION SYSTEM

A center engine LOX feedline accumulator was installed on the S-II stage as a POGO suppression device. This was the second flight stage to incorporate an accumulator system and the analysis results indicate that the accumulator suppressed the S-II POGO oscillations.

The accumulator system consists of (1) a bleed system to maintain sub-cooled LOX in the accumulator through S-IC boost and S-II engine start, and (2) a fill system to fill the accumulator with helium subsequent to engine start and maintain a helium filled accumulator through S-II CECO.

Figure 6-10 shows the required accumulator temperature at engine start, the predicted temperatures during prelaunch and S-IC boost, and the actual temperatures experienced during AS-510 flight. As can be seen, the maximum allowable temperature of -281.5°F at engine start was adequately met (-294.2°F actual).

Figure 6-11 shows the accumulator LOX level versus time during accumulator fill. As can be seen, the full time was 6.2 seconds which is within the 5 to 7 second requirement.

After the accumulator was filled with helium, it remained in that state until S-II CECO when the helium flow was terminated by closing the two fill solenoid valves. There was no sloshing or abnormal liquid level behavior in the accumulator during center engine operation. Figure 6-12 shows the helium injection accumulator fill supply bottle pressure during accumulator fill operation. As can be seen, the supply bottle pressure was within the predicted band, indicating that the helium sage rates were as predicted.

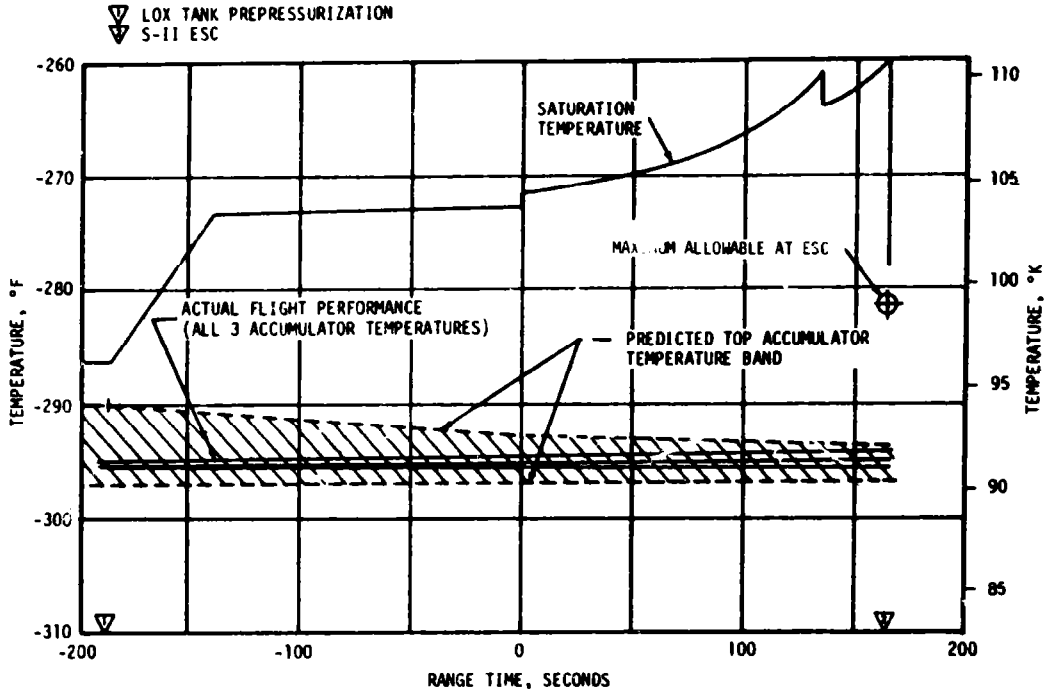

Figure 6-10. S-II Center Engine LOX Feedline Accumulator Bleed System Performance

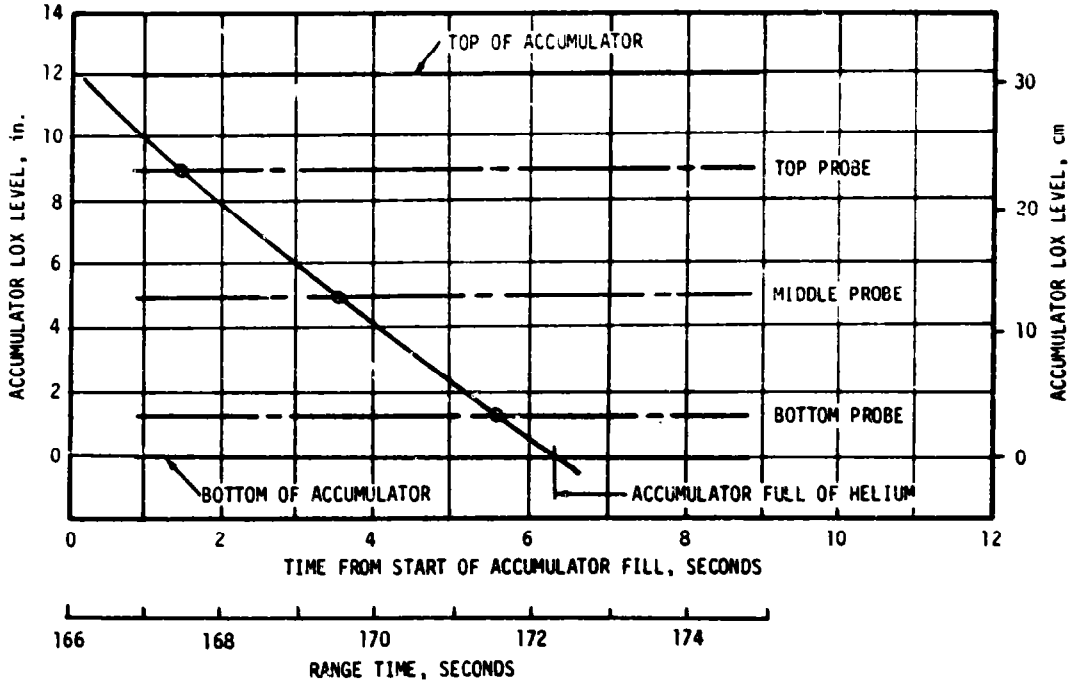

Figure 6-11. S-II Center Engine LOX Feedline Accumulator Fill Transient

6.10 S-II HYDRAULIC SYSTEM

S-II hydraulic system performance was normal throughout the flight. System supply and return pressures, reservoir volumes, and system fluid temperatures were within predicted ranges. All servoactuators responded to commands with good precision. The maximum engine deflection was approximately 1 degree in pitch on engine No. 1 at initiation of Iterative Guidance Mode (IGM). Actuator loads were well within design limits. The maximum actuator load was approximately 6300 lbf on the yaw actuator of engine No. 1 at CECO.

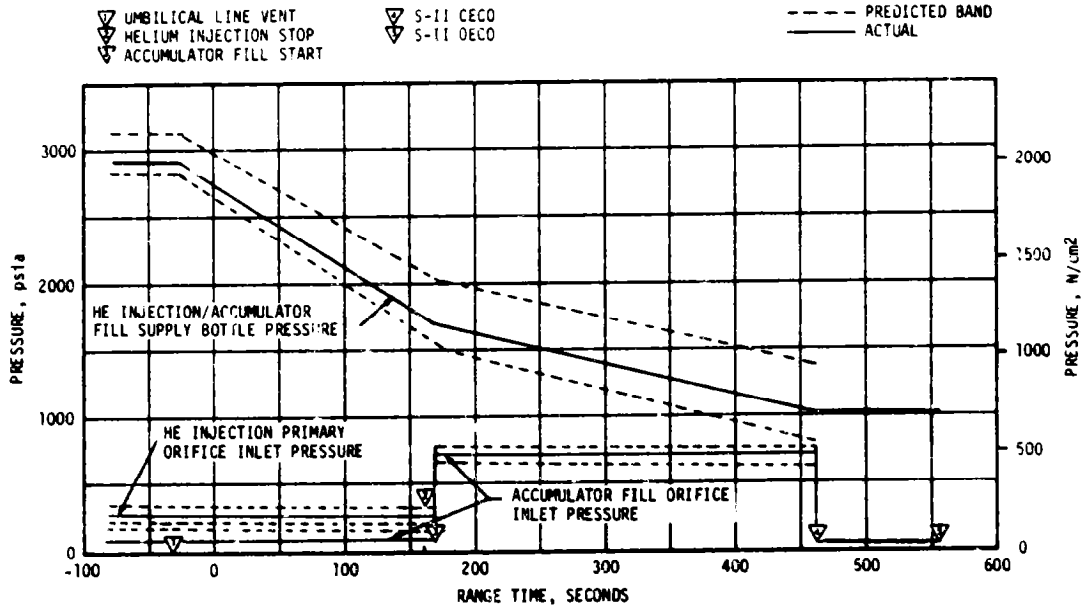

Figure 6-12. S-II Center Engine LOX Feedline Accumulator Helium Supply System Performance

SECTION 7

S-IVB PROPULSION

7.1 SUMMARY

The S-IVB propulsion system performed satisfactorily throughout the operational phase of first and second burns and had normal start and cutoff transients. S-IVB first burn time was 141.5 seconds, 3.8 seconds less than predicted. Approximately 2.6 seconds of the shorter burn time can be attributed to higher S-IVB thrust. The remainder can be attributed to S-IC and S-II stage performances. The engine performance during first burn, as determined from standard altitude reconstruction analysis, deviated from the predicted Start Tank Discharge Valve (STDV) +130-second time slice by 1.82 percent for thrust and 0.09 percent for specific impulse. The S-IVB stage first burn Engine Cutoff (ECO) was initiated by the Launch Vehicle Digital Computer (LVDC) at 694.7 seconds.

The Continuous Vent System (CVS) adequately regulated LH_2 tank ullage pressure at an average level of 19.3 psia during orbit and the Oxygen/Hydrogen (O_2/H_2) burner satisfactorily achieved LH_2 and LOX tank repressurization for restart. Engine restart conditions were within specified limits. The restart at full open Mixture Ratio Control Valve (MRCV) position was successful.

Abnormal temperatures were noted in the turbine hot gas system between first burn ECO and second burn Engine Start Command (ESC). Most noticeable was the fuel turbine inlet temperature. During LH_2 chilldown in Time Base 6 (T_6), the temperature decreased from 130 to -10°F at second ESC. The oxidizer turbine inlet temperature also indicated a small decrease in temperature. In addition, fuel turbine inlet temperature indicated an abnormally fast temperature decrease after first burn ECO. The cause of the decrease in turbine inlet temperature was a small leak past the teflon seal of the fuel poppet gas generator fuel inlet valve.

S-IVB second burn time was 350.8 seconds, which was 5.4 seconds less than predicted. The engine performance during second burn, as determined from the standard altitude reconstruction analysis, deviated from the STDV +130-second time slice by 1.89 percent for thrust and 0.09 percent for specific impulse. Second burn ECO was initiated by the LVDC at 10,553.7 seconds (02:55:53.7).

A trend to slightly higher than predicted propulsion systems performance during first and second burn has also been noted on several preceding flights. Therefore, the preflight predictions for AS-511 are being reassessed.

Subsequent to second burn, the stage propellant tanks and helium spheres were safed satisfactorily. Sufficient impulse was derived from LOX dump, LH_2 CVS operation and Auxiliary Propulsion System (APS) ullage burns to achieve a successful lunar impact.

7.2 S-IVB CHILLDOWN AND BUILDUP TRANSIENT PERFORMANCE FOR FIRST BURN

The thrust chamber temperature at launch was well below the maximum allowable redline limit of -130°F. At S-IVB first burn ESC, the temperature was -151°F, which was within the requirement of -189.6 ±110°F.

The chilldown and loading of the engine GH_2 start tank and pneumatic control bottle prior to liftoff was satisfactory.

The engine control sphere pressure and temperature at liftoff were 3000 psia and -168°F. At first burn ESC the start tank conditions were within the required region of 1325 ±75 psia and -170 ±30°F for start. The discharge was completed and the refill initiated at first burn ESC +3.8 seconds. The refill was satisfactory and in good agreement with the acceptance test.

The propellant recirculation systems operation, which was continuous from before liftoff until just prior to first ESC, was satisfactory. Start and run box requirements for both fuel and LOX were met, as shown in Figure 7-1. At first ESC the LOX pump inlet temperature was -294.9°F and the LH_2 pump inlet temperature was -421.6°F.

The first burn start transient was satisfactory, and the thrust buildup was within the limits set by the engine manufacturer. This buildup was similar to the thrust buildups observed on AS-506 through AS-509. The MRCV was in the closed position (5.0 EMR) prior to first start, and performance indicates it remained closed during first burn. The total impulse from STDV to STDV +2.5 seconds was 213,695 lbf-s.

First burn fuel lead followed the predicted pattern and resulted in satisfactory conditions as indicated by the fuel injector temperature.

7.3 S-IVB MAINSTAGE PERFORMANCE FOR FIRST BURN

The propulsion reconstruction analysis showed that the stage performance during mainstage operation was satisfactory. A comparison of predicted and actual performance of thrust, specific impulse, total flowrate, and Mixture Ratio (MR) versus time is shown in Figure 7-2. Table 7-1 shows the thrust, specific impulse, flowrates, and MR deviations from the predicted at the STDV open +130-second time slice.

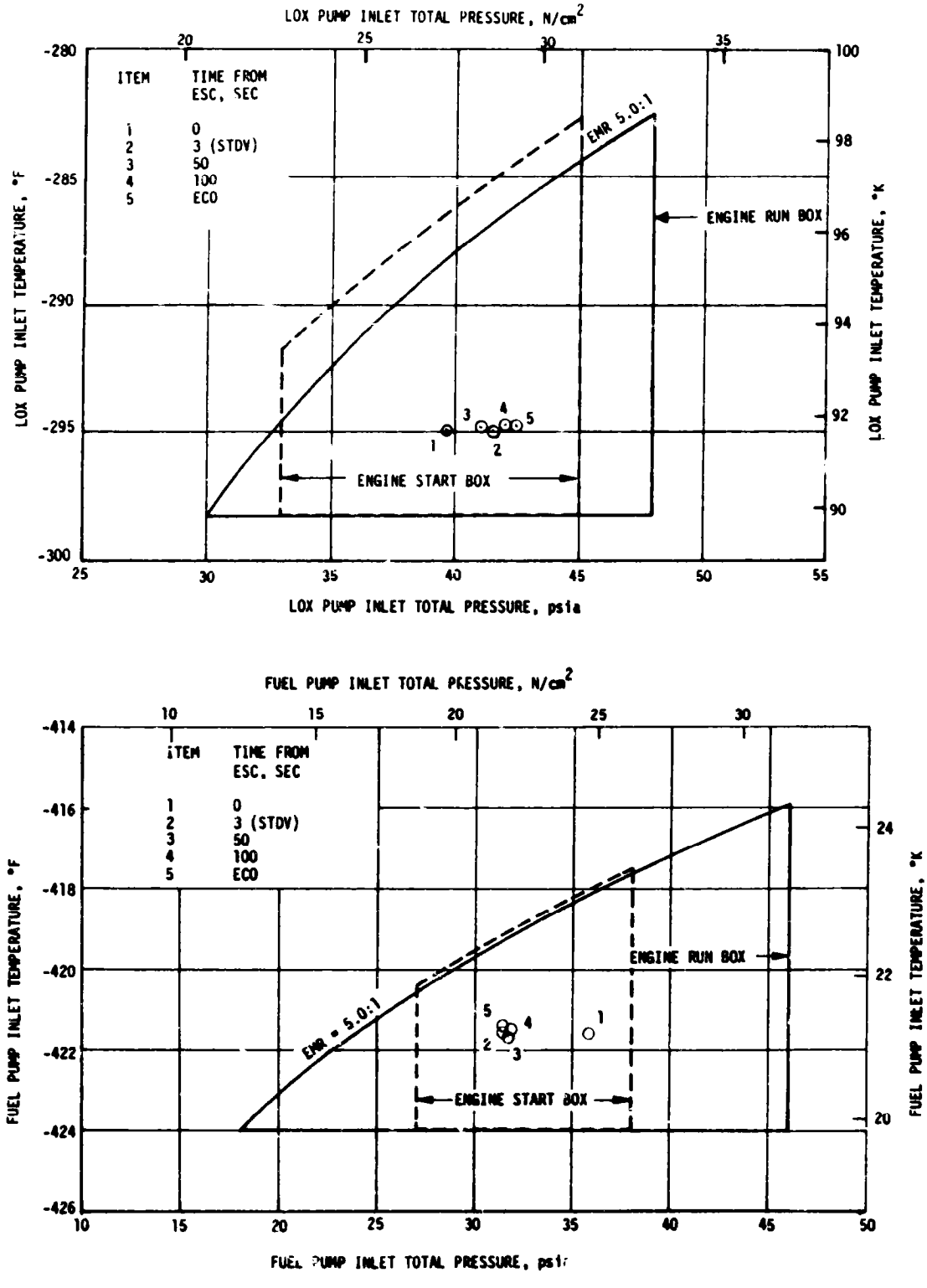

Figure 7-1. S-IVB Start Box and Run Requirements - First Burn

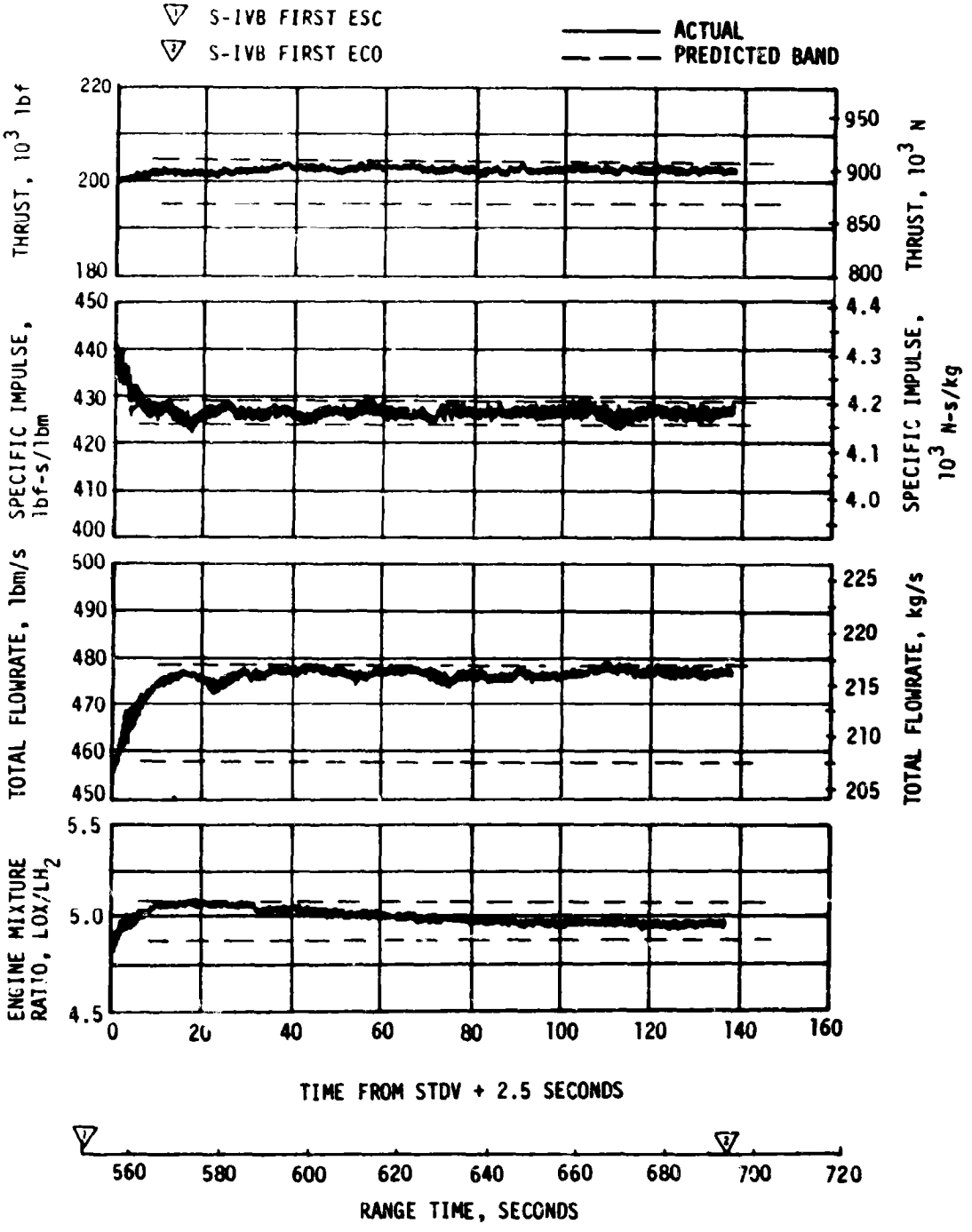

Figure 7-2. S-IVB Steady State Performance - First Burn

Table 7-1. S-IVB Steady State Performance - First Burn
(STDV +130-Second Time Slice at Standard Altitude Conditions)

PARAMETER	PREDICTED	RECONSTRUCTION	FLIGHT DEVIATION	PERCENT DEVIATION FROM PREDICTED
Thrust, lbf	199,335	202,965	3630	1.82
Specific Impulse, lbf-s/lbm	427.2	427.6	0.4	0.09
LOX Flowrate, lbm/s	387.72	394.61	6.89	1.78
Fuel Flowrate, lbm/s	79.84	80.06	1.22	1.52
Engine Mixture Ratio, LOX/Fuel	4.918	4.929	0.011	0.22

Table 7-2. S-IVB-510 J-2 Engine Performance Acceptance Test Tags

PARAMETER	ESC +280 SEC	ESC +440 SEC	PERFORMANCE CHANGE*	MIXTURE RATIO CONTROL VALVE CONTRIBUTION**	GAS GENERATOR CONTRIBUTION***
MRCV, deg	31.0	29.2	1.8		
Thrust, lbf	203,196	198,642	4554	3000	1554
EMR, LOX/Fuel	4.94	4.89	0.05	0.06	Negligible
ISP, sec	427.50	427.80	0.30	0.30	Negligible

*Performance change during acceptance
**Expected change using engine gain factors
***Gas generator shift

The specific impulse and EMR were well within the predicted bands. The thrust and propellant flowrates were higher than nominal, but also within the predicted bands. The higher thrust and flowrates for flight can be attributed to a combination of two conditions:

a. A higher nominal MRCV setting of approximately 30.8 degrees as compared to the planned predicted nominal setting of 30.0 degrees. The MRCV setting was within the requirement of 30.0 ±1.0 degrees.

b. A higher than predicted Gas Generator (GG) system performance.

It should be noted that the estimated higher MRCV setting is based on engine performance reconstruction. The MRCV position indicator can only be used for trend data.

Operation of the J-2 engine during the stage acceptance firing near the null (5.0 EMR) position exhibited a bi-level performance condition. This condition was typical of a GG system performance shift. The lower level was used for the flight prediction. Table 7-2 provides comparative results from the acceptance test data, where the equivalent MRCV angles were 31.0 and 29.2 degrees. The resulting thrust and EMR change due to the valve movement was -4554 lbf and 0.05 units, respectively. Using established engine gain factors, the corresponding thrust change should be -3000 lbf for a 1.8-degree MRCV movement. The remaining -1554 lbf thrust change is attributed to a lower level of GG performance which occurred at the 29.2-degree MRCV setting. The flight reconstruction results indicate that this lower level of GG performance did not occur during flight.

The resulting higher thrust and flowrates for flight caused shorter than expected burn times but did not significantly affect the overall S-IVB stage performance, as indicated by the near nominal specific impulse for the two burns and near nominal residuals following second burn.

Although specific impulse during first burn was near nominal as previously noted, actual flight performance values were slightly higher than predicted, as shown in Table 7-1. While the slightly higher than nominal specific impulse has little significance for a single flight, similar deviations occurred on AS-505 through AS-509 with the exception of AS-507 which had a slightly less than nominal deviation (-0.002 percent); therefore, the preflight predictions for AS-511 are being reassessed.

The performance of the J-2 engine helium control system was satisfactory during mainstage operation. The engine control bottle was connected to the stage ambient repressurization bottles; therefore, there was little pressure decay. Helium usage is estimated as 0.30 lbm during first burn.

7.4 S-IVB SHUTDOWN TRANSIENT PERFORMANCE FOR FIRST BURN

S-IVB ECO was initiated at 694.7 seconds by a guidance velocity cutoff command which resulted in a 3.8-second less than predicted burn time. Approximately 2.6 seconds of the shorter burn time can be attributed to higher S-IVB thrust. The remainder can be attributed to S-IC stage and S-II stage performance.

The ECO transient was satisfactory. The total cutoff impulse to zero percent of rated thrust was 42,482 lbf-s which was 2168 lbf-s higher than predicted. Cutoff occurred with the MRCV in the 5.0 position.

7.5 S-IVB PARKING ORBIT COAST PHASE CONDITIONING

The LH_2 CVS performed satisfactorily, maintaining the fuel tank ullage pressure at an average level of 19.3 psia. This was well within the 18 to 21 psia band of the inflight specification.

The continuous vent regulator was activated at 753.9 seconds and was terminated at 9667.1 seconds. The CVS performance is shown in Figure 7-3.

Calculations based on estimated temperatures indicate that the mass vented during parking orbit was 2293 lbm and that the boiloff mass was 2513 lbm.

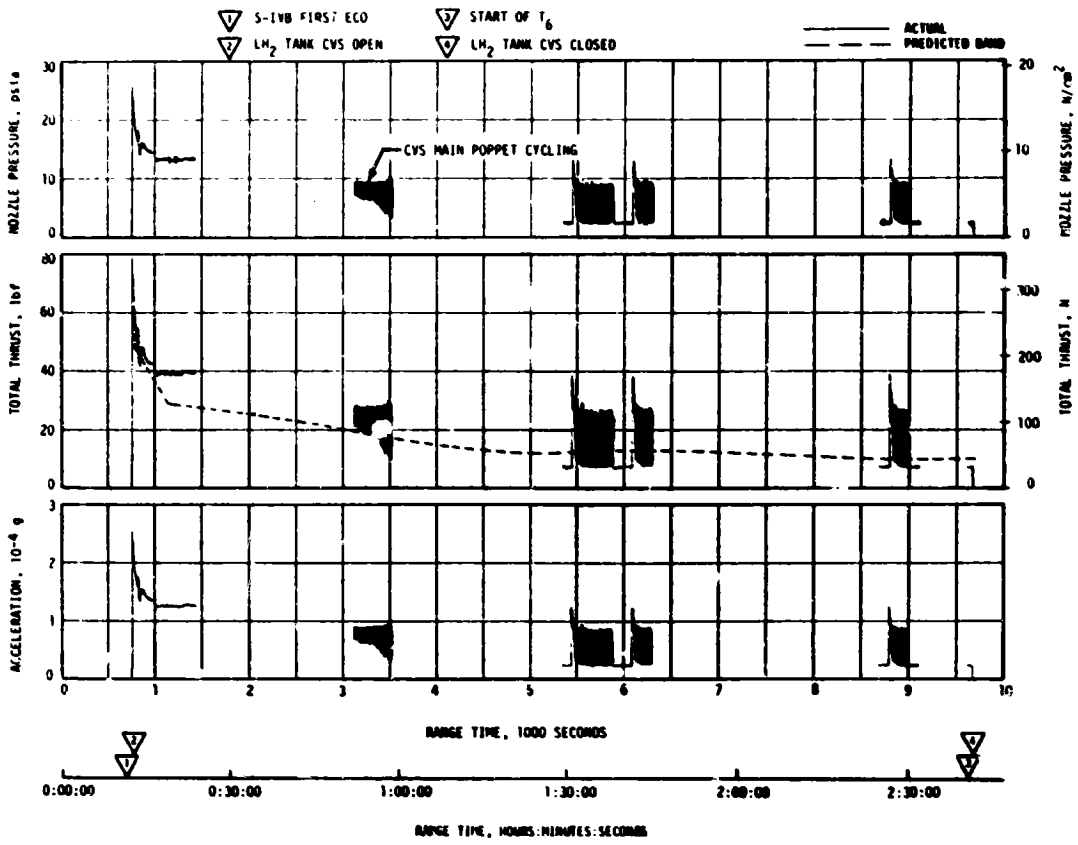

Figure 7-3. S-IVB CVS Performance - Coast Phase

7.6 S-IVB CHILLDOWN AND BUILDUP TRANSIENT PERFORMANCE FOR SECOND BURN

Repressurization of the LOX and LH_2 tanks was satisfactorily accomplished by the O_2/H_2 burner. Burner "ON" command was initiated at 9666.9 seconds. The LH_2 repressurization control valves were opened at burner "ON" +6.1 seconds, and the fuel tank was repressurized from 19.5 to 30.2 psia in 177 seconds. There were 25.6 lbm of cold helium used to repressurize the LH_2 tank. The LOX repressurization control valves were opened at burner "ON" +6.3 seconds, and the LOX tank was repressurized from 36.8 to 40.1 psia in 120 seconds. There were 3.5 lbm of helium used to repressurize the LOX tank. LH_2 and LOX ullage pressures are shown in Figure 7-4. The burner continued to operate for a total of 455 seconds providing nominal propellant settling forces. The performance of the AS-510 O_2/H_2 burner was satisfactory as shown in Figure 7-5.

The S-IVB LOX recirculation system satisfactorily provided conditioned oxidizer to the J-2 engine for restart. The LOX and fuel pump inlet conditions are plotted in the start and run boxes in Figure 7-6. At second ESC, the LOX and fuel pump inlet temperatures were -284.0 and -419.2°F, respectively. Fuel recirculation system performance was adequate and conditions at the pump inlet were satisfactory at second STDV open. The fuel prevalve "closed" indication was not received during restart chilldown. The prevalve operated normally, and the failure to pick up the "closed" indication was due to a microswitch or telemetry problem (see Table 15-3), rather than actual prevalve movement. Second burn fuel lead generally followed the predicted pattern and resulted in satisfactory conditions, as indicated by the fuel injector temperature. Since J-2 start system performance was nominal during coast and restart, no helium recharge was required from the LOX ambient repressurization system (bottle No. 2). The start tank performed satisfactorily during second burn blowdown and recharge sequence. The engine start tank was recharged properly and it maintained sufficient pressure during coast. The engine control sphere first burn gas usage was as predicted; the ambient helium spheres recharged the control sphere to a nominal level for restart.

The second burn start transient was satisfactory. The thrust buildup was within the limits set by the engine manufacturer and was similar to the thrust buildup on AS-506 through AS-509. The MRCV was in the proper full open (4.5 EMR) position prior to the second start. The total impulse from STDV to STDV +2.5 seconds was 196,985 lbf-s.

The helium control system performed satisfactorily during second burn mainstage. There was little pressure decay during the burn due to the connection to the stage repressurization system. An estimated 1.1 lbm of helium was consumed during second burn.

Abnormal temperatures were noted in the turbine hot gas system between first burn ECO and second burn ESC. Most noticeable was the fuel turbine inlet temperature. During LH_2 chilldown in T_6, the inlet temperature

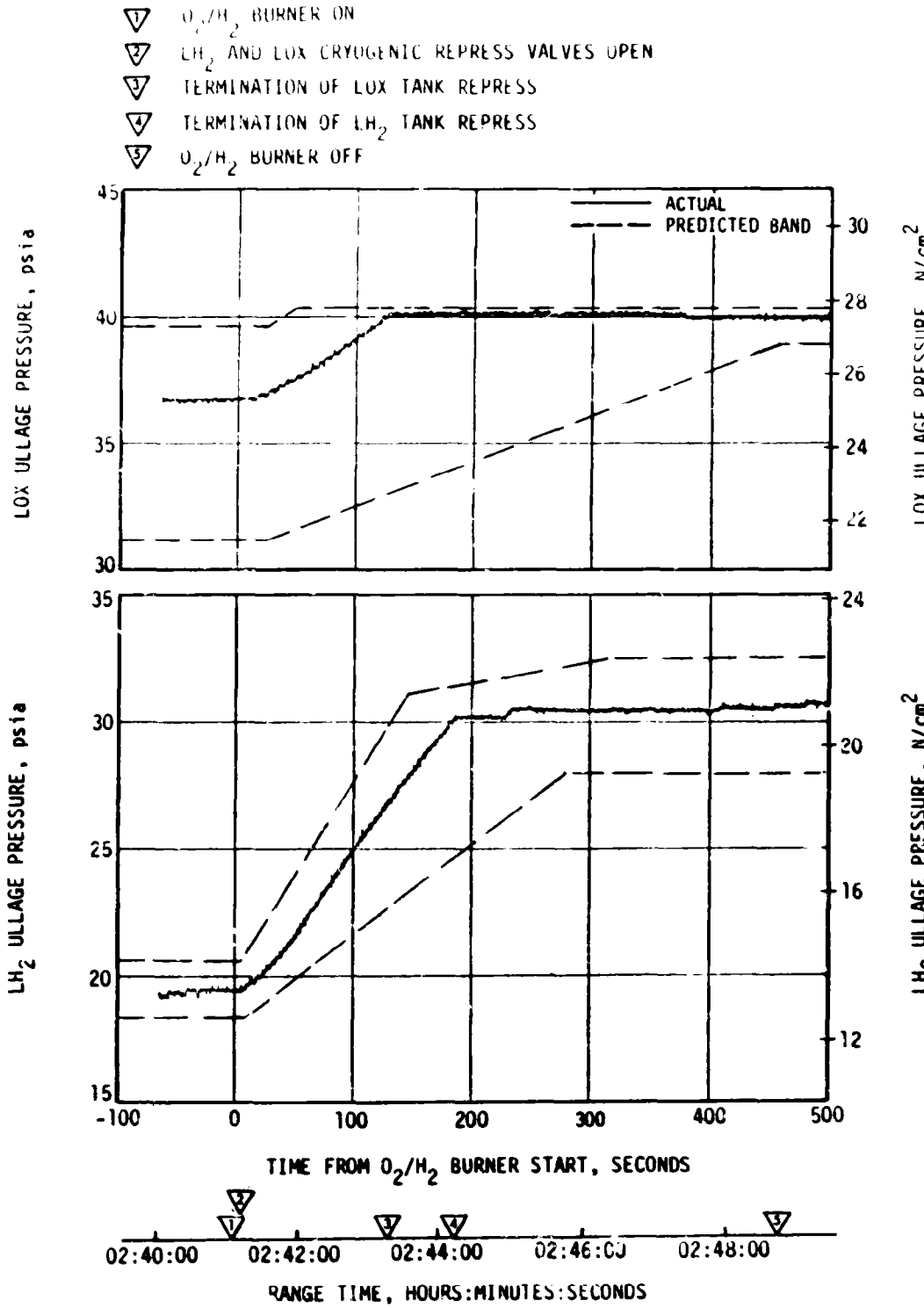

Figure 7-4. S-IVB Ullage Conditions During Repressurization Using O_2/H_2 Burner

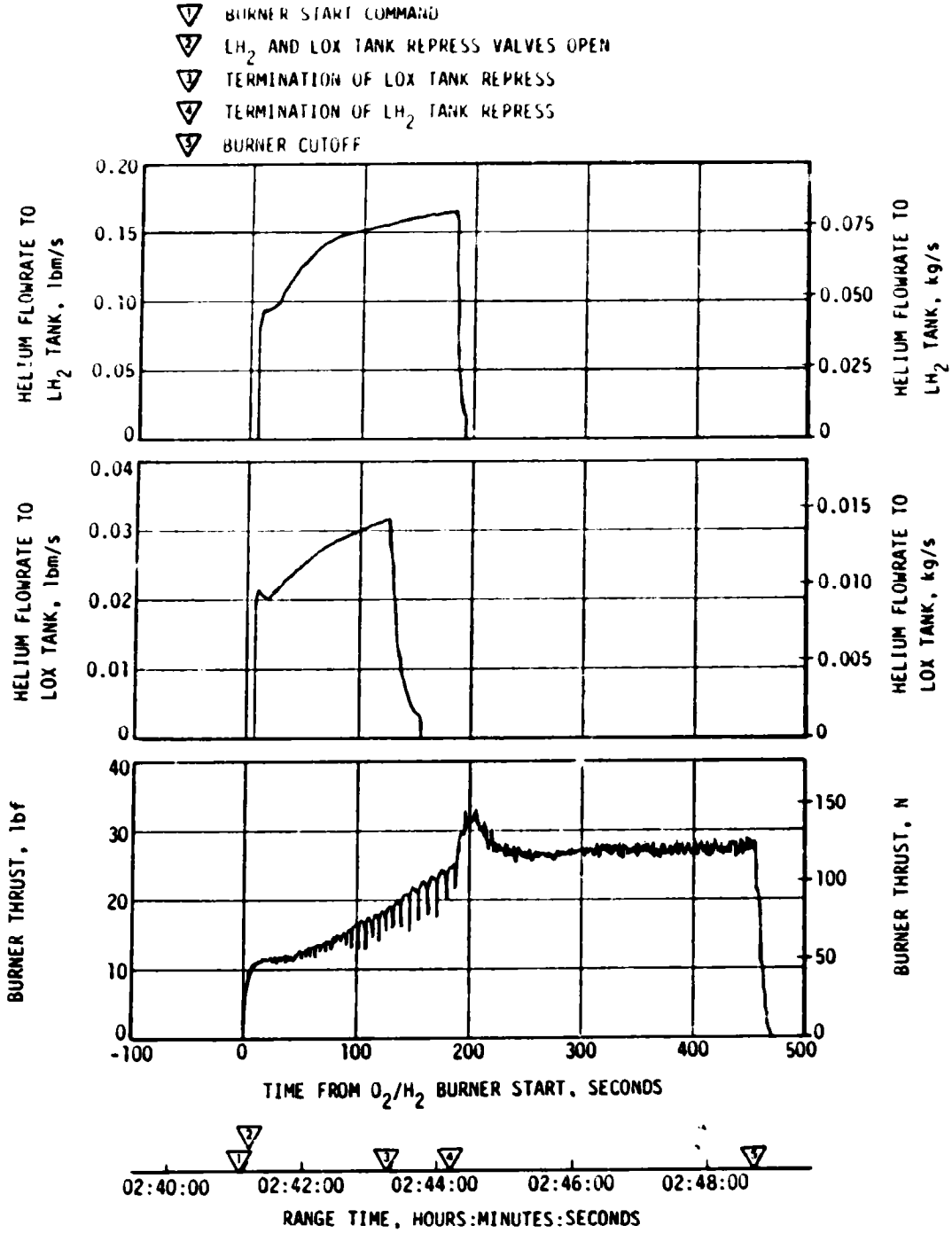

Figure 7-5. S-IVB O_2/H_2 Burner Thrust and Pressurant Flowrate

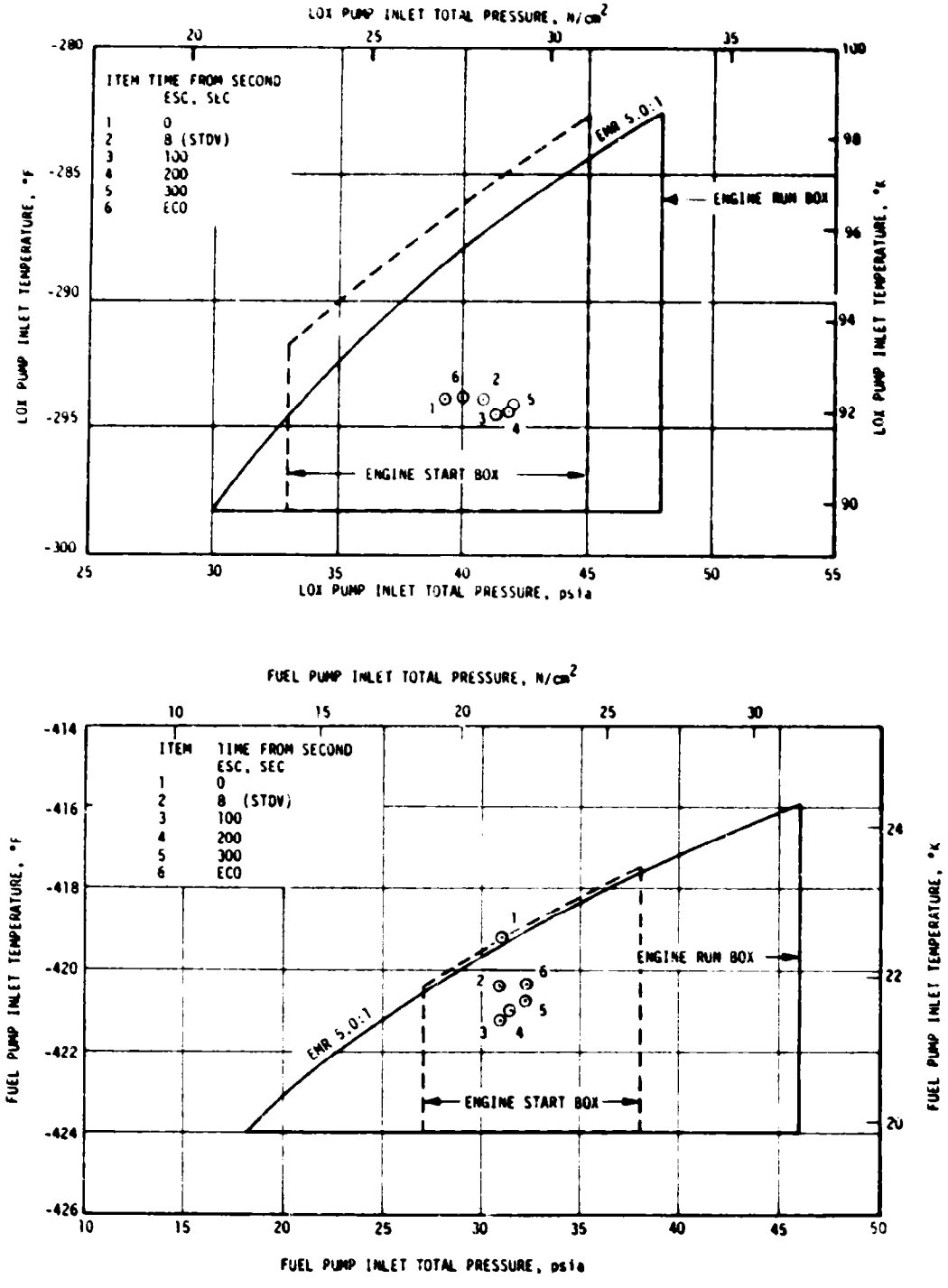

Figure 7-6. S-IVB Start Box and Run Requirements - Second Burn

decreased from 130 to -10°F at second ESC. The oxidizer turbine inlet temperature also indicated a small decrease in temperature. In addition, fuel turbine inlet temperature indicated an abnormally fast temperature decrease after first burn ECO. Fuel and oxidizer turbine inlet temperature data are presented in Figure 7-7 for first burn and Figure 7-8 for second burn. The cause of the decrease in turbine inlet temperature was a small leak past the teflon seal of the fuel poppet gas generator inlet valve.

7.7 S-IVB MAINSTAGE PERFORMANCE FOR SECOND BURN

The propulsion reconstruction analysis showed that the stage performance during mainstage operation was satisfactory.

The second burn time was also shorter than predicted. This can be primarily attributed to the higher than predicted S-IVB thrust.

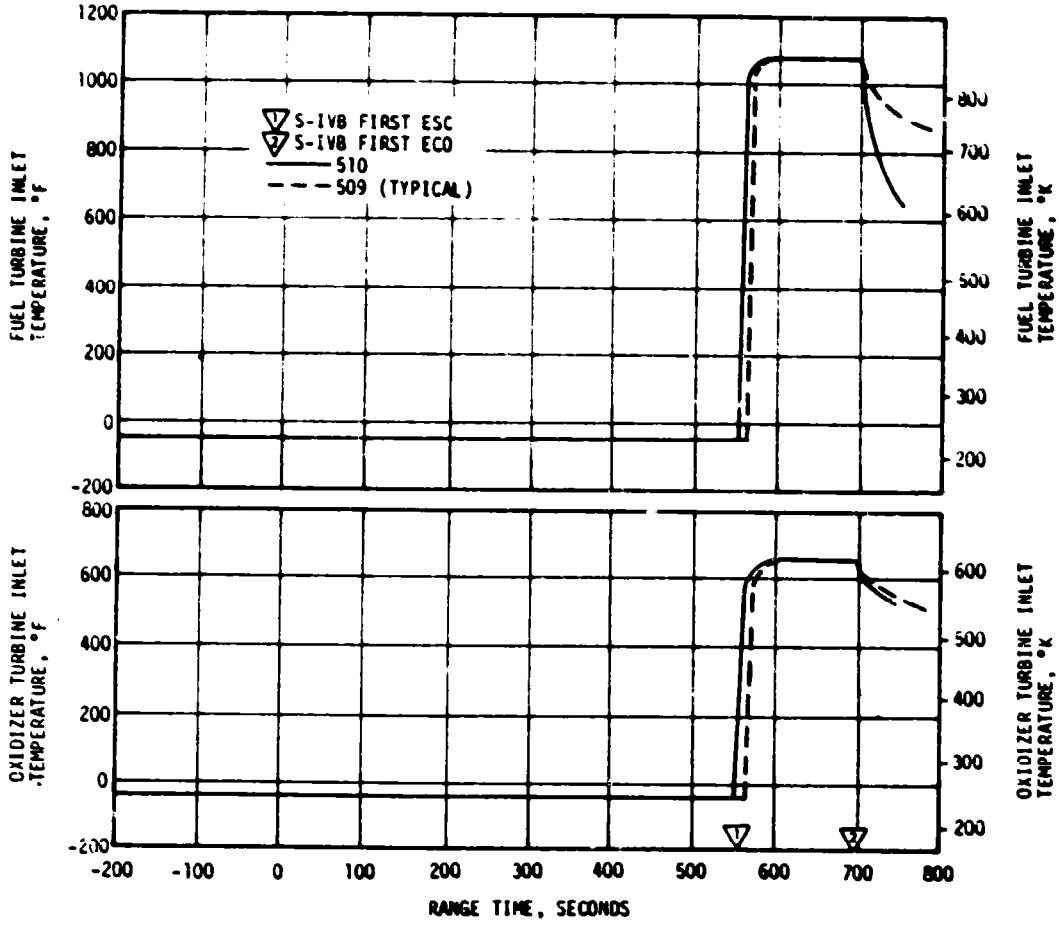

Figure 7-7. S-IVB Engine Turbine Inlet Temperatures Comparison - First Burn

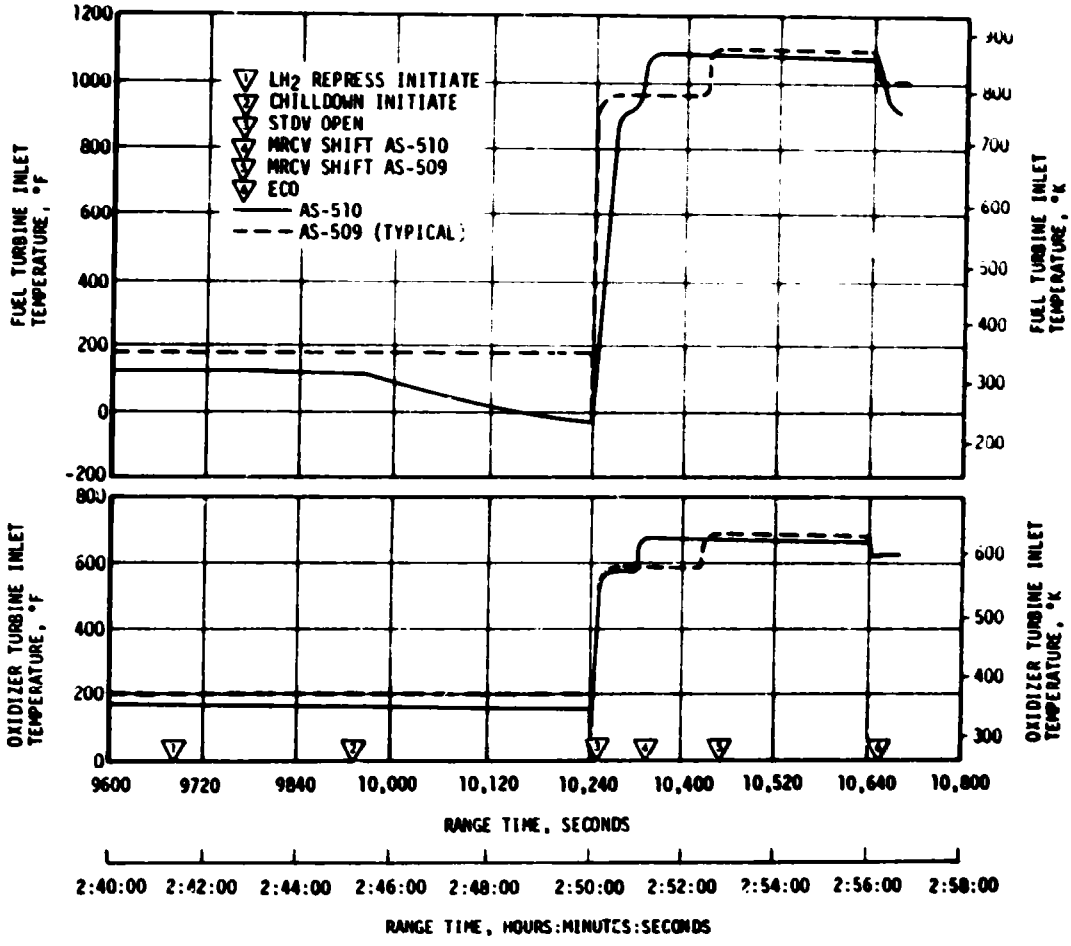

Figure 7-8. S-IVB Engine Turbine Inlet Temperatures Comparison - Second Burn

A comparison of predicted and actual performance of thrust, specific impulse, total flowrate, and MR versus time is shown in Figure 7-9. Table 7-3 shows the thrust, specific impulse, flowrates, and MR deviations from the predicted at the STDV open +130-second time slice at standard altitude conditions. The 130-second time slice thrust was 1.89 percent higher than predicted. The higher than predicted thrust during second burn is attributed to the same reason as for first burn. The MRCV position measurement can only be used as a gross measurement, since during second burn the measurement was erratic after returning to the closed position and engine performance simulations do not substantiate any MRCV movement.

The specific impulse for second burn, as discussed for first burn in paragraph 7.3, although near nominal was slightly higher than predicted, as shown in Table 7-3. While the slightly higher than nominal specific impulse has little significance for a single flight, similar deviations occurred on AS-505 through AS-509; therefore, the preflight predictions for AS-511 second burn are being reassessed.

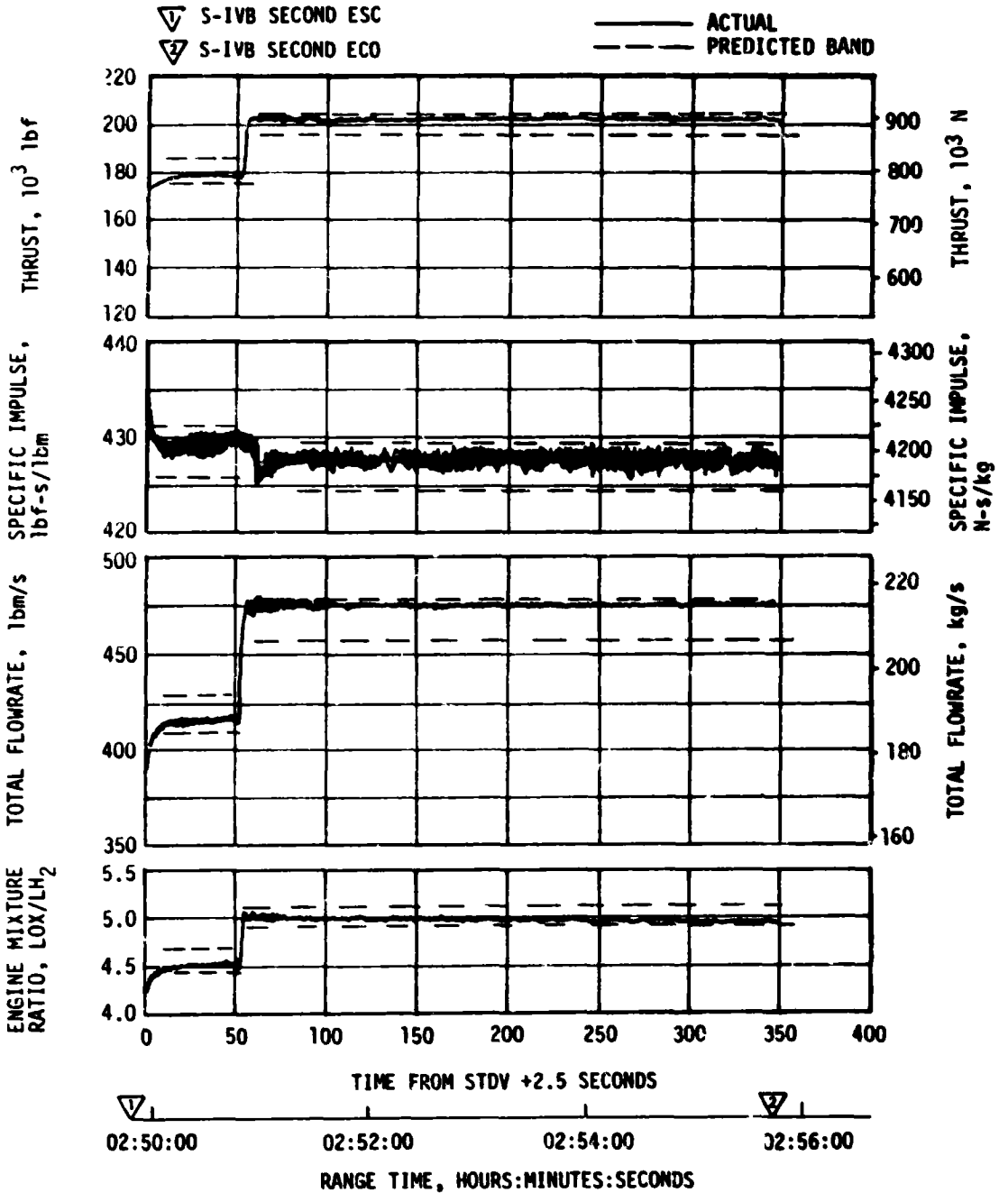

Figure 7-9. S-IVB Steady State Performance - Second Burn

Table 7-3. S-IVB Steady State Performance - Second Burn
(STDV +130-Second Time Slice at Standard Altitude Conditions)

PARAMETER	PREDICTED	RECONSTRUCTION	FLIGHT DEVIATION	PERCENT DEVIATION FROM PREDICTED
Thrust, lbf	199,335	203,111	3776	1.89
Specific Impulse, lbf-s/lbm	427.2	427.6	0.4	0.09
LOX Flowrate, lbm/s	387.72	394.87	7.15	1.84
Fuel Flowrate, lbm/s	78.84	80.17	1.33	1.69
Engine Mixture Ratio, LOX/Fuel	4.918	4.926	0.008	0.16

7.8 S-IVB SHUTDOWN TRANSIENT PERFORMANCE FOR SECOND BURN

S-IVB second ECO was initiated at 10,553.7 seconds (02:55:53.7) by a guidance velocity cutoff command for a burn time of 350.8 seconds. The burn time was 5.4 seconds less than predicted.

The ECO transient was satisfactory. The total cutoff impulse to zero thrust was 43,927 lbf-s which was 2898 lbf-s higher than predicted. Cutoff occurred with the MRCV in the full closed (5.0 MR) position.

7.9 S-IVB STAGE PROPELLANT MANAGEMENT

This was the second stage to use the pneumatically operated two-position MRCV. The operation of the valve was essentially identical to that demonstrated on AS-509.

A comparison of propellant mass values at critical flight events, as determined by various analyses, is presented in Table 7-4. The best estimate full load propellant masses were 0.07 percent greater for LOX and 0.19 percent greater for LH_2 than predicted. This deviation was well within the required loading accuracy.

Table 7-4. S-IVB Stage Propellant Mass History

EVENT	UNITS	PREDICTED		PU INDICATED (CORRECTED)		PU VOLUMETRIC		FLOW INTEGRAL		BEST ESTIMATE	
		LOX	LH_2	LOX	LH_2	LOX	LH_2	LOX	LH_2	LOX	LH_2
S-IC Liftoff	lbm	195,657	43,590	195,993	43,570	195,393	43,935	195,668	43,534	195,788	43,674
First S-IVB ESC	lbm	195,657	43,590	195,993	43,570	195,393	43,935	195,668	43,534	195,788	43,674
First S-IVB Cutoff	lbm	139,547	32,200	140,657	32,213	140,222	32,479	140,093	32,281	140,263	32,406
Second S-IVB ESC	lbm	139,359	29,742	139,996	29,708	139,606	29,916	139,460	29,726	139,665	29,789
Second S-IVB Cutoff	lbm	3821	1726	4152	1810	4192	1800	4243	1712	4243	1712

The masses shown do not include mass below the main engine valves, as presented in Section 16.

Extrapolation of best estimate residuals data to depletion, using the propellant flowrates, indicated that a LOX depletion would have occurred approximately 9.41 seconds after second burn velocity cutoff. Since LH_2 slosh amplitude was decaying at second burn ECO the fuel required, at LOX depletion, to compensate for slosh effects was less than the predicted 150 lbm.

During first burn the MRCV was positioned at the closed position for start and remained there, as programed, for the duration of the burn.

The MRCV was commanded to the 4.5 MR position 119.9 seconds prior to second ESC. The MRCV, however, did not actually move until it received engine pneumatic power at ESC +0.6 second. The MRCV took approximately 250 milliseconds to reach the open (4.5) position.

At second ESC +64.5 seconds, the valve was commanded to the closed position (approximately 5.0 MR) and remained there throughout the remainder of the flight.

7.10 S-IVB PRESSURIZATION SYSTEM

7.10.1 S-IVB Fuel Pressurization System

The LH_2 pressurization system met all of its operational requirements. The LH_2 pressurization system indicated acceptable performance during prepressurization, boost, first burn, coast phase, and second burn.

The LH_2 tank prepressurization command was received at -96.5 seconds and the tank pressurized signal was received 11.8 seconds later. Following

the termination of prepressurization, the ullage pressure reached relief conditions (approximately 31.4 psia) and remained at that level until liftoff, as shown in Figure 7-10. A small ullage collapse occurred during the first 15 seconds of boost. The ullage pressure returned to the relief level by 125 seconds due to self pressurization. A similar ullage collapse occurred at S-IC/S-II separation. The ullage pressure returned to the relief level 33 seconds later.

During first burn, the average pressurization flowrate was approximately 0.69 ibm/s, providing a total flow of 96.5 lbm. Throughout the burn, the ullage pressure was at the relief level, as predicted.

After the post insertion maneuver to the local horizontal, the No. 2 CVS Nozzle temperature dropped to the saturation point and remained there for 20 seconds. Sloshing LH_2 entered the CVS and some LH_2 (approximately 10 lbm) was vented through nozzle No. 2. Since it has been experienced on most of the previous flights (AS-501, AS-502, AS-503, AS-506, AS-507, and AS-508), the introduction of LH_2 into the CVS ducts is not a new occurrence and does not pose a problem. The effect was greater on AS-510 because the size of the post insertion maneuver was larger than those employed on previous flights. More detailed information is given in paragraph 10.4.2.

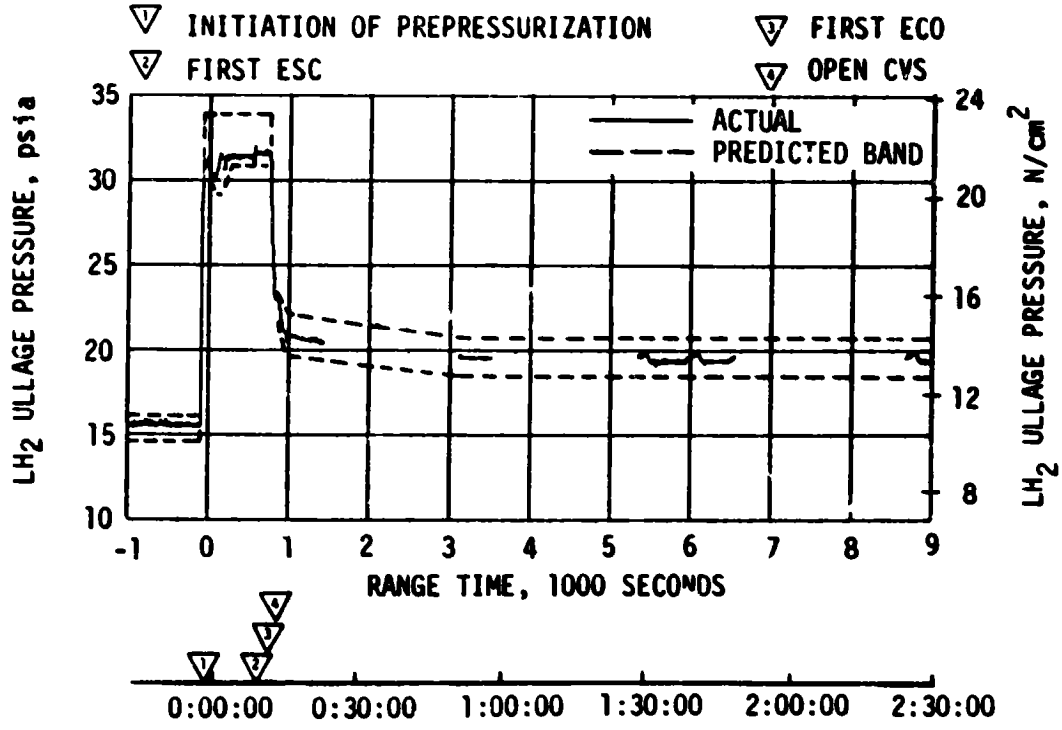

Figure 7-10. S-IVB LH_2 Ullage Pressure - First Burn and Parking Orbit

The LH_2 tank was satisfactorily repressurized for restart by the O_2/H_2 burner. The LH_2 ullage pressure was 30.8 psia at second burn ESC, as shown in Figure 7-11. The average second burn pressurization flowrate was 0.72 lbm/s until step pressurization, when it increased to 1.45 lbm/s. This provided a total flow of 309.0 lbm during second burn. Significant venting during second burn occurred at second ESC +280 seconds when step pressurization was initiated. This behavior was as predicted.

The LH_2 pump inlet NPSP was calculated from the pump interface temperature and total pressure. These values indicated that the NPSP at first burn ESC was 16.6 psi. At the minimum point, the NPSP was 7.7 psi above the required values. Throughout the burn, the NPSP had satisfactory agreement with the predicted values. The NPSP at second burn STDV was 7.9 psi, which was 3.4 psi above the required value. Figures 7-12 and 7-13 summarize the fuel pump inlet conditions for first and second burns.

7.10.2 S-IVB LOX Pressurization System

LOX tank prepressurization was initiated at -167 seconds and increased the LOX tank ullage pressure from ambient to 41.0 psia in 15.1 seconds, as shown in Figure 7-14. Five makeup cycles were required to maintain the LOX tank ullage pressure before the ullage temperature stabilized. At -96 seconds the LOX tank ullage pressure increased from 40.1 to 42.0 psia due to fuel tank prepressurization. The pressure then decreased to 40.6 psia at liftoff.

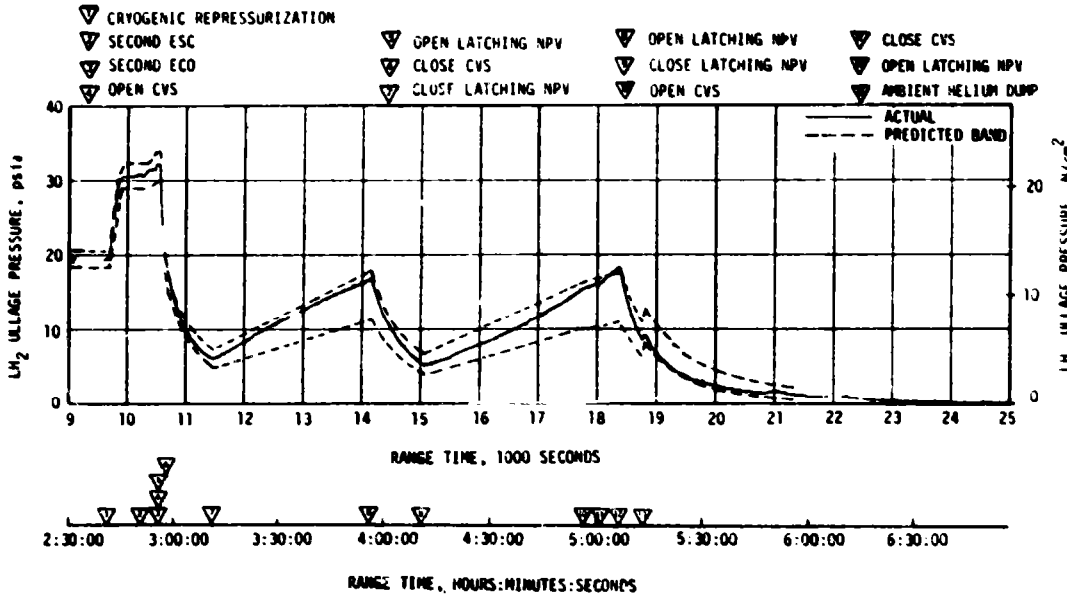

Figure 7-11. S-IVB LH_2 Ullage Pressure - Second Burn and Translunar Coast

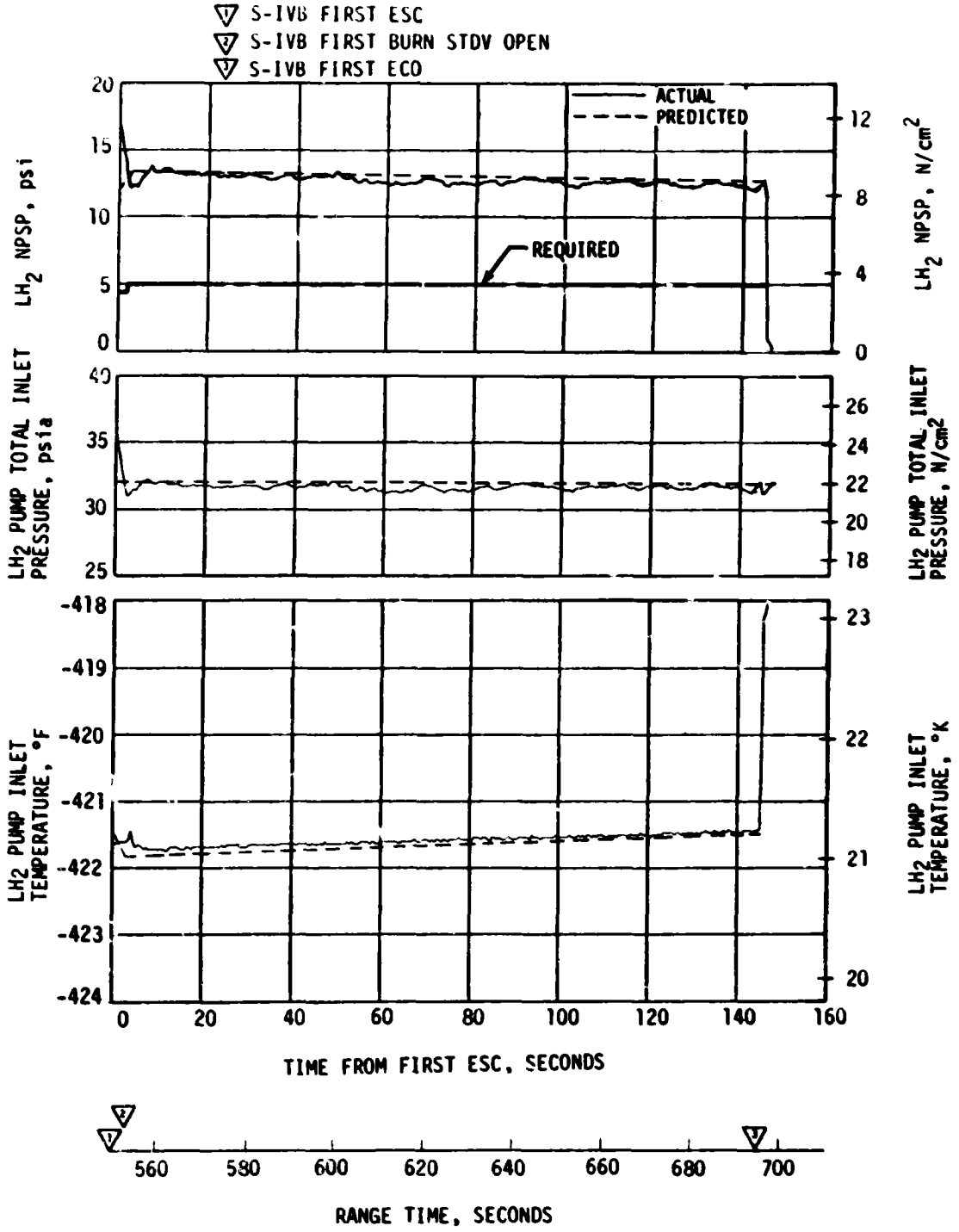

Figure 7-12. S-IVB Fuel Pump Inlet Conditions - First Burn

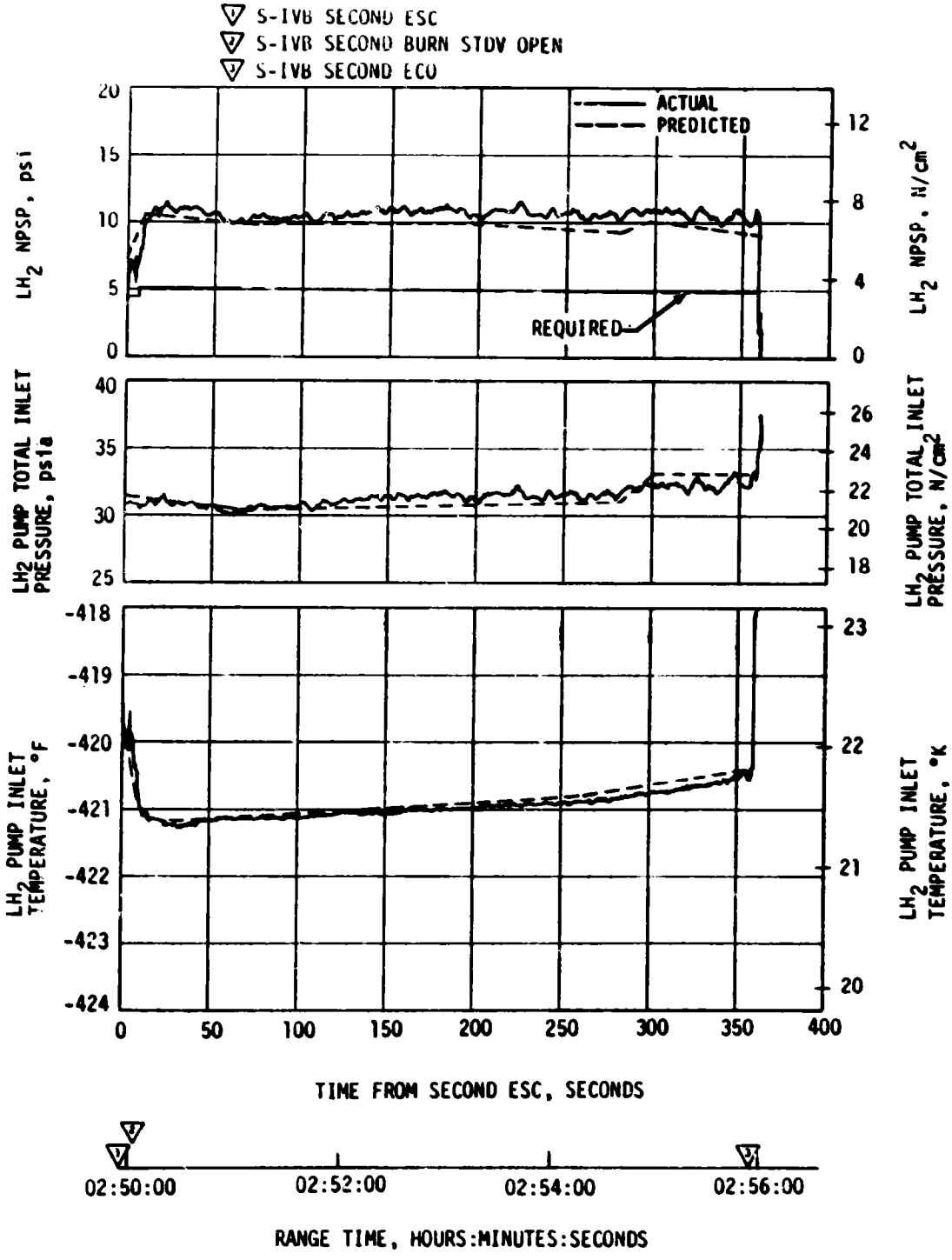

Figure 7-13. S-IVB Fuel Pump Inlet Conditions - Second Burn

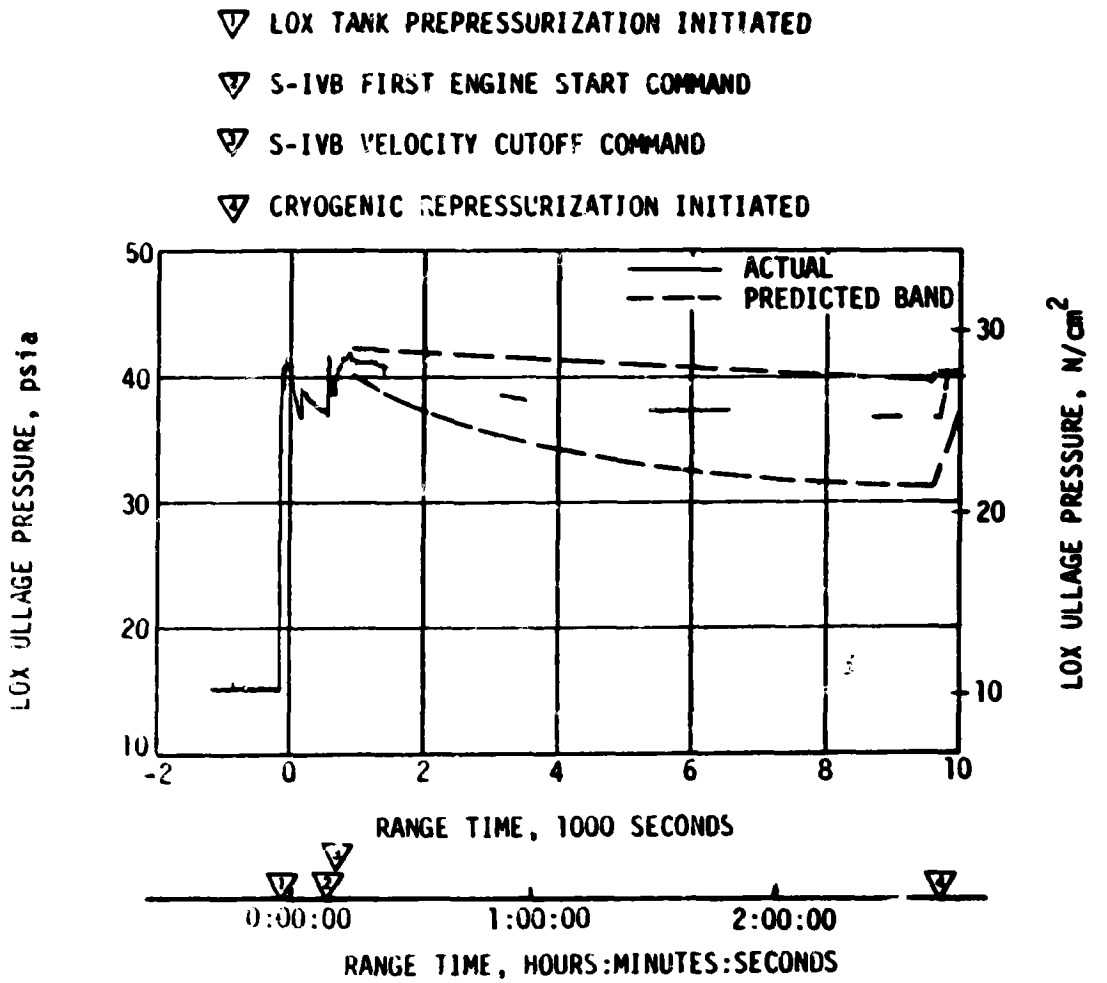

Figure 7-14. S-IVB LOX Tank Ullage Pressure - First Burn and Earth Parking Orbit

During boost there was a nominal rate of ullage pressure decay caused by an acceleration effect and ullage collapse. No makeup cycles occurred because of an inhibit until after T_4. LOX tank ullage pressure was 37.2 psia just prior to ESC and was increased at ESC due to a makeup cycle.

During first burn, five over-control cycles were initiated, including the programed over-control cycle initiated prior to ESC. The LOX tank prepressurization flowrate variation was 0.24 to 0.32 lbm/s during under-control system operation. This variation is normal and is caused by temperature effects. Heat exchanger performance during first burn was satisfactory.

During orbital coast, the LOX tank ullage pressure experienced a decay similar to that experienced on the AS-509 flight. This decay was within the predicted band, and was not a problem.

Following earth parking orbit insertion, a LOX slosh wave covered the LOX vent line diffuser. A concurrent ullage pressure increase to the relief setting resulted in liquid venting through the LOX Non-Propulsive Vent (NPV) system. The slosh wave was caused by the pitch maneuver to the local horizontal. The AS-510 90 n mi earth orbit required an 18-degree pitch maneuver, which was greater than the 6 to 10 degree maneuver required for the 100 n mi orbit on previous flights. The APS ullage engines were on to provide propellant settling, but due to the longer time requirement, the engines were shut down before the maneuver was completed. The pitch rate was arrested shortly after termination of the ullage engine firing, increasing the liquid slosh relative to the tank. More detailed information is given in paragraph 10.4.2.

LOX nonpropulsive venting occurred from approximately 750 to 1280 seconds. The lack of ullage pressure decay during the period of the high NPV nozzle pressure, 815 to 878 seconds, indicates that liquid was venting. A calculated 515 lbm of LOX was vented during this interval. During the remainder of the nonpropulsive venting, approximately 6 lbm of helium and 47 lbm of GOX were vented.

Repressurization of the LOX tank prior to second burn was required and was satisfactorily accomplished by the burner. The tank ullage pressure was 39.9 psia at second ESC and satisfied the engine start requirements.

Pressurization system performance during second burn was satisfactory. There was one over-control cycle, which was nominal. Helium flowrate varied between 0.32 to 0.39 lbm/s. Heat exchanger performance was satisfactory.

The LOX NPSP calculated at the interface was 23.7 psi at the first burn ESC. The NPSP decreased after start and reached a minimum value of 22.6 psi at 1 second after ESC. This was 7.4 psi above the required NPSP at that time. The LOX pump static interface pressure during first burn followed the cyclic trends of the LOX tank ullage pressure.

The NPSP calculated at the engine interface was 21.6 psi at second burn ESC. At all times during second burn, NPSP was above the required level. Figures 7-15 and 7-16 summarize the LOX pump conditions for first burn and second burn, respectively. The run requirements for first and secord burns were satisfactorily met.

The cold helium supply was adequate to meet all flight requirements. At first burn ESC, the cold helium spheres contained 378 lbm of helium. At the end of second burn, the helium mass had decreased to 145 lbm. Figure 7-17 shows helium supply pressure history.

7.11 S-IVB PNEUMATIC CONTROL PRESSURE SYSTEM

The stage pneumatic system performed satisfactorily during all phases of the mission.

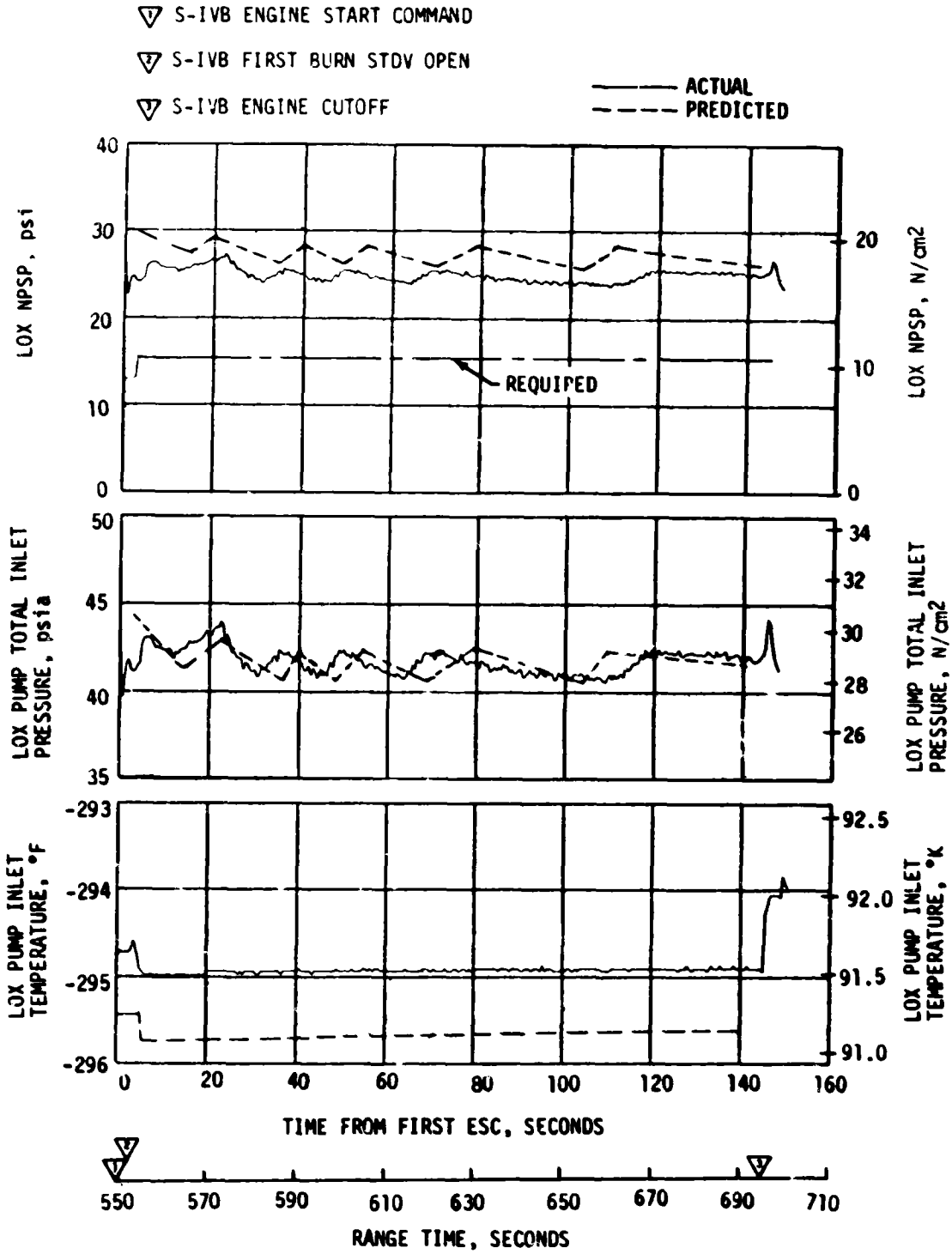

Figure 7-15. S-IVB LOX Pump Inlet Conditions - First Burn

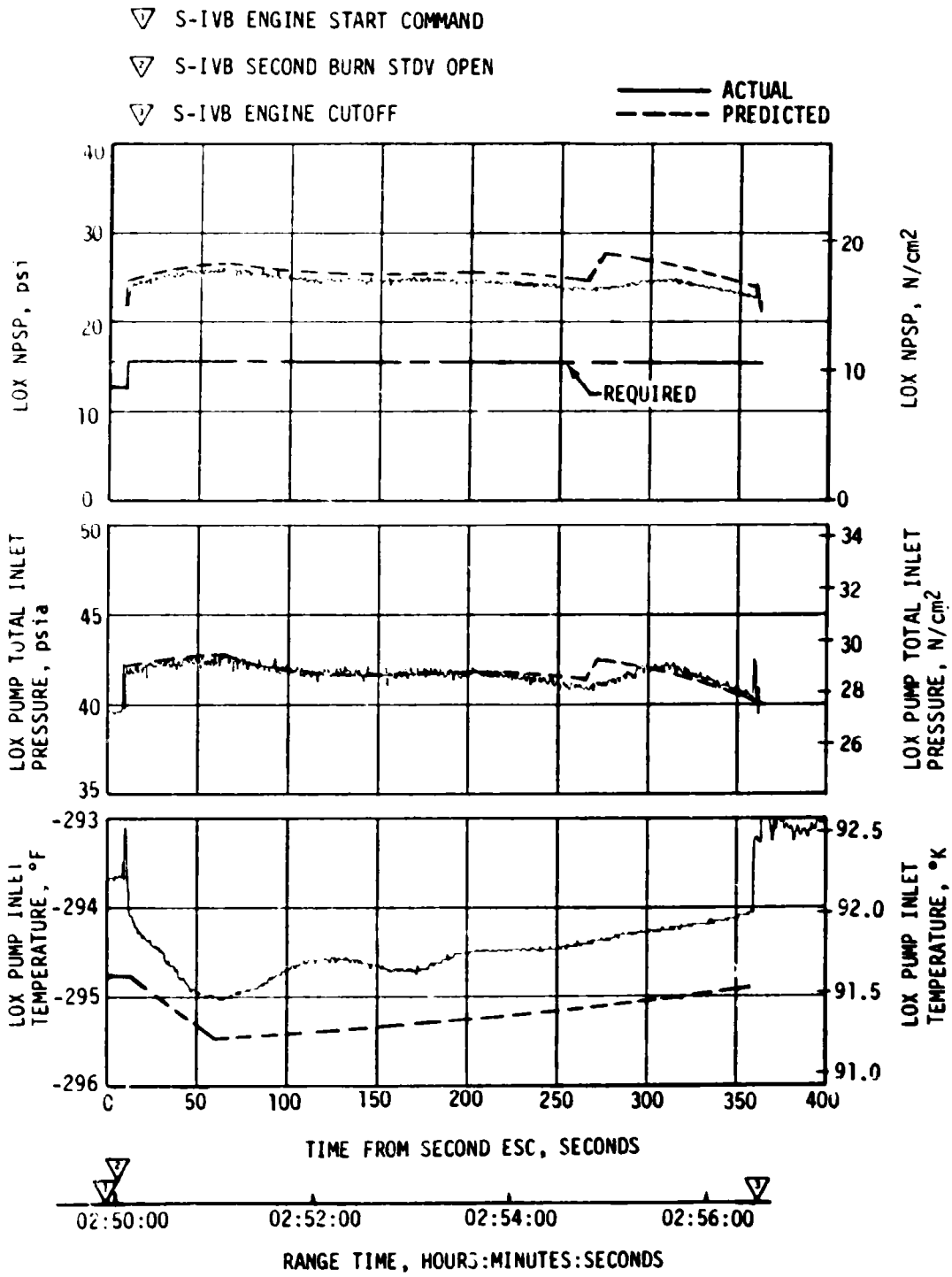

Figure 7-16. S-IVB LOX Pump Inlet Conditions - Second Burn

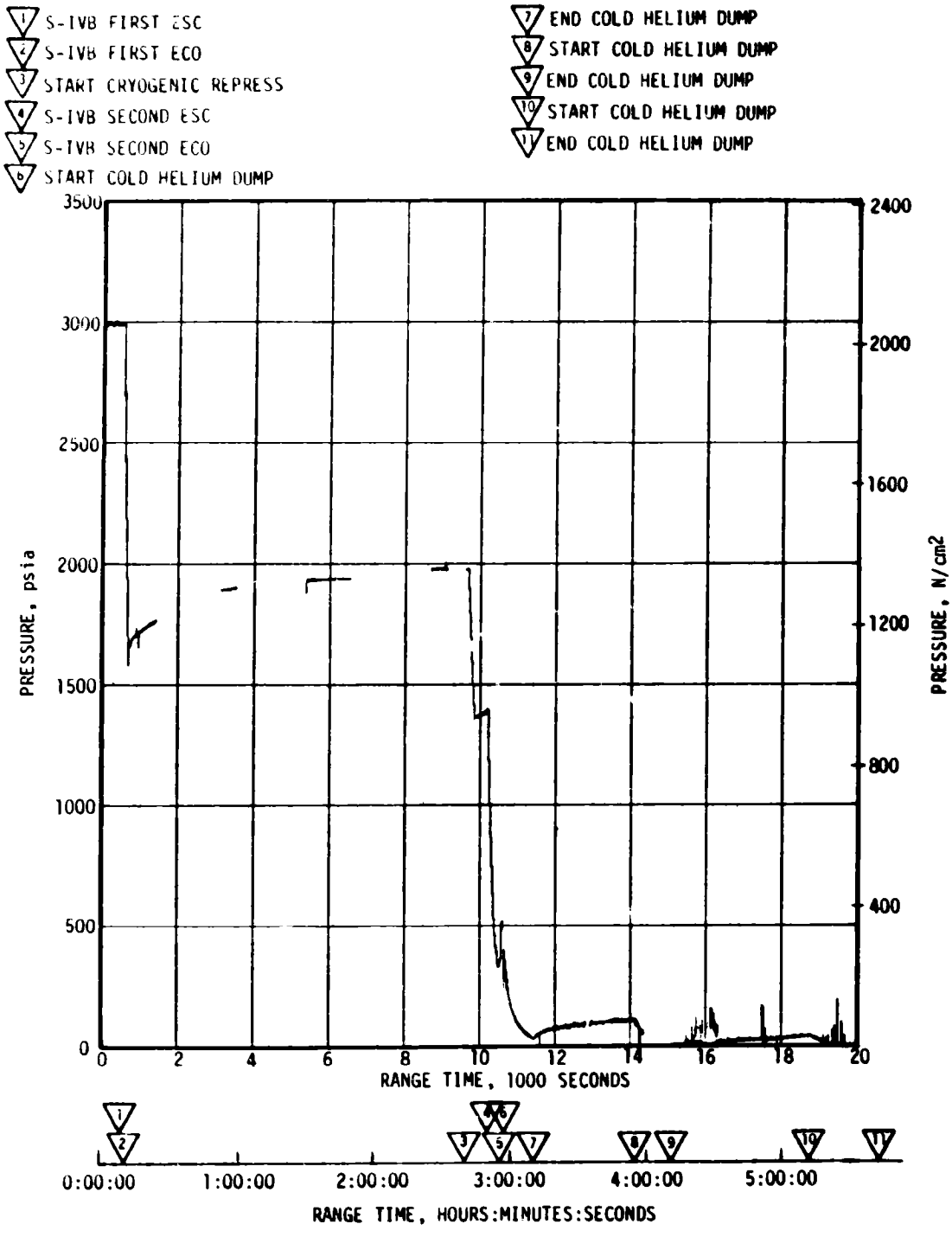

Figure 7-17. S-IVB Cold Helium Supply History

During flight, the regulator discharge pressure remained at approximately 470 psi until 30,035 seconds (08:20:35). At this time, the propellant tank vent valves were commanded closed in an attempt to isolate a disturbance that the vehicle was experiencing. During these non-programed valve actuations, the regulator discharge pressure shifted from approximately 470 to 513 psia.

The pressure remained at 513 psia until the vent valves were reopened at 32,280 seconds (08:58:00). When the vent valves were opened, the pressure dropped from approximately 513 to 470 psia and then returned to 513 psia and remained at that level (see Figure 7-18).

This observed pressure trend was probably due to leakage past the primary regulator poppet. This leakage could have resulted from low temperatures that are expected during translunar coast. When the vent valves were reopened, the demand exceeded the pilot leakage, resulting in a momentary shift back down to the primary regulator regulating band.

During qualification testing on the regulators, this type of operation was observed while flow testing the regulator below the specification temperature operating limit of -85°F.

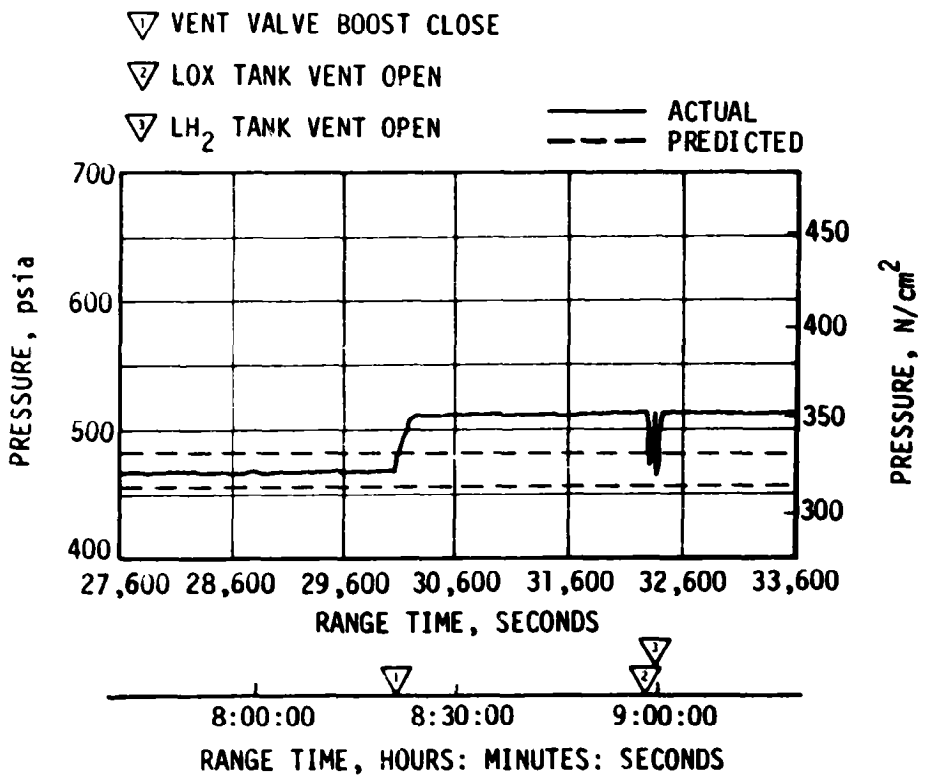

Figure 7-18. Pneumatic Regulator Discharge Pressure

7.12 S-IVB AUXILIARY PROPULSION SYSTEM

The APS demonstrated close to nominal performance throughout flight and met control system demands as required out to the time of flight control computer shutoff at approximately 37,185 seconds (10:19:45).

The oxidizer and fuel supply systems performed as expected during the flight. The propellant temperatures measured in the propellant control modules ranged from 84 to 105°F. The APS propellant usage was between the nominal and the mean +3 sigma predicted usage. Table 7-5 presents the APS propellant usage during specific portions of the mission.

During the mission the APS Apollo regulator outlet pressure increased in module No. 1 and decreased in module No. 2 as a result of thermal effects. Module No. 1 He pressurizing tank temperature decreased with regulated pressure maintained between 193 and 204 psia, and module No. 2 He pressurizing tank temperature increased with regulated pressure maintained between 189 and 194 psia. This thermal effect on the regulator outlet pressure is normal and has been observed on previous flights. The APS ullage pressures in the propellant tanks ranged from 188 to 200 psia.

The performance of the attitude control thrusters and the ullage thrusters was satisfactory throughout the mission. The thruster chamber pressures ranged from 95 to 102 psia. The ullage thrusters successfully completed the three sequenced burns of 86.7, 76.7, and 80.0 seconds; and the two ground commanded lunar impact burns of 241 seconds at 20,761 seconds (05:46:01) and 71 seconds at 36,001 seconds (10:00:01). The "Barbecue" Roll Maneuver was successfully completed prior to flight control computer shutoff.

The longest attitude control engine firing recorded during the mission was 3.523 seconds on the module No. 2 pitch engine at 785.716 seconds.

The average specific impulse of the attitude control thrusters was 200 lbf-s/lbm for Module No. 1 and 204 lbf-s/lbm for Module No. 2.

7.13 S-IVB ORBITAL SAFING OPERATIONS

The S-IVB high pressure systems were safed following J-2 engine cutoff. The thrust developed during the LOX dump was utilized to provide a velocity change for the lunar impact maneuver. The manner and sequence in which the safing was performed is presented in Figure 7-19.

7.13-1 Fuel Tank Safing

The LH_2 tank was satisfactorily safed by utilizing both the NPV and the CVS, as indicated in Figure 7-19. The LH_2 tank ullage pressure during safing is shown in Figure 7-11. At second ECO, the LH_2 tank ullage pressure was 32.2 psia; after three vent cycles, this decayed to

Table 7-5. S-IVB APS Propellant Consumption

TIME PERIOD	MODULE NO. 1				MODULE NO. 2			
	OXIDIZER		FUEL		OXIDIZER		FUEL	
	LBM	PERCENT	LBM	PERCENT	LBM	PERCENT	LBM	PERCENT
Initial Load	203.2		126.0		203.1		125.7	
First Burn (Roll Control)	0.4	0.2	0.2	0.2	0.4	0.2	0.2	0.2
ECO to End of First APS Ullaging (86.7 sec time period)	18.2	9.0	13.6	10.8	14.4	7.1	11.2	8.9
End of First Ullage Burn to Start of Second Ullage Burn	11.0	5.4	6.8	5.4	7.3	3.6	4.3	3.4
Second Ullage Burn (76.7 sec duration)	12.6	6.2	9.4	7.5	14.0	6.9	10.0	8.0
Second Burn (Roll Control)	0.3	0.1	0.2	0.2	0.3	0.1	0.2	0.2
ECO to Start of First Lunar Impact Burn at 20,761 sec	30.2	14.9	21.3	16.9	36.6	18.0	25.8	20.5
First Lunar Impact Ullage Burn (241 sec duration)	32.0	15.7	26.0	20.6	35.1	17.3	28.0	22.2
From End of First Lunar Impact Burn to Start of Second Lunar Impact Burn at 36,001 sec	16.0	7.9	10.0	7.9	14.9	7.3	9.2	7.3
From Start of Second Lunar Impact Burn to FCC Cutoff (approximately 37,185 sec)	12.0	5.9	9.3	7.4	14.7	7.2	11.0	8.8
Total Propellant Usage	132.7	65.3	96.8	76.9	137.7	67.8	99.9	79.5

NOTE: The APS propellant consumption presented in this table calculated from helium bottle pressure and temperature measurements.

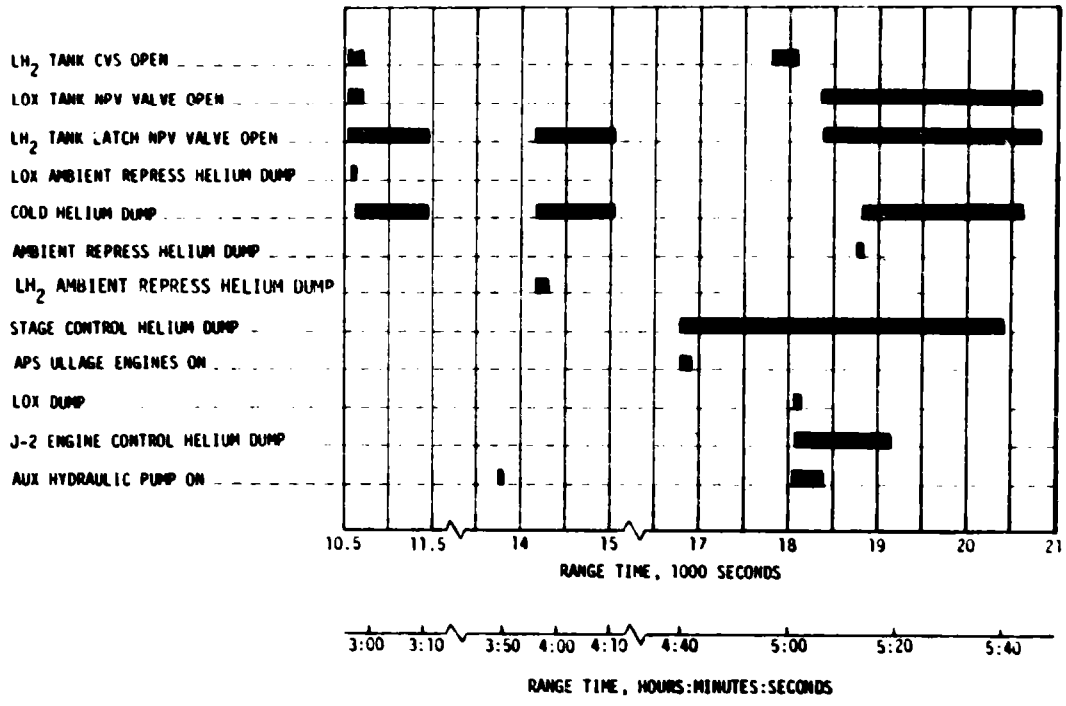

Figure 7-19. S-IVB LOX Dump and Orbital Safing Sequence

approximately zero. The ullage pressure remained at zero during the lockup period which began at 30,000 seconds (08:20:00). The mass of vented GH_2 and LH_2 agrees with the 2314 lbm of residual liquid and pressurant in the tank at the end of powered flight.

7.13.2 LOX Tank Dumping and Safing

Immediately following second burn cutoff, a programed 150-second vent reduced LOX tank ullage pressure from 39.0 to 17.8 psia, as shown in Figure 7-20. Approximately 70 lbm of helium and 125 lbm of GOX were vented overboard. As indicated in Figure 7-20, the ullage pressure then rose gradually due to self-pressurization, to 22.5 psia at the initiation of the Transposition, Docking, and Ejection (TD&E) maneuver.

The LOX tank dump was initiated at 18,080.6 seconds (05:01:20.6) and was satisfactorily accomplished. A steady-state liquid flow of 370 gpm was reached within 14 seconds. Gas ingestion did not occur during dump. The LOX residual at the start of dump was 4030 lbm. Calculations indicate that 2579 lbm of LOX was dumped. During dump, the ullage pressure decreased from 24.5 to 24.0 psia. LOX dump ended at 18,128.7 seconds (05:02:08.7) as scheduled by closure of the Main Oxidizer Valve (MOV). A steady-state LOX dump thrust of 709 lbf was attained. The

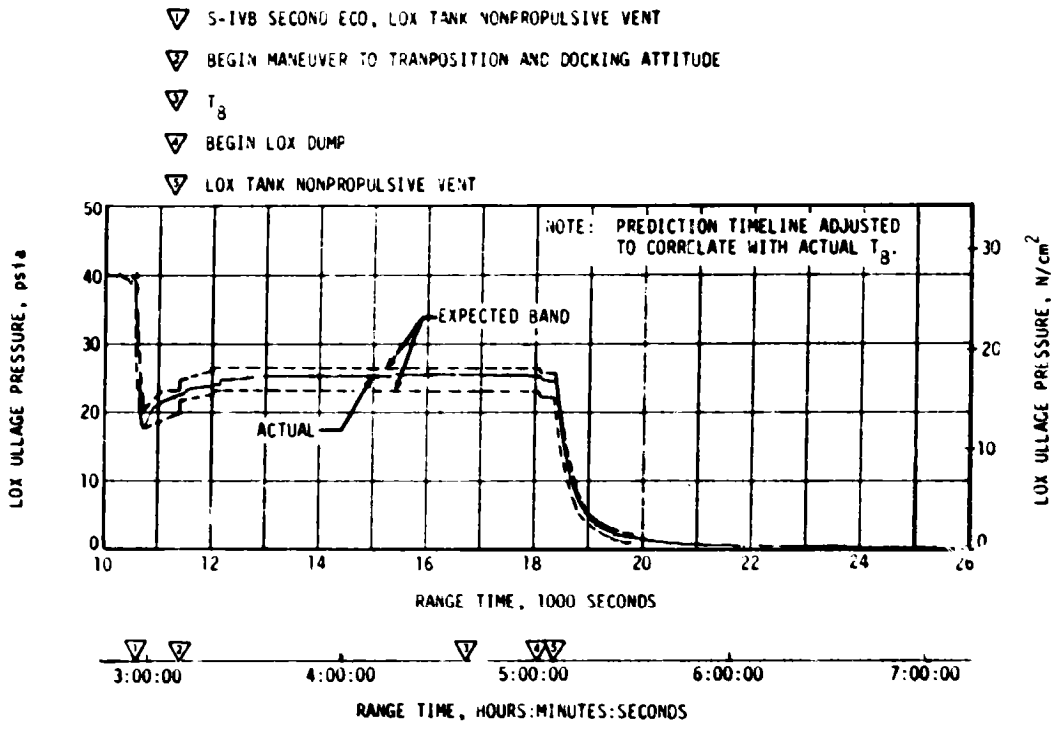

Figure 7-20. S-IVB LOX Tank Ullage Pressure - Second Burn and Translunar Coast

total impulse before MOV closure was 33,130 lbf-s, resulting in a calculated velocity change of 29.99 ft/s. Figure 7-21 shows the LOX dump thrust, LOX flowrate, oxidizer mass, and LOX ullage pressure during LOX dump.

At LOX dump termination +242 seconds, the LOX NPV valve was opened and remained open until 30,035 seconds (08:20:35). The LOX and LH_2 valves were closed to determine if nonpropulsive venting was the source of stage disturbances during translunar coast. No apparent changes resulted from the valve closures. Thus nonpropulsive venting is apparently not the source of the T_8 disturbances. The LOX NPV valve was reopened and latched at 32,280 seconds (08:58:00).

LOX tank ullage pressure decayed from 24.5 psia at 18,370 seconds (05:06:10) to near zero pressure at approximately 24,000 seconds (06:40:10). It increased to approximately 1 psia during the period the NPV valve was closed, and subsequently decayed again when the NPV valve was opened. Sufficient impulse was derived from the LOX dump, LH_2 CVS operation, and APS ullage burn to achieve a successful lunar impact. For further discussion of the lunar impact, refer to Section 17.

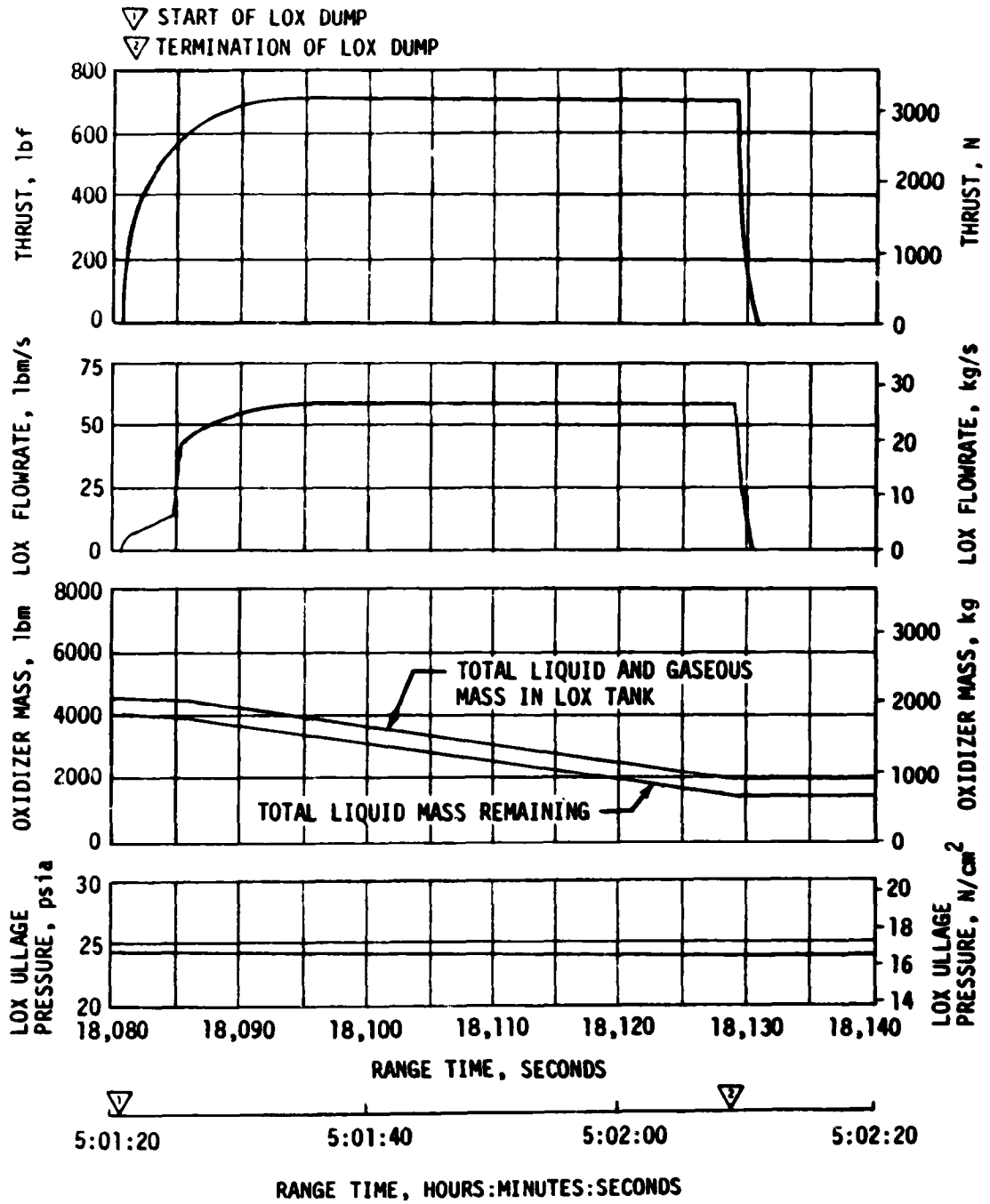

Figure 7-21. S-IVB LOX Dump Parameter Histories

7.13.3 Cold Helium Dump

A total of approximately 140 lbm of helium was dumped during the three programed dumps which occurred as shown in Figure 7-19.

7.13.4 Ambient Helium Dump

The two LOX ambient repressurization spheres were dumped through the LOX ambient repressurization control module into the LOX tank NPV system for 40 seconds. During this dump, the pressure decayed from 2890 psia to approximately 1250 psia.

The LH_2 ambient repressurization helium was dumped via the engine control sphere (26.1 lbm) and the fuel tank (15.5 lbm). The 1050-second engine control sphere safing period began at 18,081 seconds (05:01:21), and the 60-second LH_2 ambient helium dump began at 18,762 seconds (05:12:42). The pressure decayed from 2890 to 250 psia.

The helium dumped through the engine LOX dome and GG purge systems is estimated to be 31.5 lbm from 18,080.6 (05:01:20.6) to 18,821.7 seconds (05:13:41.7). This includes the helium mass from the five LH_2 ambient repressurization spheres, one LOX ambient repressurization sphere, and the J-2 engine helium control bottle. This dump was normal for the sequence and system interconnection of AS-510 but the resulting 4500 lb sec of impulse was not identified for preflight lunar impact planning. For prior flights, the ambient repressurization spheres were partially dumped through the propellant tank NPV systems during T_7. The sequence for AS-510 was changed to delay the LH_2 ambient helium dump to a later time in the mission so that the gas could be used to obtain more delta velocity if required to achieve lunar impact. It was not recognized that the LH_2 ambient helium pressurant could not be retained beyond engine helium control bottle safing. A corrective change in system sequencing is under consideration for future flights.

7.13.5 Stage Pneumatic Control Sphere Safing

The stage pneumatic control sphere and LOX repressurization sphere No. 2 were safed by initiating the J-2 engine pump purge and by flowing helium through the engine pump seal cavities for 3600 seconds. This activity began at 16,801 seconds (04:40:01) and satisfactorily reduced the pressure in the spheres from 2200 to 1100 psia.

7.13.6 Engine Start Tank Safing

The engine start tank was safed during a period of approximately 150 seconds beginning at 14,155 seconds (03:55:55). Safing was accomplished by opening the sphere vent valve. Pressure was decreased from 1290 to 10 psia with 3.0 lbm of hydrogen being vented.

7.13.7 Engine Control Sphere Safing

The safing of the engine control sphere began at 18,081 seconds (05:01:21). The helium control solenoid was energized to vent helium through the engine purge system. The initial pressure in the sphere was approximately 3100 psia. At this time, gaseous helium from the LH_2 ambient repressurization bottles began flowing to the engine control sphere. Helium from the control sphere and repressurization bottles continued to vent until 19,131 seconds (05:18:51).

During this time, the pressure in the repressurization bottles had decayed from about 2890 to 250 psia. Part of this decay was due to safing of the repressurization bottles which occurred within the time span of the control sphere safing. The control sphere pressure decayed to 125 psia. Subsequent to closing of the control solenoid, the control sphere repressurized to 225 psia witnout any noticeable decay in the ambient repressurization bottles pressure. During the safing, a total of 32.0 lbm of helium was vented.

7.14 HYDRAULIC SYSTEM

The S-IVB hydraulic system performance was satisfactory during the entire mission (S-IC/S-II boost, first and second burns of S-IVB, and orbital coast).

SECTION 8

STRUCTURES

8.1 SUMMARY

The structural loads experienced during the S-IC boost phase were well below design values. The maximum bending moment was 80 x 10^6 lbf-in at the S-IC LOX tank (30 percent of the design value). Thrust cutoff transients experienced by AS-510 were similar to those of previous flights. The maximum longitudinal dynamic responses at the Instrument Unit (IU) were ±0.25 g and ±0.30 g at S-IC Center Engine Cutoff (CECO) and Outboard Engine Cutoff (OECO), respectively. The magnitudes of the thrust cutoff responses are considered normal.

During S-IC stage boost, the expected 4 to 5 hertz first longitudinal mode responses occurred between 100 seconds range time and S-IC CECO. The maximum amplitude measured at the IU was ±0.06 g. Oscillations in the 4 to 5 hertz range have been observed on previous flights and are normal vehicle responses to the flight environment. POGO did not occur during S-IC boost.

The S-II stage center engine LOX feedline accumulator successfully inhibited the 14 to 16 hertz POGO oscillations. A peak response of ±0.6 g was measured on engine No. 5 gimbal pad during steady-state engine operation. As on previous flights, low amplitude 11 hertz oscillations were experienced near the end of S-II burn. Peak engine No. 1 gimbal pad response was ±0.06 g. POGO did not occur during S-II boost. The POGO limiting backup cutoff system performed satisfactorily during the prelaunch and flight operations. The system did not produce any discrete outputs.

The structural loads experienced during the S-IVB stage burns were well below design values. During first burn the S-IVB experienced low amplitude, 16 to 20 hertz oscillations. The ±0.04 g maximum amplitude measured on the gimbal block was comparable to previous flights responses and well within the expected range of values. Similarly, S-IVB second burn produced intermittent low amplitude responses (±0.05 g) in the 12 to 16 hertz frequency range which peaked near second burn cutoff.

8.2 TOTAL VEHICLE STRUCTURES EVALUATION

8.2.1 Longitudinal Loads

The structural loads experienced during boost were well below design values. The AS-510 vehicle liftoff occurred at a steady-state acceleration of 1.20 g. Maximum longitudinal dynamic response measured during thrust buildup and release was ±0.20 g in the IU and ±0.50 g at the Command Module (CM), Figure 8-1. Comparable values have been seen on previous flights.

The longitudinal loads experienced at the time of maximum bending moment (80.1 seconds) were as expected and are shown in Figure 8-2. The steady-state longitudinal acceleration was 2.06 g as compared to 1.9 g on AS-509 and AS-508.

Figure 8-2 also shows that the maximum longitudinal loads imposed on the S-IC stage thrust structure, fuel tank, and intertank area occurred at S-IC CECO (136.0 seconds) at a longitudinal acceleration of 3.79 g. The maximum longitudinal loads imposed on all vehicle structures above the S-IC intertank area occurred at S-IC OECO (159.6 seconds) at an acceleration of 3.97 g.

8.2.2 Bending Moments

The peak vehicle bending moment occurred during the maximum dynamic pressure phase of boost at 80.1 seconds, Figure 8-3. The maximum bending moment of 80 x 10^6 lbf-in at station 1156 was approximately 30 percent of design value.

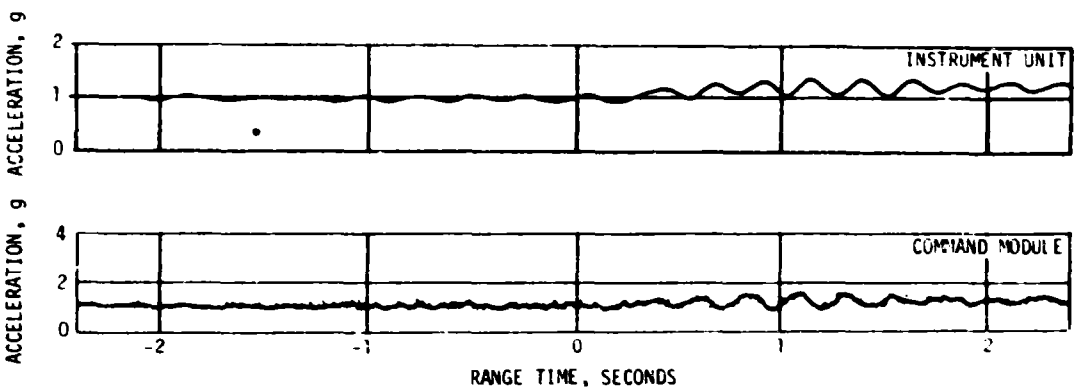

Figure 8-1. Longitudinal Acceleration at IU and CM During Thrust Buildup and Launch

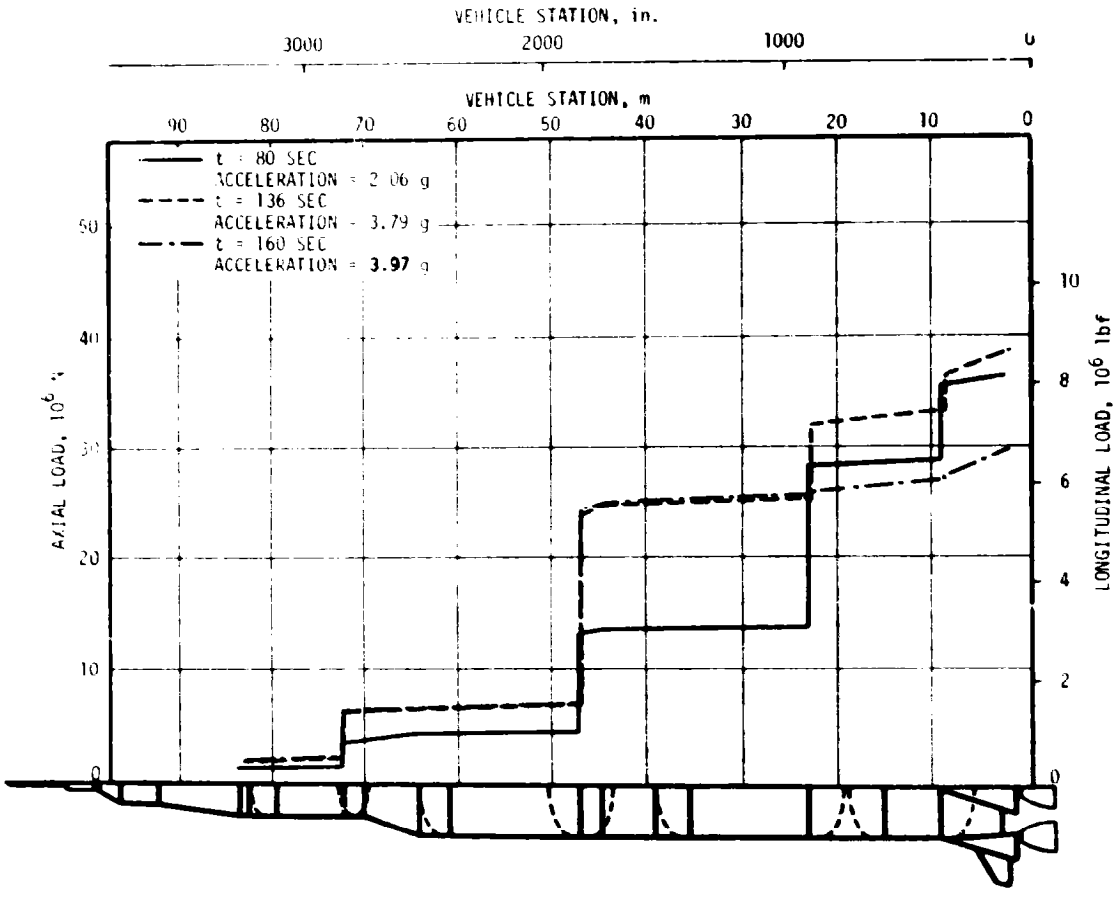

Figure 8-2. Longitudinal Load at Time of Maximum Bending Moment, CECO and OECO

Lateral response of the vehicle at liftoff was comparable to those seen on previous flights. The maximum response level seen at the CM was approximately 0.114 Grms as compared to the AS-509 maximum of 0.111 Grms.

8.2.3 Vehicle Dynamic Characteristics

8.2.3.1 Longitudinal Dynamic Characteristics

During S-IC stage boost, the significant vehicle response was the expected 4 to 5 hertz first longitudinal mode response. The low amplitude oscillations began at approximately 100 seconds and continued until S-IC CECO. The peak amplitude measured in the IU was approximately ±0.06 g, the same as seen on AS-509. The AS-510 IU response during the oscillatory period is compared with previous flight data in Figure 8-4. The change in the previous flight envelope prior to 110 seconds (Reference: AS-509 report MPR-SAT-FE-71-1) is based on further analysis of AS-509 data. Spectral analysis of engine chamber pressure measurements shows no detectable structural/propulsion coupled oscillations. POGO did not occur during S-IC boost.

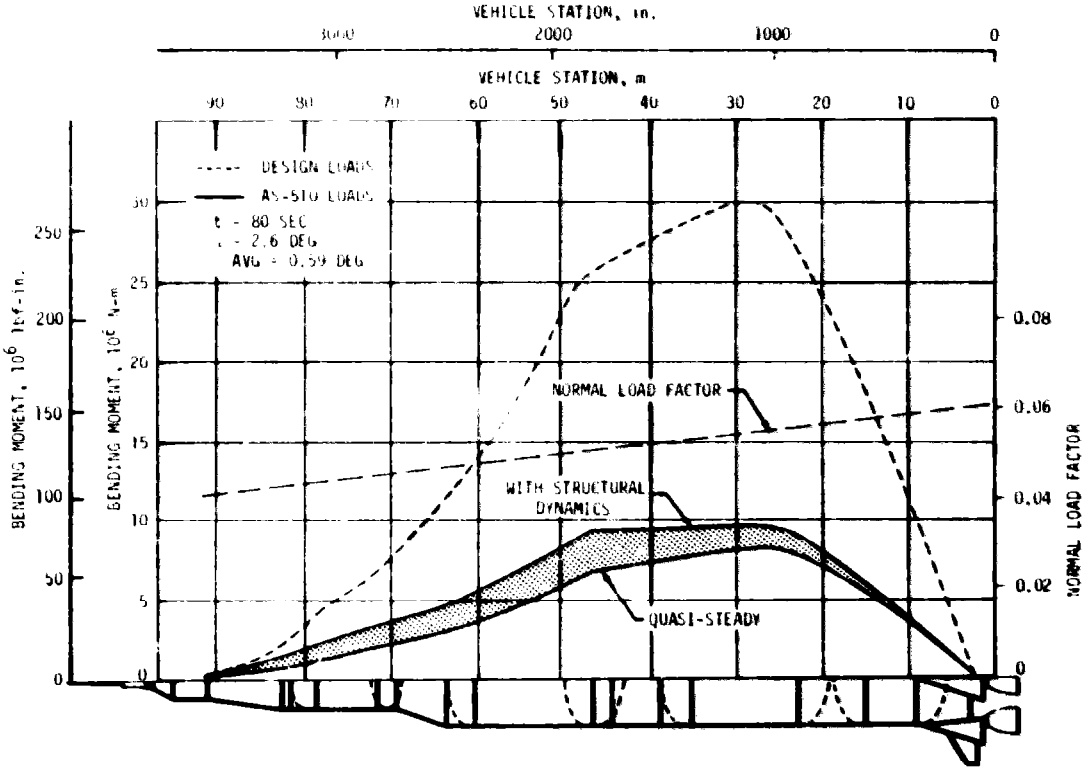

Figure 8-3. Bending Moment and Normal Load Factor Distribution at Time of Maximum Bending Moment

The AS-510 S-IC CECO and OECO transient responses were similar to those of previous flights. The maximum longitudinal dynamics resulting from CECO were ±0.25 g at the IU (the same as measured on AS-509) and ±0.55 g at the CM, Figure 8-5. For OECO the maximum dynamics at the IU were ±0.30 g (±0.35 g on AS-509) and ±1.02 g at the CM, Figure 8-6. Note that the minimum CM acceleration level of -0.80 g occurred at approximately the same time and is of the same magnitude as on previous flights, unaffected by the change in the S-IC/S-II separation sequence.

AS-510 was the second vehicle on which the S-II stage center engine accumulator was installed to suppress the 16 hertz POGO phenomenon. The flight data show that the 16 hertz oscillations were inhibited with amplitudes comparable to those seen on AS-509, Figure 8-7. The peak 14 to 20 hertz center engine gimbal response was approximately ±0.6 g, the same as observed on AS-509. POGO did not occur.

A transient response was experienced shortly after accumulator fill was initiated. The peak response of the LOX pump inlet pressure was approximately 45 psi peak-to-peak with a frequency of 68 hertz, Figure 8-8. The response of the center engine gimbal pad at the corresponding time

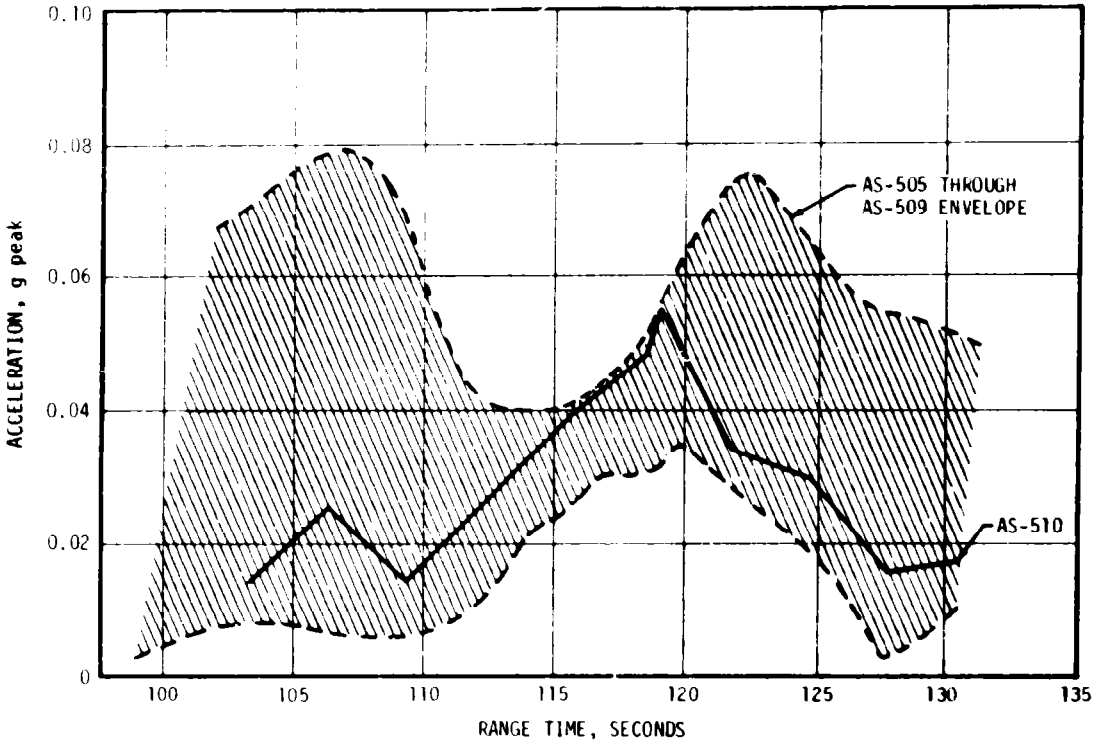

Figure 8-4. IU Accelerometer Response During Peak 4-5 Hertz Response (Longitudinal)

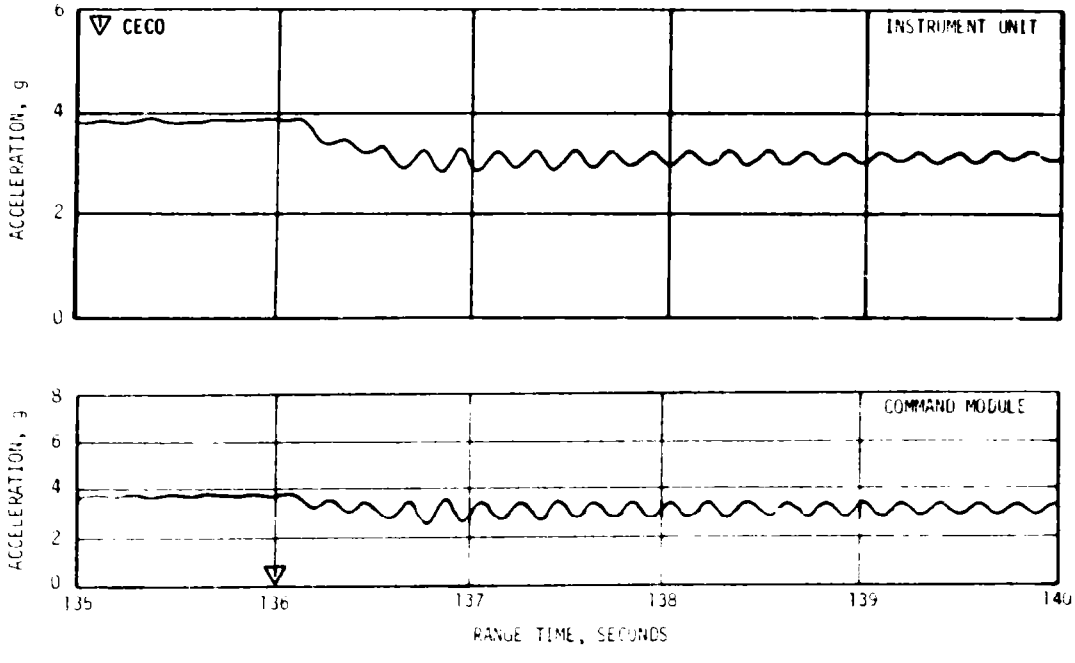

Figure 8-5. IU and CM Longitudinal Acceleration After S-IC CECO

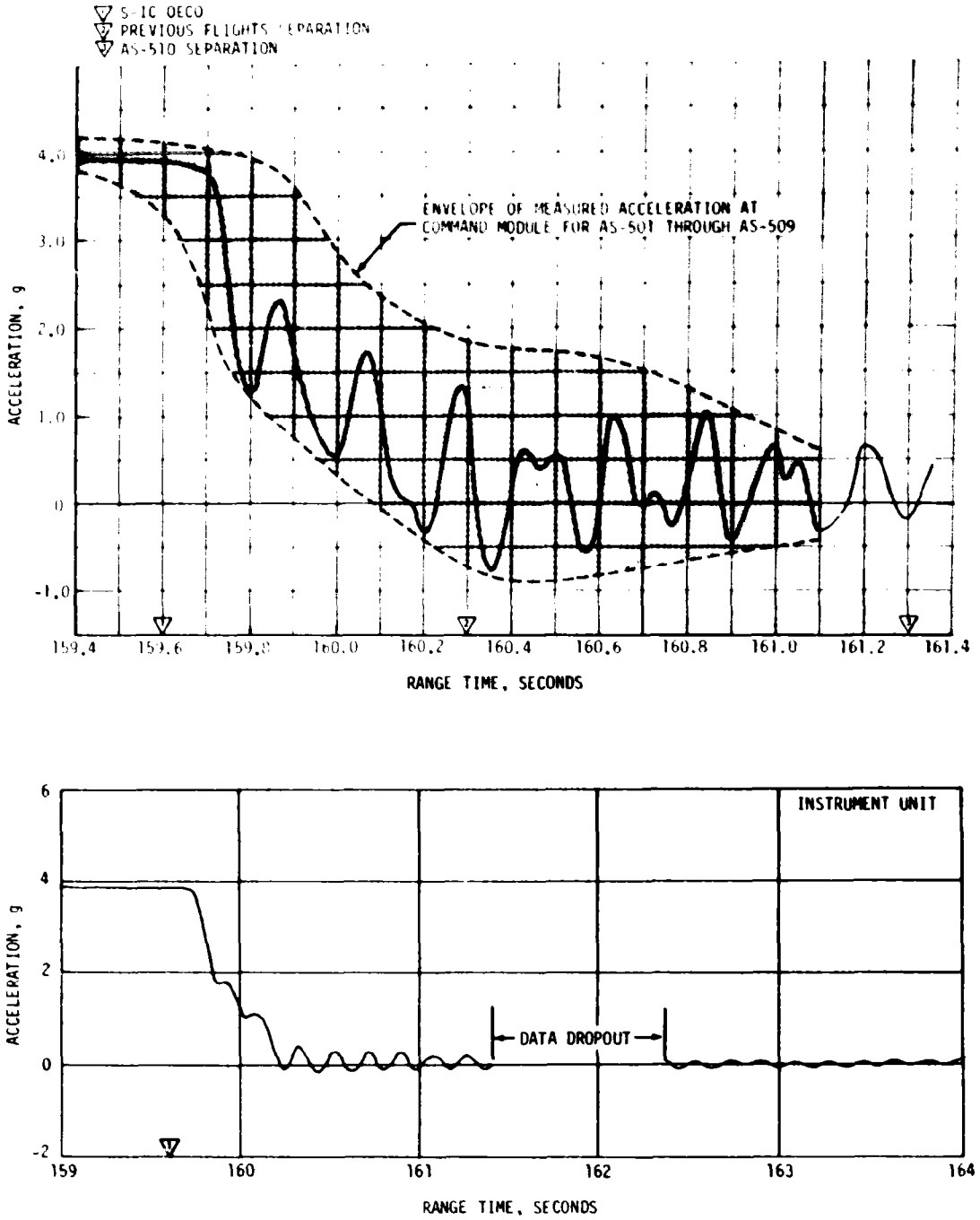

Figure 8-6. IU and CM Longitudinal Acceleration After S-IC OECO

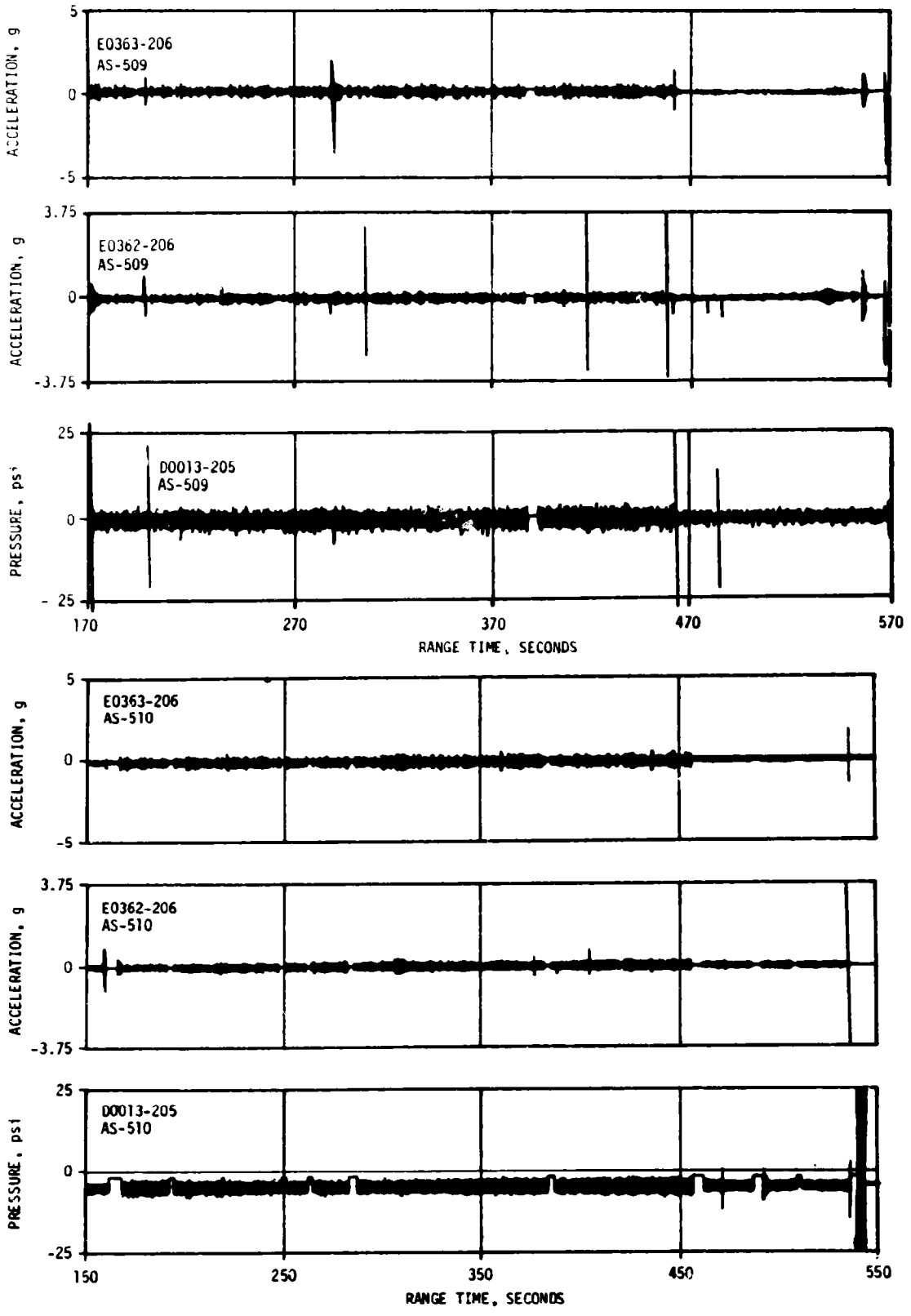

Figure 8-7. AS-510/AS-509 Acceleration and Pressure Oscillations During S-II Burn (8 to 20 Hz Filter)

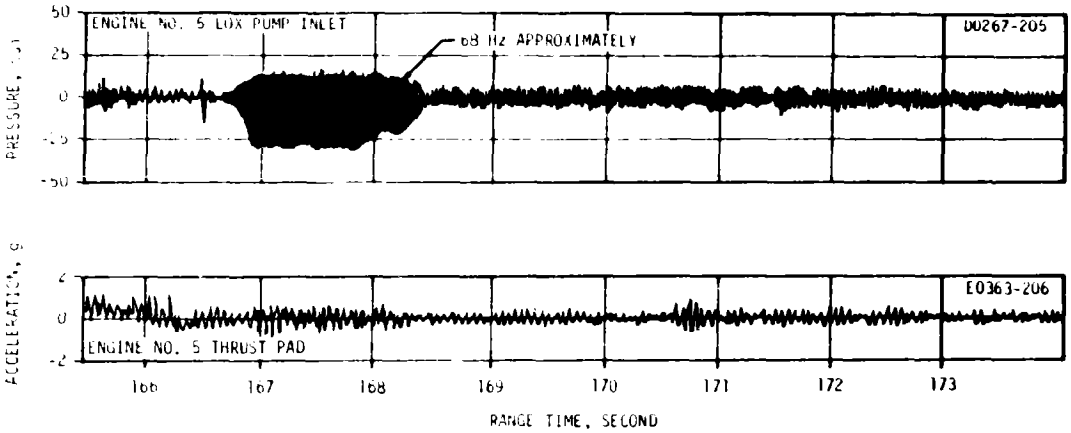

Figure 8-8. AS-510 Pump Inlet Pressure and Thrust Pad Acceleration Oscillations During Accumulator Fill Transient (1 to 110 Hz Filter)

and frequency was less than ±0.5 g. Both of these responses were comparable to those measured on AS-509.

As on prior flights, 11 hertz oscillations were noted near the end of S-II burn. The AS-510 responses were in general lower than those seen on previous flights. Table 8-1 presents a summary of peak engine No. 1 gimbal pad responses for all flights.

During AS-510 S-IVB first burn, low frequency (16 to 20 hertz) longitudinal oscillations similar to those observed on previous flights were evident. The AS-510 amplitudes (±0.04 g at gimbal block) were well below the maximum measured on AS-505 (±0.3 g) and within the expected range of values.

AS-510 S-IVB second burn produced intermittent 12 to 16 hertz oscillations similar to those experienced on previous flights. The oscillations, beginning approximately 80 seconds prior to cutoff, peaked at approximately 10 seconds prior to cutoff with ±0.05 g measured on the gimbal block. This compared to ±0.06 g on AS-509.

8.2.4 Vibration

There were no significant vibration environments identified on AS-510. A comparison of AS-510 data with data from previous flights show similar trends and magnitudes.

The data from AS-510 were limited in frequency range as compared to previous data. This was caused by the change in the data acquisition system from single-sideband/FM to FM/FM. Direct comparison of similar

Table 8-1. Post S-II CECO 11 Hertz Oscillations

FLIGHT	RANGE TIME AT PEAK AMPLITUDE (SECONDS)	ACCELERATION		LOX LEVEL AT PEAK AMPLITUDE (INCHES OF LOX)	LOX LEVELS AT 1/3 AMPLITUDE (INCHES OF LOX)	
		PEAK AMPLITUDE (G)	FREQUENCY (HZ)		START	STOP
501	NO MEASUREMENT OF ACCELERATION					
502	547	0.07	10.4	30	32	28
503	512	1.12	10.9	23	36	15
504	535	0.18	11.6	8	14	6
505	545	0.22	11.0	16	23	14
506	NO LOW FREQUENCY OSCILLATION INSTRUMENTATION					
507	545	0.09	11.4	15	27	12
508	582	0.17	11.1	19	27	9
509	542	0.16	11.0	26	32	18
510	540	0.06	11.0	18	30	14

DATA QUESTIONABLE
AS-502 - 2 ENGINES OUT
AS-502 & AS-503 - LARGE ATTENUATION AT 11 HZ ON E_1 ACCELERATION

data can not be made due to frequency roll-off characteristics. However, correlation is obtained when frequency ranges are compatible. Figure 8-9 shows a comparison of AS-510 data with previous flight data for compatible frequency ranges.

8.3 S-II POGO LIMITING BACKUP CUTOFF SYSTEM

The backup cutoff system provides for automatic S-II CECO if vibration response levels exceed predetermined levels within the preselected frequency band. The system consists of three sensors, a two-out-of-three voting logic, an engine cutoff arming function, and an automatic disable function which is effective until the arming operation has occurred.

The system did not produce discrete outputs at any time. The accelerometer analog outputs were well below the levels which would produce a discrete output even during the engine start period when the system was not armed. After arming, the analog output did not exceed 1 g.

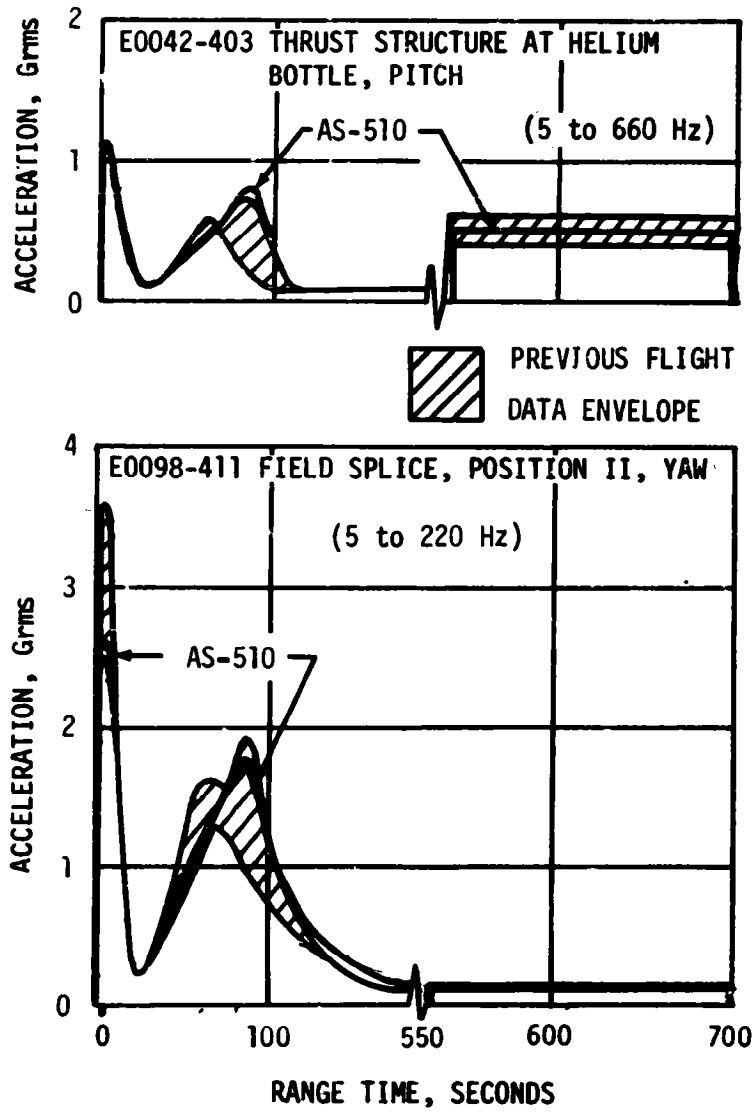

Figure 8-9. S-IVB Stage Vibration Envelopes

SECTION 9

GUIDANCE AND NAVIGATION

9.1 SUMMARY

The guidance and navigation system provided satisfactory end conditions for the boost to Earth Parking Orbit (EPO) and the boost to Translunar Injection (TLI). A navigation update was performed at the beginning of the second revolution because the difference between the Instrument Unit (IU) navigation vector and the tracking vector at Carnarvon exceeded the allowable tolerance defined in Flight Mission Rule (FMR) 7-11. The navigation differences following the update were small and were well within all allowable tolerances at TLI.

A negative shift of approximately 0.25 m/s (0.82 ft/s) occurred in the Z (down range) accelerometer output approximately one second before range zero. The precise effect of the shift on subsequent navigation errors has not been determined. The Launch Vehicle Data Adapter (LVDA) and Launch Vehicle Digital Computer (LVDC) performed satisfactorily with nominal values for component temperatures and power supply voltages.

9.2 GUIDANCE COMPARISONS

The postflight guidance error analysis was based on comparisons of the ST-124M-3 platform system measured velocities with the final postflight trajectory established from external tracking data (see paragraph 4.2). Velocity differences from Earth Parking Orbit (EPO) are shown in Figure 9-1. A positive velocity difference indicates trajectory data greater than the platform system measurement. The curves shown were generated by using a platform system error model to smooth the observed velocity differences. At EPO the differences were 1.47 m/s (4.82 ft/s), 1.36 m/s (4.46 ft/s), and 0.47 m/s (1.54 ft/s) for vertical, cross range and down range velocities, respectively. These differences are relatively small and well within the accuracy of the data compared and/or the specified limits for hardware errors. There was no indication of any accelerometer measuring head located on the ST-124M-3 platform reaching the 6-degree stop during thrust buildup. The maximum transient noted was about 3 degrees for both the down range and cross range accelerometers. However, the output of the down range accelerometer was negative from about 1.4 seconds before Time Base 1 (T_1) to about 12.8 seconds after T_1. One possible cause of the negative output was high frequency vibrations. Lack of adequate vibration measurements severely compromises rigorous

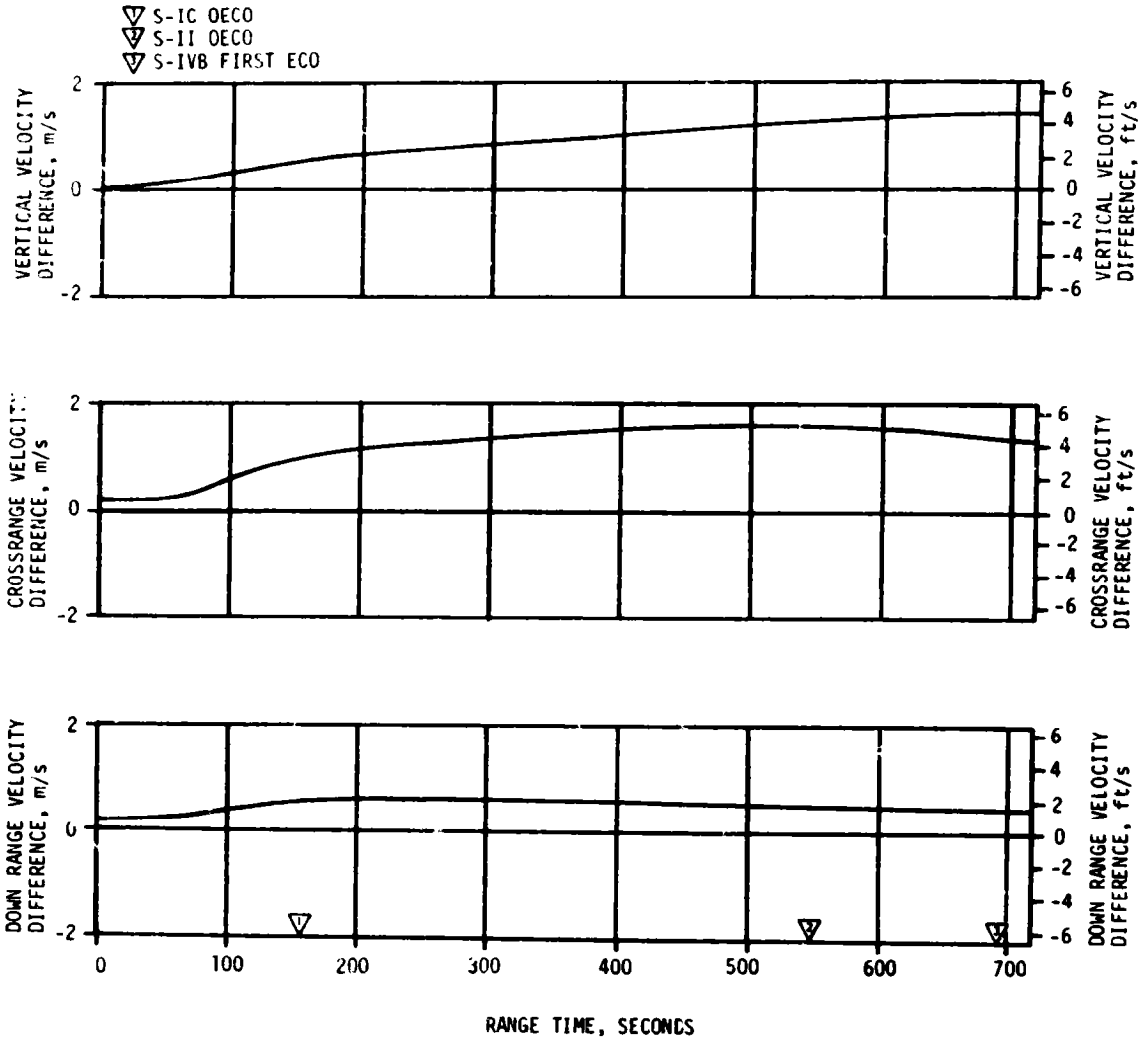

Figure 9-1. Trajectory and ST-124M-3 Platform Velocity Comparison, Boost-To-EPO (Trajectory Minus LVDC)

analysis. The resultant velocity bias was about -0.25 m/s (-0.82 ft/s). Although the velocity errors are relatively small, it should be noted that the differences are all additive, the result of which is a radius vector error at EPO greater than that observed on previous Saturn V flights.

The time history of the platform velocity comparisons for the second S-IVB burn mode are not shown. Due to insufficient tracking data, the trajectory for the out-of-orbit burn was constructed by constraining the telemetered velocities to parking orbit and translunar trajectory solutions. The LVDC and postflight trajectory state vectors are in very good agreement at TLI.

Platform system velocity measurements at significant event times are shown in Table 9-1 along with corresponding values from both the postflight and Operational Trajectories (OT). The differences between the telemetered

Table 9-1. Inertial Platform Velocity Comparisons (PACSS 12 Coordinate System)

EVENT	DATA SOURCE	VELOCITY - M/S (FT/S)		
		VERTICAL (X)	CROSSRANGE (Y)	DOWN RANGE (Z)
S-IC OECO	Guidance (LVDC)	2657.71 (8719.52)	-6.70 (-21.98)	2201.53 (7222.87)
	Postflight Trajectory	2658.32 (8721.52)	-5.57 (-18.27)	2202.09 (7224.70)
	Operational Trajectory	2662.36 (8734.78)	-1.83 (-6.00)	2189.87 (7184.61)
S-II OECO	Guidance (LVDC)	3332.15 (10,932.25)	-0.55 (-1.80)	6802.55 (22,318.08)
	Postflight Trajectory	3333.57 (10,936.91)	0.93 (3.05)	6803.00 (22,319.55)
	Operational Trajectory	3334.11 (10,938.68)	-1.33 (-4.36)	6793.87 (22,289.60)
S-IVB First ECO	Guidance (LVDC)	3167.44 (10,391.86)	-0.15 (-0.49)	7600.88 (24,937.27)
	Postflight Trajectory	3168.90 (10,396.65)	1.22 (4.00)	7601.35 (24,938.81)
	Operational Trajectory	3170.86 (10,403.08)	0.05 (0.16)	7602.30 (24,941.93)
Parking Orbit Insertion	Guidance (LVDC)	3167.10 (10,390.75)	-0.15 (-0.49)	7602.50 (24,942.59)
	Postflight Trajectory	3168.57 (10,395.57)	1.21 (3.97)	7602.97 (24,944.13)
	Operational Trajectory	3170.46 (10,401.77)	0.05 (0.16)	7603.79 (24,946.82)
S-IVB Second ECO*	Guidance (LVDC)	1618.78 (5310.96)	47.26 (155.05)	2711.09 (8894.65)
	Postflight Trajectory	1621.09 (5318.54)	51.29 (168.27)	2708.50 (8886.15)
	Operational Trajectory	1623.37 (5326.02)	48.79 (160.07)	2710.89 (8894.00)
Translunar Injection*	Guidance (LVDC)	1620.20 (5315.62)	47.35 (155.35)	2714.55 (8906.00)
	Postflight Trajectory	1622.67 (5323.72)	51.41 (168.67)	2712.06 (8897.83)
	Operational Trajectory	1624.56 (5329.92)	48.86 (160.30)	2713.89 (8903.84)

*Values represent velocity change from Time Base 6.

NOTE: Unless otherwise noted the event times quoted in this section are range time of actual occurrence as recorded at the vehicle (i.e. no transmission delay).

and postflight trajectory data reflect some combination of guidance hardware errors and tracking errors along with the probable down range velocity bias of -0.25 m/s (-0.82 ft/s) during boost-to-EPO. When the navigator was updated at about 6311.6 seconds (1:45:11.6), the velocity bias was eliminated. The differences between the telemetered and OT values reflect differences in actual and nominal performance and environmental conditions. The values shown for the second S-IVB burn mode represent component velocity changes from T_6. The characteristic velocity determined from the telemetered velocities during second burn to Engine Cutoff (ECO) was 2.20 m/s (7.22 ft/s) less than the OT due to an approximately 5.4 second shorter burn time. The telemetered data indicated 0.85 m/s (2.79 ft/s) greater than the postflight trajectory. This difference is probably due to small inaccuracies in the vector components to which the guidance velocities were constrained to generate the out-of-orbit trajectory. The measured velocity increase due to thrust decay between ECO and TLI was 0.53 m/s (1.74 ft/s) greater than the OT. The velocity increase after first S-IVB ECO was 0.13 m/s (0.43 ft/s) higher than the OT.

Comparison of navigation (PACSS 13) positions, velocities, and flight path angle at significant flight event times are shown in Table 9-2. Position and velocity component differences between the LVDC and OT values for the boost-to EPO data reflect off-nominal flight environment and vehicle performance. The navigation update is reflected in the differences at T_6, second ECO, and TLI. First guidance cutoff signal was given with only 0.03 m/s (0.10 ft/s) and a radius vector of 23 meters (75 feet) less than the OT prediction. Second S-IVB ECO was given with C_3 deviation of 7272 m^2/s^2 (OT minus LVDC). The LVDC and postflight trajectory data are in good agreement for the events shown. The magnitude of the component position and velocity differences at EPO are comparable to those noted on previous Saturn V vehicles. However, the postflight inertial coordinates of altitude and range were greater than those from the LVDC. On previous flights, the altitude and range deviations were small or of opposite sign and minimized the error in radius vector. Figures 9-2 through 9-5 show the state vector differences between the postflight trajectory and LVDC during parking orbit. The LVDC data were projected from time of update (6328.533 seconds [1:45:28.533] from Guidance Reference Release [GRR]) to T_6 to show what the deltas would have been without an update. Vent thrust was higher than the programed values used in the LVDC. Figure 9-6 presents the continuous vent thrust profile used in the LVDC along with the postflight reconstruction and nominal profiles. The continuous vent acceleration was reconstructed from telemetered velocities adjusted for acceleration bias. AS-510 vent thrust was higher than the OT nominal but within the predicted tolerance. The deviations between the postflight trajectory and the LVDC state vectors at EPO were propagated to TLI plus 9 hours to determine a Midcourse Correction (MCC). Using the programed vent, a MCC of about 6.4 m/s (21.0 ft/s) would be required. The EPO deviations combined with the reconstructed vent yielded about 8.6 m/s (28.2 ft/s) MCC. Due to the state vector differences at EPO and the buildup during parking orbit between tracking and LVDC telemetry, a decision was made to update the LVDC state vector. The basis for AS-510

Table 9-2. Guidance Comparisons (PACSS 13)

EVENT	DATA SOURCE	POSITIONS METERS (FT)				VELOCITIES M/S (FT/S)				FLIGHT PATH ANGLE (DEG)
		X_S	Y_S	Z_S	R	$\dot{X}_S$	$\dot{Y}_S$	$\dot{Z}_S$	V_S	γ
S-IC OECO	Guidance (LVDC)	6,439,574.3 (21,127,212.3)	29,652.9 (97,286.4)	159,631.5 (523,725.4)	6,441,620.7 (21,133,926.2)	934.69 (3066.57)	59.54 (195.34)	2590.62 (8499.41)	2754.72 (9037.80)	21.26006
	Postflight Trajectory	6,439,630.4 (21,127,396.5)	29,740.7 (97,574.4)	159,696.4 (523,938.5)	6,441,679.0 (21,134,117.3)	935.48 (3069.17)	60.65 (199.00)	2592.07 (8504.18)	2756.38 (9043.26)	21.26575
	Operational Trajectory	6,439,827.0 (21,128,040.0)	29,830.0 (97,869.0)	158,990.0 (521,621.0)	6,441,858.0 (21,134,705.0)	944.23 (3097.86)	64.40 (211.28)	2578.99 (8461.24)	2747.20 (9012.99)	21.5234
S-II OECO	Guidance (LVDC)	6,276,039.1 (20,590,679.1)	51,239.1 (168,107.3)	1,869,081.1 (6,132,155.8)	6,548,645.4 (21,485,057.1)	-1991.80 (-6534.78)	47.60 (156.17)	6704.61 (21,996.75)	6994.38 (22,947.44)	0.04164
	Postflight Trajectory	6,276,515.3 (20,592,241.8)	51,870.3 (170,178.3)	1,869,349.2 (6,133,035.5)	6,549,183.2 (21,486,821.7)	-1990.05 (-6529.03)	49.01 (160.80)	6705.82 (22,000.71)	6995.04 (22,949.62)	0.05939
	Operational Trajectory	6,274,978.0 (20,587,199.0)	51,382.0 (168,577.0)	1,872,731.0 (6,144,129.0)	6,548,672.0 (21,485,146.0)	-1995.05 (-6545.44)	46.71 (153.25)	6694.26 (21,962.78)	6985.37 (22,917.89)	0.0251
S-IVB First ECO	Guidance (LVDC)	5,883,387.2 (19,302,451.4)	57,548.0 (188,805.8)	2,866,607.7 (9,404,880.9)	6,544,837.5 (21,472,564.0)	-3418.24 (-11,214.70)	38.67 (126.87)	7013.80 (23,011.15)	7802.51 (25,598.79)	-0.00313
	Postflight Trajectory	5,884,137.0 (19,304,911.5)	58,364.4 (191,484.3)	2,866,935.6 (9,405,956.7)	6,545,669.9 (21,475,295.0)	-3415.93 (-11,207.13)	39.67 (130.14)	7014.20 (23,012.47)	7801.87 (25,596.69)	0.01318
	Operational Trajectory	5,869,872.0 (19,258,110.0)	57,702.0 (189,312.0)	2,894,215.0 (9,495,457.0)	6,544,861.0 (21,472,642.0)	-3451.00 (-11,322.18)	38.33 (125.74)	6997.70 (22,958.32)	7802.48 (25,598.68)	-0.0021
Parking Orbit Insertion	Guidance (LVDC)	5,848,776.8 (19,188,900.3)	57,930.7 (190,061.4)	2,936,557.3 (9,634,374.3)	6,544,838.8 (21,472,568.2)	-3502.03 (-11,489.60)	37.92 (124.41)	6974.15 (22,881.07)	7804.13 (25,604.10)	-0.00045
	Postflight Trajectory	5,849,555.2 (19,191,454.2)	58,757.4 (192,773.8)	2,936,888.9 (9,635,462.3)	6,545,690.6 (21,475,362.8)	-3499.89 (-11,482.59)	38.95 (127.79)	6974.72 (22,882.93)	7803.68 (25,602.63)	0.01506
	Operational Trajectory	5,834,941.0 (19,143,509.0)	58,082.0 (190,558.0)	2,963,999.0 (9,724,407.0)	6,544,861.0 (21,472,641.0)	-3534.66 (-11,596.64)	37.63 (123.45)	6957.54 (22,826.57)	7804.01 (25,603.70)	-0.0002
Time Base 6	Guidance (LVDC)	673,941.3 (2,211,093.5)	-95,762.2 (-314,180.4)	-6,516,853.3 (-21,380,752.3)	6,552,308.3 (21,497,074.5)	7763.65 (25,471.29)	36.57 (119.98)	797.78 (2617.39)	7804.62 (25,605.71)	0.03331
	Postflight Trajectory	676,024.7 (2,217,928.9)	-96,101.1 (-315,293.3)	-6,516,395.7 (-21,379,251.0)	6,552,072.8 (21,496,301.8)	7763.27 (25,470.04)	36.72 (120.47)	800.72 (2627.04)	7804.54 (25,605.45)	0.03005
	Operational Trajectory	665,763.0 (2,184,260.0)	-95,069.0 (-311,905.0)	-6,515,630.0 (-21,376,740.0)	6,550,246.0 (21,490,307.0)	7765.59 (25,477.67)	35.98 (118.03)	787.38 (2583.25)	7805.49 (25,608.57)	0.0408
S-IVB Second ECO	Guidance (LVDC)	6,395,354.9 (20,982,135.5)	-8802.9 (-28,880.9)	-1,934,222.1 (-6,345,873.0)	6,681,456.2 (21,920,768.1)	4376.67 (14,359.15)	168.45 (552.66)	9930.29 (32,579.69)	10,853.31 (35,607.57)	6.95644
	Postflight Trajectory	6,395,749.4 (20,983,429.7)	-8395.0 (-27,542.7)	-1,934,482.0 (-6,346,725.8)	6,681,908.5 (21,922,272.0)	4376.14 (14,357.41)	172.91 (567.29)	9930.01 (32,578.78)	10,852.91 (35,606.66)	6.95230
	Operational Trajectory	6,411,726.0 (21,035,845.0)	-7727.0 (-25,352.0)	-1,892,487.0 (-6,208,947.0)	6,685,192.0 (21,933,044.0)	4341.42 (14,243.51)	169.09 (554.76)	9942.75 (32,620.58)	10,850.57 (35,598.98)	7.1417
Translunar Injection	Guidance (LVDC)	6,438,694.1 (21,124,324.5)	-7116.4 (-23,347.8)	-1,834,786.6 (-6,019,641.1)	6,695,018.6 (21,965,284.1)	4292.53 (14,083.10)	168.76 (553.67)	9958.91 (32,673.59)	10,845.93 (35,583.76)	7.40978
	Postflight Trajectory	6,439,097.6 (21,125,648.2)	-6663.4 (-21,861.7)	-1,835,023.3 (-6,020,417.8)	6,695,471.0 (21,966,768.6)	4292.17 (14,081.92)	173.23 (568.35)	9958.67 (32,672.79)	10,845.63 (35,582.79)	7.40753
	Operational Trajectory	6,454,723.0 (21,176,914.0)	-6035.0 (-19,799.0)	-1,792,907.0 (-5,882,240.0)	6,699,105.0 (21,978,690.0)	4256.99 (13,966.49)	169.34 (555.58)	9970.24 (32,710.77)	10,842.34 (35,571.98)	7.5957

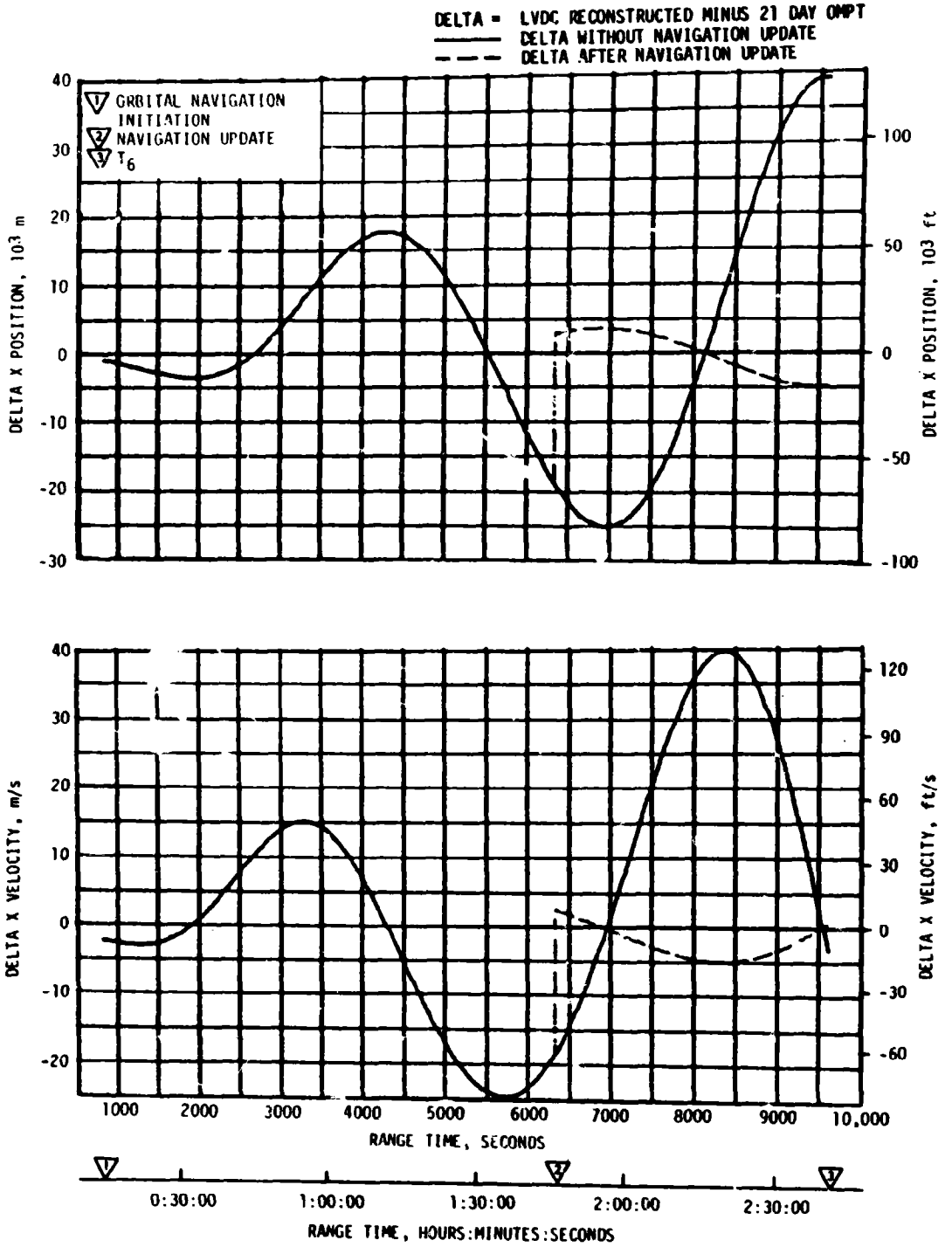

Figure 9-2. LVDC/21 Day OMPT X Position and Velocity Comparisons at EPO

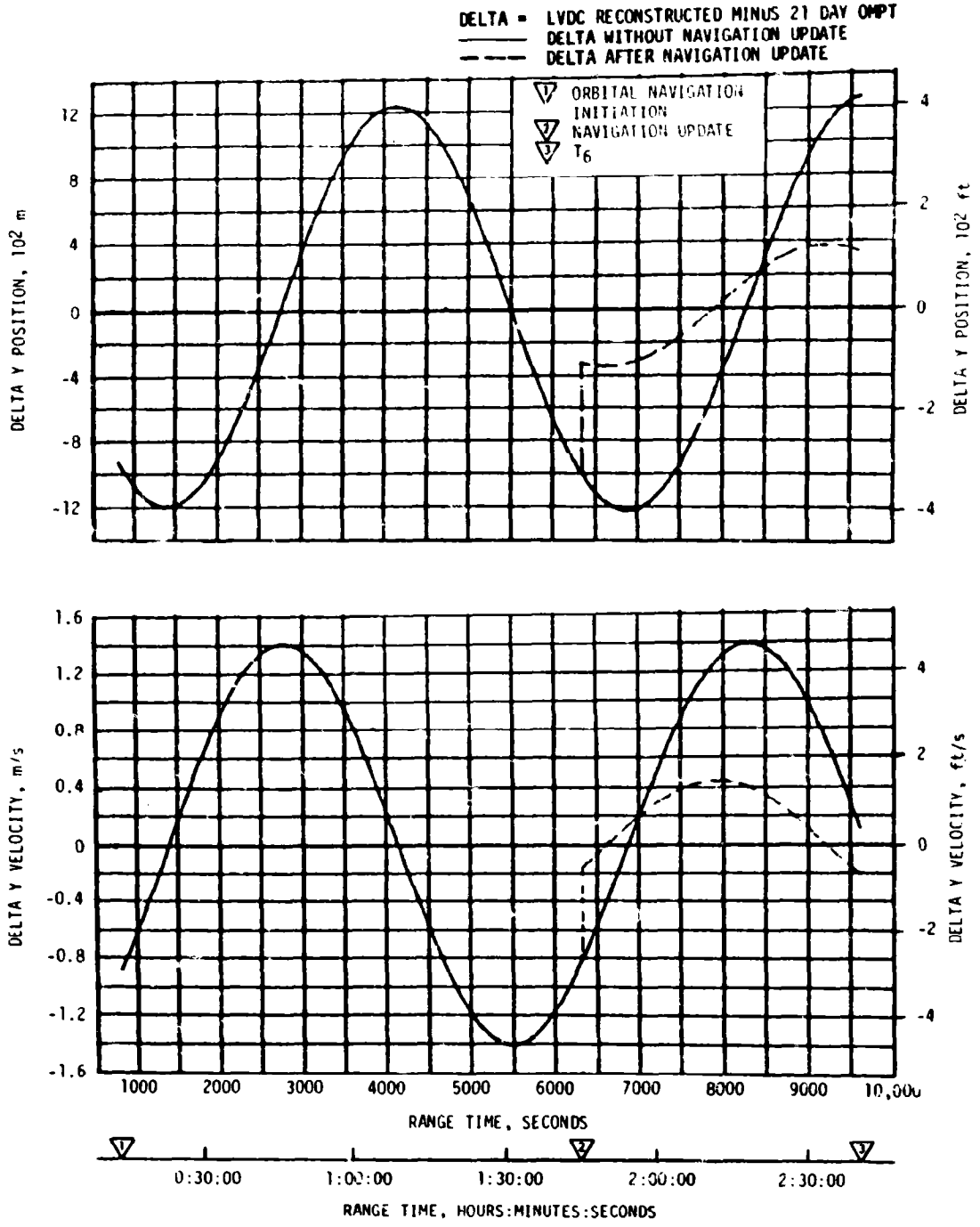

Figure 9-3. LVDC/21 Day OMPT Y Position and Velocity Comparisons at EPO

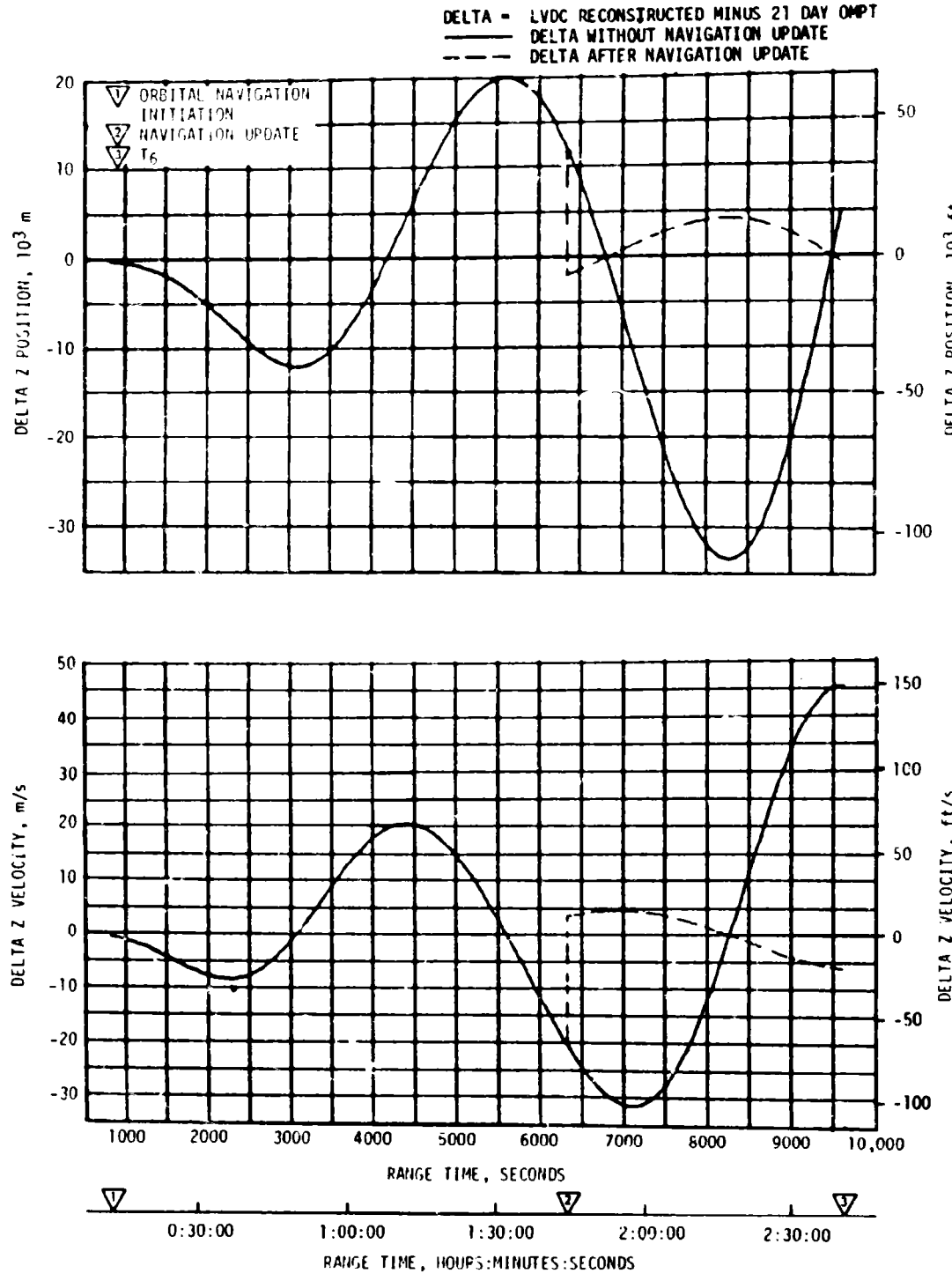

Figure 9-4. LVDC/21 Day OMPT Z Position and Velocity Comparisons at EPO

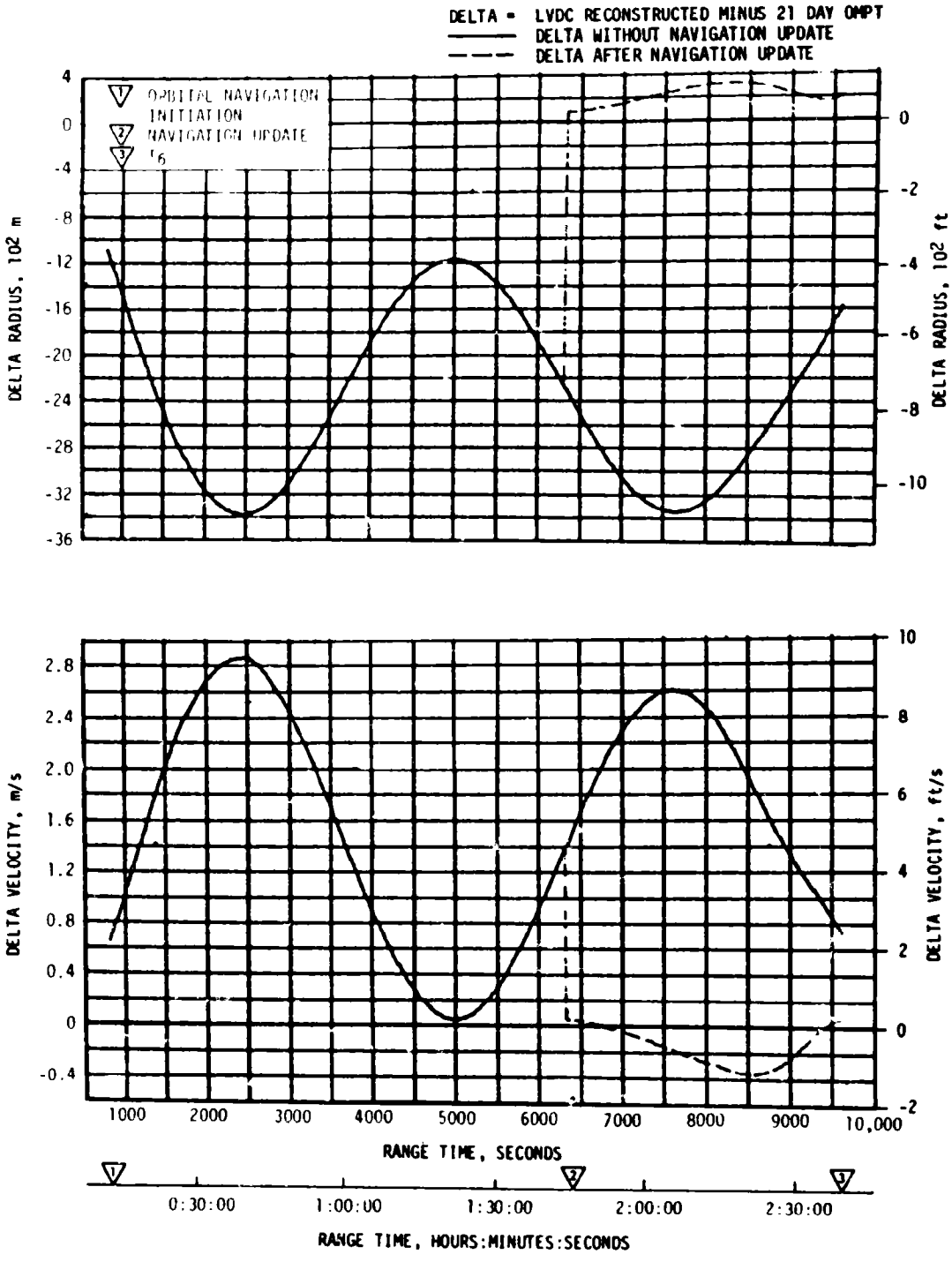

Figure 9-5. LVDC/21 Day OMPT Radius and Velocity Comparisons at EPO

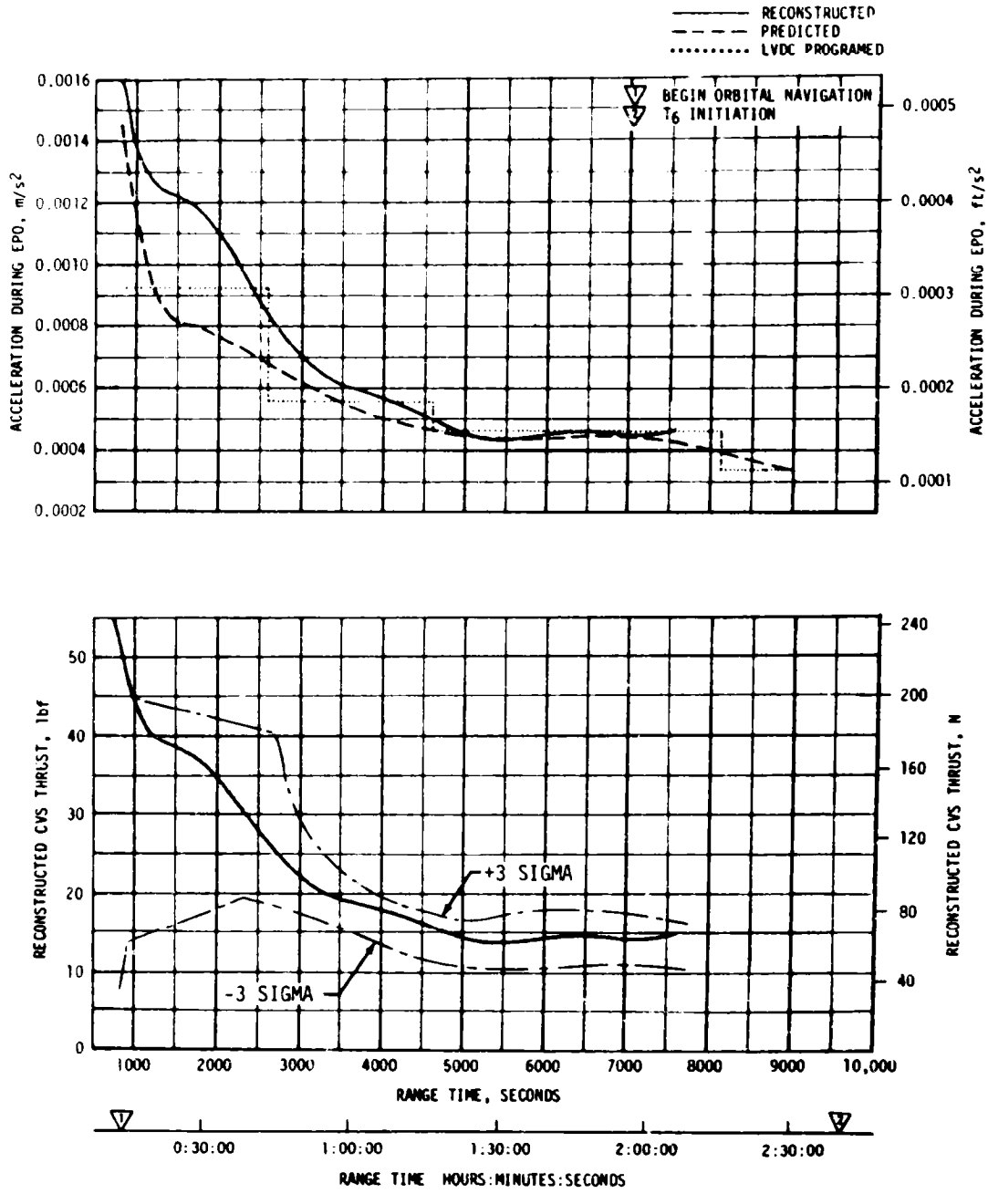

Figure 9-6. AS-510 Acceleration and CVS Thrust During EPO

update was any one of three parameters outside of 1.6 sigma. Update comparisons are discussed in paragraph 9.3 Table 9-3 presents the state vector differences at TLI between the LVDC and both the OT and postflight trajectory. The LVDC telemetry indicated a radius vector 4086 meters (13,406 ft) lower than the OT and 452 meters (1484 ft) lower than the postflight trajectory. LVDC total velocity was 3.59 m/s (11.78 ft/s) higher than the OT value and 0.30 m/s (0.98 ft/s) higher than the postflight trajectory. The LVDC and postflight trajectory were in very good agreement at TLI. Due to higher than expected S-IVB thrust, the proper cutoff conditions were met earlier than predicted. Table 9-4 shows the accuracy of the guidance system in achieving the targeted end conditions. The performance of the guidance system was satisfactory.

Table 9-3. State Vector Differences at Translunar Injection

PARAMETER	OPERATIONAL TRAJECTORY MINUS LVDC	POSTFLIGHT TRAJECTORY MINUS LVDC
ΔX_S, meters (ft)	16,029.0 (52,589.0)	403.5 (1323.7)
ΔY_S, meters (ft)	1081.0 (3549.0)	453.0 (1486.1)
ΔZ_S, meters (ft)	41,880,9 (137,401.0)	-236.7 (-776.7)
ΔR, meters (ft)	4086.0 (13,406.0)	452.4 (1484.5)
$\Delta \dot{X}_S$, m/s (ft/s)	-35.54 (-116.61)	-0.36 (-1.18)
$\Delta \dot{Y}_S$, m/s (ft/s)	0.58 (1.91)	4.47 (14.68)
$\Delta \dot{Z}_S$, m/s (ft/s)	11.33 (37.18)	-0.24 (-0.80)
ΔV_S, m/s (ft/s)	-3.59 (-11.78)	-0.30 (-0.98)

Table 9-4. First and Second Burn Terminal End Conditions

PARAMETER	TARGETED	ACTUAL	ERROR (ACT-TARG)
	FIRST BURN		
Terminal Velocity, m/s (ft/s)	7804.0613 (25,603.56)	7804.0725 (25,603.59)	0.0112 (0.037)
Radius, m (ft)	6,544,846.0 (21,472,330.8)	6,544,847.47 (21,472,335.58)	1.47 (4.823)
Path Angle, deg	0.0	-0.0008569	-0.0008569
Inclination, deg	29.684184	29.684265	0.000081
Descending Node, deg	109.33139	109.33047	-.000092
	SECOND BURN		
Eccentricity	0.976239353	0.976248033	0.000008680
Inclination, deg	29.70000941	29.70003996	0.00003055
Descending Node, deg	108.452407	108.452690	0.000283
Argument of Perigee, deg	137.040844	137.039504	-0.001340
Energy, C_3 m^2/s^2 (ft^2/s^2)	-1,438,863.99 (-15,487,414.00)	-1,438,340.30 (-15,481,777.19)	-523.69 (-5636.81)

9.3 NAVIGATION AND GUIDANCE SCHEME EVALUATION

9.3.1 Navigation Evaluation

The identification of the navigation error source has been emphasized by the implementation of a navigation update for the first time in the Saturn program. The implementation was required because the difference between the IU and tracking vectors at Carnarvon exceeded the tolerance defined in FMR 7-11. The agreement betwen tracking and the navigation solutions before and after second burn has focused attention on navigation performance during first burn and the first revolution of EPO.

Comparisons of navigation and final postflight trajectory solutions for significant event times are listed in Table 9-2. The velocity differences and position component differences at EPO are similar to those seen on the past five flights (Table 9-5). The AS-510 radius magnitude difference, however, is greater than that of any of the five preceding flights. The low navigator radius, caused by the X and Z component position errors adding rather than canceling, may have been sufficient to cause the subsequent violation of FMR 7-11. The propulsive vent during the early portion of the first revolution was higher than nominal and, therefore, tended to amplify the differences between tracking and IU navigation.

Table 9-5. Parking Orbit Insertion Difference Summary
(LVDC Telemetry - Final Trajectory)

PARAMETER	VEHICLE NUMBER				
	AS-506	AS-507	AS-508	AS-509	AS-510
X, m (ft)	464 (1522)	300 (984)	-521 (-1709)	349 (1145)	-778 (-2552)
Y, m (ft)	-1280 (-4199)	-523 (-1716)	-1573 (-5161)	-786 (-2579)	-827 (-2713)
Z, m (ft)	-243 (-797)	480 (1575)	504 (1654)	-638 (-2093)	-332 (-1089)
$\dot{X}$, m/s (ft/s)	-1.16 (-3.81)	1.05 (3.44)	-1.77 (-5.81)	0.83 (2.72)	-2.14 (-7.02)
$\dot{Y}$, m/s (ft/s)	-1.21 (-3.97)	-1.72 (-5.64)	-3.10 (-10.17)	-1.79 (-5.87)	-1.03 (-3.38)
$\dot{Z}$, m/s (ft/s)	-0.33 (-1.08)	.23 (0.75)	0.2 (0.66)	-0.37 (-1.21)	-0.57 (-1.87)
R, m (ft)	286 (938)	475 (1558)	-236 (-774)	17 (56)	-852 (-2795)
V, m/s (ft/s)	0.21 (0.69)	-0.61 (-2.00)	0.87 (2.85)	-0.72 (-2.36)	0.45 (1.48)

The inertial platform Z (down range) accelerometer output exhibited a negative shift of approximately 0.25 m/s (0.82 ft/s) (Figure 9-7). The shift was not representative of vehicle motion and remained as a Z velocity offset until the navigation update was implemented. The sampled measurement of the Z accelerometer float deflection indicated a maximum deflection of 2.9 degrees during the period where the shift first became evident (Figure 9-8). A float contact with a mechanical stop does not appear to be the probable cause of the velocity offset.

Both output pulse trains from one channel of the Z accelerometer were telemetered via FM channels having sufficient bandwidth to permit reconstruction of the Z accelerometer output (Figure 9-9). The velocity offset shift did not occur as a discrete event. The offset was accumulated over a one-second period while the output was oscillating at approximately 40 hertz.

The navigation update implemented at 6328.533 seconds (1:45:28.533), referenced to GRR, increased the orbit apogee by 2297 meters (7536 ft) and the perigee by 2752 meters (9029 ft) (Table 9-6). The estimated time remaining before restart preparations initiation was increased about seven seconds. The simulations required to determine the net effect of the navigation update have not been processed nor analyzed.

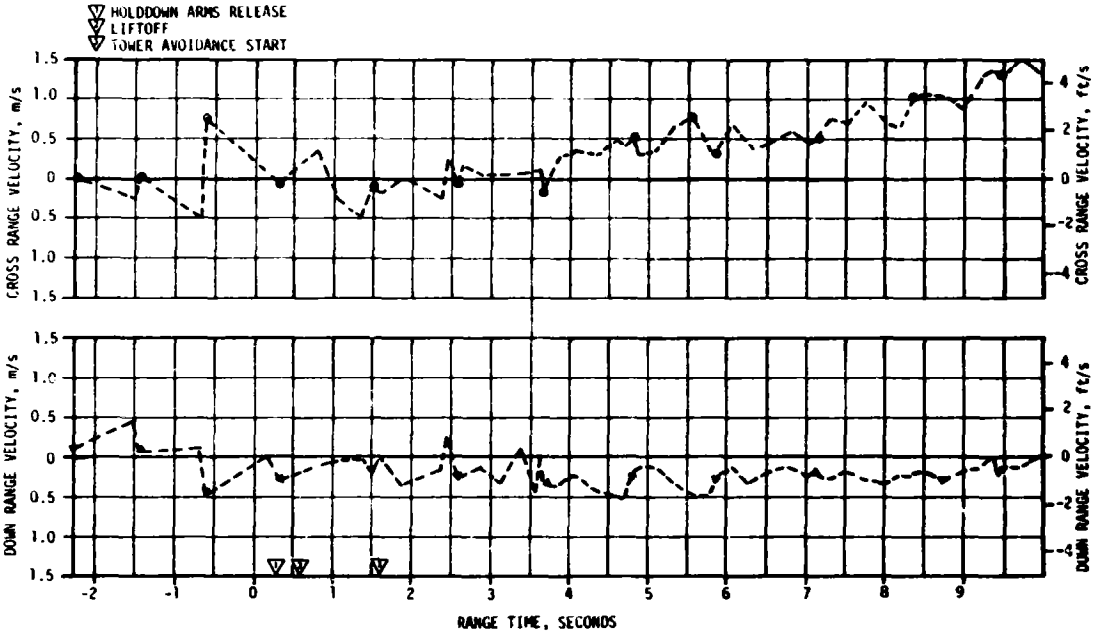

Figure 9-7. Lateral Measured Velocities at Liftoff

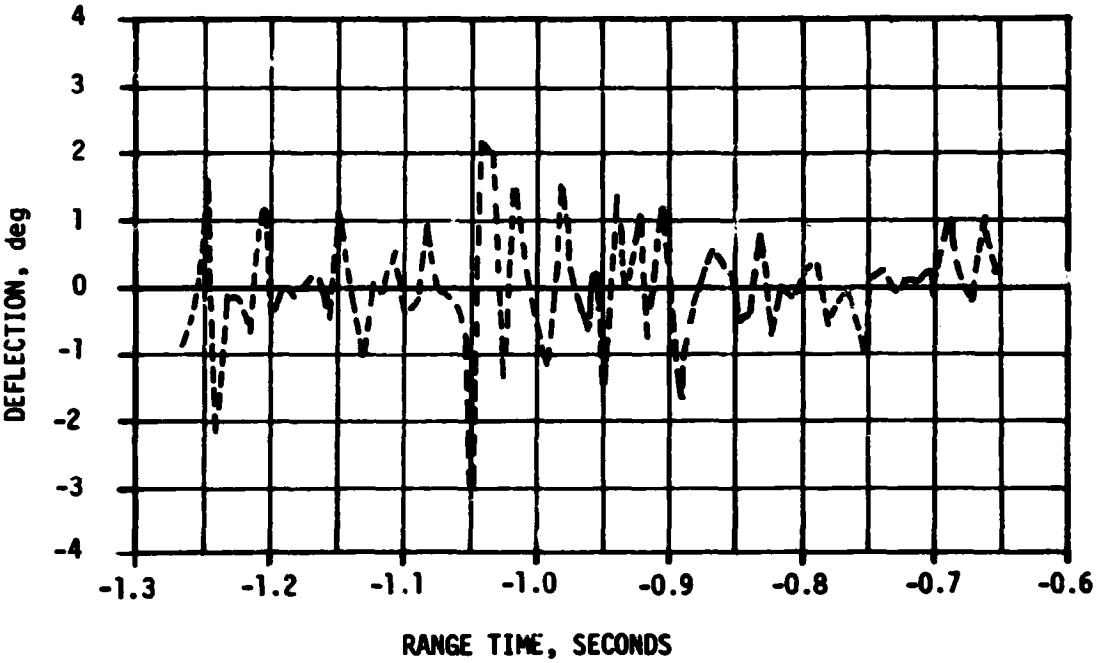

Figure 9-8. Z Accelerometer Float Deflection Before Liftoff

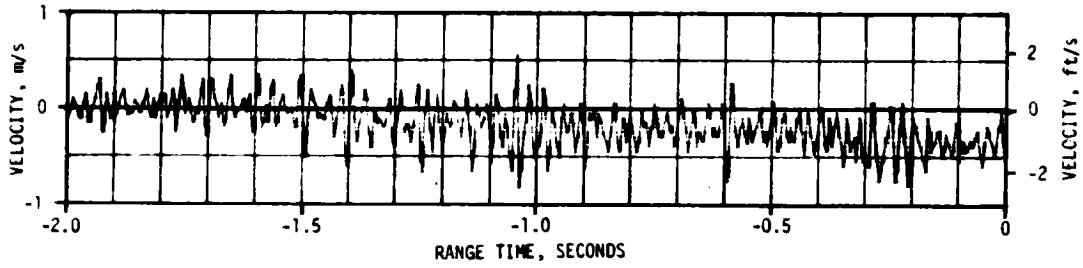

Figure 9-9. Z Inertial Velocity - Manual Pulse Count

Table 9-6. Navigation Update Comparisons

PARAMETER	NAVIGATION VECTOR PRECEDING UPDATE	ACTUAL UPDATE VECTOR	INITIAL UPDATE VECTOR
Time From GRR, sec	6324.05	6328.533*	6328.21
X, m (ft)	4,248,190.5 (13.937 x 10^6)	4,242,351.0 (13.918 x 10^6)	4,239,768.0 (13.910 x 10^6)
Y, m (ft)	81,279.0 (266.660 x 10^3)	82,104.0 (269.367 x 10^3)	82,349.0 (270.171 x 10^3)
Z, m (ft)	4,984,553.0 (16.353 x 10^6)	4,992,605.0 (16.380 x 10^6)	4,993,971.0 (16.384 x 10^6)
$\dot{X}$, m/s (ft/s)	-5940.2 (-19,488.6)	-5948.8 (-19,507.0)	-5948.2 (-19,514.9)
$\dot{Y}$, m/s (ft/s)	39.1 (128.3)	39.3 (128.9)	39.7 (130.2)
$\dot{Z}$, m/s (ft/s)	5059.4 (16,598.9)	5050.8 (16,570.7)	5048.8 (16,564.1)
R, m (ft)	6,549,770.791 (21.4885 x 10^6)	6,552,128.491 (21.4962 x 10^6)	6,551,500.622 (21.49416 x 10^6)
V, m/s (ft/s)	7802.886 (25,599.7)	7801.581 (25,595.4)	7802.118 (25,597.2)
Apogee Radius, m (ft)	6,556,125.065 (21.5094 x 10^6)	6,558,422.408 (21.5169 x 10^6)	6,558,305.644 (21.5165 x 10^6)
Perigee Radius, m (ft)	6,549,328.458 (21.4870 x 10^6)	6,552,080.3 (21.4961 x 10^6)	6,551,489.368 (21.4941 x 10^6)
Period, sec	5278.889	5281.94	5281.513

*Actual update time differs from loaded implementation time by 0.322 seconds because of LVDC navigation routine characteristics.

Tracking information and telemetered navigation data were acquired during the first pass over the Canary Islands ground station and were extrapolated forward to 3360 seconds (0:56:00). The extrapolation of the IU navigation was 16,313 meters (53,520 ft) farther down range than the tracking vector and the projected LVDC apogee was 2.46 kilometers (1.33 n mi) below that of the projected tracking vector. A comparison at Carnarvon at 3360 seconds (00:56:00) revealed differences of 14,545 meters (47,720 ft) and 2.134 kilometers (1.152 n mi). These exceeded the limits of 7268 meters (23,845 ft) and 1.759 kilometers (0.95 n mi) specified in FMR 7-11. The decision to perform a navigation update was based on Carnarvon data and a tentative update vector was generated based on Carnarvon tracking. The vector was uplinked at Goldstone to become effective at 6328.21 seconds (1:45:28.21), from GRR which was about the time of midpass over Vanguard. Goldstone tracking was then used to generate a vector for uplinking at Bermuda. The implementation time was the same as that loaded at Goldstone. This was a planned part of the procedure. The first vector was sent to assure some improvement. The implemented vector was based on later tracking data and was therefore less susceptible than the first to off-nominal vent perturbation.

9.3.2 Guidance Scheme Evaluation

Available data indicate that the events scheduled at preset times occurred within acceptable tolerances. All flight program routines, including variable launch azimuth, time tilt, iterative guidance, navigation and minor loop functions, were accomplished properly. Times of occurrence of major boost phase guidance and navigation events are shown in Table 9-7. Implementation of these events occurred within the one computation cycle tolerance following scheduled start and stop times. The navigation error apparent at parking orbit insertion may have accumulated during the boost period, but flight program navigation routines were properly implemented based upon measured input data.

9.3.2.1 First Boost Period

All first stage maneuvers were performed within predicted tolerances and Iterative Guidance Mode (IGM) performance for first boost was nominal. The steering commands telemetered during first boost are illustrated in Figures 9-10 and 9-11. Table 9-4 shows the terminal end conditions for first burn. Terminal conditions were obtained by linear forward extrapolation.

9.3.2.2 Earth Parking Orbit

Parking orbit guidance proceeded as expected. Table 9-8 presents the commanded steering angles for major events.

Real-time radar tracking data indicated a navigation error outside the allowable tolerance of FMR 7-11. Analysis of the flight program response to input data shows that the flight program performed properly based upon the data received through the LVDA.

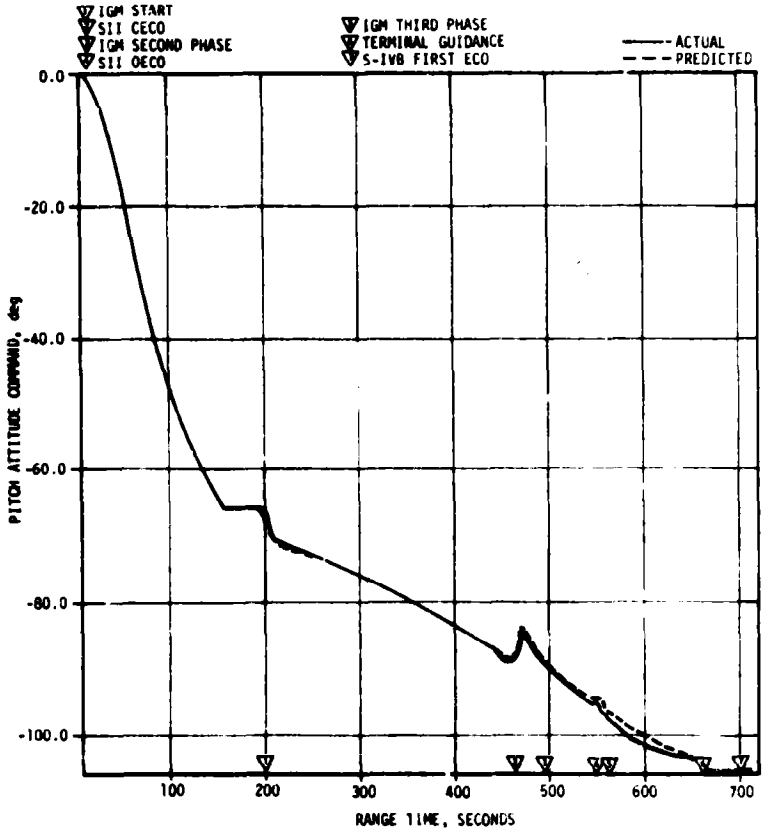

Figure 9-10. Rate-Limited Pitch Steering Command - AS-510 First Burn

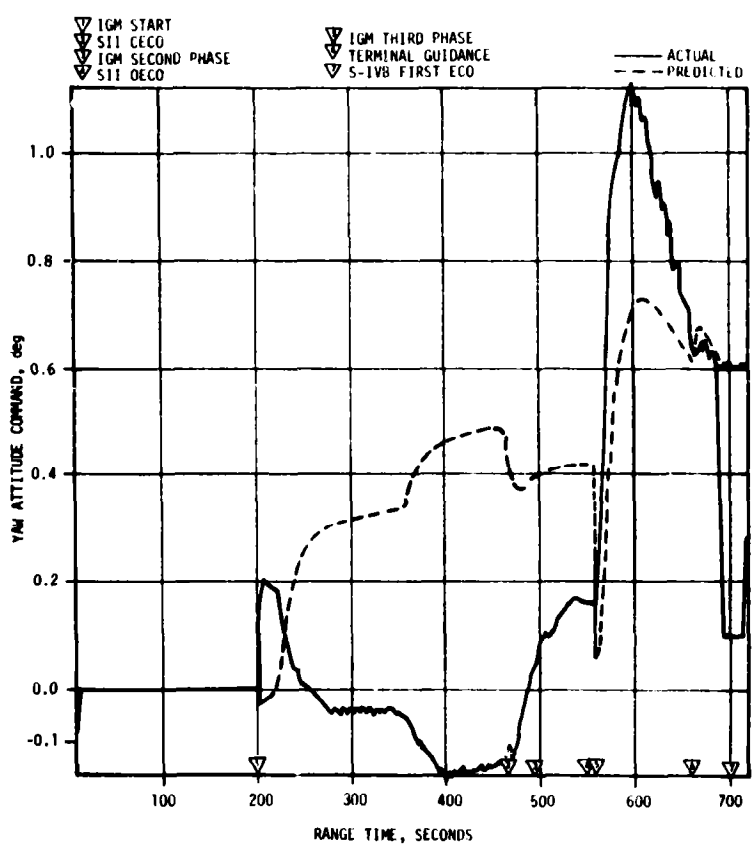

Figure 9-11. Rate-Limited Yaw Steering Command - AS-510 First Burn

Table 9-7. Boost Phase Guidance Event Times

EVENT	RANGE TIME AT THE VEHICLE, SECONDS			TIME IN BASE, SECONDS		
	ACTUAL	OPERATIONAL TRAJECTORY PREDICTED	ACTUAL MINUS OT	ACTUAL	NOMINAL	ACTUAL MINUS NOM
Begin Tower Clearance (+Yaw)	1.68	1.67	0.01	T_1 +1.107	T_1 +1.0	0.107
End Tower Clearance (-Yaw)	9.66	9.67	-0.01	T_1 +9.084	T_1 +9.0	0.084
Complete Tower Clearance	11.22	-	-	T_1 +10.644	T_1 +10.48	0.164
Start Pitch and Roll	12.21	11.64	0.57	T_1 +11.635	T_1 +11.07	0.565
End Roll	23.02	-	-	T_1 +22.443	T_1 +23.13	0.687
Freeze Pitch Command	156.17	156.00	0.17	T_2 +20.087	-	-
Stop Pitch	156.94	-	-	T_2 +20.854	-	-
Start IGM Guidance	202.62	200.64	1.98	T_3 +43.045	T_3 +41.82	1.225
SMC Enable	222.63	200.27	2.36	T_3 +63.053	T_3 +61.74	1.303
S-II CECO	459.56	459.03	0.53	T_3 +299.971	T_3 +299.96	0.011
S-II Low (4.8) EMR No. 1 On and Start Artificial Tau	483.71	483.77	-0.06	T_3 +324.128	T_3 +325.26	-1.132
End Artificial Tau	494.22	495.02	-0.80	T_3 +334.646	T_3 +336.11	-1.464
End Chi Freeze, Start 3rd Phase IGM and Artificial Tau	557.51	558.77	-1.26	T_4 +9.454	T_4 +9.49	-1.036
SMC Turn On	565.11	565.27	-0.16	T_4 +15.054	T_4 +15.20	0.854
End Artificial Tau	567.00	568.14	-1.14	T_4 +17.948	T_4 +18.92	-0.972
Start Terminal Guidance	663.00	665.64	-2.64	T_4 +113.950	T_4 +115.45	-1.500
Enter GM High Speed Cutoff (Chi Freeze)	687.80	691.77	-3.97	T_4 +138.748	T_4 +141.3	-2.552
S IVB Velocity Cutoff CMD	694.67	699.06	-4.39	T_4 +145.617	T_4 +148.66	-3.043
Start S-IVB Second Burn IGM	10,209.04	10,202.59	6.45	T_6 +584.209	T_6 +583.77	0.430
SMC Turn On	10,221.08	10,214.59	6.49	T_6 +596.248	T_6 +594.57	1.678
Mixture Ratio Control Valve Close and Start Artificial Tau	10,258.79	10,252.59	6.20	T_6 +633.953	T_6 +663.96	-0.047
End Artificial Tau	10,289.58	10,282.59	6.99	T_6 +664.753	T_6 + 663.01	1.743
Start Terminal Guidance	10,526.37	10,524.59	1.98	T_6 +901.542	T_6 +906.12	-4.578
End IGM Begin Chi Freeze	10,551.42	10,550.84	1.58	T_6 +926.590	T_6 +932.65	-6.060
S-IVB 2nd Guidance Cutoff CMD	10,553.61	10,552.73	0.88	T_6 +928.780	T_6 +934.32	-5.540

Table 9-8. Coast Phase Guidance Steering Commands at Major Events

FLIGHT PERIOD	EVENT	TIME, SECONDS	COMMANDED STEERING ANGLES, DEGREES		
			ROLL (X)	PITCH (Y)	YAW (Z)
Earth Parking Orbit	Initiate Orbital Guidance Chi Freeze	T_5 +0	-0.1646	-104.2746	0.0976
	Initiate Maneuver to Local Horizontal	T_5 +21.402	0.0000	-117.4047	0.2708
	Initiate Orbital Navigation	T_5 +100.799	-	-	-
Post TLI	Initiate Orbital Guidance Chi Freeze	T_7 +0	-0.5218	-68.0302	1.4565
	Initiate Orbital Navigation	T_7 +152.034	-	-	-
	Initiate Maneuver to Local Horizontal	T_7 +152.257	0.0000	-86.7123	0.8978
	Initiate TD&E Maneuver	T_7 +900.700	180.000	-12.8739	-39.6221
	TD&E Maneuver Complete	T_7 +1200	-	-	-
	Initiate Lunar Impact Local Reference Maneuver	T_8 +581.124	180.000	16.6985	-40.0797

A navigation update was commanded through the Goldstone telemetry station at T_5 +4682 seconds with an implementation time of T_5 +5616.4 seconds. The mode and data commands making up the navigation update were properly stored by the flight program. After further tracking a revised navigation update was commanded at T_5 +5376 seconds with an implementation time the same as for the first update. The revised update properly replaced the original update and was implemented at the proper time. At the time of implementation of the update orbital time-to-go (time until start of T_6) showed a shift of approximately 6.7 seconds. The shift in state vector parameters showed a decrease in down range displacement and an increase in altitude.

9.3.2.3 Second Boost Period

Sequencing of restart preparations occurred as scheduled relative to the start of T_6. T_6 was initiated at 9641.772 seconds (2:40:41.772) after GRR (9624.832 seconds [2:40:24.832]). Transfer ellipse target parameters were computed and telemetered just prior to initiation of second burn IGM.

The guidance steering commands are shown in Figures 9-12 and 9-13.

Table 9-4 shows the terminal end conditions for the S-IVB second burn. Terminal conditions were obtained by linear forward extrapolation. Targeted values were those telemetered at GRR and at second burn IGM start.

9.3.2.4 Post TLI Period

Post TLI guidance proceeded as expected. Table 9-8 presents the commanded steering angles for some major events.

Two lunar impact ullage burns were commanded from Mission Control Center-Houston (MCC-H) at 19,629 seconds (5:27:09.0) and 35,486 seconds (9:51:26.0), respectively. The first burn of 241 seconds duration was started at the commanded time of 20,760 seconds (5:46:00.0). The second burn was commanded to start at 36,000 seconds (10:00:00.0) with a duration of 71 seconds. Both burns were properly implemented by the flight program with the desired attitude changes occurring upon acceptance of the Digital Command System (DCS) commands and the ignition and burn durations occurring as commanded.

The solar heating avoidance roll maneuver was commanded at T_8 +20,362 seconds (5:39:22) followed by the Flight Control Computer (FCC) power off command at T_8 +20,383 seconds (5:39:43). No further maneuver capability existed after this time.

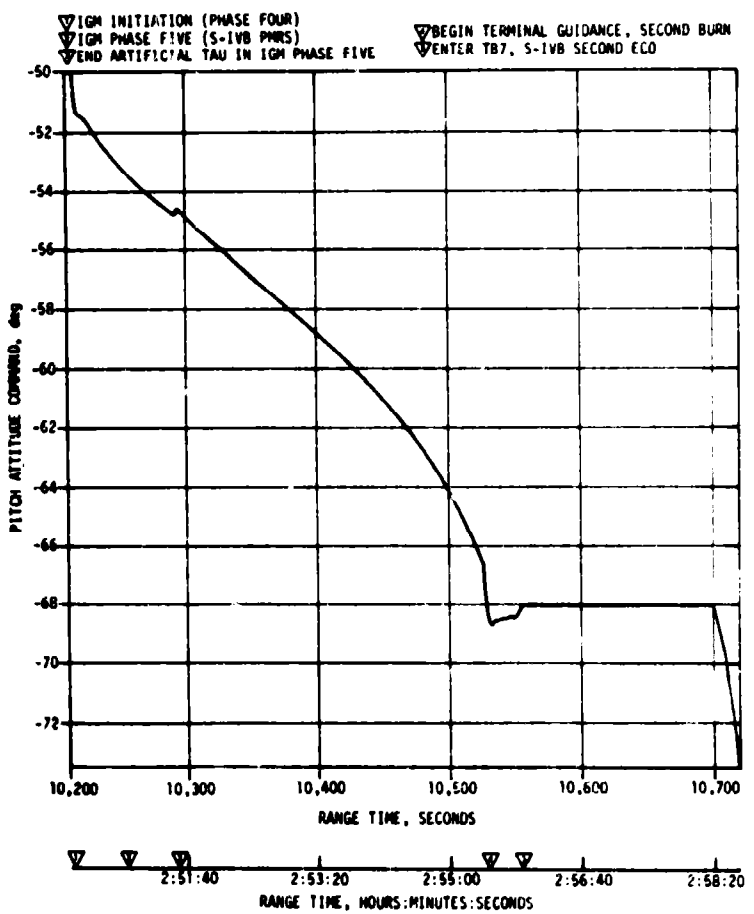

Figure 9-12. Rate-Limited Pitch Steering Command - AS-510 Second Burn

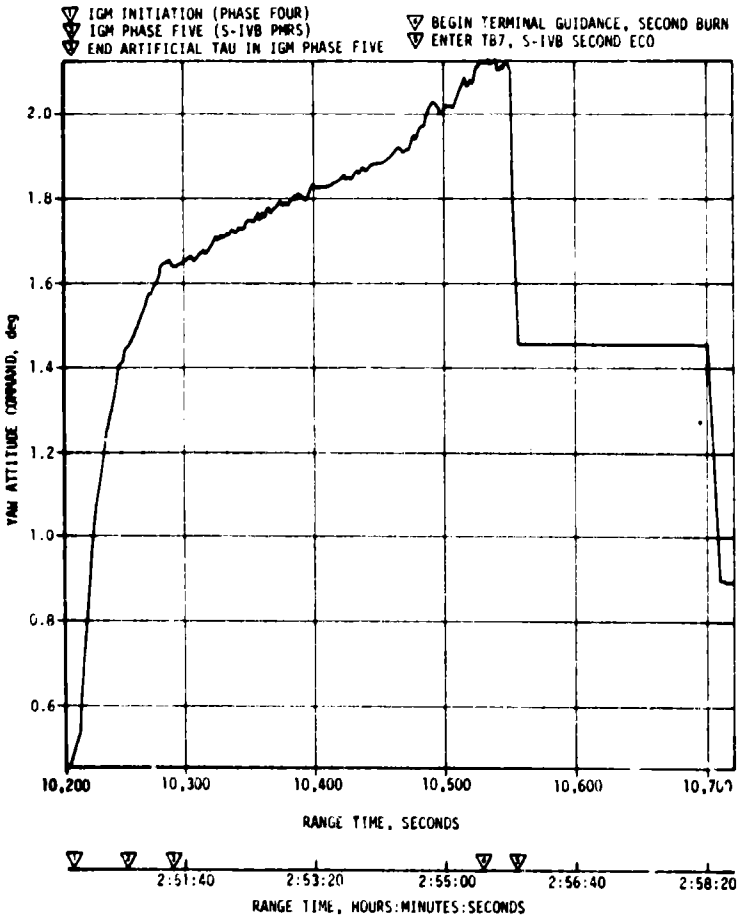

Figure 9-13. Rate-Limited Yaw Steering Command - AS-510 Second Burn

9.4 GUIDANCE SYSTEM COMPONENT EVALUATION

Data analysis results indicate that the LVDA and LVDC performed as predicted for the AS-510 mission. Component temperatures and voltages were nominal.

9.4.1 LVDC and LVDA

Two occurrences of error monitor register Bit 3 indications of a signal disagreement at the LVDA Interrupt Control Latch (INTC) were observed. The first occurred at GRR as a result of the GRR interrupt and the second occurred at GRR +5401 seconds (1:30:01) as a result of a DCS interrupt. As in previous missions, these signal disagreements were expected and did not affect mission success.

No indication of malfunction was observed in any hardware, including attitude error, telemetry, discrete, and switch selector command output circuitry.

9.4.2 ST-124M Stabilized Platform Subsystem

The ST-124M Stabilized Platform Subsystem (SPS) performed nominally throughout the mission. All electrical and environmental parameter data indicated operation was within previously observed operating limits.

A velocity shift of approximately -0.25 m/s (-0.82 ft/s) in the Z axis at approximately -1.4 seconds was indicated by LVDA data. This was verified by counting pulses on oscillograms of telemetered accelerometer outputs, (Figure 9-9). The Z accelerometer gyro pickoff was relatively quiet at the time of the velocity shift. Investigation of the cause of the velocity shift is in progress.

Typical servo loop operation was indicated by the telemetry data. Minimal excursions were observed at liftoff (see Figure 9-14). The 5 hertz oscillations were again evident before and after S-IC CECO at approximately the same amplitude of previous vehicles (0.3°P-P).

CSM separation caused the following deflections:

X gyro = 0.8°P-P
Y gyro = 0.8°P-P
Z gyro = 0.4°P-P

The accelerometer servo loop operation appeared to be nominal. On this vehicle the pickoff information was telemetered on the CP-1 link only. Figure 9-14 depicts the excursions of the three pickoffs. As can be seen the Z channel was relatively quiet at -1.4 seconds.

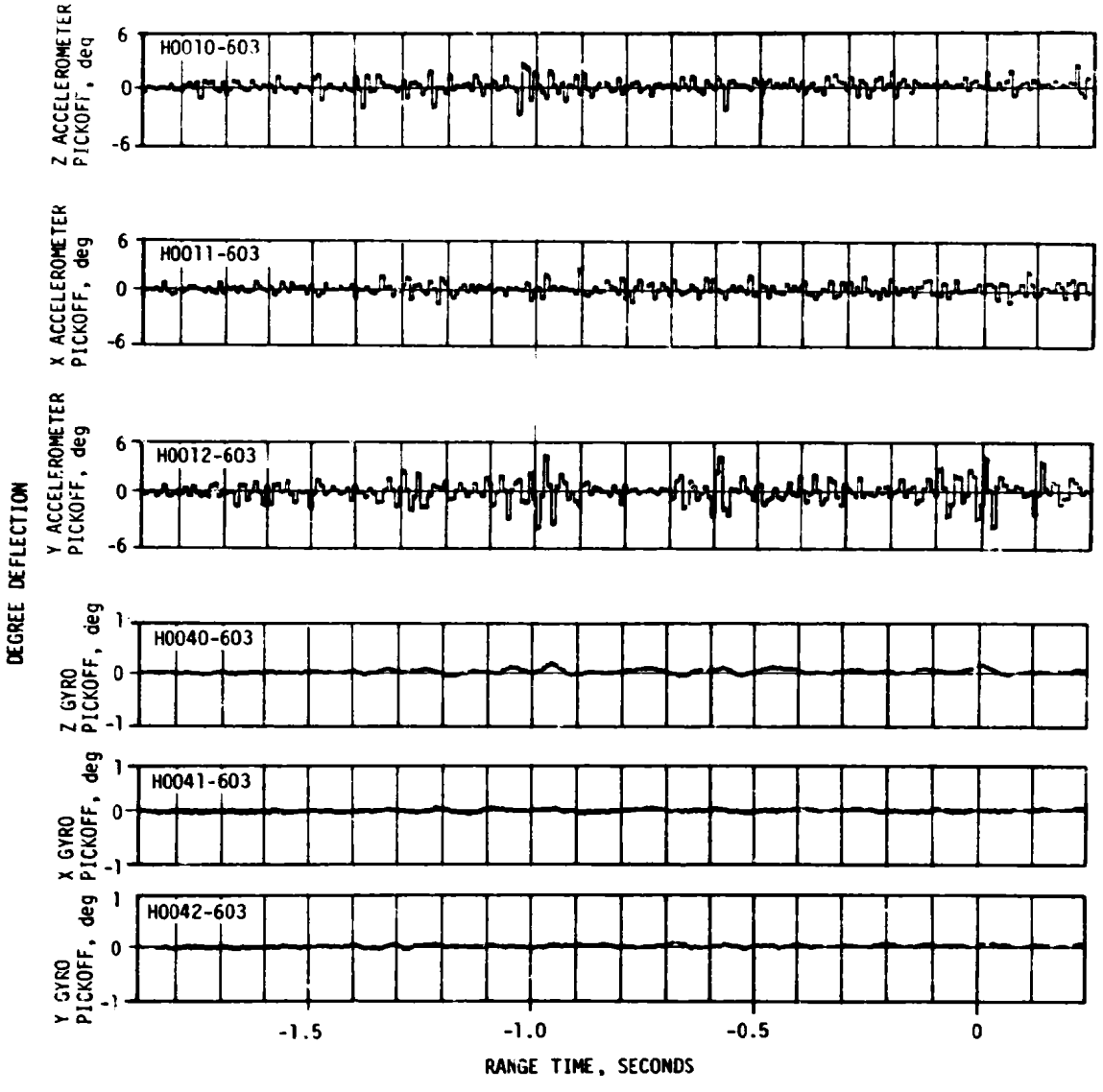

Figure 9-14. ST-124M Accelerometer and Gyro Pickoff Deflections Near Liftoff

At CSM separation the accelerometer pickoff deflections were:

X = 1.8°P-P
Y = 1.8°P-P
Z = 1.2°P-P

Proper vehicle attitude information was derived from the gimbal angle resolvers. The flight program did not switch from fine to backup gimbal resolvers.

As on the AS-509 IU, the inertial gimbal temperature at liftoff was 315°K (107°F). The typical decrease in temperature occurred after liftoff, bottoming out at 309.7°K (98.0°F) at 26,700 seconds (7:25:00.0), then rising to 310.7°K (99.5°F) at 42,200 seconds (11:43:20.0) (last data).

The gas bearing differential and internal ambient pressures remained within desired limits throughout the mission.

The platform AC power supply maintained proper voltages. Gyro and accelerometer wheel power remained constant as depicted by the summation current data.

SECTION 10

CONTROL AND SEPARATION

10.1 SUMMARY

The Flight Control Computer (FCC), Thrust Vector Control (TVC) System, and Auxiliary Propulsion System (APS) satisfied all requirements for vehicle attitude control during the flight. Bending and slosh dynamics were adequately stabilized. The prelaunch programed yaw, roll, and pitch maneuvers were properly executed during S-IC boost.

During the maximum dynamic pressure region of flight, the launch vehicle experienced winds that were slightly greater than the 95-percentile July wind from a 63 degree azimuth. The maximum average pitch engine deflection occurred in the maximum dynamic pressure region. The maximum average yaw engine deflection occurred during the yaw maneuver for tower clearance.

S-IC/S-II first and second plane separations were accomplished with no significant attitude deviations. The S-IC retro motors performed as expected. Separation distances were less than predicted because F-1 engine impulse "tailoff" was higher than expected. The effect of the closer S-II exhaust plume at engine start resulted in a more severe environment at the S-IC forward LOX dome and resulted in S-IC telemetry system damage. Analysis indicates that with an S-IC stage having only four retro motors, failure of one retro motor to ignite would result in marginal separation distances and, in the 3σ case, recontact of the two stages. Consequently, S-IC-11 and subsequent stages will be equipped with eight retro motors rather than the planned four. At Iterative Guidance Mode (IGM) initiation, guidance commanded a pitch-down maneuver as predicted. The S-II retro motors and S-IVB ullage motors performed as expected and provided a normal S-II/S-IVB separation.

Satisfactory control of the vehicle was maintained during first and second S-IVB burns and during coast in Earth Parking Orbit (EPO). After insertion the maneuver to the local horizontal required a larger change in vehicle attitude than on previous vehicles. Propellant slosh activity resulting from this pitch maneuver was greater than previously experienced and caused liquid to flow into the forward portion of the LOX tank and vent through the LOX nonpropulsive vent. For subsequent missions this condition will be corrected by reducing the pitch turning rate during the maneuver.

During the Command and Service Module (CSM) separation from the S-IVB/Instrument Unit (IU) and during the Transposition, Docking and Ejection (TD&E) maneuver, the control system maintained the vehicle in a fixed inertial attitude to provide a stable docking platform. Following TD&E, S-IVB/IU attitude control was maintained during the evasive maneuver, the maneuver to lunar impact attitude, the LOX dump, and the APS burns.

10.2 S-IC CONTROL SYSTEM EVALUATION

The AS-510 control system performed satisfactorily during S-IC boost.

Because of changes in structural dynamics, the AS-510 control system filters were different than those of the AS-509. In addition, the control system gains were increased to improve wind and engine-out response.

The peak wind speed was 18.59 m/s (36.2 knots) at 14 kilometers (7.6 n mi) with an azimuth of 63 degrees. This wind was greater than the 95-percentile July wind from this direction. Approximately 10 percent of the available pitch plane engine deflection was used (based on the average pitch engine gimbal angle). The S-IC outboard engines were canted as planned.

All dynamics were within vehicle capability. In the region of high dynamic pressure the maximum angles of attack were 2.63 degrees in pitch and 1.34 degrees in yaw. The maximum average pitch and yaw engine deflections in the maximum dynamic pressure region were 0.54 and 0.26 degree, respectively. Both deflections were due to wind shears. The absence of divergent bending or slosh dynamics shows that these modes were adequately stabilized.

Vehicle attitude errors required to trim out the effects of thrust unbalance, thrust misalignment, and control system misalignments were within predicted envelopes. Vehicle dynamics prior to S-IC/S-II first plane separation were within staging requirements.

Maximum control parameters during S-IC burn are listed in Table 10-1. Pitch and yaw time histories are shown in Figures 10-1 and 10-2. Dynamics between liftoff and 40 seconds result primarily from guidance commands. Between 40 and 100 seconds, maximum dynamics were caused by the pitch tilt program, wind magnitude, and wind shears. Dynamics from 100 seconds to separation were caused by high altitude winds, separated airflow aerodynamics, Center Engine Cutoff (CECO), and tilt arrest. The transient at CECO indicates that the center engine cant was 0.23 degree in pitch and 0.0 degree in yaw.

The attitude errors between liftoff and 20 seconds indicate that the equivalent thrust vector misalignments prior to outboard engine cant were -0.03, 0.07, and 0.07 degree in pitch, yaw, and roll, respectively. These errors are required to trim out the effects of thrust unbalance, offset center of gravity, thrust vector misalignment, and control system misalignments. The equivalent thrust vector misalignments after outboard

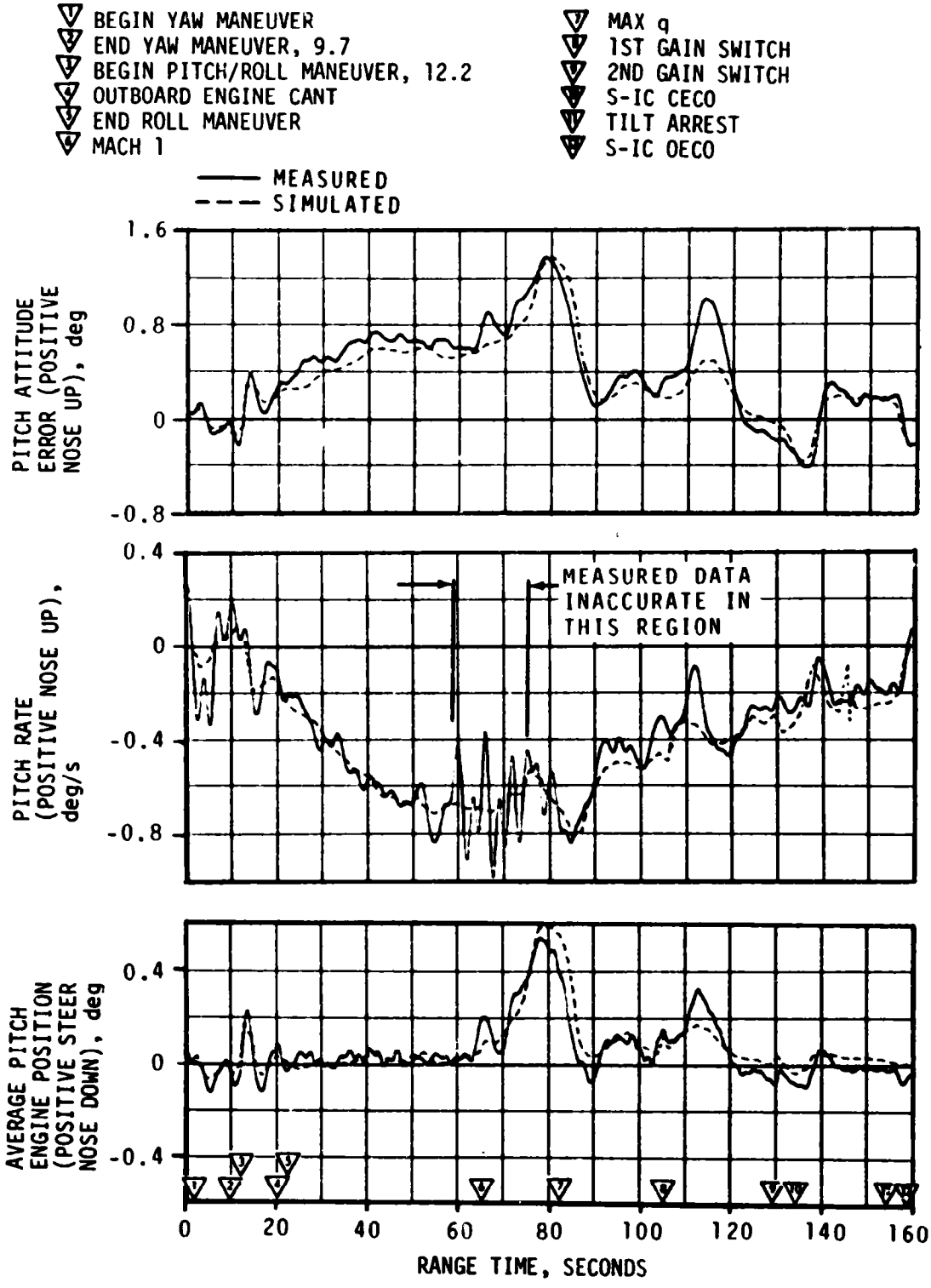

Figure 10-1. Pitch Plane Dynamics During S-IC Burn

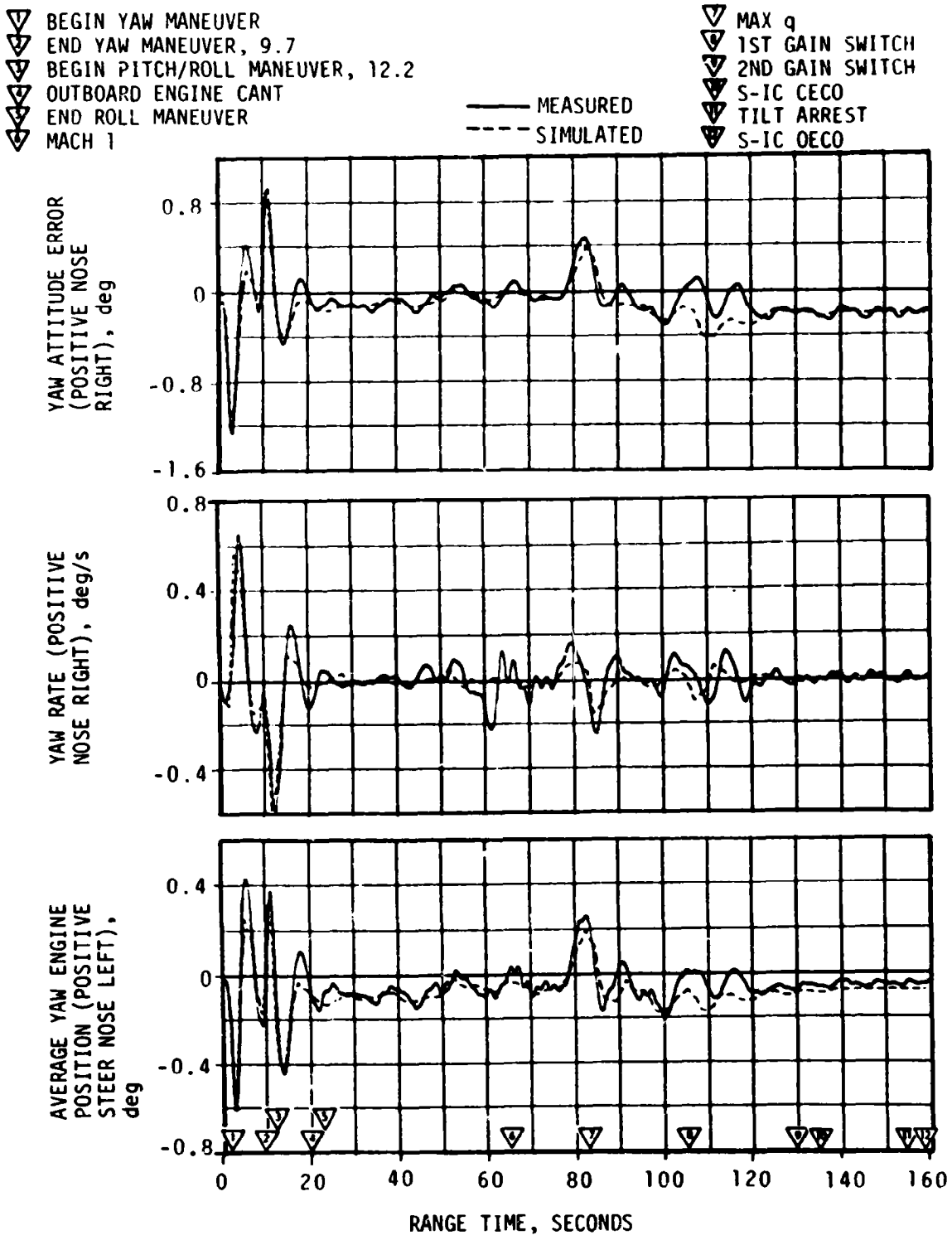

Figure 10-2. Yaw Plane Dynamics During S-IC Burn

Table 10-1. Maximum Control Parameters During S-IC Flight

PARAMETER	PITCH PLANE		YAW PLANE		ROLL PLANE	
	AMPLITUDE	RANGE TIME (SEC)	AMPLITUDE	RANGE TIME (SEC)	AMPLITUDE	RANGE TIME (SEC)
Attitude Error, deg	1.37	78.8	-1.38	3.2	-1.12	13.5
Angular Rate, deg/s	-0.84	84.7	0.65	4.8	1.33	14.3
Average Gimbal Angle, deg	0.54	78.2	-0.61	3.2		
Angle of Attack, deg	2.63	79.9	1.34	82.2		
Angle of Attack Dynamic Pressure Product, deg-N/cm^2 (deg-lbf/ft^2)	9.02 (1490)	79.9	4.95 (766)	82.2		
Normal Acceleration, m/s^2 (ft/s^2)	-.76 (-2.49)	82.4	0.61 (2.00)	85.3		

engine cant were -0.02, 0.05, and 0.09 degree in pitch, yaw, and roll, respe ively.

Figure 10-3 shows measured angle-of-attack time histories.

The predicted and measured misalignments, slow release forces, winds, and thrust-to-weight ratio are shown in Table 10-2.

10.3 S-II CONTROL SYSTEM EVALUATION

The S-II stage attitude control system performance was satisfactory. The vehicle dynamics were within expectations at all times. The maximum values of pitch parameters occurred in response to IGM Phase I initiation. The maximum values of yaw and roll control parameters occurred in response to S-IC/S-II separation conditions. The maximum control parameter values for the period of S-II burn are shown in Table 10-3.

Between S-IC OECO and initiation of IGM Phase I, commands were held constant. Significant events occurring during this interval were S-IC/S-II separation, S-II stage J-2 engine start, second plane separation, and Launch Escape Tower (LET) jettison. Pitch and yaw dynamics during this interval indicated adequate control stability as shown in Figures 10-4 and 10-5, respectively. Steady state attitudes were achieved within 10 seconds from S-IC/S-II separation.

At IGM initiation, guidance commands caused the vehicle to pitch down instead of up as for previous flights. The transient magnitudes experienced were similar to previous flights.

At S-II CECO, the guidance routines reacted properly to the decrease in total thrust. Flight and simulated data comparison, Figures 10-4 and

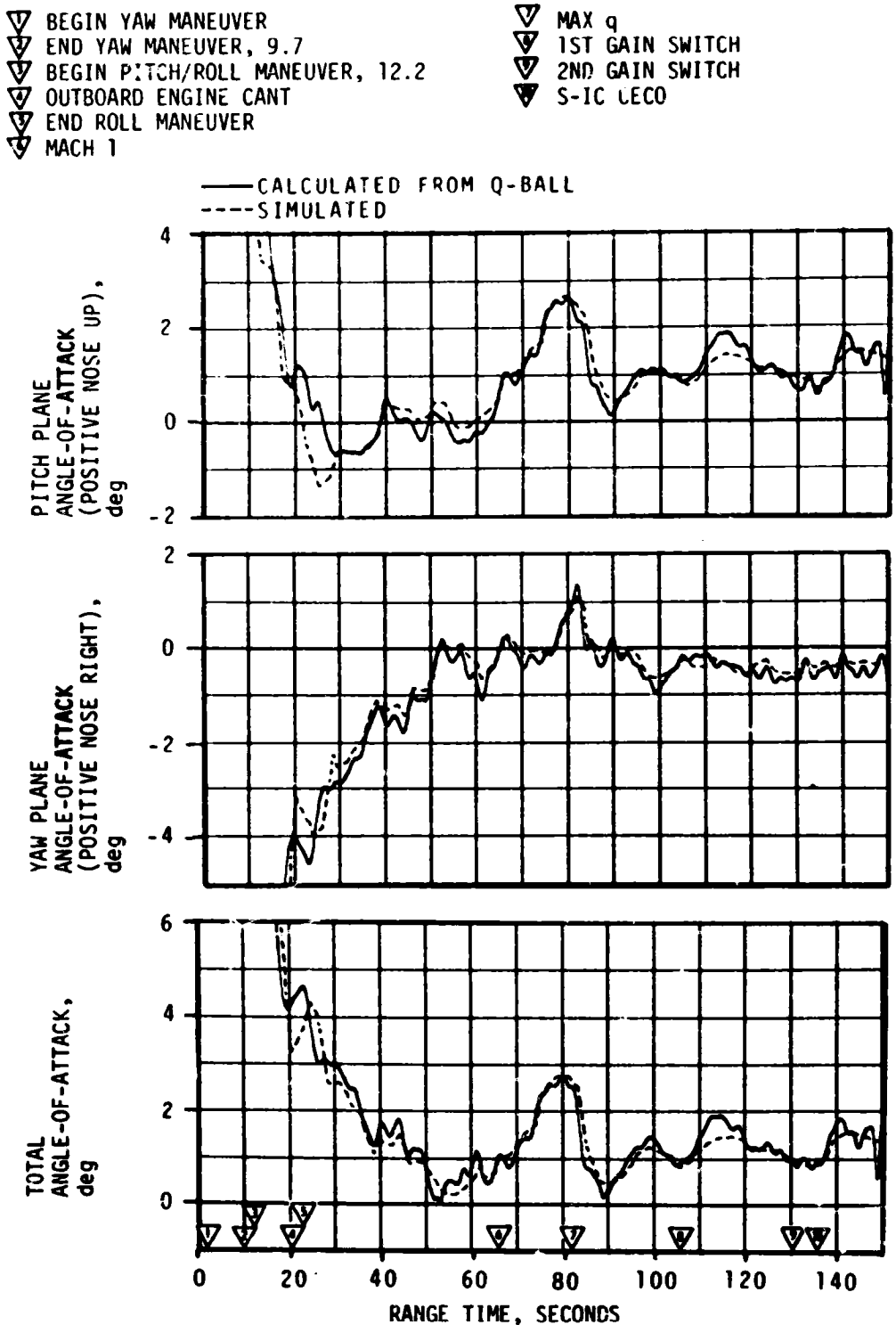

Figure 10-3. Angle-Of-Attack During S-IC Burn

Table 10-2. AS-510 Liftoff Misalignment Summary

PARAMETER	PREDICTED 3σ RANGE			LAUNCH		
	PITCH	YAW	ROLL	PITCH	YAW	ROLL
Outboard Engine Misalignment, deg	±0.34	±0.34	±0.34	-0.03	0.07	0.07
Center Engine Misalignment, deg	±0.34	±0.34	-	0.23	0.0	-
Vehicle Stacking & Pad Misalignment, deg	±0.29	±0.29	0.0	0.06	-0.04	0.0
Attitude Error at Holddown Arm Release, deg	-	-		0.0	-0.06	0.01
Peak Soft Release Force Per Rod, N (lbf)	415,900 (93,500)			Data not available		
Wind	19.55 m/s (38 knots) at 161.5 meters (530 feet)			6.2 m/s (12.0 knots) at 161.5 meters (530 feet)		
Thrust to Weight Ratio	1.212			1.224		

Table 10-3. Maximum Control Parameters During S-II Burn

PARAMETER	PITCH PLANE		YAW PLANE		ROLL PLANE	
	AMPLITUDE	RANGE TIME (SEC)	AMPLITUDE	RANGE TIME (SEC)	AMPLITUDE	RANGE TIME (SEC)
Attitude Error, deg	2.1	206.0	0.4	228.2	-2.9	164.0
Angular Rate, deg/s	-1.1	206.5	0.1	167.0	1.4	165.0
Average Gimbal Angle, deg	0.9	204.5	-0.3	164.5	-0.9	166.0

10-5, show agreement at those events of greatest control system activity. Differences between the two can be accounted for largely by engine location misalignments, thrust vector misalignments, and uncertainties in engine thrust buildup characteristics. Based on static firing tests, the effective thrust misalignments were 0.0, -0.1, and 0.14 degree for the pitch, yaw and roll axes, respectively.

10.4 S-IVB CONTROL SYSTEM EVALUATION

The TVC System provided satisfactory pitch and yaw control during powered flight. The APS provided satisfactory roll control during first and second burns.

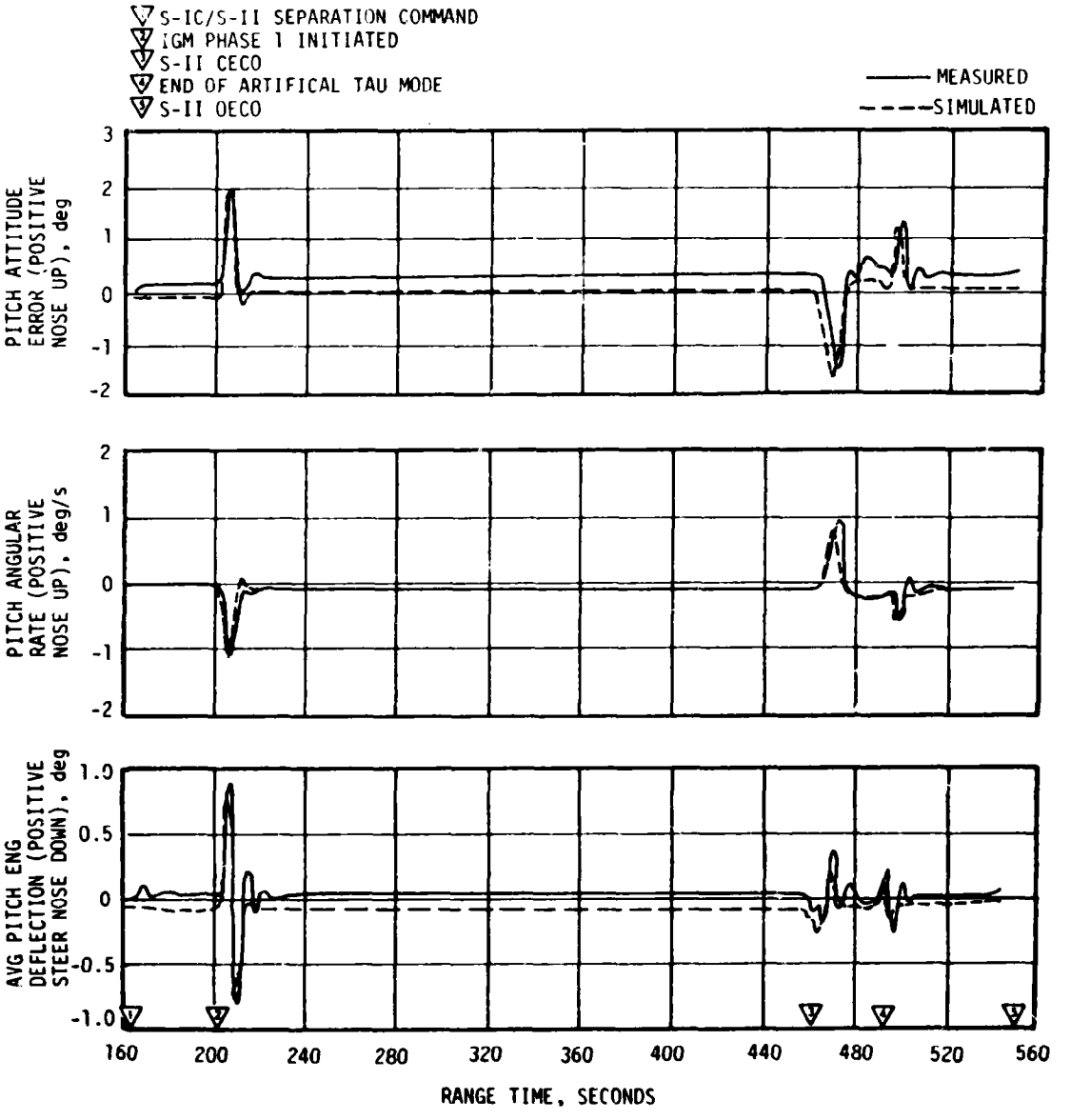

Figure 10-4. Pitch Plane Dynamics During S-II Burn

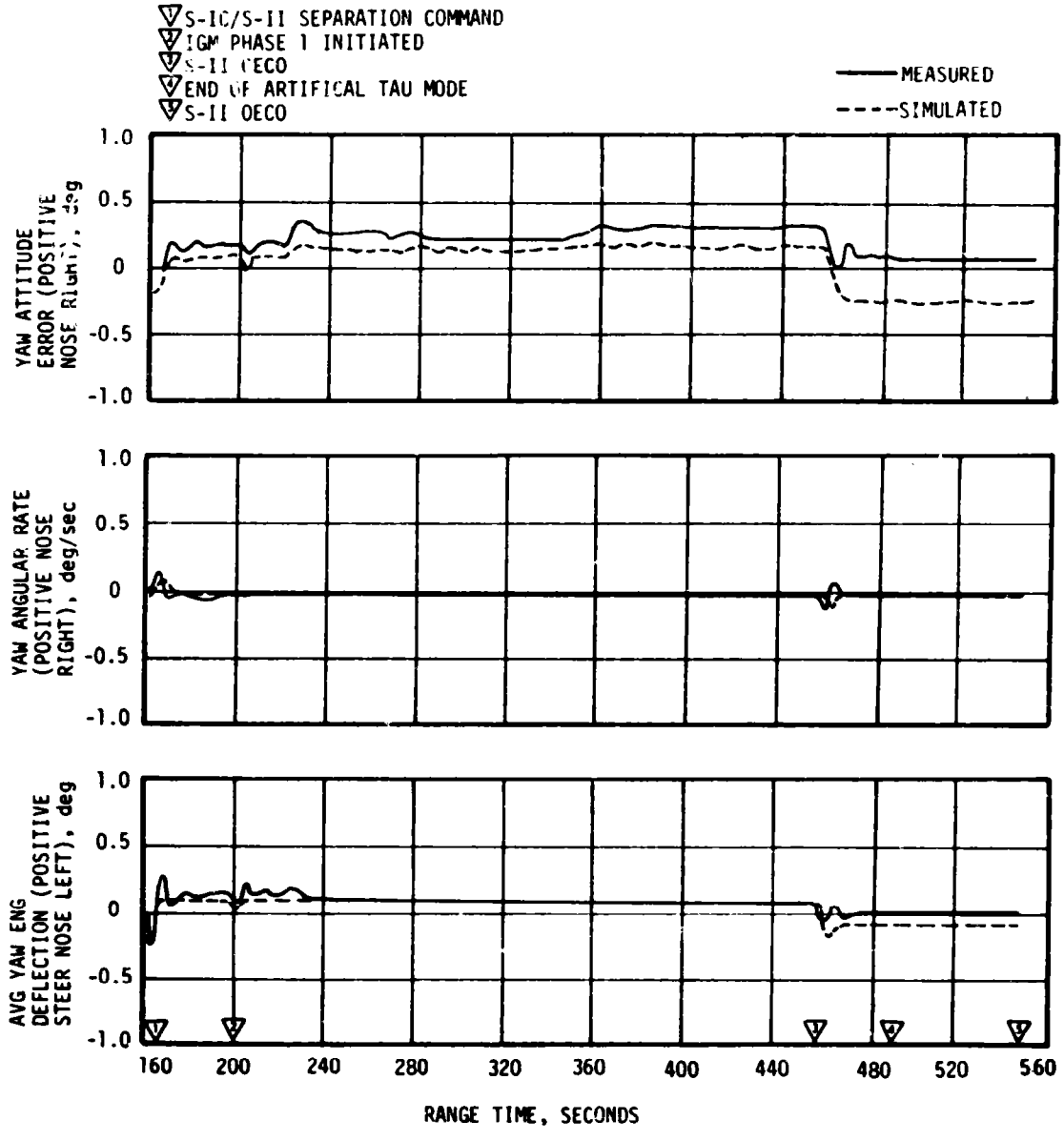

Figure 10-5. Yaw Plane Dynamics During S-II Burn

During S-IVB first and second burns, control system transients were experienced at S-II/S-IVB separation, guidance initiation, Engine Mixture Ratio (EMR) shift, terminal guidance mode, and S-IVB Engine Cutoff (ECO). These transients were expected and were well within the capabilities of the control system.

10.4.1 Control System Evaluation During First Burn

S-IVB first burn pitch attitude error, angular rate, and actuator position are presented in Figure 10-6. First burn yaw plane dynamics are presented in Figure 10-7. The maximum attitude errors and rates occurred at IGM initiation. A summary of the first burn maximum values of critical flight control parameters is presented in Table 10-4.

The pitch and yaw effective thrust vector misalignments during first burn were 0.29 and -0.30 degree, respectively. A steady state roll torque of 6.33 N-m (4.62 lbf-ft) counterclockwise looking forward required roll APS firings during first burn. The steady state roll torque experienced on previous flights has ranged between 61.4 N-m (45.3 lbf-ft) counterclockwise and 54.2 N-m (40.0 lbf-ft) clockwise.

Propellant sloshing during first burn was observed on data obtained from the Propellant Utilization (PU) mass probe sensors. The propellant slosh did not have any noticeable effect on the operation of the attitude control system.

10.4.2 Control System Evaluation During Parking Orbit

The APS provided satisfactory orientation and stabilization during parking orbit. Following S-IVB first ECO, the vehicle was maneuvered to the in-plane local horizontal, and the orbital pitch rate was established. The pitch attitude error and pitch angular rate for this maneuver are shown in Figure 10-8.

The maneuver to the local horizontal on AS-510 required a change in vehicle attitude of approximately 18 degrees in pitch (see Figure 10-8). This change in pitch attitude although predicted was considerably greater than the 6 to 10 degree maneuvers on previous Lunar Orbit Rendezvous (LOR) missions and resulted from the lower altitude parking orbit -- 90 nautical miles as compared to 100 nautical miles on previous missions.

Propellant slosh activity resulting from the pitch maneuver appeared to be greater on AS-510 than on previous missions, and the resulting large amplitude LOX slosh wave caused liquid to flow into the forward portion of the LOX tank. The LOX nonpropulsive vent opened at approximately 775 seconds GET (Time Base 5 [T_5] +80 seconds) and started venting liquid at approximately 815 seconds GET.

The larger slosh amplitudes on AS-510 were due primarily to the larger pitch maneuver which took correspondingly longer to complete. Initiation

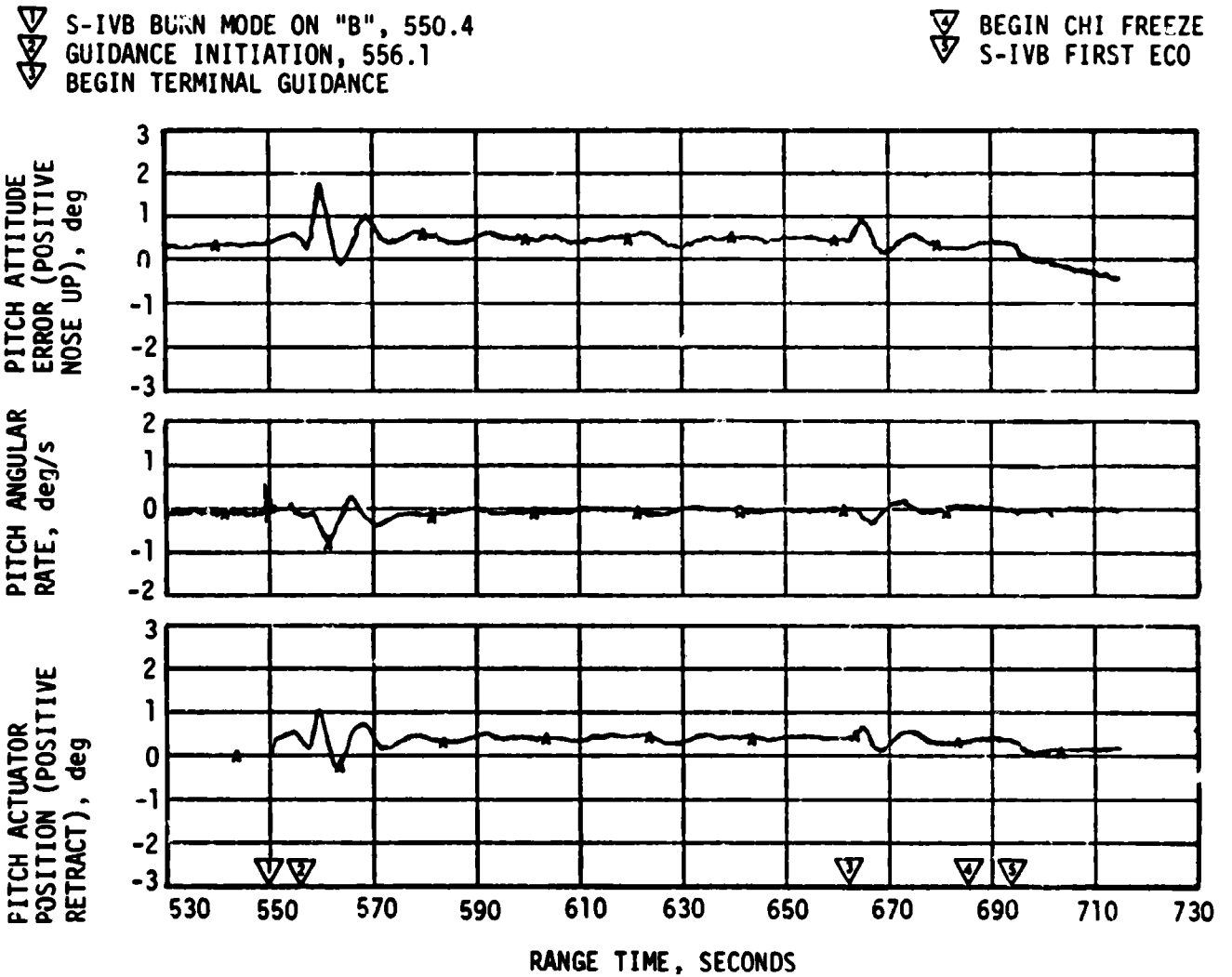

Figure 10-6. Pitch Plane Dynamics During S-IVB First Burn

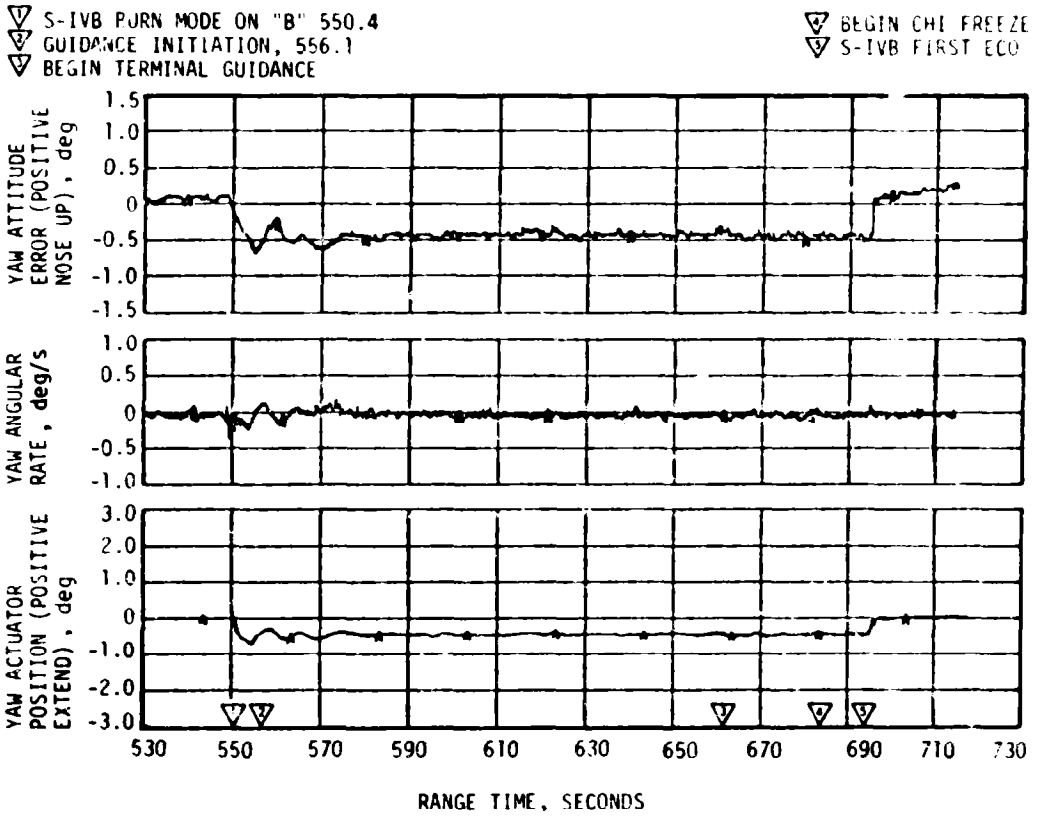

Figure 10-7. Yaw Plane Dynamics During S-IVB First Burn

Table 10-4. Maximum Control Parameters During S-IVB First Burn

PARAMETER	PITCH PLANE		YAW PLANE		ROLL PLANE	
	AMPLITUDE	RANGE TIME (SEC)	AMPLITUDE	RANGE TIME (SEC)	AMPLITUDE	RANGE TIME (SEC)
Attitude Error, deg	1.67	559.5	-0.69	554.6	-0.49	557.3
Angular Rate, deg/s	-0.79	561.3	-0.20	554.0	-0.10	555.5
Maximum Gimbal Angle, deg	1.0	559.5	-0.75	554.5	-	-

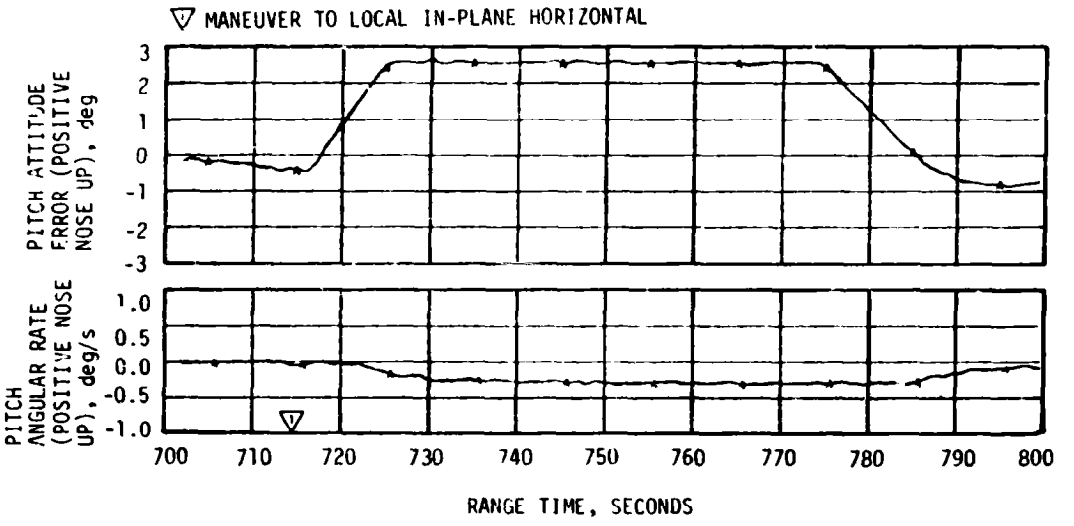

Figure 10-8. Pitch Plane Dynamics During Parking Orbit

of the maneuver by establishing a negative pitch rate of 0.3 degrees per second resulted in phase reinforcement of the slosh wave. However, the pitch rate was not arrested until after termination of the APS ullage engine burn.

A simulation of LOX slosh activity during the T_5 pitch maneuver was conducted for which it was assumed that the liquid surface was quiescent prior to maneuver initiation. The simulation results indicate that the slosh wave amplitude following the maneuver was larger by a factor of two than on previous missions, and the amplitude reached a maximum near the time that LOX was vented.

For subsequent missions the condition will be corrected by reducing the commanded pitch rate during the maneuver from 0.4 to 0.14 deg/s.

10.4.3 Control System Evaluation During Second Burn

S-IVB second burn pitch attitude error, angular rate, and actuator position are presented in Figure 10-9. Second burn yaw plane dynamics are also presented in Figure 10-10. The maximum attitude errors and rates occurred at guidance initiation. A summary of the second burn maximum values of critical flight control parameters is presented in Table 10-5.

Control system attitude error transients resulted from pitch and yaw attitude commands at the termination of the artificial Tau guidance mode (28 seconds before ECO).

The pitch and yaw effective thrust vector misalignments during second burn were approximately 0.33 and -0.25 degree, respectively. The steady state roll torque during second burn ranged from 3.36 N-m (2.47 lbf-ft) clockwise

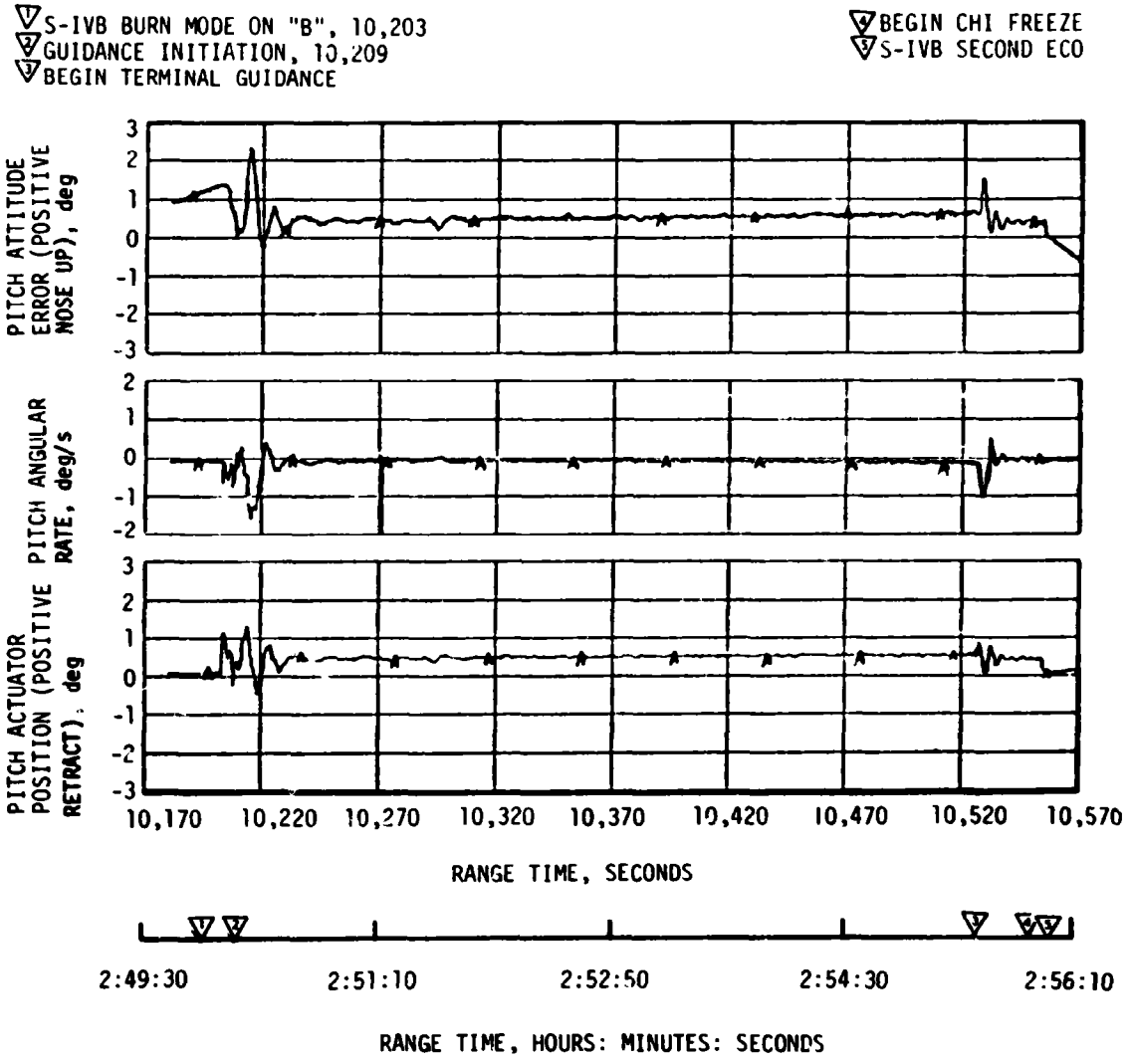

Figure 10-9. Pitch Plane Dynamics During S-IVB Second Burn

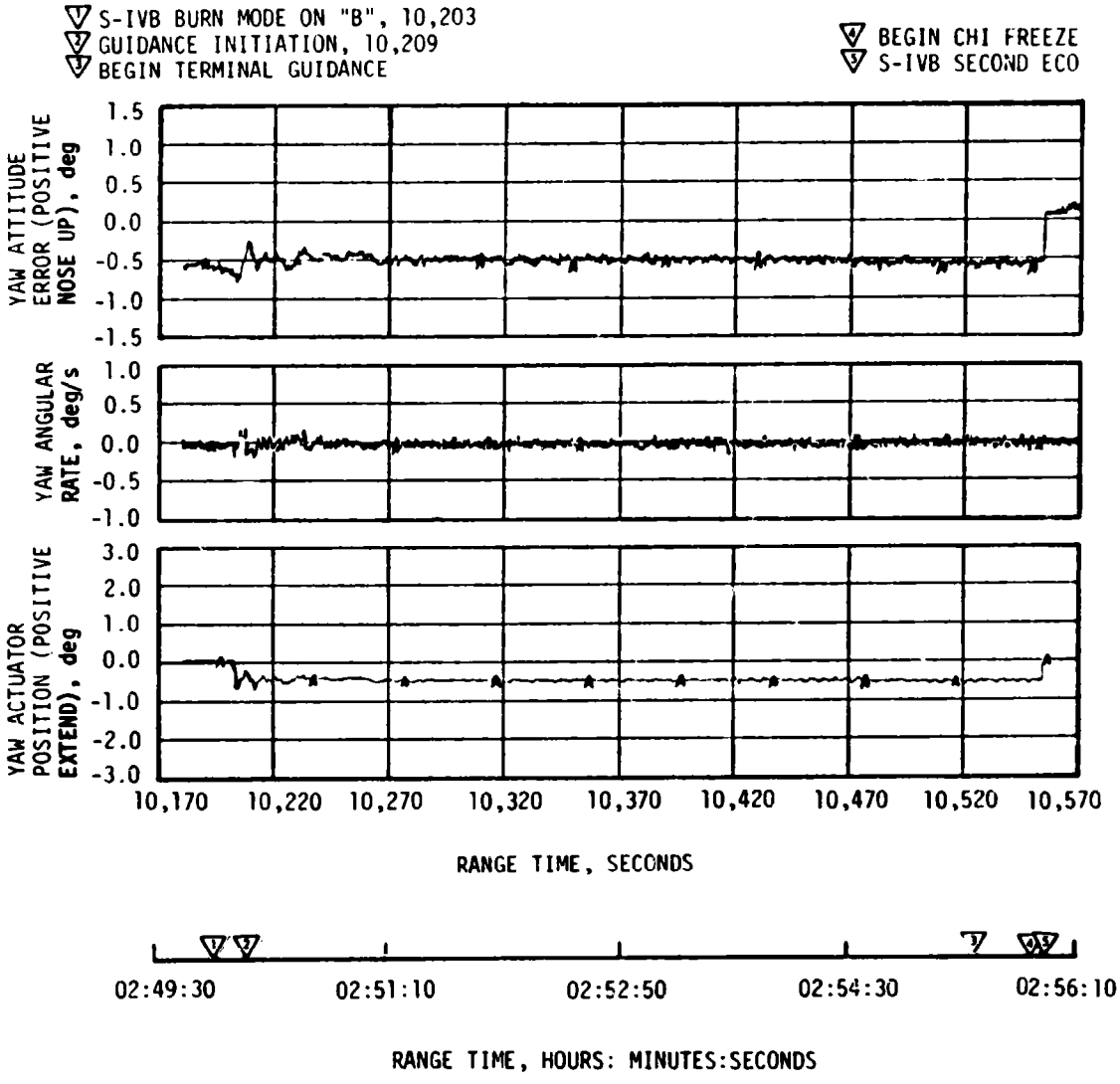

Figure 10-10. Yaw Plane Dynamics During S-IVB Second Burn

Table 10-5. Maximum Control Parameters During S-IVB Second Burn

PARAMETER	PITCH PLANE		YAW PLANE		ROLL PLANE	
	AMPLITUDE	RANGE TIME (SEC)	AMPLITUDE	RANGE TIME (SEC)	AMPLITUDE	RANGE TIME (SEC)
Attitude Error, deg	2.4	10202.2	-0.79	10203.4	0.8	10320
Angular Rate, deg/s	-1.58	10215.1	0.18	10204.7	-0.1	10240
Maximum Gimbal Angle, deg	1.3	10213.5	-0.75	10211.3	-	-

looking forward at the low EMR to 7.54 N-m (5.55 lbf-ft) counterclockwise at the 5.0:1.0 EMR.

Propellant sloshing during second burn was observed on data obtained from the PU mass probe sensors. The propellant slosh did not have any noticeable effect on the operation of the attitude control system.

10.4.4 Control System Evaluation After S-IVB Second Burn

The APS provided satisfactory orientation and stabilization from Translunar Injection (TLI) through the S-IVB/IU passive thermal control maneuver ("Barbecue Maneuver"). Each of the planned maneuvers was performed satisfactorily.

Significant periods of interest related to translunar coast attitude control were the maneuver to the inplane local horizontal following second burn ECO, the maneuver to the TD&E attitude, spacecraft separation, spacecraft docking, lunar module ejection, the maneuver to the evasive ullage burn attitude, the maneuver to the LOX dump attitude, the maneuver to the lunar impact ullage burn attitude, the maneuver to the vernier ullage burn attitude, the second maneuver to the LOX dump attitude, and the "Barbecue Maneuver." The pitch attitude error and angular rate for events during which telemetry data were available are shown in Figure 10-11.

Following S-IVB second ECO, the vehicle was maneuvered to the inplane local horizontal at 10,706 seconds (2:58:26) (through approximately -26 degrees in pitch and -0.6 degree in yaw), and an orbital pitch rate was established. At 11,455 seconds (3:10:55), the vehicle was commanded to maneuver to the separation TD&E attitude (through approximately 120, -40, and -180 degrees in pitch, yaw, and roll, respectively).

Spacecraft separation, which occurred at 12,147 seconds (3:22:27), appeared normal, as indicated by the relatively small disturbances induced on the S-IVB.

Distrubances during spacecraft docking, which occurred at 12,830 seconds (3:33:50), were larger than on previous flights. Docking disturbances required 3,480 N-s (783 lbf-s) of impulse from Module 1 and 3,040 N-s (683 lbf-s) of impulse from Module 2. The largest docking disturbances on previous flights occurred on AS-508 and required 2,930 N-s (658 lbf-s) of impulse from Module 1 and 2,180 N-s (490 lbf-s) of impulse from Module 2. Lunar module ejection occurred at 15,481 seconds (4:18:01) with normal disturbances.

At 16,260 seconds (4:31:00), a maneuver was initiated to attain the desired attitude for the evasive ullage burn. This involved maneuvering from the TD&E yaw attitude of -39.6 degrees to +40.0 degrees. At 16,802 seconds (4:40:02) the APS ullage engines were commanded on for 80 seconds to provide the necessary separation distance between the S-IVB and spacecraft.

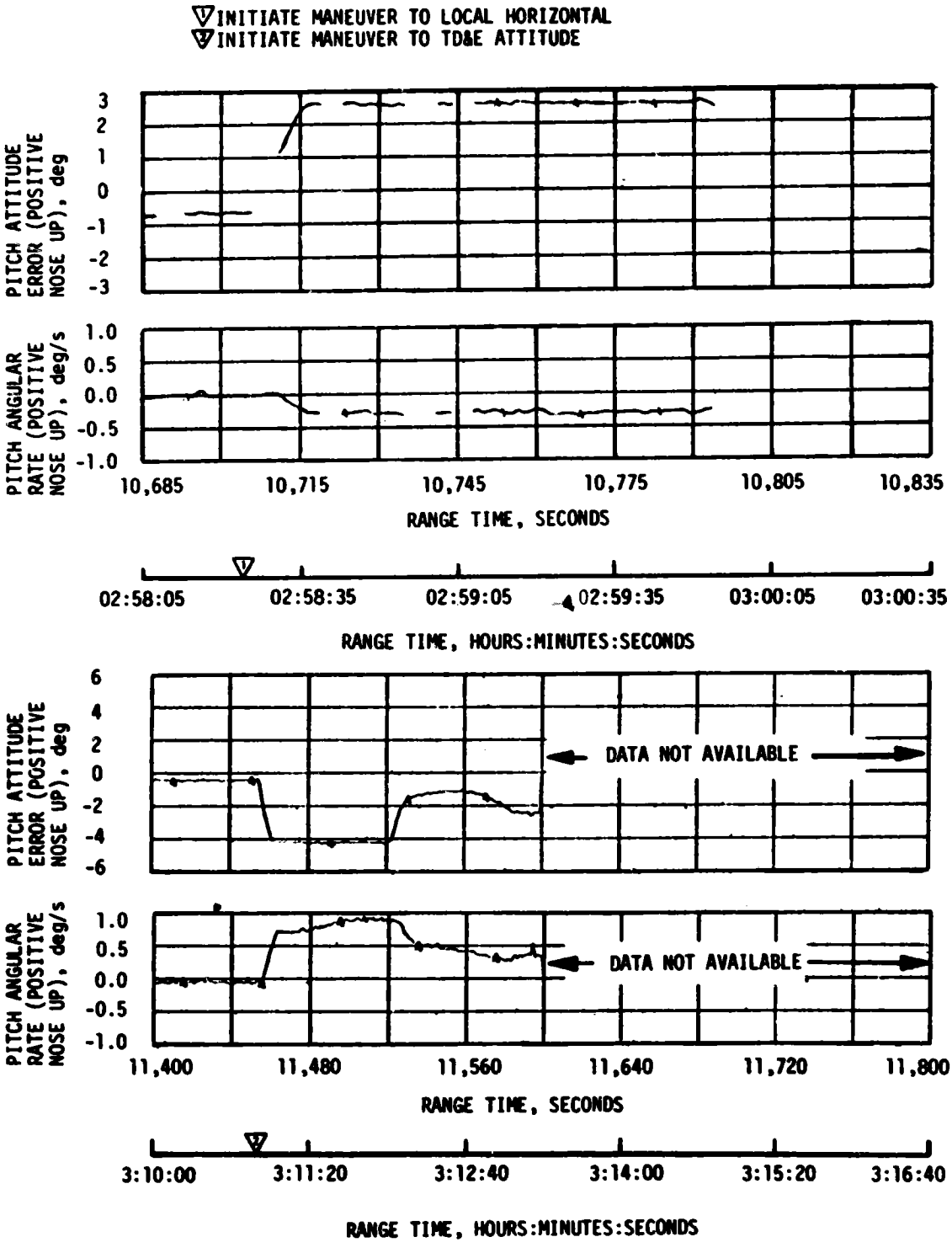

Figure 10-11. Pitch Plane Dynamics During Translunar Coast (Sheet 1 of 5)

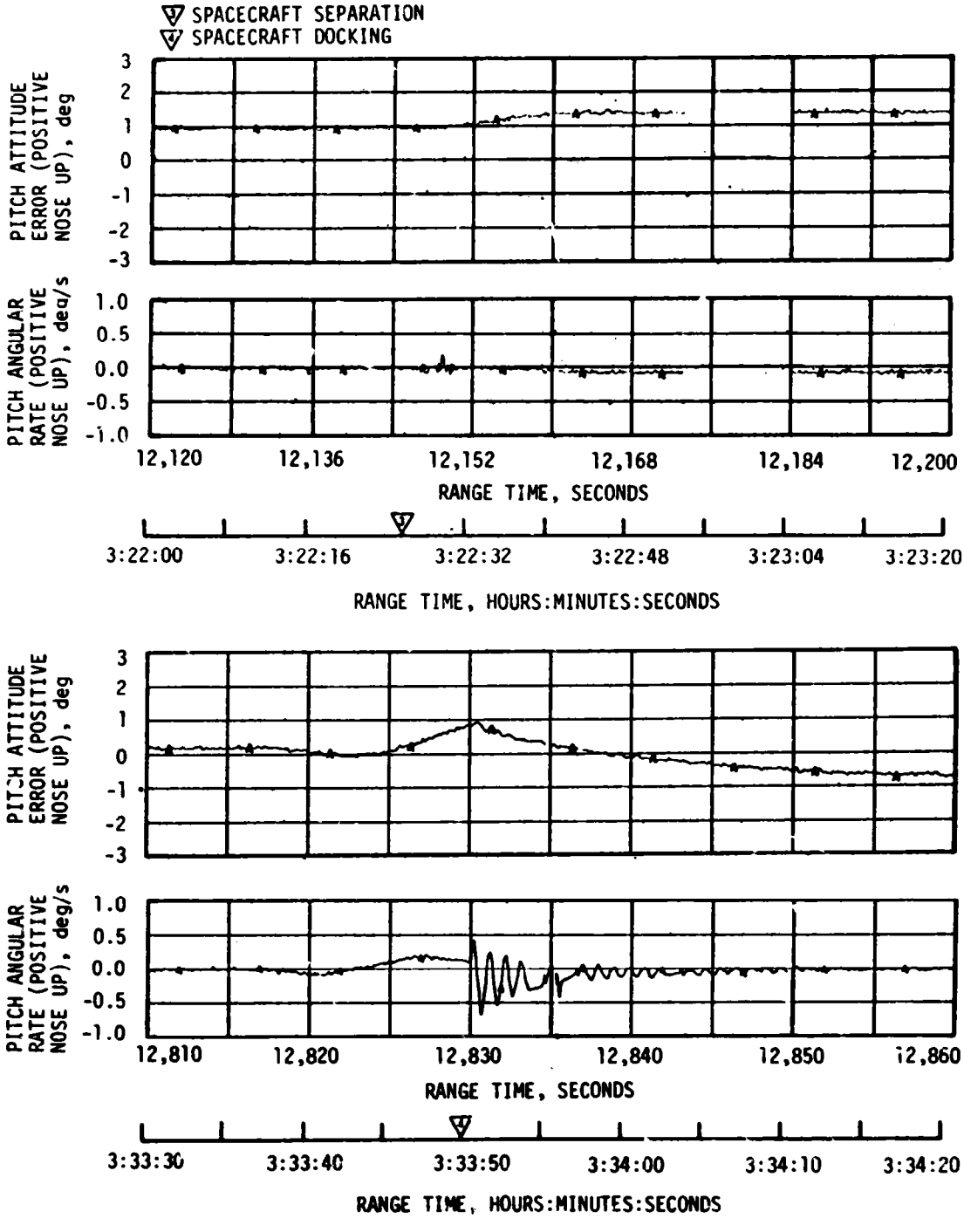

Figure 10-11. Pitch Plane Dynamics During Translunar Coast (Sheet 2 of 5)

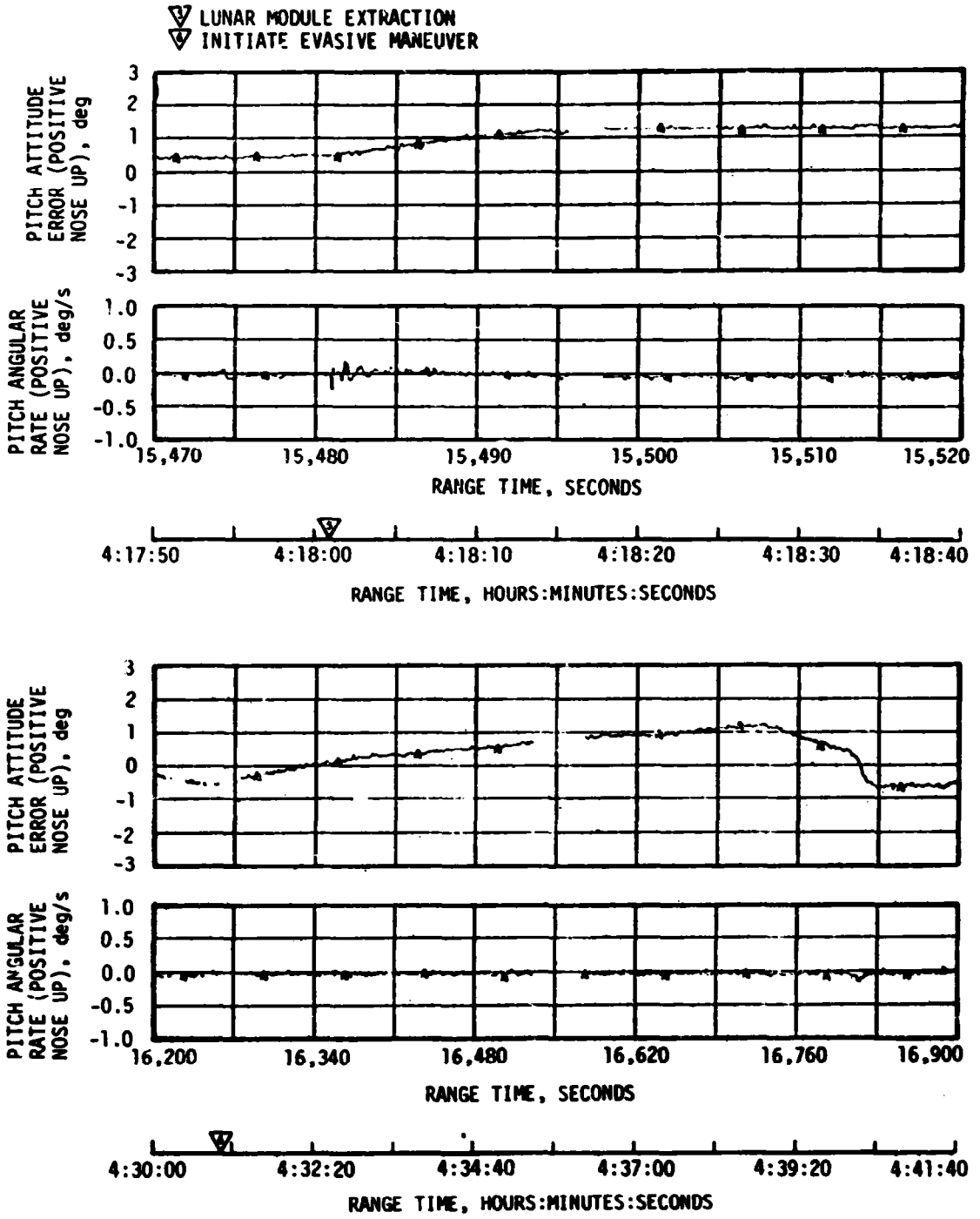

Figure 10-11. Pitch Plane Dynamics During Translunar Coast (Sheet 3 of 5)

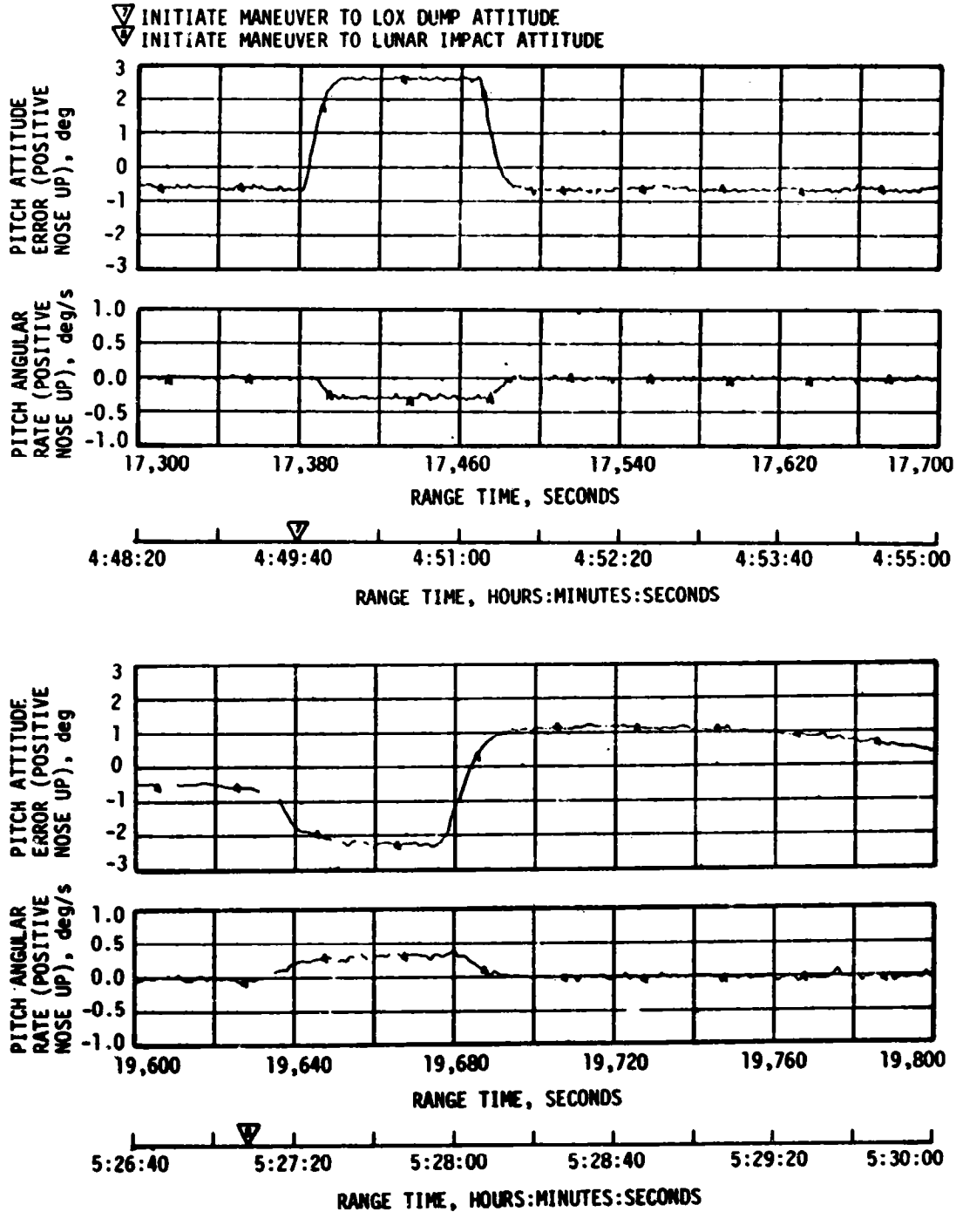

Figure 10-11. Pitch Plane Dynamics During Translunar Coast (Sheet 4 of 5)

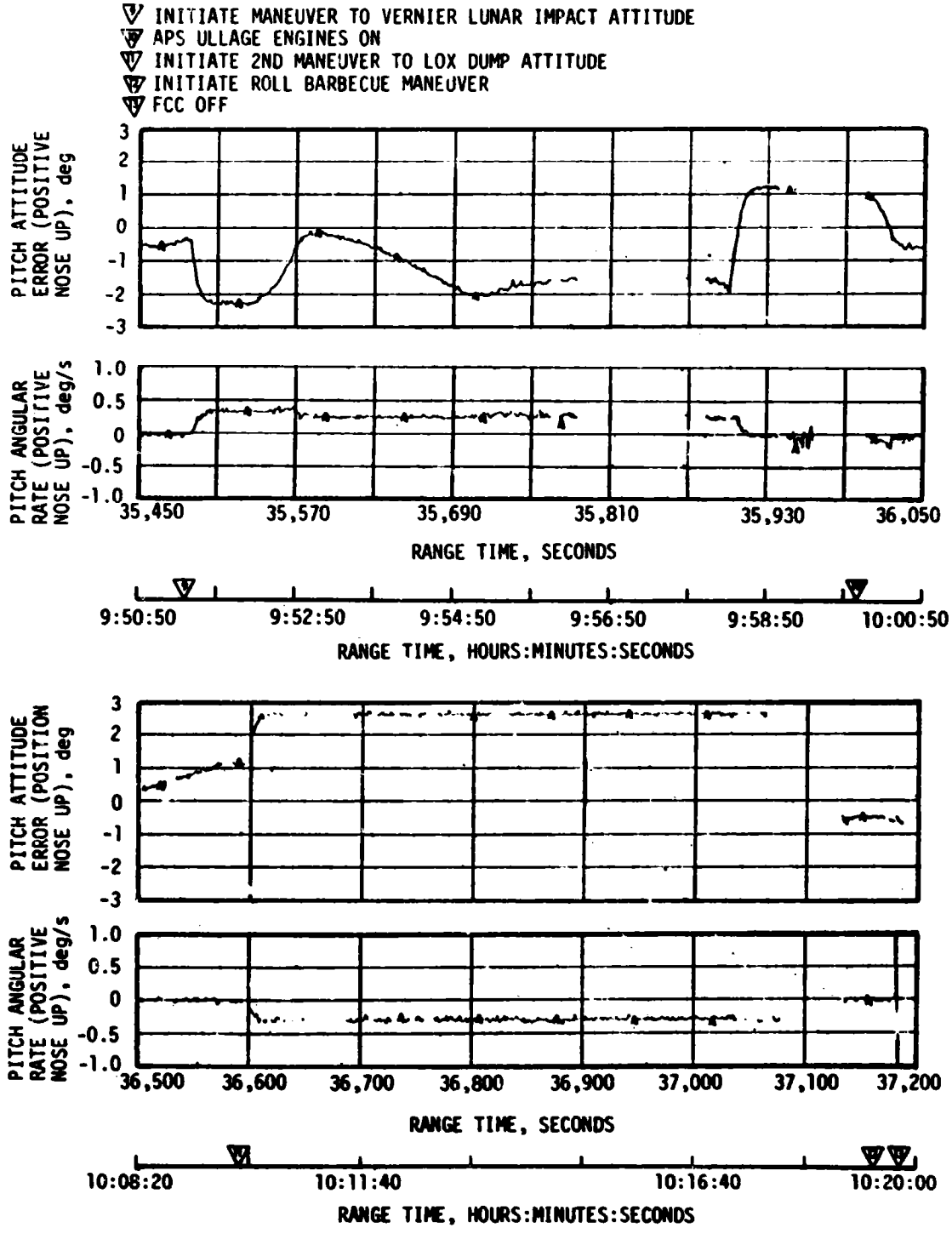

Figure 10-11. Pitch Plane Dynamics During Translunar Coast (Sheet 5 of 5)

The maneuver to the LOX dump attitude was performed at 17,382 seconds (4:49:40). This was a two-axis maneuver with pitch commanded from 179.1 to 209.0 degrees and yaw from 40.0 to -40.0 degrees referenced to the in-plane local horizontal. LOX dump occurred at 18,081 seconds (5:01:21) and lasted for 48 seconds.

At 19,629 seconds (5:27:09), a ground command was sent to perform a maneuver to the desired attitude for the APS ullage burn for lunar target impact. This was also a two-axis maneuver and resulted in a pitch maneuver change from 209.0 to 192.0 degrees and a yaw attitude maneuver change from -40.0 to -22.0 degrees referenced to the inplane local horizontal. At 20,761 seconds (5:46:01) the APS ullage engines were commanded ON for 241 seconds to provide ΔV for lunar target impact.

Beginning at 35,486 seconds (9:51:26), a series of ground commands were sent to maneuver the vehicle to the desired attitude for a vernier lunar impact APS ullage burn. This maneuver was a two-axis maneuver with the yaw maneuver delayed 33 seconds. The maneuver resulted in a pitch attitude change from 192.0 to 28.0 degrees (in a negative direction) and a yaw attitude change from -22.0 to -40.0 degrees referenced to the inplane local horizontal. At 36,001 seconds (10:00:01) the APS engines were commanded ON for 71 seconds to provide ΔV for a more accurate lunar target impact.

During the period between the first and second APS ullage burn for the lunar impact (approximately 22,000 seconds [6:06:40] to 35,000 seconds [9:43:20]) the APS made corrections for cyclic low level lateral disturbances. Figure 10-12 presents the average pitch control thruster thrust between the lunar impact APS ullage burns. Also shown on Figure 10-12 is the IU Thermal Conditioning System (TCS) water valve operation. The figure shows that the disturbance increased for 20 minutes after the IU TCS water valve was cycled open. There appears to have been a low level force after the 20 minute period following the opening of the water valve until the next water valve cycle. Figure 10-13 shows the pitch, yaw, and roll plane dynamics during a single IU TCS water cycle. Computer simulations of the IU TCS sublimator forces on the S-IVB stage resulted in pitch, yaw, and roll plane dynamics similar to Figure 10-13. The one-sided attitude control system firings were controlling a negative pitch yaw disturbing torque located approximately 45 degrees between position planes I and II.

The average lateral force on the vehicle between the lunar impact APS ullage burns is approximately 0.85 N (0.19 lbf). The average lateral force on the vehicle between the 20-minute period following the opening of the water valve, and the next cycle is approximately 0.36 N (0.08 lbf). The effect of this lateral force on the stage between the two APS ullage burns was sufficient to cause a significant lunar impact point perturbation, see Section 17.

At 36,593 seconds (10:09:53) a series of ground commands were sent to maneuver the vehicle back to the LOX dump attitude for the passive thermal

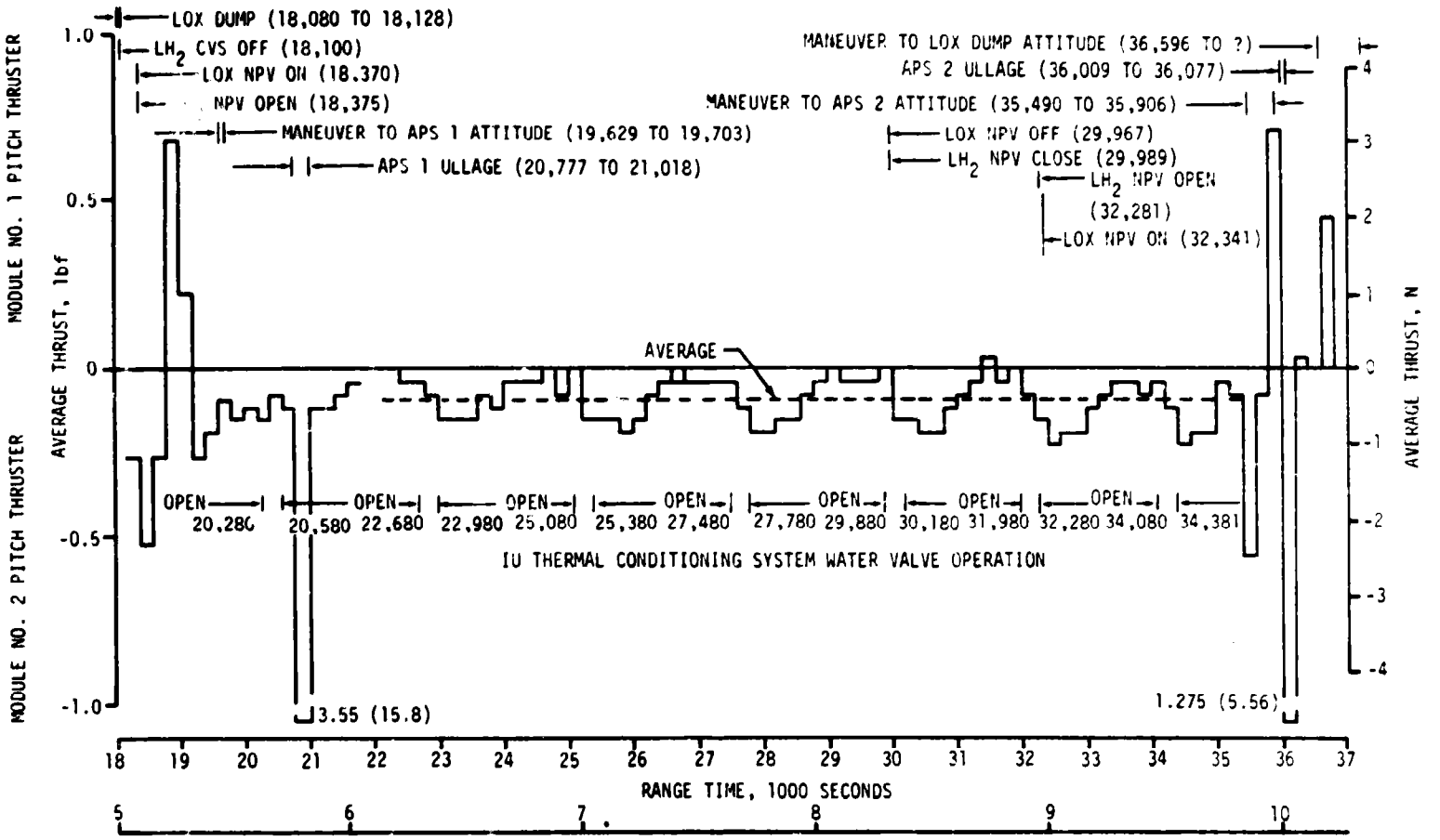

Figure 10-12. Average Pitch Control Thruster Thrust After LOX Dump

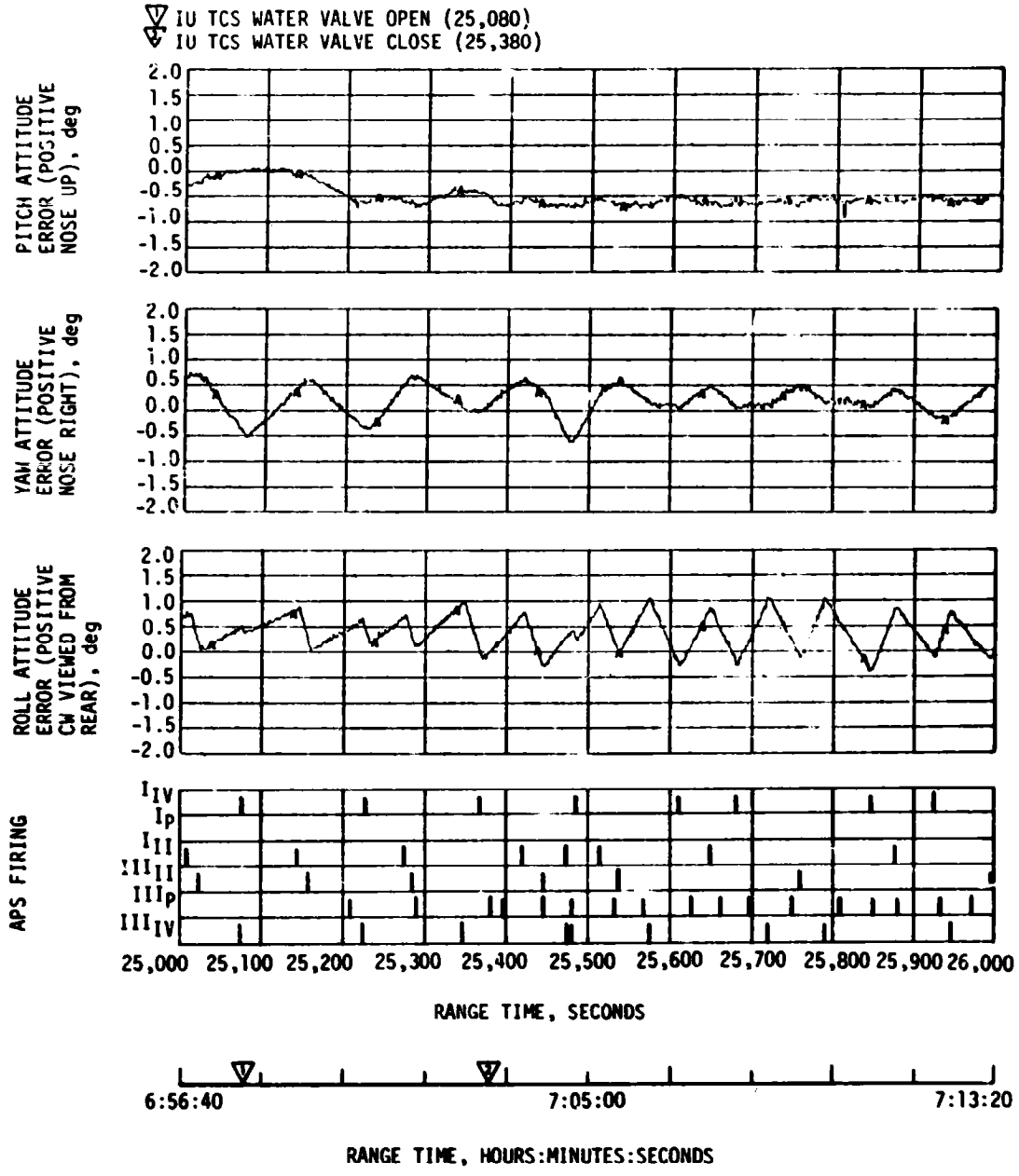

Figure 10-13. Pitch, Yaw, and Roll Plane Dynamics During T_8 (Sheet 1 of 2)

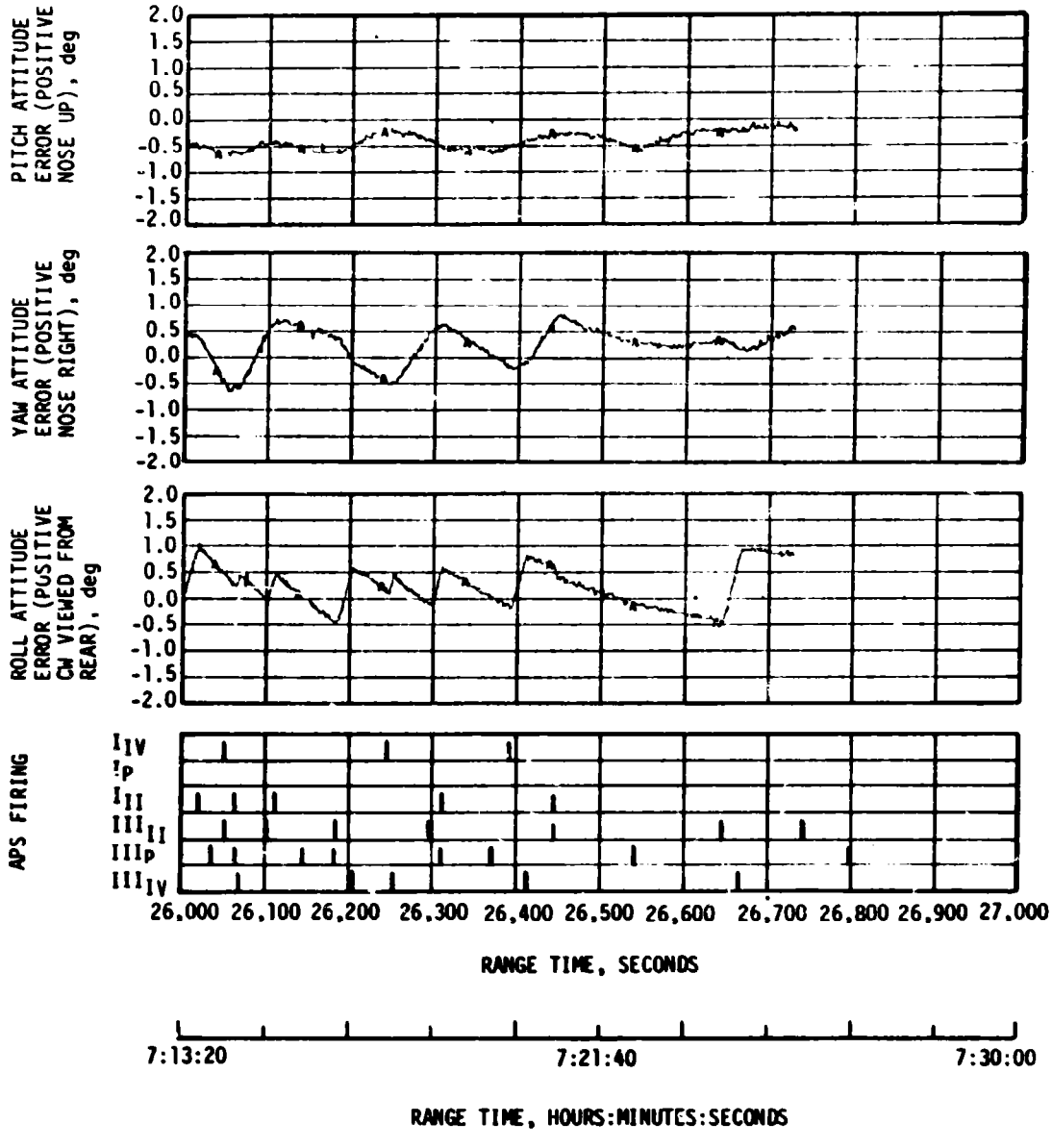

Figure 10-13. Pitch, Yaw, and Roll Plane Dynamics During T_8 (Sheet 2 of 2)

control maneuver ("Barbecue Maneuver"). This maneuver was a single-axis pitch maneuver since the yaw attitude was already at the LOX dump attitude. The maneuver resulted in a pitch maneuver change from 28.0 degrees to 209.0 degrees (in a positive direction) referenced to the inplane local horizontal.

At 37,162 seconds (10:19:22) the S-IVB was ground commanded to maneuver in the positive roll direction and established a corresponding roll angular rate of approximately 0.5 deg/s. Following initiation of the "Barbecue Maneuver," a Digital Command System (DCS) command was received at 37,185 seconds (10:19:45) to inhibit the IU FCC leaving the S-IVB stage in a "Barbecue" or tumble mode until lunar impact.

APS propellant consumption for attitude control and propellant settling prior to the APS burn for lunar target impact was higher than the mean predicted requirements. This is attributed to the higher usage during T_5. The total propellant (fuel and oxidizer) used prior to ullaging for lunar impact ΔV was 56.4 kilograms (124.2 lbm) and 56.5 kilograms (124.7 lbm) for Modules 1 and 2, respectively. This was 37.4 and 37.9 percent of the total available in each module (approximately 149.3 kilograms [329 lbm]). APS propellant consumption is tabulated in Section 7, Table 7-5.

10.5 INSTRUMENT UNIT CONTROL COMPONENTS EVALUATION

The flight program minor loop implemented all guidance commands, providing satisfactory attitude error outputs through the Launch Vehicle Data Adapter (LVDA) to the FCC. No minor loop error telemetry occurred during the mission. The FCC and control rate gyros functioned satisfactorily throughout the mission.

10.6 SEPARATION

All separations and associated sequencing were accomplished as planned, however the S-IC/S-II separation distance at the time of S-II ignition was less than previous flights and less than predicted for the AS-510 flight. See Figure 10-14. Changes that affected the separation distance were deletion of four of the eight S-IC retro motors, deletion of the S-II ullage motors, and delaying of all events in T_3 for one second to increase the separation distance. The difference between the observed and predicted separation distance, Figure 10-15, is attributed to a greater F-1 engine "tailoff" impulse than that used in the separation distance prediction. See Figure 10-16. The F-1 thrust decay was normal and not appreciably different from previous (AS-505 through 509) flights. The effect of the S-II exhaust plume at engine start resulted in a more severe environment at the S-IC forward LOX dome than seen on previous flights (Figure 10-17) and resulted in S-IC telemetry system damage as discussed in Section 15.3.2.

Analysis indicates that with an S-IC stage having only four retro motors, failure of one retro motor to ignite would result in marginal separation distances and, in the 3σ case, recontact of the two stages. See Figure 10-18. Consequently, S-IC-11 and subsequent will be equipped with eight retro motors rather than the planned four.

Second plane separation occurred as predicted. There were no significant vehicle attitude disturbances attributable to the second plane separation. Calculations indicate that the separation dynamics were similar to previous flight experience and were completed at 192.4 seconds.

S-II/S-IVB separation was normal with nominal S-II retro motor and S-IVB ullage motor performance. Vehicle dynamics were well within staging limits.

Vehicle dynamics were normal during CSM separation and the TD&E maneuver. The vehicle maintained a stable docking platform during the docking attempt.

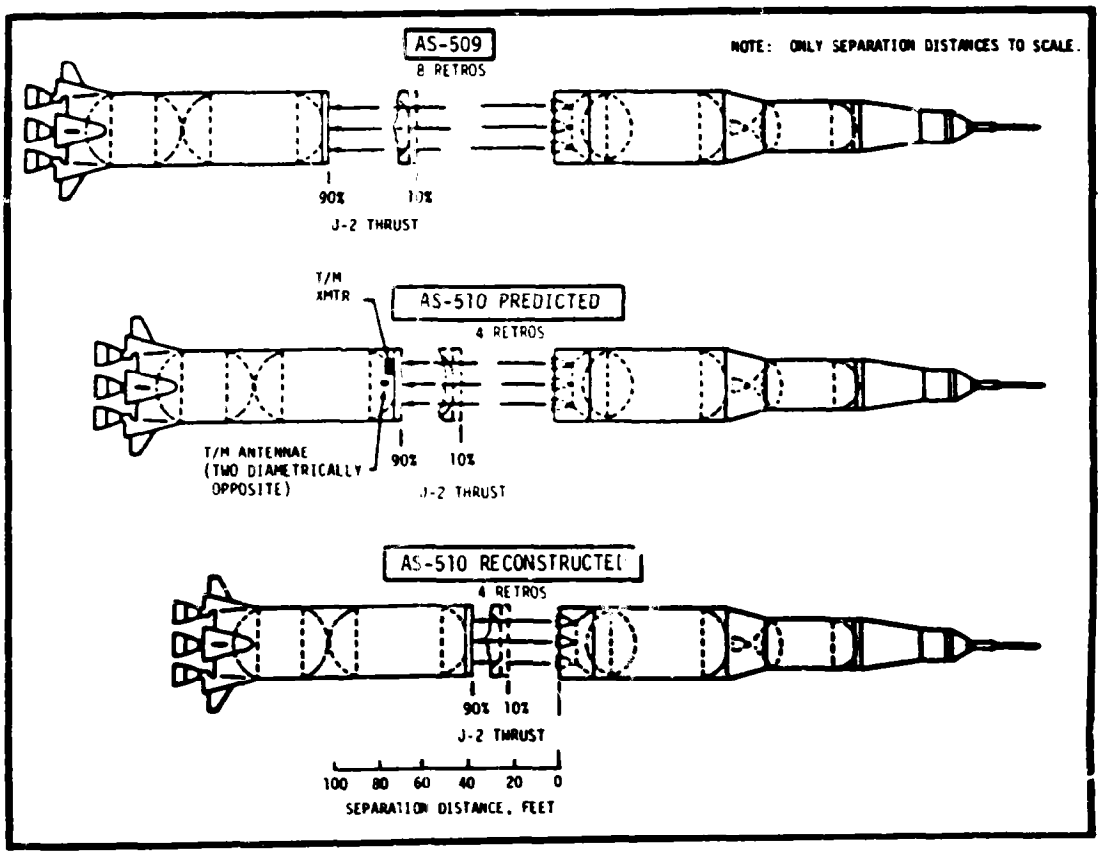

Figure 10-14. Saturn V Staging Motion

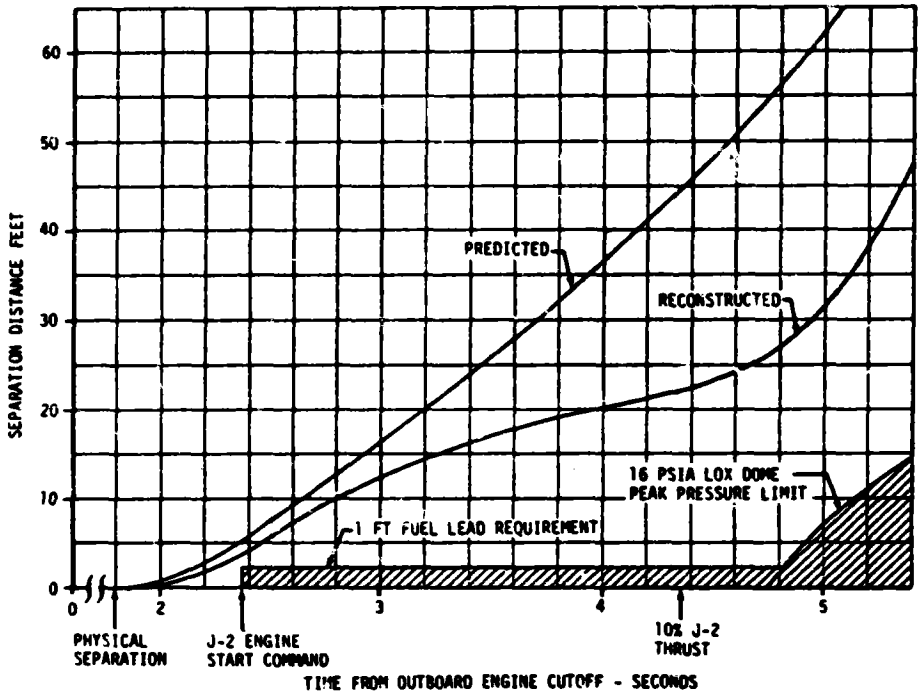

Figure 10-15. AS-510 Separation Distance

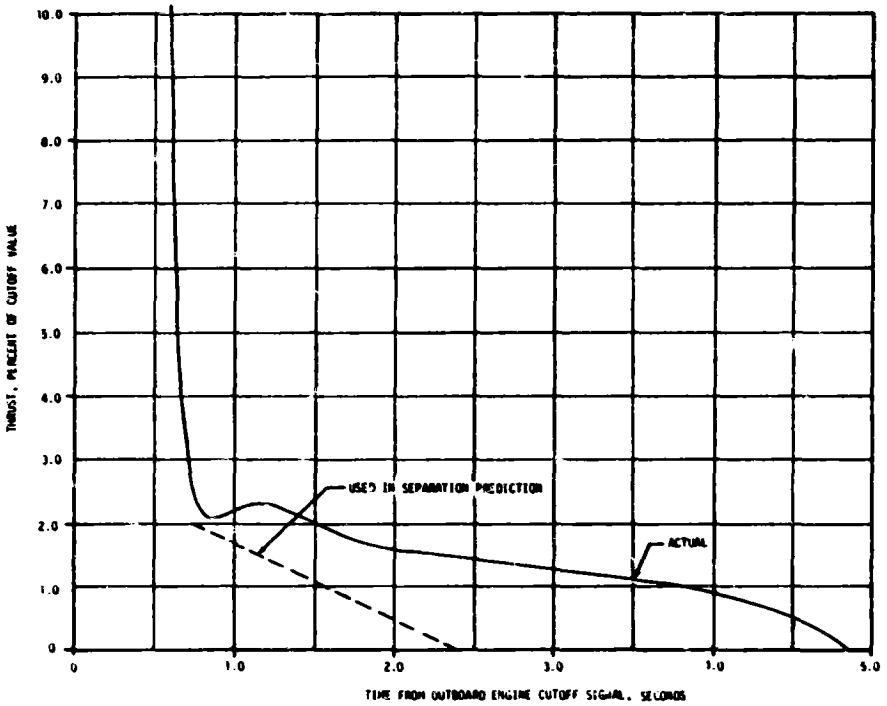

Figure 10-16. AS-510 Thrust Decay

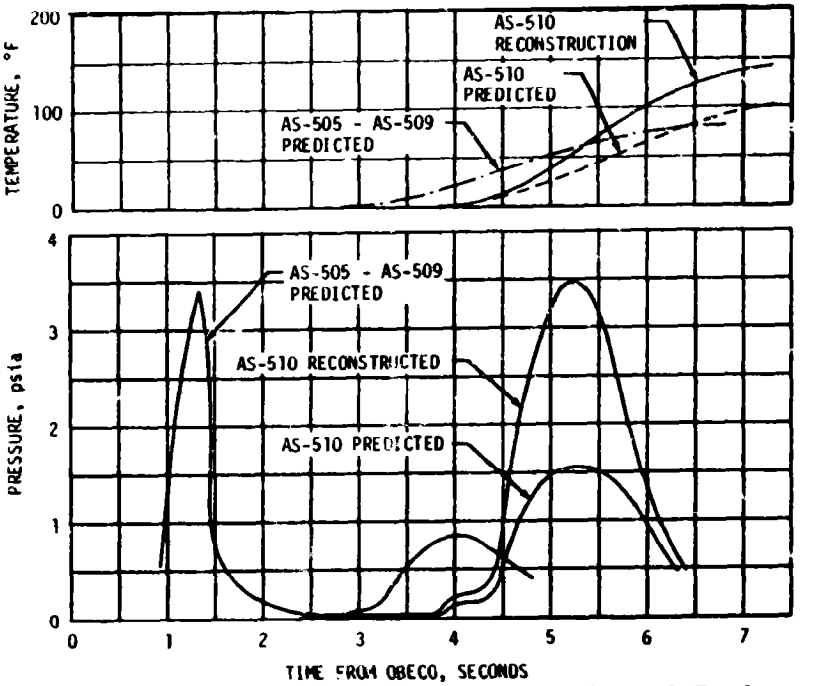

Figure 10-17. S-IC LOX Dome Pressure and Thermal Environment

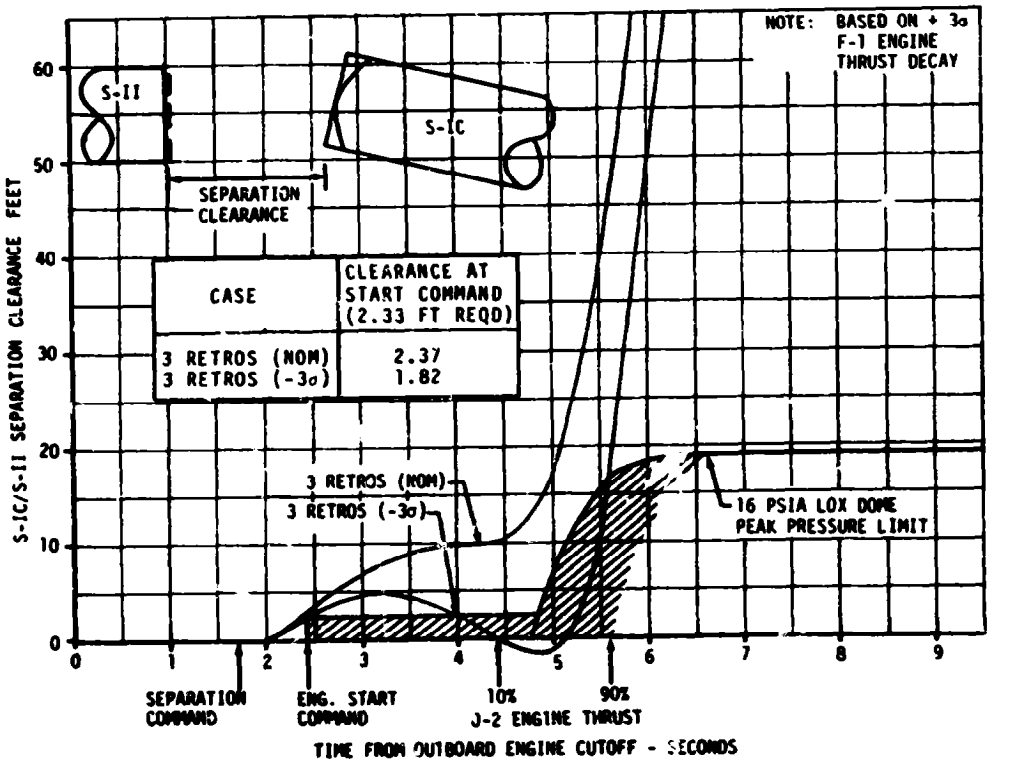

Figure 10-18. S-IC/S-II Separation Distance With Three Retro Motors

SECTION 11

ELECTRICAL NETWORKS AND EMERGENCY DETECTION SYSTEM

11.1 SUMMARY

The AS-510 launch vehicle electrical systems and Emergency Detection System (EDS) performed satisfactorily throughout all phases of flight. The S-IVB forward battery No. 2 depleted sooner than on previous flights and did not deliver its rated capacity of 24.75 ampere hours. Operation of all other batteries, power supplies, inverters, Exploding Bridge Wire (EBW) firing units and switch selectors was normal.

11.2 S-IC STAGE ELECTRICAL SYSTEM

The S-IC stage electrical system performance was satisfactory. Battery voltages were within performance limits of 26.5 to 32.0 vdc during powered flight. The battery currents were near predicted and below the maximum limits of 50 amperes for each battery. Battery power consumption was within the rated capacity of each battery, as shown in Table 11-1.

Table 11-1. S-IC Stage Battery Power Consumption

BATTERY	BUS DESIGNATION	RATED CAPACITY (AMP-MIN)	POWER CONSUMPTION*	
			AMP-MIN	PERCENT OF CAPACITY
Operational	1D10	500	27.6	5.5
Instrumentation	1D20	500	88.4	17.6

*Battery power consumptions were calculated from power transfer (T -50 seconds) until S-IC/S-II separation.

The two measuring power supplies were within the 5 ±0.05 vdc limit during powered flight.

All switch selector channels functioned as commanded by the Instrument Unit (IU) and were within required time limits.

The separation and retromotor EBW firing units were armed and triggered as programed. Charging time and voltage characteristics were within performance limits.

The range safety command system EBW firing units were in the required state-of-readiness for vehicle destruct, had it been necessary.

11.3 S-II STAGE ELECTRICAL SYSTEM

The S-II stage electrical system performed satisfactorily. Battery voltages remained within specified limits through the prelaunch and flight periods. Bus currents also remained within required and predicted limits. Main bus current averaged 32 amperes during S-IC boost and varied from 45 to 51 amperes during S-II boost. Instrumentation bus current averaged 21 amperes during S-IC and S-II boost. Recirculation bus current averaged 89 amperes during S-IC boost. Ignition bus current averaged 27 amperes during the S-II ignition sequence. Battery power consumption was within the rated capacity of each battery, as shown in Table 11-2.

Table 11-2. S-II Stage Battery Power Consumption

BATTERY	BUS DESIGNATION	RATED CAPACITY (AMP-HR)	POWER CONSUMPTION*		TEMPERATURE (°F)	
			AMP-HR	PERCENT OF CAPACITY	MAX	MIN
Main	2D11	35	14.01	40.0	93.0	84.0
Instrumentation	2D21	35	10.21	29.2	87.0	83.0
Recirculation No. 1	2D51	30	12.87	42.9	86.0	81.0
Recirculation No. 2	2D51 and 2D61	30	12.91	43.0	80.0	74.5

*Battery power consumptions were calculated from activation until S-II/S-IVB separation and include 6.5 to 6.9 AMP-HR consumed during the battery activation procedure.

The five temperature bridge power supplies, the three instrumentation power supplies, and the five LH_2 inverters all performed within acceptable limits.

All switch selector channels functioned as commanded by the IU and were within required time limits.

Performance of the EBW circuitry for the separation systems was satisfactory. Firing units charge and discharge responses were within predicted time and voltage limits. The range safety command system EBW firing units were in the required state-of-readiness for vehicle destruct, had it been necessary.

11.4 S-IVB STAGE ELECTRICAL SYSTEM

The S-IVB stage electrical system performance was satisfactory. The battery voltages, currents, and temperatures remained within the normal range for the required battery lifetime, except forward No. 2 battery which depleted at 25,600 seconds (07:06:40) after supplying only 89.7 percent of the rated capacity. Battery voltage and currents are shown in Figures 11-1 through 11-4. Battery power consumption and capacity for each battery are shown in Table 11-3.

The three 5-vdc and seven 20-vdc excitation modules all performed within acceptable limits. The LOX and LH_2 chilldown inverters performed satisfactorily.

All switch selector channels functioned as commanded by the IU and were within required time limits.

Performance of the EBW circuitry for the separation system was satisfactory. Firing units charge and discharge responses were within predicted time and voltage limits. The range safety command system EBW firing units were in the required state-of-readiness for vehicle destruct, had it been necessary.

11.5 INSTRUMENT UNIT ELECTRICAL SYSTEM

11.5.1 Summary

The IU power distribution network for AS-510 was modified to provide redundant power to the ST-124M platform and its associated components. The redundant power modification was accomplished by diode "OR"ing the 6D10 and 6D30 batteries. This configuration performed satisfactorily throughout the flight (see paragraph 11.5.2). All battery voltages, currents, and temperatures remained in the normal range during launch and coast periods of flight. Available data extend through 42,200 seconds (11:43:20) of the flight. Battery voltages, currents, and temperatures

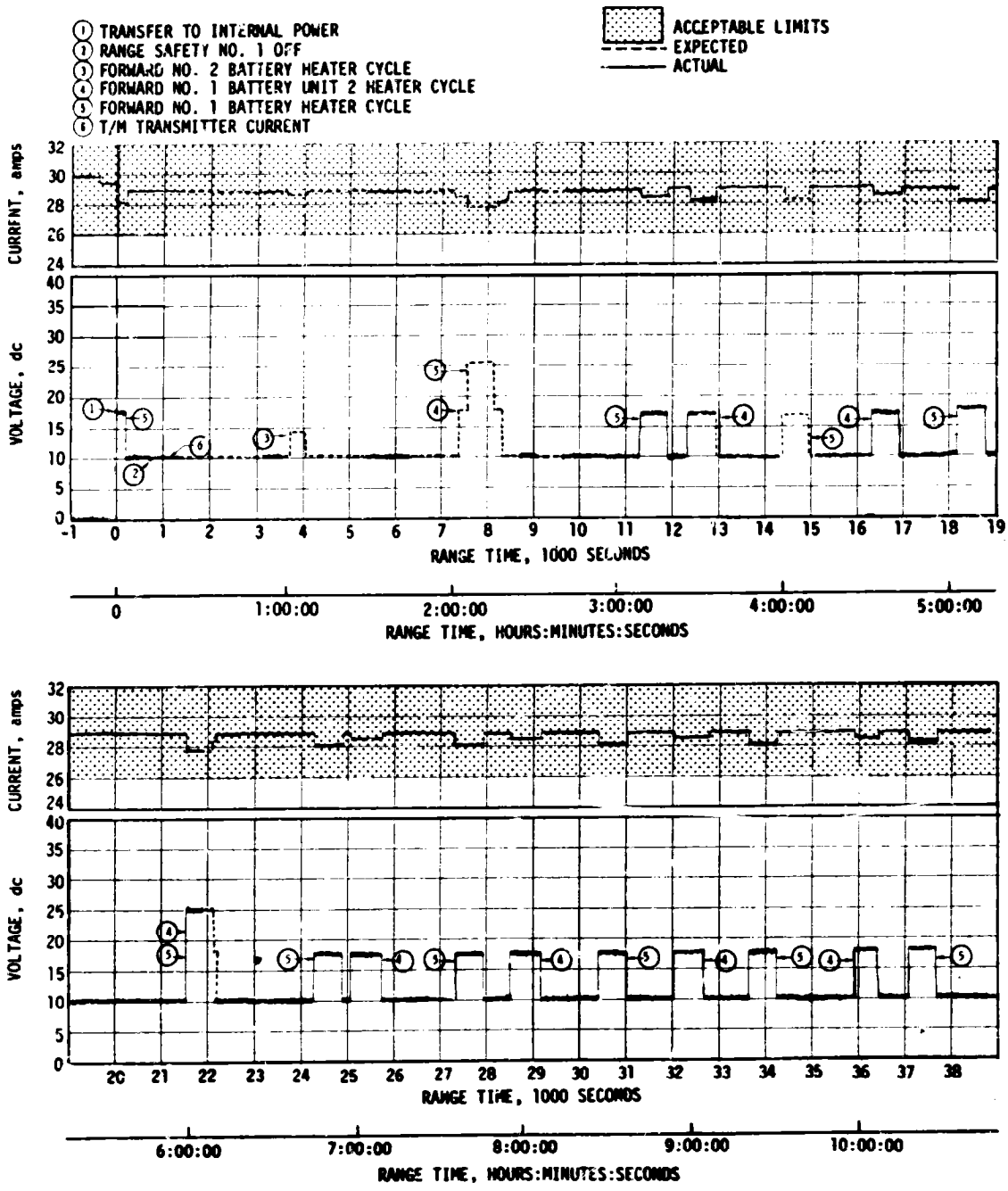

Figure 11-1. S-IVB Stage Forward No. 1 Battery Voltage and Current

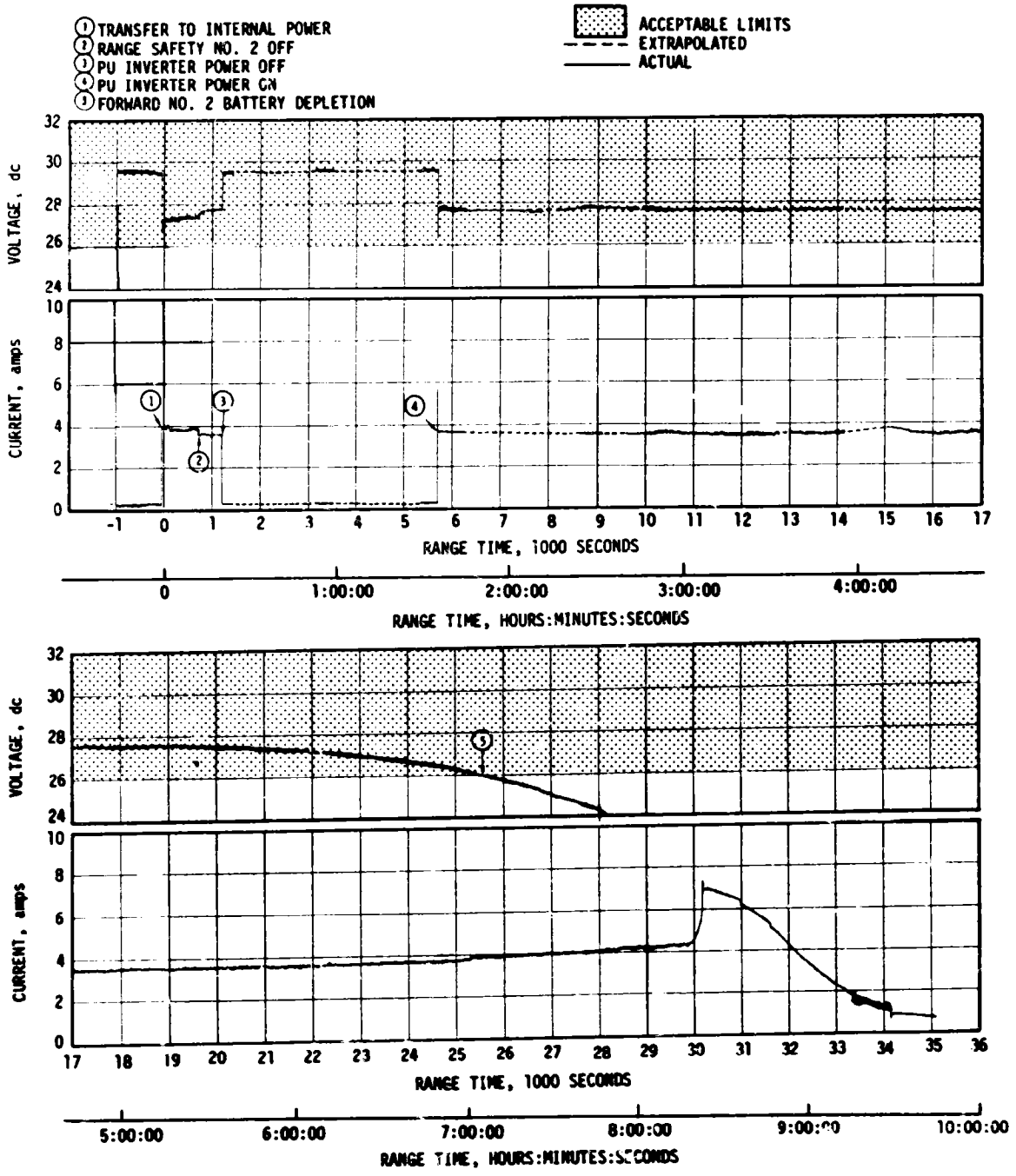

Figure 11-2. S-IVB Stage Forward No. 2 Battery Voltage and Current

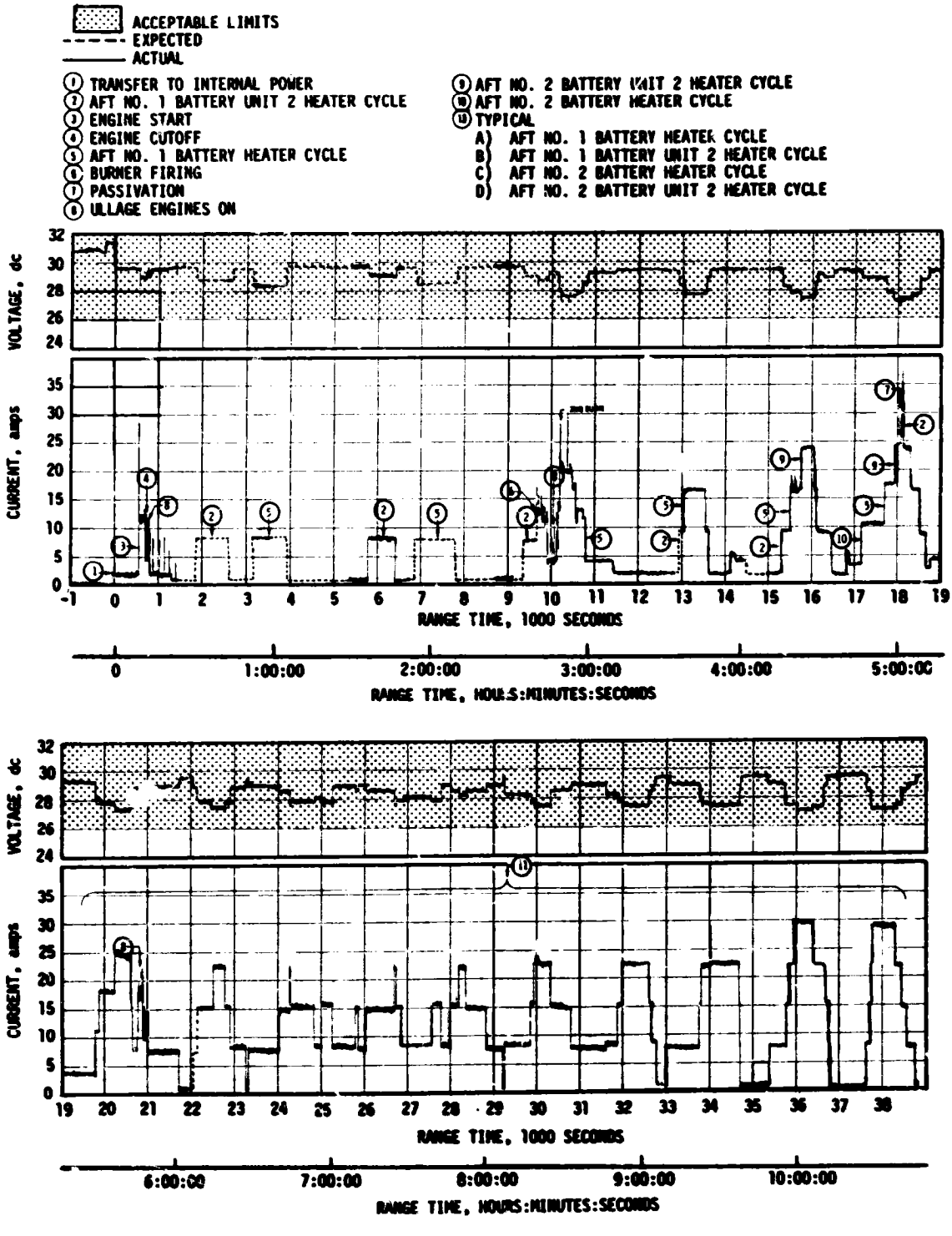

Figure 11-3. S-IVB Stage Aft No. 1 Battery Voltage and Current

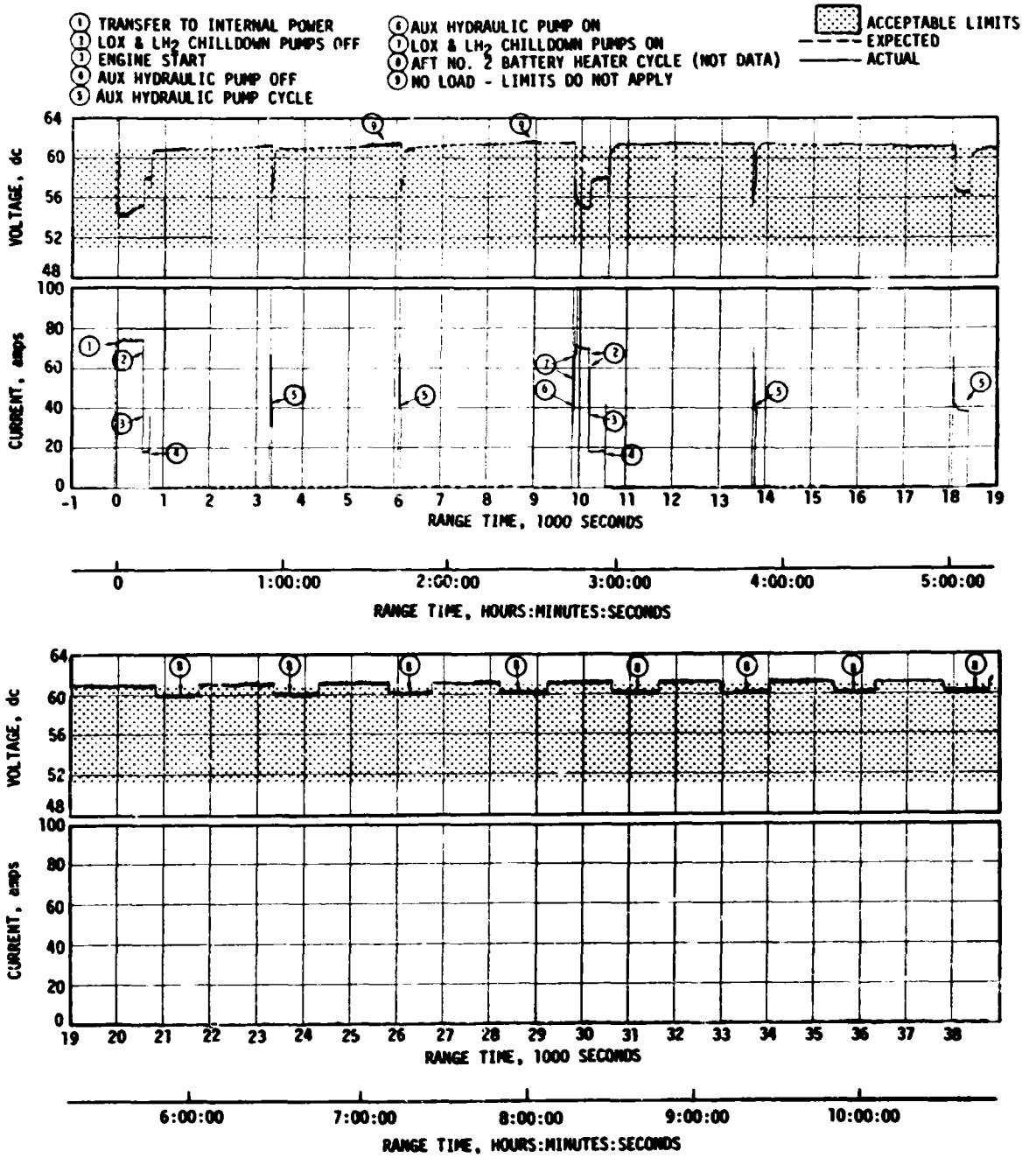

Figure 11-4. S-IVB Stage Aft No. 2 Battery Voltage and Current

Table 11-3. S-IVB Stage Battery Power Consumption

BATTERY	RATED CAPACITY (AMP-HR)	POWER CONSUMPTION	
		AMP-HR*	PERCENT OF CAPACITY
Forward No. 1	300.0	150.89	50.2
Forward No. 2	24.75	22.21**	89.7
Aft No. 1	300.0	113.15	37.7
Aft No. 2	75.0	32.94	43.9

* Actual usage was computed from battery activation to 37,162 seconds (11:43:20).

** The battery voltage fell below the defined depletion level of 26.0 volts at 25,600 seconds (07:06:40). Calculations of actual power consumption was terminated at this time.

are shown in Figures 11-5 through 11-8. Battery power consumption and capacity for each battery are shown in Table 11-3.

The 56-vdc power supply maintained an output voltage of 55.8 to 56.6 vdc, well within the required tolerance of 56 ±2.5 vdc.

The 5-vdc measuring power supply performed nominally, maintaining a constant voltage within specified tolerances.

The switch selector, electrical distributors, and network cabling performed nominally.

11.5.2 Battery 6D10 and 6D30 Load Sharing Analysis

The ST-124M platform and associated components requires 9.75 amperes. The original current sharing predictions shown in Table 11-5 were made based on an assumption of a 50/50 sharing ratio for the diode "OR" configuration between batteries 6D10 and 6D30. Flight data indicate a voltage difference existed between the 6D11 and 6D31 bus. This voltage difference requires correcting the predicted 50/50 assumption to an 80/20 sharing ratio basis.

Table 11-4. IU Battery Power Consumption

BATTERY	RATED CAPACITY (AMP-HR)	POWER CONSUMPTION	
		AMP-HR*	PERCENT OF CAPACITY
6D10	350	196.0	56.0
6D20	350	341.5**	97.3**
6D30	350	280.0	80.2*
6D40	350	324.8	92.8

* Actual usage was computed from battery activation to 37,162 seconds (10:19:22).

** The CCS transponder which was powered by the 6D20 battery was operating at S-IVB/IU lunar impact which occurred at 285,882 seconds (79:24:42). Power consumption until S-IVB/IU lunar impact was calculated based on nominal operation.

Table 11-5. IU Load Sharing Comparison

BATTERY BUS	ORIGINAL PREDICTED (AMPS)	REVISED PREDICTED (AMPS)*	ACTUAL (AMPS)*	DELTA (AMPS)*
6D10 6D11	15.08	18.01	19.40	1.39
6D30 6D31	26.68	23.76	24.20	0.44

* Based on flight data for first 750 seconds.

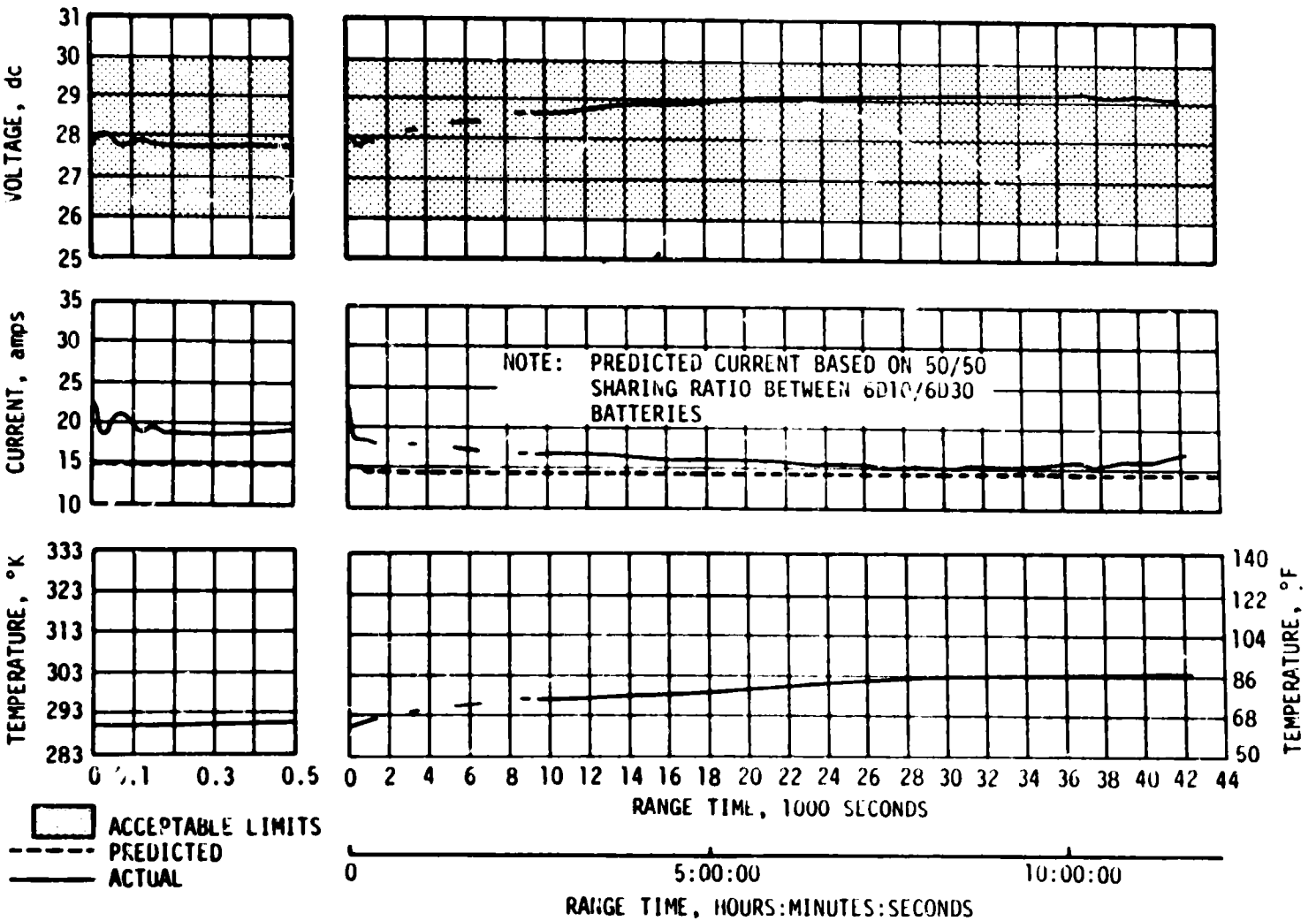

Figure 11-5. 6D10 Battery Measurements

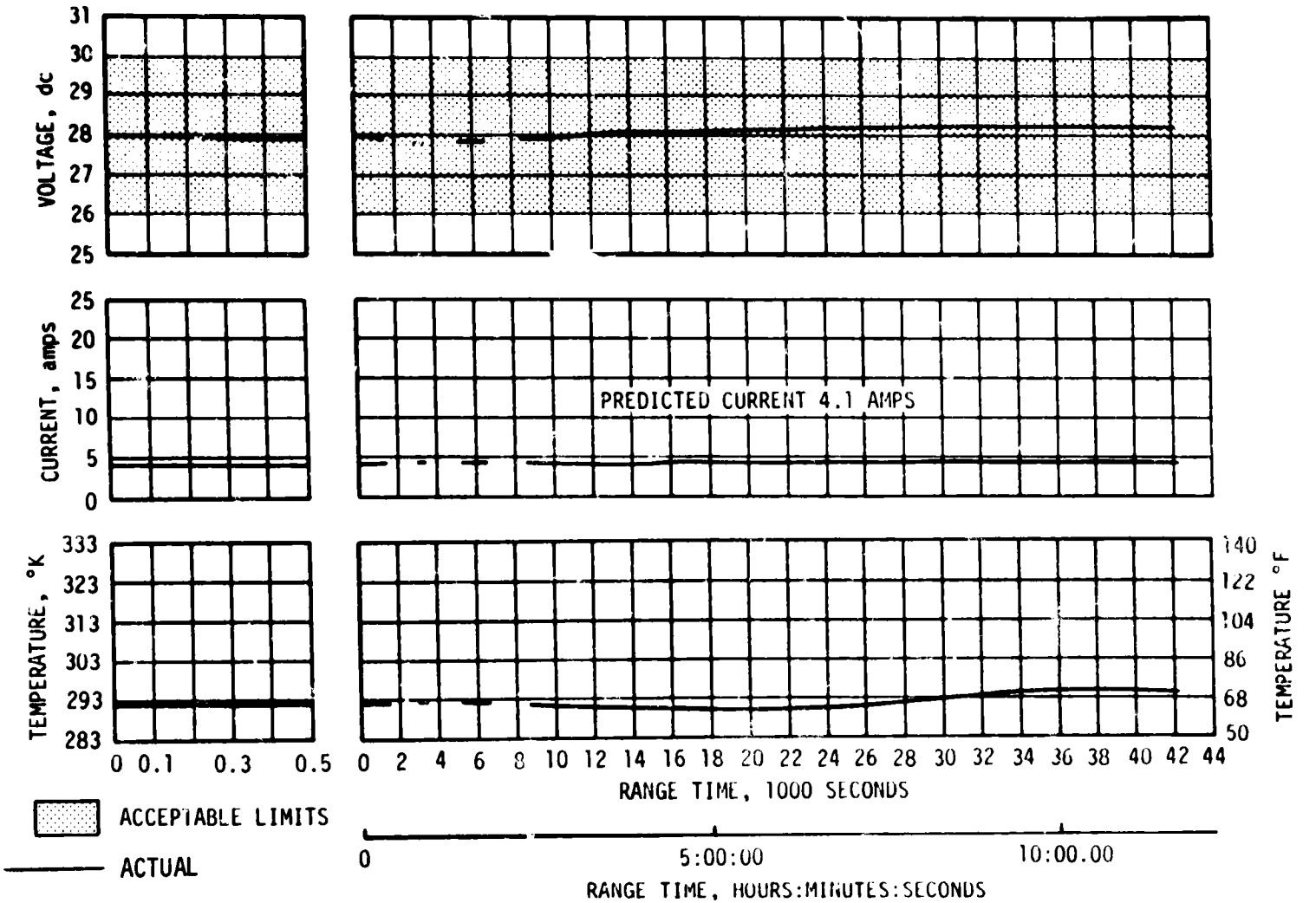

Figure 11-6. 6D20 Battery Measurements

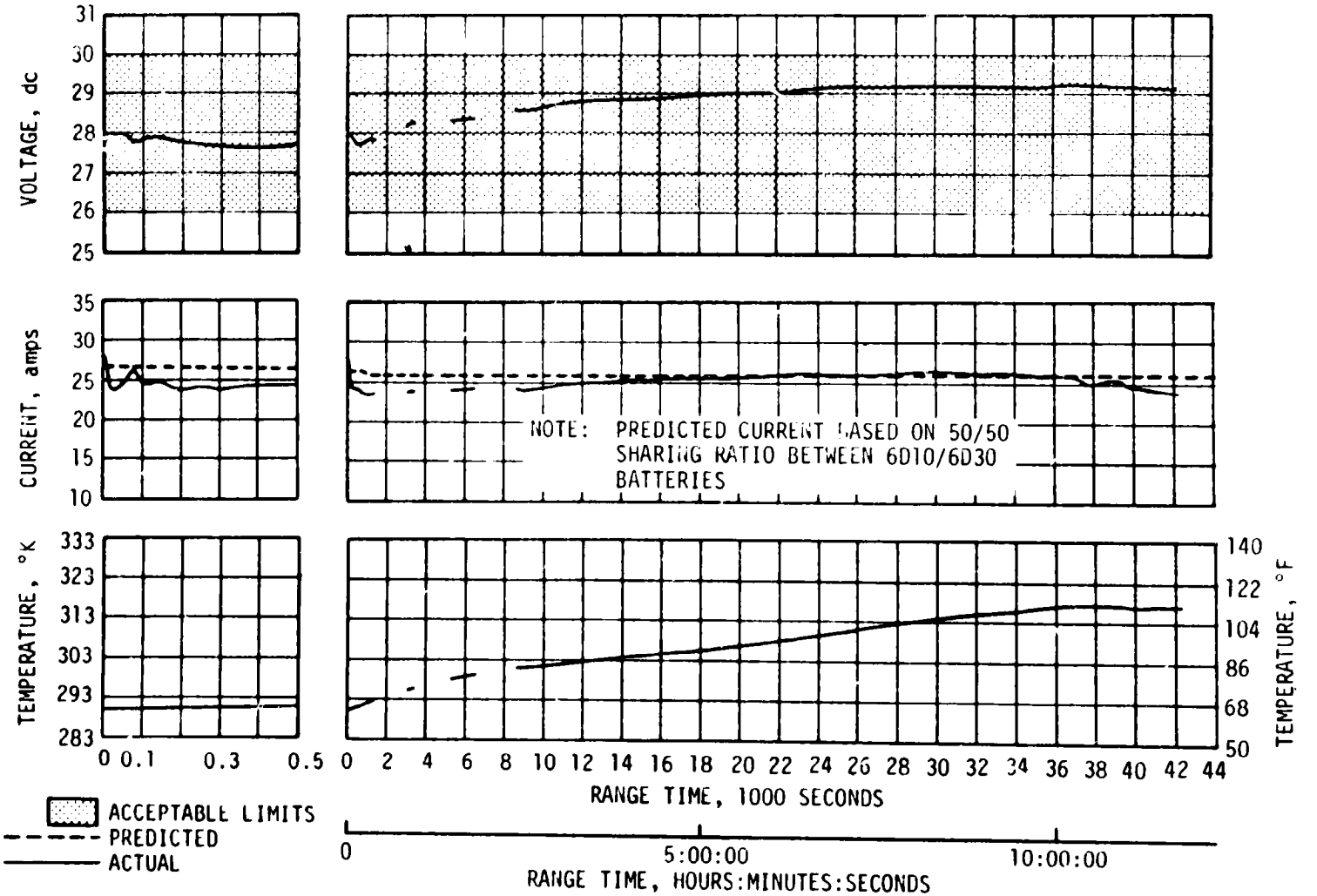

Figure 11-7. 6D30 Battery Measurements

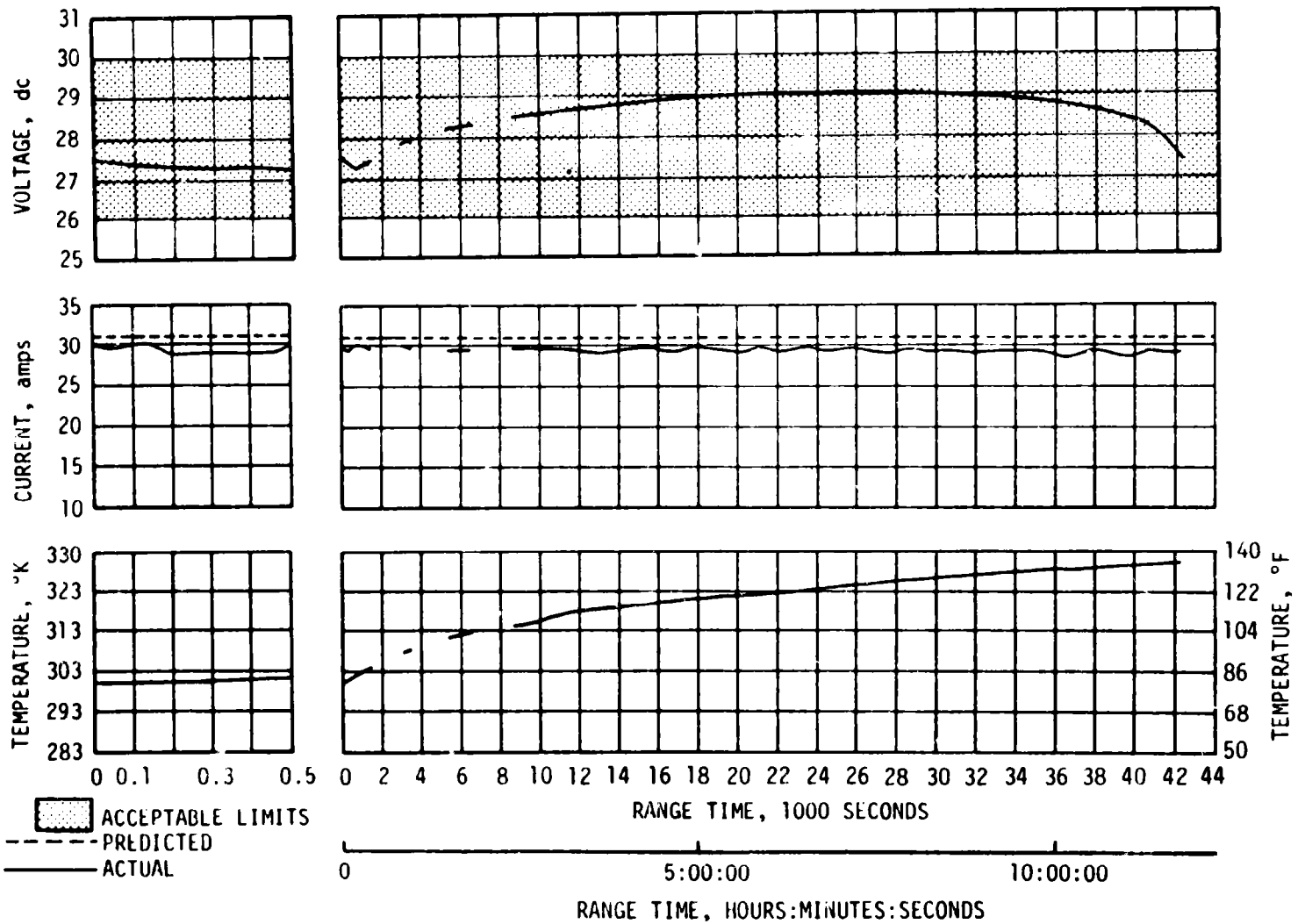

Figure 11-8. 6D40 Battery Measurements

Throughout flight, a shifting in the current sharing ratio between 6D10 and 6D30 batteries may be seen in Figures 11-5 through 11-8. This shifting is to be expected for this network configuration as the 6D11 and 6D31 voltage differential changes. Complete shifting of the total redundant load to either battery is not indicated in the AS-510 flight data.

11.6 SATURN V EMERGENCY DETECTION SYSTEM (EDS)

The performance of the AS-510 EDS was normal and no abort limits were exceeded. All switch selector events associated with EDS for which data are available were issued at the nominal times. The discrete indications for EDS events also functioned normally. The performance of all thrust OK pressure switches and associated voting logic, which monitors engine status, was nominal insofar as EDS operation was concerned. S-II and S-IVB tank ullage pressures remained within the abort limits, and displays to the crew were normal.

The maximum dynamic pressure difference sensed by the Q-ball was 0.84 psid at 79.9 seconds. This pressure was only 27 percent of the EDS abort limit of 3.2 psid.

As noted in Section 10, none of the rate gyros gave any indication of angular overrate in the pitch, yaw, or roll axis. The maximum angular rates were well below the abort limits.

SECTION 12

VEHICLE PRESSURE ENVIRONMENT

12.1 SUMMARY

The S-IC base heat shield was instrumented with two differential pressure measurements. The AS-510 flight data have trends and magnitudes similar to those seen on previous flights.

The AS-510 S-II base pressure environments are consistent with the trends and magnitudes seen on previous flights.

12.2 BASE PRESSURES

12.2.1 S-IC Base Pressures

The S-IC base heat shield was instrumented with two differential (internal minus external) pressure measurements. The AS-510 flight data, Figure 12-1, show good agreement with previous flight data with similar trends and magnitudes. The maximum differential pressure of approximately 0.20 psid occurred at an altitude of approximately 3.7 n mi.

12.2.2 S-II Base Pressures

The S-II stage base heat shield forward face pressures are presented in Figure 12-2 together with the postflight analytical values and the data band from previous flights. The AS-510 data compare favorably with previous flight data.

Figure 12-3 presents the S-II thrust cone pressure history. The flight data are slightly higher than the data band of the previous flights and are in good agreement with the postflight analysis.

The heat shield aft face pressures, Figure 12-4, were within the previous flight data band. The reduction of the J-2 engine precant angle from 1.3 to 0.6 degree was not reflected in increased heat shield aft face pressures.

12.3 S-IC/S-II SEPARATION PRESSURES

The AS-510 S-IC/S-II staging sequence was different from previous flights. The resulting forward skirt pressure environment was greater than previously experienced. A detailed discussion of the staging conditions and increased pressure environment is found in Section 10-6.

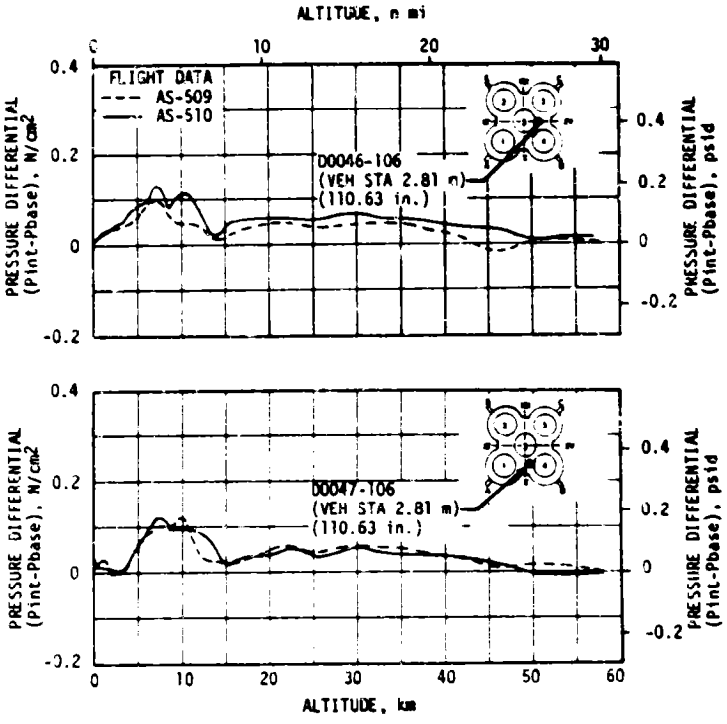

Figure 12-1. S-IC Base Heat Shield Differential Pressure

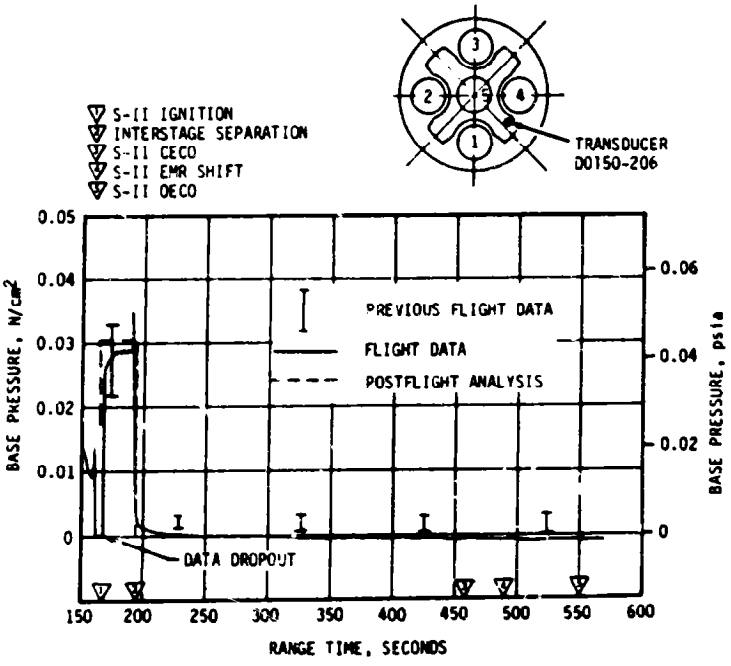

Figure 12-2. S-II Heat Shield Forward Face Pressure

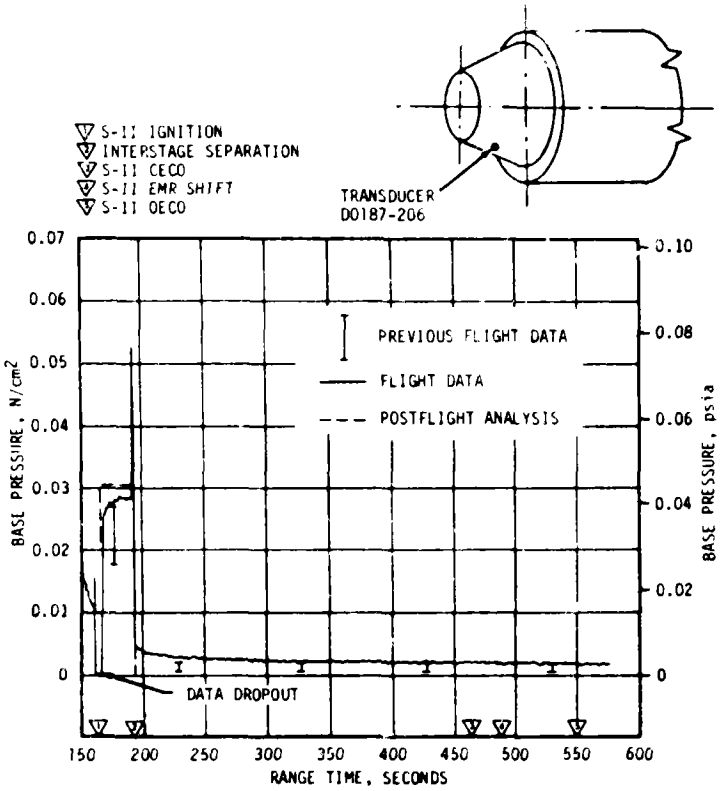

Figure 12-3. S-II Thrust Cone Pressure

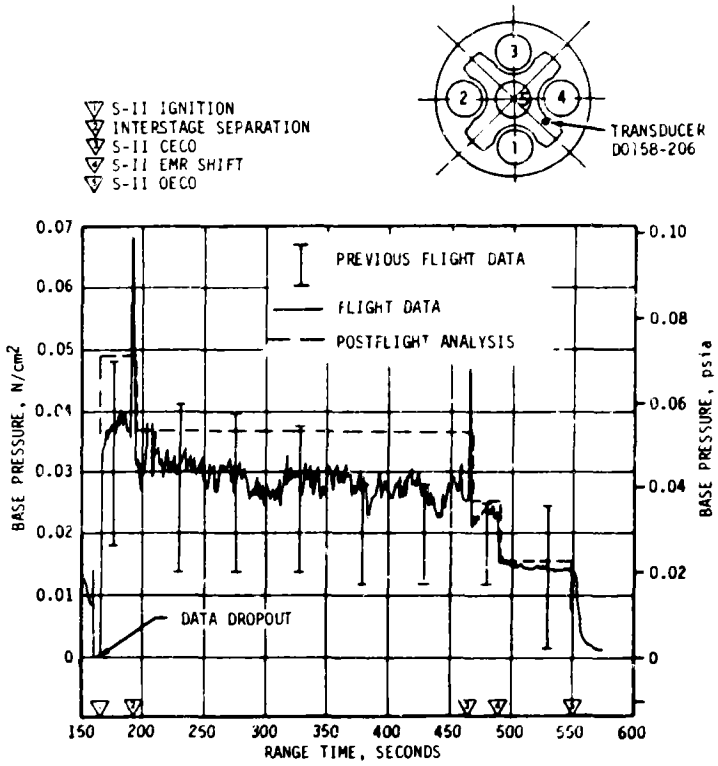

Figure 12-4. S-II Heat Shield Aft Face Pressure

SECTION 13

VEHICLE THERMAL ENVIRONMENT

13.1 SUMMARY

The AS-510 S-IC base region thermal environments exhibited trends and magnitudes similar to those seen on previous flights.

The base thermal environments on the S-II stage were consistent with the trends and magnitudes seen on previous flights and were well below design limits.

Aerodynamic heating environments and S-IVB base thermal environments were not measured on AS-510.

13.2 S-IC BASE HEATING

Thermal environments in the base region of the AS-510 S-IC stage were recorded by two total calorimeters and two gas temperature probes which were located on the base heat shield. The sensing surfaces of the total calorimeters were mounted flush with the heat shield surface. The base gas temperature sensing surfaces were mounted at distances aft of the heat shield surface of 0.25 inch (C0050-106) and 2.50 inches (C0052-106). Data from these instruments are compared with AS-509 flight data and are presented in Figures 13-1 and 13-2. The AS-510 data exhibit similar trends and magnitudes as previous flights. The maximum recorded total heating rate was approximately 24.67 Btu/ft^2-s and occurred at an altitude of 10.8 n mi. The maximum gas temperature was approximately 1664°F, recorded 2.5 inches aft of the heat shield, at an altitude of 11.3 n mi. In general, CECO on AS-510 produced a spike in the thermal environment data with a magnitude and duration similar to previous flight data.

Ambient gas temperatures under the engine cocoons (measurements C0242-101 through C0242-105) were within the band of previous flight data and within predicted values. These temperatures are shown in Figure 13-3.

13.3 S-II BASE HEATING

Figure 13-4 presents the AS-510 total heating rate throughout S-II burn, as recorded by transducer C0722-206 on the aft face of the base heat shield. The postflight analytical curve for this transducer and the previous flight data band are also shown for comparison. The analytical

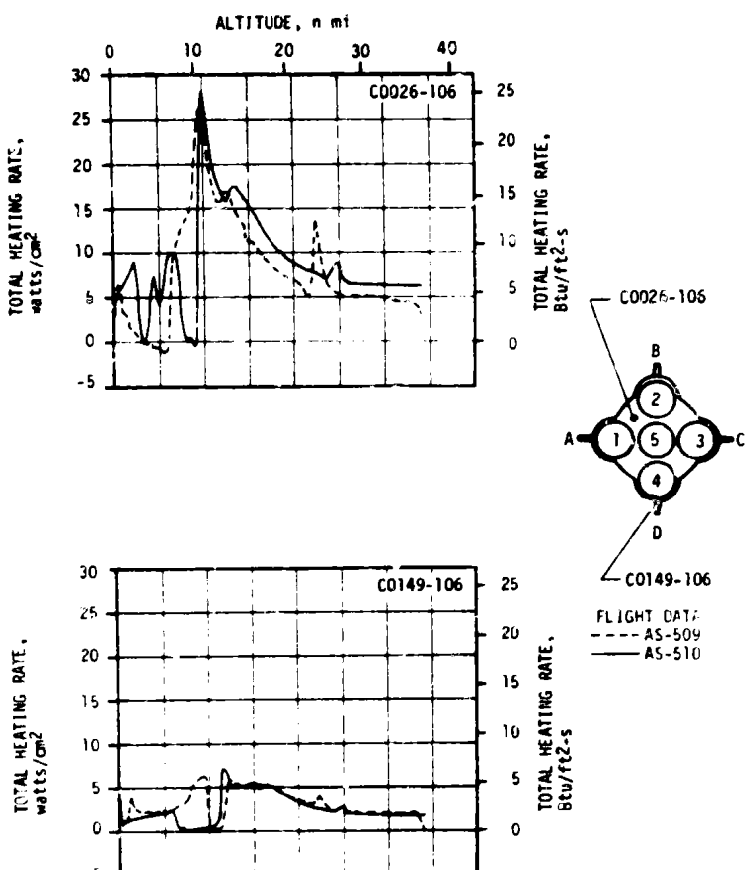

Figure 13-1. S-IC Base Region Total Heating Rate

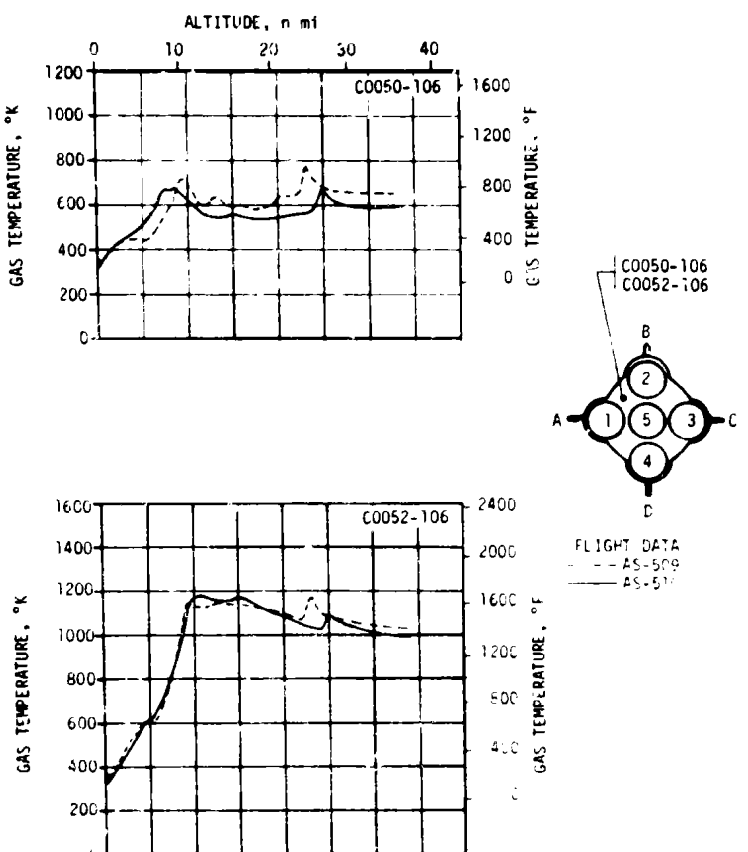

Figure 13-2. S-IC Base Region Gas Temperature

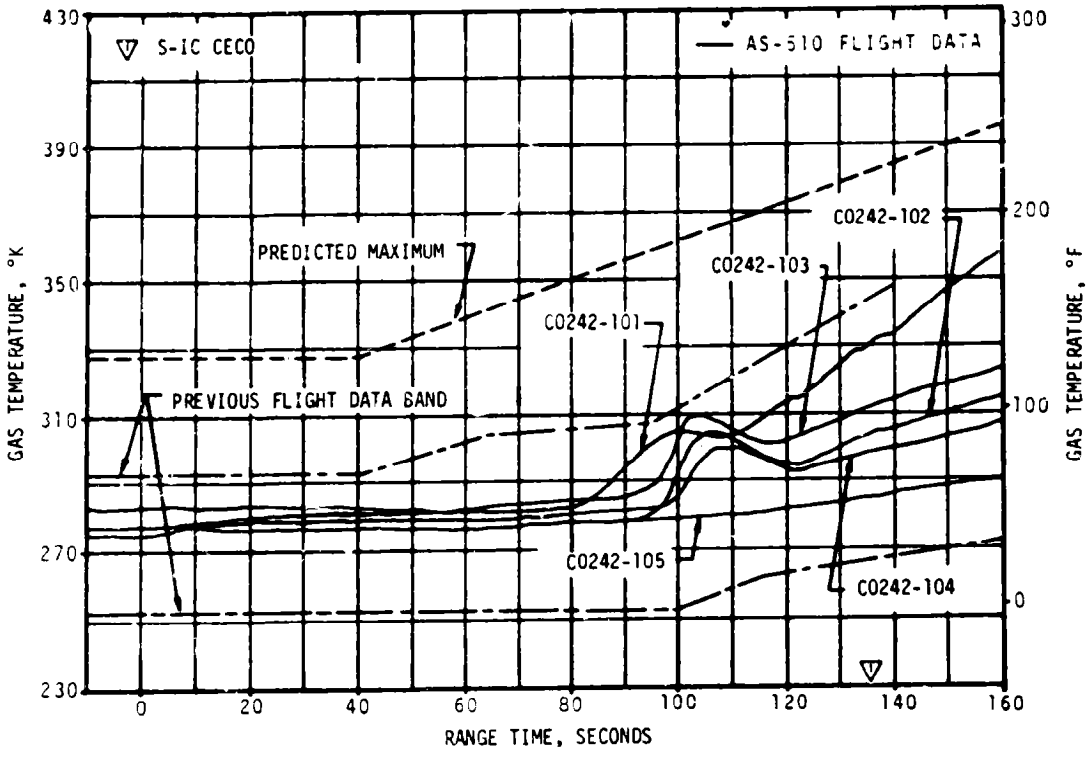

Figure 13-3. S-IC Ambient Gas Temperature Under Engine Cocoon

heat rate represents the theoretical response of the transducer to the total thermal environment reflected by thermal math models. Key flight parameters relating to engine performance, engine position, and reference temperatures are used in the postflight analysis. The math models are based on both theoretical and empirical postulates. The flight data for AS-510 are higher than that recorded during previous flights. This was expected since the J-2 engine precant on the S-II-10 stage was reduced from 1.3 degrees to 0.6 degree. Due to the uncertainty of engine deflections during the period CECO to performance mixture ratio shift, no attempt was made to predict the effect of CECO on heat shield aft face heating rates. The flight measured heating rates were well below the maximum design allowable values.

Figure 13-5 shows the AS-510 flight data and postflight analysis of the heat shield recovery temperature transducer, C0731-206. The analytical temperature curve represents a calculated transducer reading based on math models using key flight parameters. The gas recovery temperature is an analytically derived value computed from the flight measurement data. Note that the flight values are the probe temperatures and not the gas recovery temperatures. The AS-510 flight gas recovery temperature values were expected to be on the high side of the previous flight data due to the reduction of the S-II-10 stage J-2 engine precant angle. Figure 13-5 shows that this is not substantiated by the flight data. However, as indicated by the data envelope from previous flights, a

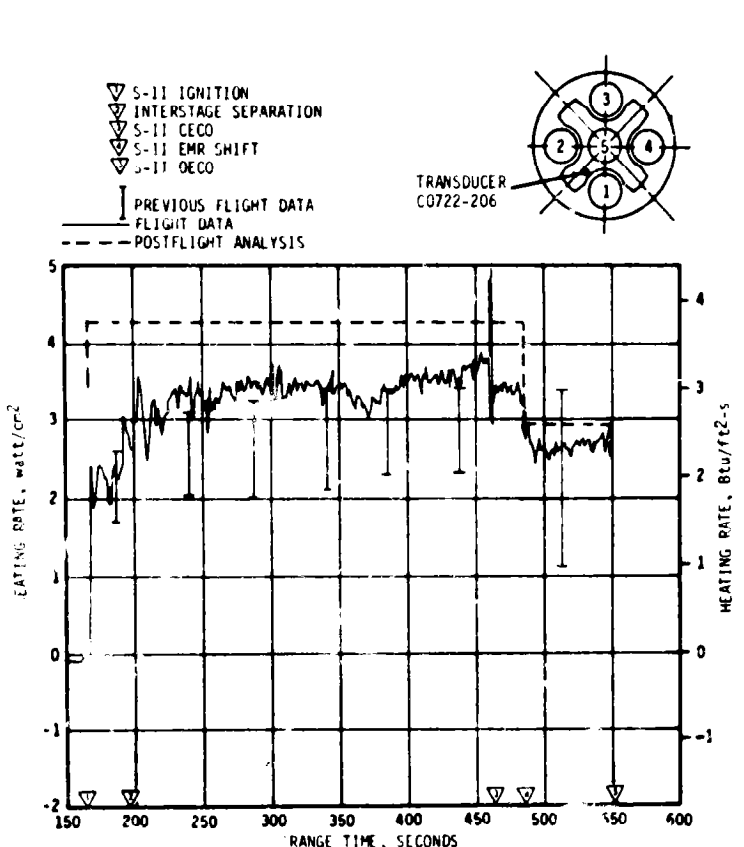

Figure 13-4. S-II Heat Shield Aft Heat Rate

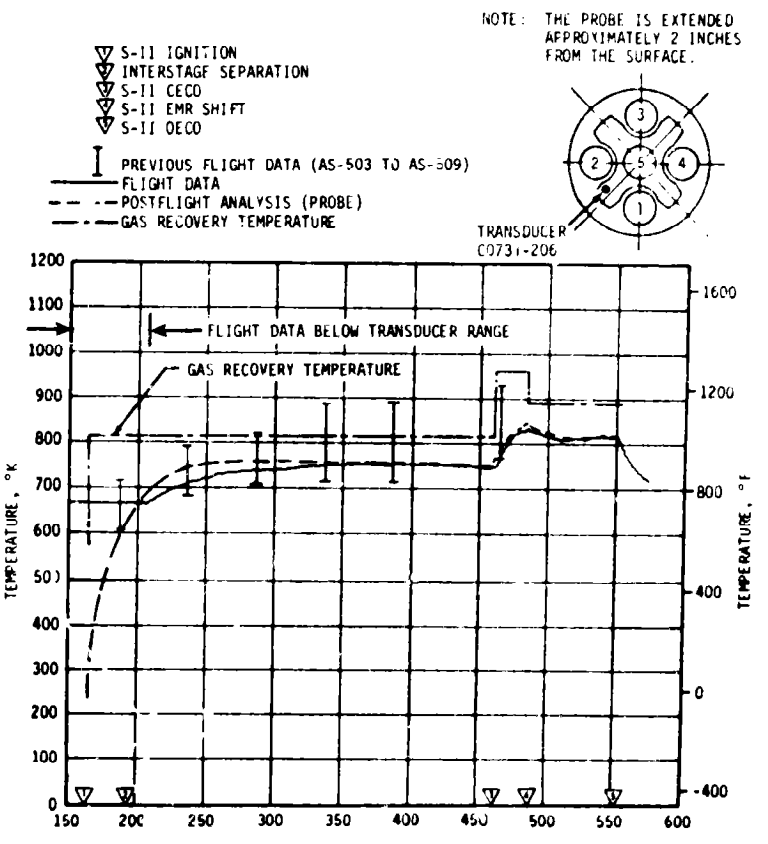

Figure 13-5. S-II Heat Shield Gas Recovery Temperature

considerable probe temperature variation exists between different flights which cannot be explained by the variation of the parameters considered in the analysis alone. Also, since the initial temperature is below the probe range, it is not possible to determine if the probe temperature is biased.

Figure 13-6 shows the AS-510 flight data and postflight analysis of the heat shield aft radiation heat rate. The analytical radiation heat rate represents the heat rate at the transducer location and is derived from a math model. Good agreement is obtained between flight and the post-flight analytical values and with previous flight data.

There were no structural temperature measurements on the base heat shield and only three thrust cone forward surface temperature measurements in the base region. To evaluate the structural temperatures on the aft

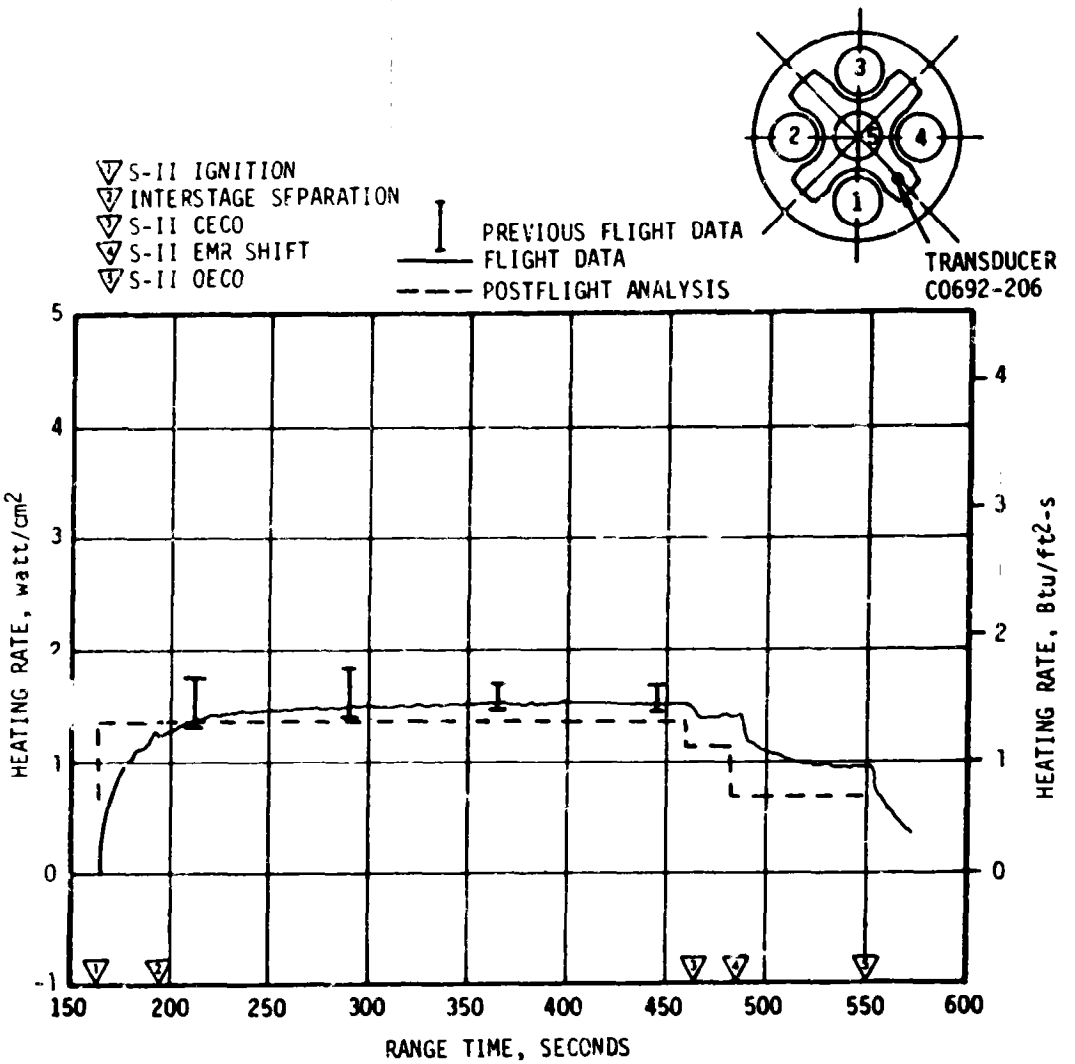

Figure 13-6. S-II Heat Shield Aft Radiation Heat Rate

surface of the heat shield, a postflight analysis was performed using maximum AS-510 postflight analysis base heating rates. The maximum postflight analysis temperature was 950°F which compares favorably with previous flights, and was well below the maximum design temperatures of 1460°F (no engine out) and 1550°F (one control engine out). The effectiveness of the heat shield and flexible curtains was evidenced by the relatively low temperatures recorded on the thrust cone forward surface. The maximum measured temperature on the thrust cone forward surface was 29°F The measured temperatures were well below design values.

13.4 VEHICLE AEROHEATING THERMAL ENVIRONMENT

Aerodynamic heating environments were not measured on the AS-510 S-IC stage. Due to the similarity in the trajectory, the aerodynamic heating environments are believed to be approximately the same as previous flight environments. Flow separation on the AS-510 vehicle was observed from ground optical data (Melbourne Beach) to occur at approximately 110 seconds. The forward point of flow separation versus flight time is presented in Figure 13-7. The effects of CECO during the AS-510 flight were similar to previous flights. At higher altitudes the measured location of the forward point of flow separation is questionable due to loss of resolution in the ground optical data.

13.5 S-IC/S-II SEPARATION THERMAL ENVIRONMENT

The AS-510 S-IC/S-II staging sequence was different from previous flights. The resulting forward skirt thermal environment was more severe than previously experienced. A detailed discussion of the staging conditions and thermal environment is found in Section 10-6.

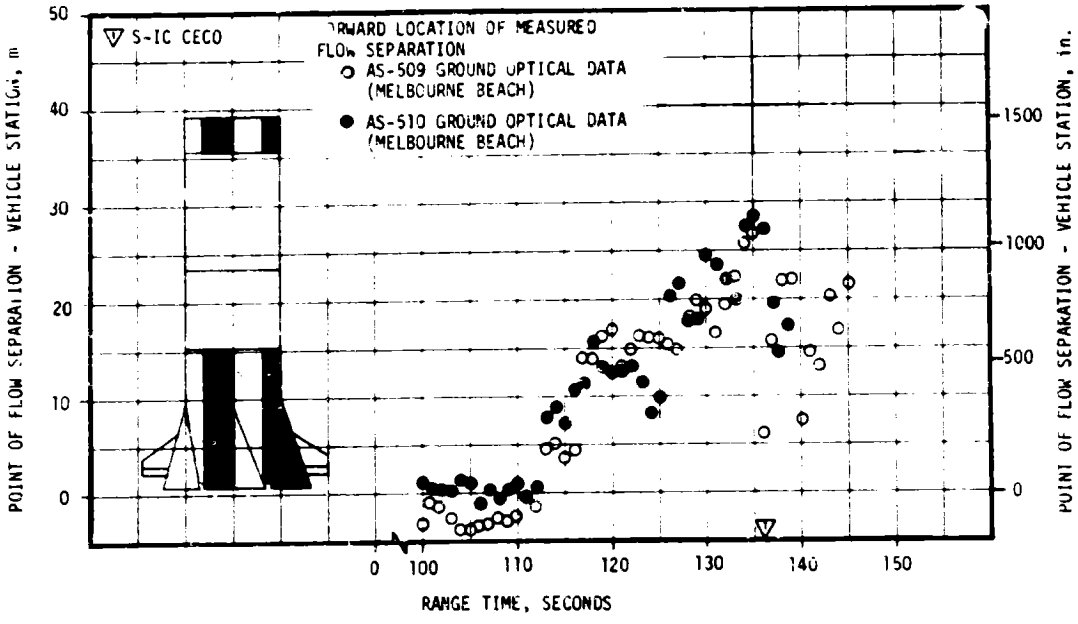

Figure 13-7. Forward Location of Separated Flow on S-IC Stage

SECTION 14

ENVIRONMENTAL CONTROL SYSTEMS

14.1 SUMMARY

The S-IC stage forward compartment ambient temperatures were maintained above the minimum performance limit during AS-510 countdown. The S-IC stage aft compartment environmental conditioning system performed satisfactorily.

The S-II thermal control and compartment conditioning system apparently performed satisfactorily since the ambient temperatures external to the containers were normal, and there were no problems with the equipment in the containers.

The Instrument Unit (IU) Environmental Control System (ECS) performed satisfactorily for the duration of its mission. Coolant temperatures, pressures, and flowrates were maintained within the required limits.

14.2 S-IC ENVIRONMENTAL CONTROL

The S-IC stage forward skirt ECS has three phases of operation during prelaunch operations. When onboard electrical systems are energized, but prior to cryogenic loading, conditioned air is used to maintain the desired environment. When cryogenic loading begins, warmed GN_2 is substituted for the conditioned air. The third phase uses a warmer GN_2 flow to offset the cooling effects caused by S-II stage J-2 engine thrust chamber chilldown. All three phases functioned satisfactorily as evidenced by ambient temperature readings.

The most severe prelaunch forward compartment thermal environment (-77°F at C0206-120) occurred during J-2 engine chilldown and was above the minimum performance limit of -90°F. During flight the lowest forward compartment temperature measured was -135.6°F at instrument location C0206-120.

After the initiation of LOX loading, the temperature in the vicinity of the battery (12K10) decreased to 65°F which is within the battery qualification limits of 35 to 95°F. The temperature increased to 79°F at liftoff. Just prior to liftoff, the other ambient temperatures ranged from 70°F at instrument location C0203-115 to 90.3°F at instrument location C0205-115. During flight the lowest aft compartment temperature recorded was 60.8°F at instrument location C0203-115.

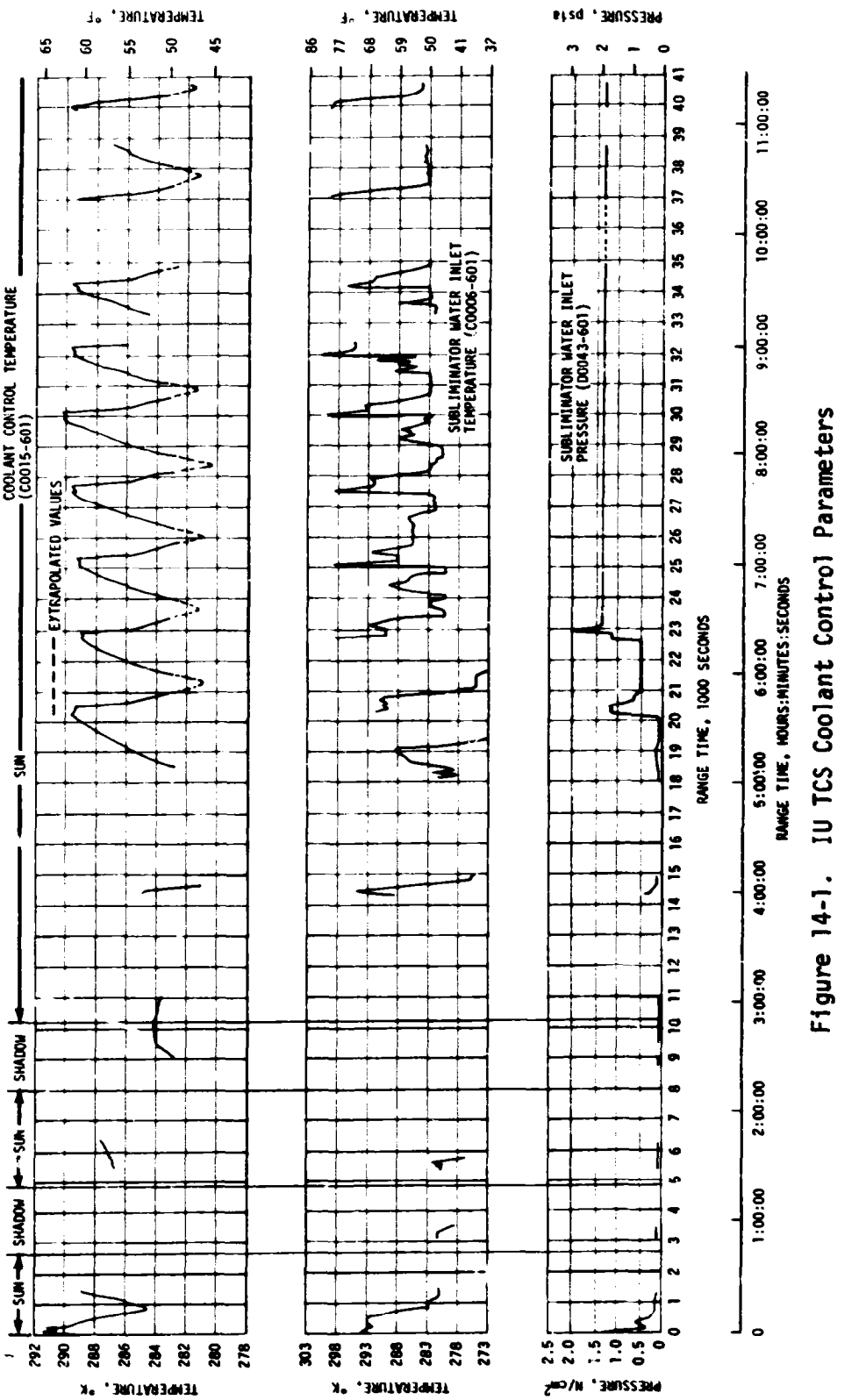

Figure 14-1. IU TCS Coolant Control Parameters

14.3 S-II ENVIRONMENTAL CONTROL

The engine compartment conditioning system maintained the ambient temperature and thrust cone surface temperatures within design ranges throughout the launch countdown. The system also maintained an inert atmosphere within the compartment as evidenced by the absence of H_2 or O_2 indications on the hazardous gas monitor.

No equipment container temperature measurements were taken. However, since the ambient measurements external to the containers were satisfactory and there were no problems with the equipment in the containers, it is assumed that the thermal control system performed adequately.

14.4 IU ENVIRONMENTAL CONTROL

14.4.1 Thermal Conditioning System

Performance of the IU Thermal Conditioning System (TCS) was satisfactory throughout flight. The temperature of the coolant supplied to the coldplates and internally cooled components was continuously maintained within the required 45 to 68°F temperature band.

Figure 14-1 shows the TCS coolant control temperature (C0015-601) out to 41,000 seconds (11:23:20). The range of measurement C0015-601 does not allow reading the minimum coolant temperature; however, extrapolation of the data indicates that the coolant temperature did not drop below the specification limit.

Sublimator performance during ascent is presented in Figure 14-2. The water control valve opened at approximately 183 seconds allowing water to flow to the sublimator. Significant cooling of the sublimator was evidenced at approximately 215 seconds at which point the temperature of the coolant began to rapidly decrease. This high cooling rate during the first 120 seconds after water valve opening is typical of a fast starting sublimator. At the first thermal switch sampling (480 seconds) the coolant temperature was below the actuation point, hence the water valve was closed. At the second thermal switch sampling, the coolant temperature was still below the actuation point and the water valve remained closed.

Figure 14-1 shows temperature control parameters over the time span for which data has been received. Sublimator cooling was nominal as evidenced by normal (C0015-601) coolant temperature cycling through 40,000 seconds (11:06:40) into the flight. Following water valve closure at approximately 20,580 seconds (05:43:00) the water line pressure, as indicated by measurement D0043-601, leveled off at about 0.72 psia rather than continuously decreasing to zero as normally observed during the sublimator drying out cycle. The indicated pressure remained at this level until the water valve reopened at approximately 22,680 seconds (06:18:00), at which time the indicated pressure rose to approximately 3.0 psia. Once the

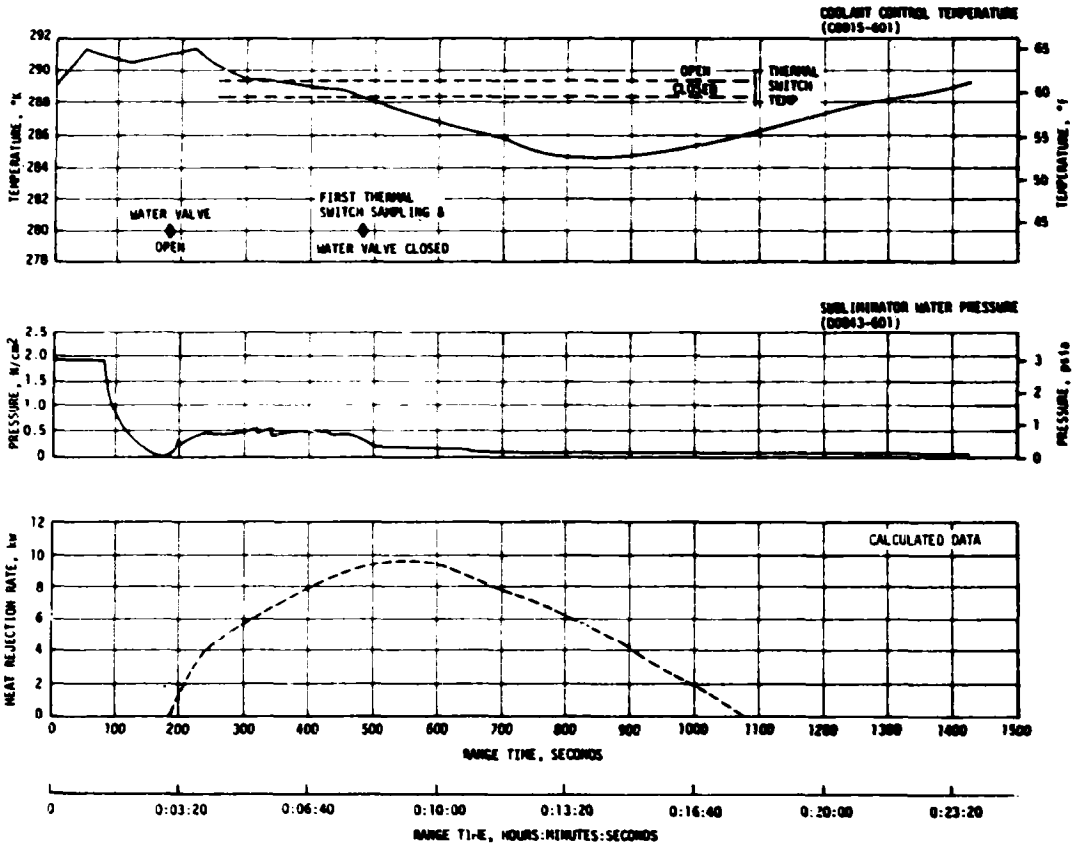

Figure 14-2. IU Sublimator Performance During Ascent

water valve closed at approximately 22,980 seconds (06:23:00), the indicated pressure decreased to a level of 1.95 psia and remained at this level throughout the remaining data even though several water valve cycles were experienced. At the time of each occurrence and thereafter, sublimator cooling was evidenced by cycling of coolant control temperature, water inlet temperature, and water flowrate. The water line temperature sensor indicated a value less than 32°F just prior to the initial and final leveling off of pressure (D0043-601). This suggests that the probable cause for the pressure inconsistency was ice formation at or on the pressure transducer. Such an inconsistency could occur if the water immediately adjacent to the transducer diaphragm were to freeze leaving a small hole which allowed the pressure to instantaneously increase during the next water valve cycle and allowing more water to reach the transducer diaphragm. The water induced through the small hole could freeze, completely sealing off the transducer diaphragm with a positive pressure entrapped. This ice blockage would physically prevent the diaphragm from returning to its undistended (zero pressure) position. In any case, the erroneous pressure indication had no effect on TCS operation.

Hydraulic performance of the TCS was as expected throughout the time period for which data have been evaluated. System flowrates and pressures are presented in Figure 14-3. No significant changes in performance were noted throughout this time span.

The TCS GN_2 supply pressure decay, which is indicative of GN_2 usage rate, was nominal, as shown in Figure 14-4.

All component temperatures remained within their expected ranges throughout the primary IU mission, (Figure 14-5) and continued under ECS control throughout the time span for which data have been evaluated.

The thermal shrouds were effective in shielding the IU components from solar heating as evidenced by the low-normal component temperatures. This is especially significant since the IU was never in the earth's shadow after 10,200 seconds (02:50:00).

14.4.2 ST-124M-3 Gas Bearing System (GBS)

The gas bearing system performance was nominal throughout the IU mission. Figure 14-6 depicts ST-124M-3 platform pressure differential (D0011-603) and platform internal ambient pressure (D0012-603).

The GBS GN_2 supply sphere pressure decay was nominal, as shown in Figure 14-7.

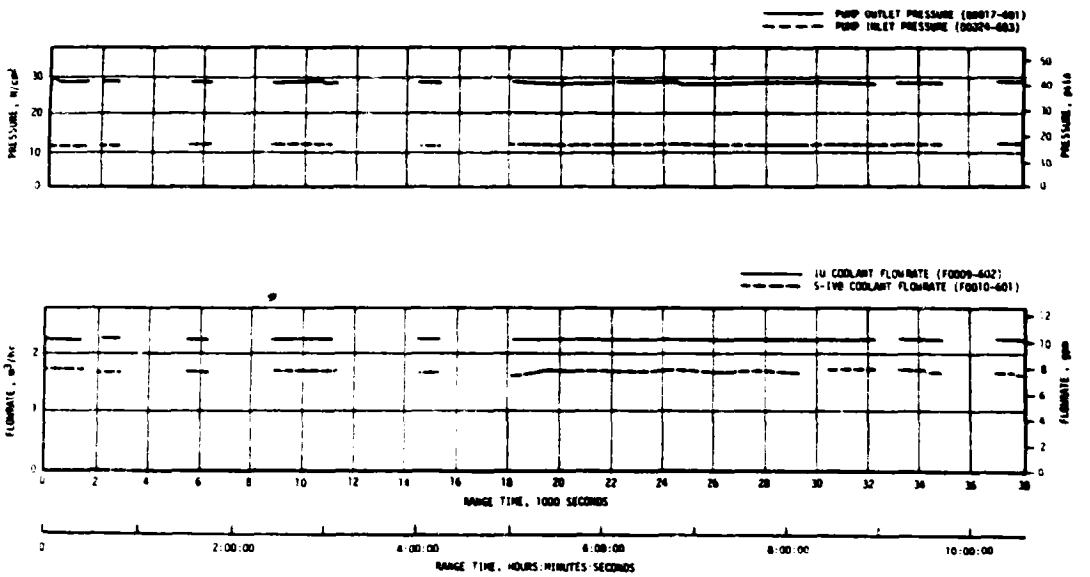

Figure 14-3. IU TCS Hydraulic Performance

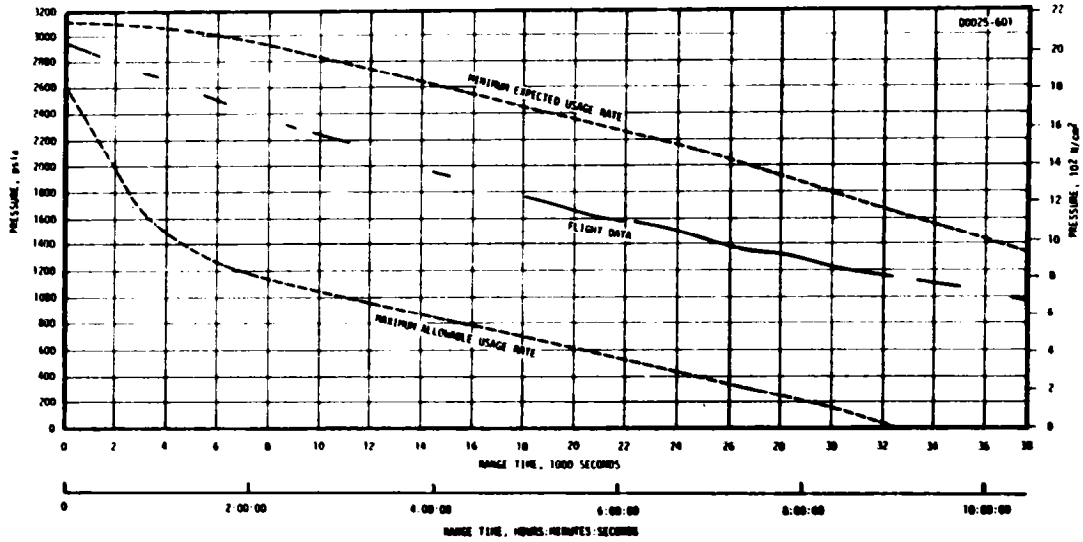

Figure 14-4. IU TCS GN_2 Sphere Pressure

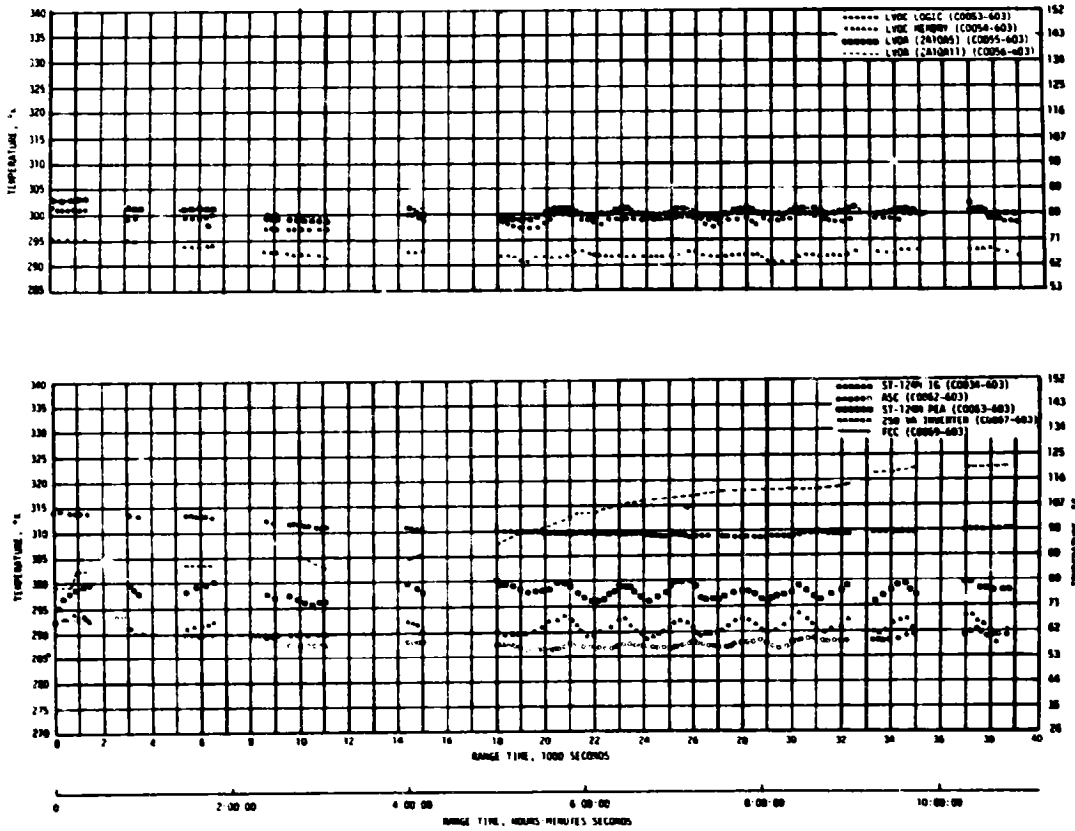

Figure 14-5. Selected IU Component Temperatures

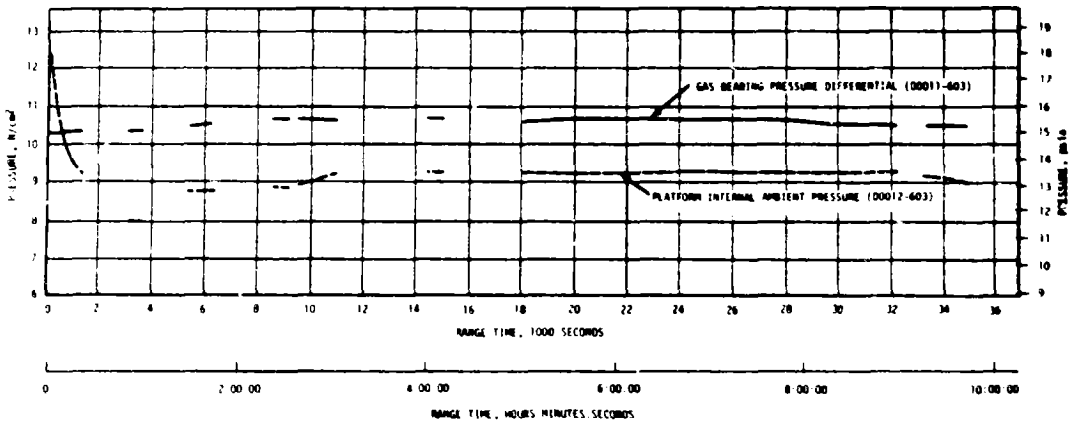

Figure 14-6. IU Inertial Platform GN_2 Pressures

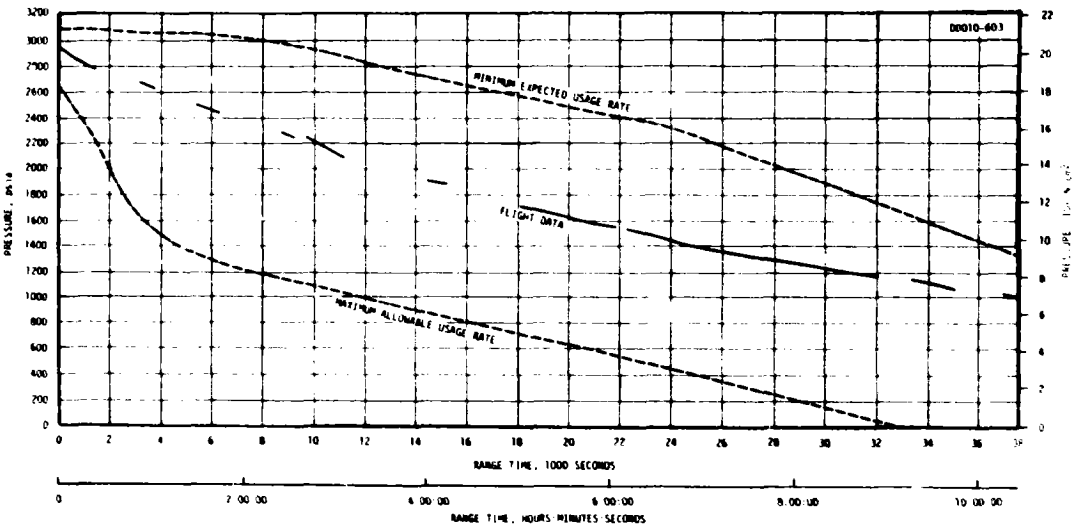

Figure 14-7. IU GBS GN_2 Sphere Pressure

SECTION 15

DATA SYSTEMS

15.1 SUMMARY

All data systems performed satisfactorily throughout the flight. Flight measurements from onboard telemetry were 99.8 percent reliable.

Telemetry performance was normal except that the S-IC telemetry was lost after S-IC/S-II separation. Radio Frequency (RF) propagation was generally good, though the usual problems due to flame effects and staging were experienced and an additional dropout occurred when S-II stage flame impinged on the S-IC stage at S-II stage ignition. Usable VHF data were received until 23,225 seconds (6:27:05). The Secure Range Safety Command Systems (SRSCS) on the S-IC, S-II, and S-IVB stages were ready to perform their functions properly, on command, if flight conditions during launch phase had required destruct. The system properly safed the S-IVB on a command transmitted from Bermuda (BDA) at 701.5 seconds. The performance of the Command and Communications System (CCS) was excellent. Usable CCS telemetry data were received to 48,240 seconds (13:24:00) at which time the telemetry subcarrier was inhibited. Ascension (ACN), Canary Island (CYI), Goldstone (GDS), Madrid (MAD), and Merritt Island Launch Area (MILA) were receiving CCS signal carrier at S-IVB/IU lunar impact at 285,882 seconds (79:24:42). Good tracking data were received from the C-Band radar, with Carnarvon (CRO) indicating final Loss of Signal (LOS) at 53,358 seconds (14:49:18).

The 58 ground engineering cameras provided good data during the launch.

15.2 VEHICLE MEASUREMENT EVALUATION

The AS-510 launch vehicle had 1353 measurements scheduled for flight; three measurements were waived prior to start of the automatic countdown sequence leaving 1350 measurements active for flight. Three measurements failed during flight resulting in an overall measurement system reliability of 99.8 percent.

A summary of measurement reliability is presented in Table 15-1 for the total vehicle and for each stage. The waived measurements, failed measurements, and partially failed measurements are listed by stage in Tables 15-2 and 15-3. None of these listed failures had any significant impact on postflight evaluation.

Table 15-1. AS-510 Measurement Summary

MEASUREMENT CATEGORY	S-IC STAGE	S-II STAGE	S-IVB STAGE	INSTRUMENT UNIT	TOTAL VEHICLE
Scheduled	296	553	275	229	1353
Waived	3	0	0	0	3
Failures	0	0	3	0	3
Partial Failures	5	0	2	0	7
Questionable	0	0	0	0	0
Reliability, Percent	100.0	100.0	98.9	100.0	99.8

15.3 AIRBORNE VHF TELEMETRY SYSTEM EVALUATION

15.3.1 Performance Summary

Performance of the eight VHF telemetry links was generally satisfactory, however, as indicated in Table 15-4, several data dropouts occurred.

All inflight calibrations occurred as programed and were within specifications.

Data degradation and dropouts were experienced at various times during boost, as on previous flights, due to the attenuation of RF signals. Signal attenuation was caused by main flame effects, S-IC/S-II staging, S-II ignition, and S-II second plane separation. In addition to the normal expected data dropouts at S-IC/S-II separation, an unexpected data dropout was experienced approximately three seconds after separation and S-IC telemetry was lost at 164.7 seconds. On AS-510 the expected dropout occurred at about 161.3 seconds followed by a second dropout observed in all stage telemetry channels at approximately 164 seconds. The apparent cause was a reflected plume effect when the S-II stage flame impinged on the S-IC stage, since the S-IC was closer to the S-II engines at ignition than on previous missions. Loss of this data, however, posed no problem since losses were of such short duration as to have little or no impact on flight analysis. The second unexpected dropout was the loss of both S-IC telemetry links at 164.7 seconds. This occurrence is discussed in paragraph 15.3.2.

Table 15-2. AS-510 Flight Measurements Waived Prior to Flight

MEASUREMENT NUMBER	MEASUREMENT TITLE	NATURE OF FAILURE	REMARKS
	S-IC STAGE		
L0002-119	LOX Level, Sensor Segment, Position II	Shorted Probe Segment or Cabling Inside LOX Tank	KSC Waiver I-B-510-4
L0010-119	Segment Identification Position II	Shorted Probe Segment or Cabling Inside LOX Tank	KSC Waiver I-B-510-4
L0013-119	LOX Level, Time Correlation Position II	Shorted Probe Segment or Cabling Inside LOX Tank	KSC Waiver I-B-510-4

Table 15-3. AS-510 Measurement Malfunctions

MEASUREMENT NUMBER	MEASUREMENT TITLE	NATURE OF FAILURE	TIME OF FAILURE (RANGE TIME)	DURATION SATISFACTORY OPERATION	REMARKS
		MEASUREMENT FAILURES, S-IVB STAGE			
C0199-401	Temperature, Thrust Chamber Jacket	Slow response to temperature change	-300 seconds	Prior to -300 seconds	Probably the result of inadequate sensor-to-jacket thermal contact
D0264-403	Pressure-Oxidizer Pump Inlet, CI Coupled	Data offset, erratic during burn periods	-100 seconds	Prior to -100 seconds	Transducer probably sensitive to thermal shock and/or humidity
K0112-404	Event, Fuel Prevalve Closed	Failed to indicate "closed" when prevalves were closed	9884 seconds	Prior to 9884 seconds	Probably due to high contact resistance in talkback microswitch
		PARTIAL MEASUREMENT FAILURES, S-IC STAGE			
A0001-118	Acceleration, Longitudinal	Rectification error at liftoff	-2.5 to 11 seconds	150 seconds	Same phenomena seen on previous flight
C0003-102	Temperature, Turbine Manifold, Engine No. 2	Failed Off scale high	45 seconds	45 seconds	Probable transducer failure
C0003-104	Temperature, Turbine Manifold, Engine No. 4	Failed Off scale high	5 to 145 seconds	21 seconds	Probable transducer failure
K0124-120	LOX Tank Vent Valve	Data noisy	0 to 96 seconds	65 seconds	Noisy switch contacts
T0001-102	Turbopump RPM	Data erratic	20 seconds	20 seconds	Some usable data after 20 seconds
		PARTIAL MEASUREMENT FAILURES, S-IVB STAGE			
D0221-415	Pressure Ullage Control Chamber No. 2-4	Data erratic. Should be zero psia	25,400 seconds	Prior to 25,400 seconds	Probable transducer amplifier failure
D0256-403	Pressure - Ambient Helium Pneumatic Sphere	Lower than normal data level	12,400 seconds	Prior to 12,400 seconds	Probable transducer or transducer amplifier failure

Table 15-4. AS-510 Launch Vehicle Telemetry Links

LINK	FREQUENCY (MHZ)	MODULATION	STAGE	FLIGHT PERIOD (RANGE TIME, SEC)	PERFORMANCE SUMMARY
AF-1	256.2	FM/FM	S-IC	0 to 164.7	Data Dropouts
AP-1	244.3	PCM/FM	S-IC	0 to 164.7	Range Time (sec) — Duration (sec) 161.4 — 1.5 164.5 — - 164.7 — See paragraph 15.3.2
BF-1	241.5	FM/FM	S-II	0 to 800	Data Dropouts
BF-2	234.0	FM/FM	S-II	0 to 800	Range Time (sec) — Duration (sec)
BP-1	248.6	PCM/FM	S-II	0 to 800	136.5 — 0.8 137.6 — 2.4 161.3 — 2.5 163.9 — 3.1 168.7 — 0.6 192.4 — 1.4
CP-1	258.5	PCM/FM	S-IVB	Flight Duration	Data Dropouts Range Time (sec) — Duration (sec) 161.3 — 1.1 164.5 — 1.5
DF-1	250.7	FM/FM	IU	Flight Duration	Data Dropouts
DP-1	245.3	PCM/FM	IU	Flight Duration	Range Time (sec) — Duration (sec)
DP-1B (CCS)	2282.5	PCM/FM	IU	Flight Duration	161.4 (DP-1) — 0.9 163.0 (DP-1B) — 7.0 164.6 (DP-1) — 0.9 193.0 (DP-1B) — 2.0

The performance of S-IVB and IU VHF telemetry systems was normal during earth orbit, S-IVB second burn, and final coast. Usable VHF telemetry data were received to 22,680 seconds (6:18:00) for the IU VHF and to 23,225 seconds (6:27:05) for the S-IVB VHF telemetry system. A summary of available VHF telemetry coverage showing Acquisition of Signal (AOS) and LOS for each station is shown in Figure 15-1.

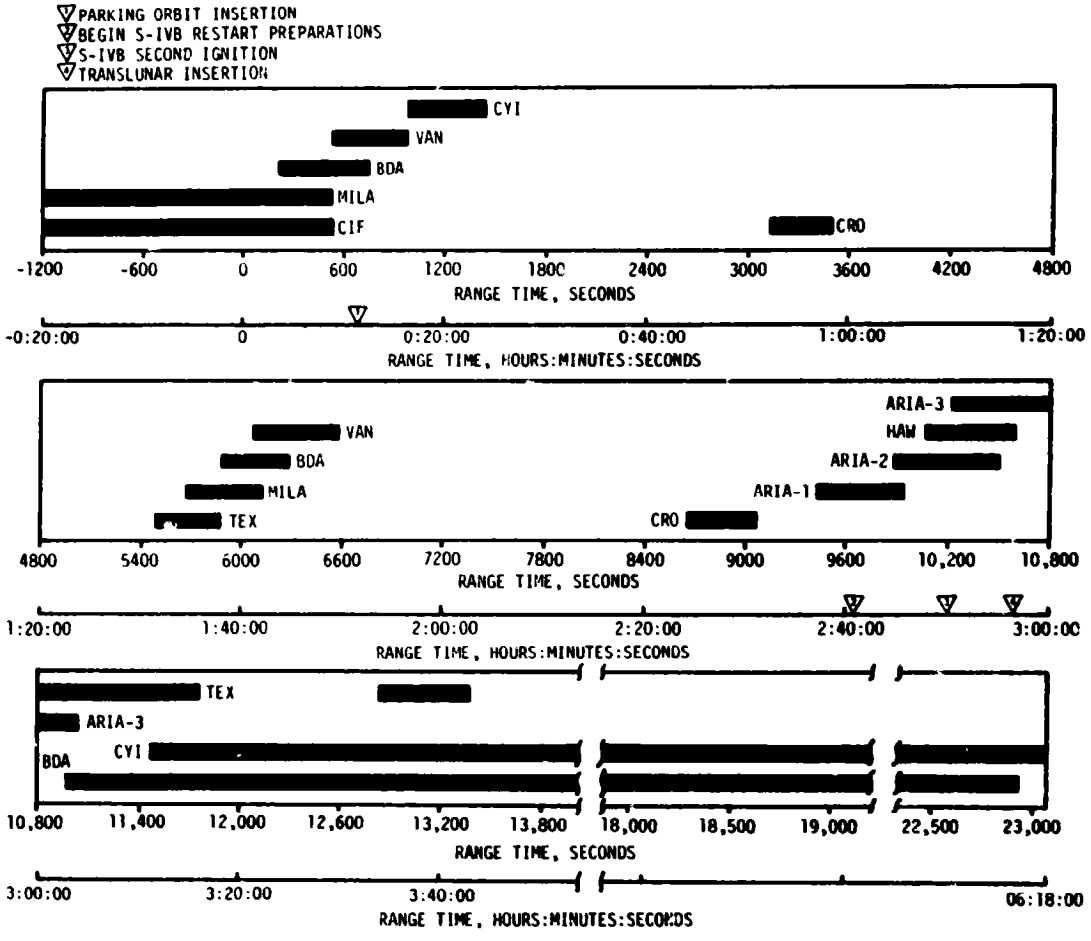

Figure 15-1. VHF Telemetry Coverage Summary

15.3.2 S-IC Telemetry Data Loss After Separation

The S-IC stage AP-1 and AF-1 telemetry links RF signal degraded to a level that caused data dropout at about 164.7 seconds, shortly after S-IC/S-II separation. Weak S-IC stage RF signals continued to be received at ground stations up to 225 seconds. The continuing RF signal indicated that S-IC stage transmitters were functioning but antenna gain was severely attenuated. The received signal strengths were about the level to be expected from the RF radiating from a coaxial cable without antenna. It appears the problem occurred in the RF link between S-IC RF canister and antennas. Previous flights have experienced random instrumentation losses in the S-IC forward skirt area due to the pressure and temperature environment during separation. The more severe environment (see paragraph 10.6) created by slower S-IC/S-II separation apparently damaged the equipment associated with RF output. Possible

failure modes are: (1) Severed RF coaxial cables; (2) Shorted RF coaxial cables; (3) Failure within cable bundle to RF canister applying power to coaxial switch; and (4) Damage to RF canister.

Since S-IC stage operational telemetry is not required after separation, there is no impact on RF system for subsequent flights.

15.4 C-BAND RADAR SYSTEM EVALUATION

The C-Band radar performed satisfactorily during flight, although several of the ground stations experienced problems with their equipment which caused some loss of signal. The phase front disturbance reported on previous missions occurred only once and was not as severe as on some previous missions.

The BDA FPQ-6 and FPS-16 radar reported a large amount of modulation on the downlink signal during launch, however, this did not affect tracking.

The Carnarvon ground station had acquisition problems during the second revolution. This was due to initially locking on a sidelobe.

MILA achieved late acquisition during Translunar Coast (TLC) because of antenna pointing problems; however, once MILA acquired the signal, they maintained track for 9.5 hours. Carnarvon was the last station to maintain track and indicated final LOS at 53,358 seconds (14:49:18).

A summary of available C-Band radar coverage showing AOS and LOS for each station is shown in Figure 15-2.

15.5 SECURE RANGE SAFETY COMMAND SYSTEMS EVALUATION

Telemetered data indicated that the command antennas, receivers/decoders, Exploding Bridge Wire (EBW) networks, and destruct controllers on each powered stage functioned properly during flight. They were in the required state-of-readiness if flight conditions during the launch had required vehicle destruct. Since no arm/cutoff or destruct commands were required, all data except receiver signal strength remained unchanged during the flight. Power to the S-IVB stage range safety command systems was cut off at 701.5 seconds by ground command from BDA, thereby deactivating (safing) the systems.

15.6 COMMAND AND COMMUNICATION SYSTEM EVALUATION

The performance of the CCS was excellent. No onboard equipment malfunctions occurred. Ground stations were able to acquire and maintain two-way lock with the CCS until S-IVB/IU lunar impact.

The RF portion of the CCS performed satisfactorily with minor exceptions during boost, earth orbit, and translunar coast. Downlink data dropouts occurred during S-IC/S-II staging and at S-II second plane separation.

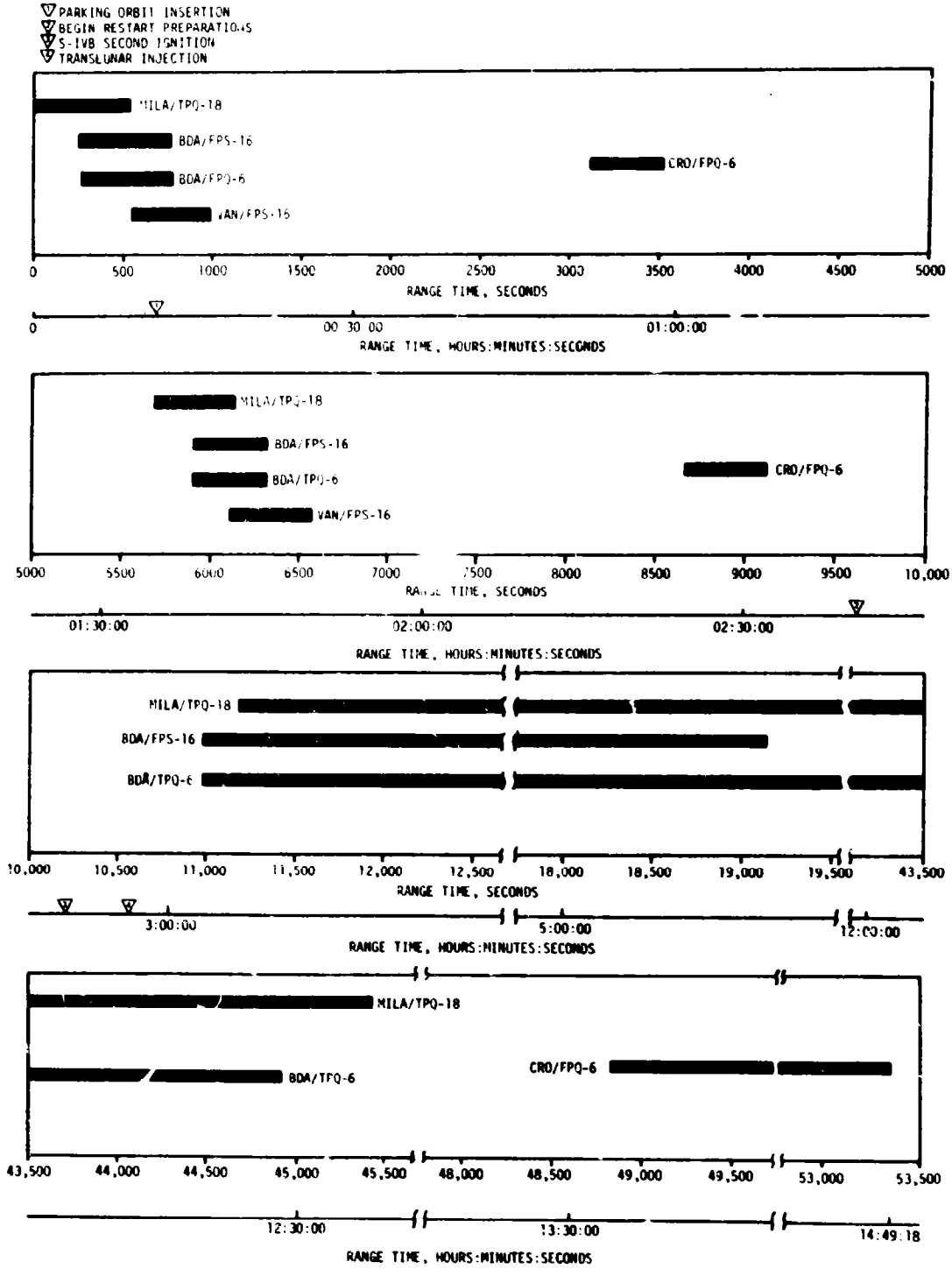

Figure 15-2. C-Band Radar Coverage Summary

Other downlink dropouts were caused by vehicle antenna nulls, multipath effects, and station handover. None of these dropouts caused any significant loss of data.

Uplink dropouts occurred during S-IC/S-II staging and at S-II second plane separation. The usual ground station handover dropouts during TLC were of extremely short duration.

The last CCS telemetry data were received at 48,240 seconds (13:24:00) when the telemetry subcarrier was inhibited by a scheduled switch selector command. ACN, CYI, GDS, MAD, and MILA indicated tracking LOS at lunar impact at 285,882 seconds (79:24:42). A summary of CCS coverage giving AOS and LOS for each station is shown in Figure 15-3.

The performance of the command section of the CCS was satisfactory. All ground commands were accepted by the onboard equipment on the first transmission. The multi-word lunar impact commands were transmitted in the Message Acceptance Pulse (MAP) override mode so that command transmission would not be interrupted. The CCS command history is shown in Table 15-5.

15.7 GROUND ENGINEERING CAMERAS

In general, ground camera coverage was good. Fifty-eight items were received from KSC and evaluated. Seven items had unusable timing. As a result of these seven failures, system efficiency was 88 percent. Tracking coverage was excellent, with all cameras acquiring data. Specific emphasis was given to the modified separation sequence of the S-IC/S-II stages and the flame impingement on the S-IC upper dome. The separation rate of the stages was reduced from Melbourne Beach tracking films.

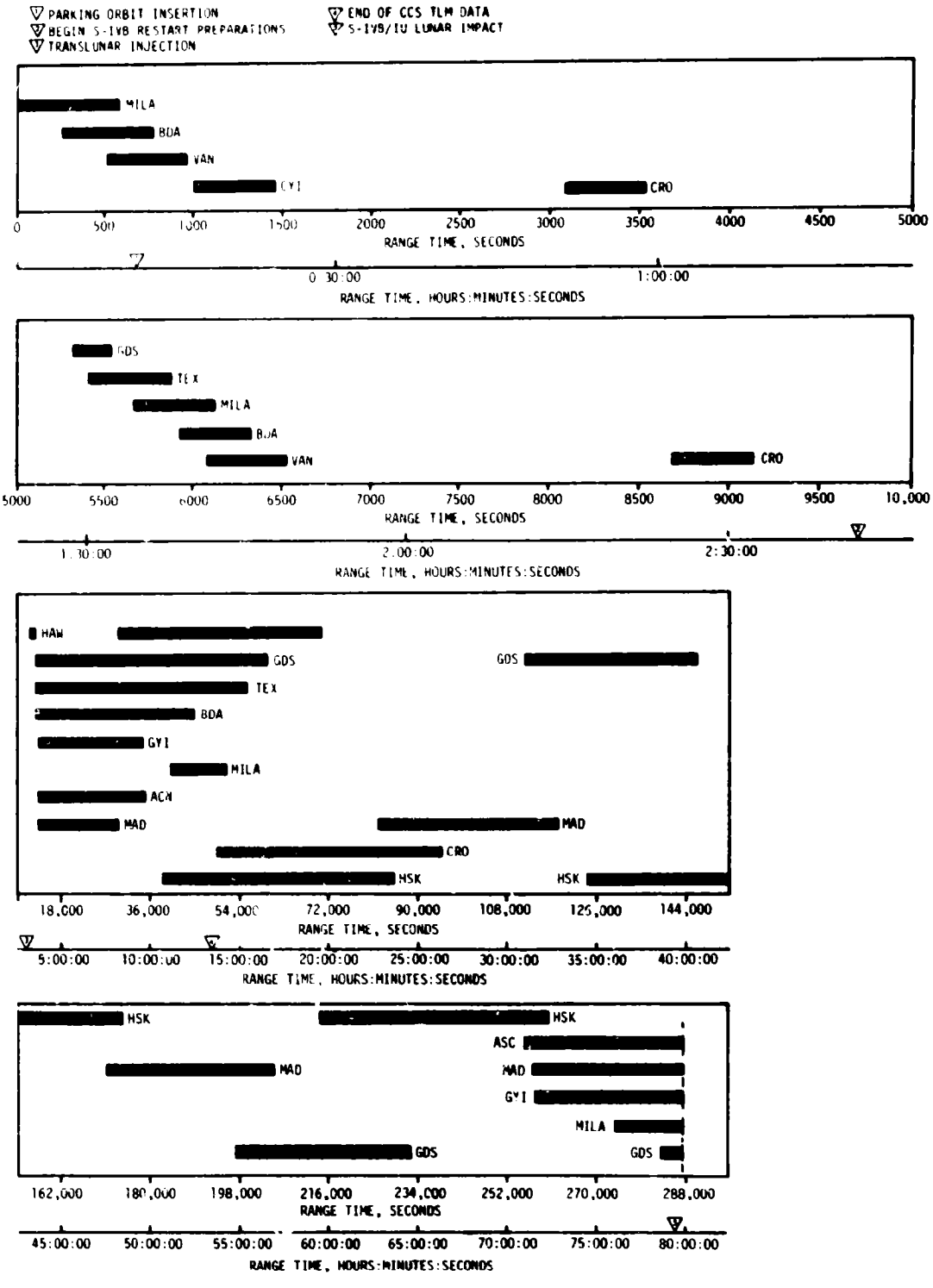

Figure 15-3. CCS Coverage Summary

Table 15-5. Command and Communication System Command History, AS-510

RANGE TIME SECONDS	RANGE TIME HRS:MINS:SECS	TRANSMITTING STATION	COMMAND	NUMBER OF WORDS TRANSMITTED	REMARKS
5,377	1:29:37	GDS	Navigation Update (NU)	36	Accepted
5,403	1:30:03	GDS	Sector Dump for NU	3	Accepted
6,071	1:41:11	BDA	Navigation Update	36	Accepted
6,118	1:41:58	BDA	Sector Dump for NU	3	Accepted
16,200	4:[illegible]1:00	MAD	Yaw Attitude Maneuver	1	Accepted
16,800	:40:00	MAD	T_B Initiate	1	Accepted
19,629	5:27:09	MAD	Lunar Impact (5 hr 30 min)	8	Accepted
19,665	5:27:45	MAD	Lunar Impact Dumps	28	Accepted
22,123	6:[illegible]:43	MAD	Set Antenna Low Gain	1	Accepted
29,967	8:19:27	GDS	LOX NPV Valve Unlatch and Closed	9	Accepted
29,989	8:19:49	GDS	LH_2 Latch Relief Valve Unlatch and Closed	9	Accepted
30,009	8:20:09	GDS	LH_2 Tank Vent BST Close Cycle	9	Accepted
30,027	8:20:27	GDS	LOX Tank Vent BST Close Cycle	9	Accepted
32,281	8:58:01	GDS	LH_2 Latch Relief Valve Open and Latch	21	Accepted
32,341	8:59:01	GDS	LOX NPV Valve Open and Latch	21	Accepted
34,979	9:42:59	GDS	Set Antennas Omni	1	Accepted
35,486	9:51:26	GDS	2nd Lunar Impact Burn (10 hr 0 min)	8	Accepted
35,492	9:51:32	GDS	2nd Lunar Impact Burn	8	Accepted
35,497	9:51:37	GDS	2nd Lunar Impact Burn	8	Accepted
35,502	9:51:42	GDS	2nd Lunar Impact Burn	8	Accepted
35,507	9:51:47	GDS	2nd Lunar Impact Burn	8	Accepted
35,519	9:51:59	GDS	2nd Lunar Impact Burn	8	Accepted
35,671	9:54:31	GDS	2nd Lunar Impact Dumps	28	Accepted
36,593	10:09:53	GDS	Lunar Impact +30 deg Pitch	8	Accepted
36,598	10:09:58	GDS	Lunar Impact +30 deg Pitch	8	Accepted
36,603	10:10:03	GDS	Lunar Impact +30 deg Pitch	8	Accepted
36,607	10:10:07	GDS	Lunar Impact +30 deg Pitch	8	Accepted
36,612	10:10:12	GDS	Lunar Impact +30 deg Pitch	8	Accepted
36,617	10:10:17	GDS	Lunar Impact +30 deg Pitch	8	Accepted
37,162	10:19:22	GDS	31 deg Lunar Impact Roll	8	Accepted
37,183	10:19:43	GDS	FCC Power "A" Off	3	Accepted
37,193	10:19:53	GDS	FCC Power "B" Off	3	Accepted

SECTION 16

MASS CHARACTERISTICS

16. SUMMARY

Total vehicle mass, determined from postflight analysis, was within 0.52 percent of prediction from ground ignition through S-IVB stage final shutdown. This small variation indicates that hardware weights, propellant loads and propellant utilization during powered flight were close to predicted values.

16.2 MASS EVALUATION

Postflight mass characteristics are compared with final predicted mass characteristics (MSFC Memorandum S&E-ASTN-SAE-71-60) and the final operational trajectory (MSFC Memorandum S&E-AERO-FMT-95-71).

The postflight mass characteristics were determined from an analysis of all available actual and reconstructed data from S-IC ignition through S-IVB second burn cutoff. Dry weights of the launch vehicle are based on actual stage weighings and evaluation of the weight and balance log books (MSFC Form 998). Propellant loading and utilization was evaluated from propulsion system performance reconstructions. Spacecraft data were obtained from the Manned Spacecraft Center (MSC).

Differences in dry weights of the inert stages and the loaded spacecraft were all within 0.39 percent of predicted, which was well within acceptable limits.

During S-IC burn phase, the total vehicle mass was less than predicted by 3677 kilograms (8107 lbm) (0.13 percent) at holddown arm release, and by 3086 kilograms (6804 lbm) (0.37 percent) at S-IC/S-II separation. These differences are attributed to S-IC stage burn characteristics, dry weight, and propellant loading. S-IC burn phase total vehicle mass is shown in Tables 16-1 and 16-2.

During S-II burn phase, the total vehicle mass was more than predicted by 575 kilograms (1269 lbm) (0.09 percent) at ignition, and by 595 kilograms (1312 lbm) (0.28 percent) at S-II/S-IVB separation. These differences are due primarily to S-II and S-IVB stage propellant loading which was higher than predicted. Total vehicle mass for the S-II burn phase is shown in Tables 16-3 and 16-4.

Total vehicle mass during both S-IVB burn phases, as shown in Tables 16-5 through 16-8, was within 0.33 percent of the predicted values. A difference of 140 kilograms (309 lbm) (0.08 percent) from predicted at first burn ignition was due largely to a greater than predicted propellant loading. The difference at completion of second burn was 216 kilograms (475 lbm) (0.33 percent), reflecting a larger than expected LOX residual. Total vehicle mass at spacecraft separation was 236 kilograms (520 lbm) (1.43 percent) greater than predicted.

A summary of mass utilization and loss, both actual and predicted, from S-IC stage ignition through spacecraft separation is presented in Table 16-9. A comparison of actual and predicted mass, center of gravity, and moment of inertia is shown in Table 16-10.

Table 16-1. Total Vehicle Mass--S-IC Burn Phase--Kilograms

EVENTS	GROUND IGNITION		HOLDDOWN ARM RELEASE		CENTER ENGINE CUTOFF		OUTBOARD ENGINE CUTOFF		S-IC/S-II SEPARATION	
	PRED	ACT	PRED	ACT	PRED	ACT	PRED	ACT	PRED	ACT
RANGE TIME--SEC	-6.50	-6.50	0.30	0.30	136.07	135.90	159.02	159.56	160.69	161.20
DRY STAGE	129999.	129821.	129999.	129821.	129999.	129821.	129999.	129821.	129999.	129821.
LOX IN TANK	1480310.	1491184.	1446620.	1446975.	188939.	172628.	1161.	702.	759.	706.
LOX BELOW TANK	21.15.	21127.	21875.	21887.	21859.	21871.	15240.	13160.	13113.	10738.
LOX ULLAGE GAS	190.	191.	236.	225.	2923.	2891.	3366.	3353.	3373.	3360.
FUEL IN TANK	637030.	635614.	626791.	624362.	81224.	82766.	7377.	7173.	6042.	4938.
FUEL BELOW TANK	4313.	4313.	5996.	5996.	5996.	5996.	5938.	5938.	5938.	5938.
FUEL ULLAGE GAS	39.	40.	39.	43.	216.	225.	252.	253.	254.	252.
N2 PURGE GAS	36.	36.	36.	36.	19.	19.	19.	19.	19.	19.
HELIUM IN BOTTLE	288.	288.	288.	285.	111.	108.	85.	78.	83.	76.
FROST	635.	635.	635.	635.	340.	340.	340.	340.	340.	340.
RETROROCKET PROP	513.	513.	513.	513.	513.	513.	513.	513.	513.	513.
OTHER	239.	239.	239.	239.	239.	239.	239.	239.	239.	239.
TOTAL STAGE	2274712.	2274005.	2235272.	2231021.	412381.	417417.	184520.	181051.	180688.	177028.
TOTAL S-IC/S-II IS	4132.	4119.	4132.	4119.	4132.	4119.	4132.	4119.	4132.	4119.
TOTAL S-II STAGE	488005.	498493.	488005.	488493.	487784.	488271.	487784.	488271.	487784.	488271.
TOT S-II/S-IVB IS	3645.	3641.	3645.	3641.	3645.	3641.	3645.	3641.	3645.	3641.
TOTAL S-IVB STAGE	120643.	120798.	120643.	120798.	120593.	120707.	120593.	120707.	120593.	120707.
TOTAL INSTRU UNIT	2037.	2035.	2037.	2035.	2037.	2035.	2037.	2035.	2037.	2035.
TOTAL SPACECRAFT	52773.	52723.	52773.	52723.	52773.	52723.	52773.	52723.	52773.	52723.
TOTAL UPPERSTAGE	671238.	671812.	671238.	671812.	670926.	671500.	670926.	671500.	670926.	671500.
TOTAL VEHICLE	2945950.	2945817.	2906510.	2902833.	1083307.	1088917.	855446.	852551.	851614.	848528.

Table 16-2. Total Vehicle Mass--S-IC Burn Phase--Pounds

EVENTS	GROUND IGNITION		HOLDDOWN ARM RELEASE		CENTER ENGINE CUTOFF		OUTBOARD ENGINE CUTOFF		S-IC/S-II SEPARATION	
	PRED	ACT	PRED	ACT	PRED	ACT	PRED	ACT	PRED	ACT
RANGE TIME--SEC	-6.50	-6.50	0.30	0.30	136.07	135.90	159.02	159.56	160.69	161.20
DRY STAGE	286600.	286208.	286600.	286208.	286600.	286208.	286600.	286208.	286600.	286208.
LOX IN TANK	3263527.	3265453.	3193662.	3190034.	372448.	380580.	2515.	2121.	1665.	1893.
LOX BELOW TANK	46552.	46577.	48227.	48253.	48192.	48218.	33600.	29014.	28920.	23675.
LOX ULLAGE GAS	419.	421.	520.	496.	6439.	6374.	7422.	7392.	7437.	7408.
FUEL IN TANK	1404412.	1401289.	1381839.	1376484.	179069.	182469.	16268.	14006.	13321.	10897.
FUEL BELOW TANK	9509.	9509.	13219.	13219.	13219.	13219.	13136.	13136.	13136.	13136.
FUEL ULLAGE GAS	86.	88.	86.	96.	476.	486.	554.	552.	538.	556.
N2 PURGE GAS	80.	80.	80.	80.	43.	43.	43.	43.	43.	43.
HELIUM IN BOTTLE	636.	636.	636.	628.	246.	238.	187.	172.	184.	168.
FROST	1400.	1400.	1400.	1400.	750.	750.	750.	750.	750.	750.
RETROROCKET PROP	1132.	1132.	1132.	1132.	1132.	1132.	1132.	1132.	1132.	1132.
OTHER	528.	528.	528.	528.	528.	528.	528.	528.	528.	528.
TOTAL STAGE	5014883.	5013323.	4927932.	4918560.	909144.	920247.	362718.	355057.	354256.	346187.
TOTAL S-IC/S-II IS	9110.	9083.	9110.	9083.	9110.	9083.	9110.	9083.	9110.	9083.
TOTAL S-II STAGE	1075869.	1076943.	1075869.	1076943.	1075381.	1076455.	1075381.	1076455.	1075381.	1076455.
TOT S-II/S-IVB IS	8038.	8029.	8038.	8029.	8038.	8029.	8038.	8029.	8038.	8029.
TOTAL S-IVB STAGE	265974.	266315.	265974.	266315.	265774.	266115.	265774.	266115.	265774.	266115.
TOTAL INSTRU UNIT	4492.	4487.	4492.	4487.	4492.	4487.	4492.	4487.	4492.	4487.
TOTAL SPACECRAFT	116345.	116235.	116345.	116235.	116345.	116235.	116345.	116235.	116345.	116235.
TOTAL UPPERSTAGE	1479627.	1481092.	1479627.	1481092.	1479139.	1480604.	1479139.	1480604.	1479139.	1480604.
TOTAL VEHICLE	6494710.	6494415.	6407759.	6399652.	2388284.	2400851.	1841058.	1835661.	1833396.	1826792.

Table 16-3. Total Vehicle Mass--S-II Burn Phase--Kilograms

EVENTS	S-IC IGNITION		S-II IGNITION		S-II MAINSTAGE		S-II ENGINE CUTOFF		S-II/S-IVB SEPARATION	
	PRED	ACT	PRED	ACT	PRED	ACT	PRED	ACT	PRED	ACT
RANGE TIME--SEC	-6.50	-6.50	162.39	163.00	164.39	164.90	549.69	549.06	550.69	550.10
S-IC/S-II SMALL IS	616.	615.	0.	0.	0.	0.				
S-IC/S-II LARGE IS	3519.	3504.	3515.	3504.	3515.	3504.				
S-IC/S-II PROPELLANT	0.	0.	0.	0.	0.	0.				
TOTAL S-IC/S-II IS	4132.	4119.	3515.	3504.	3515.	3504.				
DRY STAGE	35720.	35790.	35720.	35790.	35720.	35790.	35720.	35790.	35720.	35790.
LOX IN TANK	378976.	379369.	378976.	379369.	378526.	378916.	633.	622.	500.	490.
LOX BELOW TANK	737.	737.	737.	737.	800.	800.	787.	787.	787.	787.
LOX ULLAGE GAS	159.	157.	159.	157.	162.	160.	1876.	1904.	1881.	1904.
FUEL IN TANK	71974.	72000.	71967.	71994.	71755.	71781.	1359.	1700.	1304.	1649.
FUEL BELOW TANK	104.	104.	110.	111.	127.	127.	123.	123.	123.	123.
FUEL ULLAGE GAS	63.	63.	64.	63.	65.	65.	772.	805.	774.	805.
INSULATION PURGE GAS	17.	17.	0.	0.	0.	0.				
FROST	204.	204.	0.	0.	0.	0.				
START TANK	13.	13.	13.	13.	2.	2.	2.	2.	2.	2.
OTHER	34.	34.	34.	34.	34.	34.	34.	34.	34.	34.
TOTAL S-II STAGE	488005.	488493.	487784.	488271.	487194.	487678.	41309.	41771.	41128.	41588.
TOT S-II/S-IVB IS	3645.	3641.	3645.	3641.	3645.	3641.	3645.	3641.	3645.	3641.
TOTAL S-IVB STAGE	120643.	120798.	120552.	120707.	120552.	120707.	120553.	120707.	120550.	120705.
TOTAL IU	2037.	2035.	2037.	2035.	2037.	2035.	2037.	2035.	2037.	2035.
TOTAL SPACECRAFT	52773.	52723.	52773.	52723.	52773.	52723.	48604.	48591.	48604.	48591.
TOTAL UPPER STAGE	179100.	179198.	179009.	179108.	179009.	179108.	174841.	174976.	174838.	174974.
TOTAL VEHICLE	671238.	671812.	670309.	670884.	669719.	670291.	216150.	216748.	215967.	216562.

Table 16-4. Total Vehicle Mass--S-II Burn Phase--Pounds

EVENTS	S-IC IGNITION		S-II IGNITION		S-II MAINSTAGE		S-II ENGINE CUTOFF		S-II/S-IVB SEPARATION	
	PRED	ACT	PRED	ACT	PRED	ACT	PRED	ACT	PRED	ACT
RANGE TIME--SEC	-6.50	-6.50	162.39	163.00	164.39	164.90	549.69	549.06	550.69	550.10
S-IC/S-II SMALL IS	1360.	1356.	0.	0.	0.	0.				
S-IC/S-II LARGE IS	7750.	7727.	7750.	7727.	7750.	7727.				
S-IC/S-II PROPELLANT	0.	0.	0.	0.	0.	0.				
TOTAL S-IC/S-II IS	9110.	9083.	7750.	7727.	7750.	7727.				
DRY STAGE	78750.	78904.	78750.	78904.	78750.	78904.	78750.	78904.	78750.	78904.
LOX IN TANK	835500.	836366.	835500.	836366.	834508.	835368.	1396.	1373.	1103.	1082.
LOX BELOW TANK	1625.	1625.	1624.	1625.	1764.	1764.	1736.	1736.	1736.	1736.
LOX ULLAGE GAS	352.	347.	352.	347.	357.	353.	4136.	4199.	4147.	4199.
FUEL IN TANK	158675.	158735.	158662.	158721.	158192.	158250.	2996.	3750.	2875.	3636.
FUEL BELOW TANK	231.	231.	244.	245.	282.	282.	272.	272.	272.	272.
FUEL ULLAGE GAS	141.	141.	141.	141.	143.	144.	1703.	1776.	1708.	1776.
INSULATION PURGE GAS	38.	38.	0.	0.	0.	0.				
FROST	450.	450.	0.	0.	0.	0.				
START TANK	30.	30.	30.	30.	5.	5.	5.	5.	5.	5.
OTHER	76.	76.	76.	76.	76.	76.	76.	76.	76.	76.
TOTAL S-II STAGE	1075869.	1076943.	1075380.	1076455.	1074079.	1075146.	91070.	92091.	90673.	91686.
TOT S-II/S-IVB IS	8038.	8029.	8038.	8029.	8038.	8029.	8038.	8029.	8038.	8029.
TOTAL S-IVB STAGE	265973.	266315.	265773.	266115.	265773.	266115.	265773.	266115.	265768.	266110.
TOTAL IU	4492.	4487.	4492.	4487.	4492.	4487.	4492.	4487.	4492.	4487.
TOTAL SPACECRAFT	116345.	116235.	116345.	116235.	116345.	116235.	107155.	107127.	107155.	107127.
TOTAL UPPER STAGE	394848.	395066.	394848.	394866.	394848.	394866.	385458.	385758.	385453.	385753.
TOTAL VEHICLE	1479827.	1481092.	1477779.	1479048.	1476678.	1477739.	476529.	477849.	476127.	477439.

Table 16-5. Total Vehicle Mass--S-IVB First Burn Phase--Kilograms

EVENTS	S-IC IGNITION		S-IVB IGNITION		S-IVB MAINSTAGE		S-IVB ENGINE CUTOFF		S-IVB END DECAY	
	PRED	ACT	PRED	ACT	PRED	ACT	PRED	ACT	PRED	ACT
RANGE TIME--SEC	-6.50	-6.50	553.79	553.20	556.29	555.70	699.07	694.67	699.29	694.90
DRY STAGE	11385.	11429.	11362.	11406.	11362.	11406.	11300.	11345.	11300.	11345.
LOX IN TANK	88582.	88641.	88577.	88641.	88449.	88509.	63130.	63455.	63103.	63428.
LOX BELOW TANK	166.	166.	166.	166.	180.	180.	180.	180.	180.	180.
LOX ULLAGE GAS	16.	13.	20.	13.	25.	13.	100.	59.	100.	60.
FUEL IN TANK	19750.	19788.	19745.	19784.	19698.	19737.	14583.	14677.	14573.	14667.
FUEL BELOW TANK	21.	21.	26.	25.	26.	26.	26.	26.	26.	26.
FUEL ULLAGE GAS	20.	17.	20.	17.	20.	17.	68.	53.	68.	53.
ULLAGE ROCKET PROP	53.	53.	9.	9.						
APS PROPELLANT	285.	296.	285.	298.	285.	298.	283.	298.	283.	298.
HELIUM IN BOTTLES	198.	203.	198.	203.	198.	203.	177.	178.	177.	178.
FROST	136.	136.	45.	45.	45.	45.	45.	45.	45.	45.
START TANK GAS	2.	2.	2.	2.	0.	0.	3.	3.	3.	3.
OTHER	25.	25.	25.	25.	25.	25.	25.	25.	25.	25.
TOTAL S-IVB STAGE	120643.	120798.	120486.	120641.	120317.	120463.	89925.	90348.	89888.	90311.
TOTAL IU	2037.	2035.	2037.	2035.	2037.	2035.	2037.	2035.	2037.	2035.
TOTAL SPACECRAFT	48604.	48591.	48604.	48591.	48604.	48591.	48604.	48591.	48604.	48591.
TOTAL UPPERSTAGE	50642.	50627.	50642.	50627.	50642.	50627.	50642.	50627.	50642.	50627.
TOTAL VEHICLE	171286.	171425.	171128.	171268.	170959.	171090.	140567.	140976.	140530.	140938.

Table 16-6. Total Vehicle Mass--S-IVB First Burn Phase--Pounds

EVENTS	S-IC IGNITION		S-IVB IGNITION		S-IVB MAINSTAGE		S-IVB ENGINE CUTOFF		S-IVB END DECAY	
	PRED	ACT	PRED	ACT	PRED	ACT	PRED	ACT	PRED	ACT
RANGE TIME--SEC	-6.50	-6.50	553.79	553.20	556.29	555.70	699.07	694.67	699.29	694.90
DRY STAGE	25100.	25198.	25049.	25147.	25049.	25147.	24914.	25012.	24914.	25012.
LOX IN TANK	195290.	195421.	195279.	195421.	194997.	195129.	139180.	139896.	139119.	139835.
LOX BELOW TANK	367.	367.	367.	367.	397.	397.	397.	397.	397.	397.
LOX ULLAGE GAS	35.	30.	46.	30.	55.	30.	220.	132.	220.	133.
FUEL IN TANK	43542.	43626.	43531.	43617.	43428.	43513.	32152.	32358.	32129.	32330.
FUEL BELOW TANK	48.	48.	58.	57.	58.	58.	58.	58.	58.	58.
FUEL ULLAGE GAS	44.	38.	44.	38.	45.	38.	150.	117.	151.	118.
ULLAGE ROCKET PROP	118.	118.	22.	22.						
APS PROPELLANT	630.	659.	630.	659.	630.	659.	626.	657.	626.	657.
HELIUM IN BOTTLES	437.	448.	437.	448.	436.	448.	391.	394.	391.	393.
FROST	300.	300.	100.	100.	100.	100.	100.	100.	100.	100.
START TANK GAS	5.	5.	5.	5.	1.	1.	7.	7.	7.	7.
OTHER	56.	57.	56.	57.	56.	57.	56.	57.	56.	57.
TOTAL S-IVB STAGE	265974.	266315.	265626.	265968.	265254.	265577.	198252.	199185.	198169.	199103.
TOTAL IU	4492.	4487.	4492.	4487.	4492.	4487.	4492.	4487.	4492.	4487.
TOTAL SPACECRAFT	107155.	107127.	107155.	107127.	107155.	107127.	107155.	107127.	107155.	107127.
TOTAL UPPERSTAGE	111647.	111614.	111647.	111614.	111647.	111614.	111647.	111614.	111647.	111614.
TOTAL VEHICLE	377621.	377929.	377273.	377582.	376901.	377191.	309899.	310799.	309816.	310717.

Table 16-7. Total Vehicle Mass--S-IVB Second Burn Phase--Kilograms

EVENTS	S-IVB IGNITION		S-IVB MAINSTAGE		S-IVB ENGINE CUTOFF		S-IVB END DECAY		SPACECRAFT SEPARATION	
	PRED	ACT	PRED	ACT	PRED	ACT	PRED	ACT	PRED	ACT
RANGE TIME--SEC	10196.59	10202.90	10199.09	10205.80	10552.81	10553.61	10553.00	10553.80	15352.89	15480.00
DRY STAGE	11300.	11345.	11300.	11345.	11300.	11345.	11300.	11345.	11300.	11345.
LOX IN TANK	63045.	63184.	62919.	63065.	1566.	1759.	1539.	1732.	1471.	1664.
LOX BELOW TANK	166.	166.	180.	180.	180.	180.	180.	180.	166.	166.
LOX ULLAGE GAS	125.	102.	125.	102.	198.	197.	198.	197.	198.	197.
FUEL IN TANK	13454.	13479.	13406.	13428.	761.	754.	751.	744.	0.	0.
FUEL BELOW TANK	26.	26.	26.	26.	26.	26.	26.	26.	21.	21.
FUEL ULLAGE GAS	186.	144.	186.	144.	295.	278.	295.	278.	271.	254.
APS PROPELLANT	227.	237.	227.	237.	225.	237.	225.	237.	202.	214.
HELIUM IN BOTTLES	148.	165.	148.	165.	90.	97.	90.	96.	90.	96.
FROST	45.	45.	45.	45.	45.	45.	45.	45.	45.	45.
START TANK GAS	2.	2.	0.	0.	3.	3.	3.	3.	3.	3.
OTHER	25.	25.	25.	25.	25.	25.	25.	25.	25.	25.
TOTAL S-IVB STAGE	88754.	88925.	88591.	88766.	14718.	14949.	14681.	14913.	13797.	14035.
TOTAL IU	2037.	2035.	2037.	2035.	2037.	2035.	2037.	2035.	2037.	2035.
TOTAL SPACECRAFT	48604.	48591.	48604.	48591.	48604.	48591.	48604.	48591.	625.	625.
TOTAL UPPERSTAGE	50642.	50627.	50642.	50627.	50642.	50627.	50642.	50627.	2663.	2661.
TOTAL VHICLE	139396.	139552.	139233.	139393.	65360.	65576.	65323.	65540.	16461.	16697.

Table 16-8. Total Vehicle Mass--S-IVB Second Burn Phase--Pounds

EVENTS	S-IVB IGNITION		S-IVB MAINSTAGE		S-IVB ENGINE CUTOFF		S-IVB END DECAY		SPACECRAFT SEPARATION	
	PRED	ACT	PRED	ACT	PRED	ACT	PRED	ACT	PRED	ACT
RANGE TIME--SEC	10196.59	10202.90	10199.09	10205.80	10552.81	10553.61	10553.00	10553.80	15352.89	15480.00
DRY STAGE	24914.	25012.	24914.	25012.	24914.	25012.	24914.	25012.	24914.	25012.
LOX IN TANK	138991.	139298.	138712.	139035.	3454.	3876.	3394.	3819.	3244.	3669.
LOX BELOW TANK	367.	367.	397.	397.	397.	397.	397.	397.	367.	367.
LOX ULLAGE GAS	275.	225.	276.	225.	438.	436.	438.	436.	438.	436.
FUEL IN TANK	29662.	29741.	29556.	29604.	1678.	1664.	1656.	1642.	0.	0.
FUEL BELOW TANK	59.	58.	58.	58.	58.	58.	58.	58.	48.	48.
FUEL ULLAGE GAS	410.	319.	410.	319.	651.	613.	651.	614.	599.	562.
APS PROPELLANT	501.	524.	501.	524.	497.	523.	497.	523.	447.	473.
HELIUM IN BOTTLES	328.	365.	328.	365.	199.	214.	199.	213.	199.	213.
FROST	100.	100.	100.	100.	100.	100.	100.	100.	100.	100.
START TANK GAS	5.	5.	1.	1.	7.	7.	7.	7.	7.	7.
OTHER	56.	57.	56.	57.	56.	57.	56.	57.	56.	57.
TOTAL S-IVB STAGE	195669.	196047.	195311.	195697.	32449.	32957.	32367.	32878.	30419.	30944.
TOTAL IU	4492.	4487.	4492.	4487.	4492.	4487.	4492.	4487.	4492.	4487.
TOTAL SPACECRAFT	107155.	107127.	107155.	107127.	107155.	107127.	107155.	107127.	1383.	1380.
TOTAL UPPERSTAGE	111647.	111614.	111647.	111614.	111647.	111614.	111647.	111614.	5872.	5867.
TOTAL VHICLE	307316.	307661.	306958.	307311.	144096.	144571.	144014.	144492.	36291.	36811.

Table 16-9. Flight Sequence Mass Summary

MASS HISTORY	PREDICTED KG	PREDICTED LBM	ACTUAL KG	ACTUAL LBM
S-IC STAGE, TOTAL	2274712.	5014883.	2274004.	5013323.
S-IC/S-II IS, TOTAL	4132.	9110.	4119.	9083.
S-II STAGE, TOTAL	488005.	1075869.	488493.	1076943.
S-II/S-IVB IS, TOTAL	3645.	8038.	3641.	8029.
S-IVB STAGE, TOTAL	120643.	265974.	120798.	266315.
INSTRUMENT UNIT	2037.	4492.	2035.	4487.
SPACECRAFT, TOTAL	52773.	116345.	52723.	116235.
1ST FLT STG AT IGN	2945950.	6494710.	2945816.	6494415.
THRUST BUILDUP	-39440.	-86951.	-42984.	-94763.
1ST FLT STG AT HDAR	2906509.	6407759.	2902832.	6399652.
FROST	-294.	-650.	-294.	-650.
MAINSTAGE	-2069284.	-4561993.	-2068461.	-4560179.
N2 PURGE GAS	-16.	-37.	-16.	-37.
THRUST DECAY-IE	-959.	-2115.	-1005.	-2217.
ENG EXPENDED PROP	-189.	-418.	-189.	-418.
S-II INSUL PURGE	-17.	-38.	-17.	-38.
S-II FROST	-204.	-450.	-204.	-450.
S-IVB FROST	-90.	-200.	-90.	-200.
THRUST DECAY-OE	0.	0.	0.	0.
1ST FLT STG AT OECO	835452.	1841858.	832551.	1835461.
THRUST DECAY-OE	-3838.	-8461.	-4023.	-8869.
S-IC/S-II ULL RKT	0.	0.	0.	0.
1ST FLT STG AT SEP	831614.	1833396.	828527.	1826592.
STG AT SEPARATION	-160688.	-354256.	-157028.	-346187.
S-IC/S-II SMALL IS	-616.	-1360.	-615.	-1356.
S-IC/S-II ULL RKT	0.	0.	0.	0.
2ND FLT STG AT SSC	670309.	1477779.	670884.	1479048.
FUEL LEAD	0.	0.	0.	0.
S-IC/S-II ULL RKT	0.	0.	0.	0.
2ND FLT STG AT IGN	670309.	1477779.	670884.	1479048.
THRUST BUILDUP	-578.	-1276.	-582.	-1284.
START TANK	-11.	-25.	-11.	-25.
S-IC/S-II ULL RKT	0.	0.	0.	0.
2ND FLT STG AT MS	669719.	1476478.	670291.	1477739.
MAINSTAGE	-445022.	-982871.	-445843.	-982915.
LES	-4168.	-9190.	-4131.	-9108.
S-IC/S-II LARGE IS	-3515.	-7750.	-3504.	-7727.
TD & ENG PROP	-62.	-137.	-63.	-139.
2ND FLT STG AT COS	216150.	476529.	216748.	477849.
THRUST DECAY	-180.	-397.	-183.	-405.
S-IVB ULL RKT PROP	-2.	-5.	-2.	-5.
2ND FLT STG AT SEP	215967.	476127.	216562.	477439.
STG AT SEPARATION	-41128.	-90673.	-41588.	-91686.
S-II/S-IVB IS DRY	-3165.	-6978.	-3160.	-6967.
S-II/S-IVB PROP	-480.	-1060.	-481.	-1062.
S-IVB AFT FRAME	-21.	-48.	-21.	-48.
S-IVB ULL RKT PROP	-1.	-3.	-1.	-3.
S-IVB DET PKG	-1.	-3.	-1.	-3.
3RD FLT STG AT SSC	171168.	377362.	171308.	377670.

Table 16-9. Flight Sequence Mass Summary (Continued)

MASS HISTORY	PREDICTED KG	PREDICTED LBM	ACTUAL KG	ACTUAL LBM
3RD FLT STG 1ST SSC	171168.	377362.	171308.	377670.
ULLAGE ROCKET PROP	-39.	-88.	-39.	-88.
FUEL LEAD	-0.	-0.	0.	0.
3RD FLT STG 1ST IGN	171128.	377273.	171268.	377582.
ULLAGE ROCKET PROP	-9.	-22.	-9.	-22.
START TANK	-1.	-4.	-1.	-4.
THRUST BUILDUP	-156.	-345.	-165.	-365.
3RD FLT STG 1ST MS	170959.	376901.	171090.	377191.
ULLAGE ROCKET CASE	-61.	-135.	-61.	-135.
MAINSTAGE	-30328.	-66863.	-30052.	-66255.
APS	-1.	-4.	-0.	-2.
3RD FLT STG 1ST COS	140567.	309899.	140976.	310799.
THRUST DECAY	-37.	-82.	-37.	-82.
3RD FLT STG 1ST ETD	140530.	309816.	140938.	310717.
ENGINE PROP	-18.	-40.	-18.	-40.
FUEL TANK LOSS	-996.	-2197.	-1084.	-2391.
LOX TANK LOSS	-43.	-96.	-204.	-451.
APS	-56.	-125.	-60.	-133.
START TANK	-0.	-2.	-0.	-2.
O2/H2 BURNER	-7.	-16.	-7.	-16.
3RD FLT STG 2ND SSC	139406.	307339.	139563.	307684.
FUEL LEAD	-10.	-23.	-10.	-23.
3RD FLT STG 2ND IGN	139396.	307316.	139552.	307661.
START TANK	-1.	-4.	-1.	-4.
THRUST BUILDUP	-160.	-354.	-156.	-346.
3D FLT STG 2ND MS	139233.	306958.	139393.	307311.
MAINSTAGE	-73871.	-162858.	-73817.	-162739.
APS	-1.	-4.	-0.	-1.
3RD FLT STG 2ND COS	65360.	144096.	65576.	144571.
THRUST DECAY	-37.	-82.	-35.	-78.
3RD FLT STG 2ND ETD	65323.	144014.	65540.	144492.
JETTISON SLA	-1170.	-2581.	-1172.	-2584.
CSM	-30384.	-66987.	-30356.	-66925.
S-IVB STAGE LOSS	-462.	-1018.	-459.	-1012.
STRT TRANS/DOCK	33305.	73427.	33552.	73971.
CSM	30384.	66987.	30356.	66925.
END TRANS/DOCK	63690.	140414.	63909.	140896.
CSM	-30384.	-66987.	-30356.	-66925.
LM	-16423.	-36207.	-16437.	-36238.
S-IVB STAGE LOSS	-421.	-928.	-418.	-922.
LAU VEH AT S/C SEP	16461.	36291.	16697.	36811.
S/C NOT SEPARATED	-625.	-1380.	-625.	-1380.
IU	-2037.	-4492.	-2035.	-4487.
S-IVB STAGE	-13797.	-30419.	-14035.	-30944.

Table 16-10. Mass Characteristics Comparison

EVENT		MASS		LONGITUDINAL C.G. (X STA.)		RADIAL C.G.		ROLL MOMENT OF INERTIA		PITCH MOMENT OF INERTIA		YAW MOMENT OF INERTIA	
		KILO POUNDS	O/O DEV.	METERS INCHES	DELTA	METERS INCHES	DELTA	KG-M2 X10-6	O/O DEV.	KG-M2 X10-6	O/O DEV.	KG-M2 X10-6	O/O DEV.
S-IC STAGE DRY	PRED	130000.		9.342		0.0618							
		286600.		367.8		2.4351		2.541		16.539		16.479	
	ACTUAL	129622.		9.342	0.000	0.0618	0.0000						
		286208.	-0.13	367.8	0.00	2.4351	0.0000	2.538	-0.13	16.516	-0.13	16.457	-0.13
S-IC/S-II INTERSTAGE, TOTAL	PRED	4132.		41.734		0.1616							
		9110.		1643.1		6.3639		0.103		0.064		0.064	
	ACTUAL	4120.		41.734	0.000	0.1616	0.0000						
		9083.	-0.29	1643.1	0.00	6.3639	0.0000	0.103	-0.29	0.063	-0.29	0.064	-0.29
S-II STAGE, DRY	PRED	35720.		47.932		0.1772							
		78750.		1887.1		6.9778		0.582		1.984		1.997	
	ACTUAL	35790.		47.932	0.000	0.1772	0.0000						
		78904.	0.20	1887.1	0.00	6.9778	0.0000	0.583	0.20	1.988	0.20	2.001	0.20
S-II/S-IVB INTERSTAGE, TOTAL	PRED	3646.		66.438		0.0647							
		8038.		2615.7		2.5495		0.064		0.043		0.044	
	ACTUAL	3642.		66.436	-0.002	0.0647	0.0000						
		8029.	-0.10	2615.6	-0.10	2.5495	0.0000	0.064	-0.10	0.043	-0.10	0.044	-0.10
S-IVB STAGE, DRY	PRED	11385.		72.542		0.2265							
		25100.		2856.0		8.9196		0.082		0.298		0.298	
	ACTUAL	11430.		72.542	0.000	0.2265	0.0000						
		25198.	0.39	2856.0	0.00	8.9196	0.0000	0.083	0.39	0.299	0.39	0.299	0.39
VEHICLE INSTRUMENT UNIT	PRED	2038.		82.407		0.4750							
		4492.		3244.4		18.7042		0.019		0.010		0.009	
	ACTUAL	2035.		82.407	0.000	0.4750	0.0000						
		4487.	-0.10	3244.4	0.00	18.7042	0.0000	0.019	-0.10	0.010	-0.10	0.009	-0.10
SPACECRAFT, TOTAL	PRED	52773.		91.452		0.0975							
		116345.		3600.5		3.8418		0.099		1.688		1.688	
	ACTUAL	52723.		91.440	-0.012	0.0991	0.0016						
		116235.	-0.08	3600.0	-0.50	3.9051	0.0632	0.099	-0.08	1.679	-0.53	1.679	-0.53

Table 16-10. Mass Characteristics Comparison (Continued)

EVENT		MASS		LONGITUDINAL C.G. (X STA.)		RADIAL C.G.		ROLL MOMENT OF INERTIA		PITCH MOMENT OF INERTIA		YAW MOMENT OF INERTIA	
		KILO POUNDS	O/O DEV.	METERS INCHES	DELTA	METERS INCHES	DELTA	KG-M2 X10-6	O/O DEV.	KG-M2 X10-6	O/O DEV.	KG-M2 X10-6	O/O DEV.
1ST FLIGHT STAGE AT IGNITION	PRED	2945951.		30.493		0.0047							
		6494710.		1200.5		0.1886		3.593		889.635		889.571	
	ACTUAL	2945317.		30.505	0.012	0.0050	0.0002						
		6494415.	0.00	1200.9	0.47	0.1972	0.0085	3.594	0.04	889.458	-0.01	889.393	-0.01
1ST FLIGHT STAGE AT HOLDDOWN ARM RELEASE	PRED	2906511.		30.439		0.0050							
		6407759.		1198.4		0.1972		3.628		890.598		890.533	
	ACTUAL	2902833.		30.452	0.012	0.0048	-0.0001						
		6399652.	-0.12	1198.9	0.47	0.1923	-0.0048	3.629	0.03	890.314	-0.02	890.250	-0.02
1ST FLIGHT STAGE AT OUTBOARD ENGINE CUTOFF SIGNAL	PRED	835453.		46.836		0.0170							
		1841858.		1843.9		0.6711		3.612		443.057		442.996	
	ACTUAL	832551.		46.993	0.156	0.0172	0.0002						
		1835461.	-0.34	1850.1	6.17	0.6797	0.0085	3.612	0.00	438.331	-1.06	438.270	-1.06
1ST FLIGHT STAGE AT SEPARATION	PRED	831615.		47.004		0.0172							
		1833396.		1850.5		0.6799		3.610		437.900		437.840	
	ACTUAL	828529.		47.172	0.167	0.0174	0.0002						
		1826592.	-0.36	1857.1	6.61	0.6887	0.0087	3.610	-0.00	432.758	-1.16	432.697	-1.16
2ND FLIGHT STAGE AT START SEQUENCE COMMAND	PRED	670310.		55.986		0.0192							
		1477779.		2204.1		0.7580		0.954		139.768		139.775	
	ACTUAL	670885.		55.982	-0.004	0.0194	0.0002						
		1479048.	0.09	2204.0	-0.15	0.7665	0.0085	0.956	0.20	139.728	-0.02	139.743	-0.01
2ND FLIGHT STAGE AT MAINSTAGE	PRED	669719.		55.987		0.0192							
		1476478.		2204.2		0.7580		0.956		139.763		139.770	
	ACTUAL	670291.		55.983	-0.004	0.0194	0.0002						
		1477739.	0.09	2204.0	-0.15	0.7665	0.0085	0.958	0.20	139.723	-0.02	139.738	-0.01
2ND FLIGHT STAGE AT CUTOFF SIGNAL	PRED	216150.		71.490		0.0579							
		476529.		2814.5		2.2826		0.866		44.961		44.967	
	ACTUAL	216749.		71.445	-0.045	0.0580	0.0000						
		477849.	0.28	2812.7	-1.78	2.2848	0.0021	0.868	0.26	45.186	0.50	45.199	0.52

Table 16-10. Mass Characteristics Comparison (Continued)

EVENT		MASS		LONGITUDINAL C.G. (X STA.)		RADIAL C.G.		ROLL MOMENT OF INERTIA		PITCH MOMENT OF INERTIA		YAW MOMENT OF INERTIA	
		KILO POUNDS	O/O DEV.	METERS INCHES	DELTA	METERS INCHES	DELTA	KG-M2 X10-6	O/O DEV.	KG-M2 X10-6	O/O DEV.	KG-M2 X10-6	O/O DEV.
		215968.		71.511		0.0579							
	PRED	476127.		2815.4		2.2826		0.866		44.835		44.841	
2ND FLIGHT STAGE AT SEPARATION		216563.		71.467	-0.044	0.0580	0.0000						
	ACTUAL	477439.	0.28	2813.6	-1.74	2.2848	0.0021	0.868	0.26	45.059	0.50	45.072	0.52
		171169.		77.295		0.0385							
3RD FLIGHT STAGE AT 1ST START SEQUENCE COMMAND	PRED	377362.		3043.1		1.5185		0.207		13.953		13.950	
		171308.		77.290	-0.004	0.0385	-0.0000						
	ACTUAL	377670.	0.08	3042.9	-0.18	1.5163	-0.0022	0.207	0.24	13.952	0.00	13.949	-0.00
		171128.		77.296		0.0385							
3RD FLIGHT STAGE AT 1ST IGNITION	PRED	377273.		3043.1		1.5185		0.207		13.952		13.949	
		171268.		77.291	-0.004	0.0385	-0.0000						
	ACTUAL	377582.	0.08	3042.9	-0.18	1.5163	-0.0022	0.207	0.24	13.951	0.00	13.948	-0.00
		170960.		77.297		0.0385							
3RD FLIGHT STAGE AT 1ST MAINSTAGE	PRED	376901.		3043.2		1.5185		0.207		13.951		13.948	
		171091.		77.292	-0.004	0.0385	-0.0000						
	ACTUAL	377191.	0.08	3043.0	-0.18	1.5163	-0.0022	0.207	0.24	13.951	0.00	13.947	0.00
		140558.		78.183		0.0464							
3RD FLIGHT STAGE AT 1ST CUTOFF SIGNAL	PRED	309899.		3078.1		1.8288		0.206		13.135		13.132	
		140976.		78.165	-0.018	0.0463	-0.0000						
	ACTUAL	310799.	0.29	3077.3	-0.72	1.8266	-0.0022	0.207	0.24	13.146	0.09	13.143	0.09
		140530.		78.185		0.0467							
3RD FLIGHT STAGE AT 1ST END THRUST DECAY, START COAST	PRED	309816.		3078.1		1.8386		0.206		13.134		13.131	
		140939.		78.166	-0.018	0.0463	-0.0003						
	ACTUAL	310717.	0.29	3077.4	-0.72	1.8266	-0.0120	0.207	0.23	13.145	0.08	13.142	0.08
		139407.		78.156		0.0465							
3RD FLIGHT STAGE AT 2ND START SEQUENCE COMMAND	PRED	307339.		3078.5		1.8312		0.205		13.128		13.125	
		139563.		78.185	-0.011	0.0466	0.0001						
	ACTUAL	307684.	0.11	3078.1	-0.44	1.8363	0.0051	0.206	0.27	13.132	0.03	13.129	0.03

Table 16-10. Mass Characteristics Comparison (Continued)

EVENT		MASS		LONGITUDINAL C.G. (X STA.)		RADIAL C.G.		ROLL MOMENT OF INERTIA		PITCH MOMENT OF INERTIA		YAW MOMENT OF INERTIA	
		KILO POUNDS	O/O DEV.	METERS INCHES	DELTA	METERS INCHES	DELTA	KG-M2 X10-6	O/O DEV.	KG-M2 X10-6	O/O DEV.	KG-M2 X10-6	O/O DEV.
3RD FLIGHT STAGE AT 2ND IGNITION	PRED	139396. 307316.		78.194 3078.5		0.0465 1.8312		0.205		13.130		13.127	
	ACTUAL	139553. 307661.	0.11	78.183 3078.1	-0.010 -0.41	0.0466 1.8363	0.0001 0.0051	0.206	0.27	13.133	0.03	13.131	0.02
3RD FLIGHT STAGE AT 2ND MAINSTAGE	PRED	139234. 306958.		78.199 3078.7		0.0465 1.8312		0.205		13.127		13.124	
	ACTUAL	139394. 307311.	0.11	78.188 3078.2	-0.011 -0.44	0.0466 1.8363	0.0001 0.0051	0.206	0.27	13.131	0.04	13.128	0.03
3RD FLIGHT STAGE AT 2ND CUTOFF SIGNAL	PRED	65361. 146096.		86.080 3388.9		0.0972 3.8296		0.204		5.211		5.208	
	ACTUAL	65576. 146571.	0.33	86.018 3386.5	-0.061 -2.41	0.0970 3.8199	-0.0002 -0.0097	0.205	0.24	5.276	1.24	5.272	1.23
3RD FLIGHT STAGE AT 2ND END THRUST DECAY	PRED	65324. 146014.		86.089 3389.3		0.0972 3.8296		0.204		5.201		5.198	
	ACTUAL	65540. 146492.	0.33	86.027 3386.9	-0.062 -2.44	0.0970 3.8199	-0.0002 -0.0097	0.205	0.24	5.266	1.25	5.263	1.25
CSM SEPARATED	PRED	33306. 73427.		79.256 3120.3		0.0932 3.6716		0.146		1.640		1.635	
	ACTUAL	33553. 73971.	0.74	79.192 3117.8	-0.064 -2.52	0.0930 3.6623	-0.0002 -0.0093	0.147	0.36	1.675	2.09	1.670	2.09
CSM DOCKED	PRED	63691. 140414.		85.619 3370.8		0.1171 4.6125		0.196		4.530		4.524	
	ACTUAL	63909. 140896.	0.34	85.550 3369.1	-0.068 -2.70	0.1151 4.5351	-0.0019 -0.0774	0.196	0.25	4.640	2.43	4.634	2.43
SPACECRAFT SEPARATED	PRED	16462. 36291.		73.798 2905.4		0.1639 6.4562		0.111		0.600		0.597	
	ACTUAL	16697. 36811.	1.43	73.739 2903.1	-0.058 -2.28	0.1648 6.4911	0.0008 0.0348	0.111	0.44	0.605	0.85	0.602	0.82

SECTION 17

LUNAR IMPACT

17.1 SUMMARY

All aspects of the S-IVB/IU Lunar Impact mission objectives were accomplished successfully except the precise determination of the impact point. Previous experience and the high quality and large quantity of tracking data indicate that the final impact solution will satisfy the remaining mission objective after additional analysis. At 285,881.55 seconds (79:24:41.55), the S-IVB/IU impacted the lunar surface at approximately 0.99 degrees south latitude and 11.89 degrees west longitude with a velocity of 2,577 m/s (8,455 ft/s). This preliminary impact point is approximately 154 kilometers (83 n mi) from the target of 3.65 degrees south latitude and 7.58 degrees west longitude.

The mission objectives were to maneuver the S-IVB/IU such that it would have at least a 50 percent probability of impacting the lunar surface within 350 kilometers (189 n mi) of the target, and to determine the actual impact point within 5 kilometers (2.7 n mi), and the time within 1 second. The AS-510 targeting philosophy for seismic experiment performance and data resolution defined "preferred," "acceptable," and "undesirable" impact regions about the Apollo 12 and Apollo 14 lunar seismometers. Although the impact location is not within the preferred region nor within the acceptable region of the Apollo 14 seismometer, it is within the acceptable region of the Apollo 12 seismometer, and the principle seismic experiment investigator reports that both seismometers gave valuable scientific data from the impact.

The projected impact point resulting from the APS-1 maneuver was perturbed in an easterly direction by unplanned forces acting after the LOX dump. A first force was caused by the ambient helium pressurization spheres dumping through the ambient helium engine control sphere into the J-2 engine. Other forces were apparently caused by the IU Thermal Control System (TCS) water valve operations and APS attitude engine reactions. Following the APS-2 maneuver, a small and gradually decreasing unbalanced force (also unplanned) acted during a 5-hour period to perturb the vehicle trajectory. This perturbation coupled with the inaccuracy involved in the real time tracking analyses leading to the APS-2 maneuver resulted in the lunar impact being northwest of the target.

17.2 TRANSLUNAR COAST MANEUVERS

Following Command and Service Module (CSM)/Launch Vehicle (LV) separation at 12,147 seconds (3:22:27) the CSM was docked with the Lunar Module (LM) at 12,829 seconds (3:33:49) and the CSM/LM was then ejected from the S-IVB/IU at 15,481 seconds (4:18:01). After CSM/LM ejection, the S-IVB/IU was maneuvered to the inertially-fixed attitude as required for the evasive burn. Timebase 8 (T_8) was initiated 66 seconds later than nominal at 16,801 seconds (4:40:01). The Auxiliary Propulsion System (APS) ullage engines were started 1 second following T_8 and burned for 80 seconds to provide a near-nominal spacecraft/launch vehicle separation velocity (see Table 17-1). Following a maneuver to the Continuous Vent System (CVS) and LOX dump attitude, the initial lunar targeting velocity changes were accomplished by means of a 300 second CVS vent starting 1000 seconds after T_8 and a 48 second LOX dump starting 1280 seconds after T_8. The velocity changes resulting from these two maneuvers were near nominal (see Table 17-1).

A first APS lunar impact targeting burn (APS-1) was determined in real time by the Lunar Impact Team (LIT) at the Huntsville Operations Support Center. The specifications for this APS burn (described in Tables 17-1 and 17-2) were sent from the Mission Control Center at Houston (MCC-H) by the Booster Systems Engineer (BSE) to the S-IVB/IU. At 3960 seconds after T_8, a 241 second APS burn was initiated giving a near-nominal velocity change.

Table 17-1. Comparison of Longitudinal Velocity Increments

EVENT	VELOCITY INCREMENT, M/S (FT/S)		
	ACTUAL	NOMINAL	ACT-NOM
APS Evasive Burn	2.95 (9.68)	3.10 (10.17)	-0.15 (-0.49)
CVS Vent	0.42 (1.38)	0.47 (1.54)	-0.05 (-0.16)
LOX Dump	9.14 (29.99)	8.53 (27.99)	0.61 (2.00)
APS Impact Burn 1	9.90 (32.48)	9.98 (32.74)	-0.08 (-0.26)
APS Impact Burn 2	2.98 (9.78)	2.99 (9.81)	-0.01 (-0.03)

Table 17-2. Translunar Coast Maneuvers

EVENT	INITIATION (SEC)	DURATION (SEC)	ΔV (M/S)	PITCH (DEG)	YAW (DEG)
CSM/LV Separation	12,147	-	-0.10	138	-40
CSM/LM Docking	12,829*	500*	-0.08*	148	-40
LM Ejection	15,481	-	-0.26	172	-40
APS Evasive Burn	16,802	80	2.95	176	40
CVS Venting	17,801	300	0.42	209	-40
LOX Dump	18,081	48	9.14	209	-40
Helium Dump	18,081	675	1.37	209	-40
APS Lunar Impact Burn 1	20,760	241	9.90	192	-22
TCS & APS Thrust 1	22,680	300	0.08*	262	41
TCS & APS Thrust 2	25,080	300	0.08*	262	41
TCS & APS Thrust 3	27,480	300	0.08*	262	41
TCS & APS Thrust 4	29,880	300	0.08*	262	41
TCS & APS Thrust 5	31,980	300	0.08*	262	41
TCS & APS Thrust 6	34,080	300	0.08*	262	41
APS Lunar Impact Burn 2	36,001	71	2.98	28	-40

*Calculated from tracking observations
Note: Attitudes are the local horizontal orientation of the change in velocity.

A second APS lunar impact targeting burn (APS-2) was determined by the LIT in real time following analyses by the MCC-H of tracking data obtained after the APS-1 burn. The MCC-H analysis gave a lunar impact point of 9.3 degrees south latitude and 11.0 degrees east longitude. The specifications for the APS-2 burn were commanded by the BSE from MCC-H and at 36,001 seconds (10:00:01), a 71 second APS-2 burn was initiated giving a velocity change near the real time predicted value. Shortly after APS-2 and a return to a good communication attitude, a Passive Thermal Control (PTC) "barbecue" maneuver was initiated by commanding the vehicle to roll and then turning off the Flight Control Computer (FCC).

Table 17-1 provides a comparison of the actual and nominal velocity increments resulting from the planned maneuvers. All maneuver start times, durations, and attitudes were nominal except for the APS-2 burn which started 30 minutes later than initially planned. Table 17-2 lists data for the planned maneuvers and also includes data for several unplanned velocity changes.

Figure 17-1 presents the line-of-sight range rate residuals from a Goldstone tracking station and depicts graphically several of the S-IVB/IU velocity changes. Residuals are obtained by differencing observed range rate data from a tracking station with calculated range rate data from a sophisticated orbital model fitting portions of the data (Observed minus Calculated). Figure 17-2 shows residuals from Madrid tracking data that are associated with the docking and ejection maneuvers. Figure 17-3 gives Madrid and Texas tracking data residuals for the APS evasive burn. The magnitude of the range rate residual for each maneuver is dependent upon the geometrical considerations associated with the station location, the line-of-sight, and the vehicle attitude. This is clearly evident in Figure 17-3 for the LOX Dump and the APS-1 maneuvers as well as the APS evasive maneuver. Figure 17-4 is a comparison of the real time predicted and actual accumulated longitudinal velocity changes.

17.3 TRAJECTORY PERTURBING INFLUENCES

The range rate residuals shown in Figure 17-3 give clear evidence of a significant velocity change following the LOX Dump. This velocity change was caused by an unplanned force due to the ambient helium repressurization spheres dumping through the ambient helium engine control sphere into the J-2 engine (Helium Dump). This force perturbed the projected APS-1 lunar impact point east of the target. Figure 17-5 shows this impact point at 1.67 degrees south latitude and 4.44 degrees east longitude, which is 309 kilometers (167 n mi) from a postflight impact point of 4.33 degrees south latitude and 5.40 degrees west longitude. This latter point is 69 kilometers (37 n mi) from the target point, and was obtained by propagating the postflight reconstructed CSM separation state vector through the various planned maneuvers to the moon. The 309 kilometers (167 n mi) movement was obtained by adding the Helium Dump velocity change maneuver to the analysis.

Figure 17-5 depicts the MCC-H lunar impact point at 9.3 degrees south latitude and 11.0 degrees east longitude that was obtained by analyzing tracking data in real time. The tracking data used was obtained after the APS-1 burn was completed. This impact point was used to determine the APS-2 burn for retargeting 589 kilometers (318 n mi) back to the desired location at 3.65 degrees south latitude and 7.58 degrees west longitude (see Figure 17-5). It is to be noted that the real time MCC-H determined impact point is 305 kilometers (165 n mi) southeast of the postflight reconstructed impact point which incorporated the Helium Dump. The following discussion outlines additional trajectory perturbations which may account for some of the 305 kilometers (165 n mi) distance, with tracking uncertainties probably accounting for the remainder.

Figure 17-6 shows line-of-sight range rate residuals for the Goldstone tracking station with only the first 4300 seconds of the tracking data

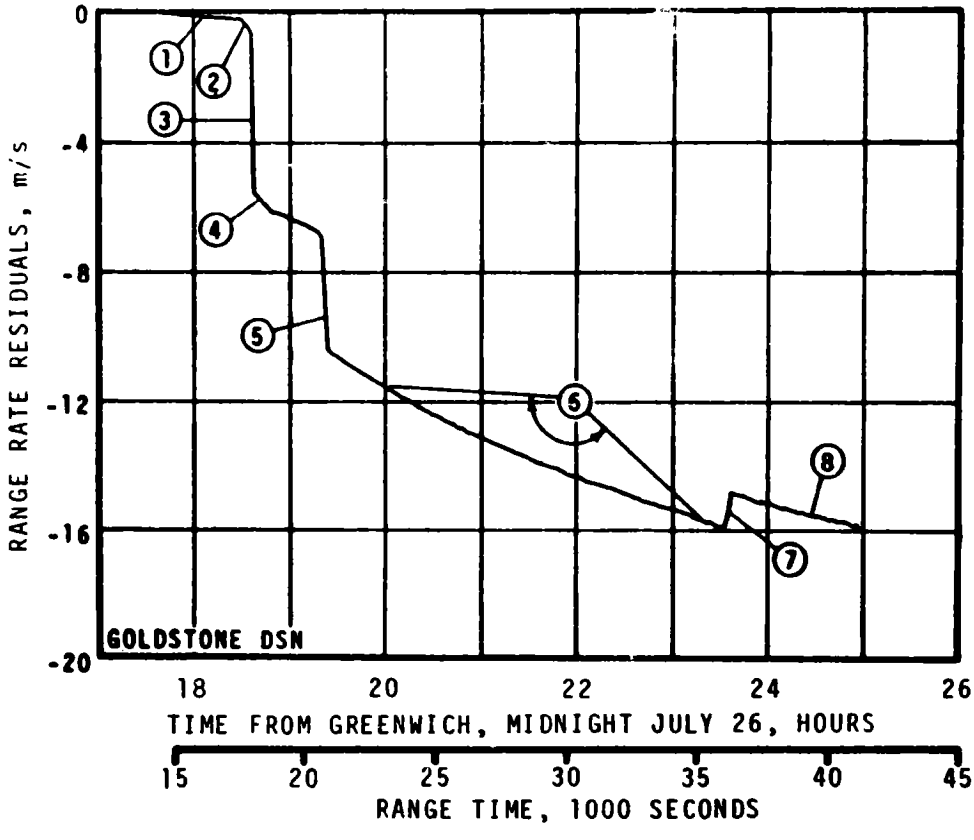

① APS EVASIVE BURN

② CVS VENTING

③ LOX DUMP

④ HELIUM DUMP

⑤ APS IMPACT BURN 1

⑥ TCS & APS THRUST

⑦ APS IMPACT BURN 2

⑧ PASSIVE THERMAL CONTROL

S-IVB/IU RANGE RATE RESIDUALS POST CSM AND DURING TB8

Figure 17-1. Translunar Coast Maneuvers Overview

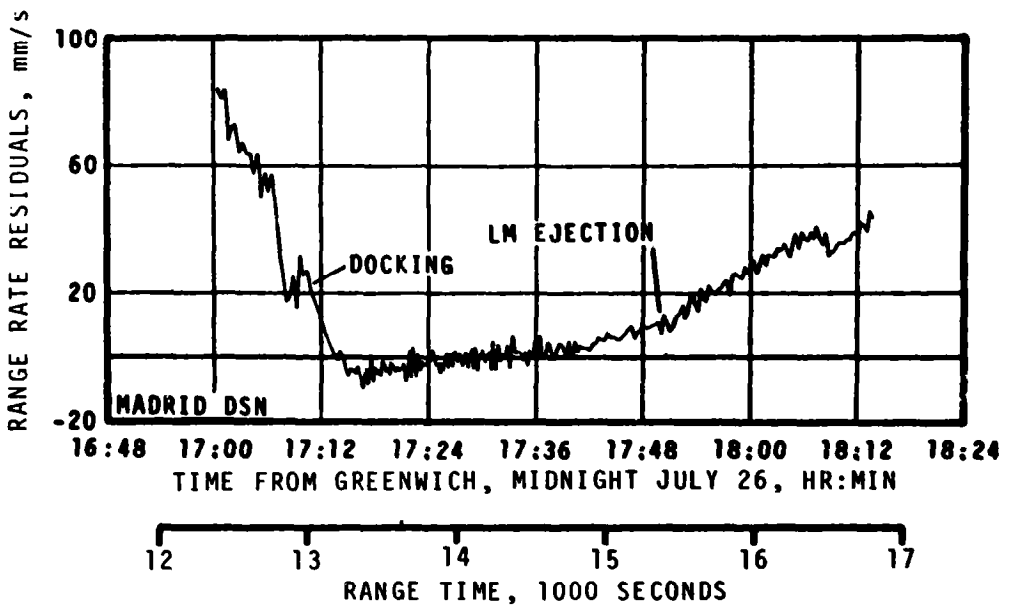

Figure 17-2. Docking and LM Ejection Maneuvers

after the anomalous thrust used to reconstruct a trajectory between the APS burns. The residuals from 25,200 seconds (7:00:00) to 36,001 seconds (10:00:01) show velocity changes that indicate non-gravitational forces were acting which slow the S/IVB/IU and perturb the lunar impact to the east. These velocity changes correlate with the times of the IU/TCS sublimator cycling and the subsequent APS reaction firings that maintain the vehicle attitude. A conservative line-of-sight residual difference of 57 mm/s (0.19 ft/s) for one of the velocity change cycles is obtained from Figure 17-6. This figure shows six similar velocity changes over the period from 22,680 seconds (6:18:00) through 35,000 seconds (9:43:20). The residual change for the first cycle is masked in Figure 17-6 because data through the first cycle were used in the trajectory reconstruction. Attributing the residual velocity changes to forces arising from the TCS/APS operations and performing the appropriate geometrical analysis leads to a force acting at 262 degrees pitch and 41 degrees yaw (relative to local horizontal) which has a total velocity change of 0.08 m/s (0.26 ft/s) per cycle. These maneuvers would be sufficient to move the impact point 155 kilometers (84 n mi) east and 46 kilometers (25 n mi) south of the projected APS-1 impact point. In addition, the perturbation of the tracking data caused difficulty in obtaining an accurate state vector on which to base the APS-2 burn.

Following the APS-2 burn at 36,001 seconds (10:00:01), that retargeted the S-IVB/IU to the desired impact point, a small unbalanced non-gravitational force perturbed the early period of the post APS-2 trajectory. This force contributes to the final impact being perturbed to

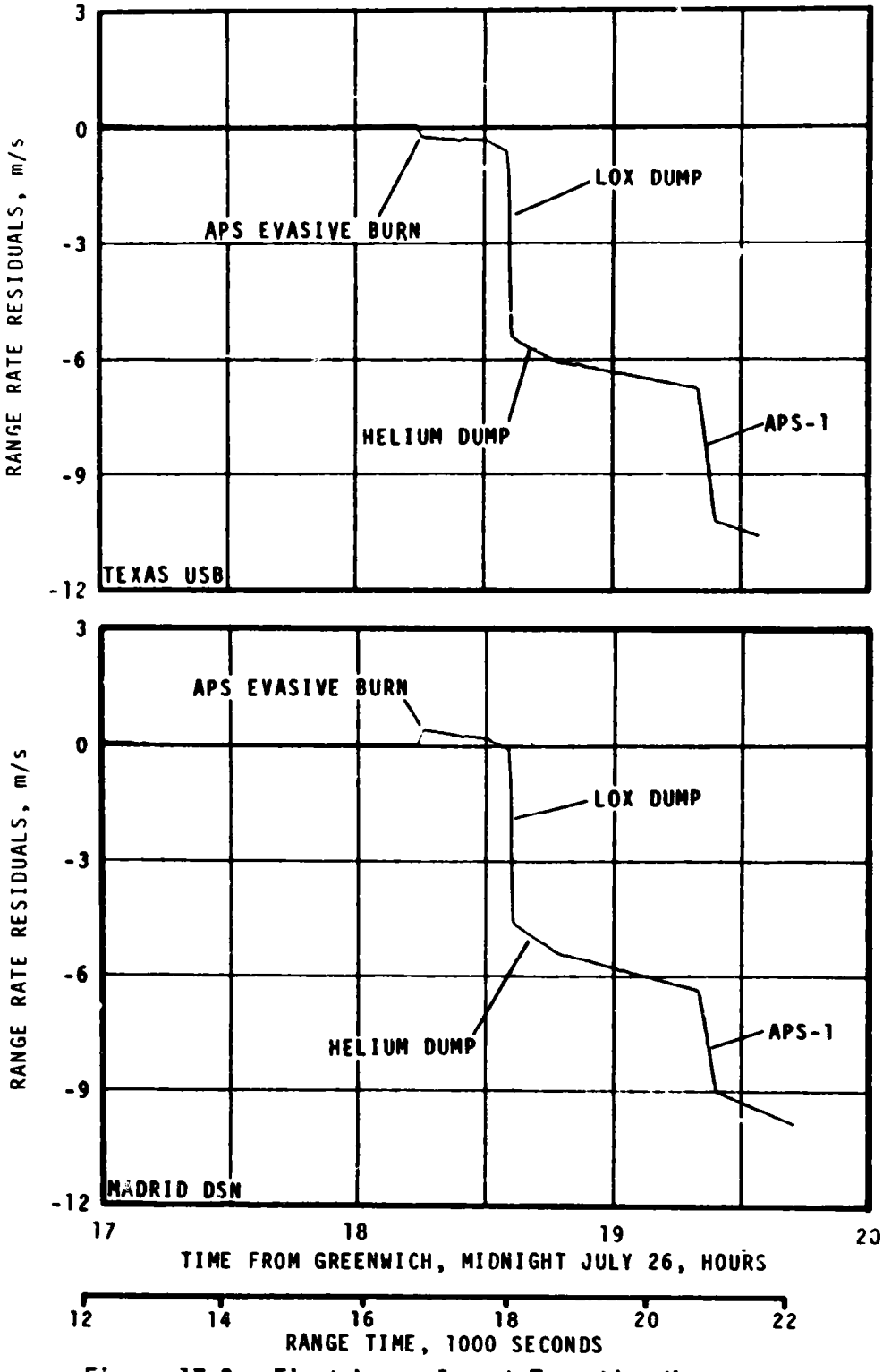

Figure 17-3. First Lunar Impact Targeting Maneuvers

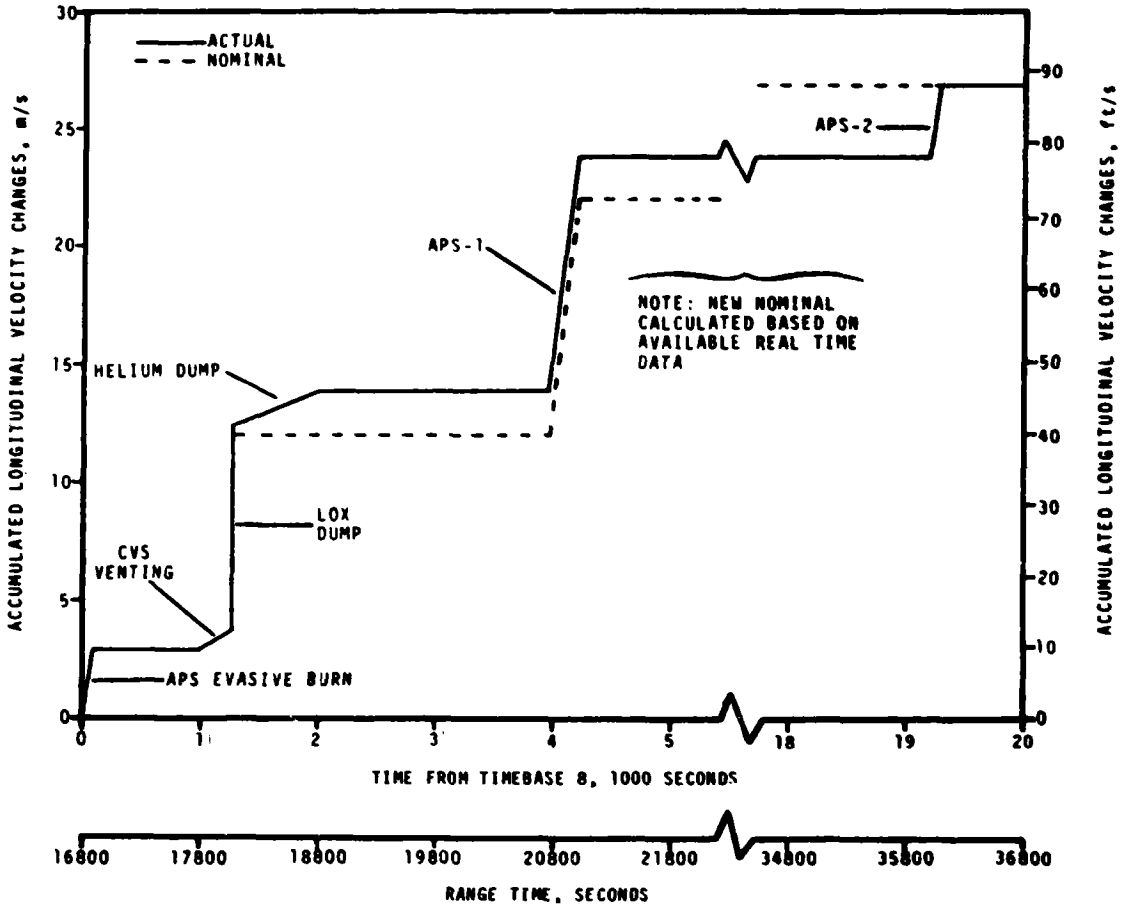

Figure 17-4. Comparison of Accumulated Longitudinal Velocity Change

a point 154 kilometers (83 n mi) northwest of the target. Figure 17-7 shows selected range rate residuals arising from the best reconstructed lunar impact trajectory to date. The analysis determined a state vector at 10:00:00 using tracking data from 26:26:00 to lunar impact. The residuals from the two Madrid tracking data sets (depicted in Figure 17-7) show an excellent fit and consistent tracking data over the total time period. The Goldstone tracking residuals, presented in Figure 17-7 and obtained from the same trajectory which gives the Madrid residuals, show a definite inconsistency in the early tracking data. An analysis of these tracking residuals indicates that the vehicle is being acted upon by a small unbalanced non-gravitational force which increases the velocity of the S-IVB/IU and perturbs the lunar impact to the west. The effect of this unbalanced force decreases gradually and after 5 hours it cannot be detected in the tracking data residuals. A low frequency oscillation (1.25 cycles per hour) modulating the higher frequency roll oscillation (13.5 cycles per hour) is evident in the Goldstone residuals

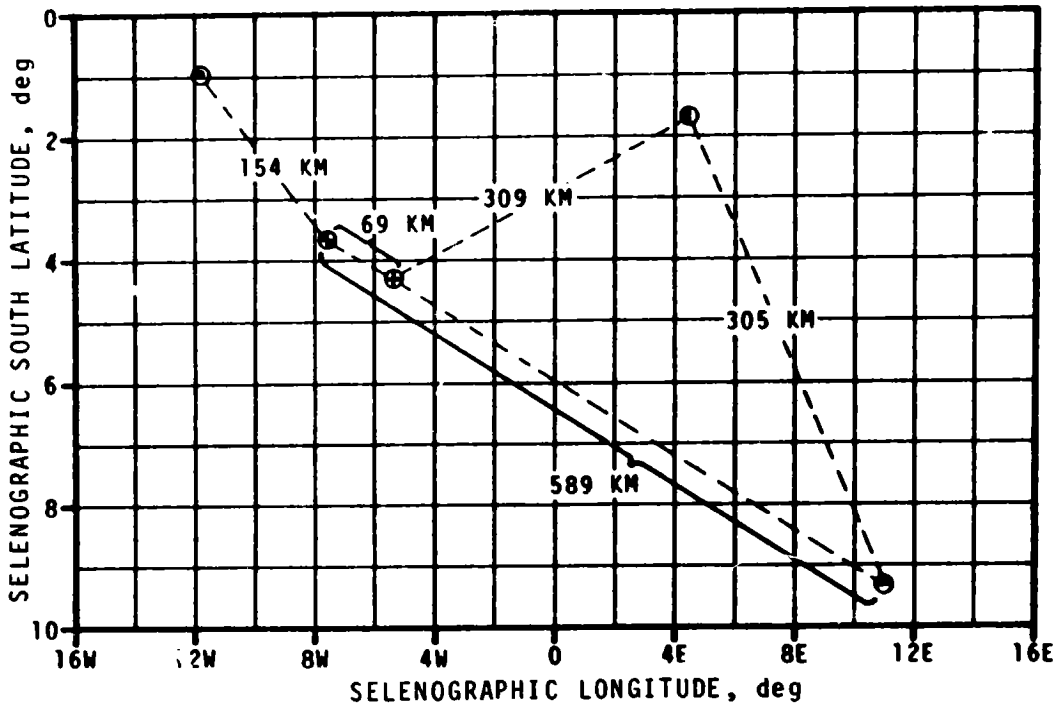

LEGEND:

- POSTFLIGHT POST APS-2 TRACKING IMPACT POINT (0.99°S, 11.89°W)
- TARGET POINT (3.65°S, 7.58°W)
- POSTFLIGHT T7 TRACKING POINT W/O HELIUM DUMP (4.33°S, 5.40°W)
- POSTFLIGHT T7 TRACKING POINT WITH HELIUM DUMP (1.67°S, 4.44°E)
- REAL TIME PRE APS-2 TRACKING POINT (9.3°S, 11.0°E)

Figure 17-5. Real Time and Postflight Lunar Impact Points

of Figure 17-7. The initial long period immediately following the "barbecue" roll initiation is 2880 seconds and roughly correlates with the 2000 to 2400 second TCS/APS periods prior to the APS-2 burn. The continuation of the TCS operation following the shutdown of the flight control computer may account for the small non-gravitational force perturbing the early portion of the post APS-2 trajectory. Since the APS system no longer maintains attitude control, the TCS forces would also produce an unbalanced moment which would perturb and greatly complicate the roll motion. After a period of time, the net force perturbing the vehicle trajectory should reduce to zero since the

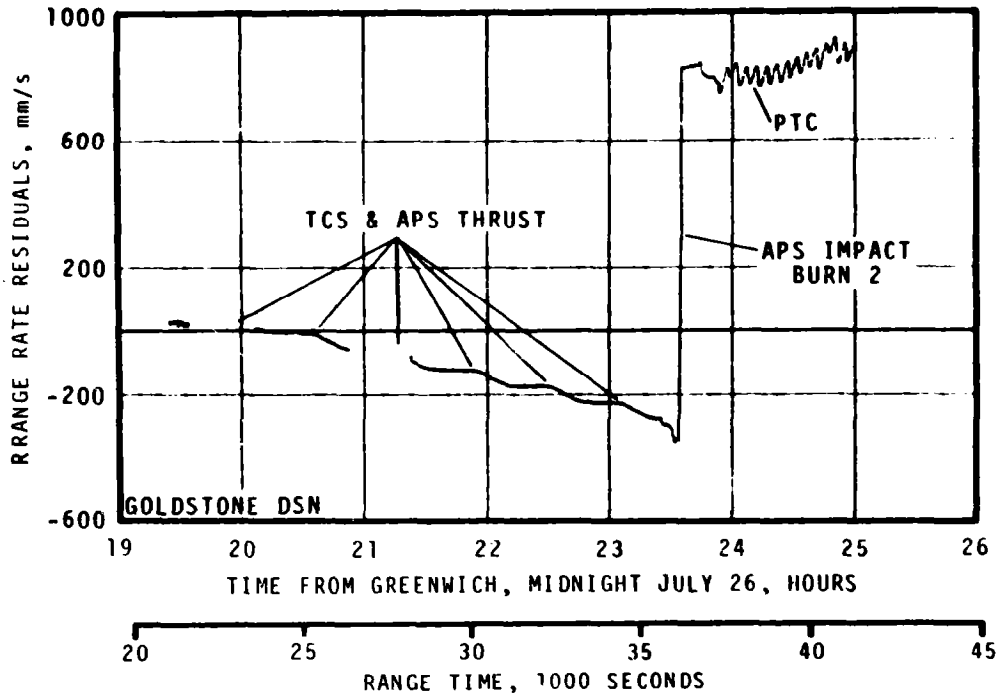

Figure 17-6. TCS and APS Thrust Perturbations

complicated rotational motion would probably distribute the TCS forces into many different directions. Additionally, the rotational frequencies should increase. These hypotheses are all supported by the evidence contained in the tracking data range rate residuals.

17.4 Trajectory Evaluation

Table 17-3 presents the actual and nominal geocentric orbit parameters of the S-IVB/IU trajectory after the APS-2 burn. These parameters are near nominal. As discussed in Paragraph 17.2, after the APS-2 burn was complete the PTC maneuver was initiated by commanding a roll rate of 5 rotations per hour. MCC-H reported a roll rate of 0.659 degree per second during the early post APS-2 tracking period. This is equivalent to 6.5 rotations per hour. The Goldstone tracking residuals presented in Figure 17-7 give a frequency of 13.5 cycles per hour for the early tracking period. This frequency is modulated by a lower frequency of 1.25 cycles per hour at 11:00:00. Since there are two omni antennas providing the tracking data, the observed frequency of 13.5 cycles per hour is twice the rotational frequency of the S-IVB/IU. A rotational rate of 6.75 revolutions per hour compares well with the reported MCC-H value of 6.59 revolutions per hour. The Madrid tracking residuals presented in Figure 17-7 show that the PTC rotation became more complex and faster at 28:00:00, 17.0 cycles per hour modulated by a

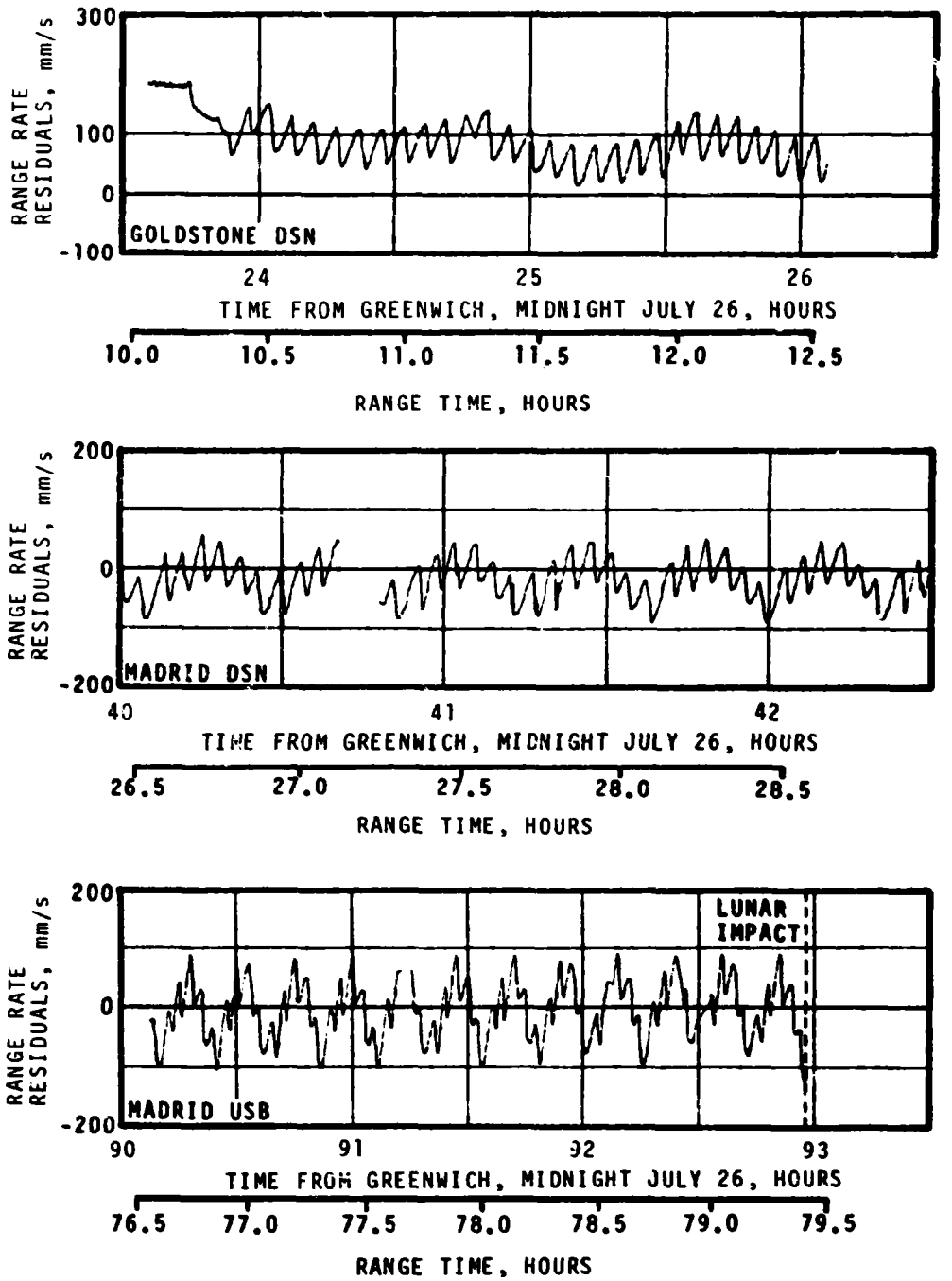

Figure 17-7. Early Tracking Inconsistency and Passive Thermal Control Oscillations

Table 17-3. Geocentric Orbit Parameters Following APS-2 Burn

PARAMETER	ACTUAL	NOMINAL	ACT-NOM
Apogee, km (n mi)	503,764 (272,011)	504,991 (272,673)	-1,227 (-662)
Eccentricity	0.974504	0.974804	-0.000300
C_3* km^2/s^2 ($n\ mi^2/s^2$)	-1.562327 (-0.455502)	-1.558768 (-0.454464)	-0.003559 (-0.001038)
Perigee Radius, km (n mi)	6,505 (3,512)	6,443 (3,479)	62 (33)

* C_3 is twice the specific energy of orbit

frequency of 2.57 cycles per hour. Again, Madrid residuals near lunar impact show an even more complex and faster PTC rotation, 20.0 cycles per hour modulated by a frequency of 4.5 cycles per hour. Considering the doubling effect mentioned above, the apparent tumble rate near lunar impact is about 10 cycles per hour or equivalently 1.0 degree per second. It is noted that the amplitude of the range rate residuals for the AS-510 S-IVB/IU is significantly less than the modulation of the AS-509 S-IVB/IU. This factor assists in more precisely determining the lunar impact point.

17.5 Lunar Impact Condition

Figure 17-8 presents the lunar landmarks of scientific interest relative to the S-IVB/IU impact. Analysis to date indicates the S-IVB/IU impacted the moon at 0.99 degree south latitude and 11.89 degrees west longitude. This impact point is accurate within about 10 kilometers (5 n mi) and will require further analysis to meet the mission objective of 5 kilometers (2.7 n mi). The high quality and large quantity of tracking data plus previous lunar impact trajectory reconstruction experience indicate the 5 kilometers objective will be met. Impact parameters and miss distances are presented in Table 17-4. The distance from the impact point to the target is 154 kilometers (83 n mi) which is within the 350 kilometers (189 n mi) mission objective. The distance to the Apollo 12 seismometer is 353 kilometers (191 n mi) and the distance to the Apollo 14 seismometer is 188 kilometers (102 n mi). The impact time presented in Table 17-4 is determined from the loss of signal (LOS) as recorded in Table 17-5 and is accurate within 0.1 second satisfying the mission objective. This table presents recorded LOS times, the range to the impact point, the transmission delay, and the corrected impact time.

Table 17-4. Lunar Impact Conditions

PARAMETER AT IMPACT	ACTUAL	NOMINAL	ACT-NOM
Stage Mass, kg (lbm)	14,007 (30,880)	13,964 (30,785)	43 (95)
Moon Centered Space-Fixed Velocity, m/s (ft/s)	2,577 (8,455)	2,579 (8,461)	-2 (-6)
Impact Angle Measured from Vertical, deg	27.83	31.04	-3.21
Incoming Heading Angle Measured From North to West, deg	83.46	81.37	2.09
Apparent Primary Tumble Rate at Impact, deg/s	~1.0	0.5	~0.5
Selenographic South Latitude, deg	0.99	3.65	-2.66
Selenographic West Longitude, deg	11.89	7.58	4.31
Impact Time, HR:MIN:SEC	79:24:41.55	79:14:35.37	00:10:06.18
Distance to Target, km (n mi)	154 (83)	0 (0)	154 (83)
Distance to Apollo 12 Seismometer, km (n mi)	353 (191)	478 (258)	-125 (-67)
Distance to Apollo 14 Seismometer, km (n mi)	188 (102)	301 (163)	-113 (-61)

Scientific influences defined desirable AS-510 lunar impact objectives which are more stringent than the mission objective of hitting within 350 kilometers (189 n mi) of the target point. For seismic purposes, regions of preferred and acceptable impact were defined.

Figure 17-9 shows these regions and the Apollo 15 impact point. The acceptable region lies greater than 250 kilometers (135 n mi) and less than 575 kilometers (310 n mi) from a seismometer. The preferred region is additionally defined to lie within a wedge of 20 degrees extending eastward from the Apollo 14 seismometer. Although the Apollo 15 impact point is not in the preferred region, the distance of 353 kilometers (191 n mi) from the Apollo 12 seismometer is acceptable.

17.6 Tracking Data

Figure 17-10 shows the tracking data available to the Trajectory Determination group. Both C-Band and S-Band data of good quality were received. Table 17-6 shows the tracking site locations and configurations.

Table 17-5. Lunar Impact Times

TRACKING STATION	RECORDED TIME ON JULY 29, 1971 (GMT-HR:MIN:SEC)	RANGE (KM)	LIGHT TIME DELAY (SEC)	CORRECTED RANGE TIME (HR:MIN:SEC)
Merritt Island	20:58.42.87	397,217	1.325	79:24:41.55
Madrid	42.88	399,534	1.333	41.55
Goldstone	42.85	399,878	1.334	41.52
Greenbelt	42.87	397,930	1.327	41.54
Ascension	42.90	396,473	1.322	41.58
NOTE: Range Zero at 13:34:00 GMT on July 26, 1971				AVERAGE 79:24:41.55 285,881.55 SEC

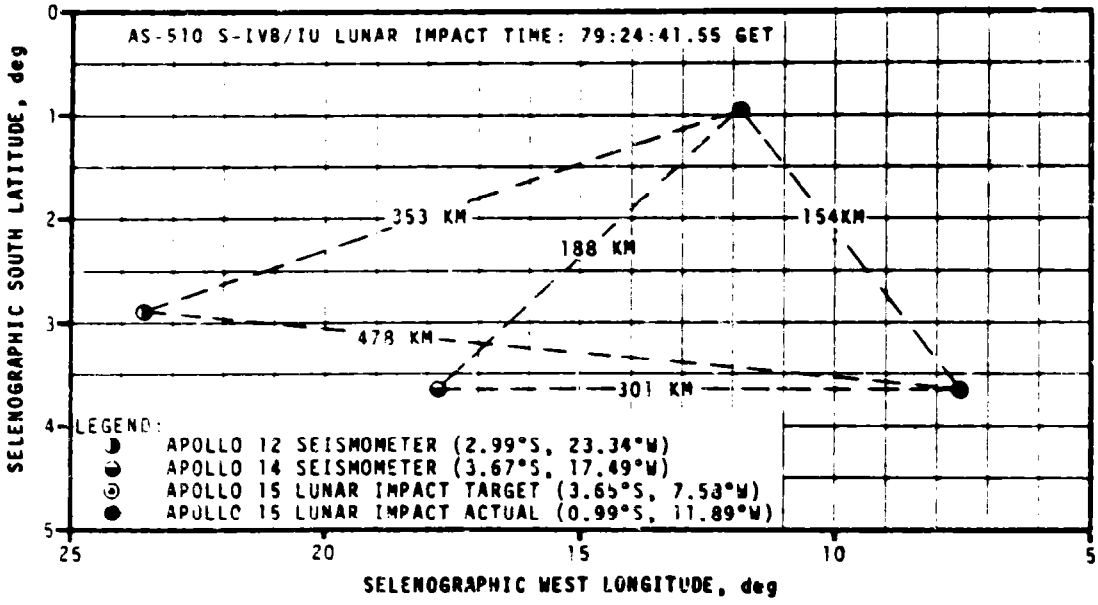

Figure 17-8. Lunar Landmarks of Scientific Interest

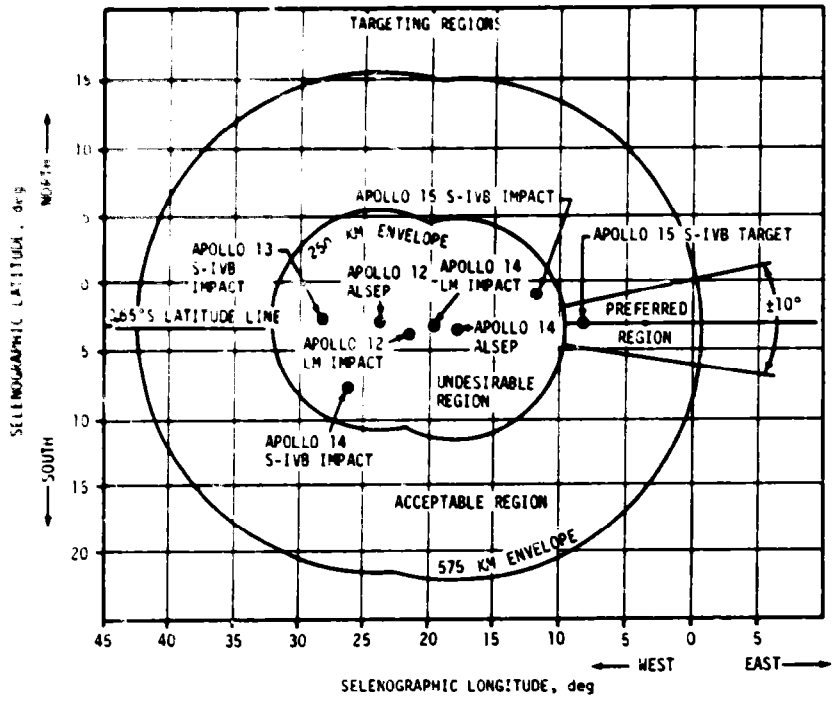

Figure 17-9. Lunar Impact Targeting Considerations

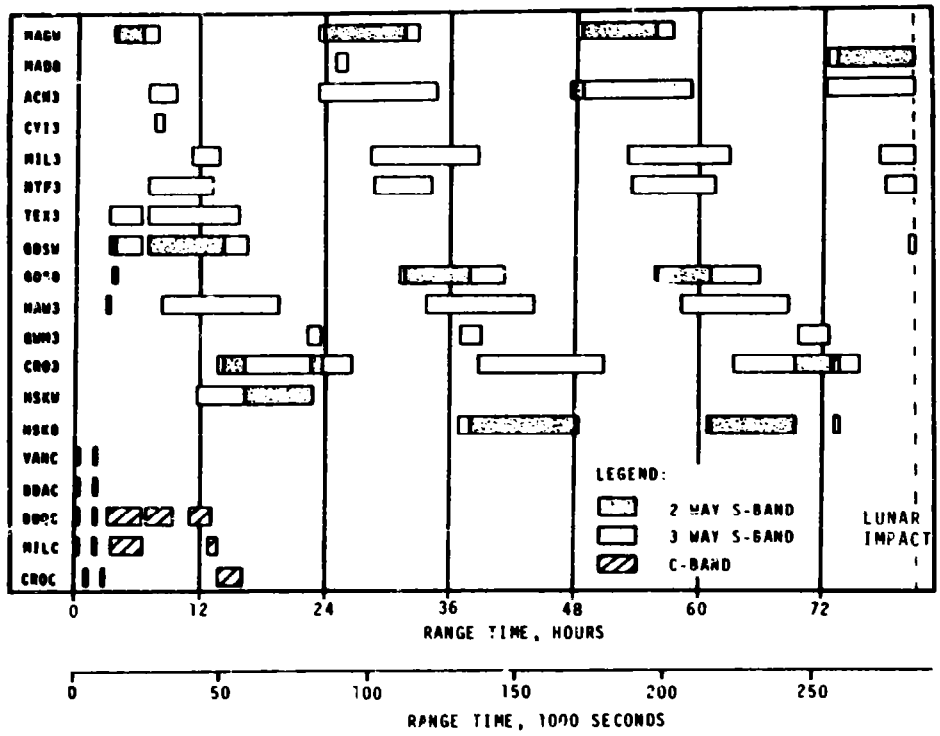

Figure 17-10. Tracking Data Availability

Table 17-6. S-IVB/IU Tracking Stations

STATION LOCATION	CONFIGURATION	ABBREVIATION
Madrid, Spain	DSN 85' S-Band	MADW
Madrid, Spain	MSFN 85' S-Band	MAD8
Ascension Island	MSFN 30' S-Band	ACN3
Canary Island	MSFN 30' S-Band	CYI3
Merritt Island, Florida	MSFN 30' S-Band	MIL3
Greenbelt, Maryland	MSFN 30' S-Band	NTF3
Corpus Christi, Texas	MSFN 30' S-Band	TEX3
Goldstone, California	DSN 85' S-Band	GDSW
Goldstone, California	MSFN 85' S-Band	GDS8
Kauai, Hawaii	MSFN 30' S-Band	HAW3
Guam Island	MSFN 30' S-Band	GWM3
Carnarvon, Australia	MSFN 30' S-Band	CRO3
Tidbinbilla, Australia	DSN 85' S-Band	HSKW
Canberra, Australia	MSFN 85' S-Band	HSK8
Insertion Ship	FPS-16M C-Band	VANC
Bermuda Island	FPS-16 C-Band	BDAC
Bermuda Island	FPQ-6 C-Band	BDQC
Merritt Island, Florida	TPQ-18 C-Band	MILC
Carnarvon, Australia	FPQ-6 C-Band	CROC

SECTION 18

SPACECRAFT SUMMARY

The Apollo 15 mission, the first of three flights in the J series of Apollo missions, was launched from Kennedy Space Center, Florida at 9:34:00 Eastern Daylight Time (13:34:00 Universal Time) on July 26, 1971. The spacecraft was manned by Colonel David R. Scott, Commander; Major Alfred M. Worden, Jr., Command Module Pilot; and Lt. Colonel James B. Irwin, Lunar Module Pilot. The spacecraft/S-IVB combination was inserted into a parking orbit of 91.5 by 92.5 miles for systems checkout and preparation for translunar injection, which was initiated about 2.75 hours after liftoff.

Shortly after the command and service module separated from the S-IVB, the color television camera was activated to observe docking with the Lunar Module (LM), and separation of the combined spacecraft from the S-IVB. The crew observed the venting of the S-IVB tanks which was followed by the auxiliary propulsion system firing which targeted the S-IVB to a lunar impact. During the separation phase, a shorted condition in the control circuit to bank A of the service propulsion system occurred, requiring bank A to be used in the manual mode for the lunar orbit insertion and transearth injection firings. The first midcourse correction was performed at about 28.75 hours with a velocity change of 5.3 ft/s, and the second midcourse correction of 5.4 ft/s was performed at about 73.5 hours. The impact of the S-IVB stage at about 79.4 hours was recorded by the Apollo 12 and 14 seismometers, and was about 83 miles from the preselected point, and approximately 102 miles east/northeast of the Apollo 14 landing site.

The service propulsion system was fired for 398.4 seconds during the lunar orbit insertion maneuver at about 78.5 hours, inserting the spacecraft into a lunar orbit 170.1 by 57.7 miles. The descent orbit insertion maneuver was performed at about 82.5 hours. Some 13 hours later, a 3.2 ft/s trim maneuver was required to raise the perilune altitude. The spacecraft were separated at about 100.75 hours, after which a 68.3 ft/s circularization maneuver was performed using the service propulsion system.

The 741-second powered descent initiation maneuver was performed at 104:30:09 and the LM landed in the Hadley Rille region of the moon at 104:42:30. At lunar touchdown, the low-level propellant light illuminated, indicating a total hover time of 111 seconds remaining. The best estimate of the landing location is 26 degrees, 6 minutes, 10 seconds north latitude

and 3 degrees, 38 minutes, 55 seconds east longitude on the Rima Hadley Lunar Photomap, First Edition, April 1970.

About 2 hours after landing, the Commander performed a 33-minute standup extravehicular activity by extending his upper body through the top hatch. From this position, he described and photographed the surrounding lunar surface.

The first lunar extravehicular activity began at 119:39:10. The crew egressed, activated the television camera, made relevant comments, and quickly became acclimated to the lunar environment. The Lunar Roving Vehicle (LRV), Apollo lunar surface experiments package, and related gear were unstowed. Some difficulty was experienced in detaching the LRV from the LM. Checkout of the LRV disclosed that front wheel steering was inoperative. After verifying that all other LRV systems were operative and that adequate vehicle control could be maintained with rear wheel steering, the crew proceeded to explore the lunar surface. The first traverse was made by passing close to Nameless, Quadrant, Pooh and Canyon Craters on the way to the first stop at Elbow Crater. An enthusiastic crew provided a colorful commentary on the lunar features as they were observed, and as samples were obtained and documented. Hadley Rille and St. George Crater were covered in exacting detail. The return traverse was made using the LRV navigation system, which provided accurate vectoring to the LM landing site. After returning to partially unload and to retrieve additional gear, the crew drove to the selected Apollo lunar surface experiments package deployment site, approximately 360 feet west/northwest of the LM. The Apollo lunar surface experiments package was deployed and two drilling operations were partially performed. The lunar surface was more difficult to drill than expected. Duration of the first lunar surface extravehicular activity was 6 hours and 32 minutes.

The second traverse began at about 142.25 hours and after recycling LRV switches and circuit breakers, the LRV front wheel steering was restored. This traverse was east of the first, but also in a southerly direction. After passing in sight of Index, Arbeit, Crescent, Dune, and Spur Craters, the crew stopped in the sampling area. The return traverse closely followed the outbound route. Drilling was completed, and the second of two probes was emplaced while the nearby area was photographed. Returning to the LM, the United States flag was erected, and samples were stowed. This traverse lasted approximately 7.25 hours and communications were satisfactory despite the fact that the LM operated with a broken antenna blade, which was repaired with tape prior to the extravehicular activity.

The third day of lunar exploration was cut short to allow the crew rest and to meet the liftoff timeline. A curtailed traverse was made to pick up the deep core samples, visit Scarp and Rim Craters, and investigate the region named The Terrace. The traverse was roughly in a westerly direction from the landing site. More samples were obtained and trouble was experienced with the 16 and 70-mm cameras. On return, the LRV was parked at a vantage point to allow television coverage of liftoff. During the three

extravehicular periods totaling 19 hours 46 minutes and 12 seconds of lunar exploration, approximately 171 pounds of lunar material were collected for return to earth. Dust and high sun angles caused some heat management problems with the communications equipment, and television picture quality was degraded; however, the crew dusted the space radiators and camera lens, and this restored near nominal operation.

After 66 hours 54 minutes and 53 seconds on the lunar surface, the ascent stage lifted off the lunar surface at 171:37:23 and attained a 42.5 by 9.0 mile orbit. From this orbit, the crew performed a nominal LM-active rendezvous, and docking was completed at about 173.5 hours.

During the lunar stay, the command and service module had orbited the moon 34 times and functioned as a scientific satellite. The LM was jettisioned one revolution later than planned because of difficulty with the tunnel venting or sealing. Jettisoning occurred at about 179.5 hours, and the LM deorbit maneuver was initiated about 1.5 hours later. The LM impact occurred at 181:29:36 at 26 degrees 21 minutes north latitude and 0 degree 15 minutes east longitude, about 12 miles from the planned impact point and about 50 miles west of the Apollo 15 landing site. Impact was recorded by the Apollo 12, 14, and 15 seismic stations.

The laser altimeter malfunctioned after 24 lunar revolutions and could not be restored to an operative condition. The lunar surface television camera which had provided good coverage of liftoff, was cycled on again at about 211.25 hours and operated normally for about 13 minutes before the downlink signal was abruptly lost. All efforts to restore video transmission failed. The subsatellite was deployed at about 222.5 hours. All systems were operating and the subsatellite orbit was approximately 76.3 by 55.1 miles. The lunar orbital phase of the Apollo 15 mission was terminated by the transearth injection maneuver at 223:48:45.

The transearth coast extravehicular activity began at about 242 hours. Television coverage was provided while the Command Module Pilot retrieved film cassettes and examined the scientific instrumentation module for any abnormalities. The extravehicular activities lasted approximately 38 minutes which was about 20 minutes shorter than planned.

The only midcourse correction of the transearth phase was performed at the seventh midcourse correction opportunity. The maneuver was 24.2 seconds in duration and provided a velocity of 5.6 ft/s. The entry flight path angle, as a result, was reduced to a nominal minus 6.51 degrees. The command module was separated from the service module 15 minutes prior to entry interface. The entry was nominal and the spacecraft was observed on the main parachutes. Later, one of the three main parachutes collapsed, but a safe landing was made at 295:11:53. The landing coordinates, determined by the onboard computer, were 26 degrees, 7 minutes, 48 seconds north latitude, and 158 degrees, 7 minutes, 12 seconds west longitude, about 1 mile from the planned landing point. The crew were brought aboard

the recovery ship by helicopter about 39 minutes after landing. The Apollo 15 mission was successfully concluded with the placing of the command module aboard the recovery ship about 1.5 hours after landing.

SECTION 19

APOLLO 15 INFLIGHT DEMONSTRATION

There were no MSFC inflight demonstrations for the Apollo 15 flight.

SECTION 20

LUNAR ROVING VEHICLE

20.1 SUMMARY

All Lunar Roving Vehicle (LRV) systems performed satisfactorily with the range capability being approximately twice the predicted value. The total range traversed during the three traverses was 27.9 kilometers at an average velocity of 9.3 km/hr; the maximum velocity was 13 km/hr and the maximum slopes negotiated were up to 12 degrees. The stopping distance was approximately 4.6 meters from 10 km/hr, and the braking and steering duty cycles were much less than predicted, with estimates as low as 5 percent of the time given by the crew. The LRV average energy consumed was 1.87 amp-hr/km with a total consumed energy of 52 amp-hr. The navigation system attained a Lunar Module (LM) closure error of less than 0.2 kilometer on each traverse while gyro drift was negligible.

The wander factor (LRV path deviation due to obstacles) plus wheel slip was approximately equal to the predicted value of 10 percent.

The following concerns occurred during the lunar surface operation:

a. Battery No. 2 volt-ammeter was inoperative at first power up.

b. Forward steering was inoperative on Extravehicular Activity (EVA)-1 but was successfully activated on EVA-2 and 3.

c. Seat belt fastening was excessively time consuming.

d. Lunar Communication Relay Unit (LCRU) TV dropped out after LM liftoff.

e. The left front fender extension was missing after EVA-1.

A detailed description of the LRV may be seen in paragraph 20.14.

20.2 DEPLOYMENT

There were three occurrences during LRV deployment which were not nominal, although their significance on the deployment operation was minimal. These occurrences were:

a. Both support arm latch mechanisms unlatched (corrected by crew during normal inspection procedures).

b. Saddle did not release although pin was out. (Crew accomplished release with manual force. Could be avoided by using proper release procedure.)

c. Two chassis pins were not flush with hinge. (Crew used deployment tool and normal procedures to push pins into latch.)

Details of nominal deployment are described in paragraph 20.14.

20.3 LRV TO STOWED PAYLOAD INTERFACES

The interfaces between the stowed payloads and LRV were adequate.

20.4 LUNAR TRAFFICABILITY ENVIRONMENT

Prior to the Apollo 15 mission a series of environmental constraints (operations envelope) were established for use as design criteria for the LRV lunar surface operations. These design criteria outlined the expected range of surface temperature, radiation levels, meteoroid flux rates, etc., as well as a spectrum of surface roughness for use in mission planning and trafficability analyses. Because premission photography (20-meter resolution) left much to be desired in providing answers to the basic questions relative to the expected vehicle trafficability, it was necessary to make certain conservative assumptions regarding these factors for the Apollo 15 landing site.

In general, the environment was more favorable than anticipated in the normal case. Premission scientific traverse planning assumed that the crew would require at least a 10 percent wander factor to reach the various scientific stations on the traverse. Based on preliminary data obtained from the real-time operations, preliminary data from analysis of soil samples, and cursory examination of available photography and discussions with the Apollo 15 crew during their debriefings, these operational envelopes were not exceeded. Based on real-time observations the premission wander factor seems to have been a good value for this landing site. During the Standup EVA (SEVA), the crew described the surface as good from a trafficability standpoint, since only a small percentage of the surface appeared to be covered with fragmental debris. See Figure 20-1 for a map showing the LRV traverses. The crew further remarked that the surface looked very much like the Apollo 14 site in terms of the amount of hummocky surface; however, the surface looked as if it would offer no problem to the LRV. The mare surface at the site, as shown by TV and surface photography, shows that the surface is indeed gently undulating (hummockh) in detail and although abundantly cratered, there is a very small percentage of the surface littered with blocky debris. Craters near the LM, although 25 to 30 meters in diameter, had smooth interiors and very small amounts of blocky ejecta indicating that the fragmental layer was relatively thick at this site. In terms of surface roughness, the entire area traversed by the LRV can now be classified a smooth mare surface; however, some photography does show blocky craters and crew comments indicate other types of roughness as indicated by the series of large depressions or swales (apparently very

NOTE: TRAVERSE CHECK POINTS ARE INDICATED BY NUMBERS

Figure 20-1. LRV Traverses

old subdued craters) which were traversed by the LRV during EVA-3. Further discussion of surface roughness is contained in paragraph 20.6. The mean regional slope distribution of the surface traversed by the LRV was much less than had been assumed prior to the Apollo 15 mission. A comparison of the premission estimates and postmission assessments of the slope distribution for EVA's 1, 2, and 3 can be made on Figures 20-2 through 20-5. The latter estimates were based on map distances corresponding to lunar surface profile segments ranging between 100 m and 500 m. The topographic data used to obtain range of slopes was a 1:15,840-scale topographic map compiled by NASA MSC from Orbiter V photographs with a photographic resolution of 20 m. In general, the fine-grained surface material of the Apennine-Hadley region is characterized by a slightly cohesive granular soil with bulky grains in the silt-to-fine-sand size range which exhibits adhesive characteristics when in contact with other surfaces. The soil conditions encountered during EVA's 1, 2, and 3 were variable. As expected, at locations of different geologic history, variations in the consistency, packing characteristics, and gradation of the lunar soil were observed to depths varying from a few centimeters to a few tens of centimeters. The LRV mobility performance could be materially affected by these soil conditions. The available information indicates that the soil conditions at the Apollo 15 landing site do not appear to be substantially different from those encountered during previous Apollo missions. In general, the material appears to be more cohesive than that encountered at the Apollo 14 site and at least as cohesive as that encountered at the Apollo 11 and Apollo 12 sites.

Figure 20-6 shows gradation curves from grain-size analyses performed at the Lunar Receiving Laboratory on several lunar soil samples obtained during the Apollo 15 mission. These curves are compared with the grain-size distribution of the crushed basalt, designated as LSS (WES Mix), that was used as a lunar soil simulant for LRV wheel-soil interaction studies performed at the U. S. Army Engineer Waterways Experiment Station (USAE WES), Vicksburg, Mississippi. The physical and mechanical properties of the five consistencies at which this simulant was placed, designated respectively as LSS_1 through LSS_5, are listed in Table 20-1 and are compared with ranges of corresponding lunar soil properties obtained during missions prior to Apollo 15.

For comparison purposes, listed below are a limited amount of preliminary quantitative or semi-quantitative lunar soil mechanics data that have been obtained from real-time observations and photographic coverage, and post-mission analyses on lunar soil samples from the Apennine-Hadley region:

(1) The bulk density of the double-core tube soil sample (#U03/L04), obtained at Station 2 of EVA 1 (near St. George Crater), is estimated to range between 1.4 g/cm^3, along the upper 27 to 29 cm, and 1.64 g/cm^3 along the lower section of the tube which is 34.9 cm long.

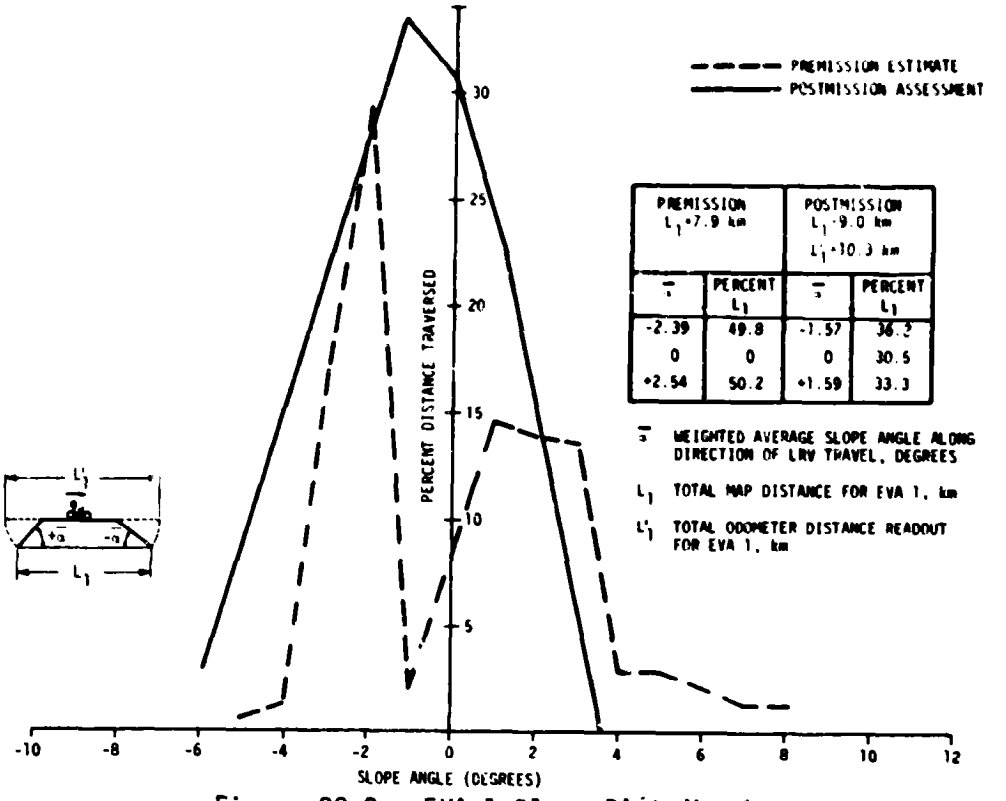

Figure 20-2. EVA 1 Slope Distribution

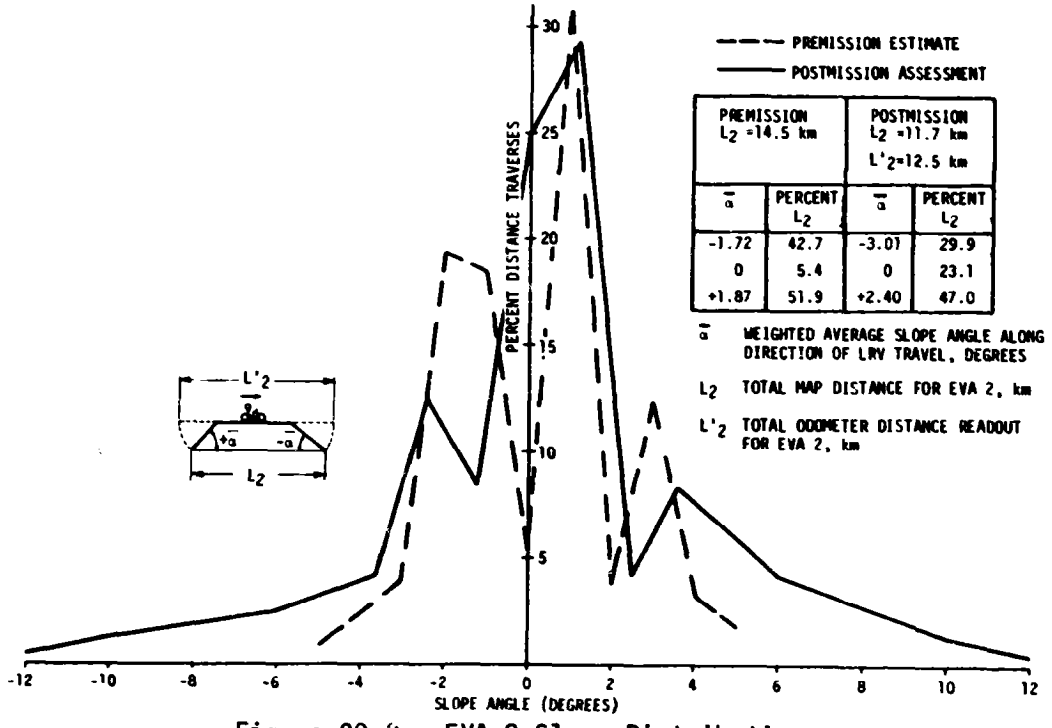

Figure 20-3. EVA 2 Slope Distribution

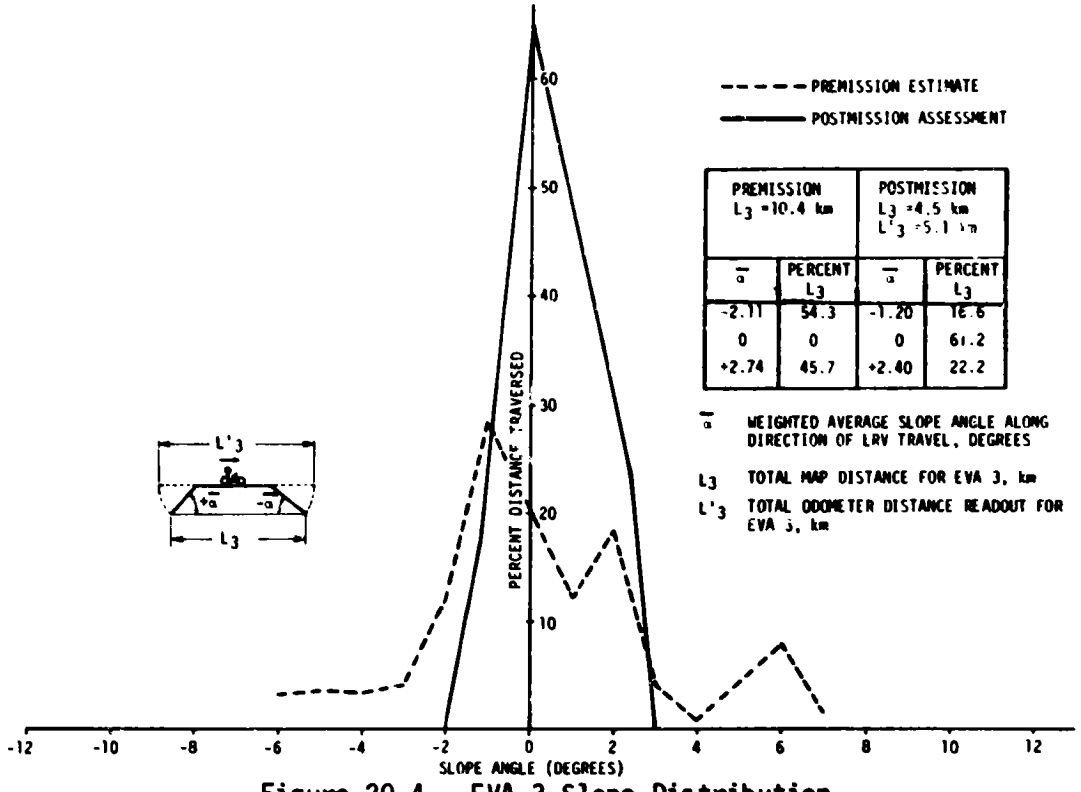

Figure 20-4. EVA 3 Slope Distribution

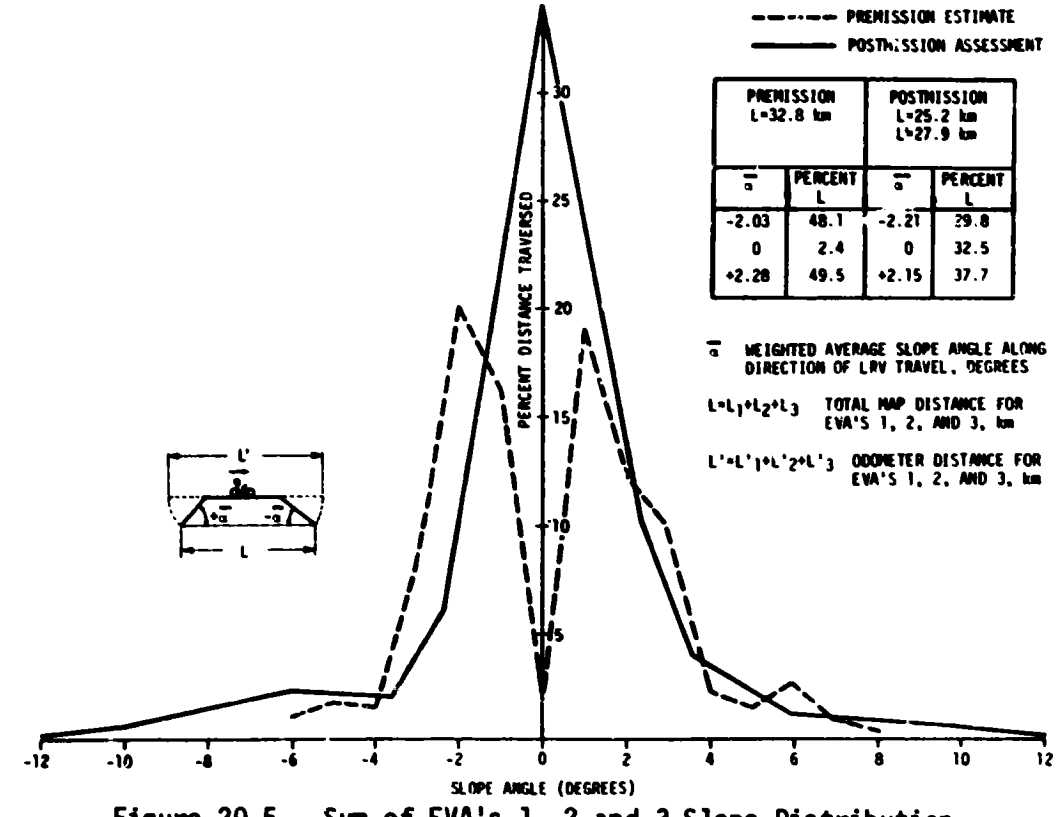

Figure 20-5. Sum of EVA's 1, 2 and 3 Slope Distribution

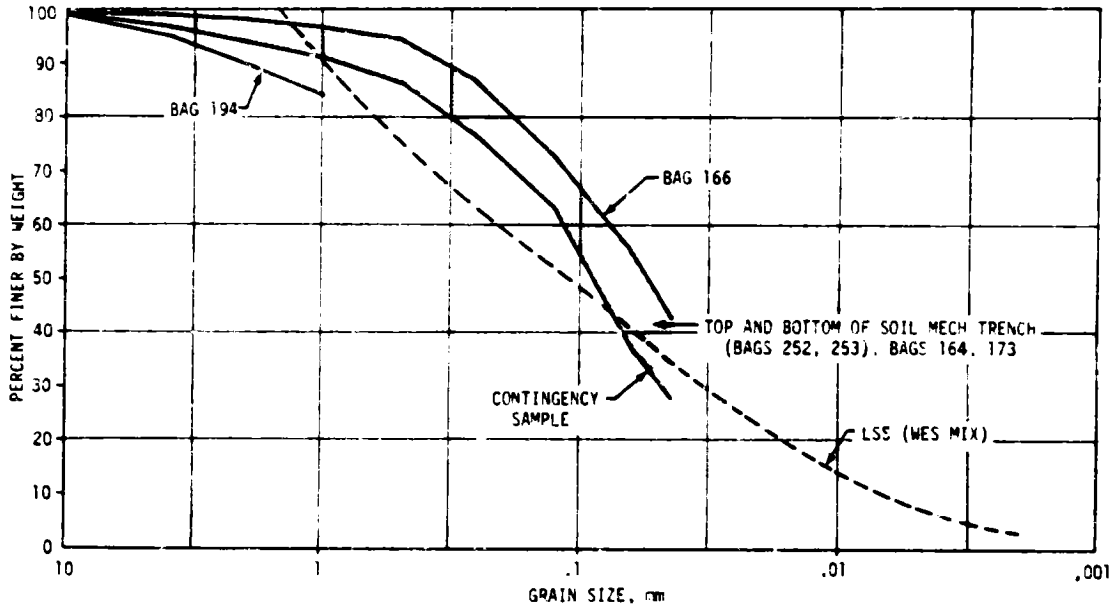

Figure 20-6. Grain Size Distribution Curves from Apollo 15 Lunar Soil Samples and LSS (WES Mix)

(2) The bulk density of the three upper sections of the deep core obtained at the ALSEP site is estimated to be 1.62 g/cm^3, 1.84 g/cm^3, and 1.75 g/cm^3 in order of increasing depth. Each of these sections is 39.9 cm long.

(3) The cohesion of the material in the vicinity of the soil mechanics trench is estimated to be 0.1 N/cm^2 (0.15 psi) and the rate of its resistance to penetration with depth to range between 4.1 N/cm^3 and 5.4 N/cm^3 (15 psi/in to 20 psi/in).

(4) The average depth of crew bootprints was 1 cm (0.4 in). However, bootprints as deep as 15 cm (6 in.) were also developed especially on soft rims of fresh craters.

It is indicated that the physical and mechanical properties of the soils traversed by the LRV were within the range of the properties of the lunar soil simulants LSS$_1$ through LSS$_5$ used in terrestrial LRV wheel-soil interaction studies.

20.5 WHEEL-SOIL INTERACTION

Information relative to the interaction of the vehicle with the lunar surface was extracted from: (1) crew descriptions; (2) photographic coverage of the EVA activities, including a short 16 mm movie taken with the Data Acquisition Camera (DAC) while the vehicle was in motion along segments of the EVA 2 traverse; and (3) LRV amp-hr integrator, odometer and speedometer readouts. On the basis of this information, the LRV interaction with the lunar surface can be summarized as follows:

Table 20-1. Physical Properties of Lunar Soil Simulant

SOURCE	VOID RATIO	BULK DENSITY		ANGLE OF INTERNAL FRICTION (deg)	COHESION		PENETRATION RESISTANCE GRADIENT	
		DRY LSS (g/cm^3)	EQUIVALENT OF LUNAR SOIL (g/cm^3)		(N/cm^2)	(psi)	(N/cm^3)	(psi/in)
Premission Estimates From Surveyor I, III, V, VI, & VII Orbiter I-V Apollo 11, 12, 14 Luna 9, 13, 16, 17 Lunokhod 1	0.55-1.1	1.50-2.00	——	35-45	0.03-0.14	(0.05-0.20)	0.4-2.6	(1.5-9.6)
LSS_1 (Loose - Air Dry)	0.90	1.52*	1.63 **	38.5	0	0	0.2	(0.8)
LSS_2 (Intermediate Density - Air Dry)	0.83	1.58	1.69	39.0	0.03	(0.05)	0.6	(2.2)
LSS_3 (Dense - Air Dry)	0.74	1.66	1.78	40.0	0.06	(0.08)	1.8	(6.5)
LSS_4 (Loose - Moist)	0.90	1.52	1.63	38.5	0.08	(0.11)	1.0	(3.7)
LSS_5 (Dense - Moist)	0.69	1.71	1.83	41.0	0.29	(0.30)	6.4	(23.6)

* - Dry Bulk Density of LSS (Specific Gravity of Solids - 2.89)
** - Equivalent Bulk Density of Lunar Soil (Specific Gravity of Solids - 3.1), Based on the Same Void Ratio

a. The general impression of the crew was that the LRV exerted a very low ground pressure on the lunar surface. This observation is also corroborated by numerous photographs obtained during the lunar surface EVA's. With both crewmen onboard the vehicle and the weight of the vehicle and its payload evenly distributed among the wheels, the depth of the wheel tracks was on the average of 1 1/4 cm (1/2 in) and varied between an imperceptible amount and 5 cm (2 in). High wheel sinkage was usually developed when the vehicle was traversing small fresh craters. Because of its light weight, on one occasion the LRV had the tendency to slide down a rather steep slope sideways as soon as the crew had stepped off the vehicle. To prevent sliding, the crew took turns holding it.

b. The 50-percent chevron-covered wire-mesh wheels of the LRV developed excellent traction with the lunar surficial material. In most cases a sharp imprint of the chevron tread was clearly discernible, indicating that the surficial soil possessed a small amount of cohesion and that the amount of wheel slip was minimal. The latter observation is also corroborated by the small error of traverse closure in the odometer and navigation systems, which were based on a constant wheel-slip bias of 2.3 percent. Also, an average LRV wheel sinkage of 1-1/4 cm (1/2 in) at a wheel slip of 2.3 percent is in agreement with data obtained from the USAE WES wheel-soil interaction tests on lunar soil simulants.

c. The crew reported driving was quite easy when the vehicle was operated on level surface which was relatively free of obstacles. On this type of surface the indicated vehicle speed, which was not corrected for wheel slip, ranged between 10 km/hr and 12 km/hr, with one maximum speed readout of 13 km/hr. In these instances the throttle setting was reported to be at or close to 100 percent. When the vehicle ran across crater fields with a high density of small craters (1 m to 2 m diameter) with low rims, the maximum indicated vehicle speed for comfortable riding was 6 km/hr to 7 km/hr. At all of these speeds, no wheel slip could be detected. From terrestrial experience, a wheel slip of less than about 20 percent is not detectable by the vehicle driver. In one instance at the ALSEP site, the wheels attained a 100 percent slip when the vehicle was being started from a stand-still position. While spinning, the wheels dug into the lunar soil to a depth of approximately 13 cm (5 in); i.e., down to the lower part of the wheel rim. This contingency did not delay the mission and did not impose undue inconvenience to the crew who lifted the vehicle out of the depression and placed it on undisturbed soil and resumed their activities.

d. During hard-over turns executed at high speeds, the momentum of the vehicle tended to maintain it along a straight line course until its speed would be reduced by a sufficient amount to allow the wheels to turn. In those instances, the vehicle would tend to slide sideways.

e. Driving on previously developed LRV tracks did not materially change the performance of the vehicle, although the crew commented that in some instances the vehicle speed tended to increase.

f. On the basis of crew debriefings and EVA photographic coverage, it appears that the LRV was operated on slopes ranging in slope angle between 0 degrees and 12 degrees. Because of its light weight and the excellent traction obtained by the LRV wire-mesh wheel on the lunar soil, the general performance of the vehicle on these slopes was reported to be very satisfactory. On the basis of wheel-soil interaction tests performed on lunar soil simulants prior to the mission, the maximum slope angle that could be negotiated by the LRV had been estimated to be 20 degrees. It appears that the slopes actually negotiated at the Apennine-Hadley region represented about 60 percent of the vehicle's maximum slope climbing capability.

g. Maneuvering the vehicle on slopes did not present any serious problems. It was reported that the vehicle could be controlled more easily on up-slope than down-slope. When the vehicle was traversing along slope contours, the resulting ride was somewhat uncomfortable and the wheels on the down-slope side tended to displace the soil laterally and to sink by a greater amount than the wheels on the up-slope side. It was also reported that the most preferable way to cross a crater was not to drive cross-slope, but: (1) to drive the vehicle down to the bottom of the crater along the gradient of the crater slope; (2) to drive it across the bottom of the crater; and (3) to drive it up-slope, again along the gradient of the slope.

h. Based on crew observations, it appears that no perceptible amount of soil was collected inside the wheel when the vehicle was in motion. This observation is in agreement with the behavior of the lunar soil simulant used in the USAE WES wheel-soil interaction tests within the range of wheel slip realized during the LRV operation on the lunar surface.

i. During the performance of the wheel-soil interaction task ("Grand Prix") at high vehicle accelerations, a "rooster tail" was developed by fine-grained material ejected from the wheels. The maximum height of the trajectory of the ejected material was 4.5 m (15 ft). Because of the presence of the fenders the material was being ejected forward from the uncovered sides of the wheels. As reported by the crew, ejected dust was below the level of vision.

j. During the "Grand Prix" exercise, the crew observed that some of the vehicle wheels were airborn in some instances, although the crewman driving the vehicle, had no sensation of this vehicle behavior.

k. The vehicle's response to braking was reported to be excellent. The wheels tended to completely lock and the vehicle came to a complete stop within one to three vehicle lengths.

1. As a result of the vehicle interaction with the lunar surface a thin layer of very fine-grained material tended to cover the surface of the vehicle components over a long period of time. The accumulated particles appeared to be evenly distributed over the vehicle surface. However, the material could be easily brushed off.

In summary, it appears that the LRV wheel-soil interaction at the Apennine-Hadley region is consistent with expectations based on premission terrestrial wheel-soil interaction studies on lunar soil simulants. Accordingly, the existing MSFC lunar soil model appears to be adequate for LRV performance evaluation purposes.

20.6 LOCOMOTION PERFORMANCE

The locomotion performance of the LRV was satisfactory and met all of the demands required by the Apollo 15 mission. However, as the mission profile was well within the expected capabilities of the LRV, the vehicle was never operated under performance-limiting conditions or under degraded operating modes. Consequently no direct quantitative information exists regarding its limiting mobility performance capabilities at the Apennine-Hadley region.

A postmission evaluation of the energy consumed by the LRV during EVA's 1, 2, and 3 was made using the MSFC power profile computer model. The results of these calculations are shown and compared with real-time LRV amp-hr integrator readouts in Figure 20-7.

On the basis of the information obtained relative to the roughness of the lunar surface traversed by the LRV, this analysis has been based on two surface roughness models: One corresponding to a Smooth Mare Low-Range PSD and the other to a perfectly smooth surface with the same regional slope distribution. These two limiting conditions were used because, on the basis of current information, the surface roughness coefficient K along the LRV traverses at the Apennine-Hadley region is estimated to be within the range of 0 to 17.5, corresponding to K values for "Perfectly Smooth Surface" and "Smooth Mare, Low-Range PSD" surface models. The premission estimates and postmission assessments of this coefficient are used as constants of proportionality to calculate power losses in the LRV dampers as a function of the square of the vehicle speed. These data are shown in Figure 20-8. By comparing the weighted average of the premission estimates on K with the current assessments, it can be seen that the power losses in the dampers may have been overestimated in premission power profile analyses by a factor of 5.2.

The MSFC LRV power profile computer program was also used to obtain estimates on the maximum steady state velocity attained by the LRV and corresponding wheel slip at full throttle as a function of slope angle. The results of these calculations are shown in Figures 20-9, 20-10 and 20-11. Inasmuch as the wheel slip calculations corresponding to a "Perfectly Smooth Surface" are almost identical to the ones obtained for

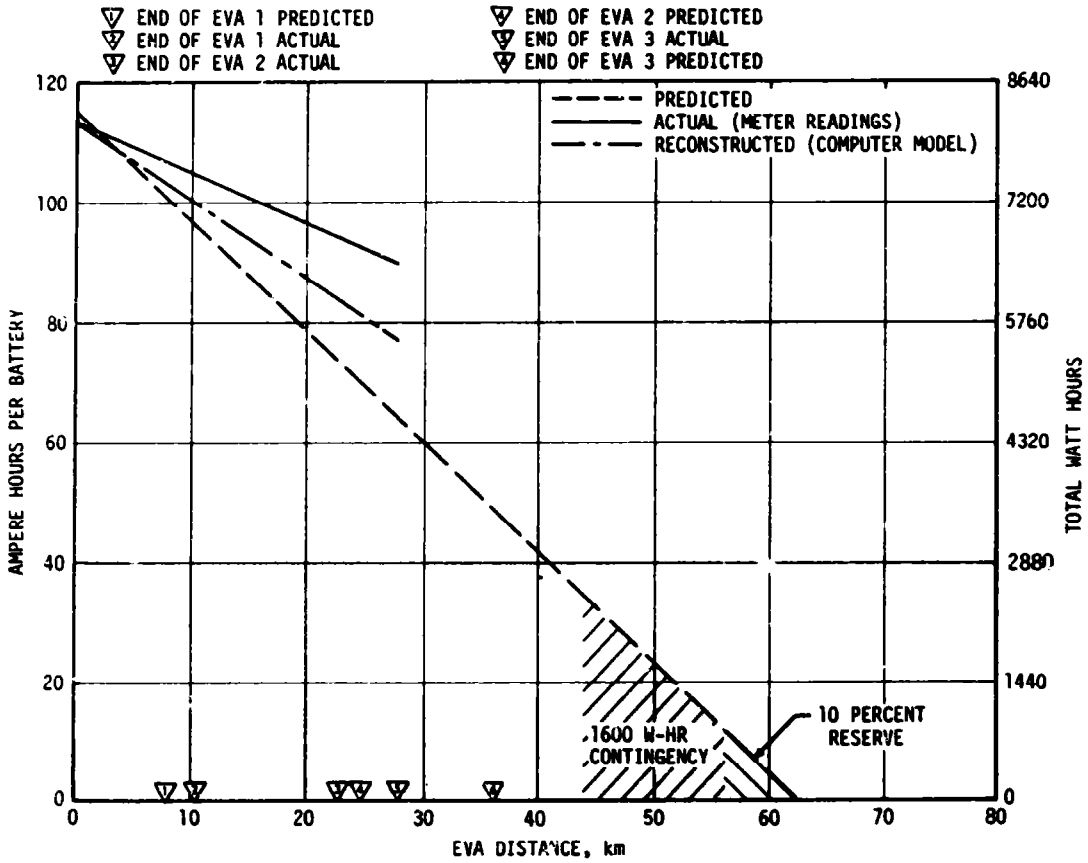

Figure 20-7. LRV Energy Consumed

the "Smooth Mare Low-Range PSD" surface, they are not shown on a separate plot. The computer estimates of both the velocity and the wheel-slip appear to be consistent with crew observations.

Finally, on the basis of the average values from the LRV amp-hr integrator readouts at the beginning and the end of each EVA, the reconstructed vehicle traverse routes and the reconstructed mission timeline estimates on the LRV range at the Apennine-Hadley region were made and are shown in Table 20-2.

On the basis of this analysis, the following conclusions can be made:

(1) Assuming that the LRV amp-hr integrator readouts are correct, the agreement between the estimated and "actual" performance of the LRV is very satisfactory, even by terrestrial vehicle mobility performance standards.

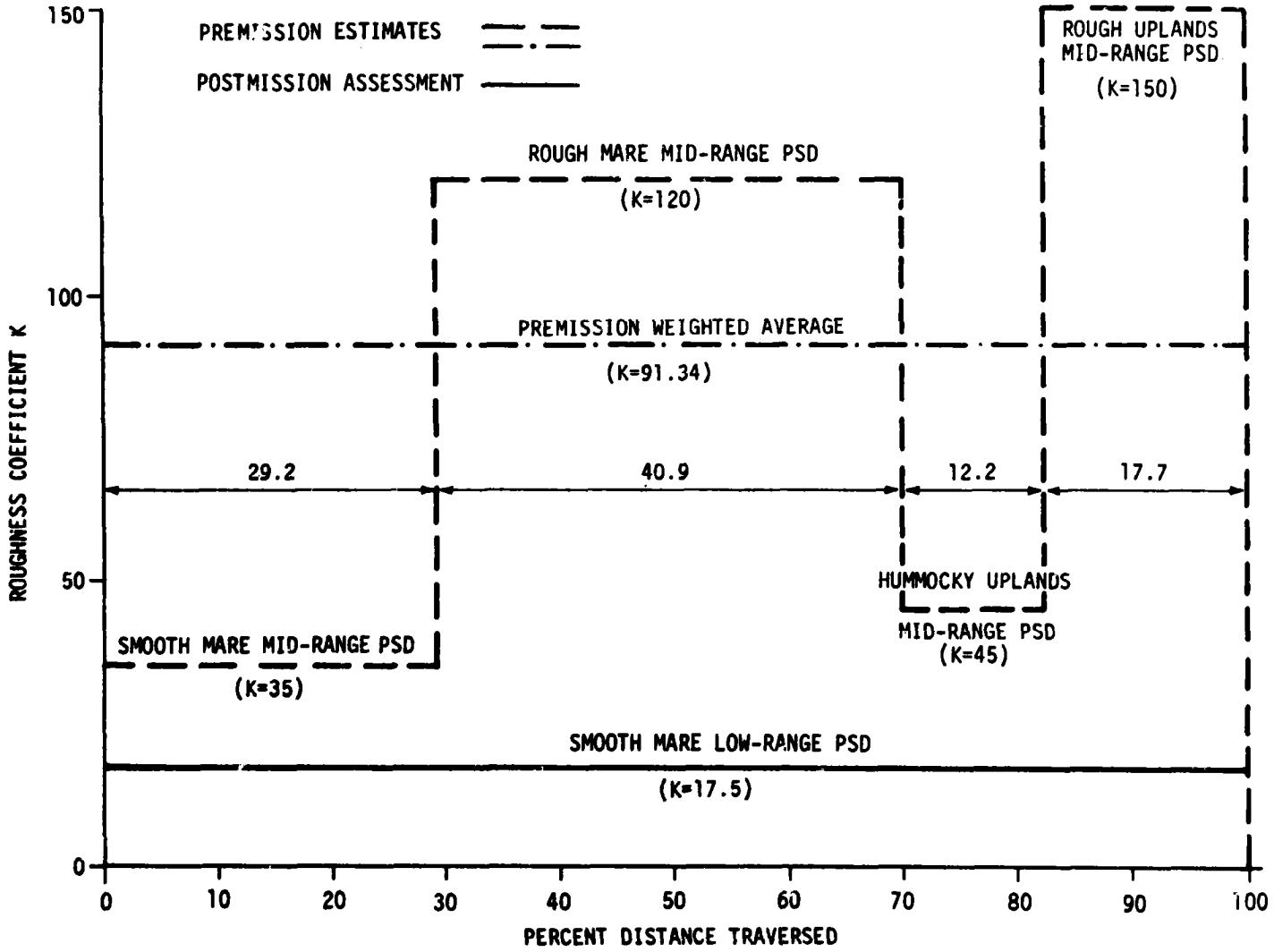

Figure 20-8. Lunar Surface Roughness

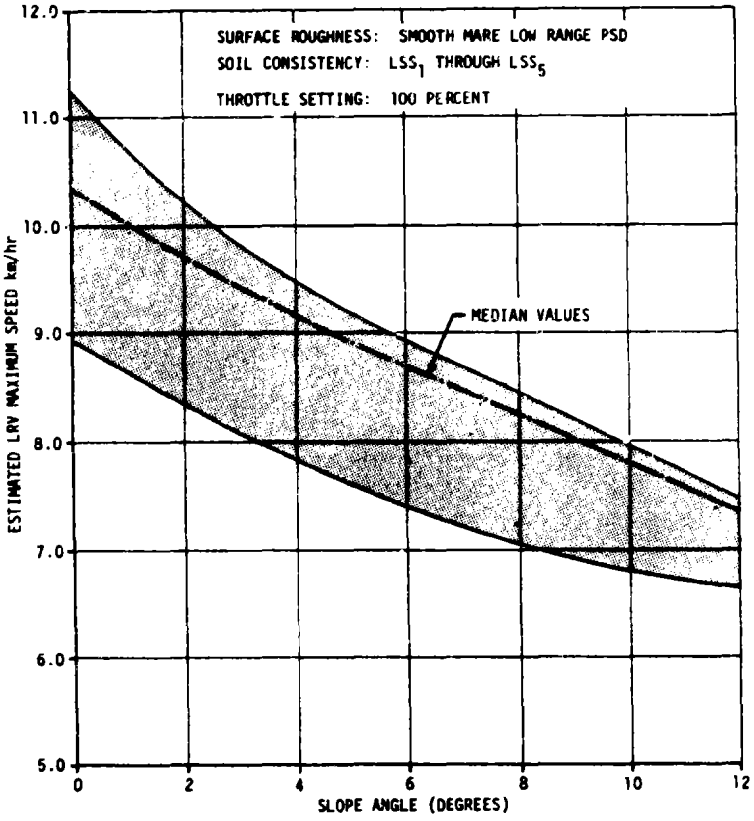

Figure 20-9. MSFC Computer Model Estimate of Maximum LRV Speed on Smooth Mare Low Range PSD Surface

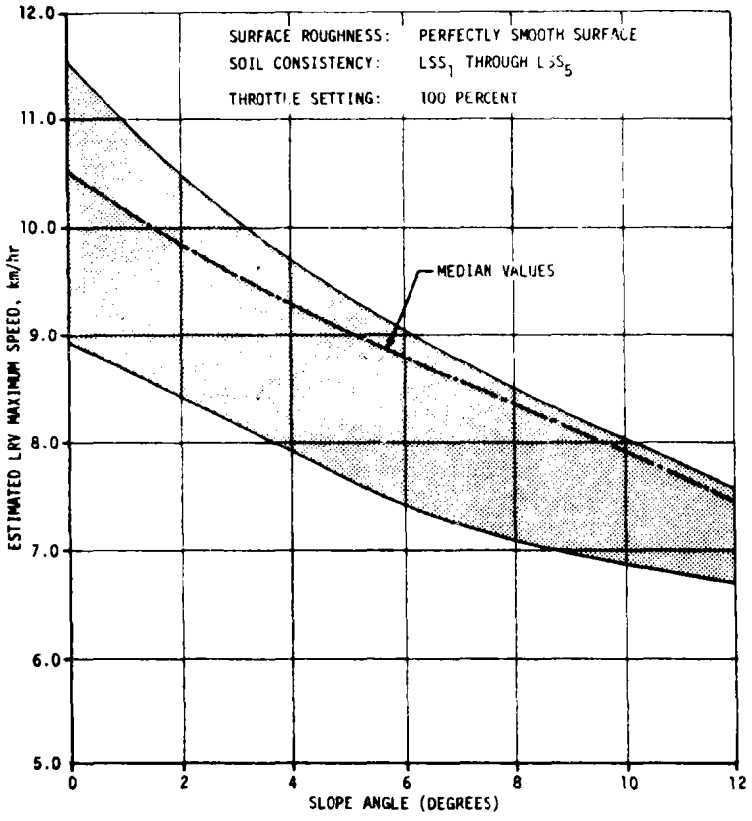

Figure 20-10. MSFC Computer Model Estimate of Maximum LRV Speed on Perfectly Smooth Surface

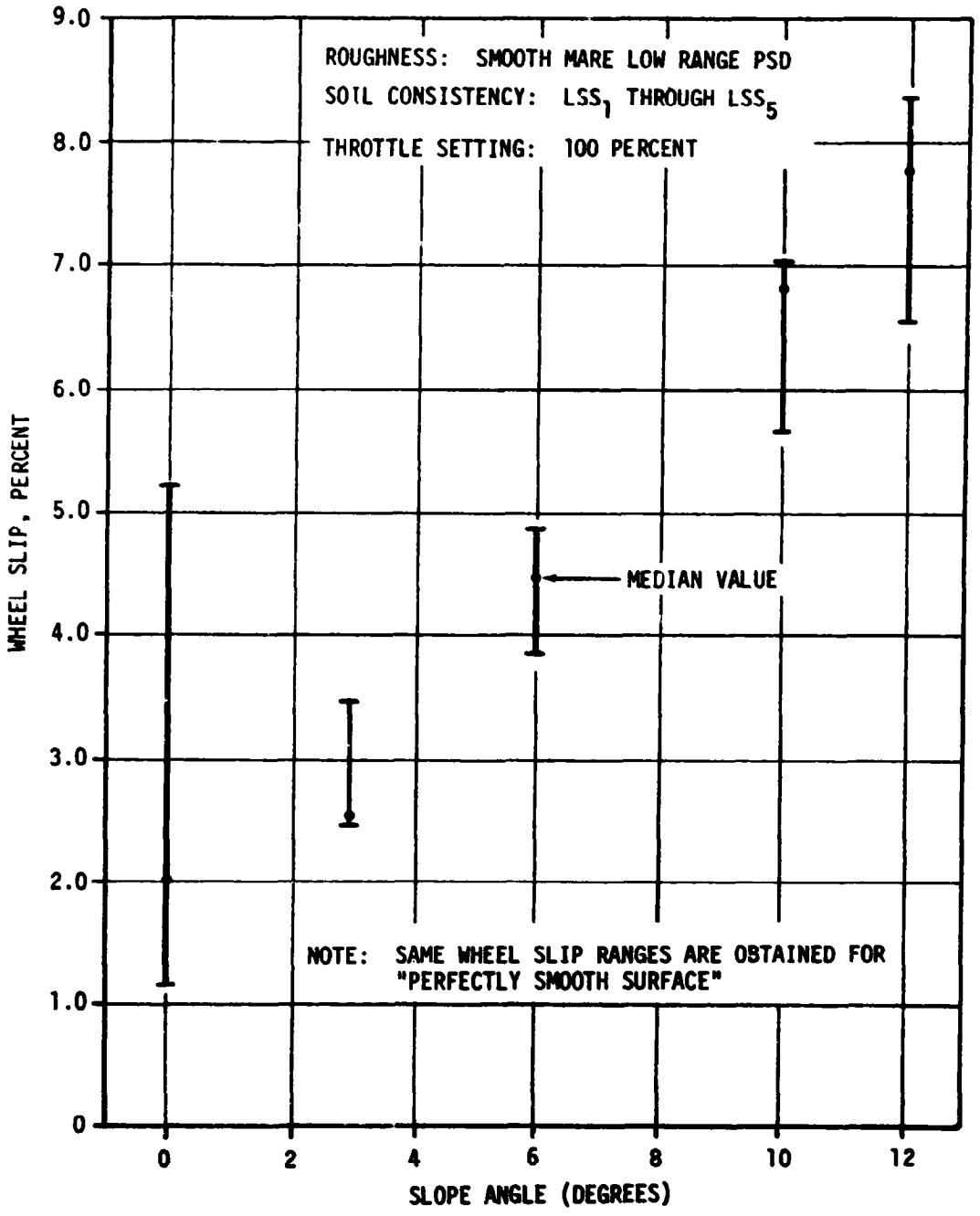

Figure 20-11. MSFC Computer Program Estimates on LRV Wheel Slip Versus Slope Angle Under Full Throttle (Maximum Velocity) Conditions

Table 20-2. Reconstructed LRV Total Range

	8712 WATT-HR BATTERY -10 PERCENT DRAWDOWN	8712 WATT-HR BATTERY -10 PERCENT DRAWDOWN -1600 WATT-HR CONTINGENCY
MSFC LRV Reconstructed Power Profile, km	$82.8^{+7.7}_{-11.8}$	$65.9^{+5.7}_{-9.4}$
LRV Amp-Hr Integrator Readouts (Based on Median Values at the Beginning and End of Each EVA), km	123.0	97.9
Percent Difference Between Computer Estimates and Amp-Hr Readouts	$32.7^{+9.6}_{-6.3}$	$32.7^{+5.9}_{-10.6}$
LRV Amp-Hr Integrator Readouts (Based on Median Values at the Beginning and End of EVA's 1, 2, and 3* (See Figure 20-7), km	117.3	93.4
Percent Difference Between Computer Estimates and Amp-Hr Readouts	$29.4^{+6.6}_{-10.1}$	$29.4^{+6.1}_{-10.1}$
*Reading at end of EVA-3 taken after meter tapped.		

(2) Appreciable deviation between premission LRV power consumption estimates and actual LRV data on the Apennine-Hadley region can be attributed mainly to conservative estimates of the slope distribution and roughness characteristics of the lunar surface.

(3) The lunar soil model used in LRV performance evaluation is adequate and consistent with lunar soil mechanics and wheel-soil interaction data obtained from the Apollo 15 mission.

(4) Deviations between the current MSFC LRV power profile computer estimates and "actual" LRV performance data can be attributed mainly to the following sources:

(a) Inaccuracies in the LRV amp-hr integrator readouts.

(b) Errors in postmission estimates of the regional slope distribution at the Apennine-Hadley region which were made on the basis of a 20-m resolution topographic map.

(c) Inaccuracies in estimating power losses due to navigation, steering, etc., which according to the current estimates were about 30 percent of the estimated traction-drive losses.

(d) Errors in estimating actual distances traversed by the LRV.

(e) Variable soil conditions at the Apennine-Hadley region. region.

20.7 MECHANICAL SYSTEMS

20.7.1 Harmonic Drive

The harmonic drive performed satisfactorily; no excessive power consumption or temperatures were noted nor was any mechanical malfunction apparent. All wheel drives were operational throughout the mission.

20.7.2 Wheels and Suspension

The wheels and suspension systems performed as expected, verifying adequacy of the design.

20.7.3 Brakes

The crew commented that the brakes appeared to perform as they had expected although they took longer to stop than they had experienced with the 1 g trainer as anticipated. The crew also commented that they learned to brake down to 5 km/hr or less when avoiding craters or other obstacles to prevent sliding. During the "Grand Prix" exercise the vehicle was brought to a stop from 10 km/hr in about three vehicle lengths or less according to the crew. Evidence indicates that on a rolling surface of the type at Hadley base, the brake system performed as expected.

20.7.4 Suspension and Stability

The crew reported that the suspension system performed well during lunar traverse. The suspension system produced a low frequency "rocking" type ride, which was predominantly a pitching motion. Very little roll was noticed. The suspension reportedly did "bottom out" a few times. One specific instance was when the LRV encountered a 30 centimeter high obstacle at a velocity of 10 km/hr. This was expected for obstacles of this size.

The LRV was sensitive in the area of controllability. When steering with the rear wheels only, as was the case throughout EVA-1, the front wheels tended to dig in while the rear end drifted out when making a sharp turn at high speeds. The LRV did a 180 degree spin-out once under this steering mode. With the front wheel steering operable and the rear

steering electrically disconnected, as was the case for a short time during EVA-2, the rear wheels apparently drifted off center causing an undesirable crabbing motion. Subsequently, the crew chose to return to the Double Ackermann steering mode and utilized it for the remainder of EVA-2 and all of EVA-3. Double Ackermann steering proved to be very sensitive. After a little driving experience, however, the crewman driving reported that this steering mode was good although he had to pay close attention to driving.

The sliding breakpoint was estimated as being between 5 km/hr (3.125 mph) and 7 km/hr (4.375 mph). The LRV tended to slide straight ahead instead of turning when given a steering command at high speeds. With driving experience, the crew decided that the best driving practice was to brake before entering a turn.

The LRV was exceedingly stable and had no tendency to roll even when in a spin-out condition. The wheels did become airborne occasionally, but did so independent of one another and did not cause a controllability problem. The crew reported that during the "Grand Prix" all four wheels were off the ground for a short period of time. The driver, however, did not sense that the wheels were off at this time. The chassis stayed relatively horizontal while driving. Driving cross slope, although stable, proved to be an uncomfortable driving condition.

20.7.5 Hand Controller

The hand controller performed satisfactorily with no apparent problems. The manner of steering was a "bang-bang" action. The steering soft stops were of no consequence. The usual mode for applying throttle was to apply full throttle and then back off to the desired speed. The reverse mode performed satisfactorily.

20.7.6 Loads

Instrumentation was not available on the LRV to ascertain loads induced on the vehicle. In addition, the 16 mm camera failure during the "Grand Prix" nullifies the only other source of data. However, no apparent load problems were encountered since the crew reported no problems in this area.

20.8 ELECTRICAL SYSTEMS

The LRV electrical systems performed adequately with no major problems.

20.8.1 Batteries

The batteries proved to be more than adequate for this mission based on amp-hr meter readings. Configuration via current and speed indications was inconclusive due to lack of crew readouts. Amp-hour meters indicated a total usage of 52 amp-hr out of a nominal capacity of 230 amp-hr for the two batteries, leaving a residual of 178 amp-hr.

20.8.2 Traction Drive System

The traction drive system appears to have worked nominally. There were no indications of any off nominal conditions and all four units performed as expected. The crew indicated that the temperature of the units all remained below 200°F which is the lowest indication of the meter. During sorties the current readings were approximately 10 amps/battery for speeds ranging from 8 km/hr to 12 km/hr. The crew indicated at the debriefing that the throttle position was about 90 percent of full throttle which was consistent with the other data.

20.8.3 Distribution System

The electrical distribution system provided power to all functions as required with the exception of the battery No. 2 volt-ammeter which failed to function during the mission.

20.8.4 Steering

After LRV deployment, the forward steering did not respond to crew commands. Routine procedural checks were made with negative results and EVA-1 was initiated and completed using only the rear steering. The crew reported no difficulty in driving the LRV and experienced good mobility rates. Prior to initiating the LRV traverse during EVA-2, the crew performed recommended corrective action operations with the forward steering and reported that the forward steering was functioning. No further problem was encountered with the forward steering throughout EVA-2 or EVA-3.

The following information was taken from the communication link during LRV operation:

a. Steering circuit breaker depressed and power switch placed in Bus A. No steering response was noted.

b. Traction drive units were found to be operating, indicating that the ±15 volt power supply was operational.

c. Steering switch was changed to Bus C position and there was still no steering response.

d. The crew attempted to physically turn wheels and were unable to do so. (They assumed that they were to try to correct a binding condition and so applied an impulse force rather than a more desirable steady force to overcome the reverse 256:1 gear ratio.)

e. Steering drive was applied with all other power off and the ammeter observed, but no movement was detected.

f. The crew at this point turned steering power off for the front wheels and began EVA-1.

g. Wheels tracked well during entire EVA-1.

h. At the beginning of EVA-2, steering power was turned on and the front steering began to work.

i. After EVA-2 had begun, the crew found steering a little sensitive to the Double Ackerman configuration and turned the rear steering power off.

j. The crew indicated that the rear wheels were wandering and so returned to Double Ackerman. (The length of time that rear power was off was very short; approximately 1 or 2 minutes.)

From the above data the following possibilities may explain the failure:

a. Mechanically frozen motor or gear.

b. Open motor circuit:

   (1) Brush contact lost on either of the two brushes.

   (2) Front steering circuit breaker open.

   (3) Pole side of steering power switch open.

c. Wiper command potentiometer open due to lubricant or other material (something that might be removed either from exercise of the hand controller, vibration or heat).

The first possibility seems to fit the information that the steering tended to track well and that the crewmen were unable to physically move the wheels. However, tests on the quality test vehicle revealed that the meter deflects slightly when the hand control is energized, so this should have been detected by the crew. The movement is small enough, however, to be missed if not observed carefully, and with the suit on could have been missed rather readily.

The second possibility would satisfy the fact that current was not observed, but fails to explain why the wheels did not wander. Other available data give evidence that the wheels may or may not track reasonably well depending upon the operating conditions.

The third possibility would explain the fact that the current deflection was absent and would perhaps explain the inability of the crew to turn the wheels. However, it fails to explain the lack of wander when power was off. In conclusion, none of the possibilities are ruled out but at the same time none explain the situation well enough to reach a definite solution.

20.8.5 Amp-Hour Integrator

Just after deployment, the values read from the amp-hour meters showed an offset from the expected full scale reset values. Later sufficient readings were recorded that indicated proper operations, but it expected that a number of small discrepancies in the read values were result of the crew members reading the meters from different angles.

20.9 CONTROL AND DISPLAY CONSOLE

The Control and Display Console (C&DC) proved adequate in all areas with the exception of some difficulty in reading meters. Amp-hour and battery current meters were especially difficult to read due to the large scale divisions. There was an offset from the expected full scale readings on the amp-hour meters. The battery No. 2 volt-ammeter did not register during the entire mission.

20.10 NAVIGATION SYSTEM

Performance of the navigation system was satisfactory. In addition to supplying navigation support for the LRV, the system, by using range and bearing readings from known landmarks, determined the location of the LM on the moon.

Table 20-3 summarizes the navigation performance.

20.11 CREW STATION

The seat belt design was the principal problem involving the crew station. The velcro used to tie down the loose end of the seat belt prevented the seat belt from being lengthened. The crew commented that the seat belt would have been usable had they been able to lengthen it, but it would still have required too much time and effort. A modified seat belt for LRV No. 2 and No. 3 is considered necessary.

The velcro tabs on the upright portion of the seat were not used. The crew feels that had this velcro been used, their movement would have been overly restrained and the driver would have had difficulty positioning himself relative to the hand controller.

Ingress was accomplished by sitting on the edge of the seat with crewman's back to the LRV, then swinging the legs around against the foot rest, then pressing back on the foot rest to erect the body. In doing this the Portable Life Support System (PLSS) would slightly hang on the PLSS support on back of the seat. The crew stated that possibly a better ingress procedure should be used.

The outboard toeholds were not used as they were a hindrance to ingress and were removed and stowed. Egress was accomplished without difficulty.

Table 20-3. LRV Navigation System Performance

	TRAVERSE I	TRAVERSE II	TRAVERSE III
Odometer Distance	10.3 km	12.5 km	5.1 km
Map Distance	9.0 km	11.7 km	4.5 km
Ride Time	approx. 62 min	approx. 83 min	approx. 35 min
Park Time	approx. 74 min	approx. 154 min	approx. 82 min
Total Time of Traverse	approx. 136 min	approx. 237 min	approx. 117 min
Average Velocity	10.0 km/hr	9.0 km/hr	8.7 km/hr
Mobility Rate	8.7 km/hr	8.46 km/hr	7.54 km/hr
Number of Navigation Checks	1	1	0
Number of Navigation Updates	0	1	0
Navigation Closure Error	less than 200 m	less than 200 m	less than 200 m
Maximum Position Error	less than 300 m	less than 350 m	less than 250 m
GYRO Drift Rate	little or none	little or none	little or none
GYRO Misalignment	small	small	small
Percent Wander	14	7	16

Definitions

Map Distance - Map distance traveled, neglecting deviations around small craters.

Ride Time - The time spent riding, including minor stops, from departure to arrival at the LM.

Average Velocity - The odometer reading at the end of the traverse divided by the ride time.

Mobility Rate - The map distance divided by the ride time.

Navigation Closure Error - The position error in the navigation system at the end of the traverse.

Percent Wander - $\frac{\text{speed - mobility rate}}{\text{mobility rate}} \times 100$ percent

There were no apparent visibility problems caused by the LRV, although the crew commented that 1-meter diameter subdued craters were not visible more than 3 meters from the vehicle.

20.12 THERMAL

20.12.1 Summary

The LRV-1 thermal control system performed satisfactorily during the Apollo 15 mission. Although some deviations from preflight predictions occurred during the LRV-1 mission, all components were maintained within design temperature limits during the transportation, extravehicular, and cooldown periods.

Significant dust degradation of the space radiators resulted in a lack of cooldown during the post EVA-2 cooldown period. However, no restriction on LRV operation during EVA-3 resulted. Minimal design and/or crew procedure changes will be necessary to assure clean radiators for cooldown periods on subsequent missions.

20.12.2 Transportation Phase

All components were maintained within storage temperature limits during the transportation phase (translunar coast, lunar orbit, LM landed attitude).

Prior to EVA-1, the temperature readings were 298°K (78°F) and 300°K (80°F) for battery No. 1 and battery No. 2, respectively. These temperature deviations from the predicted value of 283°K (50°F) did not degrade EVA-1 capabilities. Possible explanations being investigated include a different attitude timeline and high temperature bias on meters.

20.12.3 Extravehicular Activity Periods

All components remained within operational temperature limits throughout the three lunar surface EVA's. As predicted, motor temperatures were off-scale low throughout the EVA's. Comparisons between predicted and actual battery temperatures during the three EVA's are presented in Figures 20-12 through 20-14. The temperatures were computed based on preliminary EVA timelines.

Major parameters affecting thermal performance of the LRV batteries are: soil model, damping power, vehicle orientation, driving time, and distance traversed. Correlation of analytical and actual battery temperatures will be improved with more complete definition of these influencing parameters.

Predicted and measured temperatures for the batteries during cooldown 1 are presented in Figure 20-15. Cooldown 1 is defined as the period between the end of EVA-1 and beginning of EVA-2. The predicted

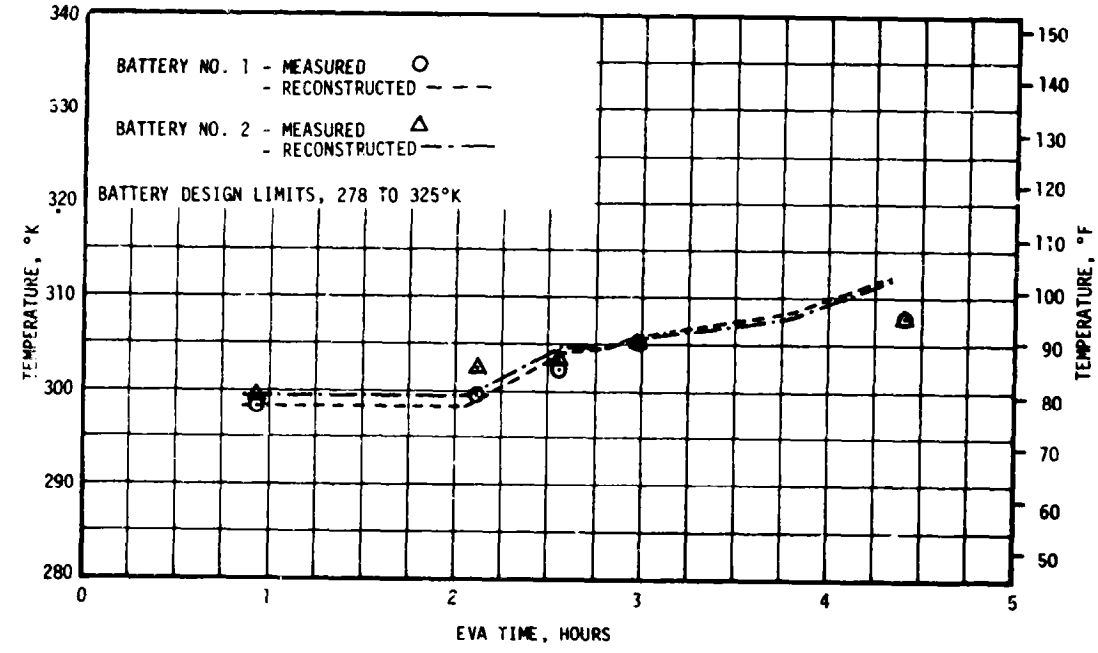

Figure 20-12. LRV Battery Temperatures for EVA-1

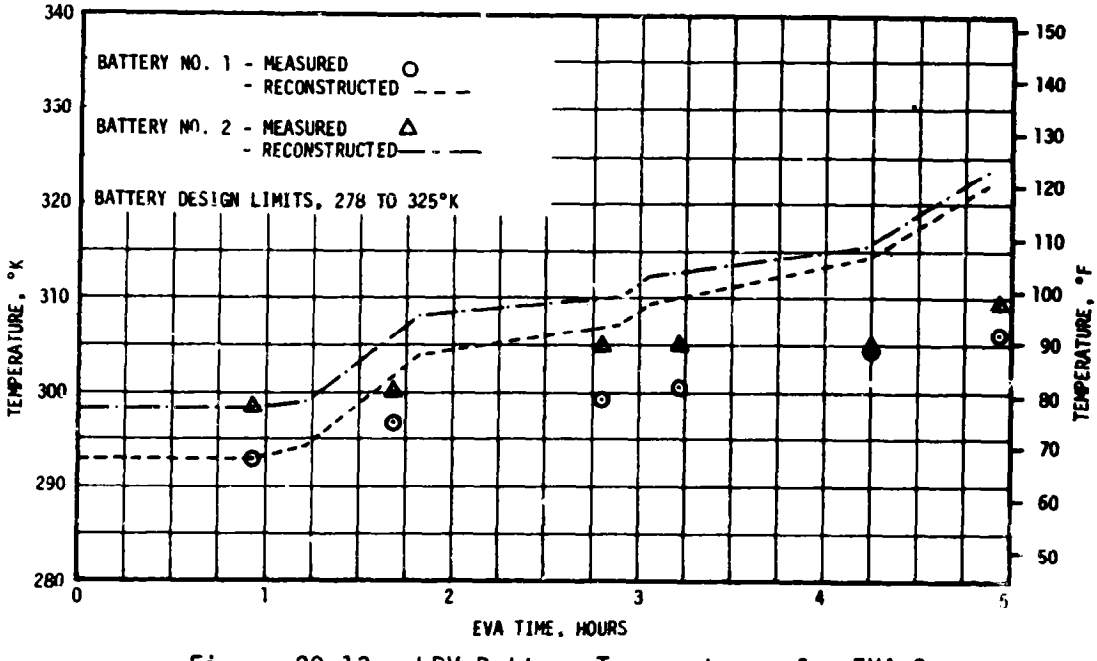

Figure 20-13. LRV Battery Temperatures for EVA-2

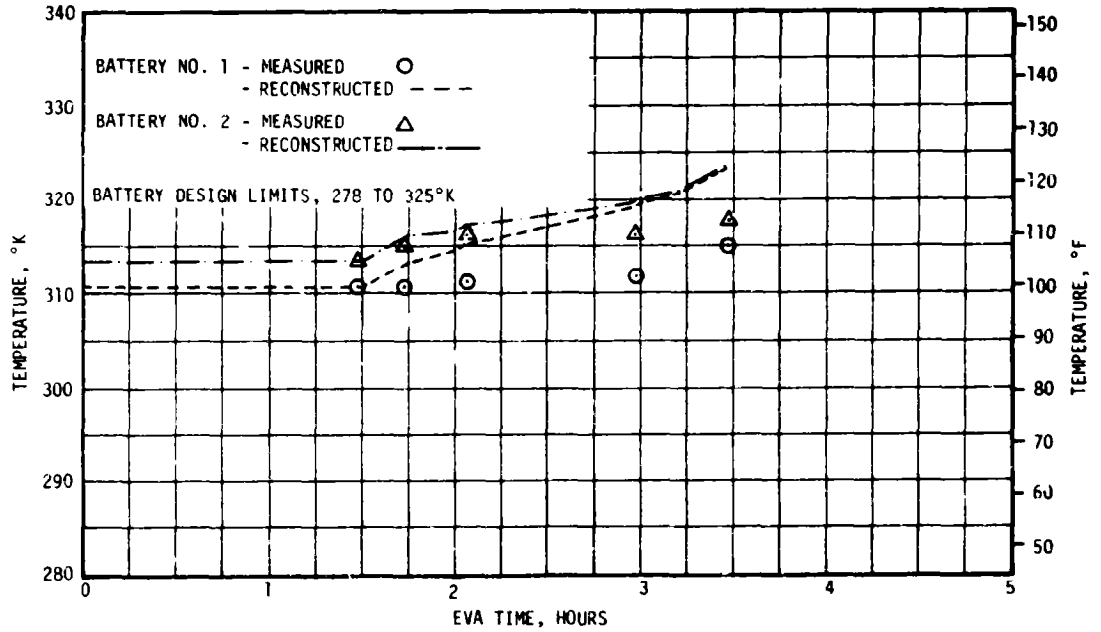

Figure 20-14. LRV Battery Temperatures for EVA-3

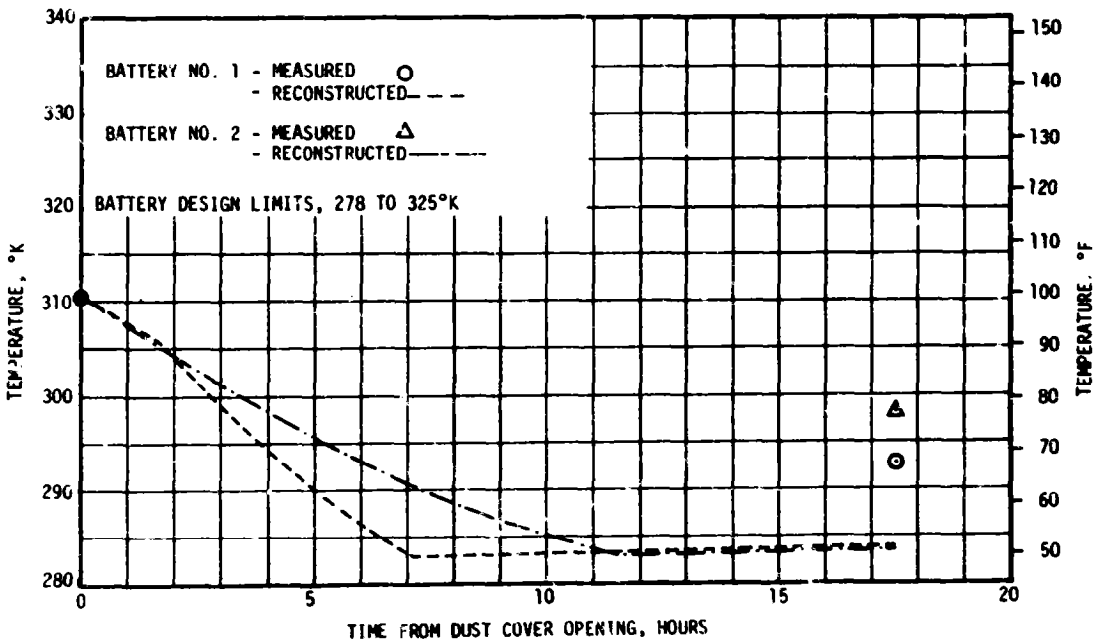

Figure 20-15. LRV Battery Temperatures During Cooldown 1

temperatures were computed using a radiator solar absorptance (α_s) of 0.07 (clean surface) and with the right side of the vehicle facing the solar vector as specified in the ICD 13M07391. The LRV was parked headed North, resulting in a slight increased radiator solar heat load and decreased cooldown rate. Dust accumulation on the radiator was not indicated during cooldown 1.

The battery dust covers should close automatically at 283°K (50°F). Battery No. 1 cover closed during cooldown 1. However, the temperature meter indicated 293°K (68°F). This indicates that either the bimetallic actuator spring malfunctioned or the temperature gage was reading high (see transportation phase).

Cooldown 2 - Predicted and measured battery temperatures during cooldown 2 are shown in Figure 20-16. The radiators' heat load was higher than predicted due to dust coverage and the northerly parking position.

Radiator temperatures with dust coverages of 5 and 15 percent in combination with the northerly parking attitude were determined. The 15 percent (α_s = 0.45) indicates temperatures slightly above the measured values.

Minor changes in the design, preflight checkout, and operational procedures are being considered to preclude dust accumulation on future missions.

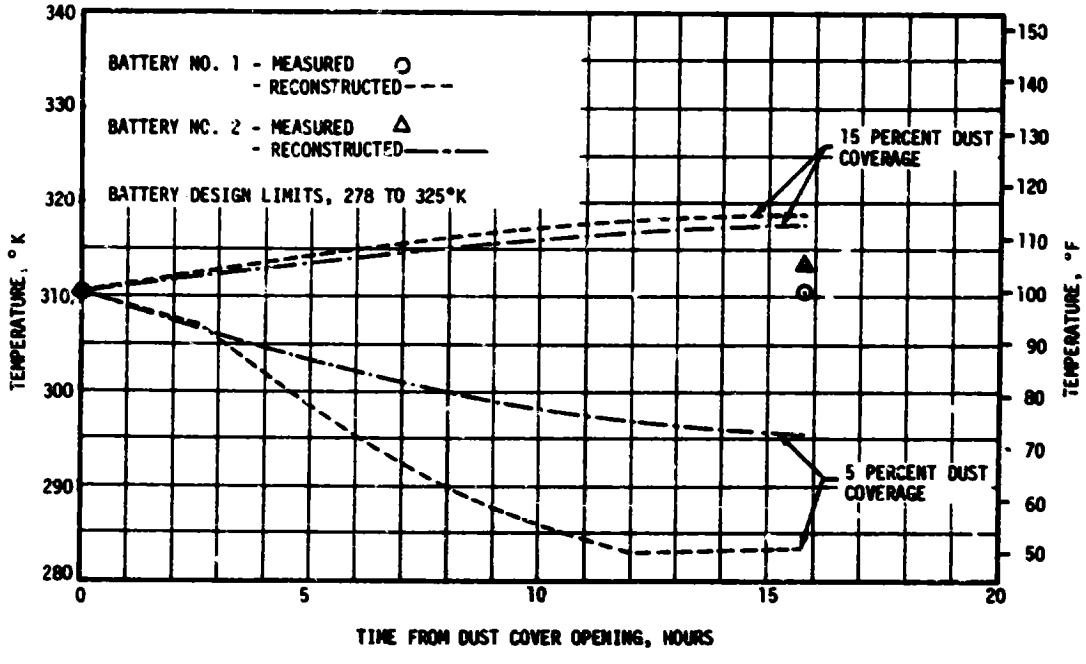

Figure 20-16. LRV Battery Temperatures During Cooldown 2

20.13 STRUCTURES

No structural damage to the LRV was noticed by the crew, although a close inspection was not performed. A preliminary review of LRV photos reveals no wheel wire mesh breakage. These photos, however, do show that the forward portion of the left front fender was missing after EVA-1. Cause of this is unknown.

20.14 LUNAR ROVING VEHICLE DESCRIPTION

The LRV was the first manned vehicle to traverse the lunar surface. The LRV was stowed in the LM stowage bay and deployed on the lunar surface after landing. This section contains general information pertaining to the LRV operational capabilities and subsystem descriptions.

20.14.1 LRV Overall Description

The LRV system on the lunar surface consists of the LRV, the structure for securing the LRV to the LM stowage bay and the mechanism for deploying the LRV from the LM onto the lunar surface.

The LRV (Figure 20-17) is a four-wheeled, self-propelled, manually controlled vehicle to be used for transporting crewmen and equipment on the lunar surface. The vehicle has accommodations for two crewmen and the stowed auxiliary equipment designed for the particular mission.

The LRV system is comprised of the Mobility Subsystem, Electrical Power Subsystem, Control and Display Console (C&DC), Navigation Subsystem, Crew Station, Thermal Control Subsystem and Space Support Equipment. Each subsystem is described in subsequent paragraphs.

20.14.2 Subsystem Description

20.14.2.1 Mobility Subsystem

The mobility subsystem consists of the chassis and equipment and controls necessary to propel, suspend, brake and steer the LRV. Each wheel includes an open wire mesh tire with chevron tread covering 50 percent of the surface contact area. The tire inner frame provides a stiff load path to accommodate high impact loads. Each wheel has a decoupling mechanism and can be decoupled from the traction drive by operating the two decoupling mechanisms which allow the wheel to "free-wheel" about a bearing independent of the drive train. This decoupling mechanism can also be used to re-engage the wheel with the traction drive. Decoupling disables the brake on the affected wheel. When the LRV is folded for stowage in the LM the front and rear wheels are compressed together. Upon deployment of the vehicle and unfolding of the wheels the wheel bulge retention wire is released and the wheel assumes its normal configuration.

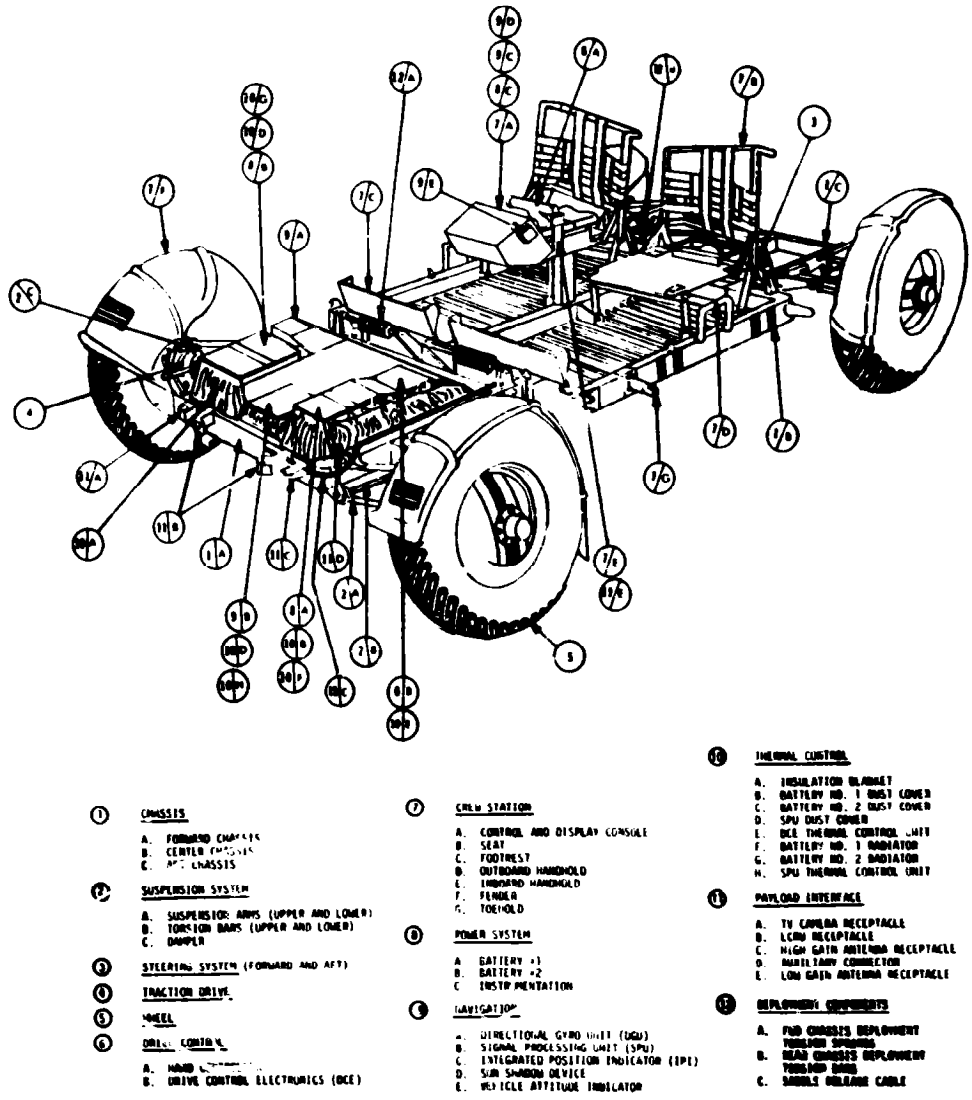

Figure 20-17. Deployed LRV Without Stowed Payload

Each LRV wheel is provided with a separate traction drive, consisting of a harmonic drive gear reduction unit, drive motor and brake assembly. Each traction drive also contains an odometer pickup which transmits a pulse to the navigation subsystem at the rate of nine pulses per wheel revolution. The four harmonic drive gear reduction units transmit torque to each wheel. Input torque to the four harmonic drives is supplied by the four electric drive motors. The harmonic drive reduces the motor speed by a ratio of 80:1.

The drive motors are direct current series, brush-type motors which operate from a nominal input voltage of 36 vdc. Speed control for the motors is furnished by pulse width modulation from the drive controller electronic

package. Each motor is instrumented for thermal monitoring. An analog temperature measurement from a thermistor at the stator field is displayed on the C&DC. In addition, each motor contains a thermal switch which closes on increasing temperature at 400°F and provides an input signal to the caution and warning system to actuate the warning flag.

Each traction drive is equipped with a mechanical brake actuated by a cable connected to a linkage in the hand controller. Braking is accomplished by moving the hand controller rearward. This operation de-energizes the drive motor and forces brake shoes against a brake drum which stops the rotation of the wheel hub. Equal braking force for the left and right wheels is accomplished by routing the cables through an equalizer device. The forward and rear brakes are actuated by separate cables.

The chassis is suspended from each wheel by two pairs of suspension arms connected between the LRV chassis and each traction drive. Loads are transmitted from the suspension arms to the chassis through torsion bars. Wheel vertical travel and rate of travel is limited by a linear damper connected between the chassis and each traction drive. The deflection of the suspension system and wheels combine to allow 14 inches of chassis ground clearance when the LRV is fully loaded and 17 inches when unloaded.

Forward movement of the hand controller about the T-handle throttle pivot axis proportionately increases forward speed. A constant torque of about 6 in.-lb is required to move the hand controller beyond the limit of the dead band. The 9-degree position corresponds to a pulse duty cycle of approximately 50 percent, at each drive motor. The maximum power setting is achieved by pivoting the hand controller to the hard stop (maximum) position at approximately 14 degrees. To decelerate, the hand controller is pivoted toward neutral. To place the vehicle in neutral, the hand controller is pivoted to the zero ±1/2 degree position. To operate the vehicle in reverse, the reverse inhibit switch is placed in the up position and the hand controller pivoted rearward about the throttle pivot point. The vehicle must be brought to a full stop before a direction change is commanded. This is required to prevent the possibility of some wheels being in forward and some in reverse upon reapplication of power. The hand controller will remain in the existing forward or reverse speed position in the crewmen "hands off" condition. Pivoting the hand controller left or right about the roll pivot point proportionally changes the wheel steering angle. The steering control, like the throttle control, has a 1/2 degree neutral dead band on either side of zero. A torque of 7 in.-lb is required to roll the hand controller beyond the neutral position to begin steering angle change. The hand controller is spring loaded to return to the neutral steering position when released. If the wheels are not aligned with the LRV centerline, they will automatically return to the aligned position when the steering system is turned on.

Braking is initiated with the LRV in either forward or reverse by pivoting the hand controller rearward about the brake pivot point. Forward and reverse power is disabled when the brake is displaced 15 degrees. A 3-inch

rearward displacement of the hand controller engages and locks the parking brake. To disengage the parking brake, the hand controller is placed in the steer left position. The Drive Control Electronics (DCE) accepts forward and reverse speed control signals from the hand controller and transmits them to the drive motors in a format which allows drive motor speed control. In addition, the DCE accepts odometer signals from the traction drives and processes the signals for speedometer readout and navigation system usage.

20.14.2.2 Electrical Power Subsystem

The electrical power subsystem consists of two batteries, distribution wiring, connectors, switches, circuit breakers and meters for controlling and monitoring electrical power.

The two batteries are of silver zinc construction and have a nominal voltage of 36 +5/-3 vdc and each has a capacity of 121 ampere hours. Both batteries are normally used simultaneously on an approximate equal load basis during LRV operation by selection of various load-to-bus combinations through circuit breakers and switch settings on the control and display console.

The batteries are located on the forward chassis enclosed by the thermal blanket and dust covers. Battery No. 1 (on the left side) is connected thermally to the navigation Signal Processing Unit (SPU), and serves as a partial heat sink for the SPU. Battery No. 2 (on the right side) is thermally tied to the navigation Directional Gyro Unit (DGU) and serves as a heat sink for the DGU.

Each battery is protected from excessive internal pressure by a pressure relief valve that is set to open at 3.1 to 7 psi differential pressure. The relief valve closes when the differential pressure is below the valve's relief pressure. Each battery is capable of carrying the entire LRV electrical load, and the circuitry is designed such that in the event one battery fails, the entire electrical load can be switched to the remaining battery.

During normal LRV operation, the navigation system power remains on during the entire sortie. To conserve power for increased range, all mobility elements (i.e., traction drives, steering motors, electronic controller, and power supplies) are turned off if a stop is to exceed 5 minutes duration.

The normally open temperature switches in the batteries and drive motors close on increasing temperatures. When either battery reaches 125°F or any drive motor reaches 400°F, the temperature switch closes, energizing the "OR" logic element and the driver. The driver then sends a 10-millisecond 36 volt pulse to the coil of the electromagnet which releases the magnetic hold on the indicator at the top of the console and a spring

loaded flag flips up. The crewman can reset the flag by pushing it down even though the cause has not been eliminated. The flag will not flip up again unless an overtemperature occurs on another battery or traction drive or the initial overtemperature subsides and then recurs. The particular high temperature item can be selected for continuous monitoring on the control and display console analog meters.

20.14.2.3 Control and Display Console

The C&DC (Figure 20-18) is separated into two main functional areas: Navigation on the upper area of the panel and monitoring and controls on

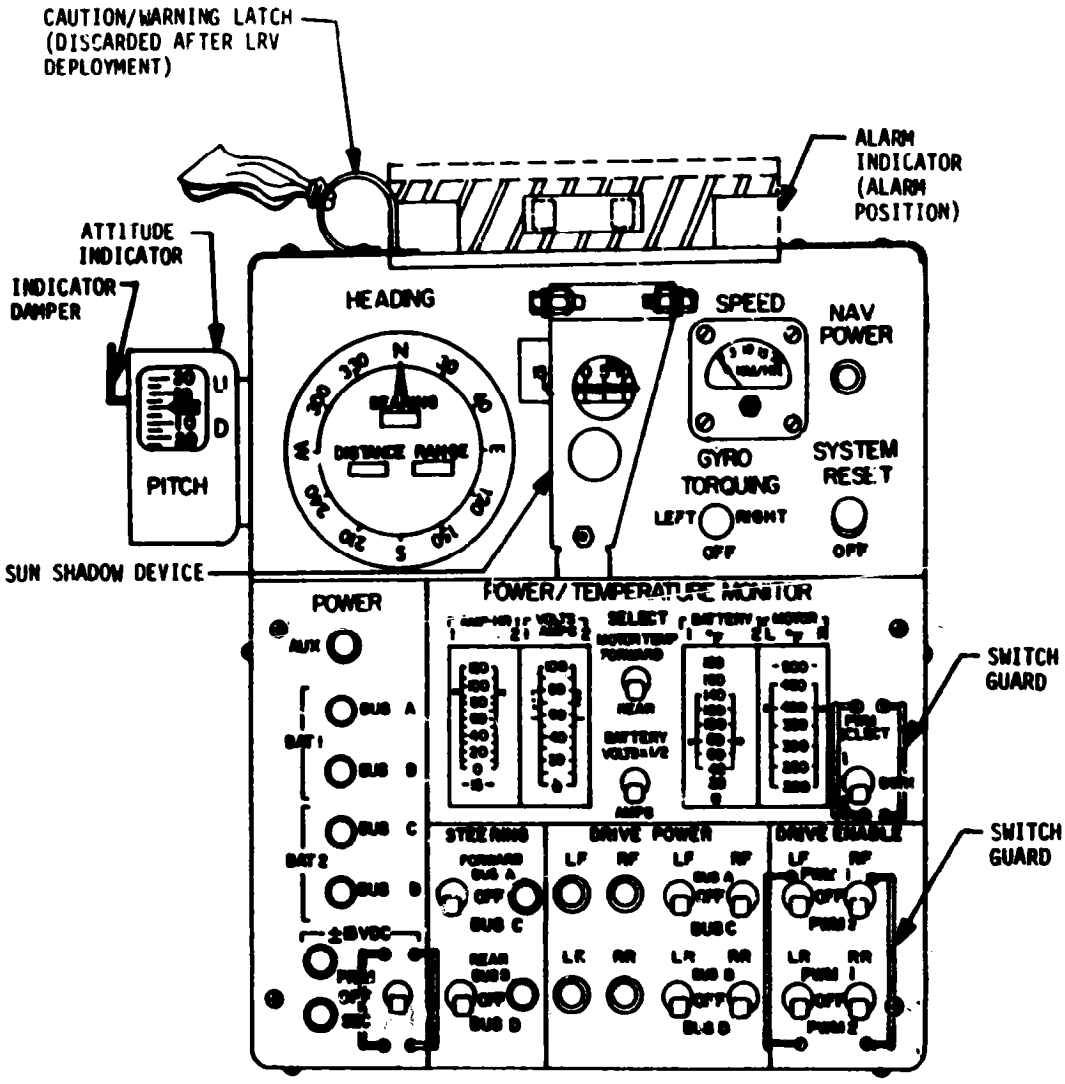

Figure 20-18. Control and Display Console

the lower area of the panel. The C&DC legends are activated with radioactive Promethium which provides visibility of displays under lunar shadow conditions.

The attitude indicator provides indications of LRV pitch and roll. It indicates PITC upslope (U) or downslope (D) within a range of +25 to -25 degrees in 5-degree increments and indicates ROLL within a range of 25 degrees left to 25 degrees right in 1-degree increments. The pitch and roll readings are transmitted to Mission Control Center (MCC) for navigation update computation. The heading indicator displays the LRV heading with respect to lunar north. The initial setting and updating of this instrument is accomplished by operating the GYRO TORQUING switch LEFT or RIGHT. The HEADING indicator was set to read 270 degrees at KSC prior to launch. This setting will allow minimum gyro torquing time on the lunar surface to adjust to the required heading.

The bearing indicator displays bearing to the LM in 1-degree digits. In the event of power loss to the navigation system, the bearing indication will remain displayed.

Distance indicator displays distance traveled by the LRV in increments of 0.1 kilometer. This display is driven from the navigation signal processing unit which receives its inputs from the third fastest traction drive odometer. Total digital scale capacity is 99.9 kilometers. Range indicator displays the distance to the LM, and is graduated in 0.1 kilometer increments with a total digital scale capacity of 99.9 kilometers. Speed indicator shows LRV velocity from 0 to 20 km/hr. This display is driven by the odometer pulses from the right rear wheel, through the SPU.

The sun shadow device is used to determine the LRV heading with respect to the sun azimuth. When deployed, the device casts a shadow on a graduated scale when the vehicle is facing away from the sun. The point at which the shadow intersects the scale is transmitted by the crew to MCC for navigation update. The scale length is 15 degrees either side of zero with 1-degree divisions. The sun shadow device can be utilized at sun elevation angles up to 75 degrees.

20.14.2.4 Navigation Subsystem

The navigation subsystem provides heading, bearing, range and distance information for the astronauts. The system consists of a directional gyro unit, a signal processing unit, an integrated position indicator, a sun shadow device and an attitude indicator. Vehicle input signals are processed in the signal processing unit and displayed as follows: heading with respect to lunar north, bearing back to the LM, range back to the LM, total distance traveled and vehicle velocity.

The navigation subsystem is initialized by momentarily transferring the system reset switch to SYSTEM RESET position and back to OFF which

initializes reset of all digital displays and internal registers to zero. Initialization is performed at the start of each EVA only. Alignment of the directional gyro is accomplished by measuring the pitch and roll of the LRV using the attitude indicator and measuring the LRV orientation with respect to the sun using the sun shadow device. This information is relayed to MCC where a heading angle is calculated. The gyro is then adjusted by slewing with the torquing switch until the heading indicator reads the same as the calculated value. The heading angle of the LRV is implicit in the output from the gyro, which is generated by a three wire synchro transmitter. The heading indicator in the Integrated Position Indicator contains a synchro control transformer and an electromechanical servo system which drives the control transformer until a null is achieved with the inputs from the gyro. There are four odometers in the system, one for each traction drive unit. Nine odometer pulses are generated for each revolution of each wheel. These signals are amplified and shaped in the motor controller circuitry and enter the line receiver in the SPU. The odometer pulses from the right rear wheel enter the velocity processor for display on the LRV SPEED indicator.

Odometer pulses from all four wheels enter the odometer logic via the SPU line receivers. This logic selects the third fastest wheel for use in the distance computation. This insures that the odometer output pulses will not be based on a wheel which is locked, nor will they be based on a wheel that has excessive slip.

20.14.2.5 Crew Station

The crew station consists of seats, footrests, inboard handholds, outboard handholds, arm rest, floor panels, seat belts, fenders, and toeholds.

LRV seats are tubular aluminum frames spanned by nylon. The seats are folded flat onto the center chassis for launch and held in place by Velcro tiedown straps. After LRV deployment on the lunar surface the tiedown straps are removed and the seats are erected to the operational position by the crew. The seat back is used to support and restrain the PLSS from lateral motion when the crew is positioned for LRV operation. Velcro pads on the seat backs mate with Velcro on the crewman's PLSS to aid in lateral restraint. These pads, at crew option, can be covered to prevent seat back/PLSS attachment. Covers for these pads are provided as part of the LRV and can be installed or removed at KSC before LRV installation in the LM. For launch, each footrest is stowed against the center chassis floor and secured by two Velcro straps. The footrests are deployed by the crew on the lunar surface. Inboard handholds are constructed of 1 inch O.D. aluminum tubing and are used to aid the crew during ingress and egress. The handholds also contain payload attach receptacles for the 16 mm data acquisition camera and the LCRU low gain antenna. Outboard handholds are integral parts of the chassis and are used to provide crew comfort and stability when seated on the LRV and for attachment of the seat belt. The arm rest is used to support the arm of crewmen during hand controller manipulation.

A seat belt is provided at each seat. The seat belts are constructed of nylon webbing. The belt end terminates in a hook which is secured to the outboard handhold. Belt length adjustment is provided by an adjustment buckle. A stretch section of the belt permits normal fastening and release.

Each wheel is covered by a fiberglass fender. To permit LRV folding for LM installation, the fenders were required to be compressed into a smaller envelope than their operational configuration, resulting in each fender having a deployable extension. The deployable portion of each fender is positioned by the crewman during LRV deployment on the lunar surface. The front fenders also have a flap at the rear end to provide increased dust protection.

There are two toeholds, one on either side of the vehicle. The toehold is used to aid the crew in ingressing and egressing the LRV. The toehold is formed by dismantling the LRV/LM interface tripods, and using the leg previously used as the tripod center member as the toehold. The tripod member is inserted into the chassis receptacle to form the operational position of the toehold. The floor panels in the crew station area are beaded aluminum panels. The floor is structurally capable of supporting the full weight of standing crewmen in lunar gravity.

All instruments on the C&DC are mounted to an aluminum plate. The external surfaces of the C&DC are coated with thermal control paint and the face plate is black anodized and isolated from the instrument mounting plate by radiation shields and fiberglass mounts. Thermal control of the C&DC is totally passive. Handholds, footrests, tubular sections of seats and center and aft floor panels are anodized. The underside of the center chassis floor panels are covered with aluminum foil insulation to prevent LRV components from becoming too cold during translunar flight. The traction drive assemblies are coated with thermal control paint to minimize solar energy absorbed and utilizes its own mass in conjunction with the suspension assembly to store heat energy released by the traction drive motor and harmonic drive. The steering motor utilizes the complete steering motor and transmission assembly and chassis to store heat energy released by the steering motor. The hand controller primary source of heating is from solar energy. The surface finish is such that a minimum of solar energy is absorbed. Each of the above units utilizes energy transfer to deep space while vehicle is parked between sorties to lower the starting temperature of each sortie.

20.14.2.6 Thermal Control

Thermal control systems are incorporated into the LRV to maintain temperature sensitive components within the appropriate temperature limits during the translunar phase of a mission and during its operational life on the lunar surface. Thermal control systems consist of special surface finishes, multilayer insulation, space radiators, thermal straps, and fusible mass

heat sinks. In addition, the LM thermal blanket encloses the lower portion of the stowed LRV to prevent heat damage to the LRV from the LM descent engine during the Fire-Until-Touchdown phase of lunar landing.

The basic concept of thermal control for forward chassis components is energy storage during operation with subsequent energy transfer to deep space while the vehicle is parked between sorties. During operation heat energy released in the DCE is stored in the DCE and the DCE thermal control unit (a fusible mass device). Heat energy released in the SPU is stored in the SPU, the SPU thermal control unit (a fusible mass device) and battery No. 1. The SPU is thermally connected to battery No. 1 by means of the SPU thermal strap. Heat energy released in the Directional Gyro Unit (DGU) is stored in the DGU, and by means of the DGU thermal strap in battery No. 2. Space radiators are mounted on the top of the SPU, DCE, battery No. 1 and Battery No. 2. Fused silica second surface mirrors are bonded to the radiators to minimize the solar energy absorbed by an exposed radiator, and to minimize the degradation of the radiating surface by the space and lunar environment. The space radiators are exposed only during the parking period between sorties. During sortie operation the space radiators are protected from lunar dust by covers on battery No. 1 and the DCE; the SPU radiator and the radiator on battery No. 2. These dust covers are opened manually at the end of a sortie. An overcenter latch holds the dust covers open until battery temperatures reach 45 ±5°F, at which time a bimetallic spring disengages the overcent latch allowing the dust covers to close. The SPU dust cover is slaved to the battery No. 1 dust cover.

In addition to the dust covers, a multi-layer insulation blanket is provided to protect the forward chassis components from the space and lunar surface environments. The exterior, and certain portions of the interior, of the multi-layer insulation blanket are covered with a layer of Beta Cloth to protect against wear and direct solar or hot gas heat loads.

In addition to protective cooling, thermal instrumentation display at the C&DC is provided for the traction drives and batteries. The display takes the form either of a discrete warning by a warning flag activated by a thermostat or an analog temperature display, (as sensed by a thermistor). Analog temperature thermistors are located on the external case of each drive motor and on the main battery bus within each battery. Thermistors located in each assembly are monitored by a bridge circuit in the C&DC and the output of the bridge drives the display meters, which are calibrated in degrees Fahrenheit. By interrogating the temperature display meters, an overtemperature condition can be isolated to the specific subassembly and corrective action initiated.

20.14.2.7 Space Support Equipment

The Space Support Equipment (SSE) consists of two basic subsystems of hardware, the structural support subsystem and the deployment hardware subsystem. The function of the structural support subsystem is to structurally support the LRV in the LM during launch boost, earth-lunar

transit and landing. The function of the deployment hardware subsystem is to deploy the LRV from the LM to the lunar surface after landing.

The deployment hardware system consists of bellcranks, linkages and pins to release the LRV from the structural support subsystem, thus allowing the LRV to deploy from the LM. It also consists of braked reels, braked reel operating tapes, braked reel cables, LRV rotation initiating push-off spring, deployment cable, telescopic tubes, chassis latches, release pin mechanisms, and LRV rotation support points. See Figure 20-19. A deployment manipulation tool is also provided. The tool provides a contingency method for pulling deployment quick release pins and cables.

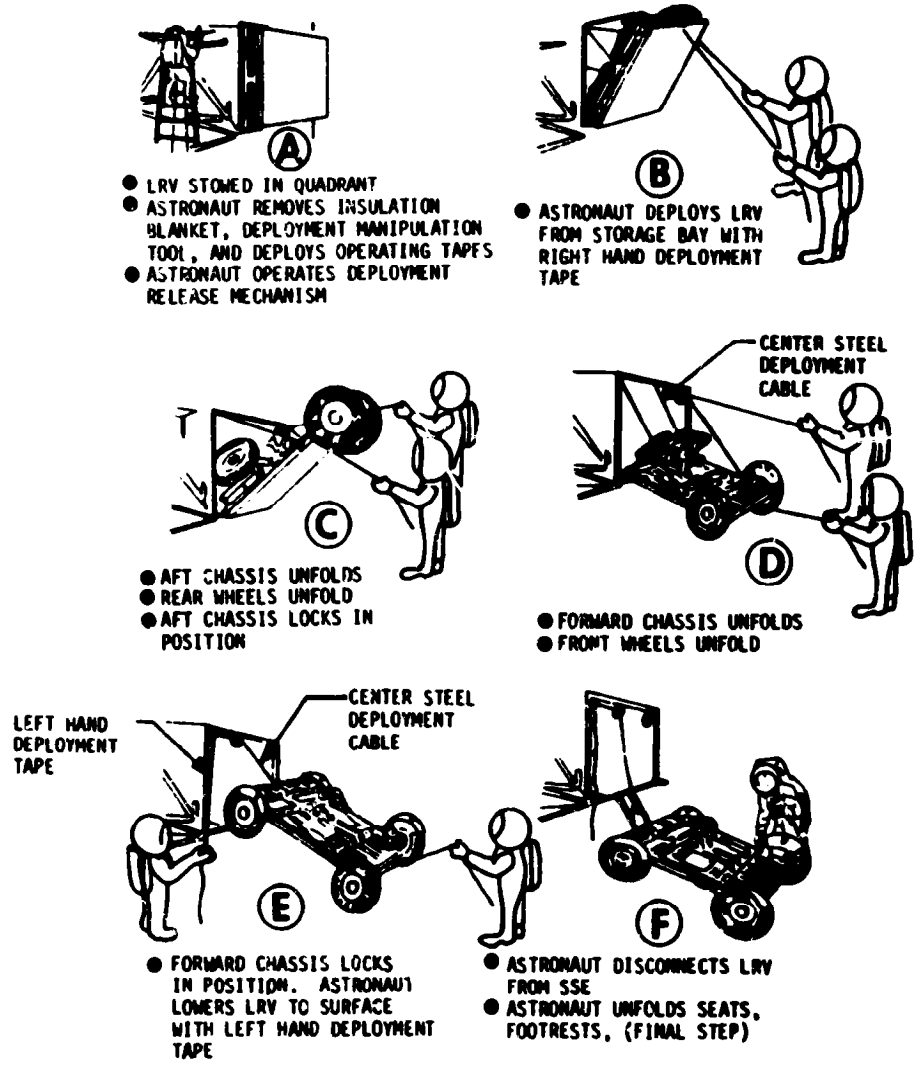

Figure 20-19. Deployment Sequence

APPENDIX A

ATMOSPHERE

A.1 SUMMARY

This appendix presents a summary of the atmospheric environment at launch time of the AS-510. The format of these data is similar to that presented on previous launches of Saturn vehicles to permit comparisons. Surface and upper levels winds, and thermodynamic data near launch time are given.

A.2 GENERAL ATMOSPHERIC CONDITIONS AT LAUNCH TIME

At launch time, the Cape Kennedy launch area was experiencing fair weather resulting from a ridge of high pressure extending westward, from the Bermuda High, through central Florida. See Figure A-1.

Surface winds in the Cape Kennedy area were light and southerly as shown in Table A-1. Wind flow aloft is shown in Figure A-2 (500 millibar level). The maximum wind belt was located north of Florida, giving less intense wind flow over the Cape Kennedy area. Winds were light and variable from the surface to 10.5 kilometer (34,450 ft) altitude.

A.3 SURFACE OBSERVATIONS AT LAUNCH TIME

At launch time, total sky cover was 7/10, consisting of high thin cirrus at 7.6 kilometers (25,000 ft). Temperature was 303°K (85.7°F). All surface observations at launch time are summarized in Table A-1. Solar radiation data are given in Table A-2.

A.4 UPPER AIR MEASUREMENTS

Data were used from three of the upper air wind systems to compile the final meteorological tape. Table A-3 summarizes the wind data systems used. Only the Rawinsonde and the Loki Dart meteorological rocket data were used in the upper level atmospheric thermodynamic analyses.

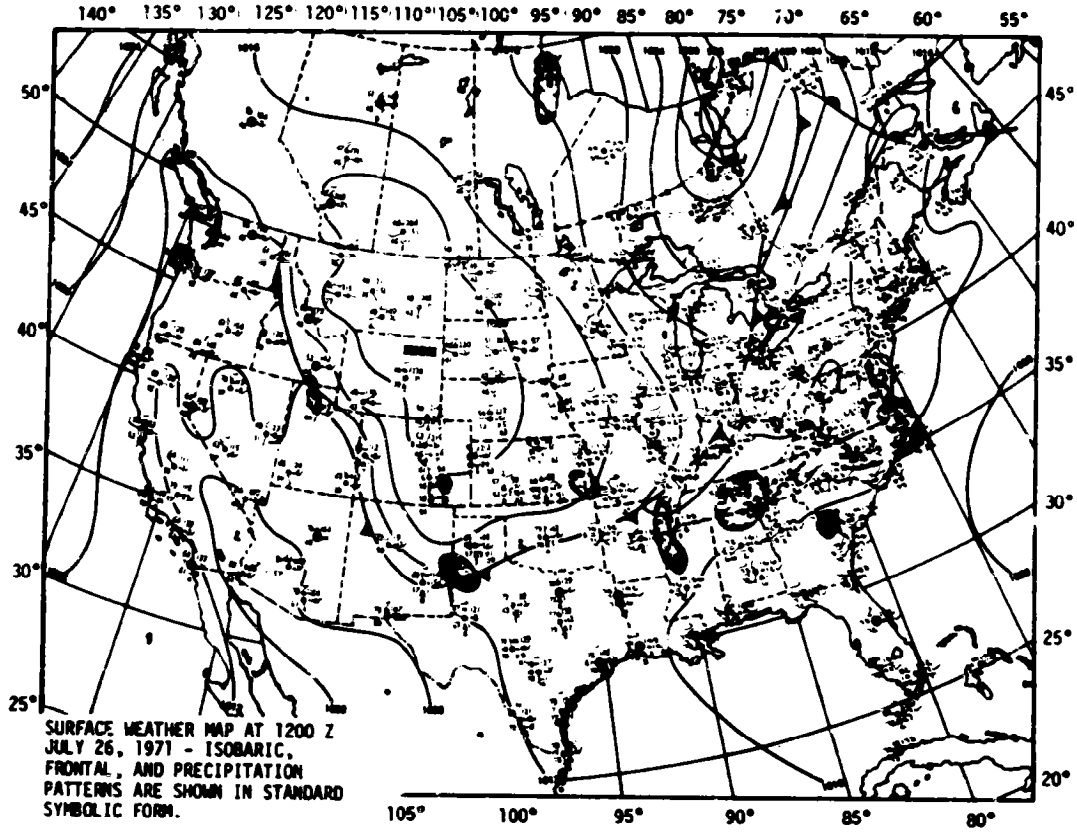

Figure A-1. Surface Weather Map Approximately 1 1/2 Hours Before Launch of AS-510

A.4.1 Wind Speed

Wind speeds were light, being 3.6 m/s (7.0 knots) at the surface, increasing to a peak of 18.59 m/s (36.2 knots) at 13.75 kilometers (45,110 ft). The winds began decreasing above this altitude, reaching a minimum of 7.0 m/s (13.6 knots) at 16.35 kilometers (53,640 ft) altitude. Above this altitude, the wind speed continued to increase, as shown in Figure A-3; a maximum speed of 76.0 m/s (147.7 knots) was measured at 55.75 kilometers (182,900 ft) altitude.

A.4.2 Wind Direction

At launch time, the surface wind direction was 160 degrees. The wind direction was quite variable with increasing altitude to 8.0 kilometers (26,000 ft). Above this level, wind direction was easterly to 58.0 kilometers (190,290 ft) altitude. Figure A-4 shows a complete wind direction versus altitude profile.

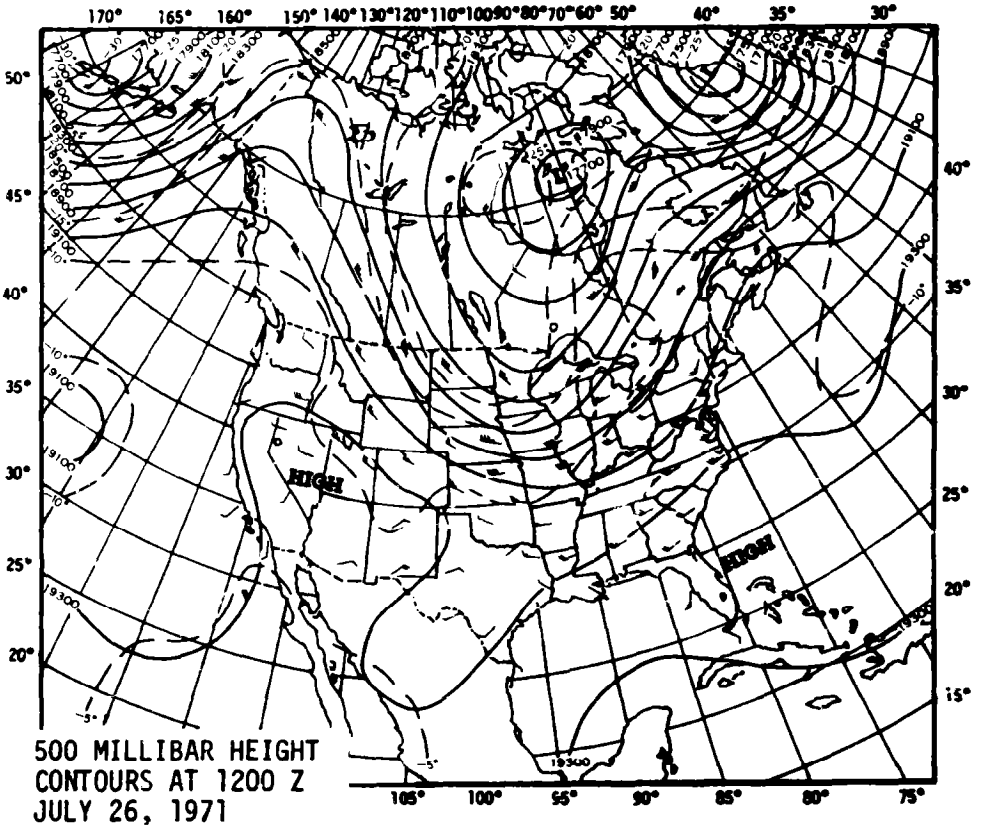

500 MILLIBAR HEIGHT CONTOURS AT 1200 Z JULY 26, 1971

CONTINUOUS LINES INDICATE HEIGHT CONTOURS IN FEET ABOVE SEA LEVEL. DASHED LINES ARE ISOTHERMS IN DEGREES CENTIGRADE. ARROWS SHOW WIND DIRECTION AND SPEED AT THE 500 MB LEVEL. (ARROWS SAME AS ON SURFACE MAP).

Figure A-2. 500 Millibar Map Approximately 1 1/2 Hours Before Launch of AS-510

A.4.3 Pitch Wind Component

The pitch wind velocity component (component parallel to the horizontal projection of the flight path) at the surface was a headwind of 0.6 m/s (1.2 knots). A maximum headwind of 17.82 m/s (34.6 knots) was observed at 13.73 kilometers (45,030 ft) altitude. See Figure A-5.

A.4.4 Yaw Wind Component

The yaw wind velocity component (component normal to the horizontal projection of the flight path) at the surface was a wind from the right of 3.54 m/s (6.9 knots). The peak yaw wind velocity in the high dynamic

Table A-1. Surface Observations at AS-510 Launch Time

LOCATION	TIME AFTER T-0 (MIN)	PRESSURE N/CM² (PSIA)	TEMPERATURE °K (°F)	DEW POINT °K (°F)	VISIBILITY KM (STAT MI)	AMOUNT (TENTHS)	SKY COVER TYPE	HEIGHT OF BASE METERS (FEET)	WIND SPEED M/S (KNOTS)	WIND DIR (DEG)
NASA 150 m (495 ft) Tower **	0	10.196 (14.79)	303.0 (85.7)	296.5 (74.0)	16 (10)	7	Cirrus	7,620 (25,000)	3.6 (7.0)	160
Cape Kennedy Rawinsonde Measurements	10	10.183 (14.77)	301.4 (82.8)	295.3 (71.8)	--	--	--	--	4.0 (7.8)	170
Pad 39A Lightpole NW 18.3 m (60.0 ft)*	0	--	--	--	---	--	--	--	5.1*** (10.0)	156***
LUT Pad 39A 161.5 m (530 ft)*	0	--	--	--	---	--	--	--	5.4*** (10.5)	158***

* Above natural grade.
** NASA 150 meter ground wind tower facility located at Cape Kennedy.
*** 1 minute average about T-0.

Table A-2. Solar Radiation at AS-510 Launch Time, Launch Pad 39A

DATE	HOUR ENDING EST	TOTAL HORIZONTAL SURFACE	NORMAL INCIDENT	DIFFUSE (SKY)
July 26, 1971	05.00	0.00	0.00	0.00
	06.00	0.01	1.01	0.01
	07.00	0.09	0.30	0.04
	08.00	0.31	0.80	0.01
	09.00	0.60	1.07	0.00
	10.00	0.81	1.15	0.00
	11.00	0.97	1.06	0.04

pressure region was from the left of 7.34 m/s (14.2 knots) at 13.43 kilometers (44,040 ft). See Figure A-6.

A.4.5 Component Wind Shears

The largest component wind shear (Δh = 1000 m) in the altitude range of 8 to 16 kilometers (26,247 to 52,493 ft) was a pitch shear of 0.0110 sec^{-1} at 11.23 kilometers (36,830 ft). The largest yaw wind shear, at these lower levels, was 0.0071 sec^{-1} at 14.43 kilometers (47,330 ft). See Figure A-7.

A.4.6 Extreme Wind Data in the High Dynamic Region

A summary of the maximum wind speeds and wind components is given in Table A-4. A summary of the extreme wind shear values is given in Table A-5.

Table A-3. Systems Used to Measure Upper Air Wind Data for AS-510

TYPE OF DATA	RELEASE TIME		PORTION OF DATA USED			
			START		END	
	TIME (UT)	TIME AFTER T-0 (MIN)	ALTITUDE M (ft)	TIME AFTER T-0 (MIN)	ALTITUDE M (ft)	TIME AFTER T-0 (MIN)
FPS-16 Jimsphere	1350	16	125 (410)	16	13,750 (45,111)	63
Rawinsonde	1344	10	14,000 (45,931)	56	24,750 (81,200)	91
Loki Dart	1505	91	58,000 (190,286)	91	25,000 (82,020)	116

A.5 THERMODYNAMIC DATA

Comparisons of the thermodynamic data taken at AS-510 launch time with the annual Patrick Reference Atmosphere, 1963 (PRA-63) for temperature, pressure, density, and Optical Index of Refraction are shown in Figures A-8 and A-9, and are discussed in the following paragraphs.

A.5.1 Temperature

Atmospheric temperature differences were small, generally deviating less than 2 percent from the PRA-63, below 45 kilometers (147,640 ft) altitude. Air temperatures were warmer than the PRA-63, from the surface and through 13 kilometers (42,650 ft). Above this altitude, temperatures deviated about the PRA-63 values. See Figure A-8.

A.5.2 Atmospheric Pressure

Atmospheric pressure deviations were greater than the PRA-63 pressure values from the surface to 58.0 kilometers (190,290 ft) altitude. All pressure values versus altitude were within 6 percent of the PRA-63 values, as shown in Figure A-8.

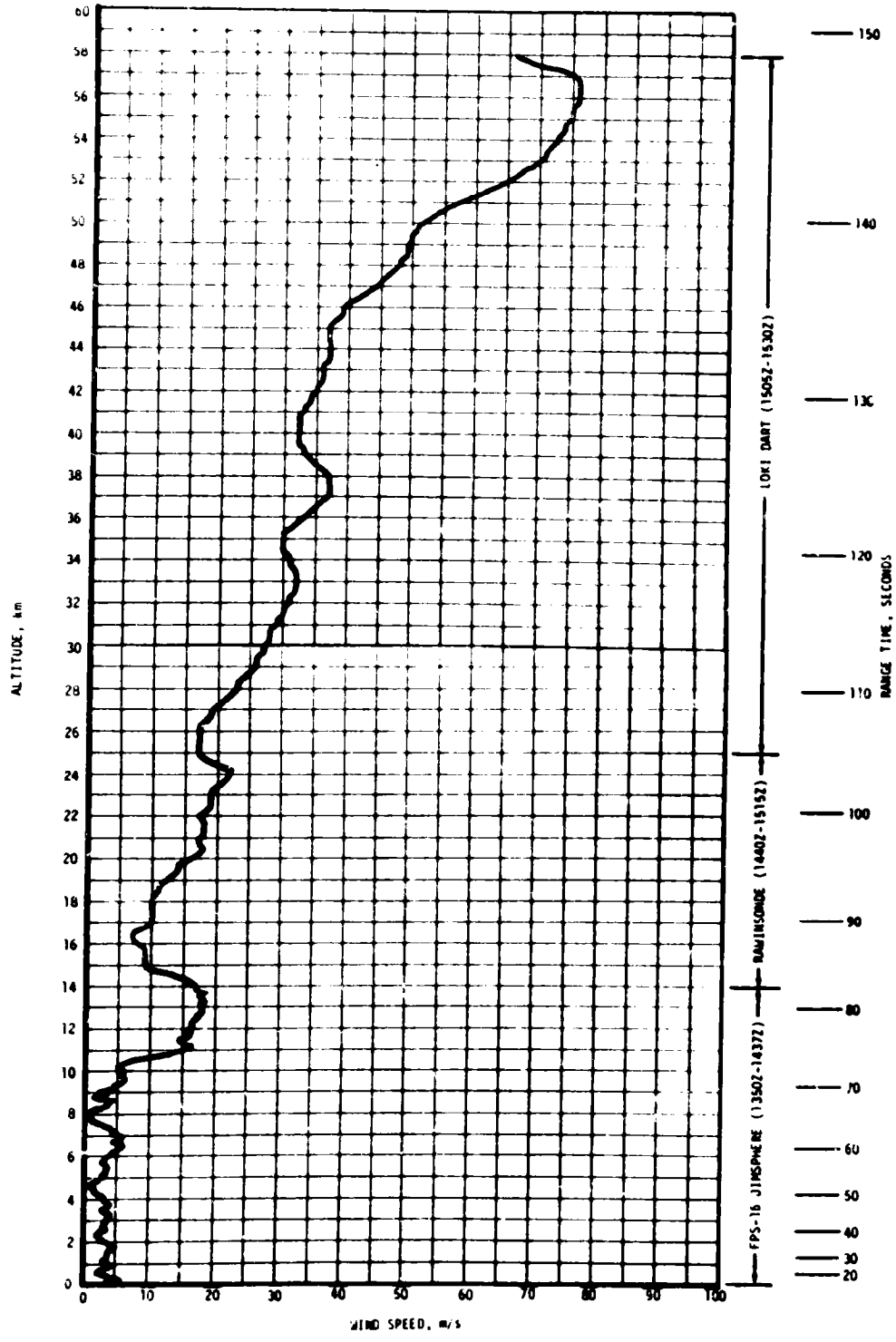

Figure A-3. Scalar Wind Speed at Launch Time of AS-510

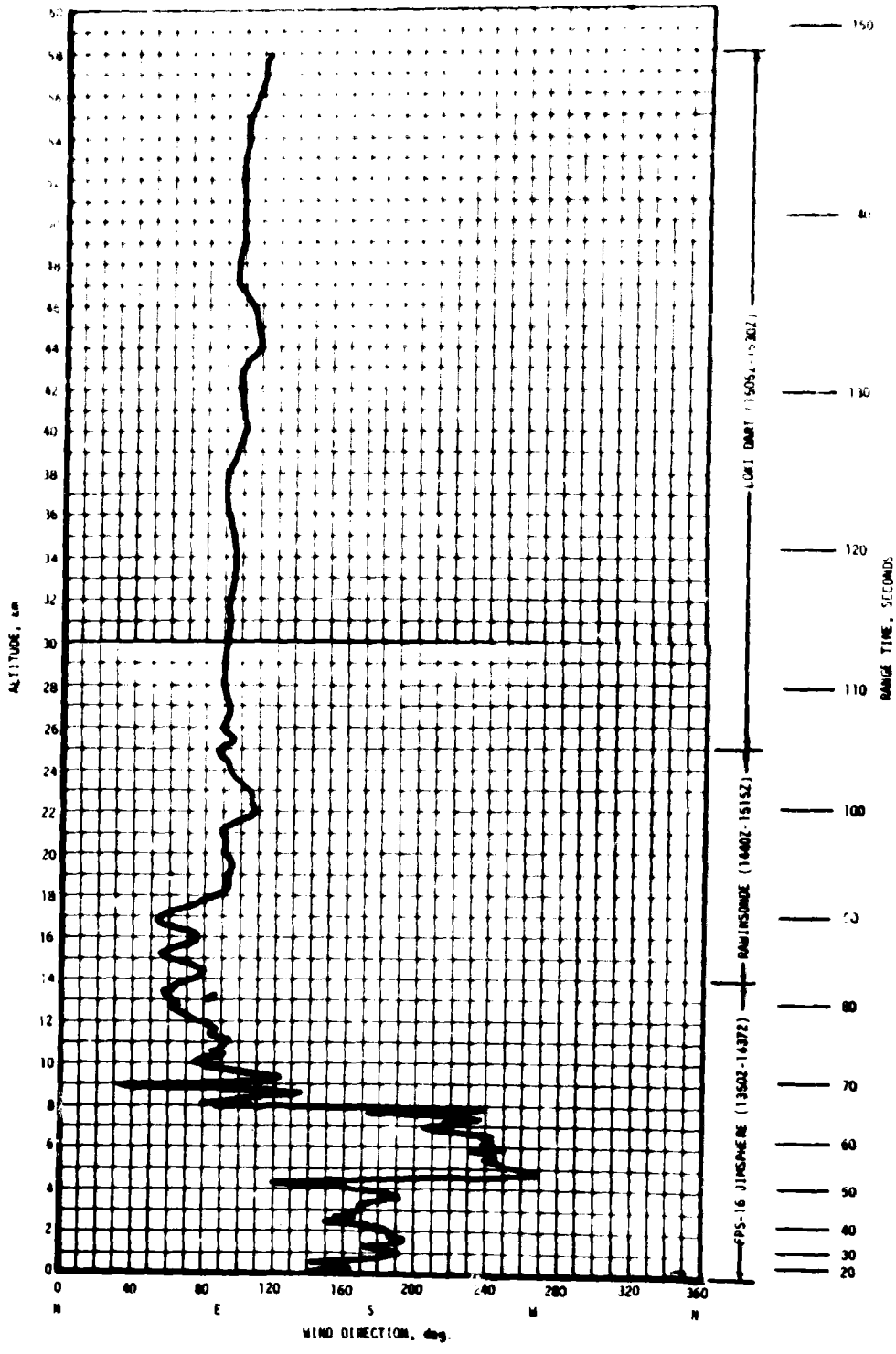

Figure A-4. Wind Direction at Launch Time of AS-510

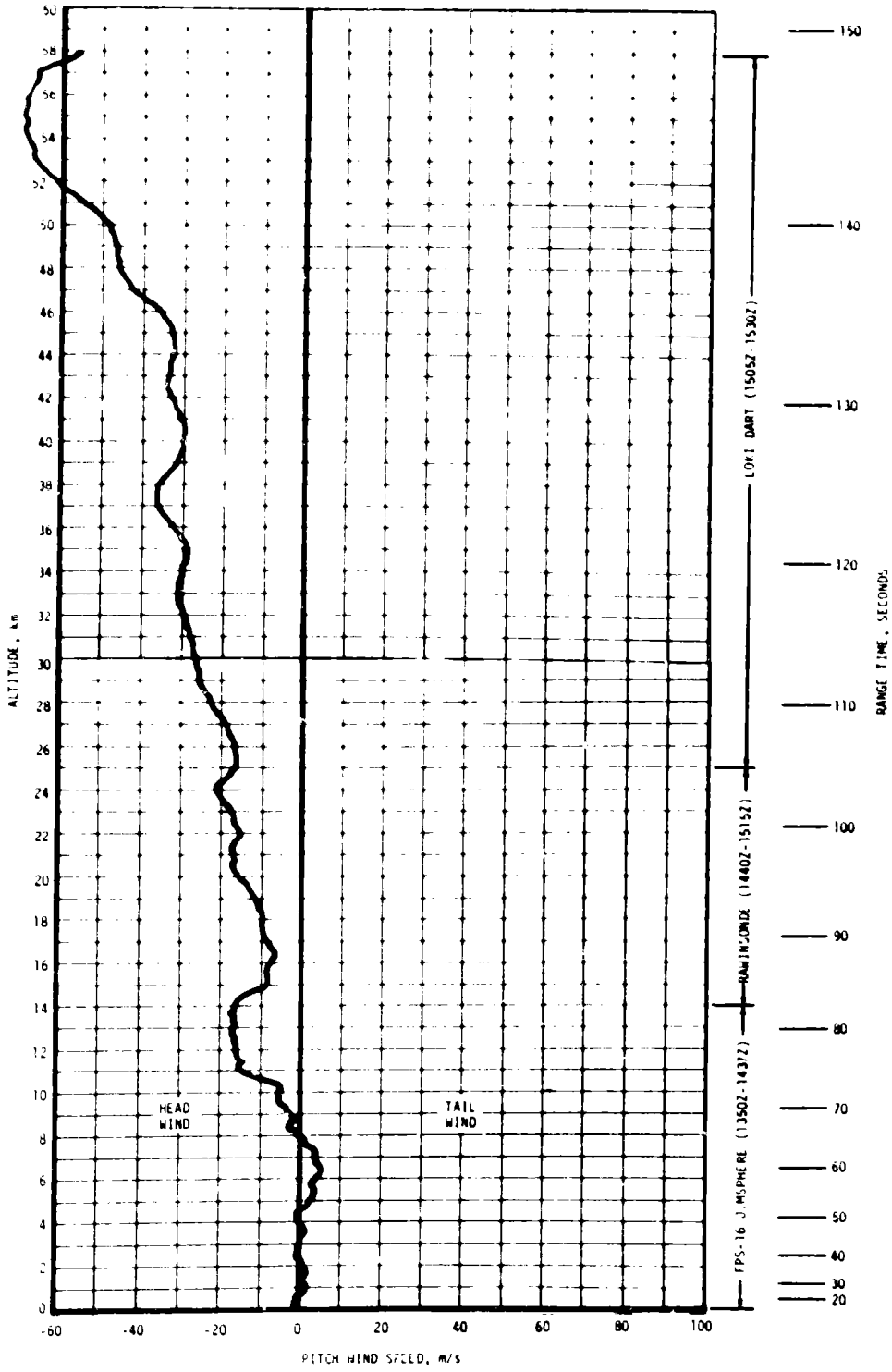

Figure A-5. Pitch Wind Velocity Component (W_X) at Launch Time of AS-510

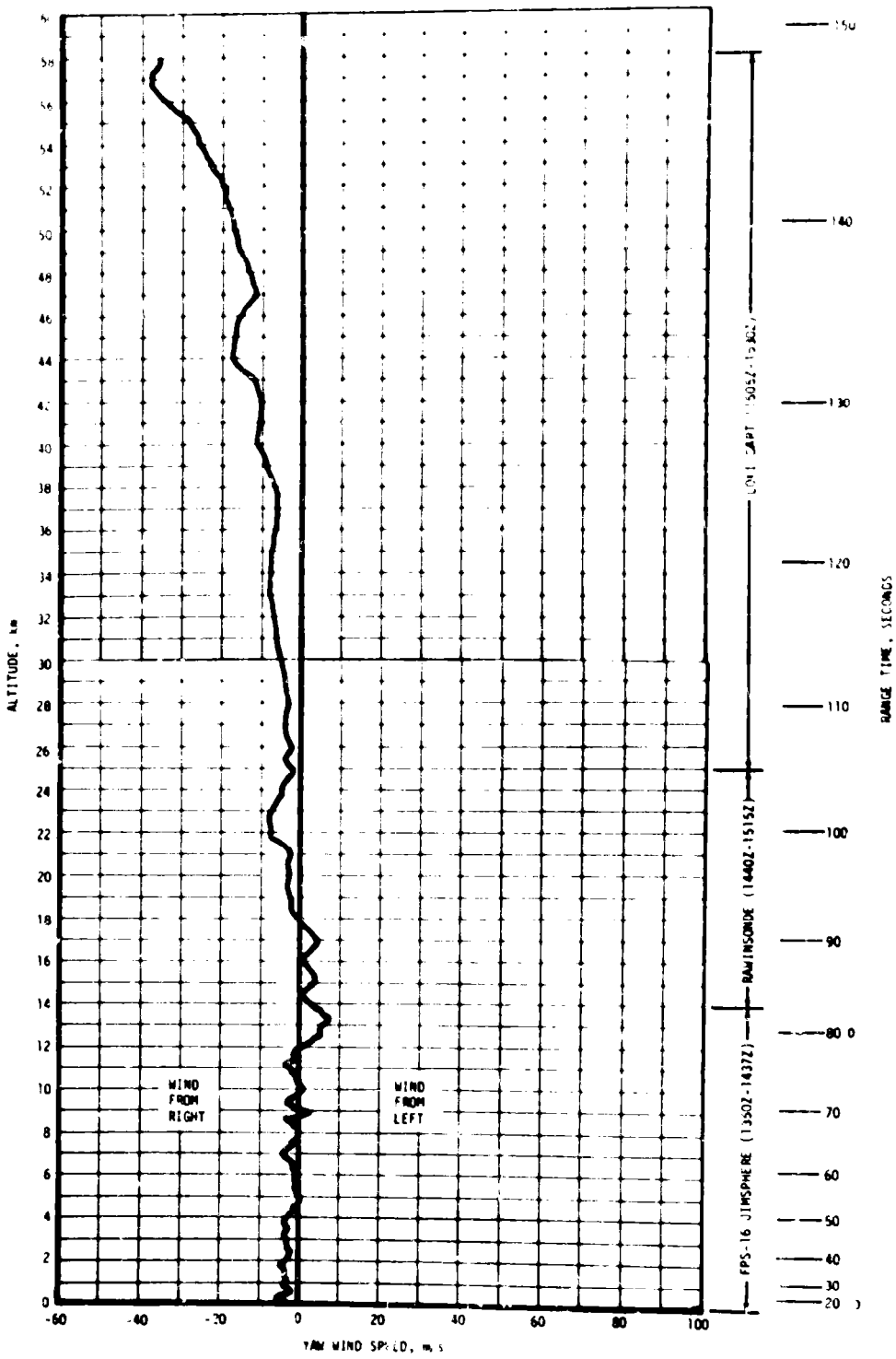

Figure A-6. Yaw Wind Velocity Component (W_z) at Launch Time of AS-510

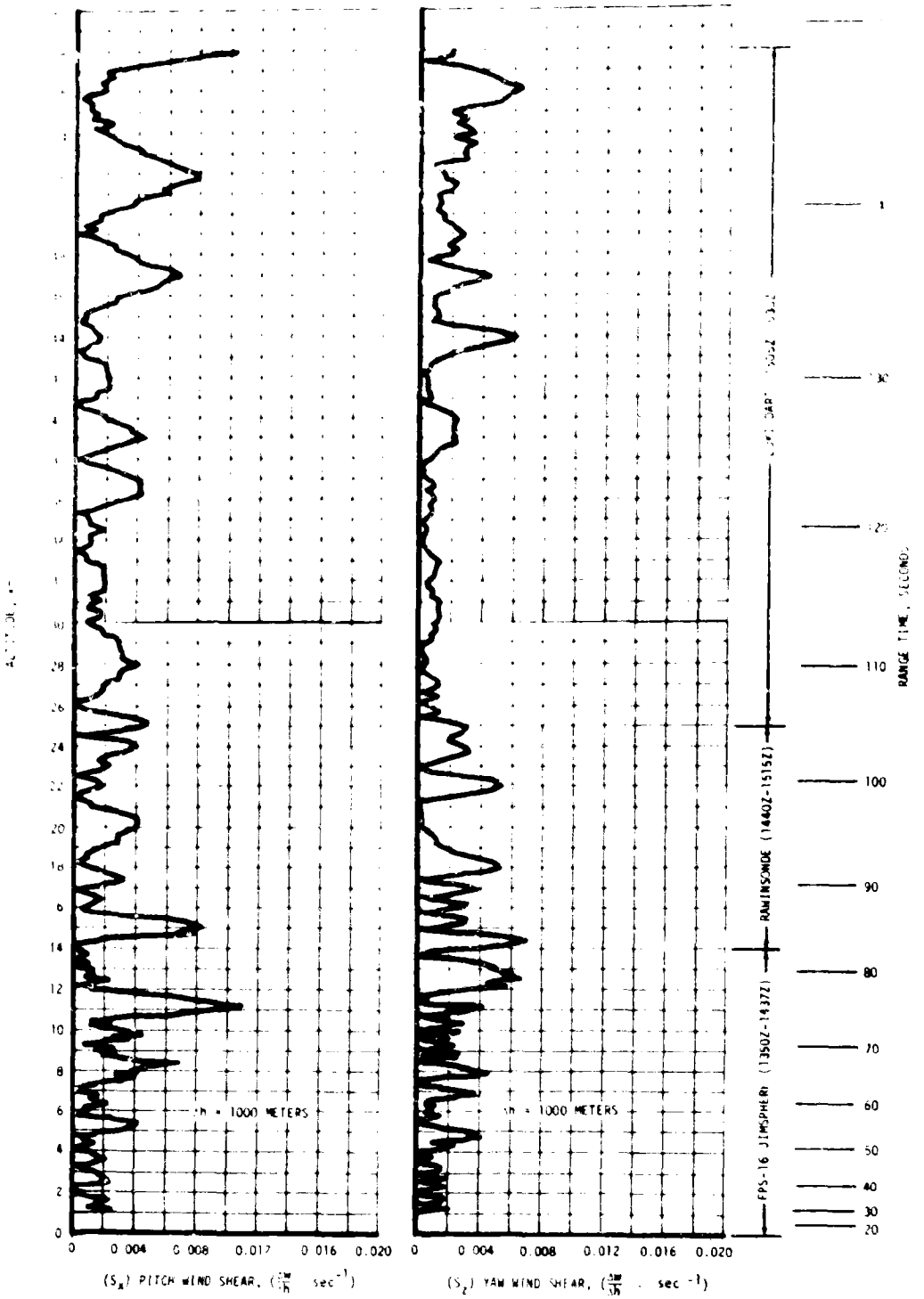

Figure A-7. Pitch (S_X) and Yaw (S_Z) Component Wind Shears at Launch Time of AS-510

Table A-4. Maximum Wind Speed in High Dynamic Pressure Region for Apollo/Saturn 501 through Apollo/Saturn 510 Venicles

VEHICLE NUMBER	MAXIMUM WIND			MAXIMUM WIND COMPONENTS			
	SPEED M/S (KNOTS)	DIR (DEG)	ALT KM (FT)	PITCH (W_X) M/S (KNOTS)	ALT KM (FT)	YAW (W_Z) M/S (KNOTS)	ALT KM (FT)
AS-501	26.0 (50.5)	273	11.50 (37,700)	24.3 (47.2)	11.50 (37,700)	12.9 (25.1)	9.00 (29,500)
AS-502	27.1 (52.7)	255	12.00 (42,600)	27.1 (52.7)	12.00 (42,600)	12.9 (25.1)	15.75 (51,700)
AS-503	34.8 (67.6)	284	15.22 (49,900)	31.2 (60.6)	15.10 (49,500)	22.6 (43.9)	15.80 (51,800)
AS-504	76.2 (148.1)	264	11.73 (38,480)	74.5 (144.8)	11.70 (38,390)	21.7 (42.2)	11.43 (37,500)
AS-505	42.5 (82.6)	270	14.18 (46,520)	40.8 (79.3)	13.80 (45,280)	18.7 (36.3)	14.85 (48,720)
AS-506	9.6 (18.7)	297	11.40 (37,400)	7.6 (14.8)	11.18 (36,680)	7.1 (13.8)	12.05 (39,530)
AS-507	47.6 (92.5)	245	14.23 (46,670)	47.2 (91.7)	14.23 (46,670)	19.5 (37.9)	13.65 (44,780)
AS-508	55.6 (108.1)	252	13.58 (44,540)	55.6 (108.1)	13.58 (44,540)	15.0 (29.1)	12.98 (42,570)
AS-509	52.8 (102.6)	255	13.33 (43,720)	52.8 (102.6)	13.33 (43,720)	24.9 (48.5)	10.20 (33,460)
AS-510	18.6 (36.2)	063	13.75 (45,110)	17.8 (34.6)	13.73 (45,030)	7.3 (14.2)	13.43 (44,040)

Table A-5. Extreme Wind Shear Values in the High Dynamic Pressure Region for Apollo/Saturn 501 through Apollo/Saturn 510 Vehicles

(Δh = 1000 m)				
VEHICLE NUMBER	PITCH PLANE		YAW PLANE	
	SHEAR (SEC-1)	ALTITUDE KM (FT)	SHEAR (SEC-1)	ALTITUDE KM (FT)
AS-501	0.0066	10.00 (32,800)	0.0067	10.00 (32,800)
AS-502	0.0125	14.90 (48,900)	0.0084	13.28 (43,500)
AS-503	0.0103	16.00 (52,500)	0.0157	15.78 (51,800)
AS-504	0.0248	15.15 (49,700)	0.0254	14.68 (48,160)
AS-505	0.0203	15.30 (50,200)	0.0125	15.53 (50,950)
AS-506	0.0077	14.78 (48,490)	0.0056	10.30 (33,790)
AS-507	0.0183	14.25 (46,750)	0.0178	14.58 (47,820)
AS-508	0.0166	15.43 (50,610)	0.0178	13.98 (45,850)
AS-509	0.0201	13.33 (43,720)	0.0251	11.85 (38,880)
AS-510	0.0110	11.23 (36,830)	0.0071	14.43 (47,330)

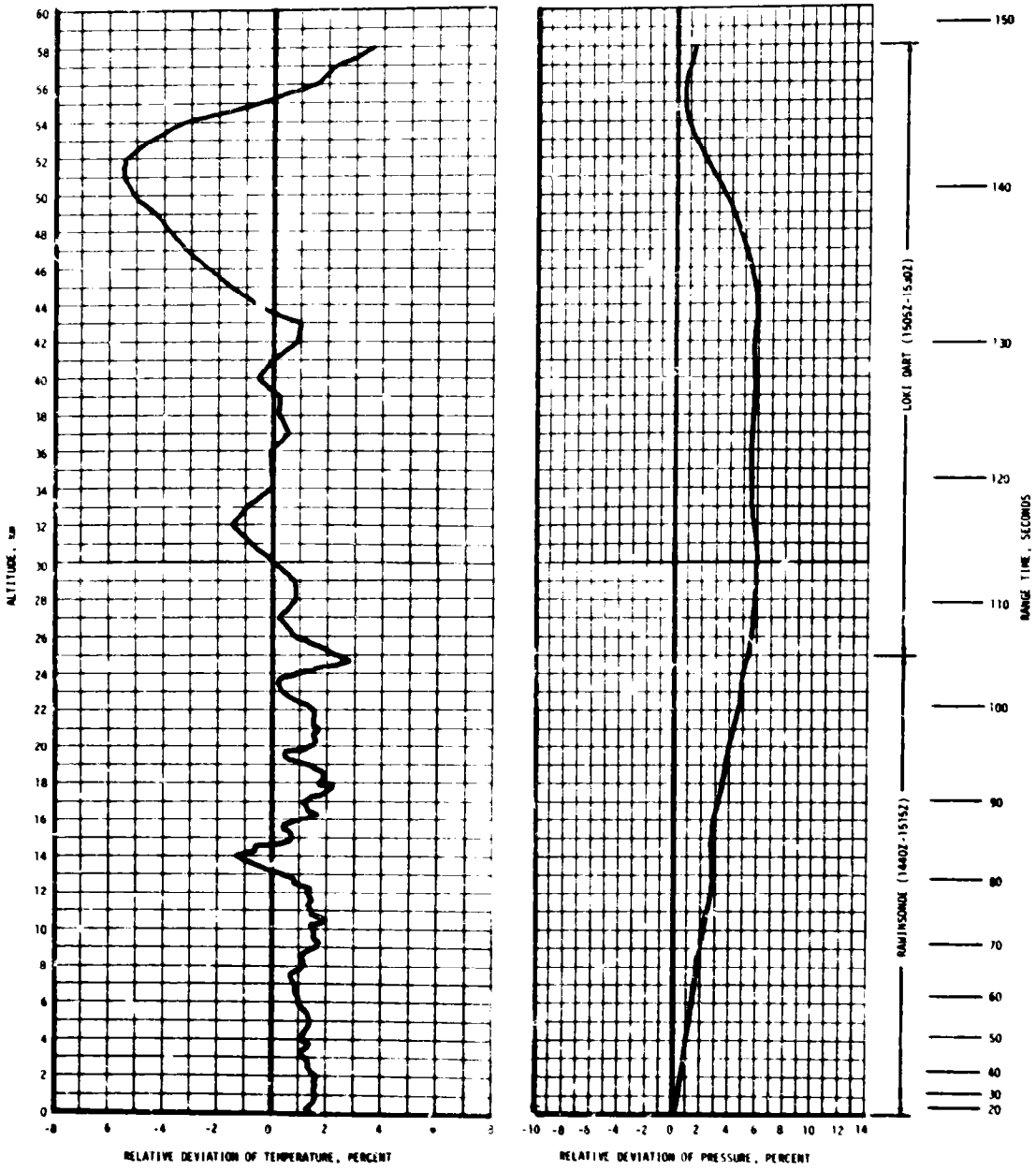

Figure A-9. Relative Deviation of Temperature and Pressure from the PRA-63 Reference Atmosphere, AS-510

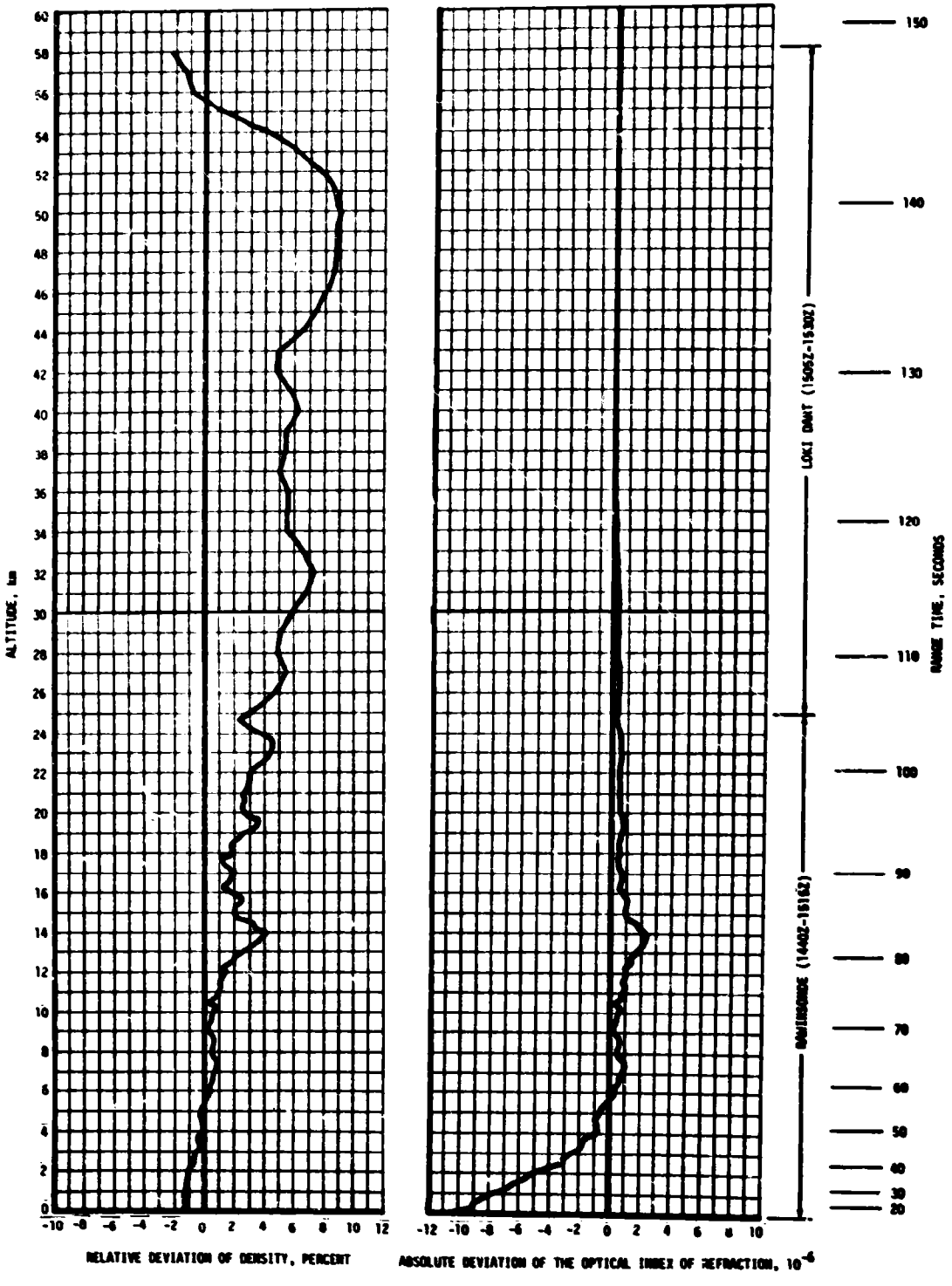

Figure A-9. Relative Deviation of Density and Absolute Deviation of the Index of Refraction from the PRA-63 Reference Atmosphere, AS-510

A.5.3 Atmospheric Density

Atmospheric density deviations were small, being within 9 percent of the PRA-63 for all altitudes. Surface density was 1.52 percent less than the PRA-63 density value. Density deviations became positive above 5.5 kilometers (18,040 ft). See Figure A-9.

A.5.4 Optical Index of Refraction

Optical Index of Refraction was 10.7 x 10^{-6} units lower than the corresponding value of the PRA-63. The deviation became less negative with altitude, and it approximated the PRA-63 at high altitudes, as is shown in Figure A-9. The maximum value of the Optical Index of Refraction was 2.37 x 10^{-6} units greater than the PRA-63 at 14 kilometers (45,930 ft).

A.6 COMPARISON OF SELECTED ATMOSPHERIC DATA FOR SATURN V LAUNCHES

A summary of the atmospheric data for each Saturn V launch is shown in Table A-6.

Table A-6. Selected Atmospheric Observations for Apollo/Saturn 501 through Apollo/Saturn 510 Vehicle Launches at Kennedy Space Center, Florida

VEHICLE DATA				SURFACE DATA						INFLIGHT CONDITIONS		
							WIND*			MAXIMUM WIND IN 8-16 KM LAYER		
VEHICLE NUMBER	DATE	TIME NEAREST MINUTE	LAUNCH COMPLEX	PRESSURE N/CM²	TEMPERATURE °C	RELATIVE HUMIDITY PERCENT	SPEED M/S	DIRECTION DEG	CLOUDS	ALTITUDE KM	SPEED M/S	DIRECTION DEG
AS-501	9 Nov 67	0700 EST	39A	10.261	17.5	55	8.0	70	1/10 cumulus	11.50	26.0	273
AS-502	4 Apr 68	0700 EST	39A	10.200	20.9	83	5.4	132	5/10 stratocumulus, 1/10 cirrus	13.00	27.1	255
AS-503	21 Dec 68	0751 EST	39A	10.207	15.0	88	1.0	360	4/10 cirrus	15.22	34.8	284
AS-504	3 Mar 69	1100 EST	39A	10.095	19.6	61	6.9	160	7/10 stratocumulus, 10/10 altostratus	11.73	76.2	264
AS-505	18 May 69	1249 EDT	39B	10.190	28.7	75	8.2	125	4/10 cumulus, 2/10 altocumulus, 10/10 cirrus	14.18	42.5	270
AS-506	16 Jul 69	0932 EDT	39A	10.203	29.4	73	3.3	175	1/10 cumulus, 2/10 altocumulus, 9/10 cirrostratus	11.40	9.5	297
AS-507	14 Nov 69	1132 EST	39A	10.081	20.0	92	6.8	280	10/10 stratocumulus with rain	14.23	47.6	245
AS-508	11 Apr 70	1413 EST	39A	10.119	24.4	57	6.3	105	4/10 altocumulus 10/10 cirrostratus	13.58	55.6	252
AS-509	31 Jan 71	1603 EST	39A	10.102	21.7	88	5.0** 8.5***	256** 275***	7/10 cumulus 2/10 altocumulus	13.33	52.8	255
AS-510	29 Jul 71	0934 EDT	39A	10.196	29.8	63	5.1** 5.4***	156** 150***	7/10 cirrus	13.75	18.6	063

*Instantaneous readings from charts at T-0 from anemometers on launch pad at 18.3 m (60.0 ft) on launch complex 39 (A&B). Heights of anemometers are above natural grade.
**Not instantaneous, but one minute average about T-0.
***One minute average readings from charts at T-0 from anemometers on LUT at 161.5 m (530 ft) above natural grade.

APPENDIX B

AS-510 SIGNIFICANT CONFIGURATION CHANGES

B.1 INTRODUCTION

The AS-510, tenth flight of the Saturn V series, was the eighth manned Apollo Saturn V vehicle. The AS-510 launch vehicle configuration was essentially the same as the AS-509 with significant exceptions shown in Tables B-1 through B-4. The Apollo 15 spacecraft structure and components were essentially unchanged from the Apollo 14 configuration. However, the Lunar Module (LM) descent stage was changed to make provisions for storing and deploying the Lunar Roving Vehicle (LRV). A detail description of the LRV is contained in paragraph 20.14. The basic launch vehicle description is presented in Appendix B of the Saturn V Launch Vehicle Flight Evaluation Report, AS-504, Apollo 9 Mission, MPR-SAT-FE-69-4.

Table B-1. S-IC Significant Configuration Changes

SYSTEM	CHANGE	REASON
F-1 Engines	Reorifice of five engines to yield 1,522,000 lbf rated thrust.	Approximately 600 pounds of additional payload capability to translunar injection is realized.
LOX	Redesign of LOX vent and relief valves. Increase outboard engine LOX depletion system time delay from 1.2 to 1.6 seconds.	To minimize the probability of valve failure during countdown. To permit an increase in payload.
S-IC/S-II Separation	Deletion of four retromotors from S-IC stage.	Weight and cost savings.
Data	Modification of PCM/DDAS and RDSM telemetry assembly. Also incorporation of new presampling filter and power supply cards.	To improve performance and increase reliability.
GSE	Replacement of APCO/Wintec regulators with grove regulators in the S-IC pneumatic console primary nitrogen regulation system.	Reduce vibration in primary regulation system.

Table B-2. S-II Significant Configuration Changes

SYSTEM	CHANGE	REASON
Instrumentation	Addition of five engine LH_2 inlet temperature transducers and four valve actuation and helium injection pressure transducers.	To provide redundant launch redline measurements.
Propulsion	Engine vent and relief valves for start bottle conditioning have replacement vent port check valves.	To improve reliability by selection of check valve used on S-II stage prevalve and recirculation valve solenoid valves.
	Addition of nonflight relief valves to LH_2 tank vent valve sensing port covers.	To protect the LH_2 tank vent valve sensing element against excessive pressure during checkout operations.
	Deletion of the four remaining ullage motors.	Analysis has verified satisfactory flight conditions without the motors.
	Reduction of engine precant angle from 1.3 to 0.6 degree outboard.	To reduce probability of interstage collision during separation.
	Replacement of propellant tank pressurization regulators with orifices.	To increase system reliability and capability.
Electrical	Addition of disable circuitry for center engine G-switch backup cutoff system.	To disable a malfunctioning G-switch prior to switch selector arming command.
Structure	Use of S-II-11 type heavier forward skirt.	An S-II-11 type structure was the only available skirt to replace the scheduled item damaged in a structural test.
GSE	Addition of S7-41 bleed orifice and redundant check valve in GH_2 start bottle pressurization system.	To provide accurate stage servicing repeatibility.
	Elimination of S7-41 propellant incompatible conditions and add a new GOX venting system.	To improve system safety.
	Addition of S7-41 GH_2 vent system, including GN_2 purge provisions.	To improve system safety.

Table B-3. S-IVB Significant Configuration Changes

SYSTEM	CHANGE	REASON
Instrumentation	Addition of two pressure and two vibration measurements to the flight telemetry system.	Incorporation of modified measurement program.
	Addition of static fire or vibration test requirement for telemetry equipment plus X-ray of reworked or new component boards.	To detect tantalum capacitor shorts in telemetry equipment due to internal solder particles in the capacitor.
Propulsion	Incorporation of new seat material in fuel tank prepressurization module check valve.	To provide new seat material of a nondelaminating material.
	Hard cap approximately 29 leak check ports in each APS module.	Reduce potential helium leakage paths in APS module conoseal joints.
Electrical	Modification of the LH_2 depletion sensor system electrical circuitry to utilize the existing (spare) fourth depletion sensor in a 3 out of 4 voting logic. The system was formerly a 2 out of 3 voting system.	To protect against a single point flight failure.

Table B-4. IU Significant Configuration Changes

SYSTEM	CHANGE	REASON
Environmental Control	The Viton-A O-ring seals in the half-inch and one-inch quick disconnect adapters and the dynamic O-ring in the one-half inch quick disconnect socket were replaced with O-rings of Ethylene Propylene (EPR). The Viton-A O-rings in the one-inch socket were replaced with a new low compression set fluorocarbon.	To improve seal and prevent leakage.
	The Buna-N O-ring on the stem of the hand valve was replaced with an O-ring of EPR material.	To improve seal and prevent leakage.
Networks	Redundant battery power for ST-124M platform. The 6D10 and 6D30 batteries provide redundant power to the platform through a diode OR circuit.	To remove potential single point of platform failure.
Instrumentation and Communications	The command and communication system transponder power supply diodes CR 17 through CR 24 were changed from UTR-11 to SIN 4942.	SIN 4942 diodes are less susceptible to physical and electrical stress.
	Added measurements B0001-601, Acoustic (sound detection by microphone); and E0029-603 and E0040-603, IU vibration mounted on ST-124M platform Panel 21.	Correlation of sound pressure levels with Panel 21 vibration.
	Added measurements A0012-403, D0266-401, D0264-403, E0042-403, and E0098-411.	S-IVB vibration measurements telemetered via IU DF-1.
	Deleted measurements E0007-603, E0008-603, and E0009-603. These measurements were ST-124M platform support vibration measurements.	Not effective for AS-510.
Flight Control	The compensating filters located in the flight control computer have been changed in accordance with the vehicle body dynamics, and propellant/oxidizer sloshing dynamics.	The addition of the Lunar Roving Vehicle to AS-510 made the filter changes necessary.
Flight Program	BOOST INITIALIZE	
	TD Test - Capability has been provided to compare the time into the launch window calculated at Guidance Reference Release with that computed in the prepare-to-launch routine.	To prevent a gross azimuth error.
	FIRST BOOST	
	Tower Avoidance - The launch tower avoidance yaw maneuver has been modified to begin the first minor loop after it is commanded.	Provides a more precise time for initiation of tower avoidance.
	Accelerometer Backups - The Z-channel accelerometer backup biases and the S-IC engine out backup biases have been added to the target tape.	To allow updating these quantities via the targeting tape.
	Tilt Arrest - Capability has been provided to modify tilt arrest time differently for S-IC center engine out than for S-IC outboard engine out.	To optimize performance for S-IC center engine out condition.

Table B-4. IU Significant Configuration Changes (Continued)

SYSTEM	CHANGE	REASON
Flight Program	FIRST BOOST (CONTINUED)	
	S-IVB Cutoff - Equal priority given to all S-IVB cutoff indications. The first cutoff indication received (INT2, INT7, DI22, or high speed loop cutoff) will be honored.	Program reliability improvement.
	SECOND BOOST	
	Mainstage Thrust Test - A test has been provided to distinguish between an unacceptable zero accelerometer change and a nonthrusting S-IVB engine between T_6 +580.5 and T_6 +590 seconds.	To avoid navigation error in the event main stage thrust is not achieved.
	Command Module Computer Cutoff - Capability has been provided to issue the S-IVB cutoff switch selector command as a function of an interrupt from the command module computer after guidance reference failure and spacecraft control.	Additional S-IVB TLI cutoff accuracy.
	ORBITAL PHASE	
	Solar Heating Avoidance - A preprogrammed maneuver has been provided for IU solar heating avoidance on the lunar impact trajectory.	To avoid overheating of command and communication system transponder.
	Lunar Impact - The following capabilities have been added to the lunar impact digital command system command: To command lunar impact maneuver changes independent of ullage burns. To negate an ullage burn commanded by a previous lunar impact command.	To be able to maneuver to a different attitude without ullage burn. The roll attitude change command provides an alternate method for achieving solar heating avoidance.
	SIGNIFICANT DATA CHANGES	
	Target to a 90 n mi parking orbit.	Required because of additional Lunar Roving Vehicle weight.
	Change launch window opening and closing to 80 and 100 degrees, respectively.	Increased payload caused limits change.
	Delay the S-IC retromotor fire signal, S-II start command, arming the S-II engine-out indications and enabling the S-II/S-IVB early staging capability.	Necessary because of S-II ullage engine removal and removal of 4 of 8 S-IC retromotors.

APPROVAL

SATURN V LAUNCH VEHICLE FLIGHT EVALUATION REPORT

AS-510, APOLLO 15 MISSION

By Saturn Flight Evaluation Working Group

The information in this report has been reviewed for security classification. Review of any information concerning Department of Defense or Atomic Energy Commission programs has been made by the MSFC Security Classification Officer. The highest classification has been determined to be unclassified.

Stanley L. Fragge
Security Classification Officer

This report has been reviewed and approved for technical accuracy.

George H. McKay, Jr.
Chairman, Saturn Flight Evaluation Working Group

Herman K. Weidner
Director, Science and Engineering

Richard G. Smith
Saturn Program Manager

END

DATE

FILMED

DEC 14 1973